Dissertation zur Erlangung des Doktorgrades
der Fakultät für Chemie und Pharmazie
der Ludwig-Maximilians-Universität München

Entwicklung und Anwendung von MS-Bindungsstudien für die MB327-PAM-1-Bindungsstelle des nikotinischen Acetylcholinrezeptors mit UNC0642 als Reporterligand

Valentin Nitsche

aus

München, Deutschland

2024

Erklärung

Diese Dissertation wurde im Sinne von § 7 der Promotionsordnung vom 28. November 2011 von Herrn Prof. Dr. Klaus T. Wanner betreut.

Eidesstattliche Versicherung

Diese Dissertation wurde eigenständig und ohne unerlaubte Hilfe erarbeitet.

München, 29.04.2024

_____

Valentin Nitsche

Dissertation eingereicht am	29.04.2024
1. Gutachter	Prof. Dr. Klaus T. Wanner
2. Gutachter	Prof. Dr. Franz F. Paintner
Mündliche Prüfung am	06.06.2024

Die vorliegende Arbeit entstand in der Zeit vom Oktober 2019 bis April 2024
am Department für Pharmazie – Zentrum für Pharmaforschung – der
Ludwig-Maximilians-Universität München auf Anregung und unter Leitung von

Herrn Prof. Dr. Klaus T. Wanner

Für die hervorragende und sehr engagierte Betreuung und Förderung meiner Arbeit
danke ich Herrn Prof. Dr. Klaus T. Wanner sehr herzlich.

Herrn Prof. Dr. Franz F. Paintner danke ich sehr herzlich für die ausgezeichneten
Forschungsbedingungen und für die Übernahme des Korreferats.

Danksagung

Zuerst möchte ich mich auch an dieser Stelle nochmal aufrichtig bei Prof. Dr. Klaus T. Wanner für die exzellente Betreuung dieser Arbeit bedanken. Auch Prof. Dr. Franz F. Paintner danke ich sehr herzlich für sein unermüdliches Wirken in diesem Projekt. Danke Ihnen beiden für die gute und respektvolle Zusammenarbeit!

Ein immens großes „Danke!“ gilt Georg Höfner für seine jahrelange Unterstützung. Georg auf einem Hocker neben mir sitzend, die Beine angewinkelt, einen Apfel in der Hand, den Blick konzentriert auf ein Problem auf dem Bildschirm gerichtet – dieses Bild werde ich nie vergessen. Nur selten ging es mir nach so einem Treffen nicht besser als davor. Schön, dass wir trotzdem nicht nur über Probleme geredet haben.

Danke an Karin V. Niessen und Thomas Seeger sowie an deren Arbeitsgruppen am Institut für Pharmakologie und Toxikologie der Bundeswehr für die gute Kooperation über all die Jahre. Besonders bei Sabrina Brockmöller und Sebastian Muschik möchte ich mich herzlich für die Hilfe beim „Fisch aufarbeiten“ bedanken.

Auch Prof. Dr. Holger Gohlke, sowie dessen Mitarbeitern Christoph G. W. Gertzen und Jesko Kaiser gilt mein uneingeschränkter Dank für die tolle Zusammenarbeit.

Bei Claudia Glas und Lars Allmendinger möchte ich mich für unzählige spaßige Mittagspausen bedanken. Bei Problemen jeder Art konnte ich mich stets auf Lars verlassen und seine regelmäßigen Besuche im Labor steigerten immer die Stimmung.

Danke an alle Mitarbeitenden des AK Wanner bzw. des AK Merk – im Laufe der Jahre verschwammen die Grenzen. Speziell Konstanten, wie Silke Duensing-Kropp und Jörg Pabel, die mich seit meinem ersten Praktikum im AK begleitet und mir bei Bedarf immer geholfen haben, dürfen nicht unerwähnt bleiben.

Meine Promotion war geprägt von wunderbaren Laborkollegen. Danke Janina Andreß, Heinrich Rudy, Thomas Ackermann, Jürgen Gabriel, Mark Währa und Tamara Bernauer für eure Unterstützung und für jede Lachträne, die ich im Labor geweint habe. Besonders Tamara danke ich für die gemeinsame Arbeit und ihre Freundschaft.

Mein größter Dank gilt meiner Familie und meinen Freunden. Ohne die Liebe meiner Eltern Elisabeth und Kai, meiner Schwester Fanny und meiner Freundin Franziska wäre ich verloren. Dass es mir nicht mehr möglich ist, alle vier in den Arm zu schließen, fühlt sich nicht richtig an. Ich kann nicht in Worte fassen, wie dankbar ich euch bin.

Die vorliegende kumulative Dissertation basiert auf folgenden Publikationen:

Erste Publikation:

Sonja Sichler, Georg Höfner, **Valentin Nitsche**, Karin V. Niessen, Thomas Seeger, Franz Worek, Franz F. Paintner, Klaus T. Wanner. „Screening for new ligands of the MB327-PAM-1 binding site of the nicotinic acetylcholine receptor". *Toxicology Letters*, vol. 394, 2024, pp. 23-31.

Zweite Publikation:

Valentin Nitsche, Georg Höfner, Jesko Kaiser, Christoph G. W. Gertzen, Thomas Seeger, Karin V. Niessen, Dirk Steinritz, Horst Thiermann, Franz Worek, Holger Gohlke, Franz F. Paintner, Klaus T. Wanner. "MS Binding Assays with UNC0642 as reporter ligand for the MB327 binding site of the nicotinic acetylcholine receptor". *Toxicology Letters*, vol. 392, 2024, pp. 94-106.

Dritte Publikation:

Jesko Kaiser, Christoph G. W. Gertzen, Tamara Bernauer, **Valentin Nitsche**, Georg Höfner, Karin V. Niessen, Thomas Seeger, Franz F. Paintner, Klaus T. Wanner, Dirk Steinritz, Franz Worek, Holger Gohlke. „Identification of ligands binding to MB327-PAM-1, a binding pocket relevant for resensitization of nAChRs". *Submitted*.

Vierte Publikation:

Tamara Bernauer, **Valentin Nitsche**, Jesko Kaiser, Christoph G. W. Gertzen, Georg Höfner, Karin V. Niessen, Thomas Seeger, Dirk Steinritz, Franz Worek, Holger Gohlke, Klaus T. Wanner, Franz F. Paintner. „Synthesis and Biological Evaluation of Novel MB327 Analogs as Resensitizers for Desensitized Nicotinic Acetylcholine Receptors after Intoxication with Nerve Agents". *Submitted*.

Fünfte Publikation (Manuskript):

Tamara Bernauer, **Valentin Nitsche**, Georg Höfner, Karin V. Niessen, Thomas Seeger, Dirk Steinritz, Franz Worek, Klaus T. Wanner, Franz F. Paintner. „Structure-Affinity Relationship of Quinazoline Derivatives as Potential Resensitizers of Desensitized nAChRs After Nerve Agent Intoxication".

Inhaltsverzeichnis

1 Einleitung

1.1 Organische Phosphorverbindungen: über Insektizide und Nervenkampfstoffe

Die Entwicklung von Phosphorsäure- und Thiophosphorsäureestern als Insektizide geht auf den deutschen Chemiker Gerhard Schrader zurück [1]. Unter den zahlreichen von ihm erstmals synthetisierten Verbindungen befanden sich auch Tabun und Sarin, die aber wegen ihrer enormen Toxizität nicht im Geringsten als Pflanzenschutzmittel in Betracht kamen [2]. Dafür erregten diese Verbindungen das Interesse der deutschen Wehrmacht, die schließlich während des Zweiten Weltkriegs Organophosphorverbindungen in Deutschland als chemische Waffen im Tonnenmaßstab herstellen ließ [3]. Inzwischen ist eine große Vielfalt an weiteren Nervenkampfstoffen bekannt, die sich von diesen Organophosphorverbindungen ableiten und im Laufe des vergangenen Jahrhunderts in zahlreichen Ländern entwickelt wurden. Tabun und Sarin werden dabei heute als G-Kampfstoffe klassifiziert, mit dem Buchstaben „G“ für Germany, da sie in Deutschland hergestellt wurden. Weitere bekannte Vertreter aus dieser Gruppe sind die Nervenkampfstoffe Cyclosarin und Soman. Die Entwicklung dieser Verbindungen fand in Deutschland in etwa in der Zeit von Anfang bis Mitte des 20. Jahrhunderts statt. An dieser Stelle sei noch erwähnt, dass Gerhard Schrader im Rahmen seiner Forschung zur Entwicklung von Insektiziden ein beachtlicher Erfolg beschieden war. Der von ihm bereits 1944 hergestellte Thiophosphorsäureester Parathion wurde wegen seiner insektiziden und akariziden Wirkung zu einem über viele Jahre weltweit verwendeten Pflanzenschutzmittel.

Nervenkampfstoffe aus dem Vereinigten Königreich Großbritannien werden unter dem Begriff V-Reihe zusammengefasst, von denen als der wohl berühmteste Vertreter VX zu nennen ist, während Kampfstoffe der Nowitschok-Reihe (russisch „Nowitschok“ ≙ Neuling) ihren Ursprung in der Sowjetunion haben [4, 5]. Ob Insektizid oder Nervenkampstoff – in der Regel lassen sich diese Verbindungen mit der „Schrader-Formel“ beschreiben (siehe Abbildung 1) [6]. Obwohl es sich bei der Vielzahl der inzwischen entwickelten Verbindungen, die mit dieser Formel beschrieben werden können, nicht ausschließlich um Phosphorsäureester handelt, wird zu ihrer Beschreibung häufig der Begriff „Organophosphate“ verwendet. Streng genommen ist dieser Begriff chemisch ebenso wenig korrekt, wie „Organophosphorverbindungen“,

welcher in diesem Kontext auch häufig als Oberbegriff für diese Art von Insektiziden und Nervenkampstoffen genutzt wird. Im streng chemischen Sinne umfasst der erste Begriff, Organophosphate, keine Phosphonsäurederivate wie etwa Sarin, während sich der zweite, Organophosphorverbindungen, im Prinzip nur auf diese, d.h. Verbindungen mit einer Phosphor-Kohlenstoff-Bindung bezieht (und somit z.B. Parathion oder GV nicht miteinbezieht). Der Einfachheit halber und auch weil in der Literatur so geläufig, sollen die Begriffe Organophosphorverbindung(en) und Organophosphat(e), bzw. die Abkürzung „OP(s)“ aber auch in dieser Arbeit verwendet werden, um Insektizide und Nervenkampfstoffe zu beschreiben, die dem durch die „Schrader-Formel“ gegebenen Schema folgen.

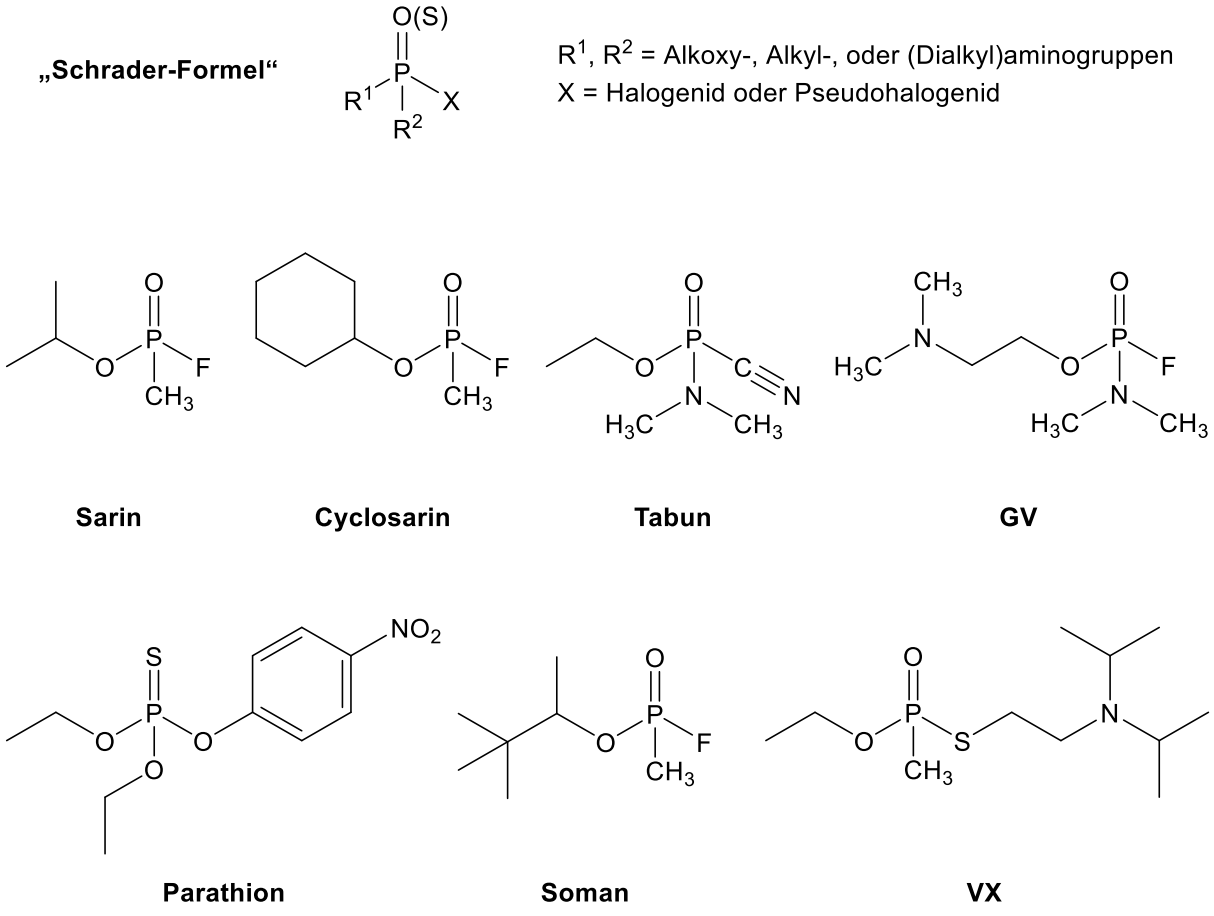

Abbildung 1: „Schrader-Formel“ (nach Quitschau et al. [6]) und prominente Vertreter von OPs (vereinfachte Darstellung ohne Angabe der Stereochemie).

Obwohl die eingangs beschriebenen Nervenkampfstoffe im 20. Jahrhundert in sehr großen Mengen hergestellt worden waren, kamen sie zum Glück nur in vergleichsweise beschränktem Maße zum Einsatz [3, 7]. Einsätze von Nervenkampfstoffen im

20. aber auch im 21. Jahrhundert gibt es leider dennoch zu verzeichnen. Einmal im ersten Golfkrieg sowie im syrischen Bürgerkrieg in Form größerer Giftgasanschläge, aber auch bei Attentaten auf Einzelpersonen wie bei dem Anschlag auf den russischen Ex-Spion Sergei Skripal oder den russischen Politiker Alexei Nawalny und wie bei der Ermordung von Kim Jong-nam, dem Halbbruder des nordkoreanischen Staatschefs Kim Jong-un [7-17]. Mit über 190 Unterzeichnerstaaten hat die Chemiewaffenkonvention, die seit 1997 in Kraft ist und den Gebrauch, die Lagerung und Herstellung chemischer Waffen untersagt, bis heute zu einer Vernichtung großer Bestände chemischer Waffen geführt, den Einsatz von Nervenkampfstoffen konnte sie aber wie beschrieben, trotz der Ächtung dieser Verbindungen, nicht gänzlich verhindern [7, 18].

So wie der Einsatz von Nervenkampfstoffen zu militärischen oder terroristischen Zwecken unverändert eine realistische Bedrohung darstellt, geht auch weiterhin von den in Insektiziden enthaltenen Organophosphatverbindungen eine Gefahr aus. Auch wenn immer mehr organophosphathaltige Pflanzenschutzmittel wegen ihrer Toxizität in den Industrieländern verboten sind (das oben aufgeführte Parathion hat in der Europäischen Union z.B. seit 2001 keine Zulassung mehr), stellen sie besonders in weniger entwickelten Ländern unverändert eine große Gefahr dar, wo durch Unfälle oder unsachgemäßen Gebrauch verursachte Organophosphatvergiftungen, oft mit Todesfolge, keine Seltenheit sind [19-22].
Im folgenden Kapitel sollen nun die Mechanismen und die Folgen einer Vergiftung mit Organophosphorverbindungen sowie der derzeitige Stand bei der medizinischen Behandlung beschrieben werden.

1.2 Störung der cholinergen Neurotransmission durch Organophosphate

Angriffspunkt der im vorangegangenen Abschnitt beschriebenen Organophosphorverbindungen ist das cholinerge System. Für ein besseres Verständnis werden nachfolgend die Grundlagen der cholinergen Neurotransmission erklärt, bevor OP-Vergiftungen und ihre Therapie näher behandelt werden.

1.2.1 Überblick: das cholinerge System

Der Neurotransmitter des cholinergen Systems, Acetylcholin, spielt sowohl im zentralen als auch im peripheren Nervensystem eine bedeutende Rolle [23-26].

Im zentralen Nervensystem ist Acetylcholin unter anderem an Vorgängen beteiligt, die für kognitive Prozesse wie die Aufrechterhaltung von Aufmerksamkeit, das Lernen und die Erinnerung von Bedeutung sind. Die cholinerge Neurotransmission im zentralen Nervensystem ist deshalb auch zentraler Gegenstand der Alzheimerforschung [27-30]. Aber auch bei diversen weiteren neurologischen Erkrankungen, wie zum Beispiel der Schizophrenie, Epilepsie und Parkinson, aber auch bei Autismus und Suchterkrankungen scheint die Acetylcholin-vermittelte Reizweiterleitung im zentralen Nervensystem eine bedeutende Rolle zu spielen, weshalb sie auch hier Gegenstand der Forschung ist [31-37].

Im peripheren Nervensystem vermittelt Acetylcholin die Signale an der neuromuskulären Endplatte der Nerven- auf die Muskelzellen und ist damit essenziell für die Auslösung von Muskelkontraktionen. Acetylcholin ist als Botenstoff außerdem maßgeblich an der Regulierung des vegetativen Nervensystems beteiligt und hat damit erheblichen Einfluss auf Blutdruck, Herzfrequenz, Verdauung und Atmung.

Die wichtigsten Bestandteile der cholinergen Synapse – ob im zentralen oder im peripheren Nervensystem – sind in Abbildung 2 schematisch dargestellt.

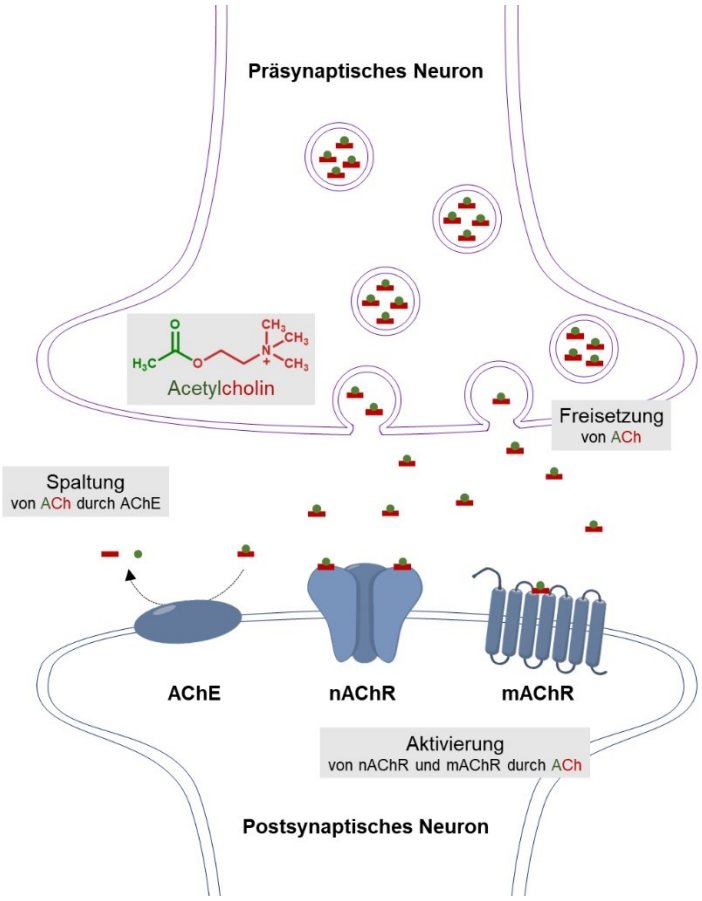

Abbildung 2: Schematische Darstellung der wichtigsten Bestandteile einer cholinergen Synapse nach Oleksak et al. [38].

Wie in der Abbildung veranschaulicht, werden die durch Acetylcholin vermittelten Effekte von zwei verschiedenen Transmembranrezeptoren übertragen: dem muskarinischen Acetylcholinrezeptor (mAChR), einem G-Protein gekoppeltem Rezeptor, und dem nikotinischen Acetylcholinrezeptor (nAChR), einem Liganden-gesteuerten Ionenkanal. Die jeweiligen Rezeptoren existieren dabei in Form diverser Subtypen. Abhängig vom Gewebetyp, in welchem der mAChR exprimiert wird, liegt er in den Isoformen M_1-M_5 vor, wobei auf die genauen Unterschiede dieser Subtypen an dieser Stelle nicht weiter eingegangen werden soll. Auch der nAChR weist, je nachdem aus welchen Untereinheiten er besteht, verschiedene Subtypen auf. Da der nAChR für die Fragestellung dieser Arbeit eine besondere Rolle einnimmt (die Gründe hierfür sollen im Verlauf dieses Kapitels weiter ausgeführt werden), ist dem Aufbau des nAChRs ein eigener Abschnitt gewidmet (siehe Kapitel 1.3.1).

Neben den beiden verschiedenartigen Rezeptoren ist das Enzym Acetylcholinesterase (AChE) das dritte wesentliche Protein, welches bei der cholinergen Neurotransmission eine essenzielle Rolle spielt, da es die Signalübertragung von Acetylcholin beendet.

Im Gegensatz zu vielen anderen Neurotransmittern erfolgt für Acetylcholin kein aktiver Abtransport des Neurotransmitters, um dessen Konzentration im synaptischen Spalt nach der Ausschüttung wieder zu verringern. Im Fall der cholinergen Reizweiterleitung wird dies stattdessen durch die AChE erreicht, welche Acetylcholin hydrolytisch in Cholin und Acetat spaltet [23-26].

An dieser Stelle kommen nun auch wieder die in der Einleitung behandelten OPs ins Spiel, da diese die AChE in ihrer Funktionsweise einschränken und damit das cholinerge System aus dem Gleichgewicht bringen. Zu welchen Konsequenzen dies führen kann, und welche Optionen zur Wiederherstellung der Funktionsfähigkeit des cholinergen Systems bestehen, soll im Weiteren beschrieben werden.

1.2.2 Organophosphatvergiftung

Vergiftungen mit OPs liegt unabhängig von der jeweiligen Substanz immer der gleiche Mechanismus zugrunde: die Hemmung der Acetylcholinesterase [39]. Wie bereits beschrieben ist die AChE für den Abbau von Acetylcholin und damit für die Beendigung des durch den Neurotransmitter vermittelten Signals zuständig. Die AChE hydrolysiert Acetylcholin mit sehr hoher Effizienz (bis zu 600000 Moleküle pro Minute [31]) zu Cholin und Acetat. Dieser Prozess wird im Wesentlichen durch drei Aminosäuren, Serin, Histidin und Glutamat, vermittelt, die im Zentrum des Enzyms vorliegen und als katalytische Triade bezeichnet werden. Bei der Spaltung des Acetylcholins wird unter katalytischer Beteiligung der beiden anderen Aminosäuren zunächst der Acetylrest des Substrats auf Serin übertragen (Abbildung 3a, **1** und **2**) und sodann aus der Esterfunktion freigesetzt (Abbildung 3a, **2** und **3**). Wenn jedoch anstelle eines Acetylcholinmoleküls ein OP-Molekül in das katalytische Zentrum der AChE gelangt, wird dieses anstelle des Acetylrestes des Acetylcholins unter Abspaltung einer Abgangsgruppe auf die OH-Funktion des Serins übertragen (Abbildung 3b, **4** und **5**). Wegen seiner hohen Stabilität kann dieses aus dem in der katalytischen Triade vorhandenen Serin und dem OP gebildete Produkt nicht weiter abgebaut werden. Die AChE ist somit blockiert [40-42]. Abhängig von der jeweiligen Organophosphatverbindung ist zwar nicht ganz ausgeschlossen, dass auch die Bindung zwischen der OH-Funktion des Serinrests der katalytischen Triade und dem OP, ähnlich wie bei dem AChE-Acetyl-Addukt, wieder gespalten wird, die Wahrscheinlichkeit hierfür ist aber gering (Abbildung 3b, **5** und **6**). Dies gilt insbesondere für OPs, die als Nervenkampfstoffe zum Einsatz kommen, da diese in der Regel, indem sie zu besonders stabilen Addukten führen, besonders toxisch sind [43, 44]. Abbildung 3

zeigt die durch die AChE katalysierte Hydrolyse von Acetylcholin bzw. die Inhibierung der AChE durch OPs am Beispiel von Tabun.

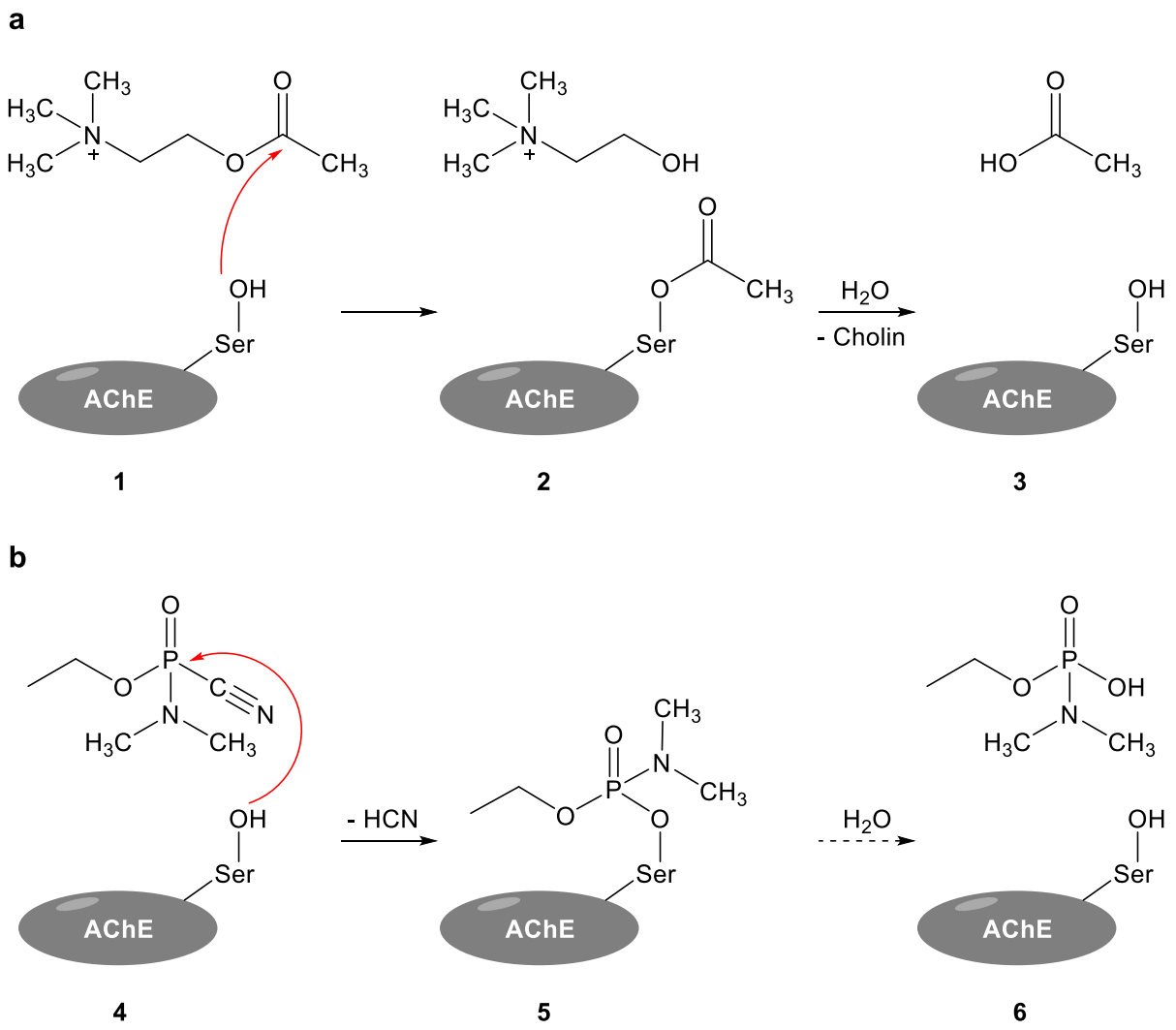

Abbildung 3: a) Abbau von Acetylcholin durch Acetylcholinesterase. b) Inhibierung der Acetylcholinesterase durch Tabun (vereinfachte Darstellung ohne Angaben zur Stereochemie).

Die eigentliche Vergiftungssymptomatik nach Exposition gegenüber OPs entsteht, wenn nicht mehr ausreichend funktionsfähige AChE vorhanden ist und der Neurotransmitter deshalb im synaptischen Spalt akkumuliert. Eine Überstimulation von muskarinischen wie auch nikotinischen AChRs sind die Folgen, wobei letztere nach andauernder Überstimulation schließlich in einen dauerhaft inaktiven („desensitisierten“) Zustand übergehen. Die anhaltende Störung der cholinergen Neurotransmission mündet letztendlich in einer sogenannten cholinergen Krise. Einer erhöhten Sekretion der Speicheldrüsen und der in den Atemwegen befindlichen Drüsen folgen häufig

Bronchospasmen, Schwindel, Erbrechen, Krampfanfälle, Bewusstseinsverlust und Muskelschwäche bzw. -lähmung. Der Tod durch eine OP-Vergiftung tritt in der Regel durch Atemstillstand ein [45-47].

Obwohl allen OP-Vergiftungen der gleiche Mechanismus zugrunde liegt, sind die Therapieansätze, die im folgenden Kapitel skizziert werden, doch oft sehr unterschiedlich.

1.2.3 Ansatzmöglichkeiten bei der Therapie von Organophosphatvergiftungen

OP-Vergiftungen beruhen, wie im vorigen Kapitel beschrieben, auf einer Hemmung der AChE durch einen im katalytischen Zentrum kovalent gebundenen OP-Rest. Eine Reaktivierung des Enzyms durch Entfernung des blockierenden OP-Rests ist ein naheliegender und auch regelmäßig verfolgter therapeutischer Ansatz. Hierfür kommen sogenannte Oxime zum Einsatz, von denen insbesondere die Wirkstoffe Pralidoxim und Obidoxim therapeutisch relevant sind (siehe Abbildung 4) [48-50].

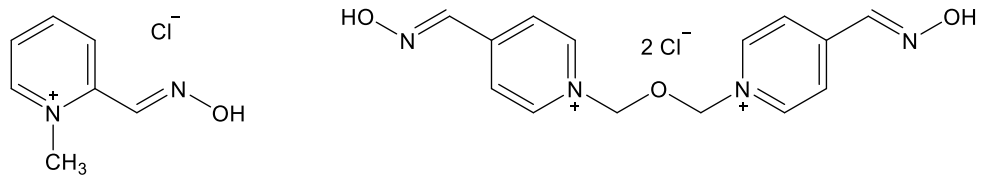

Pralidoximchlorid **Obidoximchlorid**

Abbildung 4: Zur Therapie von OP-Vergiftungen eingesetzte Oxime: Pralidoximchlorid und Obidoximchlorid.

Wegen ihrer positiven Ladung binden diese Oxime in einer zur katalytischen Triade benachbarten anionischen Stelle der AChE (im AChE-OP-Komplex), wodurch sie eine für eine Reaktion mit der Esterbindung des AChE-OP-Komplexes geeignete Vororientierung einnehmen. Durch Angriff der OH-Funktion der Oxim-Einheit am Phosphoratom des AChE-OP-Addukts kann sodann – erleichtert durch den aus Bindung an das anionische Zentrum resultierenden Templateffekt – der OP-Rest abgelöst und die AChE reaktiviert werden [40-42, 51]. Dieser Vorgang ist für ein durch Sarin blockiertes AChE-Molekül mit Pralidoxim als Reaktivator schematisch in Abbildung 5 dargestellt.

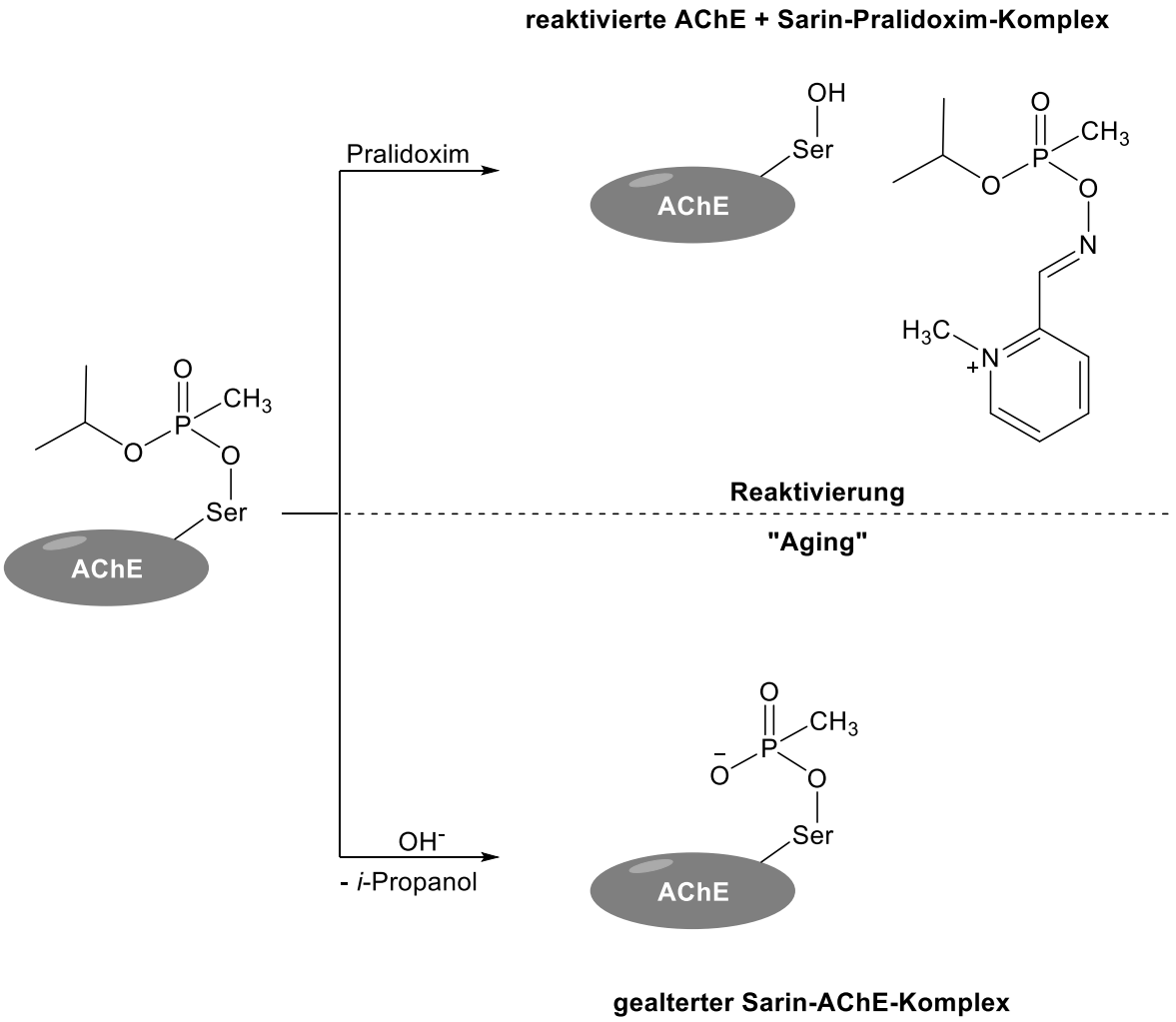

Abbildung 5: Oben: Reaktivierung einer Sarin-gehemmten AChE mit Pralidoxim. Unten: Entstehung eines nicht reaktivierbaren Sarin-AChE-Komplexes durch dessen Alterung (vereinfachte Darstellung ohne Stereochemie).

Dieser Ansatz ist aber nur bedingt erfolgreich. In einem als „aging“ (deutsch: Alterung) bezeichneten Prozess können AChE-OP-Komplexe in eine stabilere Form übergehen. Meist geschieht dies durch Abspaltung eines Alkylrests aus einer jener Esterfunktionen des OP-Rests, die bereits im ursprünglichen OP-Derivat enthalten waren (siehe Abbildung 5) [52]. Je nachdem, auf welches konkrete OP die Intoxikation zurückgeht, variiert die Geschwindigkeit des Alterungsprozesses und damit die Effizienz der Oxim-Therapie [43, 53]. Für einige der als Nervengas eingesetzten OPs ist der Alterungsprozess aber besonders schnell (z.B. Soman in wenigen Minuten [54]) mit der Folge, dass Therapieversuche mit Oximen wenig aussichtsreich sind.

Außerdem ist die Therapie mit Oximen, unabhängig vom Alterungsprozess, nicht bei jedem OP effektiv (z.B. bei einer Tabunvergiftung) – die Suche nach einer Art Breitband-Oxim, welches gegen die verschiedenen OP-Vergiftungen gleichermaßen

wirkt, ist bisher erfolglos geblieben [49, 55].
Zusammenfassend lässt sich also sagen, dass die Reaktivierung der mit einem OP-Rest blockierten AChE mit Oximen einen wichtigen Ansatz zur Therapie von OP-Vergiftungen darstellt, in der Praxis allerdings an Grenzen stößt.

Neben der Strategie, den bei einer OP-Vergiftung vorliegenden Überschuss an Acetylcholin im synaptischen Spalt durch Reaktivierung der AChE wieder zu reduzieren, besteht der zweite klassische therapeutische Ansatz darin, die Wirkung des Neurotransmitters an seinen Rezeptoren zu antagonisieren und so einer Überstimulation entgegenzuwirken. Um die durch muskarinische AChRs vermittelten Vergiftungssymptome zu lindern, hat sich Atropin bewährt [56, 57]. Jedoch bedarf es zudem des Einsatzes von Stoffen, welche die Wirkung des Acetylcholins an den nikotinischen AChRs entsprechend verringern. Derzeit sind aber keine Substanzen verfügbar, die hierfür geeignet wären [58]. nAChR-Antagonisten (wie z.B. Tubocurarin) sind zwar bekannt, ihre therapeutische Breite für einen Einsatz bei OP-Vergiftungen ist aber zu gering.
Einen alternativen, vielversprechenden Ansatz bei der Therapie von OP-Vergiftungen stellt die Behandlung mit allosterischen Modulatoren dar, die direkt an den nAChRs angreifen und diese nach einer Desensitisierung wieder in einen funktionalen Zustand überführen. Dieser Ansatz unter Verwendung sogenannter „Resensitizer“ soll im folgenden Kapitel genauer beschrieben werden.

1.3 Der nikotinische Acetylcholinrezeptor als Target bei Organophosphatvergiftungen

Wie im vorangegangenen Kapitel erläutert, beruht die derzeitige Therapie von OP-Vergiftungen hauptsächlich auf der Reaktivierung der von OPs inhibierten AChE durch Oxime und auf der Antagonisierung der durch die mAChR vermittelten Vergiftungssymptome durch Atropin. Eine therapeutische Lücke besteht bei der direkten Behandlung des nAChRs. Dieser befindet sich bei einer OP-Vergiftung vorrangig in einem nicht aktivierbaren, geschlossenen („desensitisierten“) Zustand, was unter anderem zu fatalen Vergiftungssymptomen führt. Sogenannte „Resensitizer“, also allosterische Modulatoren, die den nAChR von ebenjenem Zustand zurück in einen funktionalen Zustand überführen können, werden deshalb derzeit intensiv erforscht, um diese therapeutische Lücke zu schließen. Zum besseren Verständnis soll im Folgenden zunächst das Wichtigste zum Aufbau des nAChRs beschrieben werden, bevor im Weiteren ein kurzer Überblick zum derzeitigen Stand der Forschung zum Thema nAChR-„Resensitizer“ folgt.

1.3.1 Aufbau des nikotinischen Acetylcholinrezeptors

Der nAChR ist sicherlich einer der am besten untersuchten Vertreter aus der Gruppe der Cys-Loop-Rezeptoren. Diese Rezeptoren, zu denen unter anderem auch der 5-HT_3-, der $GABA_A$- und der Glycin-Rezeptor zählen, stellen aus fünf Untereinheiten bestehende Liganden-gesteuerte Ionenkanäle dar [59-61].

Beim nAChR handelt es sich um einen kationenselektiven, membranständigen Ionenkanal, der nach Aktivierung permeabel für Natrium- und Kalium-Ionen wird. Abhängig von den im Ionenkanal vorhandenen Untereinheiten, kann dieser auch für Calcium-Ionen durchlässig sein [62, 63]. Der Übergang des Rezeptors von seinem Ruhezustand (geschlossener Ionenkanal) in seinen aktiven, Ionen-leitenden Zustand (offener Ionenkanal) wird durch die Bindung von Liganden an die orthosteren Bindungsstellen des Rezeptors ausgelöst. Neben diesen beiden Zuständen ist für den nAChR außerdem bekannt, dass er in einen desensitisierten Zustand übergehen kann, wenn er anhaltend durch Agonisten stimuliert wird. Die Desensitisierung hängt dabei z.B. von der Agonistkonzentration, von der Dauer der Exposition des Rezeptors gegenüber Agonisten, vom Rezeptorsubtyp, sowie vom jeweiligen, konkreten Agonisten ab. Im desensitisierten Zustand ist der Ionenkanal geschlossen, im Gegensatz zum Ruhezustand aber vorübergehend nicht aktivierbar [64-70]. Die

Desensitisierung an sich, sowie der Wechsel zwischen den beschriebenen Zuständen des Rezeptors sind komplexe Prozesse und seit Langem Gegenstand der Forschung [71, 72]. An dieser Stelle soll darauf nicht weiter eingegangen werden, da im Kontext dieser Arbeit lediglich die Unterscheidung der drei genannten Zustandsmöglichkeiten von Bedeutung ist, um die Rolle des nAChRs bei einer OP-Vergiftung bzw. bei deren Therapie besser einordnen zu können.

Wie bereits beschrieben setzt sich der nAChR aus fünf Untereinheiten zusammen. Bei diesen wird grundsätzlich zwischen den Subtypen α, β, γ, δ und ε unterschieden, wobei für den α- bzw. β-Subtyp wiederum zehn bzw. vier weitere Varianten existieren [73]. Unterschiedliche Kombinationen der verschiedenen Untereinheiten ermöglichen eine Vielzahl von Isoformen des nAChRs, welche sich in ihren pharmakologischen Eigenschaften und ihrer Gewebeverteilung unterscheiden können [74]. Vereinfacht lässt sich dabei zwischen den muskulären und neuronalen nAChRs unterscheiden [75]. Im Weiteren soll der Fokus auf den nAChR vom Muskeltyp gelegt werden. Dieser ist verantwortlich für die Reizübertragung von Nerven- auf Muskelzellen an der motorischen Endplatte. Weil gerade die Störung der neuromuskulären Transmission zu fatalen Konsequenzen – wie z.B. einer Lähmung der Atemmuskulatur – führen kann, fällt ihm im Kontext dieser Arbeit eine zentrale Rolle zu [47, 76].

Der Muskeltyp-nAChR wird seit langem erforscht, häufig anhand des nAChRs von Zitterrochen (z.B. *Tetronarce californica*, vor allem bekannt als *Torpedo californica*) [77]. Dies liegt zum einen darin begründet, dass die Rezeptoren in einer sehr hohen Dichte in den Elektroorganen dieser Tiere vorliegen und damit, gerade im Vergleich zu humanen Muskeltyp-nAChRs, leicht zugänglich sind. Zum anderen weisen die nAChRs aus den Elektroorganen der Zitterrochen eine hohe Homologie zu humanen Muskeltyp-nAChRs auf [78, 79]. So setzen sich der embryonale Muskeltyp-nAChR des Menschen und der nAChR des Elektroorgans der Zitterrochen beide aus zwei α-, einer β-, einer δ- und einer γ-Untereinheit zusammen. Beim humanen, adulten Muskeltyp-nAChR ist die γ- jedoch durch eine ε-Untereinheit ersetzt [80, 81]. Nichtsdestotrotz gilt der „*Torpedo*-nAChR“ seit jeher als besonders geeignetes Modell zur Erforschung des humanen Muskeltyp-nAChRs.

Als Meilenstein bei der Erforschung des *Torpedo*-nAChRs kann die Arbeit von Unwin et al. [82] gelten, auch wenn sie laut neuer Untersuchungen die eine oder andere Schwäche bzgl. einzelner Strukturdetails aufweist [83-85]. Abbildung 6 zeigt die

dreidimensionale Struktur des *Torpedo*-nAChRs, wie sie von Unwin et al. beschrieben wird.

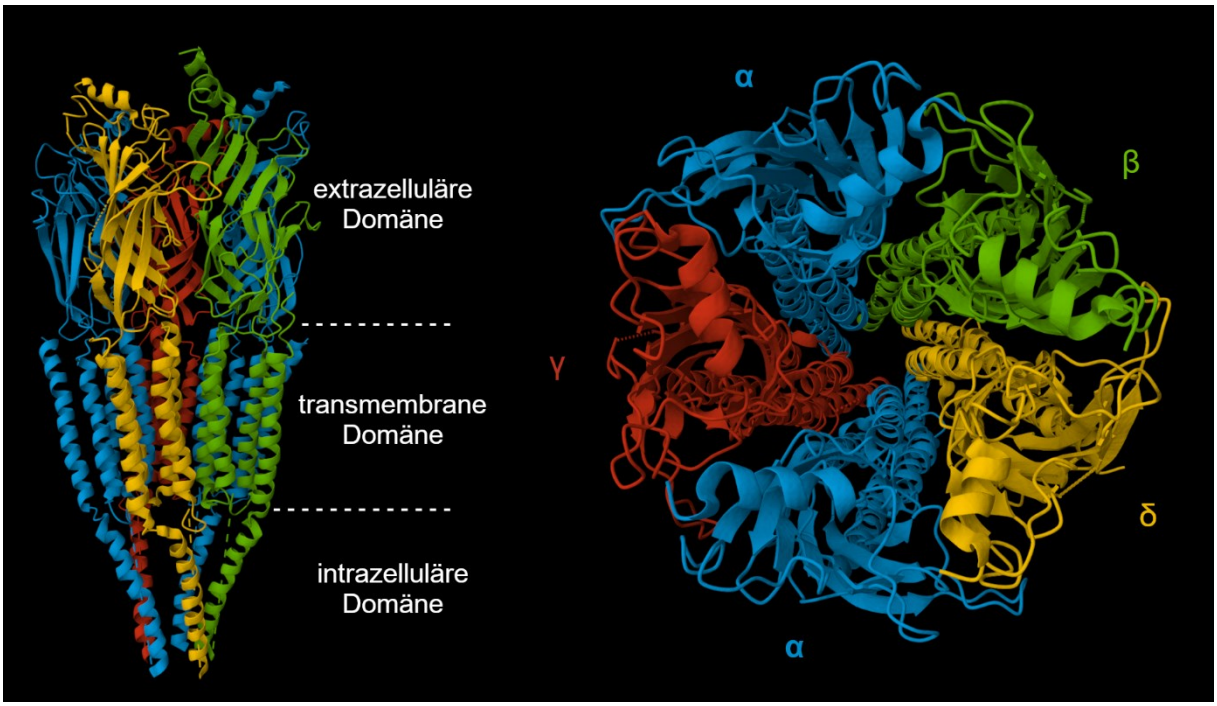

Abbildung 6: Struktur des *Torpedo*-nAChRs nach Unwin et al. (PDB: 2BG9, [82]), links: Seitenansicht des Rezeptors, rechts: Perspektive von extrazellulär nach intrazellulär. Die Abbildung wurde via RSCB.org [86] mit dem Mol* Viewer [87] erstellt.

Der Muskeltyp-nAChR besitzt zwei Bindungsstellen für den Neurotransmitter Acetylcholin, welche als orthosterische Bindungsstellen bezeichnet werden. Entsprechend des natürlichen Liganden, des Acetylcholins, ist auch häufig von „Acetylcholin-Bindungsstellen“ die Rede [67, 88, 89]. Neben den Bindungsstellen für den Neurotransmitter besitzen nAChRs zahlreiche weitere, allosterische Bindungsstellen, welche die Funktion des Rezeptors beeinflussen können, weshalb der nAChR in der Literatur auch als „allosteric machine“ beschrieben wird [90-92]. Wie bereits erwähnt, stellen ebenjene Bindungsstellen eine überaus vielversprechende Möglichkeit zur Therapie von OP-Vergiftungen dar. Der aktuelle Stand der Forschung bezüglich des Einsatzes allosterer Modulatoren des nAChRs zur Therapie von OP-Vergiftungen, d.h. sogenannter „Resensitizer“, soll im folgenden Kapitel skizziert werden.

1.3.2 Bispyridiniumverbindungen ohne Oxim-Funktion als potenzielle „Resensitizer“ des nikotinischen Acetylcholin-rezeptors

Die Entwicklung von Wirkstoffen, welche den nAChR bei OP-Vergiftung über einen allosterischen Mechanismus vom desensitisierten zurück in einen funktionalen Zustand bringen (sogenannte „Resensitizer“), würde die Therapie von OP-Vergiftungen maßgeblich verbessern. Eine Substanzklasse, die sich in diesem Rahmen als besonders vielversprechend erwiesen hat und intensiv untersucht wurde, sind die Bispyridiniumverbindungen mit MB327 (siehe Abbildung 7) als dem wohl bekanntesten und am besten untersuchten Vertreter.

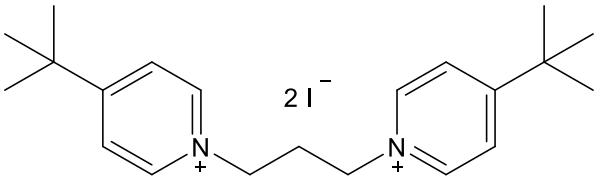

MB327

Abbildung 7: Modellsubstanz potenzieller „Resensitizer“ des nAChRs: MB327.

MB327 galt dabei nicht von Vornherein als „Resensitizer“. Noch bevor der Mechanismus, über den MB327 bei der Therapie von OP-Vergiftungen wirkt, aufgeklärt war, wurden *ex vivo* und *in vivo* Experimente mit MB327 durchgeführt, die das pharmakologische Potenzial dieser und verwandter Bispyridiniumverbindungen deutlich machten. So erhöhte MB327 als Teil einer Kombinationstherapie beispielsweise die Überlebenschance von mit OPs vergifteten Meerschweinchen in *in vivo* Versuchen [93, 94]. Auch in *ex vivo* Experimenten ließen sich vorteilhafte Effekte von MB327 beobachten: Muskelpräparationen diverser Spezies (Mensch, Ratte, Meerschweinchen), welche mit Soman vergiftet und somit gelähmt worden waren, erlangten bei einer Behandlung mit MB327 zumindest einen Teil ihrer Muskelkraft zurück [94, 95]. Die Tatsache, dass die in diesen Versuchen durch Soman gehemmte AChE wegen des hier sehr schnell ablaufenden „Aging“-Prozesses nicht zugänglich für Reaktivierung ist, war bereits ein Indiz dafür, dass die Wirkung von MB327 nicht über eine Reaktivierung der AChE zustande kommt. Genauere Details zum tatsächlichen Wirkmechanismus von MB327 lieferten aber erst funktionale Studien am

nAChR, welche zeigten, dass MB327 in der Lage ist den Rezeptor von seinem desensitisierten zurück in einen funktionalen Zustand zu überführen – also zu resensitisieren. Der Begriff „Resensitizer“ in diesem Zusammenhang ist seitdem geläufig [96-99].

Etwa zur gleichen Zeit zeigten erste *in silico* Untersuchungen, dass MB327 Bindungsstellen am nAChR besitzt, die nicht den orthosterischen Bindungsstellen entsprechen und somit für die Vermittlung allosterischer Effekte verantwortlich sein könnten [99]. Wenngleich Details bezüglich der zunächst identifizierten Bindungsstellen durch neue Erkenntnisse überholt sind, zeigen auch neue *in silico* Studien, dass MB327 exklusive Bindungsstellen am nAChR besetzt, über die es wohl allosterische Effekte auf den nAChR ausübt („MB327-PAM-1-Bindungsstelle“) [100]. Hinweise auf eine spezifische Bindung von MB327 an den nAChR lieferten zu den *in silico* Studien auch MS-Bindungsassays (siehe auch folgendes Kapitel) mit einem deuterierten Analogon von MB327, [$^2H_6$]MB327, als Reporterligand, mit denen sich die spezifische Bindung dieser Verbindung an den nAChR – in Bindungsexperimenten mit *Torpedo*-nAChR – nachweisen ließ [98].

Trotz der beschriebenen vorteilhaften Effekte, die MB327 über allosterische Bindungsstellen des nAChRs zu vermitteln scheint, ist die Substanz nicht für die Therapie von OP-Vergiftungen geeignet [101]. Die für die Resensitisierung des nAChRs erforderliche hohe Konzentrationen an MB327 schließt eine selektive Wirkung von MB327 aus. Es ist beispielweise bekannt, dass MB327 in hohen Konzentrationen auch als Ionenkanalblocker wirkt, die AChE inhibiert und auch an den mAChR bindet [94, 102, 103]. Es besteht also ein dringender Bedarf an „Resensitizern“ des nAChRs mit deutlich höherer Affinität zur MB327-Bindungsstelle des nAChRs und mit ausgeprägter intrinsischer Aktivität. Ebensolche Substanzen zu identifizieren, welche dann idealerweise als Teil einer Therapie eingesetzt werden könnten, ist deshalb ein aktuell intensiv bearbeitetes Forschungsfeld. Ein System, welches hierbei unter anderem genutzt wird, um die Affinität solcher Substanzen zur ihrer Bindungsstelle am nAChR zu charakterisieren, stellen die bereits erwähnten MS-Bindungsassays dar, auf die im folgenden Kapitel genauer eingegangen werden soll.

1.3.3 MS-Bindungsassays und ihre Anwendung bei der Suche nach und der Weiterentwicklung von „Resensitizern“

Damit ein Wirkstoff an einem Rezeptor einen Effekt entfalten kann, muss er an diesen binden. Die Untersuchung der Bindung von Wirkstoffkandidaten an das entsprechende Zielprotein ist deshalb seit jeher ein wichtiger Bestandteil bei der Identifizierung und Entwicklung neuer Wirkstoffe. Die hierzu typischerweise eingesetzten Bindungsassays beruhen auf verschiedenen Methoden. Bei der wohl klassischsten Variante werden radioaktiv markierte Liganden, die an die zu untersuchende Bindungsstelle binden, eingesetzt [104, 105]. Über die Messung der „gebundenen Radioaktivität“ kann die Bindung des Radioliganden selbst charakterisiert werden. Indem der Radioligand als Reporterligand eingesetzt wird, kann zudem auch auf indirekte Weise die Bindung von nicht radioaktiv markierten Verbindungen an die entsprechende Bindungsstelle bestimmt werden. Eine attraktive Alternative zu Radioligand-Bindungsstudien stellen Massenspektrometrie-basierte Bindungsstudien („MS-Bindungsstudien“) dar. Diese bieten gegenüber Radioligand-Bindungsassays den Vorteil, dass sie eben ohne radioaktiv markierte Substanzen auskommen, welche in der Regel zu einem erheblichen Aufwand hinsichtlich Bürokratie, Sicherheitsvorschriften, Entsorgung, etc. führen. Außerdem sind MS-Bindungsassays deutlich flexibler, was die Wahl des Reporterliganden betrifft, da mit nativen Substanzen gearbeitet werden kann und keine radioaktiv markierten Liganden erforderlich sind. Unabhängig davon, auf welche Weise die Bindung des Liganden letztendlich gemessen wird – massenspektrometrisch (typischerweise mittels LC-MS) oder durch Messung der Radioaktivität – folgen beide Systeme demselben Prinzip und beruhen auf den gleichen theoretischen Grundlagen [106-108]. Im Folgenden soll zuerst kurz das Prinzip eines MS-Bindungsassays beschrieben werden, bevor im Anschluss die wichtigsten theoretischen Grundlagen bezüglich Rezeptor-Ligand-Bindungsassays und der für diese Arbeit relevanten Arten von Bindungsexperimenten erläutert werden.

Bei der Bindung eines Liganden an seinen Rezeptor handelt es sich um einen im Prinzip einfachen chemischen Prozess, bei dem aus den Edukten, den Ligand- und Rezeptormolekülen, Rezeptor-Ligand-Komplexe entstehen (siehe Gleichung 1). Dieser Vorgang besteht aus zwei Teilschritten, der Bildung und dem Zerfall der Rezeptor-Ligand-Komplexe, die sich die Waage halten, sobald das thermodynamische Gleichgewicht erreicht ist. Dieser Zustand kann durch Gleichung 2 beschrieben

werden. Aus dieser folgt durch Umformung Gleichung 3, in welcher zusätzlich der Quotient aus der Dissoziations- und Assoziationsgeschwindigkeitskonstante, k_{-1} und k_{+1}, durch K_d (Dissoziationsgleichgewichtskonstante) ersetzt ist. Wie man aus dieser Form des Massenwirkungsgesetzes leicht ersieht, ist der Quotient der Reaktandenkonzentrationen im Gleichgewichtszustand konstant. Diese Gleichgewichtskonstante K_d gibt die Lage des Reaktionsgleichgewichts wieder und ist damit die für die Affinität eines Liganden (L) zum Rezeptor (R) übliche Kenngröße [107, 109].

(1) $$[R] + [L] \underset{k_{-1}}{\overset{k_{+1}}{\rightleftharpoons}} [RL]$$

(2) $$k_{+1} \times [R] \times [L] = k_{-1} \times [RL]$$

(3) $$K_d = \frac{[R] \times [L]}{[RL]}$$

Gleichungen 1 bis 3: (1) Gleichgewichtsreaktion zu Bildung und Zerfall der Rezeptor-Ligand-Komplexe, (2) folgt aus (1) im Gleichgewichtszustand, (3) Zusammenhang zwischen Dissoziationsgleichgewichtskonstante und Gleichgewichtskonzentrationen. [L] = Ligandkonzentration, [R] = Rezeptorkonzentration, [RL] = Rezeptor-Ligand-Komplex-Konzentration, k_{+1} = Assoziationsgeschwindigkeitskonstante, k_{-1} = Dissoziationsgeschwindigkeitskonstante, K_d = Dissoziationsgleichgewichtskonstante.

Bestimmt werden kann K_d durch Sättigungsexperimente, in welchen eine konstant gewählte Rezeptorkonzentration [R_{total}] mit verschiedenen Konzentrationen des Liganden (typischerweise im Bereich von 0,1×K_d bis 10×K_d) inkubiert wird. Die hierdurch entstehenden Sättigungskurven – eine Musterkurve ist in Abbildung 8 dargestellt – folgen der Hill-Langmuir-Gleichung (Gleichung 4) [110].

(4) $$\frac{[RL]}{[R_{total}]} = \frac{[L]}{[L] + K_d}$$

Gleichung 4: Hill-Langmuir-Gleichung, [RL] = Rezeptor-Ligand-Komplex-Konzentration, [R_{total}] = Rezeptorgesamtkonzentration, [L] = Ligandkonzentration, K_d = Dissoziationsgleichgewichtskonstante.

Sofern keine anderen Binder vorhanden sind, gilt für die Rezeptorgesamtkonzentration [R_{total}], dass sie gleich der Summe aus der Konzentration an freiem Rezeptor [R] und der Konzentration an Rezeptor-Ligand-Komplex [RL] ist. Unter Gleichgewichtsbedingungen trifft bei einem Belegungsgrad der Rezeptoren von 50%, ferner Folgendes zu: [RL] = [R] = 0,5×[R_{total}]. Aus Gleichung 4 folgt damit, dass der mit dem 50%-Belegungsgrad (y-Achse) korrespondierende Wert der Ligandkonzentration [L] (x-Achse) dem K_d-Wert entspricht. Damit hierbei, wie in Abbildung 8 dargestellt, anstelle der freien Ligandkonzentration [L] die nominelle Ligandkonzentration eingesetzt werden kann (wie auf der x-Achse in Abbildung 8), darf die Verringerung der freien im Vergleich zur nominellen Ligandkonzentration – als typische Folge der Bildung von Rezeptor-Ligand-Komplexen (RL) – nicht zu hoch sein. Als tolerabel werden hier 10% angesehen (Abweichung von der freien von der nominellen Ligandkonzentration). Um zu erreichen, dass dies der Fall ist, die als Ligand-Depletion bezeichnete Verringerung der freien Ligandkonzentartion innerhalb dieser Grenze liegt, wird die Rezeptortotalkonzentration [R_{total}] in Bindungsversuchen typischerweise bei einem Wert deutlich unter dem K_d-Wert angesetzt. Neben K_d lässt sich aus den Sättigungskurven außerdem die Anzahl der Bindungsstellen im eingesetzten Rezeptormaterial (also R_{total} bzw. auch B_{max} genannt) ermitteln. Der B_{max}-Wert ergibt sich aus dem Plateau, welchem sich die Sättigungsisotherme bei hohen Ligandkonzentrationen annähert.

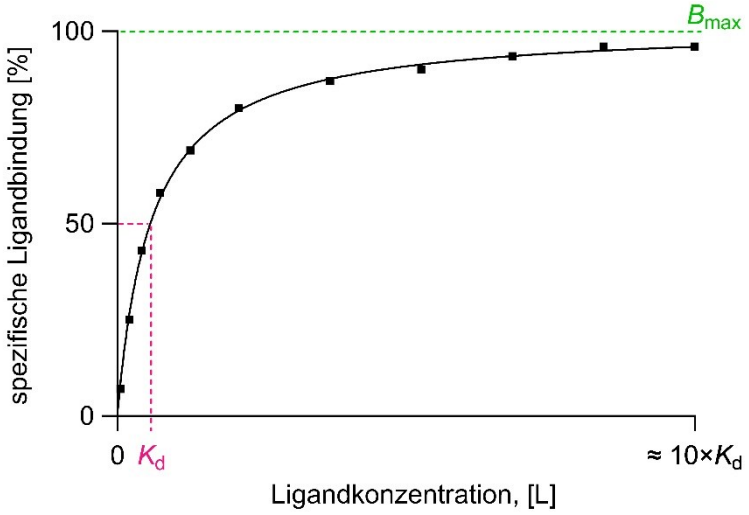

Abbildung 8: Beispiel für eine Sättigungsisotherme inklusive Darstellung der Bestimmung von K_d (pink) und B_{max} (grün).

Kompetitionsexperimente sind eine weitere Form von Bindungsexperimenten, welche für diese Arbeit besonders relevant sind. Dabei wird die Affinität kompetitiver Inhibitoren (I) indirekt mit Hilfe eines Reporterliganden bestimmt, nachdem dessen Bindungsverhalten zuvor in Sättigungsexperimenten charakterisiert wurde. Hierfür wird eine konstante Konzentration des Reporterliganden mit einer konstanten Konzentration des Rezeptors inkubiert (auch hier gilt es, Ligand-Depletion zu vermeiden). In einer Serie von Einzelexperimenten wird zusätzlich der zu untersuchende Inhibitor in verschiedenen, über mehrere Größenordnungen reichenden Konzentrationen zugegeben. Durch Darstellung der experimentell bestimmten spezifischen Bindungen des Reporterliganden (aus Gesamt- und nichtspezifischer Bindung [siehe unten]) als Funktion der logarithmischen Inhibitorkonzentration ergeben sich sogenannte Kompetitionskurven, welche durch die Gaddum-Gleichung (Gleichung 5) beschrieben werden können [111]. Aus ihnen geht der $\log IC_{50}$- bzw. der IC_{50}-Wert hervor (siehe Abbildung 9).

(5)
$$\frac{[RL]}{[R_{total}]} = \frac{[L]}{K_d \times \left(1 + \frac{[I]}{K_i}\right) + [L]}$$

Gleichung 5: Gaddum-Gleichung, [RL] = Rezeptor-Ligand-Komplex-Konzentration, $[R_{total}]$ = Rezeptorgesamtkonzentration, [L] = Ligandkonzentration, [I] = Inhibitor-konzenztration, K_d bzw. K_i = Dissoziationsgleichgewichtskonstanten des Liganden bzw. des Inhibitors.

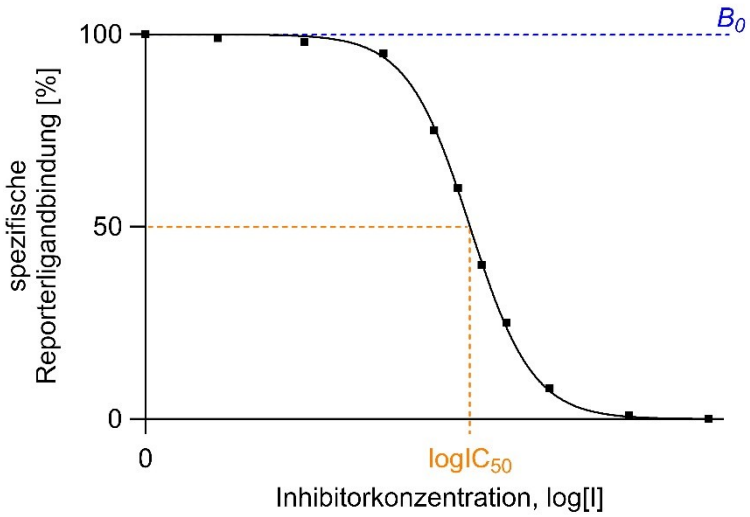

Abbildung 9: Beispiel für eine Kompetitionskurve inklusive Darstellung von B_0 (blau) und der Bestimmung von $\log IC_{50}$ (orange).

Der IC_{50}-Wert beschreibt, bei welcher Inhibitorkonzentration die spezifische Bindung des Reporterliganden um 50% reduziert wird. Es ist wichtig zu unterscheiden, dass der bei 100% spezifischer Bindung in den Kompetitionsexperimenten vorliegende B_0-Wert nicht mit dem B_{max}-Wert aus Sättigungsexperimenten identisch ist. B_0 bezeichnet im Kompetitionsexperiment die Menge an Rezeptoren bzw. Bindungsstellen, die in Abwesenheit des Inhibitors mit Reporterliganden belegt sind und ist deutlich kleiner als B_{max}, da in Kompetitionsexperimenten der Reporterligand typischerweise in einer Konzentration [L] im Bereich des K_d-Werts eingesetzt wird. Da die Größe des IC_{50}-Werts nicht konstant ist, sondern vom B_0-Wert abhängt, wird der IC_{50}-Wert meist vorteilhafterweise in die konzentrationsunabhängige Dissoziationsgleichgewichts-konstante K_i umgerechnet. Die Umrechnung kann dabei mittels der Cheng-Prusoff-Gleichung (Gleichung 6) vorgenommen werden [112].
Vor allem kompetitive Bindungsstudien sind ein wichtiges Werkzeug in der Wirkstoffentwicklung, da mit ihrer Hilfe Testverbindungen sehr effizient hinsichtlich ihrer Affinität zur untersuchten Bindungsstelle charakterisiert werden können.

(6)
$$K_i = \frac{IC_{50}}{\left(1 + \frac{[L]}{K_d}\right)}$$

Gleichung 6: Cheng-Prusoff-Gleichung, [L] = Ligandkonzentration, K_d bzw. K_i = Dissoziationsgleichgewichtskonstanten des Liganden bzw. des Inhibitors, IC_{50} = Konzentration des Inhibitors, bei welcher B_0 um 50% reduziert ist.

Die beschriebenen Bindungsexperimente bestehen in der Praxis typischerweise aus den folgenden Schritten: Inkubation des Liganden mit dem Rezeptor (ggf. Zusatz von Inhibitor), Trennung des gebundenen Liganden von dessen ungebundenem Anteil, Quantifizierung des gebundenen Liganden. Für die Quantifizierung mittels LC-MS, wie es bei den MS-Bindungsstudien der Fall ist, muss der gebundene Anteil des Liganden vor dessen Quantifizierung zusätzlich noch freigesetzt werden. Die für die Wirkstoffentwicklung interessante spezifische Bindung lässt sich hierdurch experimentell kaum bestimmen, da ein Teil des Liganden auch nicht-spezifisch, z.B. an die den Rezeptor umgebende Membran, bindet. Erfasst wird also zunächst die Gesamtbindung, welche sich aus spezifischer und nicht-spezifischer Bindung zusammensetzt. Durch Blockieren der spezifischen Bindungsstellen (beispielsweise durch einen Inhibitor mit hoher Affinität im Überschuss in separaten Experimenten),

kann aber zusätzlich auch die nicht-spezifische Bindung für den Liganden experimentell ermittelt werden. Die spezifische Bindung lässt sich im Anschluss als Differenz zwischen Gesamtbindung und nicht-spezifischer Bindung berechnen.

Wie bereits im vorangegangenen Kapitel kurz thematisiert, war es zuletzt im Arbeitskreis gelungen, auch zur Untersuchung der Bindungsstelle für MB327 am nAChR einen MS-Bindungsassay zu entwickeln [98]. Dieser MS-Bindungsassay beruht dabei auf der Verwendung von [$^2H_6$]MB327 als Reporterliganden und einer Membranaufarbeitung des Elektroplax von *Torpedo californica* als Rezeptormaterial. Letztere wurde eingesetzt, da der humane nAChR für diese Zwecke nicht verfügbar war, der *Torpedo*-nAChR diesem aber sehr ähnlich und zugleich gut zugänglich ist (siehe auch Kapitel 1.3.1). Mit dem entwickelten MS-Bindungsassay war es möglich, zum ersten Mal die Bindung von MB327 bzw. [$^2H_6$]MB327 an den nAChR in Sättigungsexperimenten zu charakterisieren. Außerdem nimmt der entwickelte MS-Bindungsassay seitdem eine zentrale Rolle bei der Suche nach und Optimierung von weiteren potenziellen Liganden für die MB327-PAM-1-Bindungsstelle ein. Wie im vorangegangenen Kapitel beschrieben, müssen diese zwingend über eine im Vergleich zu MB327 deutlich höhere Affinität und ausgeprägte intrinsische Aktivität verfügen. Der kompetitive [$^2H_6$]MB327-MS-Bindungsassay erwies sich dabei als effizientes Testsystem für die Bestimmung der Affinität von Testverbindungen zur MB327-Bindungsstelle. Von den zahlreichen damit untersuchten symmetrischen und unsymmetrischen Bispyridiniumverbindungen zeigten die meisten nur eine ähnliche oder gar geringere Affinität als das als strukturelles Vorbild verwendete MB327 ($pK_i = 4.73 \pm 0.03$) [113, 114]. Der Durchbruch bei der Suche nach deutlich höher affinen Verbindungen gelang, als Substanzbibliotheken mit einer Vielzahl strukturell unterschiedlicher Verbindungen untersucht wurden [115]. Unter den insgesamt mehr als 1300 Testverbindungen, die hierbei eingesetzt wurden, konnten einige identifiziert werden, welche teilweise eine mehr als zehnmal höhere Affinität zur MB327-Bindungsstelle des nAChRs als MB327 aufweisen. Dabei fiel eine Gruppe strukturell ähnlicher Verbindungen auf, die sich durch die bei diesen Untersuchungen höchsten gefundenen Affinitäten auszeichnen. Die Strukturen dieser Verbindungen, welche die Bezeichnungen UNC0638 ($pK_i = 6.01 \pm 0.10$), UNC0642 ($pK_i = 5.97 \pm 0.05$) und UNC0646 ($pK_i = 6.23 \pm 0.02$) tragen, sind in Abbildung 10 wiedergegeben. Abgesehen von ihrer Affinität zur MB327-Bindungsstelle des nAChRs sind für diese Verbindungen keine weiteren Daten hinsichtlich ihrer Eigenschaften gegenüber dem nAChR bekannt.

Wie aus den geschilderten Ergebnissen hervorgeht, erscheint eine genauere Untersuchung dieser Verbindungen in Bezug auf diese Eigenschaften aber eine lohnende Aufgabe, wobei sich MS-Bindungsassays als besonders hilfreiches Werkzeug erweisen dürften, wie auch bei der Suche nach weiteren „Resensitizern“ des nAChRs und deren Weiterentwicklung.

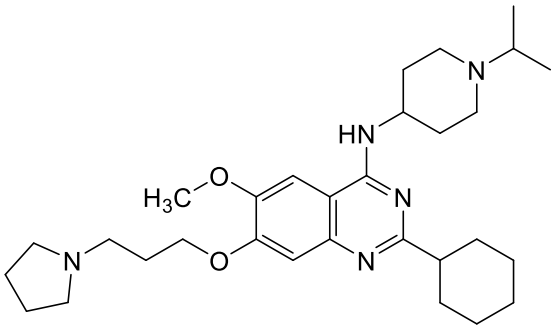

UNC0638

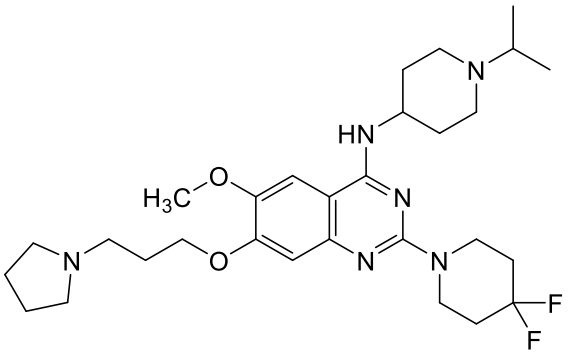

UNC0642

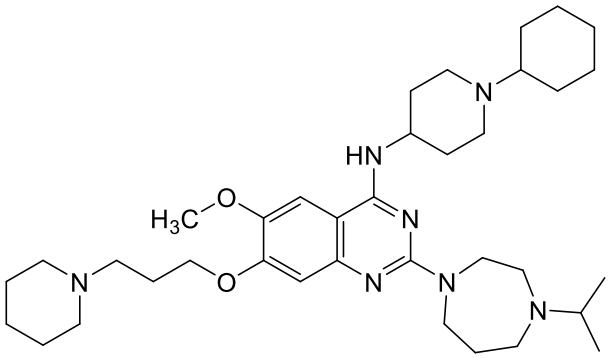

UNC0646

Abbildung 10: Strukturen der bei einem Bibliotheksscreening identifizierten Hits mit den derzeit höchsten bekannten Affinitäten zur MB327-Bindungsstelle des nAChRs: UNC0638, UNC0642 und UNC0646.

2 Zielsetzung

Vor Beginn dieser Arbeit waren im Rahmen einer Zusammenarbeit des Arbeitskreises mit dem Institut für Pharmakologie und Toxikologie der Bundeswehr die Verbindungen UNC0638, UNC0642 und UNC0646 als potenzielle „Resensitizer“ des nAChRs identifiziert worden. Diese drei strukturell ähnlichen, auf einem Chinazolin-Grundgerüst basierenden Verbindungen waren bis dahin nur als potente Inhibitoren der Methyltransferase bekannt. Bei der Suche nach neuen Liganden für die MB327-Bindungsstelle des nAChRs hatte sich nun gezeigt, dass sie auch vergleichsweise hohe, teilweise submikromolare Affinitäten und damit die höchsten bekannten Affinitäten für diese Bindungsstelle aufweisen.

Ziel dieser Arbeit war die Entwicklung und Anwendung eines MS-Bindungsassays, welcher auf einer der drei Verbindungen, UNC0638, UNC0642 oder UNC0646, als Reporterliganden basiert. Analog zum MS-Bindungsassay mit [$^2H_6$]MB327 sollte als Quelle für den nAChR eine Membranaufarbeitung des Elektroplax von *Torpedo californica* verwendet werden, da der humane nAChR für diese Zwecke nicht in ausreichenden Mengen vorliegt und der *Torpedo*-nAChR eine geeignete Alternative hierzu darstellt.

Falls die neu identifizierten Verbindungen dieselbe Bindungsstelle des nAChRs adressieren wie MB327, würde ein MS-Bindungsassay mit UNC0638, UNC0642 oder UNC0646 als Reporterligand Vorteile gegenüber dem bekannten [$^2H_6$]MB327-MS-Bindungsassay mit sich bringen. Dies liegt zum einen darin begründet, dass die Affinitäten von UNC0638 (pK_i = 6.01 ± 0.10), UNC0642 (pK_i = 5.97 ± 0.05) und UNC0646 (pK_i = 6.23 ± 0.02) zur MB327-PAM-1-Bindungsstelle deutlich höher als die von MB327 (pK_i = 4.73 ± 0.03) sind. Sowohl die Robustheit des MS-Bindungsassays als auch die Aussagekraft der damit erzielbaren Ergebnisse sollten sich durch einen höher affinen Reporterliganden verbessern. Zudem ist weder MB327 noch dessen deuteriertes Analogon, [$^2H_6$]MB327, kommerziell verfügbar – UNC0638, UNC0642 und UNC0646 sind es dagegen schon. Dies ist durchaus von Bedeutung, da dadurch nicht nur die erstmalige Entwicklung des gewünschten MS-Bindungsassays entscheidend erleichtert wird, sondern auch seine Etablierung auf der Basis einschlägiger Literaturangaben in anderen Arbeitskreisen.

Als Grundlage für den neu zu entwickelnden MS-Bindungsassay sollte zunächst eine geeignete LC-ESI-MS/MS-Methode entwickelt werden, mit der sich zumindest eine der

drei Verbindungen UNC0638, UNC0642 und UNC0646 verlässlich quantifizieren lässt. Um zu zeigen, dass die zu entwickelnde LC-ESI-MS/MS-Methode für ihren Einsatzzweck geeignet ist, sollte diese nach ausgewählten Kriterien (Selektivität, Sensitivität, Linearität, Richtigkeit, Präzision) validiert werden, und zwar unter Beachtung der von der FDA („Food and Drug Administration“) für solche Fälle herausgegebenen Richtlinien.

Die Bindung des neuen Reporterliganden an den nAChR sollte zuerst in Sättigungsexperimenten charakterisiert werden. Zusätzlich dazu sollten durch den Einsatz einiger wohl bekannter Liganden der MB327-PAM-1-Bindungsstelle in Kompetitionsexperimenten die neuen Ergebnisse anhand der alten mit dem [$^2H_6$]MB327-Bindungsassay erzielten Resultate überprüft werden. Im Anschluss daran sollte der zu entwickelnde MS-Bindungsassay schließlich als Alternative zum bisher bekannten [$^2H_6$]MB327-MS-Bindungsassay eingesetzt werden, um die Bindung von Testverbindungen an die MB327-Bindungsstelle des nAChRs zu analysieren. Bei der Auswahl der zu untersuchenden Testsubstanzen standen vor allem die folgenden Überlegungen im Vordergrund. Aufgrund von Ergebnissen aus *in silico* und *ex vivo* Experimenten, sollten neue Bispyridiniumsalze mit einem 4-Aminopyridinium-Motiv hinsichtlich ihrer Bindung am nAChR charakterisiert werden. Zudem sollten mit dem neuen MS-Bindungsassay für in *in silico* Screening-Experimenten identifizierte Hits die Affinitäten zur MB327-PAM-1-Bindungsstelle bestimmt werden. Ein Hauptaugenmerk dieser Arbeit sollte ferner auf der Untersuchung von Analoga zu den Verbindungen UNC0638, UNC0642 und UNC0646 liegen, deren Synthese im Arbeitskreis zur breiteren Abdeckung des chemischen Strukturraums geplant war. Die strukturellen Gemeinsamkeiten der drei genannten Verbindungen, UNC0638, UNC0642 und UNC0646, die alle eine vergleichsweise hohe Affinität aufweisen, legen nahe, dass Analoga mit noch höherer Affinität existieren könnten. Die Untersuchung einer Reihe von strukturanalogen Verbindungen sollte es außerdem erlauben, Struktur-Affinitäts-Beziehungen für diese Chinazolin-basierte Stoffklasse abzuleiten. Die Ergebnisse sollten für eine weitere, zielgerichtete Optimierung der Affinität von Verbindungen aus dieser Stoffklasse von „Resensitizern“ von großem Wert sein.

3 Ergebnisse und Diskussion

3.1 Erste Publikation

"Screening for new ligands of the MB327-PAM-1 binding site of the nicotinic acetylcholine receptor"

3.1.1 Zusammenfassung der Ergebnisse

Bei der Therapie von Vergiftungen mit Organophosphaten mangelt es an Wirkstoffen, welche den nikotinischen Acetylcholinrezeptor (nAChR) aus einem desensitisierten, nicht-funktionalen Zustand, welcher in Folge der Vergiftung mit Organophosphaten auftritt, in einen funktionalen Zustand rücküberführen. Verbindungen, die hierzu in der Lage sind, werden als sogenannte „Resensitizer" bezeichnet. In diesem Zusammenhang waren bisher hauptsächlich Bispyridiniumverbindungen untersucht worden. Obwohl hierbei beachtliche Erfolge erzielt werden konnten, eignen sich die bisher untersuchten Verbindungen, mit MB327 als ihrem prominentesten Vertreter, nicht als Wirkstoffe. So zeigen MB327 und die bisher untersuchten Analoga einen für eine klinische Anwendung zu geringen therapeutischen Effekt. Dies dürfte zumindest zum Teil auf die vergleichsweise geringen Affinitäten dieser Verbindungen zur MB327-PAM-1-Bindungsstelle des nAChRs zurückgehen (MB327: $pK_i = 4.73 \pm 0.03$). Über diese Bindungsstelle sollen nach derzeitigem Kenntnisstand die „resensitisierenden" Effekte dieser Verbindungen am nAChR vermittelt werden. Um Verbindungen abseits der Bispyridiniumverbindungen zu identifizieren, welche idealerweise eine deutlich höhere Affinität zur MB327-PAM-1-Bindungsstelle des nAChR als MB327 selbst aufweisen, wurden in dieser Arbeit zwei Substanzbibliotheken in Screening-Versuchen auf Testverbindungen mit Affinität zur MB327-PAM-1-Bindungsstelle untersucht. Für das Screening der „Tocriscreen Plus"- und der „ChemDiv ion channel ligand"-Bibliothek (1280 bzw. 60 Testverbindungen) wurde der [$^2H_6$]MB327-MS-Bindungsassay, der zum fraglichen Zeitpunkt als einziger für diesen Zweck zur Verfügung stand, angewendet. Hierbei konnten zehn Verbindungen identifiziert werden, die das gewählte Selektionskriterium eines IC_{50}-Werts von ≤ 10 µM erfüllten. Diese Screening-Hits wurden anschließend ausführlicher hinsichtlich ihrer Affinität zur MB327-Bindungsstelle des nAChR untersucht und offenbarten dabei teilweise niedrig- bis submikromolare Bindungsaffinitäten. Unter den zehn Verbindungen besonders auffällig ist eine Gruppe

von strukturell verwandten, Chinazolin-basierten Verbindungen, namentlich UNC0638, UNC0642 und UNC0646. Mit pK_i-Werten von respektive 6.01 ± 0.10, 5.97 ± 0.05 und 6.23 ± 0.02 weisen sie eine mehr als zehnfach höhere Affinität als MB327 auf und stellen die Verbindungen mit den bisher höchsten bekannten Affinitäten zur MB327-Bindungsstelle des nAChRs dar. Entsprechend kann festgehalten werden, dass durch das hier gezeigte Bibliothek-Screening erfolgreich Substanzen mit deutlich höheren Affinitäten identifiziert werden konnten, die es im Kontext des nAChRs unbedingt weiter zu untersuchen gilt, da sie einen vielversprechenden Ausgangspunkt für die Entwicklung potenzieller "Resensitizer“ darstellen.

3.1.2 Erklärung zum Eigenanteil

Der größte Teil der beschriebenen MS-Bindungsexperimente wurde von Sonja Sichler durchgeführt. So wurden auch nahezu alle Daten von ihr ausgewertet, nahezu alle Grafiken von ihr erstellt. Des Weiteren hat sie die erste Version des Manuskripts angefertigt. Um das Projekt abzuschließen, sollten weitere Bindungsversuche mit der im Screening auffälligen Verbindung AZ10417808 durchgeführt werden, um deren Einfluss auf die Bindung von [$^2H_6$]MB327 an die MB327-PAM-1-Bindungsstelle näher zu untersuchen. Die entsprechenden MS-Bindungsexperimente wurden eigenständig von mir durchgeführt und ausgewertet. Das bereits vorliegende Manuskript von Sonja Sichler wurde im Anschluss von mir überarbeitet und um die neuen Ergebnisse ergänzt. An der Korrektur des Manuskripts waren maßgeblich Georg Höfner, Franz F. Paintner und Klaus T. Wanner beteiligt sowie ergänzend Thomas Seeger, Karin V. Niessen und Franz Worek.

Toxicology Letters 394 (2024) 23–31

Contents lists available at ScienceDirect

Toxicology Letters

journal homepage: www.journals.elsevier.com/toxicology-letters

Screening for new ligands of the MB327-PAM-1 binding site of the nicotinic acetylcholine receptor

Sonja Sichler [a], Georg Höfner [a,1], Valentin Nitsche [a,2], Karin V. Niessen [b,3], Thomas Seeger [b,4], Franz Worek [b,5], Franz F. Paintner [a,6], Klaus T. Wanner [a,*,7]

[a] Department of Pharmacy – Center for Drug Research, Ludwig-Maximilians-Universität München, Munich, Germany
[b] Bundeswehr Institute of Pharmacology and Toxicology, Munich, Germany

ARTICLE INFO

Editor: Dr. Angela Mally

Keywords:
Nicotinic acetylcholine receptor
MS Binding Assays
Library screening
MB327-PAM-1 binding site
Quinazoline derivatives

ABSTRACT

Intoxications with organophosphorus compounds (OPCs) effect a severe impairment of cholinergic neurotransmission that, as a result of overstimulation may lead to desensitization of nicotinic acetylcholine receptors (nAChRs) and finally to death due to respiratory paralysis. So far, therapeutics, that are capable to address and revert desensitized neuromuscular nAChRs into their resting, i.e. functional state are still missing. Still, among a class of compounds termed bispyridinium salts, which are characterized by the presence of two pyridinium subunits, constituents have been identified, that can counteract organophosphate poisoning by resensitizing desensitized nAChRs. According to comprehensive modeling studies this effect is mediated by an allosteric binding site at the nAChR termed MB327-PAM-1 site. For MB327, the most prominent representative of the bispyridinium salts and all other analogues studied so far, the affinity for the aforementioned binding site and the intrinsic activity measured in *ex vivo* and in *in vivo* experiments are distinctly too low, to meet the criteria to be fulfilled for therapeutic use. Hence, in order to identify new compounds with higher affinities for the MB327-PAM-1 binding site, as a basic requirement for an enhanced potency, two compound libraries, the ChemDiv library with 60 constituents and the Tocriscreen Plus library with 1280 members have been screened for hit compounds addressing the MB327-PAM-1 binding site, utilizing the [$^2H_6$]MB327 MS Binding Assay recently developed by us. This led to the identification of a set of 10 chemically diverse compounds, all of which exhibit an IC_{50} value of $\leq$ 10 μM (in the [$^2H_6$]MB327 MS Binding Assay), which had been defined as selection criteria. The three most affine ligands, which besides a quinazoline scaffold share similarities with regard to the substitution pattern and the nature of the substituents, are UNC0638, UNC0642 and UNC0646. With binding affinities expressed as pK_i values of 6.01 ± 0.10, 5.97 ± 0.05 and 6.23 ± 0.02, respectively, these compounds exceed the binding affinity of MB327 by more than one log unit. This renders them promising starting points for the development of drugs for the treatment of organophosphorus poisoning by addressing the MB327-PAM-1 binding site of the nAChR.

1. Introduction

The use of sarin as a chemical warfare agent in a brutal civil war in Syria in recent years (OPCW 2020a) as well as the confirmed, repeated use of organophosphates in poisoning individuals as in case of Alexei Nawalny (OPCW 2020b) and of Sergei Skripal and his daughter (OPCW, 2018) show that organophosphorus compounds (OPCs) still pose a serious threat to humanity. This class of compounds exerts its detrimental pathophysiological effect via inactivation of the enzyme acetylcholinesterase (AChE). The AChE is a fundamental part of signal

* Corresponding author.
[1] 0000-0002-7957-4503
[2] 0009-0000-3351-1227
[3] 0009-0008-6810-5294
[4] 0009-0007-5713-4367
[5] 0000-0003-3531-3616
[6] 0000-0002-6795-586X
[7] 0000-0003-4399-1425

https://doi.org/10.1016/j.toxlet.2024.02.004
Received 1 August 2023; Received in revised form 8 January 2024; Accepted 18 February 2024
Available online 20 February 2024

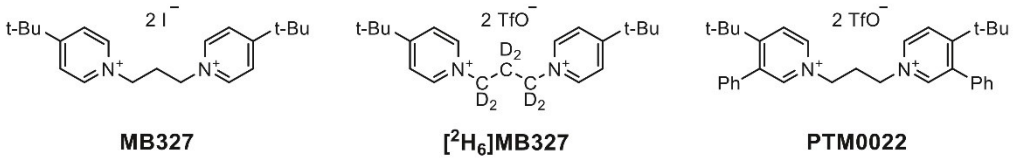

Fig. 1. Structure of MB327, [$^2H_6$]MB327 and PTM0022.

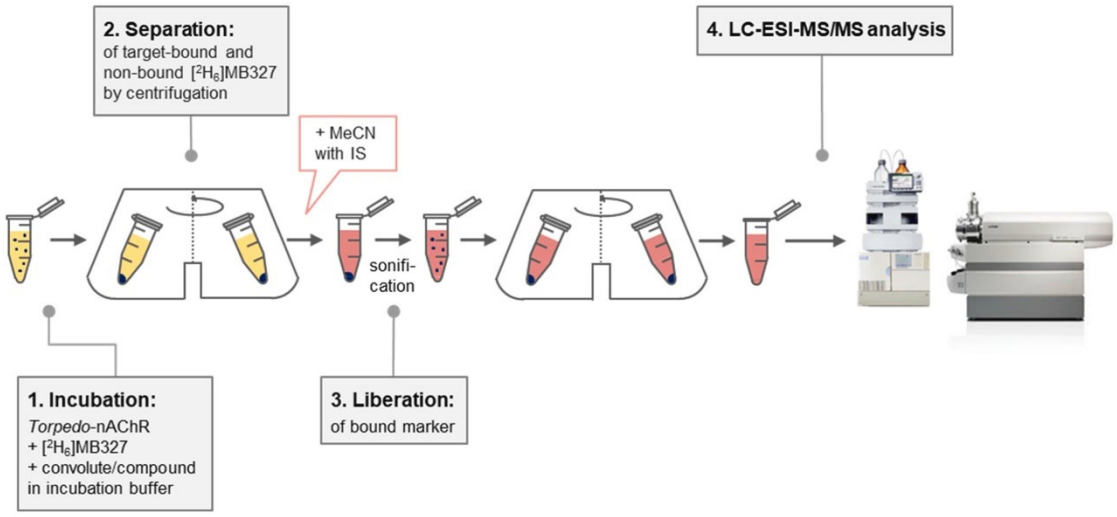

Fig. 2. MS Binding Assay workflow. The process of preparation and processing of binding samples was conducted as previously described comprising the following four steps: (1) Incubation of [$^2H_6$]MB327 as marker and aliquots of the Torpedo membrane preparation in incubation buffer, (2) Separation, (3) Liberation of bound marker and (4) LC-ESI-MS/MS analysis for quantification of bound marker. IS = internal standard {[$^2H_{18}$]MB327}.

transmission of the nervous system and responsible for the clearance of the released neurotransmitter acetylcholine from the synaptic cleft. Thus, inactivation of AChE leads to an accumulation of acetylcholine and as a consequence thereof to an overstimulation of muscarinic (mAChR) and nicotinic (nAChR) acetylcholine receptors. mAChR overstimulation can be antagonized by atropine, for instance, whereas no specific therapeutic compound is available to counteract the overstimulation of nAChR, which ultimately shifts into a non-conducting state of desensitization thereby disrupting cholinergic signaling (Papke, 2014). Desensitization of nicotinic acetylcholine receptors (nAChRs) at neuromuscular junctions leads finally to death due to respiratory paralysis.

MB327 (see Fig. 1) has been described as a potential antidote in case of organophosphate poisoning and, interestingly, has been discussed as a resensitizer of the nAChR. Recent electrophysiological studies from Niessen et al. demonstrate that the bispyridinium compound MB327 can functionally recover ("resensitize") the nAChR from desensitization (Niessen et al., 2018, 2016). In addition to the agonist, i.e. orthosteric binding site, the nAChR exhibits allosteric binding sites, as well, which have been found to allow a modulation of the function of the receptor (Arias, 2011, 2010; Changeux and Edelstein, 2005; Chatzidaki and Millar, 2015). Only recently modeling studies with MB327 identified an allosteric binding site at the nAChR termed MB327-PAM-1, which is believed to mediate its resensitizing effect on the desensitized receptor (Kaiser et al., 2023). Prior to that, pharmacological studies had demonstrated, that MB327 exerts a beneficial pharmacological effect against OPC poisoning e.g. was found to increase survival in tabun-poisoned guinea pigs *in vivo* (Turner et al., 2011). Also, for soman-impaired neuromuscular transmission in human intercostal muscle and rat diaphragm preparations, MB327 could be shown to restore muscle force (Seeger et al., 2012).

However, the toxicity of MB327 limits its use as an antidote in OPC poisoning (Price et al., 2016). To induce recovery of poisoned muscle *in vitro*, MB327 must be applied in concentrations of at least 100–200 µmol•L^{-1} to exert a clear therapeutic effect (Seeger et al., 2012), whilst its administration is accompanied with toxic effects in a concentration only marginally higher. Accordingly, its therapeutic window for effective treatment of OPC poisoning is likely to be too narrow. In fact, MB327 has been discussed to be also an AChE inhibitor and ion channel blocker at micromolar concentrations (Niessen et al., 2011; Tattersall, 1993; Turner et al., 2011). This lack of potency and selectivity of MB327 is to a large extent attributed to its low affinity for the target. In consequence, for an increased therapeutic efficacy new compounds with enhanced affinity for the MB327 binding site are to be identified.

The aim of the present study was to identify new compounds targeting the MB327-PAM-1 binding site at the nAChR, with distinctly higher affinity as compared to MB327. To this end commercially available compound libraries should be screened utilizing the [$^2H_6$]MB327 MS Binding Assay developed by us.

In a previous publication, we introduced MS Binding Assays (mass spectrometry based binding assays) as test system for the characterization of ligands binding to the MB327-PAM-1 binding site of the nAChR (Sichler et al., 2018). MS Binding Assays are based upon the same setup as conventional radioligand binding assays but use a native marker, termed MS marker, instead of a radiolabeled ligand (Höfner and Wanner, 2015). While MS Binding Assays offer a simple working principle and provide reliable results, same as radioligand binding assays, all disadvantages and restrictions, that arise from the use and the handling of radioactivity when performing radioligand binding experiments, e.g. the necessity to comply with safety regulations, the need to safely

dispose radioactive waste, etc. can be circumvented (Grimm et al., 2015; Hess et al., 2011; Neiens et al., 2015). The general setup and performance of MS Binding Assay is illustrated in Fig. 2 and involves the four following distinct steps: (1) incubation of marker, also termed reporter ligand, with the target protein, (2) separation of target protein with bound marker from the incubation system e.g. by filtration or centrifugation, (3) liberation of bound marker from the target protein and (4) LC-MS/MS analysis for the quantification of formerly bound MS marker.

For the quantification of the marker, a deuterated analogue of MB327, [$^2H_6$]MB327 (see Fig. 1), that is used in our MS Binding Assays addressing the MB327-PAM-1 binding site, a reliable, sensitive, and robust LC-ESI-MS/MS method has been developed and validated according to the recommendation of the FDA guidance for bioanalytical method validation (Sichler et al., 2018).

As target *Torpedo*-nAChR (from *Torpedo californica* also termed *Tetronarce californica*), which is a well-established substitute of the human muscle-type nAChR has been used, as the latter, unfortunately, is not available in the amounts required for this type of binding experiments (Millar, 2003; Navedo et al., 2004). In our binding assays, we had found the binding affinity of MB327 to be in the micromolar range {saturation binding experiments using [$^2H_6$]MB327 as marker yielded a K_d of 15.5 ± 0.9 μmol•L^{-1}; autocompetition binding experiments using [$^2H_6$]MB327 as marker and MB327 as competitor yielded a $K_{i,MB327}$ of 18.3 ± 2.6 μmol•L^{-1} (Sichler et al., 2018)}, which is in line with the potencies found in functional assays before (Seeger et al., 2012; Niessen et al., 2016).

In most recent work, we synthesized two series of structurally different MB327 analogues and characterized these in terms of their binding affinities towards the MB327-PAM-1 binding site (Rappenglück et al., 2018a; Rappenglück et al., 2018b). One series consisted of a set of symmetric analogues of MB327 with lipophilic and hydrophilic substituents at the pyridinium subunits. Following evidence that the putative MB327 binding sites could be non-symmetrical with regard to their polarity (Wein et al., 2018), in addition, a second series of bispyridinium salts, this time exhibiting hydrophilic on the one and lipophilic residues on the other of the two pyridinium subunits, has been synthesized. When the constituents of these two series of compounds were characterized with regard to their binding affinity for the MB327-PAM-1 binding site, PTM0022, an at both pyridinium rings 3-phenyl substituted analogue of MB327, (see Fig. 1), was identified as the most affine ligand, its pK_i value amounting to 5.16 ± 0.07.

In the pursuit to identify further ligands at the MB327 binding site with higher affinities as compared to MB327, as a second, additional route, a screening approach, as a very common technique in biomedical research, should be followed. That way, on the one hand the suitability of the [$^2H_6$]MB327 MS Binding Assay established by us for compound library screening should be demonstrated and on the other, new compounds with an affinity towards the MB327 binding site distinctly surpassing that of MB327 be discovered.

2. Material and methods

2.1. Material

MB327 and analogues [$^2H_6$]MB327 and [$^2H_{18}$]MB327 were synthesized in-house by S. Rappenglück and were of ≥ 95% purity measured by ^{1}H NMR spectroscopy (Rappenglück et al., 2018a). *Torpedo californica* (also termed *Tetronarce californica*) electroplaque tissue was obtained from Aquatic Research Consultants (San Pedro, CA, USA). Compound libraries Tocriscreen Plus and the ChemDiv ion channel ligand library were purchased from Tocris (Bristol, UK) and ChemDiv (San Diego, US), respectively. All test compounds were supplied 10 mmol•L^{-1} in DMSO. Water for incubation buffers and LC-MS-mobile phase was prepared in-house by distillation of demineralized water (prepared by reverse osmosis) and subsequent filtration using 0.45 μm filter material. For LC-MS, HPLC grade acetonitrile was obtained from VWR Prolabo (Darmstadt, Germany). Ammonium formate as additive for mobile phase buffer was purchased from Sigma-Aldrich (for mass spectrometry, ≥ 99%, Taufkirchen, Germany). All other chemicals were of analytical grade. All percentages and ratios given are specified as *v/v* ratios.

2.2. MS Binding Assays

MS Binding Assays were performed with [$^2H_6$]MB327 as marker and nAChR-enriched membranes, prepared from *Torpedo californica* electroplaque tissue, as previously described (Sichler et al., 2018; Rappenglück et al., 2018a). Membranes from frozen *Torpedo californica* electroplaque tissue were prepared as reported and stored in storage buffer (120 mmol•L^{-1} NaCl, 5 mmol•L^{-1} KCl, 8.05 mmol•L^{-1} Na_2HPO_4, 1.95 mmol•L^{-1} NaH_2PO_4, pH 7.4). Protein concentration was determined by the bicinchoninic acid method using bovine serum albumin as standard (Smith et al., 1985). All binding experiments were performed as described previously (Rappenglück et al., 2018a). For binding samples for convolute testing and deconvolution and samples for compound characterization i.e. competition experiments, aliquots of the membrane preparation (60–120 μg protein per sample) were incubated with [$^2H_6$]MB327 as marker at 10 μmol•L^{-1} in triplicates in storage buffer (= incubation buffer) in a total volume of 125 μL for 2 h at 25 °C. For each binding experiment, non-specific binding was determined by heat denaturation subjecting aliquots of the *Torpedo californica* membrane preparation to a temperature of 60 °C for 1 h in a shaking water bath prior to incubation with marker and test compounds. In competition experiments the concentrations of the competitors ranged from 1 nmol•L^{-1} - 100 μmol•L^{-1}. After incubation, binding samples were processed and analyzed exactly as previously described (Sichler et al., 2018), if not stated otherwise.

2.3. LC-MS-Instrumentation and marker quantification

LC-MS-analysis was performed on an API 3200 triple quadrupole mass spectrometer (Sciex, Darmstadt, Germany) with a Turbo-V source coupled to an Agilent 1200 HPLC system (vacuum degasser, quaternary pump, column oven; Agilent, Waldbronn, Germany) and a Shimadzu SIL-HTA autosampler (Shimadzu, Duisburg, Germany). For quantification of [$^2H_6$]MB327 as marker in MS Binding Assays the YMC Triart Diol-HILIC column (50 mm×2.0 mm, 3 μm; YMC Europe GmbH, Dinslaken, Germany) was used as stationary phase, protected by two in-line filters (0.5 and 0.2 μm, IDEX, Wertheim-Mondfeld, Germany) upstream to the column. For all experiments, the column temperature was set to 20 °C. A composition of acetonitrile and ammonium formate buffer (20 mmol•L^{-1}, pH 3.0) in a ratio of 80:20 was employed as mobile phase at a flow rate of 800 μL•min^{-1}. The samples, dissolved in acetonitrile and ammonium formate buffer (20 mmol•L^{-1}, pH 3.0) in a ratio of 90:10, were injected in a volume of 10 μL to the column. Within the API 3200 mass spectrometer, Q1 and Q3 were operated with unit resolution. [$^2H_6$]MB327 (marker) and [$^2H_{18}$]MB327 (internal standard) were monitored at the mass transitions of *m/z* 159.2/144.3 and *m/z* 165.2/147.2, respectively.

2.4. Library screening

For preparation of convolutes, we pooled 8 test compounds (10 mmol•L^{-1} in DMSO) of the respective library into one stock solution, by combining 2.5 μL of each compound solution and added incubation buffer to a final volume of 1 mL, resulting in a final concentration of 25 μmol•L^{-1} for each test compound. For testing of convolutes, we prepared and processed binding samples with [$^2H_6$]MB327 as marker at 10 μmol•L^{-1} and aliquots of the membrane preparation and the respective convolute comprising 8 test compounds at 10 μmol•L^{-1} (see MS Binding Assays for more detail). Active convolutes, i.e. convolutes that met the criteria set for selection were subjected to deconvolution experiments, where all 8 test compounds of one convolute were tested

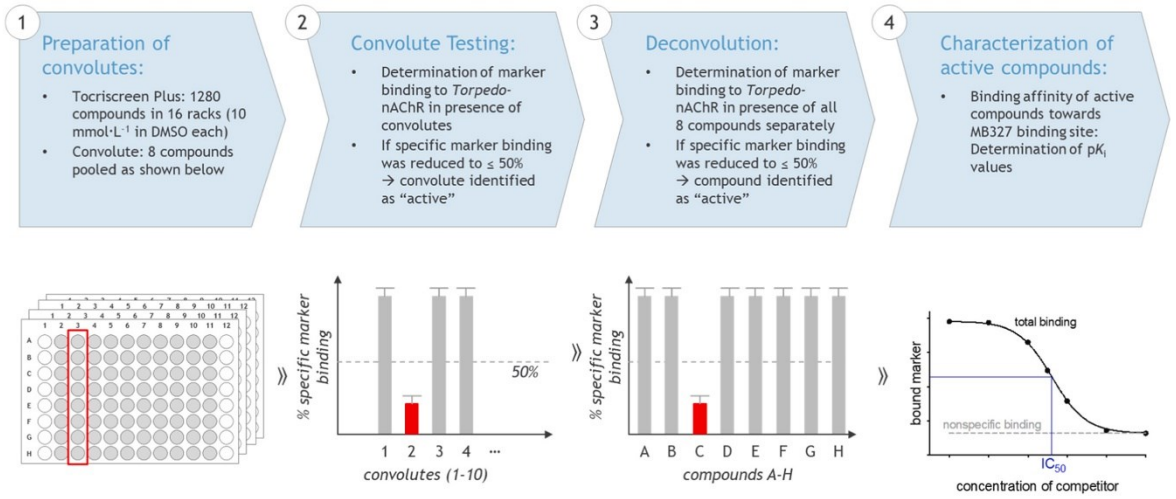

Fig. 3. Library Screening approach, illustrated with the Tocriscreen Plus library as example: For preparation of convolutes (step 1) 8 compounds in wells A-H per rack were pooled into a stock solution to be used in the binding assay. As 80 compounds were supplied per rack this makes a total of 10 convolutes per rack. Convolutes were tested in binding assays (at 10 μmol•L ^{1} for each compound) with [$^{2}H_6$]MB327 as reporter ligand and the *Torpedo*-nAChR as target. Convolutes were referred to as active, if their presence resulted in reduction of specific marker binding to a level ≤ 50% as compared to binding in absence of test compounds (shown in red for step 2). These active convolutes were subjected to deconvolution (step 3 in the screening process) i.e. single testing of each compound A-H (each at 10 μmol•L ^{1}) in the binding assay analogous to step 2. Analogous to convolute testing, a compound was considered as active, if its presence in binding samples resulted in reduction of specific marker binding to a level ≤ 50% as compared to specific binding in absence of a test compound. This is shown for compound C in the example. As final step, step 4, these compounds, identified as active, were characterized in terms of their binding affinity towards the MB327-PAM-1 binding site at the *Torpedo*-nAChR by determination of pK_i values in competition experiments.

separately at 10 μmol•L^{-1} in binding samples with [$^{2}H_6$]MB327 as marker and aliquots of the membrane preparation. Active compounds were further characterized in terms of their binding affinity towards the MB327 binding site. To this end, we conducted competition experiments with [$^{2}H_6$]MB327 as marker and active compounds as competitor in a concentration range from 1 nmol•L^{-1} to 100 μmol•L^{-1}. pK_i values were obtained by analysis of the respective competition curves with Prism v. 5.0 (GraphPad Software, La Jolla, CA, USA). Studies for the determination of the effect of AZ10417808 on [$^{2}H_6$]MB327 binding were conducted in analogy to competition experiments.

2.5. Data analysis

Based on the determined calibration function the concentration of bound marker in the binding samples was determined using Analyst v.1.6.1 (Sciex, Darmstadt, Germany). Specific binding was defined as the difference between total binding and non-specific binding. Competition curves were analyzed with the "One site - Fit Ki" regression tool (Prism v. 5.0, GraphPad Software, La Jolla, CA, USA) by means of nonlinear curve fitting, fixing top and bottom level of the sigmoidal competition curves to total binding (in absence of competitor, n = 3) and non-specific binding (determined by heat denaturation, n = 3). K_i values were calculated from the thus obtained IC_{50} values according to the Cheng-Prusoff equation by means of the aforementioned program {with K_d value for [$^{2}H_6$]MB327 from Rappenglück et al., 2018a}. If not stated otherwise, pK_i values are given as means ± SEM.

3. Results and Discussion

As already indicated, in this study compound libraries should be screened in order to identify new ligands of the MB327-PAM-1 binding site of the nAChR, that exhibit distinctly higher affinities compared to MB327. For this purpose, a compound library with a total of 60 ion channel ligands from ChemDiv Inc and a collection of 1280 compounds representing known bioactive compounds with diverse structures from Tocris, the Tocriscreen Plus library, should be studied. With the constituents of these libraries addressing ligand gated ion channels (library from ChemDiv Inc.) and dozens of pharmacological targets including GPCRs, ion channels, enzymes and transporters, to name only a few (Tocriscreen Plus library) the screening was thought to cover a broad set of different chemotypes, which might eventually lead to the identification of a reasonable number of novel binders of the MB327-PAM-1 binding site.

Fig. 3 illustrates the screening approach, we followed in this study for the screening of the Tocriscreen Plus library, which consists of the following four distinct steps: (1) Preparation of convolutes, (2) convolute testing, (3) deconvolution and (4) characterization of active compounds.

As an initial step in the screening approach all > 1300 compounds from both libraries to be tested were pooled into smaller sets of compounds, so-called convolutes. For this work, we chose to pool eight test compounds to make up one convolute, as a bigger convolute size is likely to lead to uncertain results and to a reduction of the efficiency of the screening process. In the case of the Tocriscreen Plus library, which was supplied in 16 racks with 80 compounds each, we combined all columns A to H into convolutes, i.e. 10 convolutes per rack, as illustrated in Fig. 3. As all test compounds from both libraries, the Tocriscreen Plus as well as the ChemDiv library, were supplied in a concentration of 10 mmol•L^{-1} in DMSO, dilution of one convolute i.e. eight test compounds to 10 μmol•L^{-1} in the incubation mix resulted in a final DMSO assay concentration of 0.8%. To ensure this would not adversely impact the binding experiment, we conducted autocompetition experiments, i.e. binding experiments with [$^{2}H_6$]MB327 as marker and MB327 as competitor, both in presence and absence of 0.8% DMSO in the assay, to compare affinity constants in both settings. As we did not observe any significant difference in competition curves nor corresponding pK_i values, we concluded that a concentration of 0.8% DMSO in the binding assay is well tolerated. As a next step, step 2, in the screening approach, we tested all convolutes in the binding assay with [$^{2}H_6$]MB327 as reporter ligand and the *Torpedo*-nAChR as target as previously described

Table 1
Results of convolute testing with [$^2H_6$]MB327 as reporter ligand and Torpedo-nAChR as target. Results are shown for active convolutes only.

Library	Convolute ID	Specific marker binding[a]
Tocriscreen Plus	02–05	33.1 ± 4.2
	03–02	12.1 ± 7.7
	03–04	**285.2 ± 27.8**
	05–01	48.6 ± 4.6
	07–03	41.3 ± 14.3
	09–07	28.0 ± 4.7
	11–05	27.4 ± 5.5
	12–05	17.6 ± 6.6
	12–07	15.5 ± 12.5
	14–04	4.8 ± 3.8
	14–05	5.7 ± 1.9
	14–09	12.6 ± 4.4
	14–10	19.8 ± 4.5
	15–03	32.5 ± 2.1
	15–08	40.4 ± 5.2

[a] % specific binding (mean ± SD, n = 3) of 10 µmol•L^{-1} [$^2H_6$]MB327 in presence of 8 test compounds of a convolute, each at a concentration of 10 µmol•L^{-1} as compared to specific marker binding in absence of test compounds.

(Rappenglück et al., 2018a). Accordingly, for each convolute comprising eight test compounds at a final concentration of 10 µmol•L^{-1} one binding sample was prepared, in which, in addition, the reporter ligand at the same concentration (10 µmol•L^{-1}) and aliquots of the *Torpedo* membrane preparation in incubation buffer was contained. Further, binding samples were prepared in absence of test compounds with [$^2H_6$]MB327 at 10 µmol•L^{-1} to determine total as well as non-specific binding (using heat shock as previously described) as a control. Comparing specific marker binding in presence of the convolute, i.e. the eight test compounds, with marker binding towards the *Torpedo*-nAChR in absence indicates if one or more test compounds have an effect on [$^2H_6$]MB327 binding. As we were looking for hit compounds with an IC_{50} of ≤ 10 µmol•L^{-1}, we considered a convolute as active, if its presence in binding samples resulted in a reduction of specific marker binding, defined as the difference between total and non-specific binding, to a level of ≤ 50% (specific marker binding in absence of any competitor was defined as 100%). Under these conditions, with all test compounds being present at a concentration of 10 µmol•L^{-1} in the binding assay, it is to be expected that one compound within the convolute targets the MB327 binding site with an IC_{50} value of ≤ 10 µmol•L^{-1}, provided no additive or allosteric effects are present. The phenomenon of additive effects will be discussed later in this chapter. The third step in the screening approach, called deconvolution, aims at the identification of the hit or possibly hit compounds within the active convolute responsible for the reduction of specific marker binding to ≤ 50%. As the sample size was quite small, we decided to test all compounds of the respective active convolute separately in the same setting as in convolute testing. With the focus on the identification of the hit compounds with an IC_{50} of ≤ 10 µmol•L^{-1} {in the [$^2H_6$]MB327 MS Binding Assay} the threshold for a compound to be referred to as active, remained, of course, unchanged, i.e. it had to reduce specific marker binding to a level of ≤ 50%. The final step of the screening approach aims at the characterization of the binding affinity (pK_i values) towards the

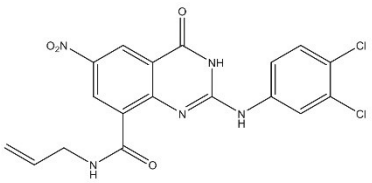

Fig. 5. AZ10417808.

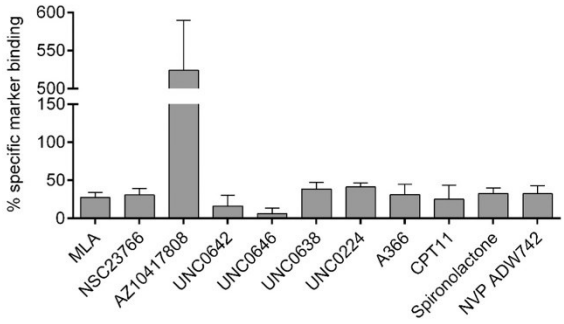

Fig. 6. Results from deconvolution experiments. Only test compounds are shown, in whose (at 10 µmol•L^{-1}) presence specific binding of [$^2H_6$]MB327 (10 µmol•L^{-1}) towards the Torpedo-nAChR was reduced below 50%, with the exception of AZ10417808, where a potentiation of marker binding was observed instead. Specific marker binding (mean ± SD, n = 3) is given as percentage compared to specific marker binding in absence of test compounds.

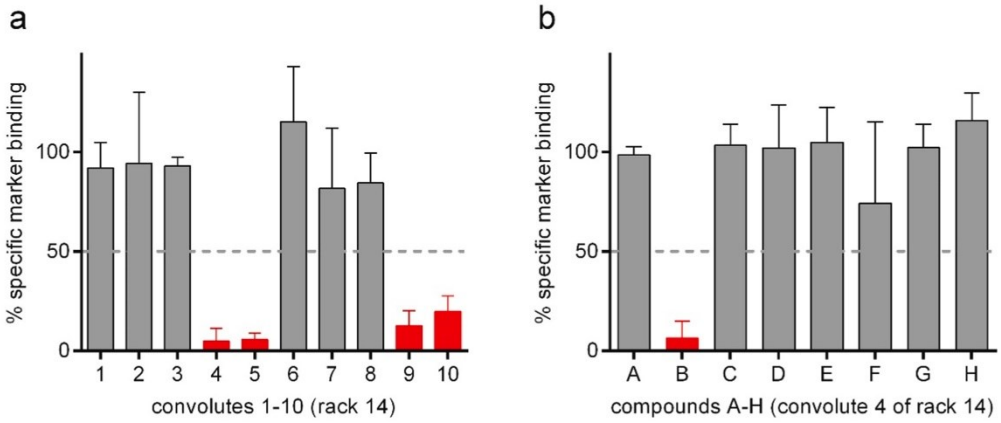

Fig. 4. Exemplary results of testing of convolutes 14–01 to 14–10 of the Tocriscreen Plus library, rack 14. Specific binding (mean ± SD, n = 3) of 10 µmol•L^{-1} [$^2H_6$]MB327 in presence of (a) 8 test compounds of a convolute or (b) one compound of the respective convolute, each at a concentration of 10 µmol•L^{-1}. Specific marker binding is given as percentage compared to specific marker binding in absence of test compounds.

Table 2
Results from competition binding experiments to determine pK_i values for active compounds. Binding experiments were conducted with 10 µmol•L^{-1} [$^2H_6$]MB327 as marker and *Torpedo*-nAChR as target.

Entry	Compound, Biological Activity[a]	Chemical Formula	pK_i[b]
1	**Methyllycaconitine** *α7 neuronal nicotinic receptor antagonist*	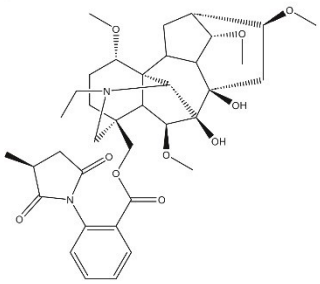	5.45 ± 0.18
2	**NSC23766** *Antioncogenic, Selective inhibitor of Rac1-GEF interaction*	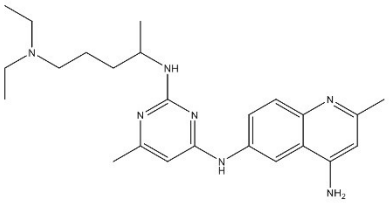	5.49 ± 0.16
3	**UNC0642** *Potent and selective G9a and GLP histone lysine methyltransferase inhibitor*	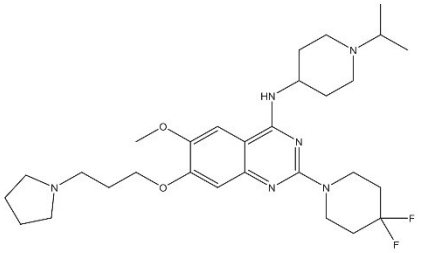	5.97 ± 0.05
4	**UNC0646** *Potent and selective G9a and GLP histone lysine methyltransferase inhibitor*	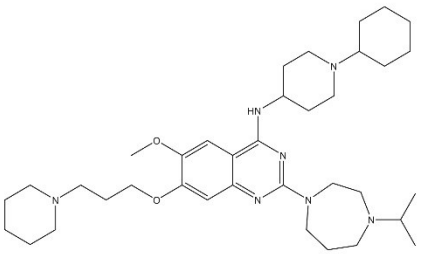	6.23 ± 0.02
5	**UNC0638** *Potent and selective G9a and GLP histone lysine methyltransferase inhibitor*	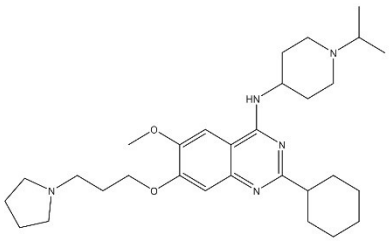	6.01 ± 0.10
6	**UNC0224** *Potent and selective G9a and GLP histone lysine methyltransferase inhibitor*	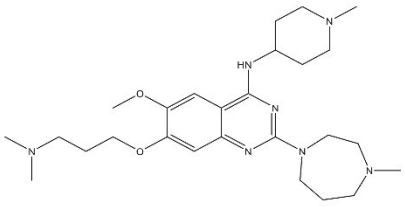	5.23 ± 0.15

(*continued on next page*)

Table 2 (*continued*)

Entry	Compound, Biological Activity[a]	Chemical Formula	pK$_I$[b]
7	**A366** *Potent and selective G9a and GLP histone lysine methyltransferase inhibitor*	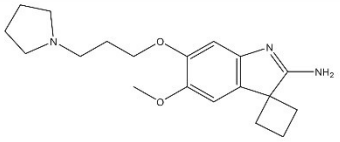	5.52 ± 0.15
8	**CPT11** *Antioncogenic, DNA topoisomerase I inhibitor*	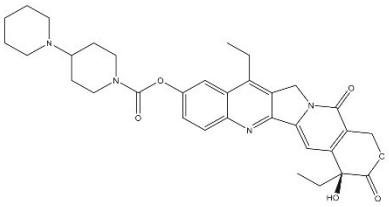	5.15 ± 0.05
9	**Spironolactone** *Mineralocorticoid receptor antagonist*	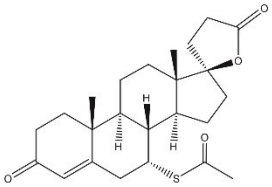	5.07 ± 0.09
10	**NVP ADW742** *ATP-competitive inhibitor of IGF1R*	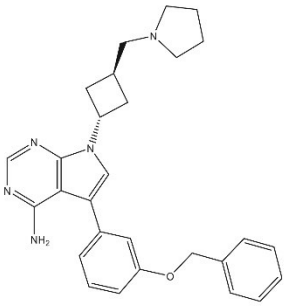	5.64 ± 0.08

[a] Data from Tocriscreen Plus.
[b] Data are given as mean ± SEM of three independent experiments.

Torpedo-nAChR of the respective hit compounds, to which end full scale competitive [$^2H_6$]MB327 MS Binding Assays should be performed.

In case of the ChemDiv compound library, convolute testing showed no distinct reduction of [$^2H_6$]MB327 binding in presence of any of the tested convolutes (see supplementary information). In contrast, testing of Tocriscreen Plus convolutes showed significant reduction of [$^2H_6$]MB327 binding in presence of convolutes (comprising eight test compounds) in several cases. In the screening 14 out of 160 convolutes were found to be active. These are listed in Table 1 (for the complete set of results of convolute testing see supplementary information). There, in Table 1, as well as in the following text, for an easier reference, convolutes originating from the Tocriscreen Plus library will be characterized by the ID XX-YY, where XX is the rack number (1−16) and YY (1−10) represents the convolute number of the corresponding rack. Interestingly, in one case, i.e. in presence of convolute 03–04, highlighted in bold in Table 1, a distinct increase of specific marker binding up to 285.2 ± 27.8% was observed.

Of the 14 convolutes identified as active four were found on rack 14. The results of the screening of the 10 convolutes (convolutes 1–10) contained in rack 14 of the Tocriscreen Plus library are exemplarily given in Fig. 4a.

Of these four active convolutes, convolute 14–04 reduced specific [$^2H_6$]MB327 binding down to a value as low as 4.8 ± 6.6% (mean ± SD, n = 3). A subsequently performed deconvolution of convolute 14–04 revealed, that the activity of this convolute arises from compound B, identified as compound UNC0646, which reduced specific marker binding to 6.4 ± 8.5% (mean ± SD, n = 3), whereas all other compounds (A and C-H) are inactive (see Fig. 4b) according to the set selection criteria {reduction of [$^2H_6$]MB327 binding to ≤ 50%}.

In case of convolute 14–10, during deconvolution even two active compounds, that reduced specific [$^2H_6$]MB327 binding to 41.4 ± 3.6% and 31.2 ± 9.5% (mean ± SD, n = 3) in the binding assay, respectively, have been identified. In contrast, though convolutes 05–01, 07–03, 09–07, 11–05 and 12–05 had fulfilled the activity criteria, deconvolution experiments did not lead to any hit compound {reduction of [$^2H_6$]MB327 binding to ≤ 50%}. This is certainly to be attributed to a so-called additive effect, where several compounds within the convolute have only minor effects on marker binding, which, however, together are large enough to reduce marker binding to ≤ 50%, wherefrom convolutes are considered as active.

Interestingly, convolute 03–04 was found to exhibit a distinct potentiation of reporter ligand binding. In subsequent deconvolution experiments, AZ10417808 was identified as the compound of this convolute, to be responsible for this effect. When tested separately in a binding sample (at 10 μmol•L^{-1}) AZ10417808, the structure of which is given in Fig. 5, caused an increase of [$^2H_6$]MB327 binding up to 523.9. ± 79.9% (mean ± SD), or in other words by a factor of about 5.

Overall, in deconvolution experiments in total 10 compounds have

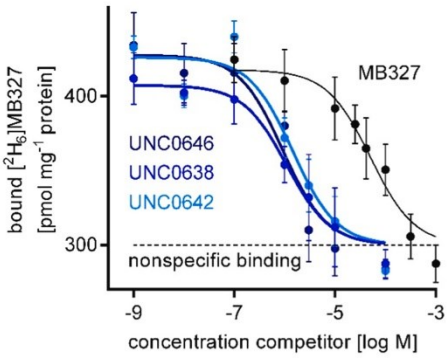

Fig. 7. Representative competition experiments conducted with 10 µmol•L^{-1} [$^2H_6$]MB327 as marker and *Torpedo*-nAChR as target employing UNC0646, UNC0638, UNC0642 and MB327 as competitor. Total binding (mean ± SD) of marker in presence of the respective competitor in a concentration range of 1 nmol•L^{-1} to 1 mmol•L^{-1}. Non-specific binding of marker was determined in triplicates by heat denaturation subjecting aliquots of the Torpedo membrane preparation to a temperature of 60 °C for 1 h in a shaking water bath prior to incubation with marker and test compounds. Nonlinear regression analysis yielded pK_i values of 6.27, 6.19, and 6.07 for UNC0646, UNC0638, UNC0642, respectively, in the particular experiments.

been identified as active. The results of the deconvolution experiments, i.e. for the compounds which due to the reduction of marker binding to ≤ 50% are considered to target the MB327 binding site with an $IC_{50} \leq 10$ µmol•L^{1}, and for AZ10417808 enhancing MB327 binding are summarized in Fig. 6.

As final step in the screening approach, each of the hit compounds has been characterized with regard to its binding affinity constant (pK_i value) for the MB327 binding site in full scale competitive [$^2H_6$]MB327 MS Binding Assays. The results, the pK_i values for active compounds determined in 3 independent binding experiments are listed in Table 2. In Table 2 also the structures of the hit compounds as well as the biological activity, they are known for in literature, is contained.

As mentioned above, AZ10417808, which is described as selective non-peptide caspase-3 inhibitor in literature, did not reduce but increase [$^2H_6$]MB327 binding. To shed some light on the effect of AZ10417808, additional [$^2H_6$]MB327 binding experiments were performed, in which the concentration of AZ10417808 has been gradually increased from 10 nmol•L^{-1} to 100 µmol•L^{-1}. This led to a continuous rise without any sign of plateauing of [$^2H_6$]MB327 binding, with a value of 9128 ± 1796% (mean ± SEM, n = 3) reached at 100 µmol•L^{-1} of AZ10417808, the highest concentration applied. With the amount of [$^2H_6$]MB327 binding {approx. 9000 pmol•[mg protein]$^{-1}$ in presence of 100 µmol•L^{-1} AZ10417808} being way above the nAChR concentration B_{max} {approx. 300 pmol•[mg protein]$^{-1}$,Sichler et al., 2018; Rappenglück et al., 2018a} in the binding experiments, it appears unlikely that the observed phenomenon may arise from any kind of specific binding. Hence, this topic was not pursued any further.

Each of the 10 hit compounds, shown in Table 2, targets the MB327 binding site at the *Torpedo*-nAChR with an affinity that is higher, than that exhibited by MB327 (pK_i = 4.73 ± 0.03, Rappenglück et al., 2018a). The pK_i values of three of these compounds, UNC0224 (Table 2, Entry 6), CPT11 (Table 2, Entry 8) and Spironolacton (Table 2, Entry 9) towards the MB327 binding site amounting to 5.23 ± 0.15, 5.15 ± 0.05 and 5.07 ± 0.09, respectively, are in the same range as the value of PTM0022 (Fig. 1, pK_i = 5.16 ± 0.07, Rappenglück et al., 2018a), which represents the compound with the highest affinity towards the MB327 binding site described so far. In comparison to MB327 (pK_i = 4.73 ± 0.03, Rappenglück et al., 2018a) the binding affinity (pK_i) for the MB327 binding site of *Torpedo*-nAChR of Methyllycaconitincitrat (MLA, pK_i = 5.45 ± 0.18, Table 2, Entry 1), which has been described as a potent antagonist of α7 nAChR, is increased by 0.70 log units. For NSC23766 (Table 2, Entry 2), A366 (Table 2, Entry 7) and NVP ADW742 (Table 2, Entry 10) the increase in binding affinity is even somewhat higher, the differences of the pK_i values amounting to 0.74, 0.77 and 0.89, respectively. The compounds with the highest affinities, UNC0638 (Table 2, Entry 5), UNC0642 (Table 2, Entry 3) and UNC0646 (Table 2, Entry 4), all of which belong to the same class of compounds, show an increase in binding affinities towards the *Torpedo*-nAChR of even more than one log unit with pK_i values of 6.01 ± 0.10, 5.97 ± 0.05 and 6.23 ± 0.02, respectively. Representative competition curves obtained for these three compounds, UNC0638, UNC0642 and UNC0646, are displayed in Fig. 7 visualizing the distinct shift and increased binding affinity of these compounds as compared to MB327, of which UNC0646 represents the first submicromolar binder. Previously, these compounds have been described as selective inhibitors of the G9a and GLP histone lysine methyltransferase. Here, we demonstrate for the first time, that they are also potent ligands of the MB327-PAM-1 binding site of the *Torpedo*-nAChR. Interestingly, the pK_i value of UNC0224 is distinctly lower than those of the other three quinazoline derivatives, UNC0638, UNC0642 and UNC0646, despite the fact, that these compounds show a high degree of structural similarities. Detailed studies are required to clarify the effect of the individual structural characteristics such as the substitution pattern and the nature of substituents and of the heterocyclic scaffold on the binding affinity to finally establish structure activity relationships for this class of compounds. Such studies as well as studies aiming at the determination of the intrinsic activity of these compounds, in particular, in *ex vivo* assays with rat diaphragm preparations impaired by OPC treatment – showing first positive results for UNC0638 and UNC0642 (Nitsche et. al., 2024) – and in animal models of organophosphate intoxication are underway.

4. Conclusion

In this study, more than 1300 compounds were tested regarding their affinity to the MB327-PAM-1 binding site of the *Torpedo californica*-nAChR within a screening approach applying the recently developed [$^2H_6$]MB327 MS Binding Assay. A set of 10 compounds was identified as active, i.e. showed a reduction of specific [$^2H_6$]MB327 binding to a level of ≤ 50%, when applied in a concentration of 10 µmol•L^{-1}, which equals an IC_{50} value of ≤ 10 µmol•L^{-1}.

These 10 active compounds were characterized in terms of their binding affinities to the MB327 binding site at the *Torpedo californica*-nAChR by means of the recently developed [$^2H_6$]MB327 MS Binding Assay. As compared to the bispyridinium salt PTM0022, a derivative of the prototypic ligand MB327 addressing the MB327-PAM-1 binding site, with the highest affinity known so far for the aforementioned binding site, the binding affinities of some of these new ligands are at least similar to that of this bispyridinium salt. For some compounds, the binding affinity even exceeds that of PTM0022 by up to one log unit (pK_i). The ligand with the highest affinity overall was identified as UNC0646 with a binding affinity towards the MB327 binding site in the submicromolar range (pK_i = 6.23 ± 0.02).

The identification of UNC0638, UNC0642 and UNC0646 representing the most affine ligands of the MB327-PAM-1 binding site known so far also nicely underlines the potency and efficiency of the [$^2H_6$]MB327 MS Binding Assay as a tool in library screening as well as for affinity characterization of identified hit compounds.

So far it is still unknown, to what extent the hit compounds identified in this study are capable to counteract organophosphate poisoning in *in vivo* models, which to clarify will have to be the subject of future experiments. Most of all UNC0638, UNC0642 and UNC0646 as the compounds with the highest affinity for the MB327-PAM-1 binding site identified so far appear as the most promising starting points for the development of antidots against organophosphate poisoning. This is, in particular, true for UNC0638 and UNC0642, which have already been found to restore muscle function of soman-poisoned muscle tissue in *ex*

vivo experiments (Nitsche et al., 2024).

CRediT authorship contribution statement

Klaus T. Wanner: Conceptualization, Funding acquisition, Supervision, Writing – review & editing. **Sonja Sichler:** Investigation, Validation, Writing – original draft. **Thomas Seeger:** Investigation, Writing – review & editing. **Franz Worek:** Writing – review & editing. **Franz F. Paintner:** Conceptualization, Funding acquisition, Supervision, Writing – review & editing. **Georg Höfner:** Conceptualization, Methodology, Validation. **Valentin Nitsche:** Investigation, Validation, Writing – original draft. **Karin V. Niessen:** Writing – review & editing.

Declaration of Competing Interest

Authors declare that they have no known competing financial interests or personal relationships that could have appeared to influence the work reported in this paper.

Data Availability

Data will be made available on request.

Acknowledgements

This study was funded by the German Ministry of Defence (E/U2AD/CF514/DF561).

Appendix A. Supporting information

Supplementary data associated with this article can be found in the online version at doi:10.1016/j.toxlet.2024.02.004.

References

Arias, H.R., 2010. Positive and negative modulation of nicotinic receptors. Adv. Protein Chem. Struct. Biol. 80, 153–203.
Arias, H.R., 2011. Allosteric modulation of nicotinic acetylcholine receptors. In: Arias, H. R. (Ed.), Pharmacology of Nicotinic Acetylcholine Receptors from the Basic and Therapeutic Perspectives. Research Signpost, Kerala, pp. 151–173.
Changeux, J.P., Edelstein, S.J., 2005. Allosteric mechanisms of signal transduction. Science 308 (5727), 1424–1428.
Chatzidaki, A., Millar, N.S., 2015. Allosteric modulation of nicotinic acetylcholine receptors. Biochem. Pharmacol. 97 (4), 408–417.
Grimm, S.H., Höfner, G., Wanner, K.T., 2015. Development and validation of an LC-ESI-MS/MS method for the triple reuptake inhibitor indatraline enabling its quantification in MS Binding Assays. Anal. Bioanal. Chem. 407, 471–485.
Hess, M., Höfner, G., Wanner, K.T., 2011. (S)- and (R)-fluoxetine as native markers in MS Binding Assays addressing the serotonin transporter. ChemMedChem 6, 1900–1908.
Höfner, G., Wanner, K.T., 2015. MS Binding Assays. In: Kool, J., Niessen, W.M.A. (Eds.), Analyzing Biomolecular Interactions by Mass Spectrometry. Wiley-VHC, Weinheim,, pp. 165–198.
Kaiser, J., Gertzen, C.G.W., Bernauer, T., Höfner, G., Niessen, K.V., Seeger, T., Paintner, F.F., Wanner, K.T., Worek, F., Thiermann, H., Gohlke, H., 2023. A novel binding site in the nicotinic acetylcholine receptor for MB327 can explain its allosteric modulation relevant for organophosphorus-poisoning treatment. Toxicol. Lett. 373, 160–171.
Millar, N.S., 2003. Assembly and subunit diversity of nicotinic acetylcholine receptors. Biochem. Soc. Trans. 31 (4), 869–874.
Navedo, M., Nieves, M., Rojas, L., Lasalde-Dominicci, J.A., 2004. Tryptophan substitutions reveal the role of nicotinic acetylcholine receptor R-TM3 domain in channel gating: differences between Torpedo and muscle-type AChR. Biochemistry 43, 78–84.
Neiens, P., Höfner, G., Wanner, K.T., 2015. MS Binding Assays for D1 and D5 dopamine receptors. ChemMedChem 10, 1924–1931.
Niessen, K.V., Tattersall, J.E., Timperley, C.M., Bird, M., Green, C., Seeger, T., Thiermann, H., Worek, F., 2011. Interaction of bispyridinium compounds with the orthosteric binding site of human alpha7 and Torpedo californica nicotinic acetylcholine receptors (nAChRs). Toxicol. Lett. 206, 100–104.
Niessen, K.V., Muschik, S., Langguth, F., Rappenglück, S., Seeger, T., Thiermann, H., Worek, F., 2016. Functional analysis of Torpedo californica nicotinic acetylcholine receptors in multiple activation states by SSM-based electrophysiology. Toxicol. Lett. 247, 1–10.
Niessen, K.V., Seeger, T., Rappenglück, S., Wein, T., Höfner, G., Wanner, K.T., Thiermann, H., Worek, F., 2018. In vitro pharmacological characterization of the bispyridinium non-oxime compound MB327 and its 2- and 3-regioisomers. Toxicol. Lett. 293, 190–197.
Nitsche, V., Höfner, G., Kaiser, J., Gertzen, C.G.W., Seeger, T., Niessen, K.V, Steinritz, D., Worek, F., Gohlke, H., Paintner, F.F., Wanner, K.T., 2024. MS Binding Assays with UNC0642 as reporter ligand for the MB327 binding site of the nicotinic acetylcholine receptor. Toxicol. Lett. 392, 94–106.
OPCW (2020a, April 8). IIT concludes units of the Syrian Arab Air Force used chemical weapons in Ltamenah, Syria in March 2017. Accessed 26.03.2020 at. ⟨https://www.opcw.org/media-centre/news/2020/04/opcw-releases-first-report-investigation-and-identification-team⟩.
OPCW (2020b, October 6). OPCW Issues Report on Technical Assistance Requested by Germany. Accessed 26.03.2020 at. ⟨https://www.opcw.org/media-centre/news/2020/10/opcw-issues-report-technical-assistance-requested-germany⟩.
OPCW (2018, September 4). OPCW Issues Report on Technical Assistance Requested by the United Kingdom Regarding Toxic Chemical Incident in Amesbury. Accessed 26.03.2020 at ⟨https://www.opcw.org/media-centre/news/2018/09/opcw-issues-report-technical-assistance-requested-united-kingdom⟩.
Papke, R.L., 2014. Merging old and new perspectives on nicotinic acetylcholine receptors. Biochem. Pharmacol. 89 (1), 1–11.
Price, M.E., Docx, C.J., Rice, H., Fairhall, S.J., Poole, S.J.C., Bird, M., Whiley, L., Flint, D. P., Green, A.C., Timperley, C.M., Tattersall, J.E., 2016. Pharmacokinetic profile and quantitation of protection against soman poisoning by the antinicotinic compound MB327 in the guinea-pig. Toxicol. Lett. 244, 154–160.
Rappenglück, S., Sichler, S., Höfner, G., Wein, T., Niessen, K.V., Seeger, T., Worek, F., Thiermann, H., Wanner, K.T., 2018a. Synthesis of a series of structurally diverse MB327 derivatives and their affinity characterization at the nicotinic acetylcholine receptor. ChemMedChem 13 (17), 1806–1816.
Rappenglück, S., Sichler, S., Höfner, S., Wein, G., Niessen, T., Seeger, K.V., Worek, T., Thiermann, F., Wanner, H., K. T, 2018b. Synthesis of a Series of Non-Symmetric Bispyridinium and Related Compounds and Their Affinity Characterization at the Nicotinic Acetylcholine Receptor. ChemMedChem 13 (24), 2653–2663.
Seeger, T., Eichhorn, M., Lindner, M., Niessen, K.V., Tattersall, J.E., Timperley, C.M., Bird, M., Green, A.C., Thiermann, H., Worek, F., 2012. Restoration of soman-blocked neuromuscular transmission in human and rat muscle by the bispyridinium nonoxime MB327 in vitro. Toxicology 294 (2-3), 80–84.
Sichler, S., Höfner, G., Rappenglück, S., Wein, T., Niessen, K.V., Seeger, T., Worek, F., Thiermann, H., Paintner, F.F., Wanner, K.T., 2018. Development of MS Binding Assays targeting the binding site of MB327 at the nicotinic acetylcholine receptor. Toxicol. Lett. 293, 172–183.
Smith, P.K., Krohn, R.I., Hermanson, G.T., Mallia, A.K., Gartner, F.H., Provenzano, M.D., Fujimoto, E.K., Goeke, N.M., Olson, B.J., Klenk, D.C., 1985. Measurement of protein using bicinchoninic acid. Anal. Biochem. 150 (1), 76–85.
Tattersall, J.E.H., 1993. Ion channel blockade by oximes and recovery of diaphragm muscle from soman poisoning in vitro. Br. J. Pharmacol. 108 (4), 1006–1015.
Turner, S.R., Chad, J.E., Price, M., Timperley, C.M., Bird, M., Green, A.C., Tattersall, J.E. H., 2011. Protection against nerve agent poisoning by a noncompetitive nicotinic antagonist. Toxicol. Lett. 206, 105–111.
Wein, T., Höfner, G., Rappenglück, S., Sichler, S., Niessen, K.V., Seeger, T., Paintner, F.F., Worek, F., Thiermann, H., Wanner, K.T., 2018. Searching for putative binding sites of the bispyridinium compound MB327 in the nicotinic acetylcholine receptor. Toxicol. Lett. 293, 184–189.

Supporting Information

Screening for New Ligands of the MB327-PAM-1 Binding Site of the Nicotinic Acetylcholine Receptor

Sonja Sichler [a], Georg Höfner [a], Valentin Nitsche [a], Karin V. Niessen [b], Thomas Seeger [b], Franz Worek [b], Franz F. Paintner [a], Klaus T. Wanner [a]
[a] Department of Pharmacy – Center for Drug Research, Ludwig-Maximilians-Universität München, Munich, Germany
[b] Bundeswehr Institute of Pharmacology and Toxicology, Munich, Germany

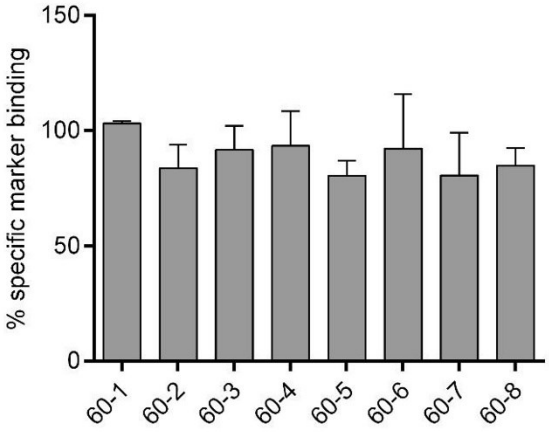

Figure SI1: Testing of the ChemDiv ion channel ligand library. Convolutes (60-1 to 60-8) were tested in MS Binding Assays with [$^2H_6$]MB327 as reporter ligand and the Torpedo-nAChR as target. Convolutes were referred to as active, if their presence resulted in reduction of specific marker binding to a level ≤ 50% as compared to binding in absence of test compounds. The ChemDiv ion channel ligand library showed no active convolute. Bars show specific binding (mean ± SD, n = 3) of 10 µmol·L^{-1} [$^2H_6$]MB327 in presence of the respective convolute [each convolute contained 8 compounds, (60-8 only 4) at a concentration of 10 µmol·L^{-1}]. Specific marker binding is given as percentage compared to specific marker binding in absence of test compounds.

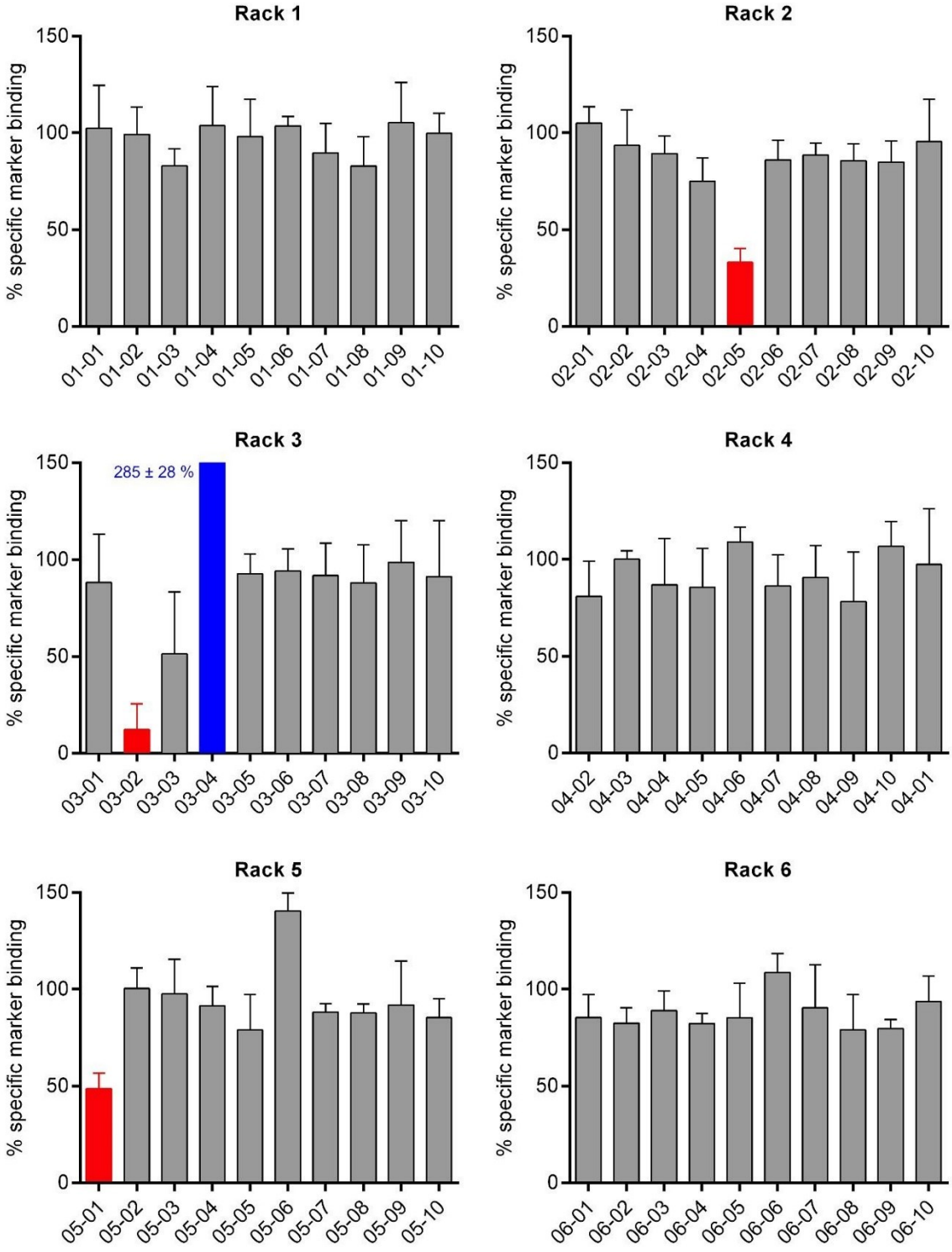

Continued next page

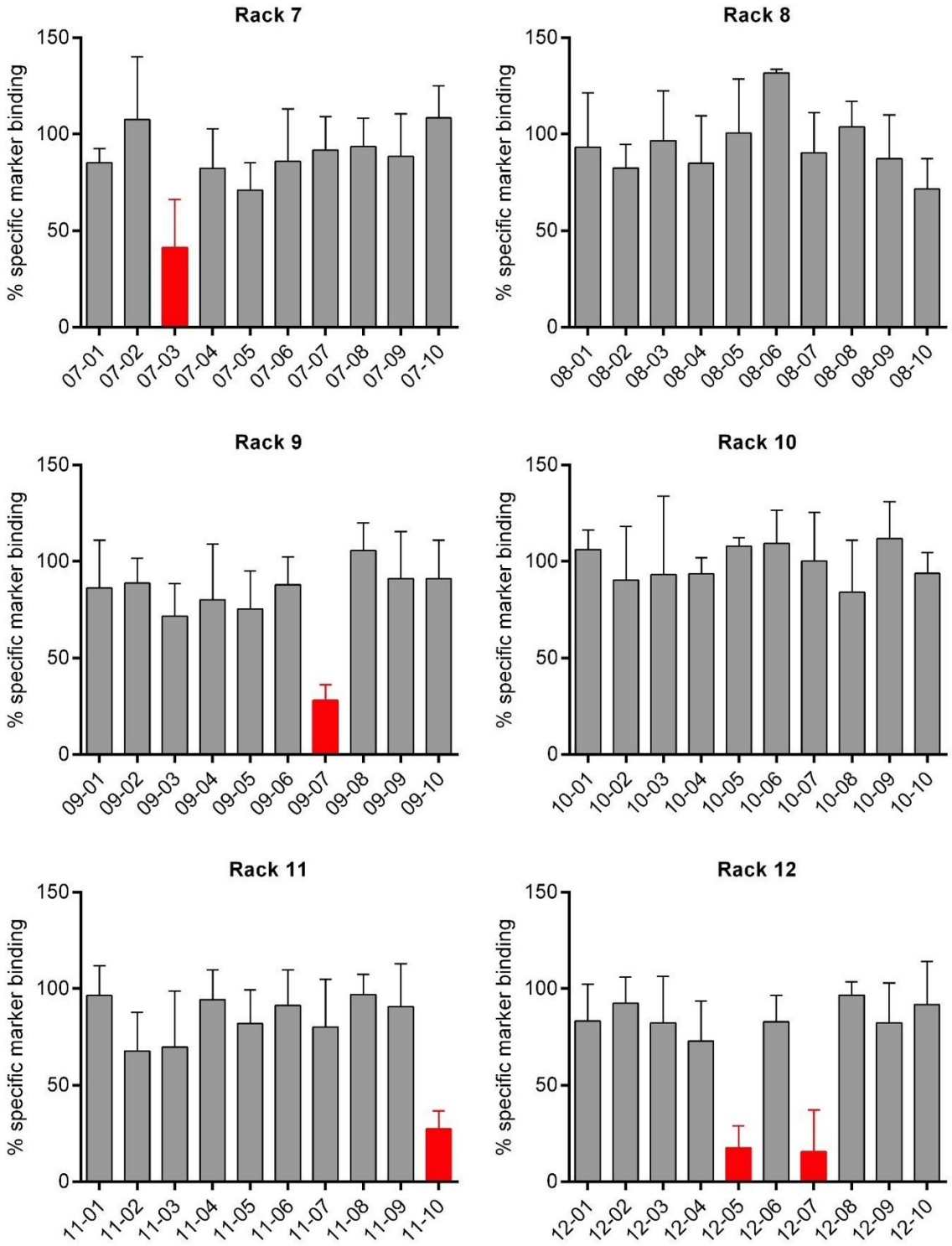

Continued next page

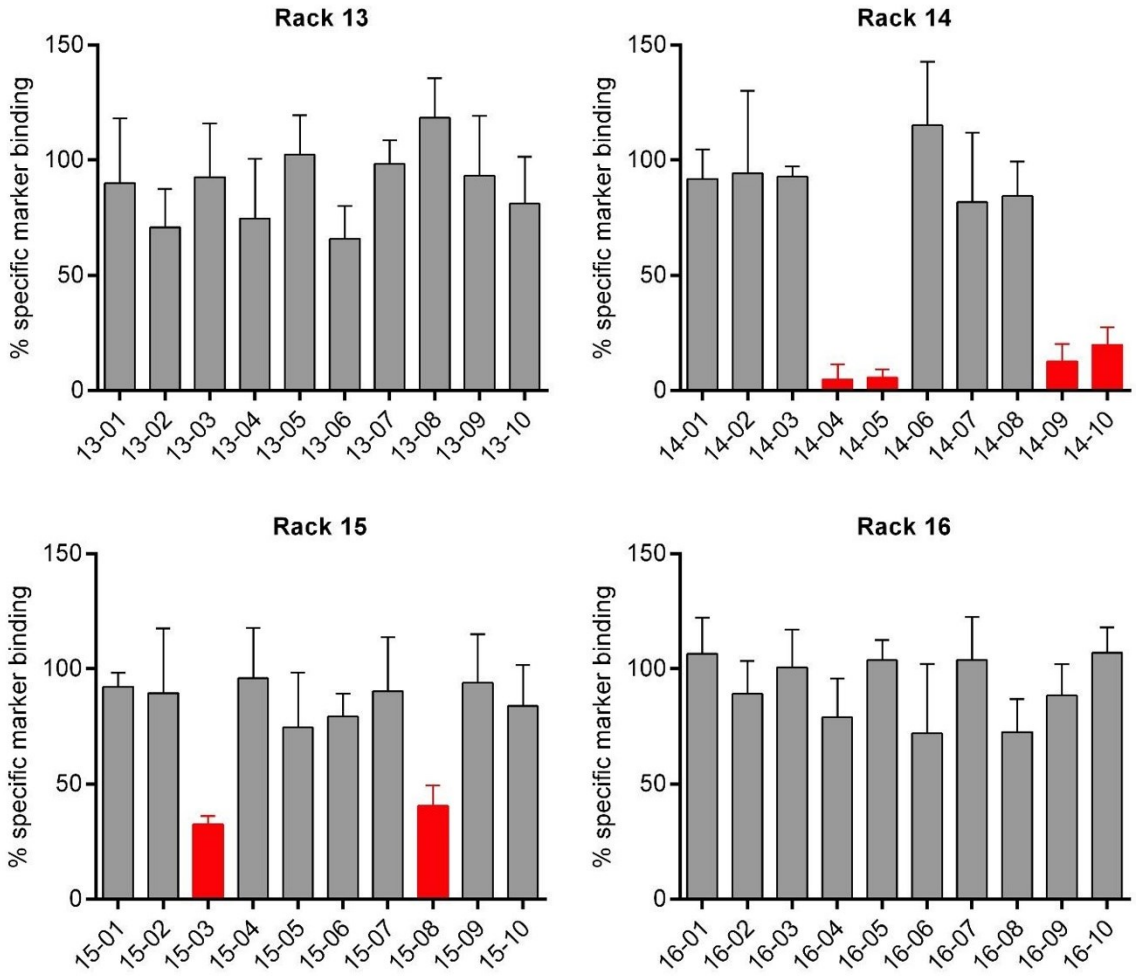

Figure SI2: Testing of the Tocriscreen Plus library. Convolutes were tested in MS Binding Assays with [$^2H_6$]MB327 as reporter ligand and the Torpedo-nAChR as target. Convolutes were referred to as active, if their presence resulted in reduction of specific marker binding to a level ≤ 50% as compared to binding in absence of test compounds. Bars show specific binding (mean ± SD, n = 3) of 10 µmol·L^{-1} [$^2H_6$]MB327 in presence of the respective convolute (each convolute contained 8 compounds at a concentration of 10 µmol·L^{-1}). Red bars mark active convolutes. Specific marker binding is given as percentage compared to specific marker binding in absence of test compounds.

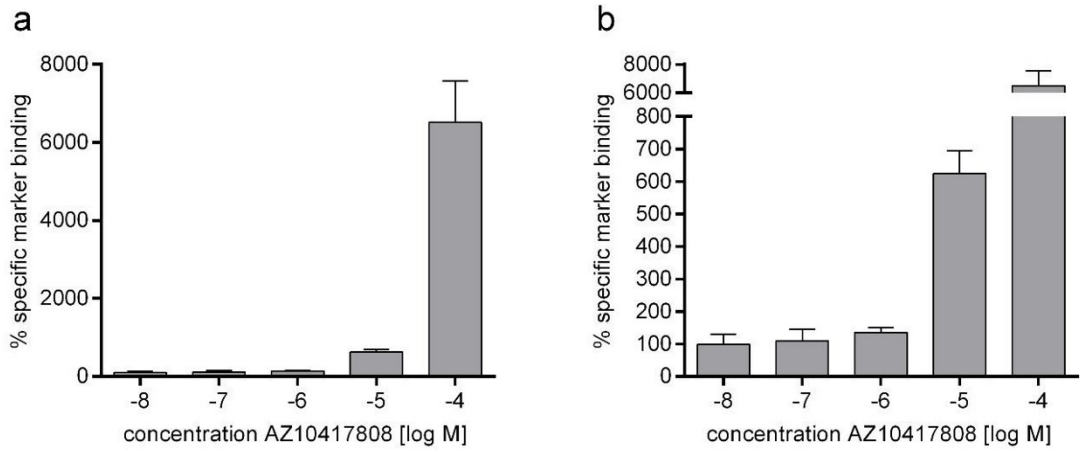

Figure SI3: Representative results of investigations regarding the influence of AZ10417808 on [$^2H_6$]MB327 binding. Experiments were carried out in analogy to competition experiments. Accordingly, 10 µmol·L^{-1} [$^2H_6$]MB327 was used as reporter ligand with Torpedo californica-nAChR as target, 100% were defined by the binding of the reporter ligand in absence of test compound, and 0% by its non-specific binding (determined by heat denaturation). The results show the increase of [$^2H_6$]MB327 binding depending on the AZ10417808 concentration. Up to a concentration of 1 µmol·L^{-1} AZ10417808 [$^2H_6$]MB327 binding rises only slowly, whereas it escalates above this value. The increase of [$^2H_6$]MB327 binding in the presence of 10 µmol·L^{-1} and 100 µmol·L^{-1} AZ10417808 as compared to [$^2H_6$]MB327 binding in the absence of a test compound corresponds to a factor of ~6 and ~70, respectively in this particular experiment.

3.2 Zweite Publikation

"MS Binding Assays with UNC0642 as reporter ligand for the MB327 binding site of the nicotinic acetylcholine receptor"

3.2.1 Zusammenfassung der Ergebnisse

Ein vielversprechender Ansatz, um die Therapie von Vergiftungen mit Organophosphaten, welche z.B. als Insektizide oder auch als Nervengase eingesetzt werden, zu verbessern, ist der Einsatz sogenannter „Resensitizer". Diese Verbindungen versetzen den bei einer OP-Vergiftung desensitisierten, inaktiven nikotinischen Acetylcholinrezeptor (nAChR) nach derzeitigem Kenntnisstand als positive allosterische Modulatoren der MB327-PAM-1-Bindungsstelle des nAChRs in einen funktionalen Zustand zurück. Die Bispyridiniumsalze mit MB327 als bekanntestem Vertreter, nach dem diese Bindungsstelle auch benannt wurde (MB327-PAM-1-Bindungsstelle), sind die in diesem Zusammenhang bisher am meisten untersuchte Verbindungsklasse. Auch wenn für die Bispyridiniumsalze bereits einige pharmakologische Vorteile bei einer Vergiftung mit Organophosphaten festgestellt wurden, ist ihre Affinität zu den genannten Bindungsstellen und damit auch ihre Potenz vergleichsweise gering, weshalb sie nicht als Wirkstoffkandidaten in Betracht kommen.

Auf der Suche nach Verbindungen, welche eine deutlich höhere Affinität zur MB327-Bindungsstelle des nAChRs aufweisen als die bisher untersuchten Bispyridiniumsalze, waren vor dieser Arbeit die strukturverwandten Chinazolinderivate UNC0638, UNC0642 und UNC0646 identifiziert worden. Im Rahmen dieser Arbeit konnte nun ein MS-Bindungsassay (Massenspektrometrie-basierter Bindungsassay) mit UNC0642 als Reporterliganden für die MB327-PAM-1-Bindungsstelle des *Torpedo californica*-nAChRs entwickelt werden, der sich sowohl in Sättigungs- als auch in Kompetitionsstudien bestens bewährte. Die Ergebnisse dieser Bindungsexperimente untermauern weiter, dass UNC0642 an dieselbe Bindungsstelle des nAChRs wie MB327 bindet. Aufgrund der höheren Affinität von UNC0642 im Vergleich zu MB327 zur MB327-PAM-1-Bindungsstelle kann der UNC0642-MS-Bindungsassay als robuster angesehen werden. Dieser MS-Bindungsassay lässt sich bei Bedarf auch unter relativ geringem Aufwand etablieren, da der Reporterligand UNC0642 kommerziell verfügbar ist, während dies beim [$^2H_6$]MB327-MS-Bindungsassay nicht der Fall ist. Der neu entwickelte UNC0642-MS-Bindungsassay stellt damit eine attraktive Alternative zu dem bisher bekannten [$^2H_6$]MB327-MS-Bindungsassay dar.

Die Annahme, dass die neu identifizierten Chinazolinderivate an dieselbe Bindungsstelle des nAChRs binden wie MB327 wird außerdem durch *in silico* Studien gestützt, die auch den Bindemodus für UNC0646 in der MB327-PAM-1-Bindungsstelle als wahrscheinlichem Wirkort beschreiben. Des Weiteren konnte in *ex vivo* Untersuchungen an Rattendiaphragma-Präparationen gezeigt werden, dass auch die neu identifizierten Chinazolinderivate in der Lage sind, die Muskelkraft in Soman-vergiftetem Muskelgewebe zumindest teilweise wiederherzustellen.

3.2.2 Erklärung zum Eigenanteil

Alle in dieser Publikation vorgestellten Arbeiten zu den MS-Bindungsstudien inklusive aller Vorarbeiten wurden von mir eigenständig durchgeführt und die dabei erzielten Daten von mir ausgewertet. Die präsentierten *in silico* Studien wurden von Jesko Kaiser durchgeführt. Thomas Seeger war verantwortlich für die beschriebenen *ex vivo* Experimente. Die entsprechenden Abschnitte des Manuskripts und die zugehörigen Grafiken bzw. Tabellen wurden von dem für den jeweiligen Abschnitt verantwortlichen Koautor angefertigt. An der Konzeption und Korrektur des Manuskripts waren Georg Höfner, Christoph G. W. Gertzen und in maßgeblicher Weise Holger Gohlke, Franz F. Paintner und Klaus T. Wanner beteiligt. Des Weiteren haben Thomas Seeger, Karin V. Niessen, Dirk Steinritz und Franz Worek an der Korrektur mitgewirkt.

Toxicology Letters 392 (2024) 94–106

Contents lists available at ScienceDirect

Toxicology Letters

journal homepage: www.journals.elsevier.com/toxicology-letters

MS Binding Assays with UNC0642 as reporter ligand for the MB327 binding site of the nicotinic acetylcholine receptor

Valentin Nitsche [a,1], Georg Höfner [a,2], Jesko Kaiser [b,3], Christoph G.W. Gertzen [b,4], Thomas Seeger [c,5], Karin V. Niessen [c,6], Dirk Steinritz [c,7], Franz Worek [c,8], Holger Gohlke [b,d,9], Franz F. Paintner [a,10], Klaus T. Wanner [a,*,11]

[a] Department of Pharmacy – Center for Drug Research, Ludwig-Maximilians-Universität München, Munich, Germany
[b] Institute for Pharmaceutical and Medicinal Chemistry, Heinrich Heine Universität Düsseldorf, Düsseldorf, Germany
[c] Bundeswehr Institute of Pharmacology and Toxicology, Munich, Germany
[d] Institute of Bio, and Geosciences (IBG-4: Bioinformatics), Forschungszentrum Jülich, Jülich, Germany

ARTICLE INFO

Editor : Dr. Angela Mally

Keywords:
Nicotinic acetylcholine receptor
UNC0642 MS Binding Assays
MB327-PAM-1 binding site
LC-MS
Resensitizer
In silico studies
Myographic studies

ABSTRACT

Intoxications with organophosphorus compounds (OPCs) based chemical warfare agents and insecticides may result in a detrimental overstimulation of muscarinic and nicotinic acetylcholine receptors evolving into a cholinergic crisis leading to death due to respiratory failure. In the case of the nicotinic acetylcholine receptor (nAChR), overstimulation leads to a desensitization of the receptor, which cannot be pharmacologically treated so far. Still, compounds interacting with the MB327 binding site of the nAChR like the bispyridinium salt MB327 have been found to re-establish the functional activity of the desensitized receptor. Only recently, a series of quinazoline derivatives with UNC0642 as one of the most prominent representatives has been identified to address the MB327 binding site of the nAChR, as well. In this study, UNC0642 has been utilized as a reporter ligand to establish new Binding Assays for this target. These assays follow the concept of MS Binding Assays for which by assessing the amount of bound reporter ligand by mass spectrometry no radiolabeled material is required. According to the results of the performed MS Binding Assays comprising saturation and competition experiments it can be concluded, that UNC0642 used as a reporter ligand addresses the MB327 binding site of the *Torpedo*-nAChR. This is further supported by the outcome of *ex vivo* studies carried out with poisoned rat diaphragm muscles as well as by *in silico* studies predicting the binding mode of UNC0646, an analog of UNC0642 with the highest binding affinity, in the recently proposed binding site of MB327 (MB327-PAM-1). With UNC0642 addressing the MB327 binding site of the *Torpedo*-nAChR, this and related quinazoline derivatives represent a promising starting point for the development of novel ligands of the nAChR as antidotes for the treatment of intoxications with organophosphorus compounds. Further, the new MS Binding Assays are a potent alternative to established assays and of particular value, as they do not require the use of radiolabeled material and are based on a commercially available compound as reporter ligand, UNC0642, exhibiting one of the highest binding affinities for the MB327 binding site known so far.

* Corresponding author.
E-mail address: klaus.wanner@cup.uni-muenchen.de (K.T. Wanner).
[1] 0009-0000-3351-1227
[2] 0000-0002-7957-4503
[3] 0000-0002-6429-0911
[4] 0000-0002-9562-7708
[5] 0009-0007-5713-4367
[6] 0009-0008-6810-5294
[7] 0000-0002-2073-5683
[8] 0000-0003-3531-3616
[9] 0000-0001-8613-1447
[10] 0000-0002-6795-586X
[11] 0000-0003-4399-1425

https://doi.org/10.1016/j.toxlet.2024.01.003
Received 19 November 2023; Received in revised form 28 December 2023; Accepted 6 January 2024
Available online 10 January 2024

1. Introduction

The poisoning with organophosphorus compounds (OPCs) as a result of exposure to respective insecticides or nerve agents represents a severe health problem (Buckley et al., 2004; Costanzi et al., 2018; Eddleston and Phillips, 2004; John et al., 2018). If not treated properly, an intoxication with OPCs can culminate in a cholinergic crisis, which can finally lead to death because of respiratory failure (Holmstedt, 1959; Newmark, 2004). As the principal mode of action, all OPCs have in common to inactivate acetylcholinesterase (AChE), an enzyme that is in charge of the breakdown of the neurotransmitter acetylcholine in the synaptic cleft of cholinergic neurons. This results in the accumulation of this neurotransmitter in the synaptic cleft whereupon the corresponding receptors, the muscarinic acetylcholine receptor (mAChR) and the nicotinic acetylcholine receptor (nAChR), become overstimulated. Being the main cause for the OPC-induced adverse health effects, medical measures aim, in general, at the elimination of this overstimulation. Thus, the standard treatment of OPC intoxication includes the application of the mAChR antagonist atropine to reduce neuronal signaling mediated by this receptor and the use of oximes, such as obidoxime, to reactivate the AChE and, thus, to lower the acetylcholine level by enzymatic breakdown (Shih et al., 2007; Thiermann and Worek, 2022; Worek et al., 2005). The use of oximes has, however, often been found to be insufficiently effective, which strongly depends on the type of OPC causing the intoxication (Thiermann et al., 2016). Hence, there is a strong need for pharmacological agents that may counteract overstimulation and resulting desensitization of the nAChRs receptors by direct intervention at this target.

Though antagonists for the acetylcholine binding site of the nAChR are known, their application to reduce nAChR overstimulation – in analogy to that of atropine for mAChR – is not feasible, as the therapeutic window of these compounds is too small (Sheridan, 2005). Yet, as an alternative, pharmacological agents that interact with nAChRs via an allosteric binding site and restore the functional activity of desensitized receptors may be applied. Among non-oxime bispyridinium salts, a series of compounds has been identified that act this way, of which MB327 (Fig. 1) can be considered the most prototypic representative. Interestingly, in electrophysiological measurements, MB327 has been demonstrated to restore the functional activity of nAChRs, which had been desensitized by overstimulation with orthosteric ligands (Niessen et al., 2016; Niessen et al., 2018). Furthermore, *in silico* studies led to the identification of a potential allosteric binding pocket for MB327 at nAChRs, termed MB327-PAM-1 binding site, where MB327 is thought to act as an allosteric modulator reestablishing receptor function (Kaiser et al., 2023). In addition, pharmacological effects for MB327 and some analogs have been recorded that demonstrate that these compounds can restore the muscle force of rat diaphragm muscles defunctionalized by soman treatment in *ex vivo* experiments (Niessen et al., 2018; Seeger et al., 2012). The ability of MB327 to reactivate soman-poisoned intercostal muscles has also been shown for tissue from humans (Seeger et al., 2012). Moreover, MB327 (respectively the corresponding methanesulfonate salt) was found to increase the survival rate of nerve agent-poisoned guinea pigs in *in vivo* studies when applied as a drug agent (Timperley et al., 2012; Turner et al., 2011). Unfortunately, with its low potency and small therapeutic window, MB327 is far from fulfilling the requirements for a drug candidate (Kassa et al., 2022). Hence, great efforts have been undertaken to identify more potent allosteric modulators of the MB327 binding site.

Sichler et al. have developed an MS Binding Assay addressing the MB327 binding site using [$^2H_6$]MB327 as a reporter ligand (Sichler et al., 2018). This has been extensively used for the characterization of the binding affinities of a plethora of bispyridinium salts related to MB327 that had been synthesized to gain insight into the structure-activity relationship of this compound class and to finally unveil representatives with distinctly higher affinities than MB327. Although binding affinities of most compounds were in the range of that of MB327 ($pK_i = 4.73 \pm 0.03$), one bispyridinium salt, PTM0022, delineated from MB327 by two additional phenyl residues, was found to surpass the binding affinity of MB327 to a small but statistically significant extent ($pK_i = 5.16 \pm 0.07$) (Rappenglück et al., 2018a, b). Significant progress was finally achieved when Sichler et al. used their [$^2H_6$]MB327-based MS Binding Assays addressing the MB327 binding site of the nAChR for the screening of a commercial compound library (Sichler et al., 2024). That way, a group of quinazoline derivatives with high affinities for the MB327 binding site was identified, with the highest affinities displayed by UNC0638 ($pK_i = 6.01 \pm 0.10$), UNC0642 ($pK_i = 5.97 \pm 0.05$), and UNC0646 ($pK_i = 6.23 \pm 0.02$) (Fig. 1).

The present study aimed to develop new MS Binding Assays for the MB327 binding site of the nAChR utilizing one of these quinazoline derivatives as reporter ligand. Such Binding Assays were expected to be more robust and specific due to the distinctly increased affinity of the employed reporter ligand as compared to that of MB327 in the [$^2H_6$]MB327-based MS Binding Assays. Moreover, such Binding Assays should provide additional solid information on the interaction of the aforementioned quinazoline derivatives with the MB327 binding site of the nAChR, which so far had only been studied in competitive [$^2H_6$]MB327 MS binding experiments. For the new Binding Assays, the concept of MS Binding Assays was followed due to simple reasons: As often discussed in the literature, this type of Binding Assays benefits from not requiring radiolabeled substances, which makes them highly flexible with regard to the compounds used as reporter ligands. Besides, MS Binding Assays do not suffer from drawbacks that commonly arise when radioactivity is

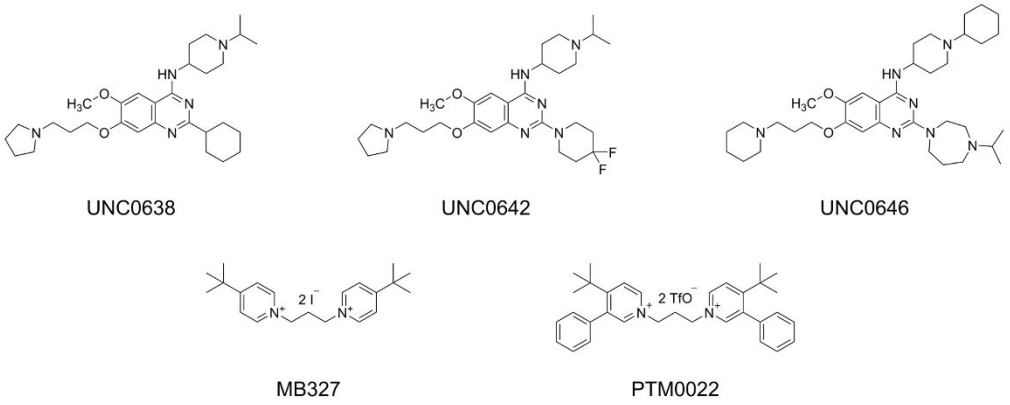

Fig. 1. Ligands of the MB327 binding site of the nAChR: MB327, PTM0022, UNC0638, UNC0642, and UNC0646.

involved in an experimental setting (Höfner and Wanner, 2015; Wanner et al., 2007).

To gain knowledge on the intrinsic activity of the newly identified quinazoline derivatives addressing the MB327 binding site, their capability to restore muscle force in *ex vivo* experiments with soman-poisoned diaphragm muscle tissues were studied, too. In addition, using docking approaches and molecular dynamics (MD) simulations, the binding mode and key interaction partners of the analog with the highest binding affinity, UNC0646, in MB327-PAM-1 were studied.

2. Materials and methods

2.1. Materials

UNC0638 and UNC0642 (purity for both ≥ 95%) were purchased from MedChemExpress (Sollentuna, Sweden). UNC0646 (purity ≥ 99%) was received from Axon Medchem (Groningen, Netherlands) and carbachol (carbamoylcholine chloride, purity ≥ 98%) from Sigma Aldrich. MB327 and PTM0022 were synthesized in-house by Rappenglück et al., purities ≥ 95% (Rappenglück et al., 2018b). Frozen tissue of *Torpedo californica* electroplaque was purchased from Aquatic Research Consultants (San Pedro, CA, USA). Water was obtained from a Sartorius arium pro ultrapure water system (Sartorius, Göttingen, Germany) for all purposes. Organic solvents for LC-MS were received from VWR Prolabo (Darmstadt, Germany) in LS-MS grade. Ammonium formate as additive for LC-MS (purity ≥ 99%) was purchased from Sigma Aldrich (Taufkirchen, Germany). All other chemicals were purchased in analytical grade. Polypropylene reaction tubes and 96-deep well plates as well as pipette tips were received from Sarstedt (Nümbrecht, Germany).

2.2. Preparation of nAChR-enriched membrane fragments

The nAChR-enriched membrane fragments were prepared from frozen electroplaque of *Torpedo californica* as described by Sichler et al. (2018).

2.3. UNC0642 centrifugation-based MS Binding Assays

In general, for MS binding experiments with UNC0642 at *Torpedo*-nAChR, the reporter ligand was incubated with aliquots of the membrane preparation from *Torpedo californica* electroplaque (approx. 75 µg protein per sample) in incubation buffer (120 mM NaCl, 5 mM KCl, 8.05 mM Na_2HPO_4 and 1.95 mM NaH_2PO_4, pH 7.4). With a total volume of 1.25 mL, each binding sample was generated in a 1.5 mL reaction tube. Incubation took place in a shaking water bath (2 h, 25 °C). After that, the reaction tubes were centrifuged for 5 min at 4 °C and 23000 rpm (approx. 49000 x *g*, Heraeus Biofuge Stratos, rotor 3331, Thermo Scientific, Waltham, USA). In the next step, the formed pellets were freed from the supernatant using a Pasteur pipette, which was connected to a vacuum pump via a vacuum filter flask. Thereafter, pellets were washed two times by the addition of 1.5 mL ice-cold incubation buffer and instant removal of the latter by a vacuum-coupled Pasteur pipette. To liberate the bound reporter ligand, 500 µL acetonitrile (containing 500 nM UNC0638 as internal standard) were given to the pellets. The mixtures were subsequently subjected to ultrasound in an ultrasonic bath (SONOREX RK100, Bandelin electronic, Berlin, Germany) for 1 h. Next, the samples were vortexed intensively before they were centrifuged again under the same conditions as described before. Of the resulting supernatants 10 µL were transferred into a 96-deep well plate and diluted by the addition of 490 µL acetonitrile to each well. The 96-deep well plate was sealed with aluminum foil before the samples were finally analyzed via LC-ESI-MS/MS. For saturation experiments, total binding was determined for fifteen reporter ligand concentrations, reaching from 200 nM to 100 µM. For the evaluation of non-specific binding, binding samples with the five lowest reporter ligand concentrations (200 nM - 1 µM) were, in addition, provided with an excess of competitor UNC0646 (100 µM). Regarding the amount of DMSO introduced by the stock solutions of the used compounds (10 mM in DMSO), all binding samples were adjusted to the same amount of 1% DMSO (*v/v*). Competition experiments were performed in analogy to saturation experiments, except that the reporter ligand concentration in the binding samples was set to a fixed concentration of 1 µM. Furthermore, binding samples contained test compounds in general in six but at least in five different concentrations (100 nM - 10 mM). Total binding in the absence of any test compound was determined by means of control samples with only 1 µM of the reporter ligand UNC0642 present in addition to the *Torpedo* membrane preparation. For the determination of non-specific binding of the reporter ligand, binding samples containing 1 µM UNC0642 and *Torpedo* membrane preparation were additionally provided with 100 µM of UNC0646 as a competitor.

2.4. Data analysis

The concentration of the reporter ligand, UNC0642, in each sample was calculated by the Analyst software v. 1.6.1 (AB Sciex, Darmstadt, Germany) based on an underlying calibration curve. To ensure a reliable quantification, calibration standards, and a corresponding calibration function were generated for each binding experiment (see "2.7 Validation of the LC-ESI-MS/MS method" for details). Further analysis (e.g., linear regression, non-linear regression, and normalization) of the data to evaluate the binding experiments was done with the Prism software v. 6.07 (GraphPad software, La Jolla, CA, USA). For saturation experiments, non-specific binding was determined only for the lowest five concentration levels (200 nM - 1 µM). By analyzing this data via linear regression forced through zero a linear regression function was established. This was subsequently used for the calculation of non-specific binding values for all reporter ligand concentrations applied in the assay. Subtracting non-specific binding from total binding yielded specific binding, which was further analyzed by the "One site binding (hyperbola)" regression tool to obtain the values for B_{max} and K_d. For competition experiments, the data received was firstly normalized with the total binding of the reporter ligand in the absence of a test compound being set to 100% and non-specific binding to 0%. The data was then analyzed with the "One site – fit Ki" regression tool, fixing top and bottom levels to 100% and 0% respectively, yielding competition curves. The derived IC_{50} values were automatically transformed into K_i values according to the Cheng-Prusoff equation by the additional input of the K_d value for the reporter ligand, UNC0642 (K_d = 6.7 µM), which was determined in saturation experiments as described above. If not stated otherwise, the results of binding experiments (B_{max}, K_d, K_i) are given as means from three experiments ± SEM.

2.5. LC-MS instrumentation

For preliminary experiments and method development, an API3200 triple quadrupole mass spectrometer with a TurboV-ESI source (Sciex, Darmstadt, Germany) was used in positive mode. After UNC0642 had been selected as a reporter ligand, all subsequent experiments were performed on an API5000. The two mass selectors, Q1 and Q3, were operated under unit resolution. For LC-ESI-MS/MS measurements the MS instrument was provided with an Agilent 1200 Series HPLC system (vacuum degasser G1379B, binary pump G1312B, oven G1316B, Agilent, Waldbronn, Germany). The stationary phase consisted of a YMC-Triart Diol-HILIC (50 mm × 2.0 mm, 3 µm; YMC Europe GmbH, Dinslaken, Germany) protected by two in-line filters (0.5 µm and 0.2 µm, IDEX, Wertheim-Mondfeld, Germany). The mobile phase consisted of a mixture of acetonitrile and an ammonium formate buffer (20 mM, pH 3.0) in a ratio of 80:20 (*v/v*). The flow rate amounted to 800 µL/min and the temperature of the column oven was set to 20 °C. For sample injection (injection volume: 10 µL), a HTS-PAL autosampler (CTC-Analytics, Zwingen, Switzerland) equipped with a 50 µL syringe was used.

For the direct infusion of compound solutions into the ESI source, the HPLC system of the LC-ESI-MS/MS unit was exchanged by a syringe pump (Harvard Apparatus, Holliston, MA, USA).

2.6. Establishing compound- and source-specific parameters

Mass transitions and compound-specific parameters for UNC0638, UNC0642, and UNC0646 were determined automatically by the "Compound optimization" tool of the Analyst software according to the manual of the respective mass spectrometer. For these experiments, the analytes were dissolved in a mixture of methanol and 0.1% aqueous formic acid [50:50 (*v/v*)]. This solution was then directly introduced into the ESI source using a syringe pump. The optimized compound-dependent parameters for the determined mass transitions that were used for the detection of the analytes via MS/MS are listed in Table 1. Source-specific parameters were optimized for the reporter ligand UNC0642 using the "Flow Injection Analysis" tool of the Analyst software, to which end a solution of acetonitrile containing 5 nM UNC0642 and 1:50 (*v/v*) matrix blank was repeatedly injected. The obtained parameters are as follows: collision gas (N_2) = 6 psi, curtain gas (N_2) = 20 psi, nebulizing gas (N_2) = 30 psi, auxiliary gas (N_2) = 50 psi, ionspray voltage = 1500 V and temperature = 600 °C.

2.7. Validation of the LC-ESI-MS/MS method

Matrix zero calibrator samples, which were necessary for the generation of calibration standards and quality control samples, were prepared in the same way as binding samples (see above: "2.3 UNC0642 centrifugation-based MS Binding Assays") with the exception that the incubation was carried out in the absence of any compounds. Instead, matrix zero calibrator samples were later spiked with a defined amount of the reporter ligand, UNC0642, in order to generate the corresponding calibration standards and quality control samples. Thus, the dilution step prior to LC-ESI-MS/MS measurement was adapted (compared to binding samples) and 10 µL supernatant (containing no UNC0642, but like binding samples 500 nM of the internal standard, UNC0638) were diluted with 440 µL acetonitrile and another 50 µL of acetonitrile, which then contained an according amount of the reporter ligand, UNC0642. Following this procedure, quality control samples investigated the subsequently given concentration levels for the reporter ligand, UNC0642, with each prepared in six replicates: 50 pM (LLOQ), 500 pM, 5 nM, 50 nM. Calibration standards were studied in eight different reporter ligand concentration levels, each generated in three replicates (50 pM, 150 pM, 400 pM, 1.2 nM, 3.5 nM, 10 nM, 30 nM, 75 nM). The data for calibration standards was plotted in a coordinate system with peak area ratios of analyte vs. internal standard on the y-axis and the concentration ratios of analyte vs. internal standard on the x-axis. Calibration curves were then obtained by linear regression with a weighting factor of $1/x^2$. Matrix blanks were prepared analogously to binding samples (see above: "2.3 UNC0642 centrifugation-based MS Binding Assays") except that there were no compounds present during the incubation and with the difference, that acetonitrile without internal standard was added to the pellet after the washing process of the samples.

Table 1
Compound-specific parameters and corresponding mass transitions used for the detection of UNC0638, UNC0642, and UNC0646. DP = declustering potential, EP = entrance potential, CE = collision energy, CXP = cell exit potential.

analyte	parent ion $[M+H]^+$ *m/z*	fragment ion *m/z*	DP [V]	EP [V]	CE [V]	CXP [V]
UNC0638	510.3	112.2	86	10	37	18
UNC0642	547.3	112.1	80	10	43	18
UNC0646	622.5	126.1	91	10	55	4

2.8. Docking of UNC0646

The structure of the *Torpedo*-nAChR [PDB-ID: 6UWZ (Rahman et al., 2020)] was used for docking. The α-neurotoxin and molecules from the crystallization buffer were removed, and the receptor was protonated using Protonate3D, as implemented in MOE v2020.09 (Chemical Computing Group, 2020) at pH 7. The termini were capped with *N*-methyl amide (NME) and acetyl (ACE) groups, respectively, using Maestro (Release 2022–3) (Schrödinger, 2021). The 3D conformation of the ligand was retrieved from the SMILES code and subsequently docked using MOE v2020.09 with default parameters for flexible docking (Chemical Computing Group, 2020).

2.9. Molecular dynamics simulations

The nAChR in complex with two UNC0646 ligands, both at the negative (i.e., between the β- and α-subunit and the γ- and α-subunit) site of the α-subunit, was embedded in a membrane consisting of 1-palmitoyl-2-oleoyl-*sn*-glycero-3-phosphocholine (POPC) lipids and solvated in a rectangular box of "optimal point charge" (OPC) water using Packmol-Memgen (Schott-Verdugo and Gohlke, 2019) from AmberTools22 (Case et al., 2023; Case et al., 2022). The edge of the box was set to be at least 12 Å away from the receptor atoms. KCl was added at a concentration of 150 mM and Cl^- ions were used to neutralize the system. The AMBER22 package of molecular simulations software (Case et al., 2005) was used to perform MD simulations in combination with the ff19SB force field (Tian et al., 2020) for the protein and the Lipid21 force field (Dickson et al., 2022) for lipids. Ligand charges were calculated according to the RESP procedure (Bayly et al., 1993) with default parameters as implemented in antechamber (Wang et al., 2006) using electrostatic potentials generated with Gaussian16 (M. J. Frisch et al., 2016) at the HF 6–31 G* level of theory; force field parameters for the ligand were taken from the gaff force field (Wang et al., 2004). Simulations were subsequently performed as described earlier (Kaiser et al., 2023). In short, first, a combination of steepest descent and conjugate gradient minimization was performed while lowering the positional harmonic restraints on receptor and ligand atoms from a force constant of 25 kcal mol^{-1} $Å^{-2}$ to one of zero. Then, the system was stepwise heated to 300 K and, subsequently, positional harmonic restraints were decreased from a force constant of 25 kcal mol^{-1} $Å^{-2}$ to one of zero.

Thereafter, 12 replicas of 500 ns length each of unbiased MD simulations were performed, using Langevin dynamics with a collision frequency of 2 ps^{-1} for temperature control and the Berendsen barostat with semi-isotropic pressure adaption. The trajectories were analyzed with CPPTRAJ (Roe and Cheatham, 2013). The per-residue effective binding energy was computed using the MM-PBSA method, as implemented in AMBER21 (Miller et al., 2012), in the presence of a heterogenous-dielectric implicit membrane model with spline fitting (Greene et al., 2019), an ionic strength of 0.15 M, and an internal dielectric constant of 4.

2.10. Binding mode of UNC0642

Based on the MD simulations with UNC0646 bound to nAChR, we clustered the binding of UNC0646 to obtain a representative binding mode using the *k-means* algorithm, as implemented in CPPTRAJ (Roe and Cheatham, 2013). Based on the biggest cluster (containing 37% of all frames), we replaced the substituents of the quinazoline ring of UNC0646 according to the substitution pattern of UNC0642 and subsequently minimized the ligand in the presence of the receptor with all receptor atoms constrained using MOE v.2022.02 (Chemical Computing Group, 2023).

2.11. Image generation

Images of nAChR were generated using PyMol v2.4.0 (Schrodinger,

2015).

2.12. Alignment of subunits

Sequences of subunits were retrieved from the UniProt database (accessed on the 30th of January, 2023) (The UniProt, 2023) and aligned using Jalview v2.11.2.6 (Waterhouse et al., 2009).

2.13. Rat diaphragm myography

All procedures using animals followed animal care regulations. Preparation of rat diaphragm hemispheres from male Wistar rats (300 ± 50 g) and experimental protocol of myography was performed as described before with slight modifications (Seeger et al., 2012; Seeger et al., 2007). The stimulation was shortened from 25 Hz to 20 Hz and the pulsewidth from 50 to 10 μs. In short, for all procedures (including wash-out steps, preparation of soman and test compound solutions) aerated Tyrode solution (125 mM NaCl, 24 mM $NaHCO_3$, 5.4 mM KCl, 1 mM $MgCl_2$, 1.8 mM $CaCl_2$, 10 mM glucose, 95% O_2, 5% CO_2; pH 7.4; 25 ± 0.5 °C) was used. After the recording of control muscle force one hour after preparation, the muscles were incubated in the Tyrode solution, containing 3 μM soman for 20 min. Following a 20 min wash-out period, the test compounds were added in ascending concentrations (0.1 μM to 100 μM). The incubation time was 20 min for each concentration. The electric field stimulation was performed with 10 μs pulse width and 2 A amplitudes. The tetanic stimulation of 20 Hz, 50 Hz, 100 Hz were applied for 1 s and in 10 min intervals. Muscle force was calculated as a time-force integral (area under the curve, AUC) and constrained to values obtained for maximal force generation (muscle force in the presence of Tyrode solution without any additives; 100%).

All results were expressed in means ± SD (n = 6 - 12). For all data analysis, Prism 5.0 (GraphPad Software, San Diego, CA, USA) was used.

3. Results and discussion

3.1. MS Binding Assays addressing the Torpedo-nAChR with quinazoline derivatives

3.1.1. LC-ESI-MS/MS method development

For performing the MS Binding Assays with one of the newly identified ligands of the MB327 binding site with a quinazoline scaffold, i.e., UNC0638, UNC0642, and UNC0646, first, a reliable LC-MS/MS method for quantification was needed. To this end, a triple quadrupole mass spectrometer in the multiple reaction monitoring (MRM) mode, in combination with a pneumatically assisted electrospray ionization source (ESI) and an HPLC system, should be used. This setup has repeatedly been demonstrated to achieve the selectivity and sensitivity required for marker quantification in MS Binding Assays and, thus, to be well suited for this purpose (Ackermann et al., 2021; Ackermann et al., 2019; Grimm et al., 2015; Hess et al., 2011; Neiens et al., 2018; Neiens et al., 2015). In the literature, for the three compounds UNC0638, UNC0642, and UNC0646, only MS studies reporting their parent ions but no mass fragmentations are known (Liu et al., 2011; Liu et al., 2013; Vedadi et al., 2011). Accordingly, first, the mass transitions of UNC0638, UNC0642, and UNC0646 were analyzed in direct infusion experiments. The most intense mass transitions found, all of which originated from the parent ion $[M+H]^+$, were (see Fig. S1 for product ion spectra): UNC0638 *m/z* 510.3/112.2, UNC0642 *m/z* 547.3/112.1, and UNC0646 *m/z* 622.5/126.1. Next, a suitable LC-ESI-MS/MS method for the quantification of these compounds had to be developed. To enable a reasonably high sample throughput of the MS Binding Assays, such a method should have a short run time while still separating the analyte from contents in the sample matrix interfering with the MS analysis, which, according to our experience, can commonly be reached when the retention factors of the analytes are > 1. In their recent work, Sichler et al. described LC-ESI-MS/MS quantification methods for MS Binding Assays that were all based on the same LC conditions, though the analytes, all polar ligands, varied (e.g., MB327 and phencyclidine) (Sichler et al., 2018). This method is based on a YMC-Triart Diol-HILIC column operated under classical HILIC conditions [mobile phase acetonitrile/ammonium formate buffer (20 mM, pH 3.0) = 80:20; flow rate 800 μL/min]. The quinazoline derivatives UNC0638, UNC0642, and UNC0646 are to be expected to be protonated and, consequently, to possess a high polarity under these chromatographic conditions. Hence, we reasoned that these conditions might also be suitable for their analysis. Indeed, the chromatograms for UNC0638 and UNC0642 obtained with these LC-parameters were satisfying, with the retention factor *k* amounting to 1.7 and 2.1 for UNC0642 and UNC0638, respectively, and the run time to < 3 min (for a chromatogram, see Fig. 2). Under the same chromatographic conditions, UNC0646, however, yielded a peak with a retention factor of > 10, which was far too high for the intended purpose and the peak shape was poor. This issue could be overcome by raising the amount of buffer in the mobile phase from 20% to 35%, whereas the flow rate had to be reduced from 800 to 600 μL/min to not exceed the limits for back pressure. This led to a retention factor $k = 1.2$ for UNC0646 (for a chromatogram, see Fig. S2), which was in the desired range. Finally, preliminary binding experiments should be performed to explore, which of the three compounds might be best suited as a reporter ligand for the planned MS Binding Assays.

3.1.2. Preliminary binding experiments and determination of final assay conditions

When developing a binding assay, irrespective of whether this is, e.g., a radioligand or MS Binding Assay, a decision regarding the technique has to be made that is used for the separation of the target protein with the bound reporter ligand from the rest of the incubation mixture containing the non-bound ligand. In general, filtration is preferred for separation, as it offers an efficient way of handling binding samples and a high sample throughput. Unfortunately, for a filtration-based binding assay, a ligand with a high binding affinity is required. According to the literature, the K_d value should be in the range of 10^{-7} to 10^{-8} M or lower (Hulme and Trevethick, 2010; McKinney and Raddatz, 2006), as otherwise the k_{off} rate (indirectly reflected by the K_d value) is too high and the loss of specifically bound reporter ligand during washing steps will exceed the 10% limit, which will affect the results to a non-tolerable extent. As an alternative to the separation process, centrifugation may be used for ligands with affinities that are too low for filtration. This approach suffers, however, from the fact that the separation step is laborious and the throughput rather low. From the pK_i values determined in the $[^2H_6]$MB327 MS Binding Assay for UNC0638 (pK_i = 6.01 ± 0.10), UNC0642 (pK_i = 5.97 ± 0.05), and UNC0646 (pK_i = 6.23 ± 0.02), it is obvious that with these compounds as reporter ligands only centrifugation can be used for the separation step. As UNC0646 has the highest affinity for the MB327 binding site compared to UNC0638 and UNC0642, it was first chosen as a reporter ligand. When following the general assay procedure Sichler et al. had developed for the centrifugation-based MS Binding Assay with $[^2H_6]$MB327 as reporter ligand addressing *Torpedo*-nAChR, we were indeed able to observe specific binding for UNC0646 in preliminary binding experiments (Rappenglück et al., 2018b; Sichler et al., 2018). For the sake of completeness, also filtration was tested as a separation technique with UNC0646 as the reporter ligand. The experiments, however, led to results suggesting that most of the target-bound ligand had been lost during this assay based on the filtration approach. Hence, centrifugation should be used for the separation step for all further experiments. Much to our surprise, when attempting to finalize the conditions for the MS Binding Assay with UNC0646 as the reporter ligand, we encountered repeatedly difficulties regarding the reproducibility of the compound quantification. Hence, we decided to test UNC0642 as a reporter ligand in MS Binding Assays, although its binding affinity is lower than that of UNC0646. Again, for the MS Binding Assays with UNC0642 as a reporter ligand, we kept close to the conditions that Sichler et al. had established

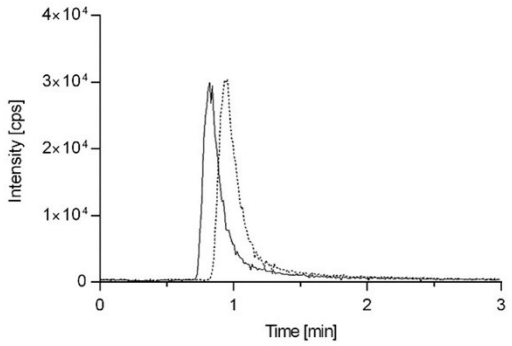

Fig. 2. LC-ESI-MS/MS-MRM chromatogram of a matrix standard containing the reporter ligand UNC0642 (solid line) at a concentration of 5 nM and the internal standard UNC0638 (dashed line) at 10 nM. For quantification, the mass transitions *m/z* 547.3/112.1 and *m/z* 510.3/112.2 for UNC0642 and UNC0638, respectively, were used. A YMC-Triart Diol-HILIC (50 mm × 2.0 mm, 3 µm) column was used as a stationary phase in combination with an 80:20 (*v/v*) mixture of acetonitrile and ammonium formate buffer (20 mM, pH 3.0) as mobile phase. The injection volume amounted to 10 µL and the flow rate to 800 µL/min.

for their centrifugation-based [$^2H_6$]MB327 MS Binding Assay addressing the *Torpedo*-nAChR (see Materials and methods for details). However, in the case of the new binding assay, non-specific binding was determined by the competitor approach, whereas Sichler et al. had applied the heat shock method, by which the target material is denatured to lose specific binding (Sichler et al., 2018). For the new Binding Assays, highly affine ligands of the MB327 binding site were available that appeared well suited for the determination of non-specific binding by the competitor approach with competitors not yet identified when Sichler et al. developed their [$^2H_6$]MB327 MS Binding Assay. Hence, we opted for this approach, as this is the most common one (Hulme and Trevethick, 2010; Motulsky and Neubig, 2002). As a competitor for the determination of non-specific binding, UNC0646 was selected as one of the two quinazoline derivatives with high affinities for the MB327 binding site, UNC0638 and UNC0646. This decision was made, as the reporter ligand should be quantified using an internal standard to improve the robustness of the quantification method. Hence, one of the two aforementioned quinazoline derivatives was needed to this end. As only UNC0638 exhibits a chromatographic behavior similar to that of the reporter ligand UNC0642 but not UNC0646 (see Section 3.1.1), which is essential for a compound to be used as an internal standard, UNC0638 could serve this function. Accordingly, for determining non-specific binding in the binding assay, quinazoline derivative UNC0646 had to be used.

3.1.3. LC-ESI-MS/MS method and method validation

With the conditions of the MS Binding Assays and, thus, also the matrix of the analytical samples being defined, the preconditions for the validation of the LC-ESI-MS/MS method for the quantification of the reporter ligand UNC0642 with UNC0638 as internal standard were given. As indicated above, the LC method was largely the same as the one developed by Sichler et al. (Sichler et al., 2018). In Fig. 2, a chromatogram of the ligand UNC0642 and the internal standard UNC0638 obtained applying these LC conditions is given with the most important parameters of the LC-ESI-MS/MS method being listed in the caption (for further details see Materials and methods). For the validation of the analytical method, the recommendations of the FDA guidance for bioanalytical method validation were followed regarding the criteria linearity, accuracy, precision, sensitivity, and selectivity (FDA, 2018). The results of the validation process are briefly discussed in the following. Detailed validation data of the corresponding three validation series can be found in the SI (see Fig. S3 and Table S1). For the validation experiments, matrix blank and matrix zero calibrator samples were prepared in analogy to the samples of the MS binding experiments. Matrix zero calibrator samples were used to create calibration standards and quality control samples (see Materials and methods for details). Calibration standards were prepared for eight different concentrations in the range from 50 pM (lower limit of quantification, LLOQ) to 75 nM and quality control samples for the four concentrations 50 pM (LLOQ), 500 pM, 5 nM, and 50 nM. In calibration standards and quality control samples, the internal standard UNC0638 was present at 10 nM. To evaluate the linearity of the quantification method in the investigated concentration range (50 pM to 75 nM), the calibration standards were analyzed via linear regression to obtain a calibration curve (see Materials and methods for details). The criteria of the FDA guideline for linearity demand calibration standard deviations from the nominal concentrations to be within a limit of ± 15% (± 20% at LLOQ). As we determined calibration standard deviations from the nominal concentrations in the range from 93% to 112%, the criteria of the FDA guideline for linearity were fulfilled. Deviations of the measured concentrations from nominal concentrations within ± 15% (± 20% at LLOQ) are required for accuracy by the FDA guidelines for quality control samples. For intra-run samples, accuracies from 91 - 103% and for inter-run samples accuracies from 94 - 101% were found, thus fulfilling the acceptance criteria of the FDA guideline for these criteria. The quality control samples were also examined regarding precision (expressed by the relative standard deviation), which amounted to 2.5 - 6.5% and 4.0 - 6.3% for intra-run and inter-run precisions, respectively, being in line with the acceptance criteria of ± 15% (± 20% at LLOQ) of the FDA guidelines. Also, the sensitivity of the LC-ESI-MS/MS method was guaranteed as the intensity of the peak corresponding to the LLOQ of 50 pM as compared to the noise signals was in line with the required signal-to-noise ratio of at least five. When a matrix blank sample was measured, no interference was found, demonstrating the selectivity of the established LC-ESI-MS/MS method. Overall, all studied validation criteria of the analytical method comply with the standards defined by the FDA guidelines.

3.1.4. UNC0642 MS Binding Assays

3.1.4.1. Saturation experiments. Next, with the validated quantification method for UNC0642 at hand, the binding of this compound to *Torpedo*-nAChR should be characterized in saturation experiments. For saturation experiments, the target is in general incubated with the reporter ligand in a concentration range from 0.1 K_d to 10 K_d for the determination of total binding. As the K_d of UNC0642 was expected to be in the very low micromolar range, we investigated fifteen different reporter ligand concentrations ranging from 200 nM to 100 µM for total binding. For the determination of non-specific binding, a further set of binding samples containing UNC0646 as competitor was prepared. Because of its low solubility, UNC0646 could only be used in an assay concentration of up to 100 µM. Since the affinity of UNC0646 ($pK_i = 6.23 \pm 0.02$) determined in [$^2H_6$]MB327 MS Binding Assays is similar to that of the reporter ligand UNC0642 ($pK_i = 5.97 \pm 0.05$), according to common rules, at least a hundredfold excess of the competitor UNC0646 over the reporter ligand UNC0642 had to be applied. Hence, because of the limited solubility of UNC0646, non-specific binding could only be measured for the five lowest reporter ligand concentrations (200 nM - 1 µM). Based on these data, a linear regression function, which was forced through zero, was established and finally used for the calculation of non-specific binding values for all reporter ligand concentrations employed in the assay (Davenport and Russell, 1996).

Specific binding as the difference between total and non-specific binding was finally analyzed by non-linear regression, generating saturation isotherms that revealed a binding affinity for UNC0642 of 6.7 ± 0.4 µM (K_d) and a maximum density of binding sites $B_{max} = 2980$

± 130 pmol/mg protein. The results of a representative saturation experiment are depicted in Fig. 3. The obtained K_d value of 6.7 ± 0.4 μM, corresponding to a pK_d of 5.17 ± 0.03, is in reasonable accordance with the pK_i value of 5.97 ± 0.05 previously determined by Sichler et al. (Sichler et al., 2024). The B_{max} value found in our experiments appears to be rather high, which may be explained by recent *in silico* experiments suggesting that there are multiple MB327 binding sites in the nAChR (Kaiser et al., 2023). Overall, the results of these saturation experiments indicate that UNC0642 binds to nAChR in a specific and saturable manner, which in combination with the data found by Sichler et al. in competition experiments with [$^2H_6$]MB327 as reporter ligand (Sichler et al., 2024), further supports the assumption that both address the same binding site, the MB327 binding pocket of *Torpedo*-nAChR.

3.1.4.2. Competition experiments. Finally, with the methodology for performing saturation experiments with UNC0642 as a reporter ligand at hand, competitive MS Binding Assays addressing the MB327 binding site of *Torpedo*-nAChR should be established. These should be used to characterize the binding affinities of a representative set of ligands of the MB327 binding pocket known from [$^2H_6$]MB327 MS Binding Assays. As the binding affinity of MB327 towards the MB327 binding site of *Torpedo*-nAChR is rather low, the results from MS Binding Assays based on [$^2H_6$]MB327 as a reporter ligand might deviate from the real value. Yet, these results should still be a reasonable basis for a comparison with the data obtained from the new MS Binding Assay with UNC0642 as a reporter ligand. The comparison might allow us to validate the results of the UNC0642 MS Binding Assay and, in addition, further support the assumption that UNC0642 and MB327 address the same binding pocket of *Torpedo*-nAChR. The set of competitors to be studied in the UNC0642 MS Binding Assays contains MB327, as the reporter ligand from the [$^2H_6$]MB327 MS Binding Assay and most prototypic representative of bispyridinium salts addressing nAChR, and PTM0022, as this compound shows the highest affinity so far found within the class of bispyridinium salts (Rappenglück et al., 2018b). Furthermore, the quinazoline derivative UNC0646 should be included in this set of test compounds, as it represents the compound with the highest affinity for the MB327 binding site so far known (Sichler et al., 2024). For control purposes, finally, also the effect of carbachol, which is a well-known ligand of the orthosteric binding site of nAChR, in the new competitive MS Binding Assays with UNC0642 as the reporter ligand should be studied. The competition experiments were performed in analogy to the saturation experiments with the following adaption. The concentration of the reporter ligand UNC0642 was kept constant at 1 μM. Binding samples were provided with increasing concentrations of the respective test compounds, usually covering a range of three orders of magnitude around the expected IC_{50}. After quantification of the reporter ligand via LC-ESI-MS/MS, the obtained data was normalized. For this, binding samples had been prepared, which contained no competitor (equivalent to 100% specific binding) or 100 μM UNC0646 as competitor (i.e., non-specific binding, 0% specific binding). Competition curves were created by non-linear regression yielding the respective IC_{50} values of the test compounds from which K_i values were calculated according to the Cheng-Prusoff equation (see Materials and methods for details). The competition curves that resulted when the above-mentioned test compounds were characterized in the new competitive MS Binding Assays with UNC0642 as reporter ligand – in three independent experiments in every case – are given in Figs. 4a and 4b.

Except for carbachol, for all other test compounds, the shape of the competition curves was well in line with theoretical models. The analysis of the curves revealed IC_{50} values from which pK_i values of 3.40 ± 0.04, 4.80 ± 0.03, and 5.83 ± 0.05 for MB327, PTM0022, and UNC0646, respectively, were calculated. Overall, pK_i values found in the new MS Binding Assay utilizing UNC0642 as reporter ligand were lower

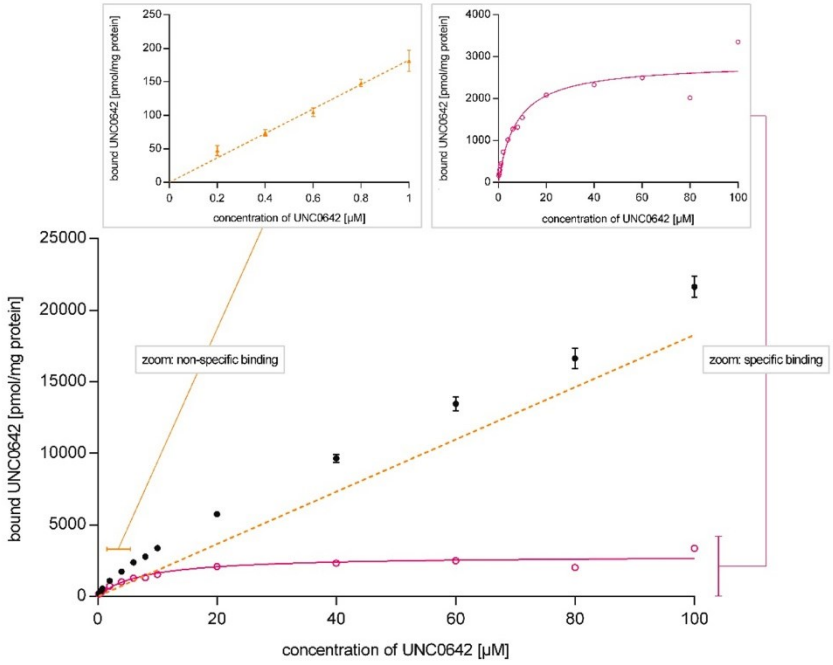

Fig. 3. Representative saturation experiment for UNC0642 binding to *Torpedo*-nAChR. Total binding (black circles) and non-specific binding (orange triangles). Linear regression of non-specific binding is shown as an orange dashed line. Total binding (black circles) was not further analyzed and only used to calculate specific binding. Accordingly, no black line is given in the figure. Specific binding (pink circles) was calculated as the difference between total binding and non-specific binding and analyzed by non-linear regression (solid pink line). Experimental values are means ± SD, n = 3.

than those determined in the [$^2H_6$]MB327 MS Binding Assay, but most importantly the rank order of affinities remained the same (MB327 < PTM0022 < UNC0646, see Table 2). Interestingly, also carbachol affected the binding of UNC0642. Up to a concentration of 1 μM carbachol, the UNC0642 binding remained largely unchanged, whereas it decreased for higher carbachol concentrations to reach a plateau of 75 - 80% at about 10 μM, which persists up to the highest concentration applied (1 mM). Notably, the change of UNC0642 binding occurs in the same range of carbachol concentration – 1 μM to 10 μM – that is known from functional studies to affect the transition of *Torpedo*-nAChR from its resting into its active state (Niessen et al., 2016). If the concentration of an orthosteric ligand present at the nAChR is far above the amount required for activation, the receptor switches into a desensitized state (Papke, 2014). This has to be taken into account for the analysis of the above-described data, as the transition of *Torpedo*-nAChR into the desensitized state likely occurs at a carbachol concentration covered in the experiments, i.e., ≥ 100 μM (Währa et al., 2023). Thus, the decrease of UNC0642 binding to the MB327 binding site upon increasing the carbachol concentration is likely the result of a conformational change due to the orthosteric ligand binding, which exerts an allosteric effect between the orthosteric and the MB327 binding site (Kaiser et al., 2023). However, for a better understanding of the interaction between the MB327 binding site and the orthosteric binding site, further studies are needed.

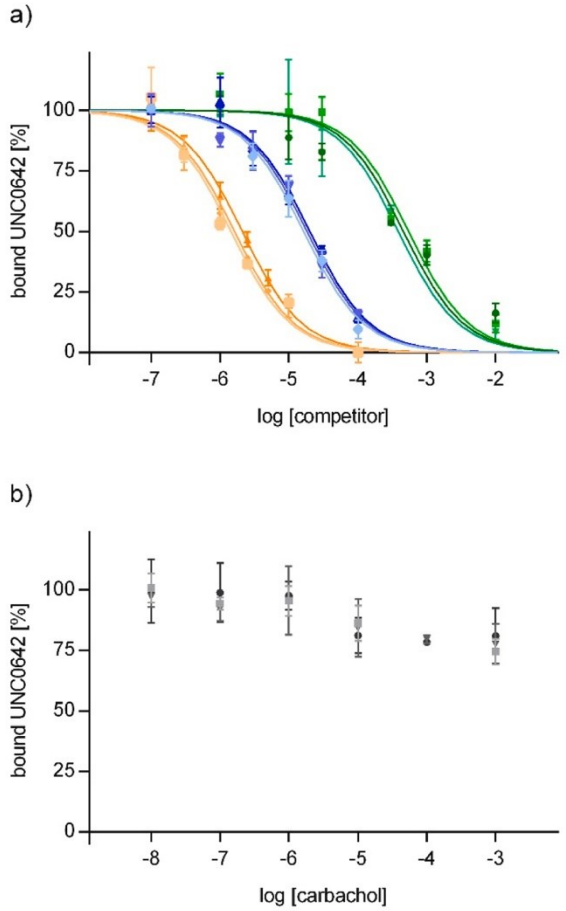

Fig. 4. a) Competition curves obtained for MB327 (green), PTM0022 (blue), and UNC0646 (orange). b) Influence of carbachol on UNC0642 binding. Data points (mean ± SD, $n = 3$) represent the specific binding of UNC0642.

Overall, according to the results of the UNC0642 MS Binding Assays, it is reasonable to conclude that UNC0642 alike MB327 addresses the MB327 binding site of the nAChR. In particular, the binding of UNC0642 can completely be inhibited by MB327, and both the MS Binding Assay based on UNC0642 and on [$^2H_6$]MB327 yield pK_i values that are in reasonable to good agreement and lead to the same rank order of potencies in competitive experiments for the set of ligands studied (see Table 2). Hence, the UNC0642 MS Binding Assays represent a valuable new tool for the characterization of the affinity of ligands of the MB327 binding site of the nAChR. With the binding affinity of UNC0642 being distinctly higher than that of [$^2H_6$]MB327, the reporter ligands of the UNC0642 and [$^2H_6$]MB327 MS Binding Assays, the former can be considered more robust with regard to its performance and results than the latter. In addition, the former MS Binding Assay has the advantage that its reporter ligand, UNC0642, is commercially available, which eases its setup.

3.2. *In silico investigation of the UNC0646 binding mode in MB327-PAM-1*

Recently, we proposed a novel binding site, MB327-PAM-1, in nAChR for binding of MB327 that can explain the allosteric modulation relevant for treating poisoning with OPC (Kaiser et al., 2023). MB327-PAM-1 is located in between two adjacent subunits at the transition of the extracellular to the transmembrane region and is different from two allosteric and one orthosteric binding pocket that had been proposed before for bispyridinium compounds using in silico methods (Epstein et al., 2021; Wein et al., 2018). To investigate the binding site of the ligand with the highest binding affinity in this study, UNC0646, first, we performed flexible docking experiments to place the ligand in MB327-PAM-1. To do so, we selected all residues within 9 Å of the centrally located E199α (respectively, Q209β, E210δ, E200γ in the other subunits) as a potential binding site. UNC0646 was placed similarly at the negative side of the two α subunits, whereas in the other three subunits, the ligand was either placed in the middle between two possible binding sites or more towards the pore, which would result in a high solvent exposure (SI Fig. S4). In between the γ- and α-subunit (binding site A), the best-scored conformation contains a twist conformation of the cyclohexane ring and a boat conformation of the piperidine ring of the side chain in the 4-position of the quinazoline ring (SI Fig. S5). As these ring conformations are energetically unfavorable, we chose the second best-scored conformation. The orientation of UNC0646 in the binding pocket is similar there but the rings have chair conformations. Overall, in both binding sites at the negative side of the α-subunits, the orientation of UNC0646 is comparable. However, while in between the β- and α-subunit (binding site B) the nitrogen of the piperidine ring in the 4-position of the quinazoline ring is interacting with E199α, the ligand is placed more deeply in the binding site A, which facilitates interaction between this nitrogen and E65γ (Fig. 5A, SI Fig. S6).

To further scrutinize interactions with surrounding amino acids, we performed 12 replicas of 500 ns long unbiased MD simulations starting from the docked conformations of UNC0646 in binding sites A and B

Table 2
pK_i values obtained from IC_{50} values determined in UNC0642 MS Binding Assays and [$^2H_6$]MB327 MS Binding Assays, respectively (Rappenglück et al., 2018b; Sichler et al., *Unpublished results*).

compound	UNC0642 MS Binding Assay pK_i	[$^2H_6$]MB327 MS Binding Assay
MB327	3.40 ± 0.04	4.73 ± 0.03
PTM0022	4.80 ± 0.03	5.16 ± 0.07
UNC0646	5.83 ± 0.05	6.23 ± 0.02

resulting in 6 μs (12 x 500 ns) of cumulative simulation time. During MD simulations, the receptor and membrane remained structurally virtually invariant (SI Fig. S7, S8). Throughout the MD simulations, UNC0646 showed smaller movements in binding site A (RMSD = 3.02 ± 0.30 Å) than binding site B (RMSD = 5.13 ± 0.58 Å, $p = 0.004$ according to a two-sided t-test). Furthermore, UNC0646 leaves the binding site B in six out of 12 replicas [distance to I65α < 5 Å in the last frame, as done previously (Kaiser et al., 2023)], whereas this does not occur in any of the 12 replicas in binding site A. Together, this suggests that the orientation of UNC0646 in binding site A is preferred.

Thus, we used this orientation to further predict important residues for interactions, in particular, salt bridge interactions of the three tertiary amines in the substituents of the quinazoline ring with the glutamates in the binding site; glutamates were ranked as the most important residues for ligand binding in per-residue decompositions of the effective binding energy computed with MMPBSA (SI Fig. S9). E65γ, previously described to be important for interactions with MB327 (Kaiser et al., 2023), shows the most conserved interactions with the piperidyl moiety in position 4 of the quinazoline ring (71.8 ± 7.4% of all frames, Fig. 5). Second, the positively charged nitrogen of the substituent in the 7-position interacts primarily with E69α (28.2 ± 10.5%). As this nitrogen is located in an area surrounded by four glutamates (E69α, E199α,

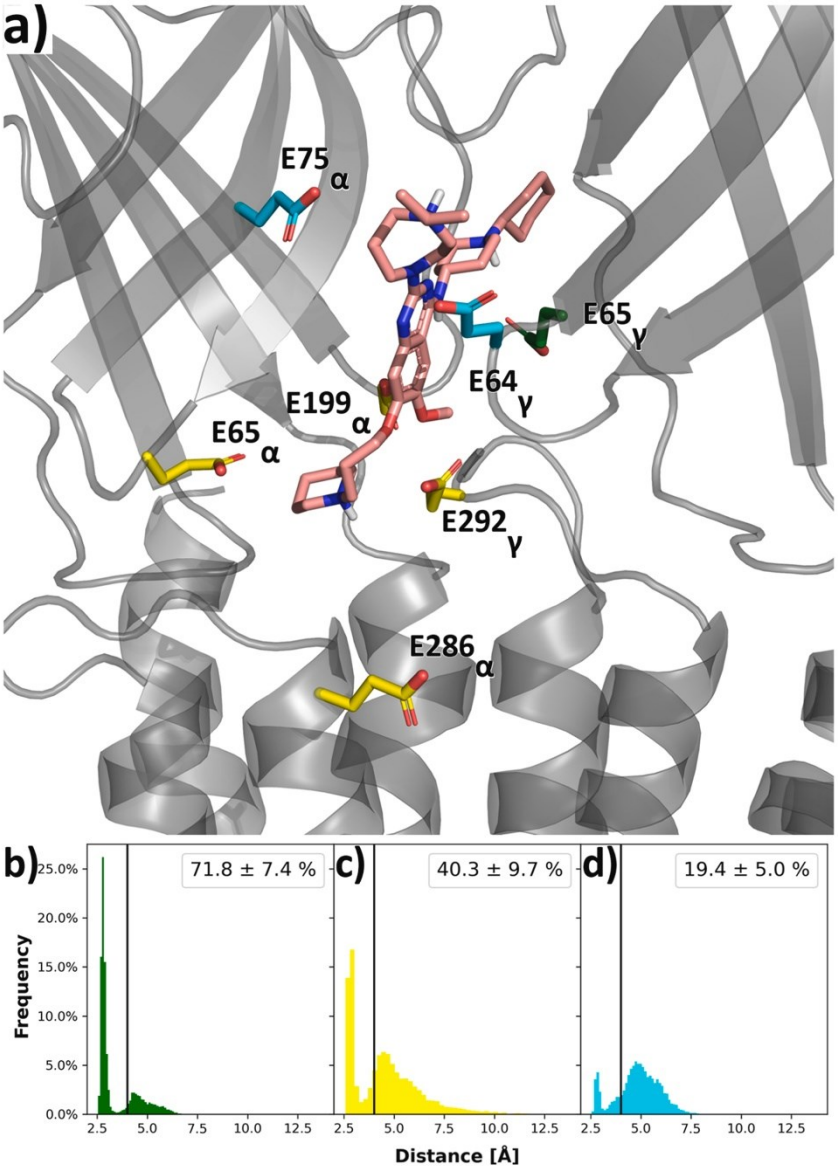

Fig. 5. UNC0646 and interacting residues in *Torpedo*-nAChR. a) Docked binding mode of UNC0646 as starting point for MD simulations. b) Minimal distance of the positively charged piperidyl nitrogen in the sidechain at position 4 to the carboxylate oxygens of E65γ. c) Minimal distance of the positively charged piperidyl nitrogen in the side chain at position 7 to the carboxylate oxygens of E65α, E199α, E286α, and E292γ. d) Minimal distance of the positively charged nitrogen in the diazepane ring to the carboxylate oxygens of E75α and E64γ. Amino acids in panel A are colored according to the plot colors in panels b) - d). The values in panels B-D indicate the mean ± SEM (taken over 12 replicas each) of the frequency of hydrogen bonds (distance of nitrogen to carboxylate oxygen < 4 Å).

Table 3
Sequence similarity of *Torpedo* and human adult muscle-type nAChR subunits. Amino acids shown in Fig. 5 are represented with green shadings. Amino acids at structurally homologous positions in other subunits are shown on a white background; amino acids with deviating physicochemical properties are shown in italics.

Human muscle-type nAChR				Torpedo nAChR			
α	β	δ	ε	α	β	δ	γ
E	E	E	E	E69	E	E	E
T	*S*	*T*	*T*	E75	*T*	*T*	*T*
E	*Q*	E	E	E199	*Q*	E	E
E	D	*K*	*Q*	E286	D	*Q*	*Q*
N	D	E	E	*N*	*I*	D	E64
Q	E	E	E	*Q*	E	E	E65
S	E	*A*	E	*S*	E	E	E292

E286α, and E292γ), additional salt bridge interactions can form. Considering all four glutamates, the nitrogen is interacting with carboxylate oxygens in 40.3 ± 9.7% of all frames. In contrast, the tertiary amine nitrogen in the diazepane ring at position 2 shows only minor interactions with the two surrounding glutamates (E75α, and E64γ; in 19.4 ± 5.0% of all frames). These results indicate that the side chain in the 4-position of the quinazoline ring is most important for forming salt bridge interactions whereas the diazepane ring is least important. These findings are in line with a structure-affinity relationship deduced from compounds UNC0646, UNC0642, and UNC0638, where removing the positive charge in the 2-position of the quinazoline ring has only minor effects on ligand affinity. Furthermore, the findings are supported by residue conservation analysis according to which E65γ, E69α, E199α, and E286α are highly conserved among different subunits of the *Torpedo* and human muscle-type nAChR such that acidic side chains at each position are available in at least three of the five subunits and hydrogen bond acceptors are available in all subunits but one (Table 3). By contrast, E292γ, E75α, and E64γ are less conserved (Table 3).

Based on a representative binding mode of UNC0646 during MD simulations in binding site A, we replaced the substituents of the quinazoline ring of UNC0646 to match those of UNC0642 using MOE and subsequently minimized the ligand in the binding site (SI Fig. S10). The substituents in 4- and 7-position of the quinazoline ring of UNC0642 interact similarly as those of UNC0646, whereas due to a lack of protonation sites interactions with the ring system in 2-position are missing.

3.3. Evaluation of the muscle force recovery of quinazoline-based compounds

To gain more knowledge on the intrinsic effects of UNC0638, UNC0642 and UNC0646 we performed myographic experiments with soman-poisoned and also un-poisoned rat diaphragms. The corresponding results of these experiments are summarized in Fig. 6. Interestingly, the compound with the highest known affinity to the MB327 binding site, UNC0646, was the only compound in this series of experiments that did not seem to have a beneficial effect on the restoration of muscle force after soman poisoning. UNC0638 and UNC0642 instead induced the regeneration of muscle force at a maximum of 30 μM and 10 μM, respectively. The highest extent of recovery was observed for a stimulation frequency of 20 Hz and amounted to 18.4 ± 16.1% for UNC0638 at 30 μM and 16.2 ± 12.8% for UNC0642 at 10 μM (mean ± SD, n = 5). The maximum amplitudes of UNC0638 and UNC0642 are thus lower than the maximum amplitude observed for MB327 [approximately 30% at 20 Hz (Niessen et al., 2018; Seeger et al., 2012)], but favorably the concentration needed to generate the described effect was distinctly lower for UNC0638 and UNC0642 than for MB327, which showed its maximum effect at a concentration of 300 μM. To obtain a recovery comparable to that exhibited by UNC0638 and UNC0642 at a concentration of 30 μM and 10 μM, respectively, MB327 had to be used at 100 μM (Niessen et al., 2018; Seeger et al., 2012). Noteworthy, the muscle force restoration effected by UNC0638 and UNC0642 declined at higher concentrations after the maximum had been reached at 30 μM and 10 μM, respectively. This phenomenon has been observed for MB327 and some MB327 analogs before (Niessen et al., 2018). It has been speculated, that counteracting effects, mediated by different binding sites may be responsible for the observed course of muscle force as a function of the compound concentration. In the present case, i.e. for UNC0638, UNC0642, and UNC0646, this theory is supported by results, that have been obtained in myographic experiments performed in analogy to those above except for using native, functionally active instead of soman-poisoned rat-diaphragms.

Here, the muscle force of the functionally active muscle decreased when UNC0638 and UNC0642 were applied at high concentrations (i.e. ≥ 10 μM). This effect was even more pronounced for UNC0646, as it started at distinctly lower concentrations and led to a nearly complete inhibition of the muscle force at 1 μM (see Fig. 6). Hence, the "bell-shape" of the curve of muscle-force recovery in soman-poisoned rat diaphragms upon treatment with UNC0638 and UNC0642 may be attributed to the above-described counteracting effect, which is, however, moderate, so that at lower concentration a positive effect still prevails. In contrast, in the case of UNC0646 no positive effect on muscle force recovery remains, as here the counteracting effect starts at distinctly lower concentrations and is more pronounced.

Finally, it should be mentioned, that the muscle force decreasing potential of the studied compounds appears to be reversible, as the muscle force partly recovers when the respective samples are subjected to a washing step (see Fig. 6).

Overall, the quinazoline derivatives UNC0638, UNC0642 and UNC0646 identified as binders of the MB327-PAM-1 binding site of the nAChR are in principle also able to restore muscle function of soman-poisoned muscle tissue. Though the maximum amplitudes for muscle force recovery of UNC0638 and UNC0642 are lower than those found for MB327, the maximum values are, remarkably, reached for the two quinazoline derivatives at distinctly lower concentrations than for MB327, which is likely to result from their higher binding affinities. Future studies will have to aim on a better understanding of the factors responsible for the counteracting effects regarding the recovery of muscle force in soman-poisoned rat diaphragms that might finally lead to more potent compounds.

4. Conclusion

The quinazoline-based compounds UNC0638, UNC0642, and UNC0646 had been identified as hits in a recent library screening campaign using competitive [$^2H_6$]MB327 MS Binding Assays in the search for new ligands addressing the MB327-PAM-1 binding site of the nAChR. In the present study, these compounds, which exhibit the

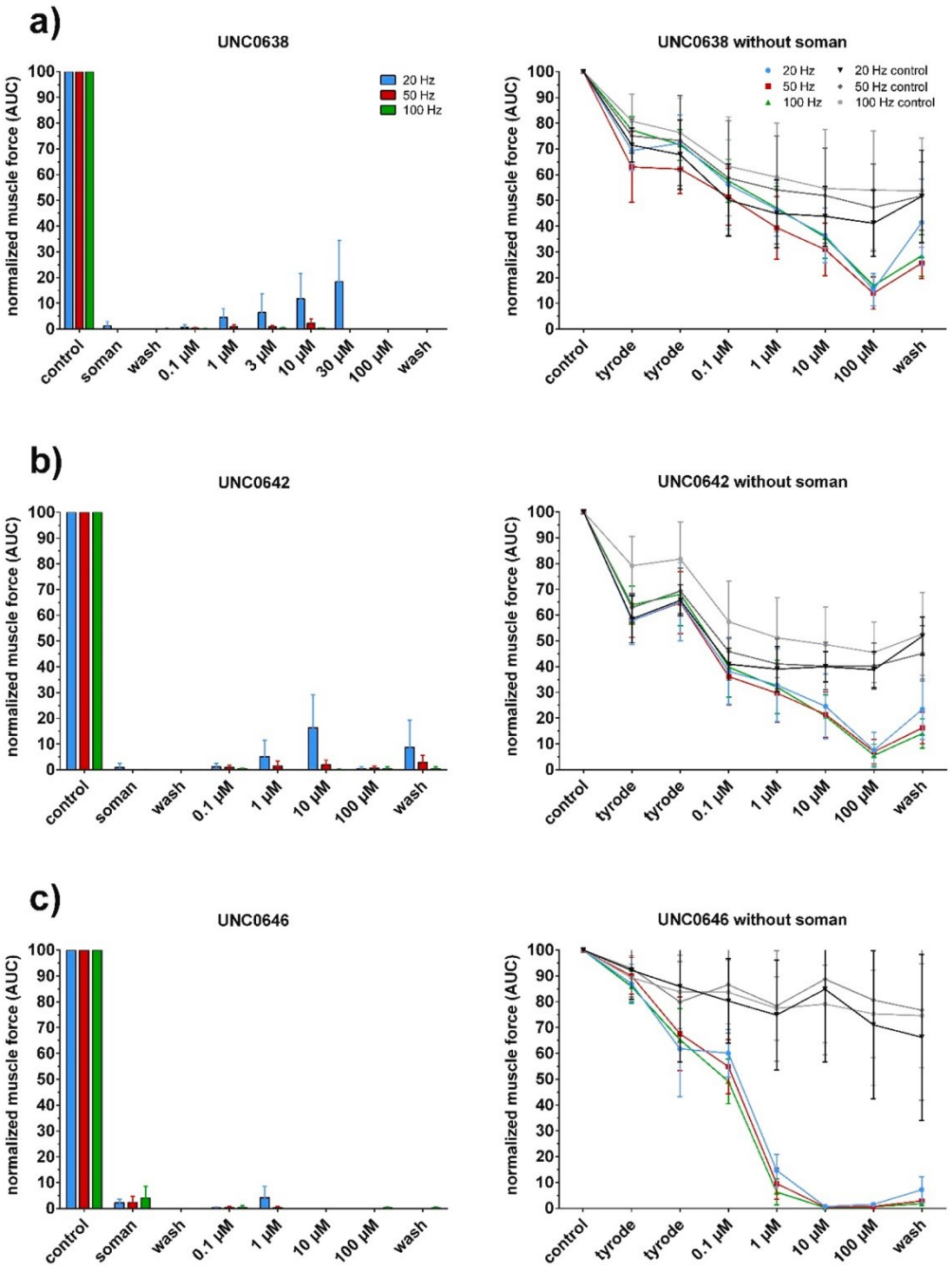

Fig. 6. Muscle force of soman-poisoned (left) and un-poisoned (right) rat diaphragms after treatment with a) UNC0638, b) UNC0642, and c) UNC0646. Left: Muscle force of diaphragm muscle was blocked by 3 µM soman. Right: Muscle force generation of un-poisoned muscle. Muscle force generation was measured as the area under the curve normalized to muscle force under control conditions at the start of the measurement (n = 6 - 12).

highest affinities known so far for the MB327-PAM-1 binding site, have been used for the development of new MS Binding Assays for the aforementioned binding site of the nAChR with UNC0642 serving as reporter ligand, UNC0638 as internal standard and UNC0646 as competitor for the determination of non-specific binding. The new UNC0642 MS Binding Assays comprised the characterization of the binding of UNC0642 to the MB327-PAM-1 binding site of *Torpedo*-nAChR in saturation experiments and the determination of the binding affinity of a set of ligands of the aforementioned binding site in competition experiments. The results were in good accord with those obtained from the [$^2H_6$]MB327 MS Binding Assays, that had been used so far for the determination of binding affinities for the MB327 binding

site. Carbachol used as a control had only a very small effect on reporter ligand binding in respective competition experiments. As this compound, carbachol, represents a ligand of the orthosteric binding site of the nAChR the observed effect on reporter ligand binding is likely to be attributed to an allosteric interaction between both binding sites. Based on the results obtained with the new UNC0642 MS Binding Assay it is reasonable to conclude, that this binding assay addresses the same binding site as the [$^2H_6$]MB327 MS Binding Assay, i.e. the MB327-PAM-1 binding site of the nAChR. Hence, the UNC0642 MS Binding Assays represent a valuable alternative to the [$^2H_6$]MB327 MS Binding Assays and profit from the high affinity of the reporter ligand, which will contribute to the robustness of the Binding Assays, and from the commercial availability of said compound.

By using docking approaches and molecular dynamics simulations, the binding mode and key interactions of UNC0646 in the recently proposed allosteric binding site of the nAChR, the MB327-PAM-1 binding site, could be successfully unveiled.

Ex vivo studies revealed a beneficial effect of UNC0638 and UNC0642 on muscle force recovery of soman-poisoned rat diaphragms. In experiments with un-poisoned muscle tissues, a muscle force-reducing effect was uncovered for all three test compounds, which in the case of UNC0646 is likely to be so strong that it overcompensates the positive effect, that might originate from this compound on soman-poisoned muscle tissue, as well. This may explain the observed lack of such an effect for this compound. Though the maximum effect in muscle force recovery mediated by UNC0638 and UNC0642 was lower than that observed for MB327 and some analogs, this effect was reached at distinctly lower concentrations for UNC0638 and UNC0642 than that needed in the case of MB327. This might reflect the distinctly higher binding affinities of UNC0638 and UNC0642 for the MB327-PAM-1 binding site as compared to MB327 and analogs.

Overall, UNC0638, UNC0642, and UNC0646 have been found to address the MB327-PAM-1 binding site of the nAChR with high affinity, which renders quinazoline derivatives a promising class of compounds for further studies aiming at the development of drugs for the treatment of the nAChR-mediated pathological effects of organophosphorus poisoning.

CRediT authorship contribution statement

Worek Franz: Writing – review & editing. **Gohlke Holger:** Writing – review & editing, Supervision, Software, Conceptualization. **Steinritz Dirk:** Writing – review & editing. **Kaiser Jesko:** Writing – original draft, Methodology, Investigation. **Gertzen Christoph G.W.:** Writing – review & editing, Supervision. **Seeger Thomas:** Writing – original draft, Methodology, Investigation. **Niessen Karin V.:** Writing – review & editing, Investigation. **Paintner Franz F.:** Writing – review & editing, Supervision, Funding acquisition, Conceptualization. **Wanner Klaus T.:** Writing – review & editing, Supervision, Funding acquisition, Data curation, Conceptualization. **Nitsche Valentin:** Writing – original draft, Methodology, Investigation. **Höfner Georg:** Writing – review & editing, Methodology.

Declaration of Competing Interest

Authors declare that they have no known competing financial interests or personal relationships that could have appeared to influence the work reported in this paper.

Data Availability

Data will be made available on request.

Acknowledgments

This work was supported by the German Ministry of Defence (E/U2AD/KA019/IF558). We are grateful for computational support and infrastructure provided by the "Zentrum für Informations- und Medientechnologie" (ZIM) at the Heinrich Heine University Düsseldorf and the computing time provided by the John von Neumann Institute for Computing (NIC) to HG on the supercomputer JUWELS at Jülich Supercomputing Center (JSC) (user IDs: HKF7, VSK33, nAChR).

Appendix A. Supporting information

Supplementary data associated with this article can be found in the online version at doi:10.1016/j.toxlet.2024.01.003.

References

Ackermann, T.M., Bhokare, K., Höfner, G., Wanner, K.T., 2019. MS Binding Assays for GlyT1 based on Org24598 as nonlabelled reporter ligand. Neuropharmacology 161, 107561.

Ackermann, T.M., Allmendinger, L., Höfner, G., Wanner, K.T., 2021. MS Binding Assays for glycine transporter 2 (GlyT2) employing Org25543 as reporter ligand. ChemMedChem 16, 199–215.

Bayly, C.I., Cieplak, P., Cornell, W., Kollman, P.A., 1993. A well-behaved electrostatic potential based method using charge restraints for deriving atomic charges: the RESP model. J. Phys. Chem. 97, 10269–10280.

Buckley, N.A., Roberts, D., Eddleston, M., 2004. Overcoming apathy in research on organophosphate poisoning. BMJ 329, 1231–1233.

Case, D.A., Cheatham 3rd, T.E., Darden, T., Gohlke, H., Luo, R., Merz Jr., K.M., Onufriev, A., Simmerling, C., Wang, B., Woods, R.J., 2005. The Amber biomolecular simulation programs. J. Comput. Chem. 26, 1668–1688.

Case, D.A., H.M, A., Belfon, K., Ben-Shalom, I.Y., Berryman, J.T., Brozell, S.R., Cerutti, D. S., Cheatham 3rd, T.E., Cisneros, G.A., Cruzeiro, V.W.D., Darden, T.A., Duke, R.E., Giambasu, G., Gilson, M.K., Gohlke, H., Goetz, A.W., Harris, R., Izadi, S., Izmailov, S. A., Kasavajhala, K., Kaymak, M.C., King, E., Kovalenko, A., Kurtzmann, T., Lee, T.S., Le Grand, S., Li, P., Lin, C., Liu, J., Luchko, T., Luo, R., Machado, M., Man, V., Manathunga, M., Merz, K.M., Miao, Y., Mikhailovskii, O., Monard, G., Nguyen, H., O'Hearn, K.A., Onufriev, A., Pan, F., Pantano, S., Qi, R., Rahnamoun, A., Roe, D.R., Roitberg, A., Sagui, E., Schott-Verdugo, S., Shajan, A., Shen, J., Simmerling, C.L., Skrynnikov, N.R., Smith, J., Swails, J., Walker, R.C., Wang, J., Wang, J., Wei, H., Wolf, R.M., Wu, X., Xiong, Y., Xue, Y., York, D.M., Zhao, S., Kollmann, P.A., 2022. Amber 2022. vol. Amber 2022. University of California, San Francisco.

Case, D.A., Aktulga, H.M., Belfon, K., Cerutti, D.S., Cisneros, G.A., Cruzeiro, V.W.D., Forouzesh, N., Giese, T.J., Gotz, A.W., Gohlke, H., Izadi, S., Kasavajhala, K., Kaymak, M.C., King, E., Kurtzman, T., Lee, T.S., Li, P., Liu, J., Luchko, T., Luo, R., Manathunga, M., Machado, M.R., Nguyen, H.M., O'Hearn, K.A., Onufriev, A.V., Pan, F., Pantano, S., Qi, R., Rahnamoun, A., Risheh, A., Schott-Verdugo, S., Shajan, A., Swails, J., Wang, J., Wei, H., Wu, X., Wu, Y., Zhang, S., Zhao, S., Zhu, Q., Cheatham 3rd, T.E., Roe, D.R., Roitberg, A., Simmerling, C., York, D.M., Nagan, M. C., Merz Jr., K.M., 2023. AmberTools. J. Chem. Inf. Model 63, 6183–6191.

Chemical Computing Group, U., 2020. Molecular Operating Environment (MOE). vol. 2020.09, 1010 Sehrbooke St. West, Suite #910, Montreal, QC, Canada, H3A, 2R7.

Chemical Computing Group, U., 2023. Molecular Operating Environment (MOE). vol. 2022.02, 1010 Sehrbooke St. West, Suite #910, Montreal, QC, Canada, H3A, 2R7.

Costanzi, S., Machado, J.H., Mitchell, M., 2018. Nerve agents: what they are, how they work, how to counter them. ACS Chem. Neurosci. 9, 873–885.

Davenport, A.P., Russell, F.D., 1996. Radioligand Binding Assays: theory and practice. In: Mather, S.J. (Ed.), Current Directions in Radiopharmaceutical Research and Development. Springer Netherlands, Dordrecht, pp. 169–179.

Dickson, C.J., Walker, R.C., Gould, I.R., 2022. Lipid21: complex lipid membrane simulations with AMBER. J. Chem. Theory Comput. 18, 1726–1736.

Eddleston, M., Phillips, M.R., 2004. Self poisoning with pesticides. BMJ 328, 42–44.

Epstein, M., Bali, K., Piggot, T.J., Green, A.C., Timperley, C.M., Bird, M., Tattersall, J.E. H., Bermudez, I., Biggin, P.C., 2021. Molecular determinants of binding of non-oxime bispyridinium nerve agent antidote compounds to the adult muscle nAChR. Toxicol. Lett. 340, 114–122.

FDA, 2018. FDA (United States Food and Drug Administration), 2018. Guidance for industry: Bioanalytical method validation, ⟨https://www.fda.gov/files/drugs/published/Bioanalytical-Method-Validation-Guidance-for-Industry.pdf⟩ from 04.04.2022.

Frisch, M.J., G.W.T, Schlegel, H.B., Scuseria, G.E., Robb, M.A., J.R.C, Scalmani, G., Barone, V., Petersson, G.A., H.N, Li, X., Caricato, M., Marenich, A.V., Bloino, J., B.G. J, Gomperts, R., Mennucci, B., Hratchian, H.P., Ortiz, J.V., A.F.I, Sonnenberg, J.L., Williams-Young, D., Ding, F., F.I, Egidi, F., Goings, J., Peng, B., Petrone, A., Henderson, T., D.R, Zakrzewski, V.G., Gao, J., Rega, N., Zheng, G., W.L, Hada, M., Ehara, M., Toyota, K., Fukuda, R., Hasegawa, J., M.I, Nakajima, T., Honda, Y., Kitao, O., Nakai, H., Vreven, T., K.T, Montgomery Jr., J.A., Peralta, J.E., Ogliaro, F., M.J.B, Heyd, J.J., Brothers, E.N., Kudin, K.N., Staroverov, V.N., T.A.K, Kobayashi, R., Normand, J., Raghavachari, K., A.P.R, Burant, J.C., Iyengar, S.S., Tomasi, J., M.C, Millam, J.M., Klene, M., Adamo, C., Cammi, R., Ochterski, J.W., R.L.M, Morokuma, K., Farkas, O., Foresman, J.B., a.D.J.F, 2016. Gaussian16. vol. Revision A.03. Gaussian Inc., Wallingford CT.

Greene, D.A., Qi, R., Nguyen, R., Qiu, T., Luo, R., 2019. Heterogeneous dielectric implicit membrane model for the calculation of MMPBSA binding free energies. J. Chem. Inf. Model. 59, 3041–3056.

Grimm, S.H., Höfner, G., Wanner, K.T., 2015. MS Binding Assays for the three monoamine transporters using the triple reuptake inhibitor (1R,3S)-indatraline as native marker. ChemMedChem 10, 1027–1039.
Hess, M., Höfner, G., Wanner, K.T., 2011. (S)- and (R)-fluoxetine as native markers in mass spectrometry (MS) Binding Assays addressing the serotonin transporter. ChemMedChem 6, 1900–1908.
Höfner, G., Wanner, K.T., 2015. MS Binding Assays. Anal. Biomol. Interact. Mass Spectrom. 165–198.
Holmstedt, B., 1959. Pharmacology of organophosphorus cholinesterase inhibitors. Pharmacol. Rev. 11, 567.
Hulme, E.C., Trevethick, M.A., 2010. Ligand Binding Assays at equilibrium: validation and interpretation. Br. J. Pharm. 161, 1219–1237.
John, H., van der Schans, M.J., Koller, M., Spruit, H.E.T., Worek, F., Thiermann, H., Noort, D., 2018. Fatal sarin poisoning in Syria 2013: forensic verification within an international laboratory network. Forensic Toxicol. 36, 61–71.
Kaiser, J., Gertzen, C.G.W., Bernauer, T., Höfner, G., Niessen, K.V., Seeger, T., Paintner, F.F., Wanner, K.T., Worek, F., Thiermann, H., Gohlke, H., 2023. A novel binding site in the nicotinic acetylcholine receptor for MB327 can explain its allosteric modulation relevant for organophosphorus-poisoning treatment. Toxicol. Lett. 373, 160–171.
Kassa, J., Timperley, C.M., Bird, M., Green, A.C., Tattersall, J.E.H., 2022. Influence of experimental end point on the therapeutic efficacy of essential and additional antidotes in organophosphorus nerve agent-intoxicated mice. Toxics 10.
Liu, F., Barsyte-Lovejoy, D., Allali-Hassani, A., He, Y., Herold, J.M., Chen, X., Yates, C.M., Frye, S.V., Brown, P.J., Huang, J., Vedadi, M., Arrowsmith, C.H., Jin, J., 2011. Optimization of cellular activity of G9a inhibitors 7-aminoalkoxy-quinazolines. J. Med Chem. 54, 6139–6150.
Liu, F., Barsyte-Lovejoy, D., Li, F., Xiong, Y., Korboukh, V., Huang, X.P., Allali-Hassani, A., Janzen, W.P., Roth, B.L., Frye, S.V., Arrowsmith, C.H., Brown, P.J., Vedadi, M., Jin, J., 2013. Discovery of an in vivo chemical probe of the lysine methyltransferases G9a and GLP. J. Med Chem. 56, 8931–8942.
, 2006McKinney,M., Raddatz, R., 2006. Practical aspects of radioligand binding. Curr ProtocPharmacol Chapter 1, Unit1 3.
Miller 3rd, B.R., McGee Jr., T.D., Swails, J.M., Homeyer, N., Gohlke, H., Roitberg, A.E., 2012. MMPBSA.py: an efficient program for end-state free energy calculations. J. Chem. Theory Comput. 8, 3314–3321.
Motulsky, H., Neubig, R., 2002. Analyzing radioligand binding data. Curr Protoc Neurosci Chapter 7, Unit 7 5.
Neiens, P., Höfner, G., Wanner, K.T., 2015. MS Binding Assays for D1 and D5 dopamine receptors. ChemMedChem 10, 1924–1931.
Neiens, P., De Simone, A., Höfner, G., Wanner, K.T., 2018. Simultaneous multiple ms Binding Assays for the dopamine, norepinephrine, and serotonin transporters. ChemMedChem 13, 453–463.
Newmark, J., 2004. Therapy for nerve agent poisoning. Arch. Neurol. 61, 649–652.
Niessen, K.V., Muschik, S., Langguth, F., Rappenglück, S., Seeger, T., Thiermann, H., Worek, F., 2016. Functional analysis of Torpedo californica nicotinic acetylcholine receptors in multiple activation states by SSM-based electrophysiology. Toxicol. Lett. 247, 1–10.
Niessen, K.V., Seeger, T., Rappenglück, S., Wein, T., Höfner, G., Wanner, K.T., Thiermann, H., Worek, F., 2018. In vitro pharmacological characterization of the bispyridinium non-oxime compound MB327 and its 2- and 3-regioisomers. Toxicol. Lett. 293, 190–197.
Papke, R.L., 2014. Merging old and new perspectives on nicotinic acetylcholine receptors. Biochem Pharm. 89, 1–11.
Rahman, M.M., Teng, J., Worrell, B.T., Noviello, C.M., Lee, M., Karlin, A., Stowell, M.H. B., Hibbs, R.E., 2020. Structure of the native muscle-type nicotinic receptor and inhibition by snake venom toxins. Neuron 106, 952–962 e955.
Rappenglück, S., Sichler, S., Höfner, G., Wein, T., Niessen, K.V., Seeger, T., Paintner, F.F., Worek, F., Thiermann, H., Wanner, K.T., 2018a. Synthesis of a series of non-symmetric bispyridinium and related compounds and their affinity characterization at the nicotinic acetylcholine receptor. ChemMedChem 13, 2653–2663.
Rappenglück, S., Sichler, S., Höfner, G., Wein, T., Niessen, K.V., Seeger, T., Paintner, F.F., Worek, F., Thiermann, H., Wanner, K.T., 2018b. Synthesis of a series of structurally diverse MB327 derivatives and their affinity characterization at the nicotinic acetylcholine receptor. ChemMedChem 13, 1806–1816.
Roe, D.R., Cheatham 3rd, T.E., 2013. PTRAJ and CPPTRAJ: software for processing and analysis of molecular dynamics trajectory data. J. Chem. Theory Comput. 9, 3084–3095.
Schott-Verdugo, S., Gohlke, H., 2019. PACKMOL-memgen: a simple-to-use, generalized workflow for membrane-protein-lipid-bilayer system building. J. Chem. Inf. Model 59, 2522–2528.
Schrödinger, 2021. Maestro. vol. 2022–3. Schrödinger, LLC, New York, NY.
Schrodinger, L.L.C., 2015. The PyMOL Molecular Graphics System, Version 1.8.
Seeger, T., Worek, F., Szinicz, L., Thiermann, H., 2007. Reevaluation of indirect field stimulation technique to demonstrate oxime effectiveness in OP-poisoning in muscles in vitro. Toxicology 233, 209–213.
Seeger, T., Eichhorn, M., Lindner, M., Niessen, K.V., Tattersall, J.E., Timperley, C.M., Bird, M., Green, A.C., Thiermann, H., Worek, F., 2012. Restoration of soman-blocked neuromuscular transmission in human and rat muscle by the bispyridinium non-oxime MB327 in vitro. Toxicology 294, 80–84.
Sheridan, R.D., 2005. Nicotinic antagonists in the treatment of nerve agent intoxication. J. R. Soc. Med. 98, 114–115.
Shih, T.M., Rowland, T.C., McDonough, J.H., 2007. Anticonvulsants for nerve agent-induced seizures: The influence of the therapeutic dose of atropine. J. Pharm. Exp. Ther. 320, 154–161.
Sichler, S., Höfner, G., Rappenglück, S., Wein, T., Niessen, K.V., Seeger, T., Worek, F., Thiermann, H., Paintner, F.F., Wanner, K.T., 2018. Development of MS Binding Assays targeting the binding site of MB327 at the nicotinic acetylcholine receptor. Toxicol. Lett. 293, 172–183.
Sichler, S., Höfner, G., Nitsche, V., Niessen, K.V., Seeger, T., Worek, F., Paintner, F.F., Wanner, K.T., 2024. Screening for New nAChR-Ligands at the MB327-Binding Site by Means of MS Binding Assays. Toxicol. Lett., submitted.
The UniProt, C., 2023. UniProt: the Universal Protein Knowledgebase in 2023. Nucleic Acids Res. 51, D523–D531.
Thiermann, H., Worek, F., 2022. Pro: Oximes should be used routinely in organophosphate poisoning. Br. J. Clin. Pharm. 88, 5064–5069.
Thiermann, H., Aurbek, N., Worek, F., 2016. CHAPTER 1 Treatment of Nerve Agent Poisoning. Chemical Warfare Toxicology: Volume 2: Management of Poisoning, vol. 2. The Royal Society of Chemistry, pp. 1–42.
Tian, C., Kasavajhala, K., Belfon, K.A.A., Raguette, L., Huang, H., Migues, A.N., Bickel, J., Wang, Y., Pincay, J., Wu, Q., Simmerling, C., 2020. ff19SB: amino-acid-specific protein backbone parameters trained against quantum mechanics energy surfaces in solution. J. Chem. Theory Comput. 16, 528–552.
Timperley, C.M., Bird, M., Green, C., Price, M.E., Chad, J.E., Turner, S.R., Tattersall, J.E. H., 2012. 1,1′-(Propane-1,3-diyl)bis(4-tert-butylpyridinium) di(methanesulfonate) protects guinea pigs from soman poisoning when used as part of a combined therapy. Med Chem. Commun. 3, 352–356.
Turner, S.R., Chad, J.E., Price, M., Timperley, C.M., Bird, M., Green, A.C., Tattersall, J.E., 2011. Protection against nerve agent poisoning by a noncompetitive nicotinic antagonist. Toxicol. Lett. 206, 105–111.
Vedadi, M., Barsyte-Lovejoy, D., Liu, F., Rival-Gervier, S., Allali-Hassani, A., Labrie, V., Wigle, T.J., Dimaggio, P.A., Wasney, G.A., Siarheyeva, A., Dong, A., Tempel, W., Wang, S.C., Chen, X., Chau, I., Mangano, T.J., Huang, X.P., Simpson, C.D., Pattenden, S.G., Norris, J.L., Kireev, D.B., Tripathy, A., Edwards, A., Roth, B.L., Janzen, W.P., Garcia, B.A., Petronis, A., Ellis, J., Brown, P.J., Frye, S.V., Arrowsmith, C.H., Jin, J., 2011. A chemical probe selectively inhibits G9a and GLP methyltransferase activity in cells. Nat. Chem. Biol. 7, 566–574.
Währa, M., Allmendinger, L., Höfner, G., Wanner, K.T., 2023. Benocyclidine (BTCP) as non-labelled reporter ligand for ms Binding Assays for the PCP Ion channel binding site of the desensitized torpedo nicotinic acetylcholine receptor (nAChR). ChemMedChem, e202300048.
Wang, J., Wolf, R.M., Caldwell, J.W., Kollman, P.A., Case, D.A., 2004. Development and testing of a general amber force field. J. Comput. Chem. 25, 1157–1174.
Wang, J., Wang, W., Kollman, P.A., Case, D.A., 2006. Automatic atom type and bond type perception in molecular mechanical calculations. J. Mol. Graph. Model. 25, 247–260.
Wanner, K.T., Höfner, G., Mannhold, R., Kubinyi, H., Folkers, G., 2007. Mass Spectrometry in Medicinal Chemistry: Applications in Drug Discovery. Wiley.
Waterhouse, A.M., Procter, J.B., Martin, D.M.A., Clamp, M., Barton, G.J., 2009. Jalview Version 2—a multiple sequence alignment editor and analysis workbench. Bioinformatics 25, 1189–1191.
Wein, T., Hofner, G., Rappengluck, S., Sichler, S., Niessen, K.V., Seeger, T., Worek, F., Thiermann, H., Wanner, K.T., 2018. Searching for putative binding sites of the bispyridinium compound MB327 in the nicotinic acetylcholine receptor. Toxicol. Lett. 293, 184–189.
Worek, F., Szinicz, L., Eyer, P., Thiermann, H., 2005. Evaluation of oxime efficacy in nerve agent poisoning: development of a kinetic-based dynamic model. Toxicol. Appl. Pharm. 209, 193–202.

Supporting Information

Figure S1. Product ion spectra of UNC0638 (a), UNC0642 (b), and UNC0646 (c).

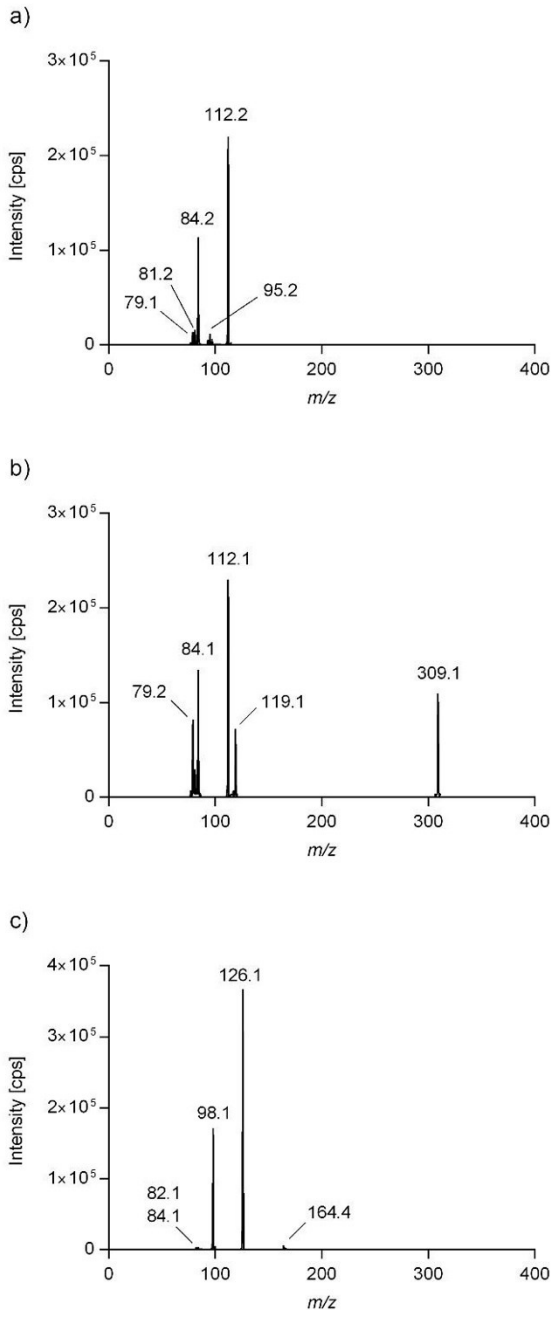

Figure S2. Representative LC-ESI-MS/MS-MRM chromatogram of UNC0646 (*m/z* 622.5/126.1, 10 nM in acetonitrile) recorded at an API3200, using the following chromatographic parameters. Stationary phase: YMC-Triart Diol-HILIC (50 mm x 2.0 mm, 3 µm). Mobile Phase: 65:35 (*v/v*) acetonitrile and ammonium formate buffer (20 mM, pH 3.0), 20 °C. Flow rate: 600 µL/min. Injection volume: 10 µL.

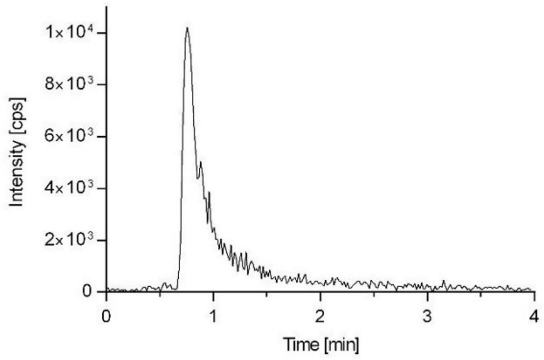

Table S1. Validation results of the LC-ESI-MS/MS method for the quantification of UNC0642

Sample (n)	Intra-Series									Inter-Series		
	Series 1			Series 2			Series 3					
	M	A	P	M	A	P	M	A	P	M	A	P
50 pM Cal (3)	0.0502	100	11.4	0.0514	103	11.1	0.0507	101	9.51	0.0508	102	9.31
150 pM Cal (3)	0.148	98.7	0.676	0.141	93.8	7.67	0.144	96.0	5.24	0.144	96.1	5.08
400 pM Cal (3)	0.399	99.7	4.40	0.375	93.8	3.53	0.386	96.4	4.31	0.386	96.6	4.45
1.2 nM Cal (3)	1.22	102	2.96	1.23	102	0.471	1.28	106	0.452	1.24	103	2.62
3.5 nM Cal (3)	3.41	97.3	4.78	3.54	101	5.67	3.33	95.2	1.25	3.43	97.9	4.65
10 nM Cal (3)	11.1	111	2.38	10.9	109	1.92	11.2	112	3.73	11.0	110	2.72
30 nM Cal (3)	27.9	92.9	2.10	28.5	95.1	1.42	27.8	92.6	1.62	28.1	93.5	1.98
75 nM Cal (3)	73.6	98.1	1.13	77.1	103	1.40	74.7	100	2.70	75.1	100	2.63
Equation of the calibration curve [a]	y = 1.57 * x + 0.00292 (r = 0.9973)			y = 1.74 * x + 0.00217 (r = 0.9971)			y = 1.86 * x + 0.00182 (r = 0.9914)			-		
50 pM QC (6)	0.0471	94.2	5.45	0.0467	93.5	6.51	0.0502	100	5.15	0.0480	96.0	6.31
500 pM QC (6)	0.484	96.8	3.84	0.467	93.5	5.80	0.460	91.1	4.89	0.470	94.1	5.09
5 nM QC (6)	4.93	98.6	2.60	5.16	103	5.28	5.03	101	2.46	5.04	101	4.01
50 nM QC (6)	47.5	95.0	2.69	49.1	98.0	5.68	46.0	92.1	2.66	47.6	95.1	4.66

M = mean concentration [nM], **A** = accuracy [%], **P** = precision [%], [a] weighting factor: $1/x^2$

Figure S3. Representative LC-ESI-MS/MS-MRM chromatograms of UNC0642 (*m*/*z* 547.3/112.1) recorded as part of the validation process of the applied LC-ESI-MS/MS quantification method. Chromatographic conditions: stationary phase, YMC-Triart Diol-HILIC (50 mm x 2.0 mm, 3 µm); mobile phase, 80:20 (*v*/*v*) acetonitrile and ammonium formate buffer (20 mM, pH 3.0), 20 °C; flow rate: 800 µL/min; injection volume: 10 µL. (a) LLOQ of 50 pM, (b) Matrix blank.

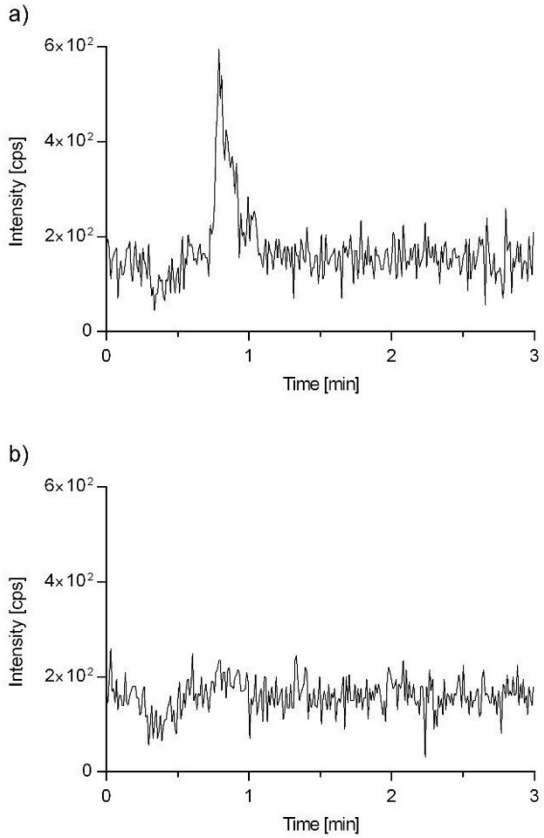

Figure S4. Conformations of UNC0646 in MB327-PAM-1 in each subunit after blind docking experiments. a) Extracellular view of the receptor. The two α-subunits are colored yellow and green, the δ-subunit pink, the β-subunit cyan, and the γ-subunit salmon. Binding mode of UNC0646 in between the b) γ- and α-subunit, c) α- and δ-subunit, d) δ- and β-subunit, e) β- and α-subunit, and f) α- and γ-subunit. The receptor is shown as ribbon, the surface as a grey contour, and the ligand as sticks.

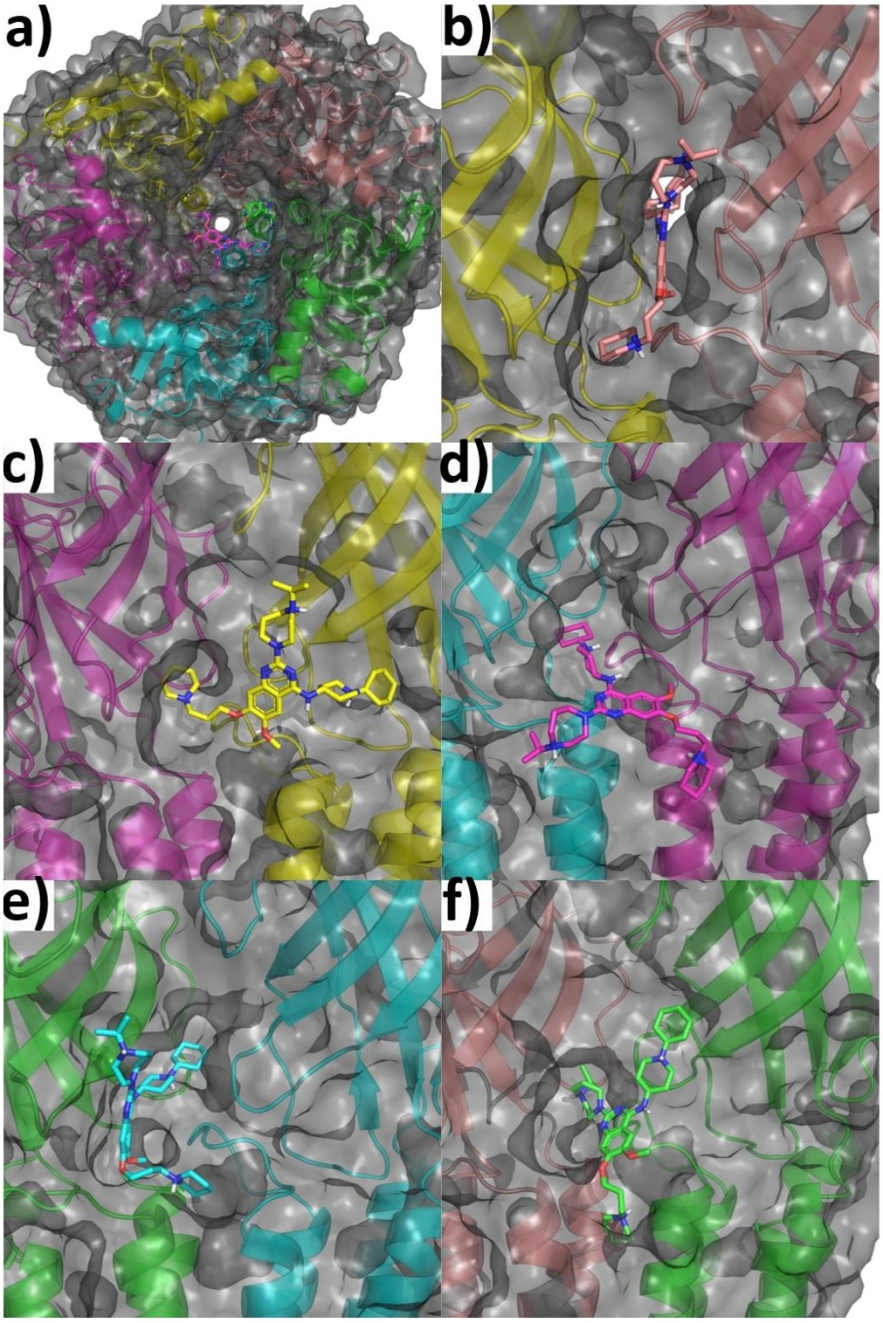

Figure S5. Docked orientation of UNC0646 between the γ- and α-(yellow) subunit. The γ-subunit has been omitted for clarity. The substituent in position 4 of the quinazoline ring is oriented in a) in a boat-twist conformation in the best-ranked pose and b) in a chair-chair conformation in the second-best-ranked conformation.

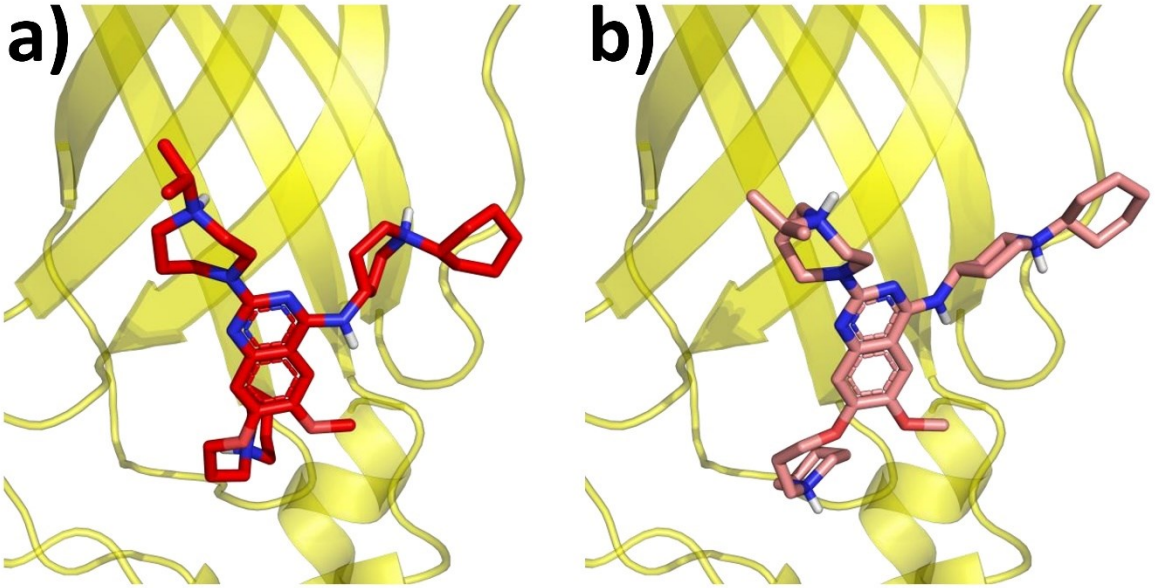

Figure S6. Docked binding mode of UNC0646 in between the β- and α-subunit. The ligand is shown in cyan and side chains similar to those in Figure 1 are shown in forest green.

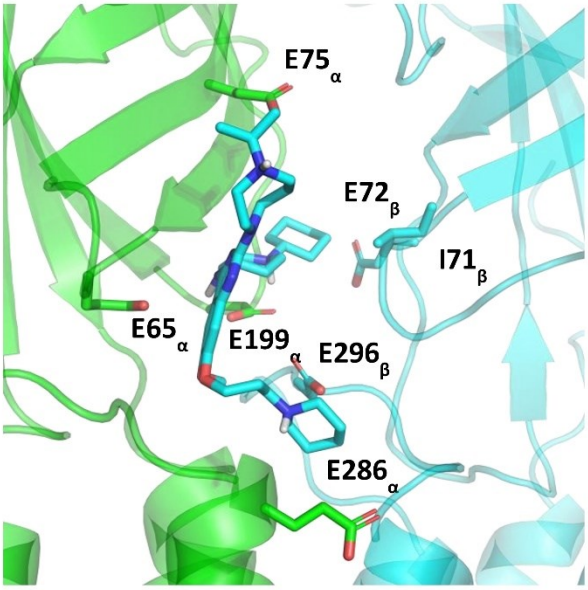

Figure S7. Backbone (C, CA, N) RMSD of nAChR during 12 replicas of 500 ns long MD simulations compared to the first frame of the production runs.

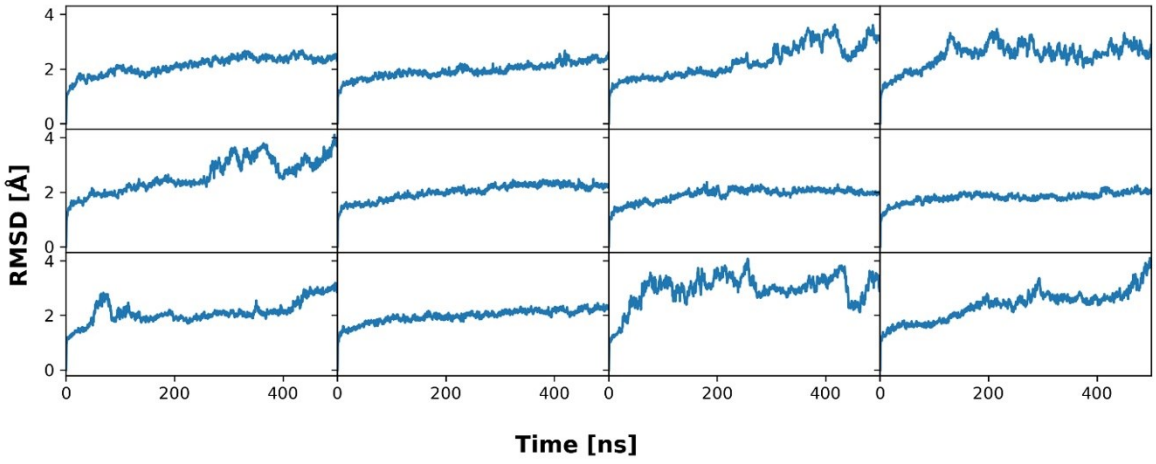

Figure S8. Electron density of water and membrane components over all 12 replicas of 500 ns long MD simulations. The electron density is plotted against the z-coordinate with the membrane centered at 0 Å for phosphatidylcholine (PC), oleic acid (OL), palmitoyl acid (PA), and water (WAT).

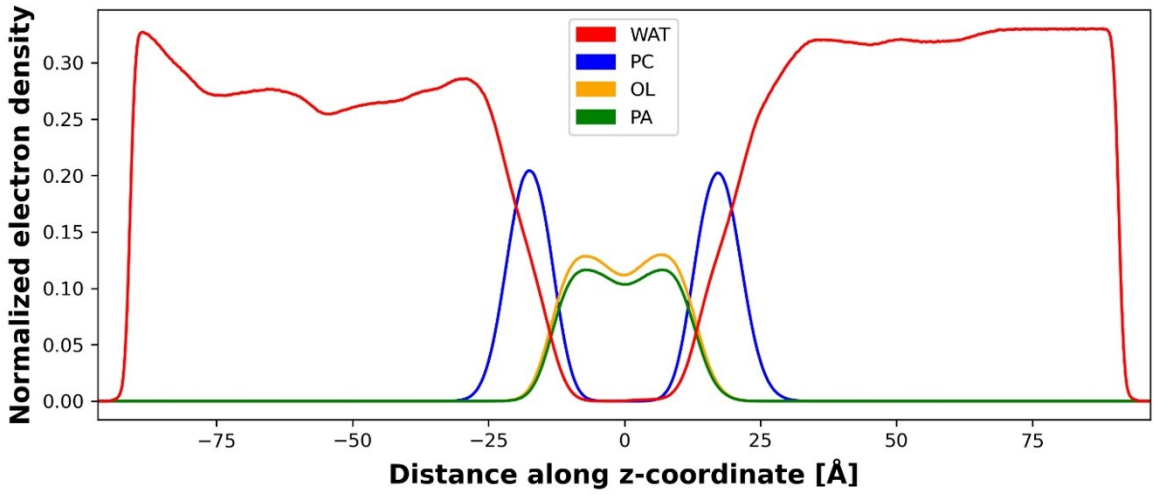

Figure S9. MMPBSA per-residue decomposition of the binding effective energy of UNC0646 in the subunits composing binding site A (γ- and α-subunit). Glutamates are shown in red.

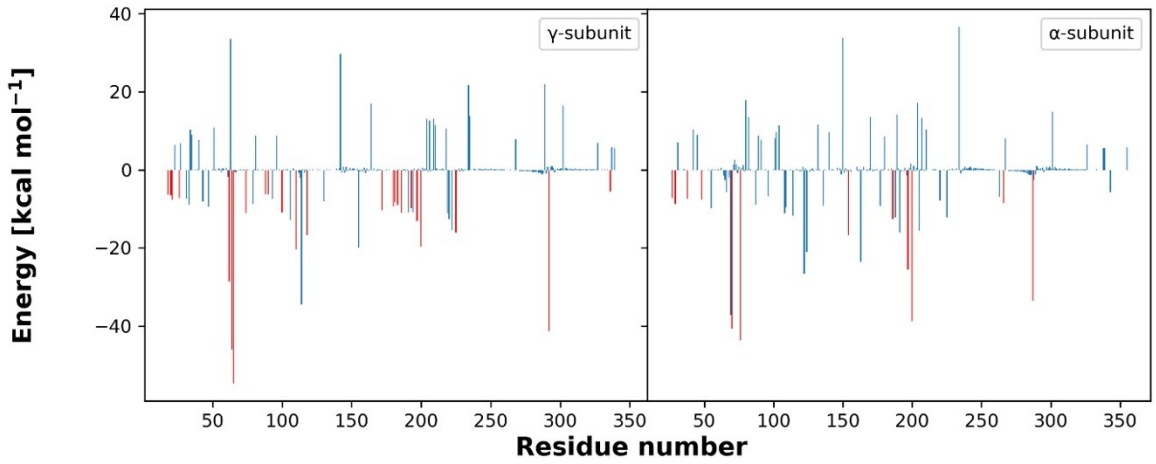

Figure S10. Binding mode of UNC0642 in MB327-PAM-1. The binding mode was obtained from a representative binding mode of UNC0646 in binding site A (between the γ- and α-subunit) and subsequent minimization of the ligand in the binding site.

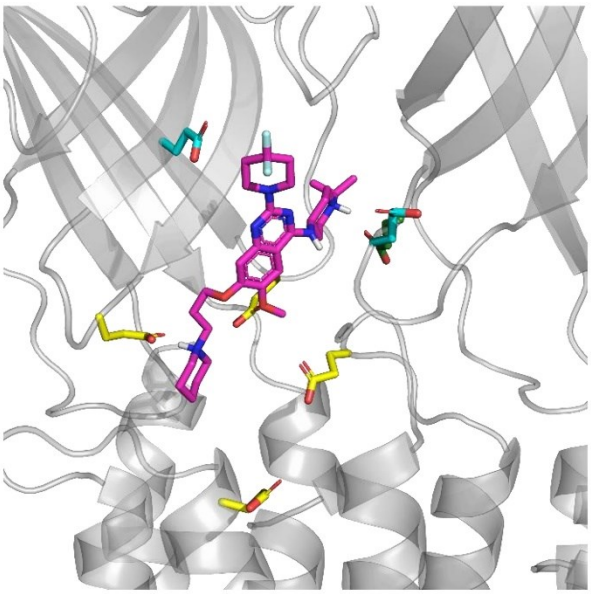

3.3 Dritte Publikation

„Identification of ligands binding to MB327-PAM-1, a binding pocket relevant for resensitization of nAChRs"

3.3.1 Zusammenfassung der Ergebnisse

Als „Resensitizer" des nikotinischen Acetylcholinrezeptors (nAChR) werden Substanzen bezeichnet, die in der Lage sind, den Rezeptor durch eine Interaktion mit einer allosterischen Bindungsstelle von einem nicht funktionalen, desensitisierten Zustand in einen funktionalen Zustand zu überführen. Substanzen mit dieser Eigenschaft sind ein vielversprechender Ansatz für eine verbesserte Therapie von Organophosphatvergiftungen, welche beispielsweise nach Exposition gegenüber Nervenkampfstoffen auftritt, da desensitisierte nAChRs zu einem Großteil der schwerwiegenden Vergiftungssymptome beitragen, welche bislang nicht adäquat behandelt werden können. Die bisher am intensivsten untersuchte Substanzklasse in diesem Zusammenhang stellt die der Bispyridiniumsalze mit MB327 als dem wohl prominentesten Vertreter MB327 dar. Von dieser Verbindung leitet sich auch die Bezeichnung „MB327-PAM-1" für die entsprechende allosterische Bindungsstelle am nAChR ab. Zuletzt wurde eine Gruppe strukturanaloger Verbindungen mit einem Chinazolin-Grundgerüst identifiziert, welche mit deutlich höheren Affinitäten an diese Bindungsstelle binden als die bisher untersuchten Bispyridiniumsalze. Eine dieser Substanzen, UNC0646, gilt derzeit als jene mit der bisher höchsten bekannten Affinität.

Im Rahmen dieser Publikation wurden nun diverse *in silico* Studien durchgeführt, um den Strukturraum rund um UNC0646 weiter zu untersuchen und somit die Struktur-Affinitäts-Beziehungen dieser Verbindungen besser zu verstehen. Die auf Basis der virtuellen Screenings identifizierten Hits, die entweder kommerziell verfügbar oder eigens synthetisiert worden waren, wurden mit Hilfe des kürzlich entwickelten UNC0642-MS-Bindungsassays hinsichtlich Ihrer Affinität zur MB327-PAM-1-Bindungsstelle charakterisiert. So konnte beispielsweise gezeigt werden, dass es für die Bindungsaffinität vorteilhaft ist, wenn sich ein flexibler Rest in 4-Position des Chinazolinringsystems befindet. Auf der Grundlage der neu gewonnenen Erkenntnisse konnte die Verbindung PTMD01-0050 entwickelt werden, deren Charakterisierung der Affinität im UNC0642-MS-Bindungsassay nahelegt, dass sie eine noch höhere Bindungsaffinität als UNC0646 aufweist.

Erste Berechnungen bezüglich Pharmakokinetik und Toxizität, die im Rahmen dieser Studie durchgeführt wurden, kommen zu dem Ergebnis, dass die entsprechenden Werte für UNC0646 nicht im Idealbereich liegen. Deshalb wurden, mit dem Ziel weitere Liganden für die MB327-PAM-1-Bindungsstelle mit gänzlich neuen molekularen Grundstrukturen zu identifizieren, weitere *in silico* Screenings durchgeführt. Hierdurch konnten vier neue Chemotypen identifiziert werden, welche potenziell die Basis für weitere Liganden darstellen. Für zwei dieser Chemotypen wurden bereits Verbindungen identifiziert, die UNC0642 (1 µM) im UNC0642-MS-Bindungsassay bei einer Testkonzentration von 10 µM signifikant von der Bindungsstelle verdrängen. Diese Verbindungen (Cycloguanil und PTMD99-0016C) besitzen trotz ihrer besonders geringen Molekülmasse eine nennenswerte Affinität zur MB327-PAM-1-Bindungsstelle. Vor allem Cycloguanil, ein mehrfach substituiertes Triazinderivat, erscheint besonders vielversprechend, da es in *ex vivo* Versuchen mit Soman-vergifteten Rattendiaphragmen ähnliche Ergebnisse wie MB327 zeigte, was erwarten lässt, dass es auch *in vivo* eine Muskelkraft-wiederherstellende Wirkung nach Somanvergiftung besitzt. Für die Therapie von Organophosphatvergiftungen dürfte diese Verbindung noch nicht geeignet sein, alleine schon wegen ihrer geringen Affinität, gleichwohl eröffnet sie zusammen mit den für die untersuchte Wirkstoffklasse neu identifizierten Chemotypen weitere Ansatzmöglichkeiten für die Entwicklung von „Resensitizern“.

3.3.2 Erklärung zum Eigenanteil

Alle *in silico* Studien wurden von Jesko Kaiser angefertigt, der bis auf einzelne ergänzende Beiträge das gesamte Manuskript verfasste. Die in dieser Publikation gezeigten MS-Bindungsstudien, mit denen die Affinitäten der in den *in silico* Screenings identifizierten Hits bestimmt wurden, lagen in meiner Verantwortung. Die entsprechenden Experimente wurden eigenständig von mir durchgeführt und die Ergebnisse von mir ausgewertet. Die beschriebenen Synthesen wurden von Tamara Bernauer und die *ex vivo* Experimente von Thomas Seeger durchgeführt und im Manuskript beschrieben. Das Konzept für das Manuskript wurde von Jesko Kaiser zusammen mit Holger Gohlke und Christoph G. W. Gertzen erstellt und das Manuskript zum entscheidenden Anteil von Holger Gohlke und Christoph G. W. Gertzen korrigiert. Zudem flossen Korrekturbeiträge von Georg Höfner, Karin V. Niessen, Franz F. Paintner, Klaus T. Wanner, Dirk Steinritz und Franz Worek in das Manuskript ein.

Identification of ligands binding to MB327-PAM-1, a binding pocket relevant for resensitization of nAChRs

Jesko Kaiser[1], Christoph G.W. Gertzen[1], Tamara Bernauer[2], Valentin Nitsche[2], Georg Höfner[2], Karin V. Niessen[3], Thomas Seeger[3], Franz F. Paintner[2], Klaus T. Wanner[2], Dirk Steinritz[3], Franz Worek[3], Holger Gohlke[1,4,*]

[1]Institute for Pharmaceutical and Medicinal Chemistry, Heinrich Heine University Düsseldorf, Düsseldorf, Germany

[2]Department of Pharmacy – Center for Drug Research, Ludwig-Maximilians-Universität München, München, Germany

[3]Bundeswehr Institute of Pharmacology and Toxicology, München, Germany

[4]Institute of Bio- and Geosciences (IBG-4: Bioinformatics), Forschungszentrum Jülich, Jülich, Germany

Running title: Identification of ligands binding to MB327-PAM-1

Keywords: nAChR; virtual screening; molecular dynamics simulations; MS Binding Assay

Author ORCID

Jesko Kaiser: 0000-0002-6429-0911

Christoph Gertzen: 0000-0002-9562-7708

Tamara Bernauer: 0000-0001-9570-1253

Valentin Nitsche: 0009-0000-3351-1227

Georg Höfner: 0000 0002 7957 4503

Karin V. Niessen: 0009-0008-6810-5294

Thomas Seeger: 0009-0007-5713-4367

Franz Paintner: 0000-0002-6795-586X

Klaus T. Wanner: 0000-0003-4399-1425

Dirk Steinritz: 0000-0002-2073-5683

Franz Worek: 0000-0003-3531-3616

Holger Gohlke: 0000-0001-8613-1447

*Corresponding Author:

Address: Universitätsstr. 1, 40225 Düsseldorf, Germany.

Phone: (+49) 211 81 13662

E-mail: gohlke@uni-duesseldorf.de

Abstract

Desensitization of nicotinic acetylcholine receptors (nAChRs) can be induced by overstimulation with acetylcholine (ACh) caused by an insufficient degradation of ACh after poisoning with organophosphorus compounds (OPCs). Currently, there is no generally applicable treatment for OPC poisoning that directly targets the desensitized nAChR. The bispyridinium compound MB327, an allosteric modulator of nAChR, has been shown to act as a resensitizer of nAChRs, indicating that drugs binding directly to nAChRs can have beneficial effects after OPC poisoning. However, MB327 also acts as an inhibitor of nAChRs at higher concentrations and can thus not be used for OPC poisoning treatment. Consequently, novel, more potent resensitizers are required. To successfully design novel ligands, the knowledge of the binding site is of utmost importance. Recently, we performed *in silico* studies to identify a new potential binding site of MB327, MB327-PAM-1, for which a more affine ligand, UNC0646, has been described. In this work, we performed ligand-based screening approaches to identify novel analogs of UNC0646 to help further understand the structure-affinity relationship of this compound class. Furthermore, we used structure-based screenings and identified compounds representing four new chemotypes binding to MB327-PAM-1. One of these compounds, cycloguanil, is the active metabolite of the antimalaria drug proguanil and shows a higher affinity towards MB327-PAM-1 than MB327. Furthermore, cycloguanil can reestablish the muscle force in soman-inhibited rat muscles. These results can act as a starting point to develop more potent resensitizers of nAChR and to close the gap in the treatment after OPC poisoning.

Introduction

Chemical warfare agents remain a serious threat to the military and civilian population. Organophosphorus compounds (OPCs) are one class of chemical warfare agents and block acetylcholinesterase (AChE) covalently [1]. This inhibits the decomposition of acetylcholine causing inflated acetylcholine (ACh) concentrations in the synaptic gap and, thereby, an overstimulation of muscarinic (mAChR) and nicotinic (nAChR) acetylcholine receptors. The overstimulation leads to structural rearrangements of nAChR, resulting in a non-functional, desensitized state [1-3].

While the overstimulation of mAChRs can be treated with atropine, only antidotes (oximes) with insufficient efficiency are available to treat the overstimulation of nAChRs indirectly by reactivating AChE. However, these oximes are ineffective against several OPCs, in particular, when aging leads to altered OPC-enzyme complexes that are less susceptible to reactivation [4, 5]. Thus, novel antidotes are required to treat OPC poisonings.

The compound MB327 can reestablish the muscle force of OPC-poisoned muscles by interacting directly with nAChRs from several species via an allosteric modulation [6-10]. Furthermore, administration of MB327 can prolong the survival rates of guinea pigs after tabun poisoning compared to the oxime HI-6, both in combination with physostigmine and hyoscine [11]. While these results are promising, MB327 cannot be used in the treatment of OPC poisoning so far because the therapeutic range is too narrow. Restoration of the muscle force in a rat diaphragm myography assay by MB327 increases up to concentrations of 300 µM but decreases at higher concentrations [9, 10]. Similarly, MB327 initially shows positive allosteric effects on nicotine binding, which decrease at micromolar concentrations. Likewise, MB327 increases the binding of the orthosteric ligand epibatidine up to micromolar concentrations but at higher concentrations decreases it [7, 9]. These results indicate that MB327 transmits inhibitory effects on nAChR via binding to the orthosteric binding site, which has recently been experimentally validated for related bispyridinium compounds [12]. Additionally, we observed the binding of MB327 to the orthosteric binding site using free ligand diffusion molecular dynamics (MD) simulations [13]. Hence, novel compounds that are more affine and more selective to the allosteric binding site than MB327 need to be identified. A first step in this direction was recently done by us by identifying UNC0646 as an allosteric nAChR ligand with a higher affinity than MB327 (Sichler et al., submitted to Tox. Lett. on the 1st of August 2023).

One way to identify novel binders and improve the affinity of known ligands is by using computer-aided drug design methods [14]. In ligand-based screening, one can search for analogs based on two- (topological) or three- (structural) dimensional ligand representations. In two-dimensional similarity screening, the importance of the three-dimensional conformation in the binding site is not taken into account. This can lead to unsatisfactory results, especially for highly flexible ligands. Thus, three-dimensional ligand screening approaches can be more effective in identifying binders that can fit into the binding site and have been used for identifying novel binders successfully in the past [15-20]. However, ligand-based screening approaches neglect explicit knowledge of the receptor structure. Additionally, ligand-based screening may only identify hits with more similar chemical scaffolds compared to the query. Thus, structure-based screening is a popular approach to identifying novel ligands for biological targets and can help to identify novel chemical scaffolds [21-28]. Recently, we identified a novel allosteric binding site of MB327 (MB327-PAM-1) and described a potential binding mode of UNC0646 in MB327-PAM-1 [13, 29], providing necessary input for three-dimensional ligand-based screening and structure-based screening.

Here, we used this information to perform all three described screening approaches to increase the chance of success and validated hits by a mass spectrometry-based affinity determination (MS Binding Assay). We identified novel substituents (**1a-k, 2b-e, 2g**) at the UNC0646 quinazoline scaffold that lead

to higher affinity and ligands with novel chemotypes [PTMD99-0001C (**3**), PTMD99-0016C (**4**), PTMD99-0026C (**5**), and cycloguanil (**6**)] binding to MB327-PAM-1.

Materials and Methods

Two-dimensional similarity search

The MolPort database was searched for compounds similar to UNC0646 using a two-dimensional search as implemented on the MolPort website (https://molport.com, accessed on October 21st, 2020). All compounds identified by the similarity search using default parameters were selected. From 22 compounds identified, twelve compounds were ordered for testing in this study.

Homology modeling of nAChR

The homology modeling of the human and *Torpedo* (recently reclassified as *Tetronarce*) nAChR was performed as previously described [13]. In short, homology models were generated using MODELLER version 9.19 [30] with the PDB structures 6PV8 [31], 5KXI [32], 2WN9 [33], and 6CNK [34] as templates. Water molecules and molecules from the crystallization buffer were removed. Amino acids not resolved in the templates were not included in the models; these amino acids are located within the intracellular loop, the *N*- and *C*-terminal region and, hence, not in the region that forms the MB327-PAM-1 pocket. The final models were selected based on the DOPE potential [35], TopScore [36], and visual inspection and subsequently protonated using PROPKA, v3.4.0 [37, 38] as implemented in Schrödinger Maestro, v2021-1 [39] at pH 7.4. The termini were capped with *N*-methyl amide (NME) and acetyl (ACE) groups, respectively.

Ligand-based screening with subsequent template-based docking

Based on our proposed binding mode of UNC0646 [29], we used the binding mode of PTMD01-0004 (**2a**) [Bernauer *et al.*, in preparation], a structurally reduced analog of UNC0646 that lacks the quinazoline substituent in 2-position, as input for ligand-based screening. We created a database from feasible organic reactions of building blocks of PTMD01-0004 (**2a**) with MolPort (https://molport.com) building blocks as implemented in the PINGUI webserver (https://scubidoo.pharmazie.uni-marburg.de/pingui/, accessed on May 19th, 2021) (SI Figure S1) [40], resulting in 69,223 in principle synthesizable compounds. We protonated the constituents of the database using OpenEye FixpKa, v2.1.1.0 [41] and filtered the database to only use compounds that are at least double positively charged as PTMD01-0004 (**2a**), resulting in 14,396 compounds and generated conformers using OpenEye OMEGA, v4.1.1.0 [42, 43] with default parameters except setting the *strictstereo* parameter to false. Initially, we used OpenEye vROCS, v3.4.1.0 [44, 45] (SI Figure S2) to filter the database by applying default parameters and the TanimotoCombo score. The best 1000 hits from the vROCS screening were further investigated using CCG MOE, v2020 [46] using a template-based docking with an upstream pharmacophore filter (SI Figure S3). The hits were analyzed based on visual inspection, and four compounds were selected for synthesizing.

Synthesis

All target compounds synthesized in the context of this study were cataloged with a PTMD number (Pharmacy and Toxicology Munich and Düsseldorf). All chemicals were used as purchased from commercial sources. Solvents used for purification were distilled before use. 5-Pyrrolidin-1-ylpentan-1-amine, which could only be purchased as the respective hydrochloride salt was converted into the free base before use [47]. Anhydrous reactions were carried out under an argon atmosphere in vacuum-dried glassware. For microwave reactions, a Discover SP microwave system by CEM GmbH was used. TLC-Analysis was performed on plates purchased from Merck (silica gel $60F_{254}$ on aluminum sheet). Flash chromatography was carried out using silica gel 60 (40-63 mm mesh size) as stationary phase, purchased from Merck. All synthesized compounds were dried under a high vacuum. ^{1}H and ^{13}C NMR spectra were recorded with a Bruker BioSpin Avance III HD 400 and 500 MHz at 25 °C. For data

processing, MestReNova (Version 14.1.0) from Mestrelab Research S.L. 2019, and for calibration, the solvent signal (CD_2Cl_2, CD_3OD or DMSO-d_6) was used. The purity of the test compounds was ≥ 95%, determined by means of quantitative NMR using TraceCERT® ethyl 4-(dimethylamino)benzoate from Merck as an internal calibrant [48, 49]. High-resolution mass spectra were recorded on a Finnigan MAT 95 (EI) or a Finnigan LTQ FT (ESI). Melting points were determined with a Büchi 510 melting point instrument and are uncorrected. For IR spectroscopy, an FT-IR Spectrometer 1600 from PerkinElmer was used. The analytical data of the synthesized compounds described below, obtained using the described methods, can be found in the Supporting Information.

Synthesis of 2,4-dichloro-6-methoxy-7-[3-(piperidin-1-yl)propoxy]quinazoline (**7**) recently reported by Vital *et al.* [50] and of *N*-(1-cyclohexylpiperidin-4-yl)-6-methoxy-7-[3-(piperidin-1-yl)propoxy]-quinazolin-4-amine (**2a**) was accomplished according to Bernauer *et al.* [Bernauer *et al.*, in preparation].

General Procedure: Synthesis of quinazolin-4-amines (GP): A solution of the respective 4-chloroquinazoline (**8**) or (**9**) (1.0 equiv), the corresponding amine (2.0 equiv - 10 equiv) and *N*,*N*-diisopropylethylamine (DIEA) (3.0 equiv) in *i*-PrOH (5 mL/mmol) was stirred at 160 °C for 15 to 60 min under microwave irradiation (200 W). The reaction mixture was concentrated in vacuo and the crude product was purified by flash chromatography [5% to 15% 3 M NH_3 (in MeOH) in CH_2Cl_2 or 10% MeOH in CH_2Cl_2 + 0.5% DMEA].

6-Methoxy-2-(piperidin-1-yl)-7-[3-(piperidin-1-yl)propoxy]-*N*-[5-(pyrrolidin-1-yl)pentyl]quinazolin-4-amine (1k): According to GP with **8** (126 mg, 0.300 mmol, 1.0 equiv), 5-(pyrrolidin-1-yl)pentan-1-amine (93.8 mg, 0.600 mmol, 2.0 equiv) and DIEA (160 µL, 119 mg, 0.900 mmol, 3.0 equiv) in *i*-PrOH (1.5 mL) for 15 min. **1k** (117 mg, 72% yield, 96% purity) was isolated by flash chromatography [7% to 15% 3 M NH_3 (in MeOH) in CH_2Cl_2] as a colorless solid.

***N*^{1}-Cyclohexyl-*N*^{2}-{6-methoxy-7-[3-(piperidin-1-yl)propoxy]quinazolin-4-yl}-*N*^{1}-methylethane-1,2-diamine (2b):** According to GP with **9** (101 mg, 0.300 mmol, 1.0 equiv), *N*^{1}-cyclohexyl-*N*^{1}-methylethane-1,2-diamine (104 µL, 93.8 mg, 0.600 mmol, 2.0 equiv) and DIEA (160 µL, 119 mg, 0.900 mmol, 3.0 equiv) in *i*-PrOH (1.5 mL) for 1 h. **2b** (127 mg, 93%) was isolated by flash chromatography [10% 3 M NH_3 (in MeOH) in CH_2Cl_2] as a yellow oil (96% purity).

6-Methoxy-*N*-[3-(4-methylpiperazin-1-yl)butyl]-7-[3-(piperidin-1-yl)propoxy]quinazolin-4-amine (2c): According to GP with **9** (101 mg, 0.300 mmol, 1.0 equiv), 3-(4-methylpiperazin-1-yl)butan-1-amine (114 µL, 108 mg, 0.600 mmol, 2.0 equiv) and DIEA (160 µL, 119 mg, 0.900 mmol, 3.0 equiv) in *i*-PrOH (1.5 mL) for 1 h. **2c** (110 mg, 78% yield, 97% purity) was isolated by flash chromatography [10% 3 M NH_3 (in MeOH) in CH_2Cl_2] as a pale yellow solid.

6-Methoxy-7-[3-(piperidin-1-yl)propoxy]-4-[4-(pyrrolidin-1-yl)piperidin-1-yl]quinazoline (2d): According to GP with **9** (101 mg, 0.300 mmol, 1.0 equiv), 4-(pyrrolidin-1-yl)piperidine (97.4 mg, 0.600 mmol, 2.0 equiv) and DIEA (160 µL, 119 mg, 0.900 mmol, 3.0 equiv) in *i*-PrOH (1.5 mL) for 1 h. **2d** (122 mg, 89%) was isolated by flash chromatography [10% 3 M NH_3 (in MeOH) in CH_2Cl_2] as a yellow oil (97% purity).

***N*-[1-(Azepan-1-yl)-2-methylpropan-2-yl]-6-methoxy-7-[3-(piperidin-1-yl)propoxy]quinazolin-4-amine (2e):** According to GP with **9** (134 mg, 0.400 mmol, 1.0 equiv), 1-(azepan-1-yl)-2-methylpropan-2-amine (717 mg, 4.00 mmol, 10 equiv) and DIEA (213 µL, 158 mg, 1.20 mmol, 3.0 equiv) in *i*-PrOH (2.0 mL) for 1 h. **2e** (46.4 mg, 25% yield, 97% purity) was isolated by flash chromatography [1. 10% 7 M NH_3 (in MeOH) in CH_2Cl_2, 2. 10% MeOH in CH_2Cl_2 + 0.5% DMEA] as a yellow oil. In addition, a further product fraction of lower purity was obtained (21% yield, 72% purity).

***N*-(1-Propan-2-ylpiperidin-4-yl)-6-methoxy-7-[3-(piperidin-1-yl)propoxy]quinazolin-4-amine (2f):** According to GP with **9** (33.6 mg, 0.100 mmol, 1.0 equiv), 1-propan-2-ylpiperidin-4-amine (31.6 µL, 28.4 mg, 0.200 mmol, 2.0 equiv) and DIEA (53.3 µL, 39.6 mg, 0.300 mmol, 3.0 equiv) in *i*-PrOH (0.5 mL) for 15 min. **2g** (41.2 mg, 93%) was isolated by flash chromatography [5% to 10% 3 M NH_3 (in MeOH) in CH_2Cl_2] as a colorless solid (96% purity).

***N*-(1-Propan-2-ylpiperidin-4-yl)-6-methoxy-7-[3-(piperidin-1-ylmethyl)pyrrolidin-1-yl]quinazolin-4-amine (2g):** A mixture of **10** (111 mg, 0.350 mmol, 1.0 equiv), 1-(pyrrolidin-3-ylmethyl)piperidine (310 mg, 1.75 mmol, 5.0 equiv) and potassium carbonate (53.2 mg, 0.385 mmol, 1.1 equiv) in *N*-methyl-2-pyrrolidone (NMP) (455 µL) was stirred at 135 °C for 20 h. The reaction mixture was concentrated and purified by flash chromatography [5% to 20% 3 M NH_3 (in MeOH) in CH_2Cl_2] to afford **2f** (147 mg, 90%) as a pale yellow solid (99% purity).

4-Chloro-6-methoxy-2-(piperidin-1-yl)-7-[3-(piperidin-1-yl)propoxy]quinazoline (8): A solution of **7** (370 mg, 1.00 mmol, 1.0 equiv) and 1-methylpiperidine (244 µL, 200 mg, 2.00 mmol, 2.0 equiv) in 1,4-dioxane (2.5 mL) was stirred at 150 °C for 1 h under microwave irradiation (300 W). **8** was isolated by flash chromatography (10% to 20% MeOH in CH_2Cl_2) as a yellow solid (327 mg, 78% yield, 95% purity).

4-Chloro-6-methoxy-7-[3-(piperidin-1-yl)propoxy]quinazoline (9) [51, 52]: To a slurry of **11** (22.2 mg, 0.100 mmol, 1.0 equiv), 3-piperidin-1-ylpropan-1-ol (19.9 µL, 18.8 mg, 0.125 mmol, 1.25 equiv), PPh_3 (34.4 mg, 0.130 mmol, 1.3 equiv) and dry THF (1.0 mL) was added di-*tert*-butyl azodicarboxylate (DBAD) (30.5 mg, 0.130 mmol, 1.3 equiv) in portions at 0 °C. The resulting solution was stirred overnight at rt and concentrated under reduced pressure. Purification by flash chromatography [5% 3 M NH_3 (in MeOH) in CH_2Cl_2] afforded **9** as a pale yellow solid (34.5 mg, > 99% yield, 96% purity).

7-Fluoro-*N*-(1-propan-2-ylpiperidin-4-yl)-6-methoxyquinazolin-4-amine (10): A mixture of **12** (20.2 mg, 0.100 mmol, 1.0 equiv), PyBOP (69.0 mg, 0.130 mmol, 1.5 equiv), diazabicycloundecene (DBU) (22.9 µL, 23.3 mg, 0.150 mmol, 1.5 equiv) and 1-propan-2-ylpiperidin-4-amine (23.7 µL, 21.3 mg, 0.150 mmol, 1.5 equiv) in acetonitrile (0.5 mL) was stirred at rt for 1 h. The mixture was concentrated in vacuo. **10** (29.3 mg, 92%) was isolated after flash chromatography [5% 3 M NH_3 (in MeOH) in CH_2Cl_2] as a colorless solid (97% purity).

Structure-based screening

The SMILES codes of in-stock compounds in the lead-like (3,434,621 compounds) and the double-protonated (129,606 compounds) subsets were downloaded from the ZINC20 database [53]. All compounds were protonated using OpenEye FixpKa, v2.1.1.0 , and conformers were generated using OpenEye OMEGA, v4.1.0.0 [42] with default parameters except setting the *strictstereo* parameter to false [42, 43]. The human and *Torpedo* homology models of nAChR were prepared for docking using OpenEye MakeReceptor, v4.0.0.0, and all compounds were docked using OpenEye FRED, v4.0.0.0 [54-56], writing out a maximum of one pose per compound. The best 1000 hits in each binding pocket were visually inspected, and 30 compounds were ordered for testing.

Commercially obtained compounds

The 42 commercially obtainable compounds were purchased from several suppliers with purities of at least 85%. A corresponding, detailed list can be found in the Supporting Information (SI Table S1). For affinity testing in MS Binding Assays, the compounds were applied as described in SI Table S1.

Molecular dynamics simulations of cycloguanil bound to nAChR

The receptor with the docked ligand was embedded in a membrane of 1-palmitoyl-2-oleoyl-*sn*-glycero-3-phosphocholine (POPC) lipids and solvated using Packmol-Memgen [57] in a rectangular box of TIP3P water [58]. KCl was added at a concentration of 150 mM and the system was neutralized using Cl^- ions. The edge of the box was set to be at least 12 Å away from receptor atoms. The AMBER22 package of molecular simulations software [59, 60] was used in combination with the *ff14SB* force field for the protein [61], the Lipid21 force field for the lipids [62], and the Joung and Cheatham parameters for monovalent ions [63]. Ligand charges were calculated according to the RESP procedure [64] with default parameters as implemented in antechamber [65] using electrostatic potentials generated by Gaussian16 [66] at the HF-6-31G* level of theory; ligand force field parameters were derived from the gaff2 force field. Since cycloguanil (**6**) should carry one positive charge (pK_a = 11.4 [67]) on the nitrogen atoms in the 1,6-dihydro-1,3,5-triazine-2,4-diamine ring system, *N*-3 was protonated.

Molecular dynamics (MD) simulations were performed as described earlier [13] using AMBER22. In short, a combination of steepest descent and conjugate gradient minimization was performed while lowering positional restraints with force constants from 25 kcal mol^{-1} $Å^{-2}$ to zero. Stepwise heating to 300 K and a subsequent reduction of harmonic restraints from 25 kcal mol^{-1} $Å^{-2}$ to zero followed.

Subsequently, 10 replicas of 1 µs length each of unbiased MD simulations were performed; for temperature control, the Langevin dynamics were applied with a collision frequency of 2 ps^{-1}, and the Berendsen barostat with semi-isotropic pressure adaption was used.

Based on the four replicas in which cycloguanil (**6**) remained within the binding site, we computed representative binding structures of cycloguanil (**6**) using the *k*-means clustering algorithm, as implemented in CPPTRAJ [68]. We then restarted simulations from the representative binding mode. Because the hydrogen bonds to $E62_\gamma$ and $E200_\gamma$ were highly conserved among all clusters except the largest one (containing 18.3% of all frames), we decided to restart simulations from the second largest cluster (containing 14.1% of all frames) (SI Figure S4). Therefore, we started directly with the production run with similar settings as for the docked structure. The first 10 ns of each replica were removed for further analysis.

All simulations were analyzed using CPPTRAJ [68].

Prediction of physicochemical and toxicological properties

Using OpenEye OMEGA, version 4.1.1.1 [43, 69], three-dimensional conformations of the compounds based on the SMILES code were generated using the default setting with the exception that only one conformation was generated for each compound. Pharmacokinetic properties and hERG inhibition were predicted using Schrödinger QikProp, version 2022-2 [70].

For PAINS filtering, the PAINS-remover webserver, v0.99 (https://www.cbligand.org/PAINS/) [71], was used. For the prediction of further toxicological properties, we used NEXUS Derek, v6.0.1 [72].

Image generation

Images of nAChR were created using UCSF Chimera [73].

Rat diaphragm myography

All procedures using animals followed animal care regulations and were approved by the responsible ethics committee. Preparation of rat diaphragm hemispheres and experimental protocol of myography were performed as described before [9]. In short, for all procedures (including wash-out steps,

preparation of soman and bispyridinium compound solutions) aerated Tyrode solution (125 mM NaCl, 24 mM $NaHCO_3$, 5.4 mM KCl, 1 mM $MgCl_2$, 1.8 mM $CaCl_2$, 10 mM glucose, 95 % O_2, 5% CO_2; pH 7.4; 25 ± 0.5 °C) was used. After the recording of control muscle force, the muscle preparations were incubated in the Tyrode solution, containing 3 µM soman. Following a 20 min wash-out period, the test compound cycloguanil (Merck KGaA) was added in ascending concentrations (1 µM, 10 µM, 30 µM, 70 µM, 100 µM, 150 µM, 200 µM, 300 µM, 500 µM, 1000 µM). In each preparation, four concentrations were measured to avoid the fatigue effects of muscle force generation. The incubation time was 20 min for each concentration. The electric field stimulation was performed with 10 µs pulse width and 0.2 A amplitudes. The titanic trains of 20 Hz, 50 Hz, 100 Hz were applied for 1 s and in 10 min intervals. Measurements on non-toxic muscle were carried out according to the same scheme. Instead of soman, pure Tyrode was incubated. Muscle force was calculated as a time-force integral (area under the curve, AUC) and constrained to values obtained for maximal force generation (muscle force in the presence of Tyrode solution without any additives; 100 %).

UNC0642 MS Binding Assays

Competitive MS Binding Assays were performed as described previously [29]. In short, the reporter ligand (UNC0642, 1 µM) and the corresponding test compound (varying concentrations) were incubated with aliquots of a membrane preparation from *Torpedo californica* electroplaque (approx. 75 µg protein per sample) in incubation buffer (120 mM NaCl, 5 mM KCl, 8.05 mM Na_2HPO_4 and 1.95 mM NaH_2PO_4, pH 7.4). Samples were generated in triplicates. After separating the protein-bound from non-bound reporter ligand by centrifugation, the protein-bound portion of UNC0642 was liberated and finally quantified via LC-ESI-MS/MS. Total binding of UNC0642 was normalized to 100% (i.e. reporter ligand binding in the absence of test compound) and 0% (i.e. non-specific reporter ligand binding, determined by the presence of 100 µM UNC0646 instead of test compound). Applying the non-linear regression function "One site – fit Ki" yielded competition curves, which then revealed IC_{50} and K_i values, respectively (Prism software v. 6.07, GraphPad software, La Jolla, CA, USA). Top and bottom levels were fixed at 100% and 0%, respectively, for that purpose. K_i values are given as mean pK_i values from three experiments ± SEM, if not stated otherwise. Next to the full-scale competition experiments, also competition experiments with only a single concentration of test compound (i.e. 10 µM) have been performed in this study. Compared to full-scale competition experiments, the obtained data was not analyzed via non-linear regression in this case and only normalized as described above to reveal the remaining reporter ligand binding as an indicator for the affinity of the respective test compound. If not stated otherwise, the remaining reporter ligand binding is given as the mean of triplicates ± SD.

Results and Discussion

Screening strategy

We used different strategies to identify novel binders of MB327-PAM-1. First, we performed ligand-based screening to identify analogs of UNC0646 using a two-dimensional similarity search as implemented on the MolPort website (https://molport.com) to identify compounds with high similarity to UNC0646 (Figure 1, blue scheme). Furthermore, we used PTMD01-0004 (**2a**), an analog with no substituent in the 2-position of the quinazoline ring, to perform ligand-based screening using its three-dimensional binding mode as a query using OpenEye vROCS [44, 45], followed by a pharmacophore-based docking of the best hits using CCG MOE [46] (Figure 1, yellow scheme). Second, to reveal new binders with novel chemical scaffolds, we performed structure-based virtual screenings (Figure 1, green scheme). There, we first docked a ZINC20 [53] lead-like library (3,434,621 compounds) into the human muscle-type nAChR using OpenEye FRED [54-56]. The lead-like library only includes compounds of a molecular weight between 250-350 g mol^{-1}. However, because a higher affinity of known ligands binding to MB327-PAM-1 generally correlates with a larger size of the ligands and most previously described binders feature at least two positive charges [29, 74, 75] (Sichler *et al.,* submitted to Tox. Lett. on the 1st of August 2023), we performed an additional screening using a ZINC20 library [53] of in-stock compounds bearing at least two positive charges (129,606 compounds). To exploit that the amino acids interacting with MB327 and UNC0646 are highly conserved among the human muscle-type and *Torpedo* nAChR [13, 29] but that the conformations of the sidechains nevertheless vary, we now used the *Torpedo* nAChR for docking to increase the search space. Also, the *Torpedo* nAChR is used in our MS Binding Assays.

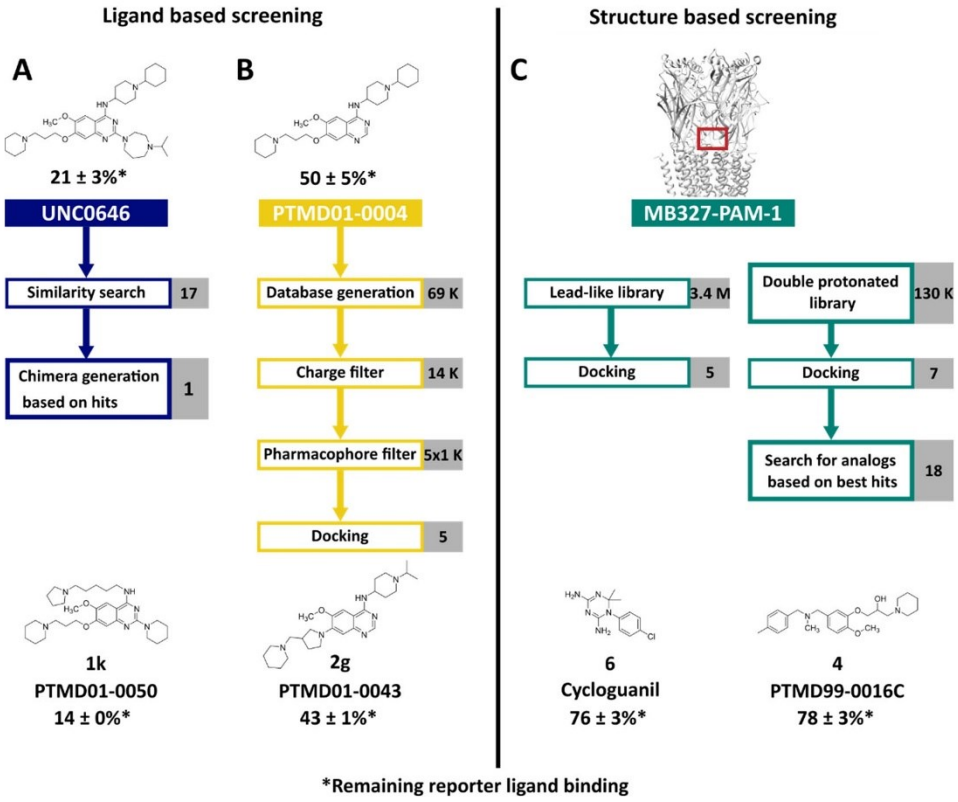

Figure 1: Screening strategies to identify novel binders of MB327-PAM-1. **A)** A two-dimensional similarity search using UNC0646 as a template was performed using MolPort (https://www.molport.com/). Based on the hits, one novel chimera compound was designed. **B)** Based on PTMD01-0004 (**2a**), a UNC0646-analog lacking the side chain in the 2-position, a database was generated based on feasible organic reactions (SI Figure S1). After applying a charge filter and a pharmacophore filter, docking experiments led to five novel analogs of UNC0646. **C)** Based on structure-based screening experiments in the human muscle type and *Torpedo* nAChR, 5 respectively 7 compounds with novel chemotypes were ordered for affinity characterization in MS Binding Assays. After the first experimental results, 18 additional compounds based on three chemical scaffolds were selected from the initial screening and ordered. This resulted in the identification of cycloguanil (**6**) and PTMD99-0016C (**4**). For each screening strategy, the best hits are shown. Percentage values indicate the remaining reporter ligand binding in the presence of test compounds (at 10 μM concentration) as compared to 100% reporter ligand binding in the absence of a competitor using the reporter ligand UNC0642 in MS Binding Assays (1 μM UNC0642) (mean ± SD, n = 3).

Two-dimensional similarity search yields affine UNC0646 analogs with small substituents in 4-position

Based on a two-dimensional screening of the MolPort library using UNC0646 as a template (Figure 1, blue scheme), 12 compounds were tested in our MS Binding Assay for MB327-PAM-1 [29]. Of these, 10 compounds displaced the reporter ligand UNC0642 from the binding site at 10 μM (**1a**-**1j**; remaining reporter ligand binding at most 90 ± 7%, n = 3; Table 1, SI Table S2). The best result was obtained for PTMD01-0019C (**1a**). In contrast to previously described UNC0646 analogs (Sichler et al., submitted to Tox. Lett. on the 1st of August 2023) [29], this is the only compound that does not have a side chain in 7-position with an aliphatic amino group, although mainly acidic amino acid side chains are available for ligand binding in MB327-PAM-1 [13, 29]. However, a study with related 4-amino-2-(*N,N*-diethylamino)quinazoline derivatives revealed that the two amino substituents impact the pK_a values of quinazolines resulting in pK_a values of up to 8.31 [76] compared to 3.51 of the unsubstituted quinazoline [77]. Thus, PTMD01-0019C (**1a**) can still be protonated under experimental and physiological conditions, similar to all previously described binders in MB327-PAM-1 [13, 29, 74, 75]. Furthermore, 4-aminopyridine has a pK_a of 9.17, indicating that even the residue in the 2-position of

PTMD01-0019C (**1a**) may be protonated [78]. These results are in line with suggestions that a positive charge is crucial for binding in MB327-PAM-1 but also indicate that the location of the positive charge is less important, which can be explained by the many acidic amino acids in MB327-PAM-1 [13, 29]. To verify the results obtained from the competition experiments by applying a single concentration, we performed full-scale competition studies for the best-binding compound PTMD01-0019C (**1a**), resulting in a pK_i of 5.19 ± 0.05 (SI Figure S5).

The second strongest reduction of reporter ligand binding was observed for UNC0379 (**1b**), a ligand with a substituent with increased flexibility at the 4-position compared to UNC0646. Along these lines, the results for ZT-12-037-01 (**1c**), C-021 (**1d**), MS012 (**1e**), PTMD01-0020C (**1f**), PTMD01-0021C (**1g**), PTMD01-0024C (**1h**), and PTMD01-0025C (**1i**) indicate that for affinity towards MB327-PAM-1, the positively charged amino side chain can be present at either position 2 or position 4 of the quinazoline building block. Furthermore, bunazosin (**1j**) has no basic side chains at the quinazoline ring but only the two electron donating groups in 2- and 4-positions, further indicating that the positive charge of the ligand might also be located within the heteroaromatic ring. This confirms the above observation that the location of the positive charge is not crucial for the binding of UNC0646 analogs. Based on these results, we synthesized PTMD01-0050 (**1k**), a chimera inspired by UNC0646, UNC0642, and UNC0379. The synthesis consisting of two steps started from **7** [Bernauer *et al.*, in preparation] [50] (Scheme 1). In analogy to a procedure described in the literature [79], **7** was reacted with *N*-methylpiperidine (2.0 equiv) at 150 °C under microwave irradiation for 1 h affording the quinazoline **8** with a piperidine ring in 2-position after column chromatography in good yield (78%). For the subsequent substitution of chloride in 4-position, **8** was stirred with 5-(pyrrolidin-1-yl)pentan-1-amine (2.0 equiv) in the presence of DIEA (3.0 equiv) under microwave irradiation at 160 °C for 15 min. The desired product PTMD01-0050 (**1k**) could be isolated in good yield (72%). Notably, this compound shows a higher reporter ligand displacement than UNC0646 (Table 1).

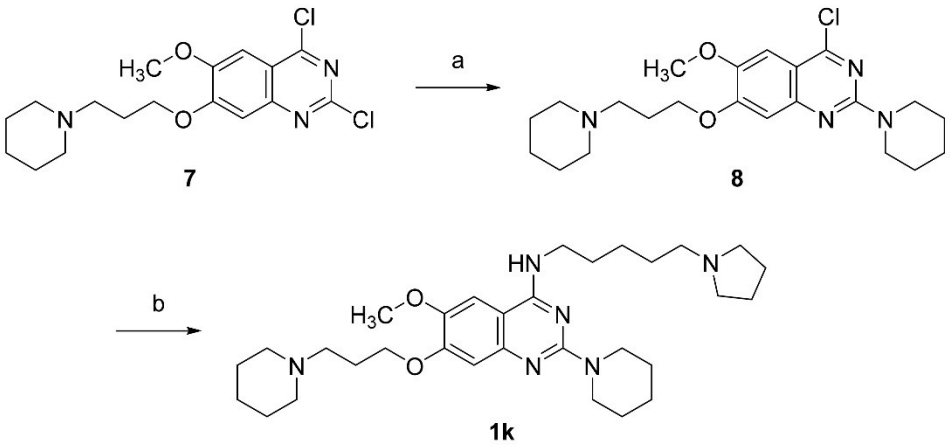

Scheme 1: Reagents and conditions: (a) 1-methylpiperidine (2.0 equiv), 1,4-dioxane, 150 °C (300 W), 1 h, 78%; (b) 5-(pyrrolidin-1-yl)pentan-1-amine (2.0 equiv), DIEA (3.0 equiv), *i*-PrOH, microwave: 200 W, 160 °C, 15 min, 72%.

Table 1: Selected analogs of UNC0646 identified by a two-dimensional similarity search and their affinities to MB327-PAM-1 in nAChR determined in MS Binding Assays.

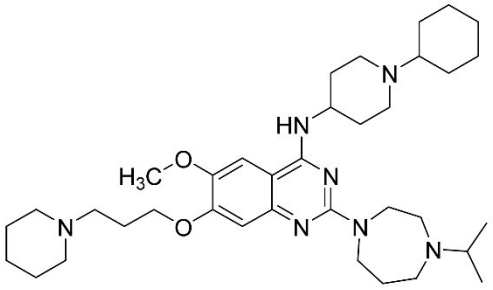

UNC0646

pK_i = 5.83 ± 0.05[a]

Remaining reporter ligand binding: 21 ± 3 %[b]

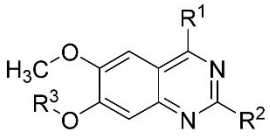

1a-k

Compound	Name / PTMD code	R^1	R^2	R^3	Remaining reporter ligand binding [%][b]
1a	PTMD01-0019C		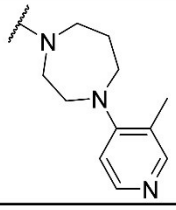		47 ± 3
1b	UNC0379	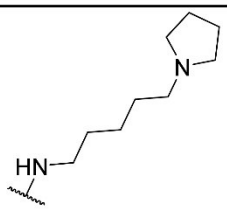	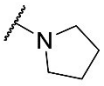		59 ± 4
1k	PTMD01-0050	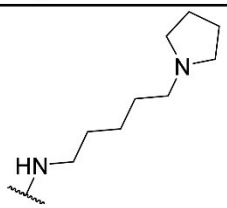	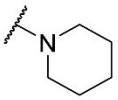	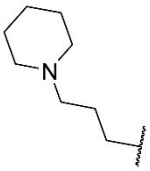	14 ± 0
1c	ZT-12-037-01	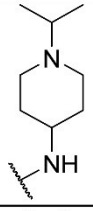	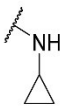		66 ± 5
1d	C-021	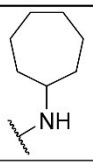	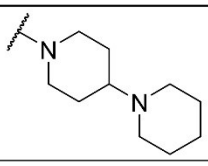		63 ± 2

1e	MS012	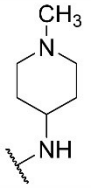	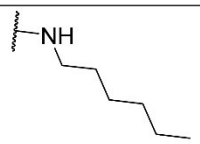		83 ± 6
1f	PTMD01-0020C		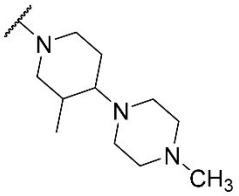		73 ± 7
1g	PTMD01-0021C		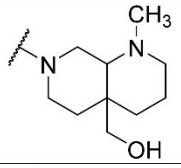		87 ± 2
1h	PTMD01-0024C		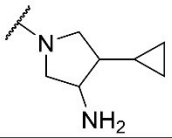		83 ± 4
1i	PTMD01-0025C		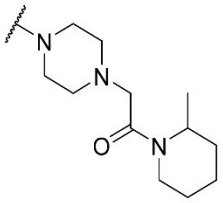		81 ± 5
1j	Bunazosin		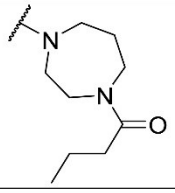		90 ± 7

[a] The pK_i value has been reported in ref. [29].

[b] Characterized by UNC0642 MS Binding Assays; Percentage of remaining reporter ligand binding in the presence of test compounds as compared to 100% reporter ligand binding in the absence of a competitor. Results are based on thirty measurements for UNC0646 and three measurements for all other compounds at a test compound concentration of 10 µM and a reporter ligand concentration of 1 µM. Mean and standard deviation are displayed.

Ligand-based screening using PTMD01-0004 (2a) as a template representing an analog of UNC0646 with a reduced molecular structure

While the two-dimensional similarity search based on UNC0646 yielded new, affine molecules binding to MB327-PAM-1, this approach did not consider the position and orientation of the ligand in MB327-PAM-1. Thus, we also performed a ligand-based screening in MB327-PAM-1 using PTMD01-0004 (**2a**) [Bernauer *et al.*, in preparation] as a template (Figure 1, yellow scheme). We started with this analog of UNC0646 because the substituent in the 2-position of UNC0646 shows minor interactions with the receptor in our proposed binding mode [29], and UNC0646 violates the molecular weight rule of Lipinski's "rule of five" [80], in contrast to PTMD01-0004 (**2a**). Furthermore, the absence of an electron-

donating group in the 2-position only has a minor impact on the affinity (Sichler *et al.*, submitted to Tox. Lett. on the 1st of August 2023).

We performed a two-step screening (see Materials and Methods) using a database of synthesizable compounds based on the building blocks of PTMD01-0004 (**2a**) (SI Figure S1). We selected five compounds that we synthesized (see below) and tested for affinity towards MB327-PAM-1 (**2b**-**2e**, **2g**, Table 2). The substituents chosen for position 4 did not increase the affinity in any compound compared to PTMD01-0004 (**2a**). Still, slight modifications in this substituent can influence reporter ligand displacement significantly.

As to the UNC0646 building block, our two-dimensional similarity search revealed that substituting it with flexible linkers in the 4-position can lead to highly affine compounds as seen for PTMD01-0050 (**1k**). The compound with increased flexibility between the quinazoline ring and the basic side chain nitrogen located within the cyclohexyl ring, PTMD01-0032 (**2b**), has a higher affinity than PTMD01-0053 (**2c**). However, the piperazine ring of PTMD01-0053 (**2c**) might also result in an alternative distance between the positive charge of the side chain and the quinazoline moiety, depending on the protonation site. Still, the relation between linker flexibility and affinity is also observed in PTMD01-0027 (**2d**), PTMD01-0030 (**2e**), and PTMD01-0032 (**2b**), where the distance between the quinazoline ring to the positively charged nitrogen is 3-4 heavy atoms long. However, to verify this trend, further compound testing will be required. Additionally, this trend does not always apply. PTMD01-0053 (**2c**) with a more flexible side chain than PTMD01-0030 (**2e**) has a lower affinity. Thus, the additional polar atom and the additional methyl substituent of the piperazine ring as well as the different distance between the positive charge in the side chain and the quinazoline moiety of PTMD01-0053 (**2c**) may also lead to a decrease in affinity.

In the 7-position, we identified in PTMD01-0043 (**2g**), an alternative substituent that leads to a higher reporter ligand displacement than if the same substituent as in UNC0646 is used in the in 7-position [PTMD01-0005 (**2f**)]. PTMD01-0043 (**2g**) otherwise bears the same side chains as PTMD01-0005 (**2f**) except in the 7-position of the quinazoline ring. As for the assessment of the two-dimensional similarity search, we verified our results by characterizing the binding affinity of the most affine compound according to the single point determinations [PTMD01-0043 (**2g**); remaining reporter ligand binding 43 ± 1%] in a full-scale MS Binding Assay yielding a pK_i of 5.46 ± 0.04 (SI Figure S6).

Table 2: Selected analogs of PTMD01-0004 (**2a**) identified by a ligand-based screening followed by template-based docking and their affinities to MB327-PAM-1 in nAChR determined in MS Binding Assays.

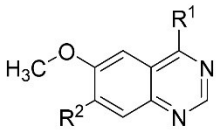

2a-g

Compound	PTMD code	R^1	R^2	Remaining reporter ligand binding [%][a]
2a	PTMD01-0004[b]	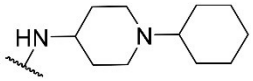	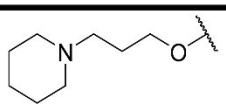	50 ± 5[c]
2b	PTMD01-0032	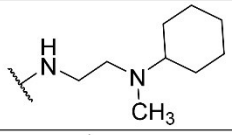	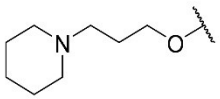	50 ± 7
2c	PTMD01-0053	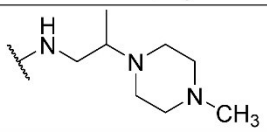	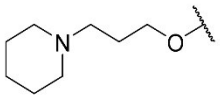	76 ± 7
2d	PTMD01-0027	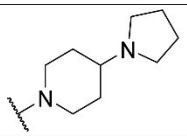	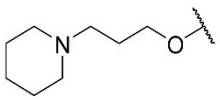	71 ± 3
2e	PTMD01-0030	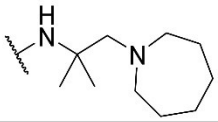	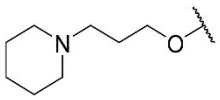	60 ± 3
2f	PTMD01-0005[b]	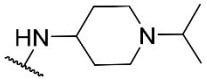	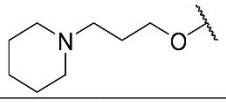	63 ± 4[d]
2g	PTMD01-0043	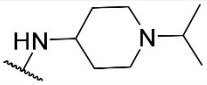	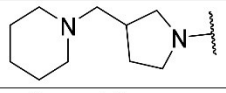	43 ± 1

[a] Characterized by UNC0642 MS Binding Assays; Percentage of remaining reporter ligand binding in the presence of test compounds as compared to 100% reporter ligand binding in the absence of a competitor. If not stated otherwise, results are based on three measurements at a test compound concentration of 10 µM and a reporter ligand concentration of 1 µM. Mean and standard deviation are displayed.

[b] PTMD01-0004 (**2a**) [Bernauer *et al.*, in preparation] and PTMD01-0005 (**2f**) were not identified in this study but are shown as reference structures to compare to PTMD01-0043 (**2g**).

[c,d] Results are based on twelve and six measurements, respectively, at a test compound concentration of 10 µM and a reporter ligand concentration of 1 µM. Mean and standard deviation are displayed.

Synthesis of compounds 2b-g:

Target compounds **2b**-**2f** were easily accessible by a two-step synthesis from commercially available building block **11** (Scheme 2). First, key intermediate **9** [51] was obtained in quantitative yield (> 99%) by reaction of quinazoline derivative **11** with 1.25 equiv 3-(piperidin-1-yl)propan-1-ol under *Mitsunobu* conditions (1.3 equiv PPh_3, 1.3 equiv DBAD, THF, rt, 20 h) following a literature procedure [81]. In the second step, the 4-amino substituents were introduced to afford the target compounds **2b**-**2f**. Nucleophilic displacement of the 4-chloro substituent was achieved according to a procedure reported in the literature [82] by heating **9** with the corresponding amines (2.0 equiv) in the presence of DIEA (3.0 equiv) to 160 °C under microwave irradiation. Thus, 4-aminoquinazolines **2b**-**2d** and **2f** were isolated in good to excellent yields (78-93%). However, the reaction with the sterically demanding amine 1-(azepan-1-yl)-2-methylpropan-2-amine to get **2e** was sluggish. Hence, a higher excess of the amine (10 equiv) was applied. This led to the target compound, which could be isolated in a yield of 25% only, which is partly due to the fact, that also a small amount of a side-product had formed being difficult to separate.

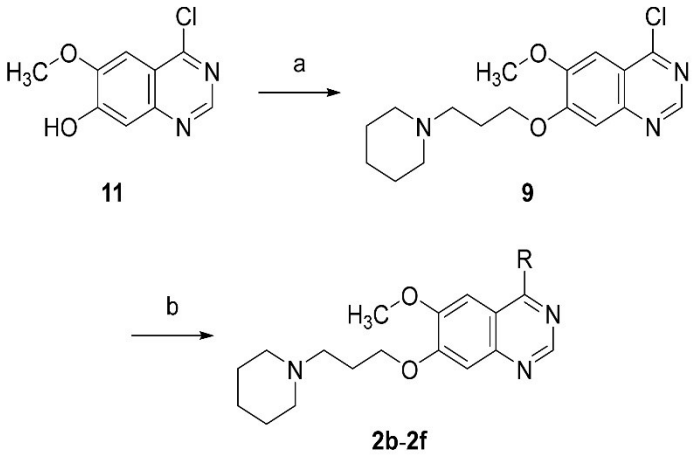

Scheme 2: Reagents and conditions: (a) 3-piperidin-1-ylpropan-1-ol (1.25 equiv), PPh_3 (1.3 equiv), DBAD (1.3 equiv), THF, rt, 20 h, > 99%; (b) amines (2.0-10 equiv), DIEA (3.0 equiv), *i*-PrOH, microwave: 200 W, 160 °C, 15 min-60 min, **2b**: 93%, **2c**: 78%, **2d**: 89%, **2e**: 25%, **2f**: 93%.

The 7-aminoquinazoline **2g** was synthesized in two steps starting from commercially available 7-fluoro substituted quinazoline-4(3*H*)-one **12** (Scheme 3). In the first step, the lactame **12** was converted to the 4-aminoquinazoline **10** by a phosphonium-mediated S_NAr reaction according to a procedure described in the literature [83]. Thus, **12** was reacted with 1.5 equiv of 1-propan-2-ylpiperidin-4-amine, PyBOP and DBU in acetonitrile at rt for 1 h, to obtain product **10** in excellent yield (92%). The subsequent substitution of the fluorine in 7-position of **10** to afford target compound **2g** was achieved by a reaction of **10** with a 5-fold excess of 1-(pyrrolidin-3-ylmethyl)piperidine in NMP at 135 °C in the presence of K_2CO_3 (1.1 equiv) according to a procedure reported in the literature [84]. In this way, the product **2g** could be isolated in 90% yield and high purity (99%).

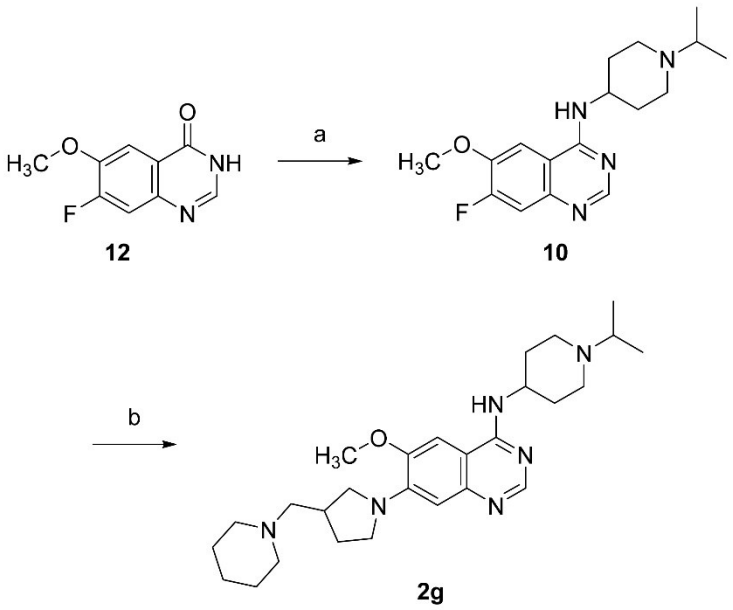

Scheme 3: Reagents and conditions: (a) 1-propan-2ylpiperidin-4-amine (1.5 equiv), PyBOP (1.5 equiv), DBU (1.5 equiv), acetonitrile, rt, 1 h, 92%; (b) 1-(pyrrolidin-3-ylmethyl)piperidine (5.0 equiv), K_2CO_3 (1.1 equiv), NMP, 135 °C, 20 h, 90%.

Structure-based screening reveals new chemotypes with a higher affinity than MB327

We first screened the lead-like library of ZINC20 [53] with 3,434,621 molecules using the homology model of the human muscle-type nAChR and OpenEye FRED [54-56] as docking engine with default parameters (Figure 1, green scheme). However, we know from previous work that larger molecules, such as UNC0646, usually bind to MB327-PAM-1 with a higher affinity than smaller ones, such as MB327. Furthermore, the two previously identified binders in MB327-PAM-1, UNC0646, and MB327, carry at least two positive charges. Thus, we decided to also screen a subset of the ZINC20 database [53] containing all doubly protonated in-stock compounds (129,606 compounds) by docking into the *Torpedo* nAChR (see also above).

We ordered 12 compounds based on visual inspection of the best 1000 hits in MB327-PAM-1 in each subunit in each of the screenings (2 x 5 x 1000 = 10,000 hits in total) (Figure 2, SI Table S3) (PTMD99-0001C – PTMD99-0015C). (In preliminary MS binding studies (the results of which had later on to be partly revised; for final results see SI Table S3), PTMD99-0006C (**13**), PTMD99-0010C (**14**), and PTMD99-0014C (**15**) showed the most promising results.) Thus, we decided to inspect the best 1000 hits in both screenings in each subunit again to find structurally similar chemotypes. We ordered three analogs of PTMD099-0006C (**13**), seven analogs of PTMD99-0010C (**14**), and eight analogs of PTMD99-0014C (**15**) (SI Table S4). In each group, at least one compound (at 10 µM concentration) displaced the reporter ligand UNC0642 (at 1 µM concentrations) from MB327-PAM-1 during single-concentration MS Binding Assay experiments indicating that these compounds show a higher affinity towards MB327-PAM-1 than MB327, which shows a remaining marker ligand binding of 102 ± 9% (n = 6) under identical conditions (1 µM reporter ligand, 10 µM test ligand) (Bernauer *et al.*, in preparation). In total, four new chemotypes, all containing at least one positive charge, were identified that displace UNC0642 from MB327-PAM-1 at concentrations of 10 µM (reporter ligand concentration of 1 µM) to any appreciable extent. However, for two of these compounds the remaining reporter ligand binding values are scarcely not significantly different from 100%, while the two other compounds differ significantly from 100% {$p < 0.05$ according to a two-sided one-sample t-test; p [PTMD99-0001C (**3**)] = 0.064, p [PTMD99-0016C (**4**)] = 0.005, p [PTMD99-0026C (**5**)] = 0.079, p [cycloguanil (**6**)] = 0.006}.

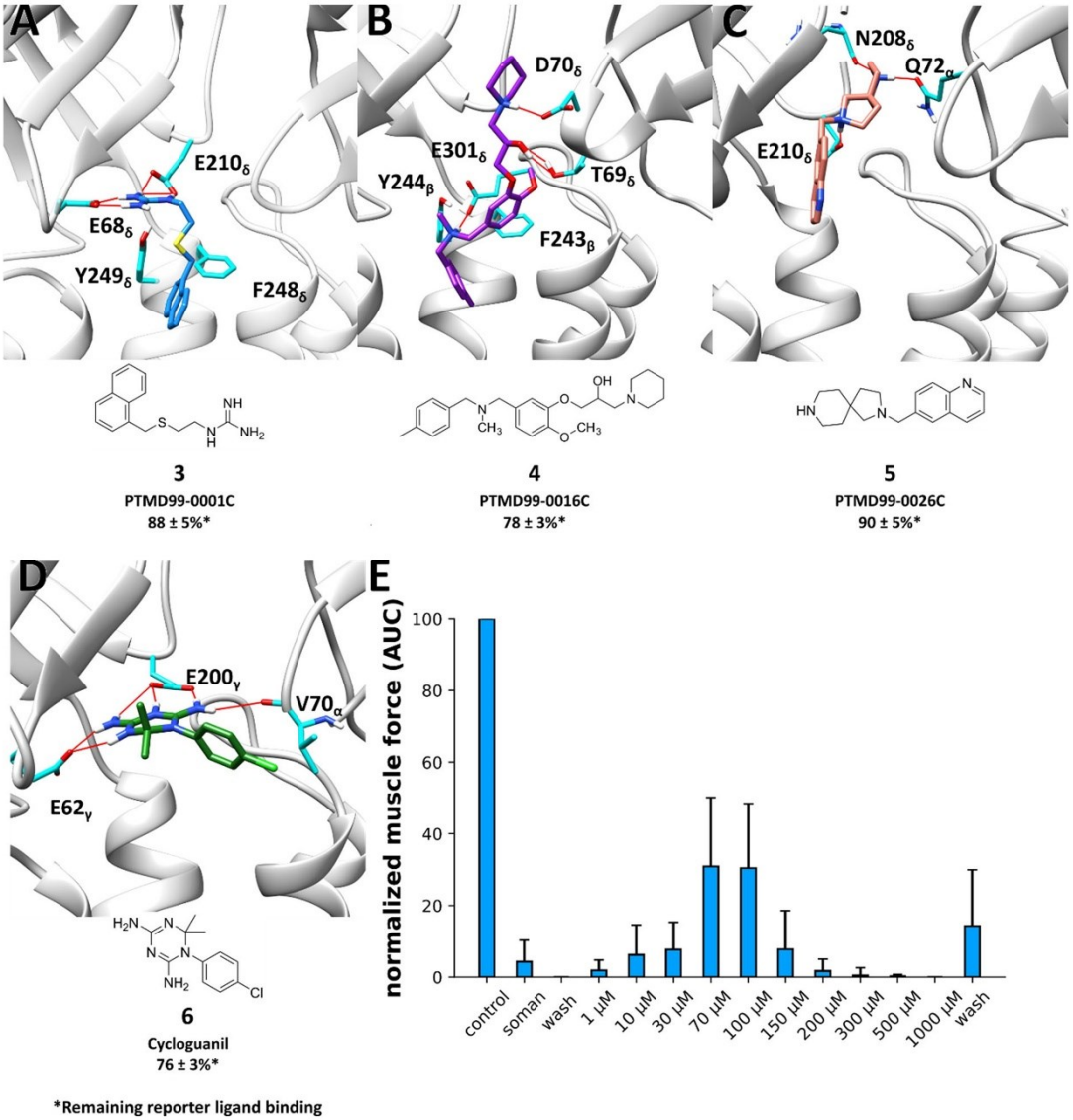

Figure 2: Docked binding mode and MS Binding Assay affinity data of selected hits from a structure-based screening in different subunits and species of nAChR. Docked binding mode of **(A)** PTMD99-0001C (**3**) in between the α- and δ-subunits of the human nAChR, **(B)** PTMD99-0016C (**4**) in between the δ- and β-subunits of the *Torpedo* nAChR, **(C)** PTMD99-0026C (**5**) in between the α- and δ-subunits of the *Torpedo* nAChR, and **(D)** cycloguanil (**6**) in between the α- and γ-subunits of *Torpedo* nAChR. Red lines indicate hydrogen bonds. Percentage values indicate the remaining reporter ligand binding in the presence of test compounds (at 10 µM concentration) as compared to 100% reporter ligand binding in the absence of a competitor using the reporter ligand UNC0642 in MS Binding Assays (1 µM UNC0642) (mean ± SD, *n* = 3). Compounds displaying chirality were tested as racemats. **(E)** Resoration of muscle force of soman-inhibited muscles after treatment with cycloguanil (**6**). Error bars indicate the standard deviation (*n* is between 5 and 27). Since the largest efficacies are observed at low stimulation frequencies [10], results are only shown for a stimulation frequency of 20 Hz (see SI Table S5 for all stimulation frequencies applied).

Of the analogs based on PTMD99-0006C (**13**), PTMD99-0016C (**4**) shows the highest affinity within this group and is the only compound able to displace UNC0642 to any appreciable extent during measurements with test compound concentrations of 10 µM and reporter ligand concentrations of 1 µM. Small changes in the 4-methylbenzyl group can have a high impact on affinity. For example, PTMD99-0020C (**16**) (SI Table S4), bearing a (3-methylpyridin-4-yl)methyl substituent instead of the 4-methylbenzyl group, does not show a displacement of the reporter ligand to any appreciable extent

anymore under identical experimental conditions. In fact, all compounds bearing a heteroaromatic ring instead of the 4-methylbenzyl group fail to displace UNC0642 to any appreciable extent under identical experimental conditions to a reasonable extent.

Based on the initial results for PTMD99-0010C (**14**), we identified PTMD99-0026C (**5**), able to displace the reporter ligand (concentration 1 µM) to any appreciable extent at 10 µM test compound concentration. However, compounds with an amide group in 3-position to the nitrogen at position 2 of the 2,8-diazaspiro[4.5]decane system do not displace the reporter ligand UNC0642 under similar experimental conditions to any appreciable extent (PTMD99-0010C (**14**), -0023C (**17**), -0024C (**18**), -0025C (**19**), -0028C (**20**) (SI Table S3, S4)). Furthermore, replacing the quinolinyl substituent by a 5-(*tert*-butyl)-pyrazol-3-yl substituent (PTMD99-0031C (**21**) (SI Table S4)) also abrogates the reporter ligand displacement indicating that hydrogen bond donors as substituents of the 2,8-diazaspiro[4.5]decane ring might be unfavorable.

Additionally, as the fourth novel chemotype binding to MB327-PAM-1, the 1,6-dihydro-1,3,5-triazine-2,4-diamine building block was identified. Most interesting, the compound showing the highest affinity, cycloguanil (**6**, 10 µM test compound concentration at 1 µM reporter ligand concentration, Figure 2D), is the active metabolite of the antimalarial drug proguanil. In competitive MS binding experiments, we observed a pK_i value for cycloguanil (**6**) of 3.64 ± 0.03 (SI Figure S7), significantly higher compared to MB327 [pK_i (MB327) = 3.40 ± 0.04 [29], $p < 0.01$, according to a two-sided *t*-test]. Cycloguanil (**6**) forms salt bridges both with $E62_\gamma$ and $E200_\gamma$ in the docked pose (Figure 2D). These two amino acids are highly conserved among different subunits of several species (Table 3), including the *Torpedo* nAChR, which is used in our MS Binding Assay, the rat muscle nAChR, which is used in our rat diaphragm assays, and in the human nAChR, in which the compounds need to exhibit an effect after OPC poisoning. Furthermore, these glutamates are crucial for the stabilization of the calcium ion in the α7 nAChR that can act as a positive allosteric modulator [85-87]. According to our screening results, we can, in general, see that larger substituents at both rings of cycloguanil (**6**) lead to a decrease in affinity (**22**-**28**, SI Table S4). Compounds based on the 1,3,5-triazin-2,4-diamin building block are overall much smaller than UNC0646 (M [UNC0646] = 621.93 g mol^{-1}; M [Cycloguanil (**6**)] = 251.72 g mol^{-1}), leading to compounds with an improved ligand efficiency.

Enough substance to conduct competition experiments with varying ligand concentrations and to perform rat diaphragm assays in order to investigate the restoration of muscle force after soman poisoning was only commercially available for cycloguanil (**6**). Treatment with cycloguanil (**6**) led to significant restoration of muscle force in rat diaphragm hemispheres after soman inhibition (Figure 2E, SI Table S5). The maximum restoration at stimulation frequencies of 20 Hz is comparable to the maximum restoration when using MB327 as a treatment option. However, while concentrations of 300 µM are necessary for the maximum effect of MB327 [26.29 ± 18.43% (mean ± SD; $n = 27$) restoration of muscle force, values taken from ref. [13]], cycloguanil (**6**) exerts a comparable effect at concentrations of 70 µM (30.87 ± 19.23%; $n = 5$). At a concentration of 100 µM, cycloguanil (**6**) leads to a significantly increased restoration of muscle force compared to MB327 [30.42 ± 18.04% vs. 17.77 ± 7.5%, values for MB327 taken from ref. [13], $p < 0.01$ according to a two-sided *t*-test ($n = 27$)]. Like MB327, cycloguanil (**6**) has a small therapeutic index, leading to muscle force inhibition at concentrations ≥ 300 µM (Figure 2E, SI Figure S8). Thus, cycloguanil (**6**) currently cannot be considered as a treatment option but as a novel lead structure for treating OPC poisoning.

To further investigate the binding mode of cycloguanil (**6**), we performed MD simulations starting from the docked conformation. In 6 out of 10 replicas over 1 µs simulation time each, the ligand left the binding site (SI Figure S9). In the replicas where cycloguanil (**6**) remained in the binding site, the binding mode shifted. Whereas the interaction with the two glutamates persisted, the aromatic system of

cycloguanil (**6**) moved towards the transmembrane region of nAChR in the direction of Y239$_\gamma$ (Figure 3A). This amino acid is located in a hydrophobic part of the binding site. Thus, we clustered the replica in which cycloguanil (**6**) remained in the binding site and performed additional 10 replicas of 1 µs long MD simulations starting from a representative structure. During the simulations, the membrane and receptor remained structurally virtually invariant (SI Figure S10, S11). Cycloguanil (**6**) continued to remain in the binding site in all replicas and showed highly conserved interactions with E62$_\gamma$ and E200$_\gamma$ (Figure 3B, C). Thus, we conclude that according to the MD-optimized binding mode, the interactions with the two glutamates persist and the hydrophobic interactions with amino acids close to Y239$_\gamma$ are important for ligand stabilization.

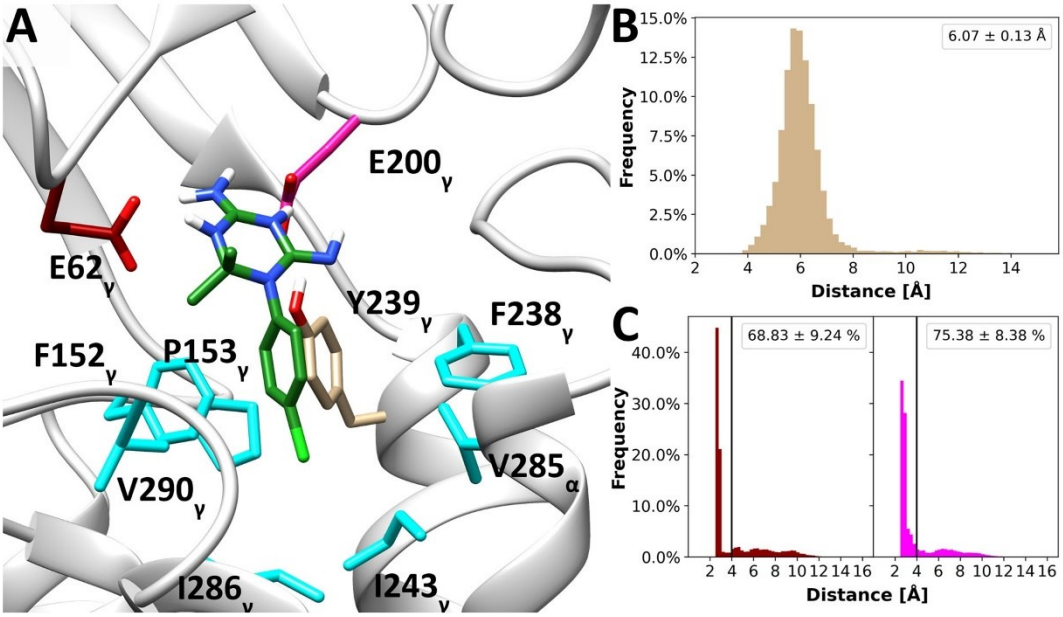

Figure 3: Binding mode of cycloguanil during MD simulations. **A)** Representative (according to a *k-means* clustering based on receptor and ligand atoms; the biggest cluster containing 48.2% of all frames is shown) binding mode of cycloguanil during 10 replicas of 1 µs long unbiased MD simulations starting from the docked conformation. **B)** Distance of the center of mass (COM) of the phenyl ring of cycloguanil to the phenyl ring of Y239$_\gamma$. The mean ± SEM distance is displayed as a legend. **C)** Distance of the nitrogens that can act as hydrogen bond donors of cycloguanil to the side chain oxygens of E62$_\gamma$ (dark red) and E200$_\gamma$ (pink). The frequency of contacts (distance < 4 Å; mean ± SEM) is displayed as a legend.

Table 3: Sequence conservation of E62$_\gamma$ and E200$_\gamma$ (green shadings) in the human muscle-type, *Torpedo*, and rat nAChR with respect to structurally homologous positions in the γ-subunit of the *Torpedo* nAChR.[a]

Human muscle type				*Torpedo*				Rat			
α	β	δ	ε	α	β	δ	γ	α	β	δ	ε
E	E	E	E	E	E	E	E62	E	E	E	E
E	*Q*	E	E	E	*Q*	E	E200	E	*Q*	E	E

[a] E62$_\gamma$ and E200$_\gamma$ are important for interactions with cycloguanil (**6**) in the docked binding mode and during MD simulations (Figure 3; see also text).

Prediction of pharmacokinetic and toxicological properties of best hits

UNC0646, the best hits of both ligand-based screenings [PTMD01-0050 (**1k**), PTMD01-0043 (**2g**)], and the best hit of each novel chemotype from the structure-based screening [PTMD99-0001C (**3**), PTMD99-0016C (**4**), PTMD99-0026C (**5**), and cycloguanil (**6**)] were initially probed in a pan interference compounds (PAINS) filter as implemented in the PAINS-remover webserver [71]; all compounds passed this filter, suggesting that they are less likely to react nonspecifically with biological targets. We further predicted the pharmacokinetic and toxicological properties using Schrödinger QikProp [70] and NEXUS Derek [72] (Table 4, Table 5). By far the most predictions for UNC0646 fall outside a 95% range for values of known drugs, questioning the drug-like properties of this compound. Along these lines, UNC0646 shows the worst Caco-2 cell permeability prediction as a model for gut-blood barrier permeation among all tested compounds and also violates two rules of Lipinski's rule of five and one rule of Jorgensen's rule of three, which are used as indicators for oral bioavailability. By contrast, all newly identified chemotypes show no violations of Lipinski's rule of five, and only PTMD99-0026C (**5**) violates one rule of Jorgensen's rule of three. Note, however, that the violated pharmacokinetic descriptors describe oral availability, whereas in the case of OPC poisoning drugs may be injected. On the other hand, improved oral bioavailability and reduced side effects might lead to the possibility to provide the antidote to a broader group of civilians and military members in the case of a high risk of OPC poisoning. Finally, the newly identified chemotypes [PTMD99-0001C (**3**), PTMD99-0016C (**4**), PTMD99-0026C (**5**), and cycloguanil (**6**)] show a reduced predicted affinity towards the HERG K^+ channel and a reduced toxicological alert count compared to UNC0646 and its analogs [PTMD01-0050 (**1k**), PTMD01-0043 (**2g**)]. Also, for the new chemotypes – except PTMD99-0026C (**5**) – no bacterial mutagenicity is predicted. In that respect, all novel compounds identified from the screenings show improved predicted pharmacokinetic properties compared to UNC0646 (Table 4) and, besides PTMD99-0026C (**5**), all novel chemotypes also display improved predicted toxicological properties (Table 5).

Table 4: Predicted pharmacokinetic properties of the best screening hits.

Compound	#stars[a]	QPlogPo/w[b]	QPPCaco[c]	RuleOfFive[d]	RuleOfThree[e]
UNC0646	7	6.014	125.427	2	1
PTMD01-0050 (**1k**)	1	5.609	428.531	2	0
PTMD01-0043 (**2g**)	0	4.541	297.484	0	0
PTMD99-0001C (**3**)	0	2.568	615.239	0	0
PTMD99-0016C (**4**)	0	3.718	277.071	0	1
PTMD99-0026C (**5**)	0	2.446	201.628	0	0
Cycloguanil (**6**)	1	1.592	446.492	0	0

[a] Number of properties falling outside the 95% range of similar values for known drugs.
[b] Octanol/water partition coefficient (recommended values: -2.0 – 6.5).
[c] Caco-2 cell permeability [nm/s] as a model for gut-blood barrier permeation (values < 25 poor, > 500 great).
[d] Number of violations of Lipinski's rule of five.
[e] Number of violations of Jorgensen's rule of three.

Table 5: Predicted toxicological properties of the best screening hits.

Compound	QPlogHERG[a]	Toxicological alert count[b]	Bacterial mutagenicity[d]
UNC0646	-8.224	4	EQUIVOCAL
PTMD01-0050 (**1k**)	-6.109	2	EQUIVOCAL
PTMD01-0043 (**2g**)	-7.460	4	EQUIVOCAL
PTMD99-0001C (**3**)	-4.980	0	INACTIVE
PTMD99-0016C (**4**)	-6.125	2	INACTIVE
PTMD99-0026C (**5**)	-6.528	4	PLAUSIBLE
Cycloguanil (**6**)	-3.989	1	INACTIVE

[a] IC_{50} value for blockage of HERG K^+ channels (recommended values: above -5).

[b] Number of alerts for toxicological predictions.

[c] Bacterial mutagenicity *in vitro*.

Conclusion

To find new compounds representing novel chemotypes that bind to MB327-PAM-1 and to better understand structure-affinity relationships of the known binder UNC0646, we performed exhaustive virtual screening followed by an MS Binding Assay. As to the importance of the substituents of UNC0646 analogs, overall, beneficial substituents in position 4 are also more flexible, suggesting that conformational adaptability may be favorable compared to the loss of conformational entropy. Furthermore, while all compounds known to bind to MB327-PAM-1 carry at least one positive charge, our results indicate that the location of the positive charge plays a minor role. Based on our results, we developed PTMD01-0050 (**1k**), which leads to a higher reporter ligand displacement at test compound concentrations of 10 µM than UNC0646.

UNC0646 analogs in general show increased binding affinity with increased molecular weight and size. Due to concerns for oral bioavailability and because for some pharmacokinetic and toxicological predictions UNC0646 lies outside the recommended value range, we also aimed to find novel chemotypes binding to MB327-PAM-1. Identified compounds with four novel chemotypes can displace UNC0642 from MB327-PAM-1 (mean ± SD < 100%) at test compound concentrations of 10 µM and reporter ligand concentrations of 1 µM. While one compound (PTMD99-0016C (**4**)) already has a molecular weight > 400 Da, the other three hits have a molecular weight < 300 Da. These compounds can be used as a starting point for optimization in terms of affinity, pharmacokinetics, and resensitization capability of a desensitized nAChR. One of those compounds, cycloguanil (**6**), was tested for its resensitizing capabilities in soman-inhibited rat muscles and leads to a significantly increased restoration of muscle force compared to MB327 at a concentration of 100 µM.

The identification of more potent resensitizers of nAChR is of utmost importance to improve the currently insufficient treatment after OPC poisonings. Identifying novel chemotypes by structure-based screening and showing with our MS Binding Assay that these compounds can bind in the same binding site as MB327 suggests that the hits also bind to the allosteric binding site MB327-PAM-1.

Acknowledgments

This work was supported by the German Ministry of Defense (E/U2AD/KA019/IF558). We are grateful for computational support and infrastructure provided by the "Zentrum für Informations- und Medientechnologie" (ZIM) at the Heinrich Heine University Düsseldorf and the computing time provided by the John von Neumann Institute for Computing (NIC) to HG on the supercomputer JUWELS at Jülich Supercomputing Centre (JSC) (user IDs: VSK33, nAChR). HG is grateful to OpenEye Scientific Software for granting a Free Public Domain Research License.

Data availability

Data will be made available on request.

Declaration of competing interest

The authors declare that they have no known competing financial or personal interests.

Author contribution

J.K. performed modeling, screening, and MD simulation experiments. C.G. supported the computational experiments. T.B. synthesized analogs of UNC0646. V.N. performed MS Binding Assays, and T.S. performed rat diaphragm assays. H.G. conceived the study and supervised the project. G.H., K.N., F.P., K.W., D.S., and F.W. supervised respective study parts. All authors contributed to writing the manuscript.

References

1. Wiener, S.W. and R.S. Hoffman, *Nerve agents: a comprehensive review.* J. Intensive Care Med., 2004. **19**(1): p. 22-37.
2. Albuquerque, E.X., et al., *Mammalian nicotinic acetylcholine receptors: from structure to function.* Physiol. Rev., 2009. **89**(1): p. 73-120.
3. Unwin, N., *Nicotinic acetylcholine receptor and the structural basis of neuromuscular transmission: insights from Torpedo postsynaptic membranes.* Q. Rev. Biophys., 2013. **46**(4): p. 283-322.
4. Thiermann, H., F. Worek, and K. Kehe, *Limitations and challenges in treatment of acute chemical warfare agent poisoning.* Chem. Biol. Interact., 2013. **206**(3): p. 435-43.
5. Worek, F., et al., *Evaluation of oxime efficacy in nerve agent poisoning: Development of a kinetic-based dynamic model.* Toxicology and Applied Pharmacology, 2005. **209**(3): p. 193-202.
6. Sichler, S., et al., *Development of MS Binding Assays targeting the binding site of MB327 at the nicotinic acetylcholine receptor.* Toxicol Lett, 2018. **293**: p. 172-183.
7. Scheffel, C., et al., *Electrophysiological investigation of the effect of structurally different bispyridinium non-oxime compounds on human alpha7-nicotinic acetylcholine receptor activity-An in vitro structure-activity analysis.* Toxicol Lett, 2018. **293**: p. 157-166.
8. Niessen, K.V., et al., *Functional analysis of Torpedo californica nicotinic acetylcholine receptors in multiple activation states by SSM-based electrophysiology.* Toxicol Lett, 2016. **247**: p. 1-10.
9. Niessen, K.V., et al., *In vitro pharmacological characterization of the bispyridinium non-oxime compound MB327 and its 2- and 3-regioisomers.* Toxicol. Lett., 2018. **293**: p. 190-197.
10. Seeger, T., et al., *Restoration of soman-blocked neuromuscular transmission in human and rat muscle by the bispyridinium non-oxime MB327 in vitro.* Toxicology, 2012. **294**(2-3): p. 80-4.
11. Turner, S.R., et al., *Protection against nerve agent poisoning by a noncompetitive nicotinic antagonist.* Toxicol Lett, 2011. **206**(1): p. 105-11.
12. Epstein, M., et al., *Molecular determinants of binding of non-oxime bispyridinium nerve agent antidote compounds to the adult muscle nAChR.* Toxicol Lett, 2021. **340**: p. 114-122.
13. Kaiser, J., et al., *A novel binding site in the nicotinic acetylcholine receptor for MB327 can explain its allosteric modulation relevant for organophosphorus-poisoning treatment.* Toxicol. Lett., 2023. **373**: p. 160-171.
14. Leelananda, S.P. and S. Lindert, *Computational methods in drug discovery.* Beilstein J. Org. Chem., 2016. **12**: p. 2694-2718.
15. Metz, A., et al., *From determinants of RUNX1/ETO tetramerization to small-molecule protein-protein interaction inhibitors targeting acute myeloid leukemia.* J. Chem. Inf. Model., 2013. **53**(9): p. 2197-202.
16. Dick, M., et al., *Pyrazolidine-3,5-dione-based inhibitors of phosphoenolpyruvate carboxylase as a new class of potential C4 plant herbicides.* FEBS Lett., 2017. **591**(20): p. 3369-3377.
17. Porta, N., et al., *Small-molecule inhibitors of nisin resistance protein NSR from the human pathogen Streptococcus agalactiae.* Biorg. Med. Chem., 2019. **27**(20): p. 115079.
18. Huo, D., et al., *Discovery of Novel Epidermal Growth Factor Receptor (EGFR) Inhibitors Using Computational Approaches.* J. Chem. Inf. Model., 2022. **62**(21): p. 5149-5164.
19. Ha, H., et al., *Discovery of Novel CXCR2 Inhibitors Using Ligand-Based Pharmacophore Models.* J. Chem. Inf. Model., 2015. **55**(8): p. 1720-1738.
20. Menendez-Gonzalez, J.B., et al., *Ligand-based discovery of a novel GATA2 inhibitor targeting acute myeloid leukemia cells.* Frontiers in Drug Discovery, 2022. **2**.
21. Gunera, J., et al., *Structure-Based Discovery of Novel Ligands for the Orexin 2 Receptor.* J. Med. Chem., 2020. **63**(19): p. 11045-11053.

22. Park, H., et al., *Structure-Based Virtual Screening and De Novo Design to Identify Submicromolar Inhibitors of G2019S Mutant of Leucine-Rich Repeat Kinase 2.* Int. J. Mol. Sci., 2022. **23**(21): p. 12825.
23. Fink, E.A., et al., *Structure-based discovery of nonopioid analgesics acting through the α_{2A}-adrenergic receptor.* Science, 2022. **377**(6614): p. eabn7065.
24. Park, H., et al., *Structure-Based Virtual Screening and De Novo Design of PIM1 Inhibitors with Anticancer Activity from Natural Products.* Pharmaceuticals, 2021. **14**(3): p. 275.
25. Benod, C., et al., *Structure-based Discovery of Antagonists of Nuclear Receptor LRH-1 *.* Journal of Biological Chemistry, 2013. **288**(27): p. 19830-19844.
26. Song, Y., et al., *Discovery of non-peptide inhibitors of Plasmepsin II by structure-based virtual screening.* Bioorg. Med. Chem. Lett., 2013. **23**(7): p. 2078-2082.
27. Diao, Y., et al., *Discovery of Diverse Human Dihydroorotate Dehydrogenase Inhibitors as Immunosuppressive Agents by Structure-Based Virtual Screening.* J. Med. Chem., 2012. **55**(19): p. 8341-8349.
28. Song, C.-H., et al., *Structure-based Virtual Screening and Identification of a Novel Androgen Receptor Antagonist *.* J. Biol. Chem., 2012. **287**(36): p. 30769-30780.
29. Nitsche, V., et al., *MS Binding Assays with UNC0642 as reporter ligand for the MB327 binding site of the nicotinic acetylcholine receptor.* bioRxiv, 2023: p. 2023.11.15.567260.
30. Eswar, N., et al., *Comparative protein structure modeling using Modeller.* Curr Protoc Bioinformatics, 2006. **Chapter 5**: p. Unit-5 6.
31. Gharpure, A., et al., *Agonist Selectivity and Ion Permeation in the α3β4 Ganglionic Nicotinic Receptor.* Neuron, 2019. **104**(3): p. 501-511.e6.
32. Morales-Perez, C.L., C.M. Noviello, and R.E. Hibbs, *X-ray structure of the human α4β2 nicotinic receptor.* Nature, 2016. **538**(7625): p. 411-415.
33. Hibbs, R.E., et al., *Structural determinants for interaction of partial agonists with acetylcholine binding protein and neuronal α7 nicotinic acetylcholine receptor.* The EMBO Journal, 2009. **28**(19): p. 3040-3051.
34. Walsh, R.M., et al., *Structural principles of distinct assemblies of the human α4β2 nicotinic receptor.* Nature, 2018. **557**(7704): p. 261-265.
35. Shen, M.Y. and A. Sali, *Statistical potential for assessment and prediction of protein structures.* Protein Sci, 2006. **15**(11): p. 2507-24.
36. Mulnaes, D. and H. Gohlke, *TopScore: Using Deep Neural Networks and Large Diverse Data Sets for Accurate Protein Model Quality Assessment.* J. Chem. Theory Comput., 2018. **14**(11): p. 6117-6126.
37. Sondergaard, C.R., et al., *Improved Treatment of Ligands and Coupling Effects in Empirical Calculation and Rationalization of pKa Values.* J. Chem. Theory Comput., 2011. **7**(7): p. 2284-95.
38. Olsson, M.H., et al., *PROPKA3: Consistent Treatment of Internal and Surface Residues in Empirical pKa Predictions.* J. Chem. Theory Comput., 2011. **7**(2): p. 525-37.
39. Schrödinger, *Maestro*. 2020, Schrödinger, LLC.: New York, NY, USA.
40. Chevillard, F., et al., *Binding-Site Compatible Fragment Growing Applied to the Design of beta2-Adrenergic Receptor Ligands.* J Med Chem, 2018. **61**(3): p. 1118-1129.
41. *QUACPAC 2.1.1.0*. 2020, OpenEye Scientific Software: Santa Fe, NM.
42. *OMEGA 4.1.0.0*. 2020, Openeye Scientific Software: Santa Fe, NM, USA.
43. Hawkins, P.C.D., et al., *Conformer Generation with OMEGA: Algorithm and Validation Using High Quality Structures from the Protein Databank and Cambridge Structural Database.* J. Chem. Inf. Model., 2010. **50**(4): p. 572-584.
44. Hawkins, P.C., A.G. Skillman, and A. Nicholls, *Comparison of shape-matching and docking as virtual screening tools.* J Med Chem, 2007. **50**(1): p. 74-82.
45. *ROCS 3.4.1.0*. OpenEye Scientific Software: Santa Fe, NM.
46. Chemical Computing Group, U., *Molecular Operating Environment (MOE)*. 2021: 1010 Sehrbooke St. West, Suite #910, Montreal, QC, Canada, H3A, 2R7.

47. Mellsted, H., et al., *2-phenyl-3H-imidazo [4, 5-B] pyridine derivates useful as inhibitors of mammalian tyrosine kinase ROR1 activity (WO/2016/124553)*, W.I.P. Organization, Editor. 2016.
48. Pauli, G.F., et al., *Importance of Purity Evaluation and the Potential of Quantitative 1H NMR as a Purity Assay.* J. Med. Chem., 2014. **57**(22): p. 9220-9231.
49. Cushman, M., et al., *Absolute Quantitative 1H NMR Spectroscopy for Compound Purity Determination.* J. Med. Chem., 2014. **57**(22): p. 9219-9219.
50. Vital, T., et al., *MS0621, a novel small-molecule modulator of Ewing sarcoma chromatin accessibility, interacts with an RNA-associated macromolecular complex and influences RNA splicing.* Front. Oncol., 2023. **13**: p. 1099550.
51. Hennequin, L.F., et al., *Quinazoline Derivatives as Angiogenesis Inhibitors (WO-2000047212-A1)*, W.I.P. Organization, Editor. 2000.
52. Ravez, S., et al., *Inhibition of tumor cell growth and angiogenesis by 7-Aminoalkoxy-4-aryloxy-quinazoline ureas, a novel series of multi-tyrosine kinase inhibitors.* Eur. J. Med. Chem., 2014. **79**: p. 369-381.
53. Irwin, J.J., et al., *ZINC20-A Free Ultralarge-Scale Chemical Database for Ligand Discovery.* J Chem Inf Model, 2020. **60**(12): p. 6065-6073.
54. *OEDOCKING 4.0.0.0*. 2020, OpenEye Scientific Software: Santa Fe, NM, USA.
55. McGann, M., *FRED and HYBRID docking performance on standardized datasets.* J. Comput. Aided Mol. Des., 2012. **26**(8): p. 897-906.
56. McGann, M., *FRED Pose Prediction and Virtual Screening Accuracy.* J. Chem. Inf. Model., 2011. **51**(3): p. 578-596.
57. Schott-Verdugo, S. and H. Gohlke, *PACKMOL-Memgen: A Simple-To-Use, Generalized Workflow for Membrane-Protein-Lipid-Bilayer System Building.* J. Chem. Inf. Model., 2019. **59**(6): p. 2522-2528.
58. Jorgensen, W.L., et al., *Comparison of simple potential functions for simulating liquid water.* The Journal of Chemical Physics, 1983. **79**(2): p. 926-935.
59. Case, D.A., et al., *The Amber biomolecular simulation programs.* J. Comput. Chem., 2005. **26**(16): p. 1668-88.
60. Case, D.A., et al., *Amber 2022*. 2022, University of California: San Francisco.
61. Maier, J.A., et al., *ff14SB: Improving the Accuracy of Protein Side Chain and Backbone Parameters from ff99SB.* J. Chem. Theory Comput., 2015. **11**(8): p. 3696-3713.
62. Dickson, C.J., R.C. Walker, and I.R. Gould, *Lipid21: Complex Lipid Membrane Simulations with AMBER.* J. Chem. Theory Comput., 2022. **18**(3): p. 1726-1736.
63. Joung, I.S. and T.E. Cheatham, III, *Determination of Alkali and Halide Monovalent Ion Parameters for Use in Explicitly Solvated Biomolecular Simulations.* The Journal of Physical Chemistry B, 2008. **112**(30): p. 9020-9041.
64. Bayly, C.I., et al., *A well-behaved electrostatic potential based method using charge restraints for deriving atomic charges: the RESP model.* The Journal of Physical Chemistry, 1993. **97**(40): p. 10269-10280.
65. Wang, J., et al., *Automatic atom type and bond type perception in molecular mechanical calculations.* Journal of Molecular Graphics and Modelling, 2006. **25**(2): p. 247-260.
66. M. J. Frisch, G.W.T., H. B. Schlegel, G. E. Scuseria,, et al., *Gaussian16*. 2016, Gaussian Inc.: Wallingford CT.
67. Charman, S.A., et al., *An in vitro toolbox to accelerate anti-malarial drug discovery and development.* Malaria Journal, 2020. **19**(1): p. 1.
68. Roe, D.R. and T.E. Cheatham, 3rd, *PTRAJ and CPPTRAJ: Software for Processing and Analysis of Molecular Dynamics Trajectory Data.* J. Chem. Theory Comput., 2013. **9**(7): p. 3084-95.
69. *OMEGA 4.1.1.1*. 2021, Openeye Scientific Software: Santa Fe, NM, USA.
70. *Schrödinger Release 2022-2: QikProp*. 2022, Schrödinger, LLC: New York, NY.

71. Baell, J.B. and G.A. Holloway, *New Substructure Filters for Removal of Pan Assay Interference Compounds (PAINS) from Screening Libraries and for Their Exclusion in Bioassays.* J. Med. Chem., 2010. **53**(7): p. 2719-2740.
72. Greene, N., et al., *Knowledge-based expert systems for toxicity and metabolism prediction: DEREK, StAR and METEOR.* SAR QSAR Environ Res, 1999. **10**(2-3): p. 299-314.
73. Pettersen, E.F., et al., *UCSF Chimera—A visualization system for exploratory research and analysis.* J. Comput. Chem., 2004. **25**(13): p. 1605-1612.
74. Rappengluck, S., et al., *Synthesis of a Series of Non-Symmetric Bispyridinium and Related Compounds and Their Affinity Characterization at the Nicotinic Acetylcholine Receptor.* ChemMedChem, 2018. **13**(24): p. 2653-2663.
75. Rappengluck, S., et al., *Synthesis of a Series of Structurally Diverse MB327 Derivatives and Their Affinity Characterization at the Nicotinic Acetylcholine Receptor.* ChemMedChem, 2018. **13**(17): p. 1806-1816.
76. Zieliński, W. and A. Kudelko, *A study concerning the synthesis, basicity and hydrolysis of 4-amino-2-(N,N-diethylamino)quinazoline derivatives.* Journal of Heterocyclic Chemistry, 2002. **39**(6): p. 1289-1292.
77. Armarego, W.L.F., *Quinazolines*, in *Advances in Heterocyclic Chemistry*, A.R. Katritzky, Editor. 1963, Academic Press. p. 253-309.
78. Albert, A., R. Goldacre, and J. Phillips, *455. The strength of heterocyclic bases.* Journal of the Chemical Society (Resumed), 1948(0): p. 2240-2249.
79. Yoshida, K. and M. Taguchi, *Reaction of N-substituted cyclic amines with 2,4-dichloroquinazoline, 2,4-dichloropyrimidine, and its 5-methyl derivative.* J. Chem. Soc., Perkin Trans. 1, 1992(7): p. 919-922.
80. Lipinski, C.A., et al., *Experimental and computational approaches to estimate solubility and permeability in drug discovery and development settings.* Adv. Drug Del. Rev., 1997. **23**(1): p. 3-25.
81. Tasler, S., et al., *Substituted 2-arylbenzothiazoles as kinase inhibitors: Hit-to-lead optimization.* Biorg. Med. Chem., 2009. **17**(18): p. 6728-6737.
82. Liu, F., et al., *Optimization of Cellular Activity of G9a Inhibitors 7-Aminoalkoxy-quinazolines.* J. Med. Chem., 2011. **54**(17): p. 6139-6150.
83. Wan, Z.-K., et al., *The Scope and Mechanism of Phosphonium-Mediated SNAr Reactions in Heterocyclic Amides and Ureas.* The Journal of Organic Chemistry, 2007. **72**(26): p. 10194-10210.
84. Harris, C.S., J.G. Kettle, and E.J. Williams, *Facile synthesis of 7-amino anilinoquinazolines via direct amination of the quinazoline core.* Tetrahedron Lett., 2005. **46**(43): p. 7381-7384.
85. Niessen, K.V., et al., *Affinities of bispyridinium non-oxime compounds to [(3)H]epibatidine binding sites of Torpedo californica nicotinic acetylcholine receptors depend on linker length.* Chem. Biol. Interact., 2013. **206**(3): p. 545-54.
86. Galzi, J.L., et al., *Identification of calcium binding sites that regulate potentiation of a neuronal nicotinic acetylcholine receptor.* EMBO J, 1996. **15**(21): p. 5824-32.
87. Noviello, C.M., et al., *Structure and gating mechanism of the alpha7 nicotinic acetylcholine receptor.* Cell, 2021. **184**(8): p. 2121-2134 e13.

Supporting Information

Identification of ligands binding to MB327-PAM-1, a binding pocket relevant for resensitization of nAChRs

Jesko Kaiser[1], Christoph G.W. Gertzen[1], Tamara Bernauer[2], Valentin Nitsche[2], Georg Höfner[2], Karin V. Niessen[3], Thomas Seeger[3], Franz F. Paintner[2], Klaus T. Wanner[2], Dirk Steinritz[3], Franz Worek[3], Holger Gohlke[1,4,*]

[1]Institute for Pharmaceutical and Medicinal Chemistry, Heinrich Heine University Düsseldorf, Düsseldorf, Germany

[2]Department of Pharmacy – Center for Drug Research, Ludwig-Maximilians-Universität München, München, Germany

[3]Bundeswehr Institute of Pharmacology and Toxicology, München, Germany

[4]Institute of Bio- and Geosciences (IBG-4: Bioinformatics), Forschungszentrum Jülich, Jülich, Germany

Table of Content

Supplemental Figures and Tables

Supplemental Figures

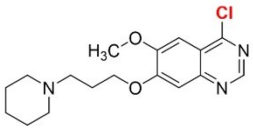

Buchwald-Hartwig
Heck
Negishi
Stille

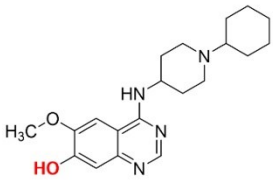

Mitsunobu

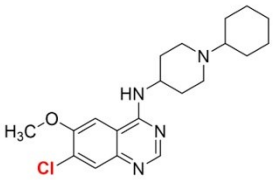

Buchwald-Hartwig
Heck
Negishi
Stille
Suzuki

Figure S1: Building blocks of PTMD01-0004 (**2a**) for the generation of a virtual database. For each building block, the stated virtual syntheses have been performed with building blocks available on MolPort (https://molport.com) using PINGUI [1]. Functional groups that participate in the respective reaction are shown in red.

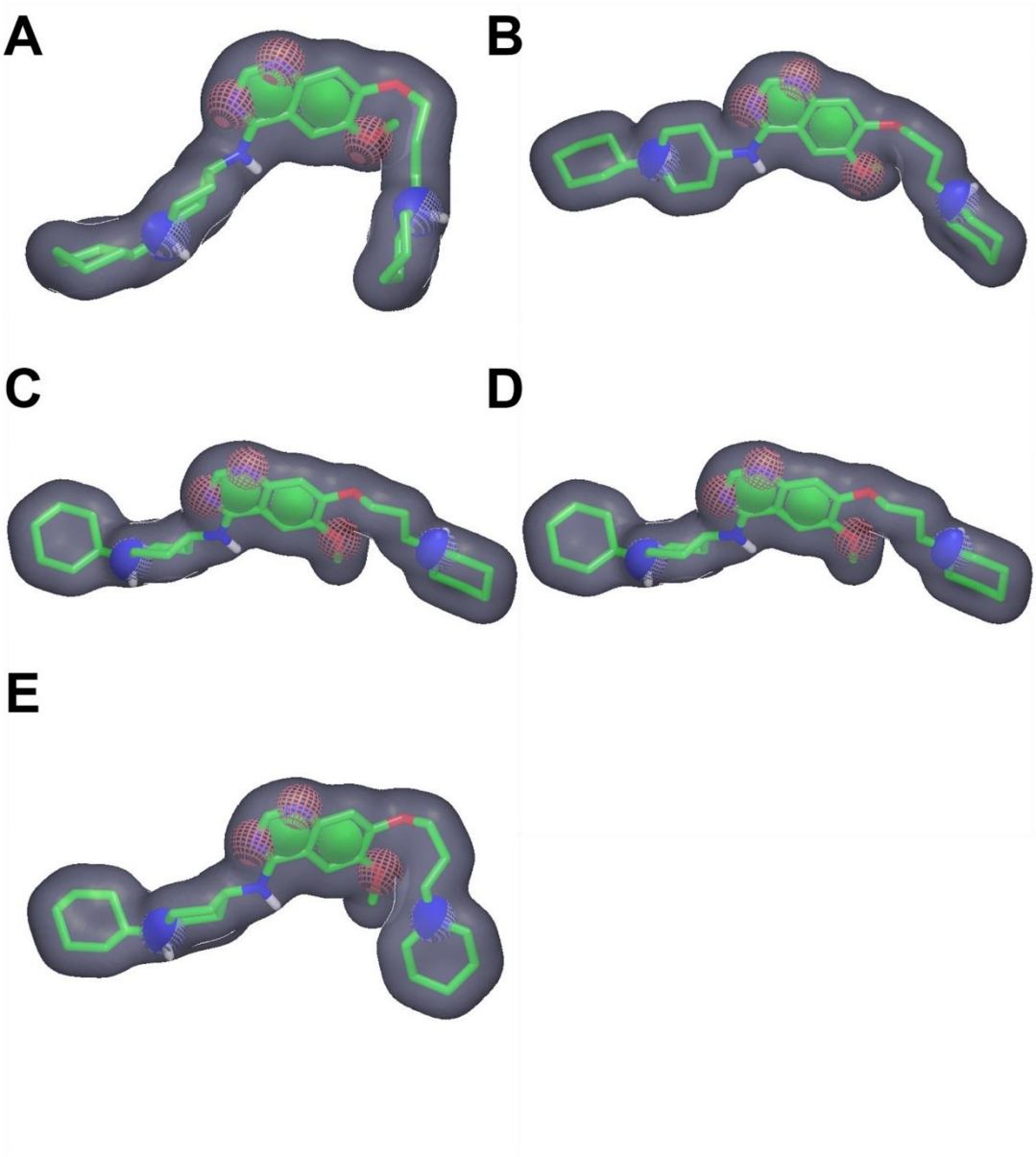

Figure S2: Pharmacophore models used for database filtering during template-based docking. Conformations of PTMD01-0004 (**2a**) (green) are shown as sticks between the **A)** α- and δ-, **B)** δ- and β-, **C)** β- and α-, **D)** α- and γ-, and **E)** γ- and α-subunits. Colored elements indicate pharmacophore filters: the grey surface indicates the ligand surface, green circles indicate aromatic systems, blue circles indicate hydrogen bond donor cations, and red circles indicate hydrogen bond acceptors. Figures were generated using OpenEye vROCS [2].

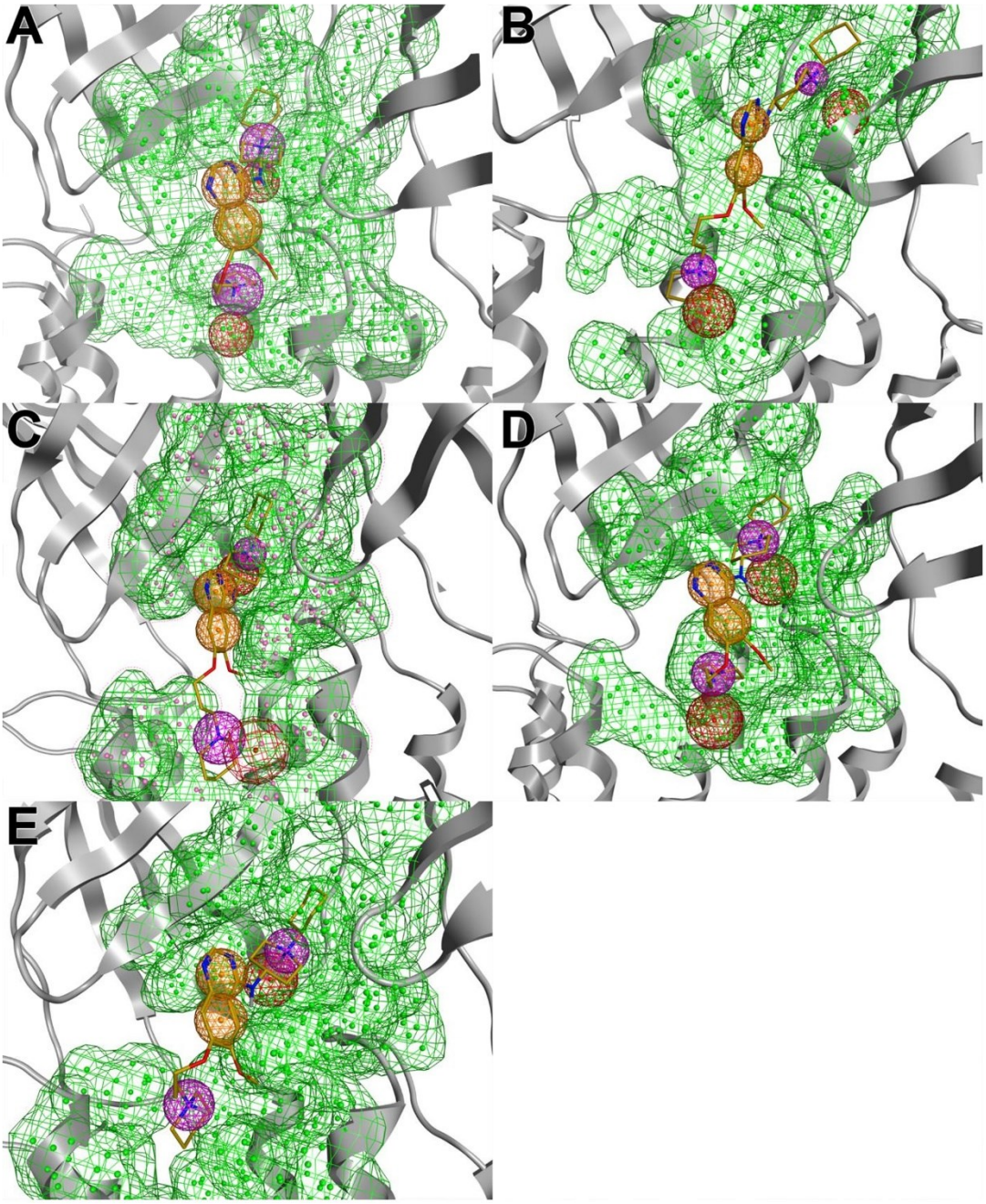

Figure S3: Binding mode of and pharmacophore model for template-based docking based on PTMD01-0004 (**2a**) (gold) shown between the **A)** α- and δ-, **B)** δ- and β-, **C)** β- and α-, **D)** α- and γ-, and **E)** γ- and α-subunits. Colored mesh areas indicate features of the pharmacophore filter: green area indicates the surface of the receptor where no atoms of the ligands are allowed to overlap, orange circles indicate the presence of an aromatic system, purple circles indicate the presence of a cation donor, and red circles indicate the direction of the hydrogen bond donor orientation. Figures were generated using Chemical Computing Group MOE [3].

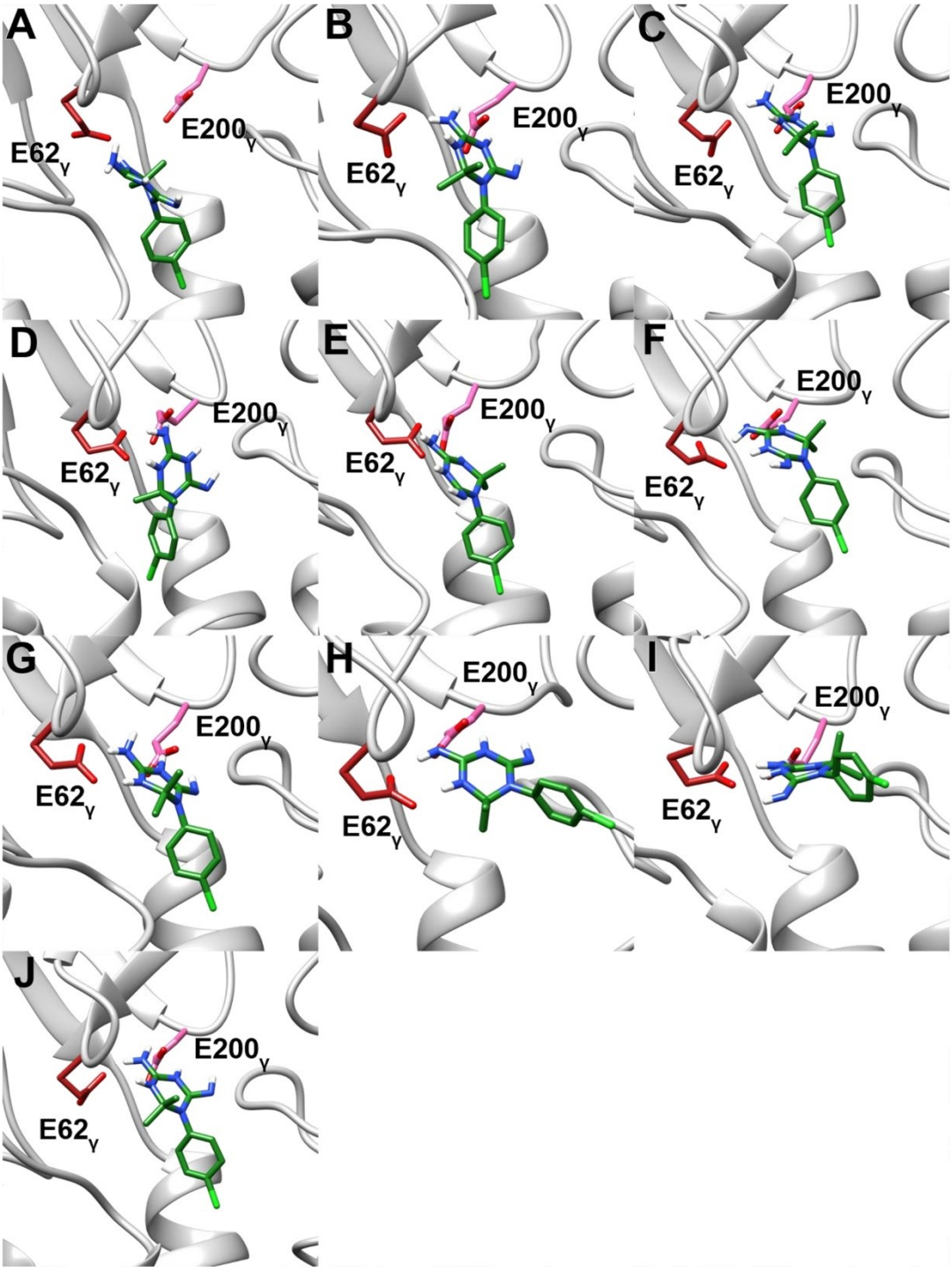

Figure S4: Representative binding modes of cycloguanil in MD simulations starting from the docked binding mode after clustering using the *k-means* algorithm as implemented in CPPTRAJ [4]. **A)** Only in the largest cluster (containing 18.3 % of all frames) cycloguanil is not interacting with $E200_{\gamma}$. In the **B)** second (containing 14.1 % of all frames), **C)** third (containing 12.4 % of all frames, **D)** fourth (containing 10.9 % of all frames), **E)** fifth (containing 10.8 % of all frames), **F)** sixth (containing 10.5 % of all frames), **G)** seventh (containing 10.1 % of all frames), **H)** eight (containing 6.7 % of all frames), **I)** ninth (containing 3.6 % of all frames), and **J)** tenth (containing 2.5 % of all frames) largest cluster, cycloguanil is interacting with $E200_{\gamma}$ and $E62_{\gamma}$.

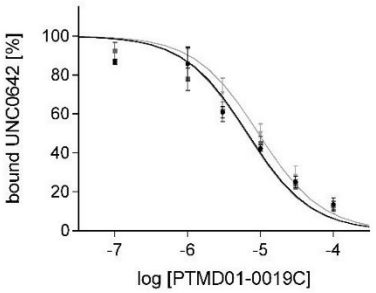

Figure S5: Competition curves obtained for PTMD01-0019C (**1a**) in UNC0642 MS Binding Assays. Data points (mean ± SD, *n* = 3) represent the specific binding of UNC0642.

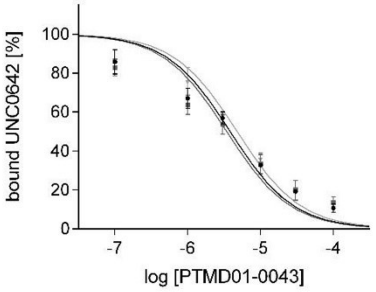

Figure S6: Competition curves obtained for PTMD01-0043 (**2g**) in UNC0642 MS Binding Assays. Data points (mean ± SD, *n* = 3) represent the specific binding of UNC0642.

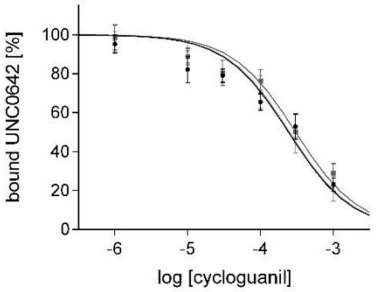

Figure S7: Competition curves obtained for cycloguanil (**6**) in UNC0642 MS Binding Assays. Data points (mean ± SD, *n* = 3) represent the specific binding of UNC0642.

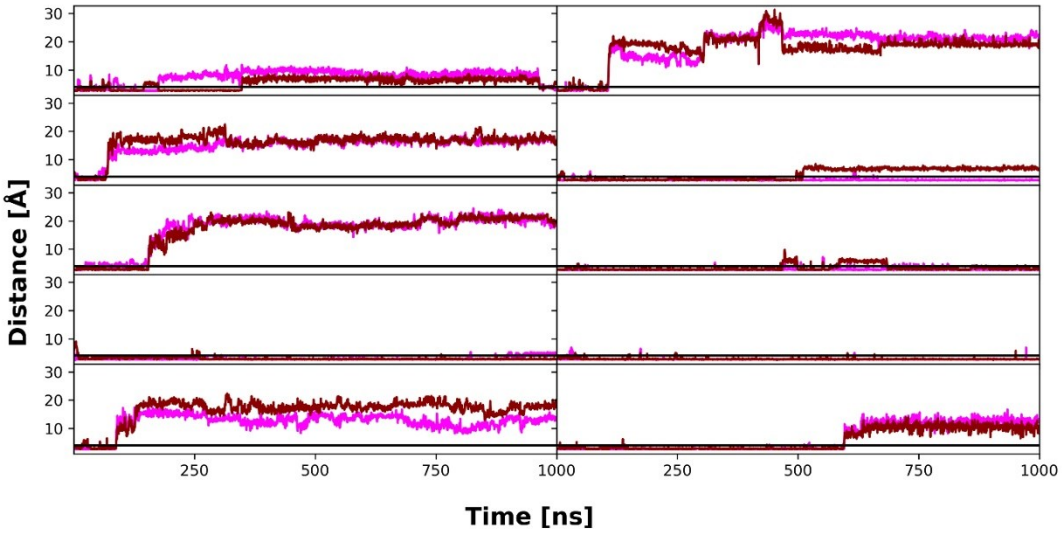

Figure S8: Distance of nitrogens that can act as hydrogen bond donors of cycloguanil to side chain oxygens of $E62_{\gamma}$ (pink) and $E200_{\gamma}$ (dark red) during 10 replicas of unbiased MD simulations.

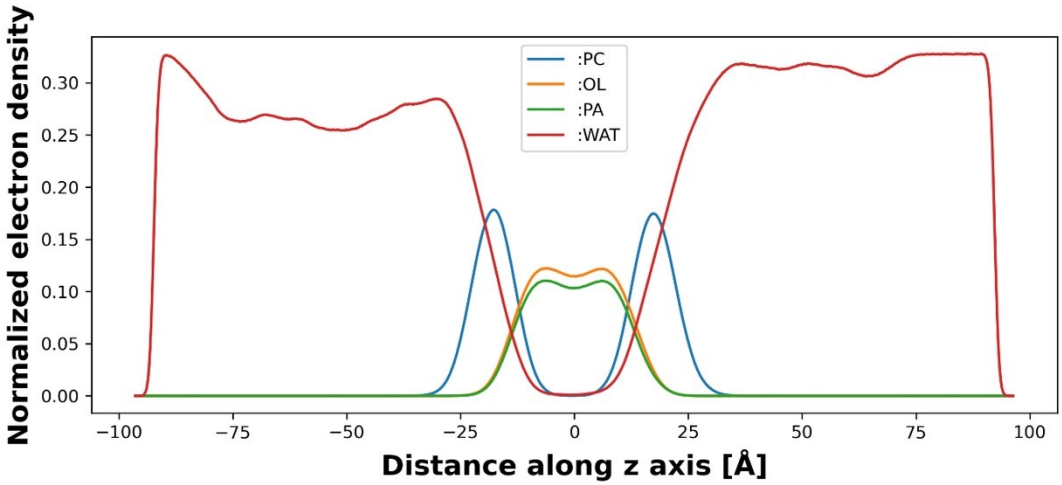

Figure S91: Normalized (number of electrons per volume [$e^{-}/Å^{3}$]) electron density of membrane components and water averaged over all 10 replicas of 1 µs long MD simulations. The electron density is plotted against the z-coordinate, which is parallel to the membrane normal. The membrane is centered at 0 Å for phosphatidylcholine (:PC), oleic acid (:OL), palmitoyl acid (:PA), and water (:WAT).

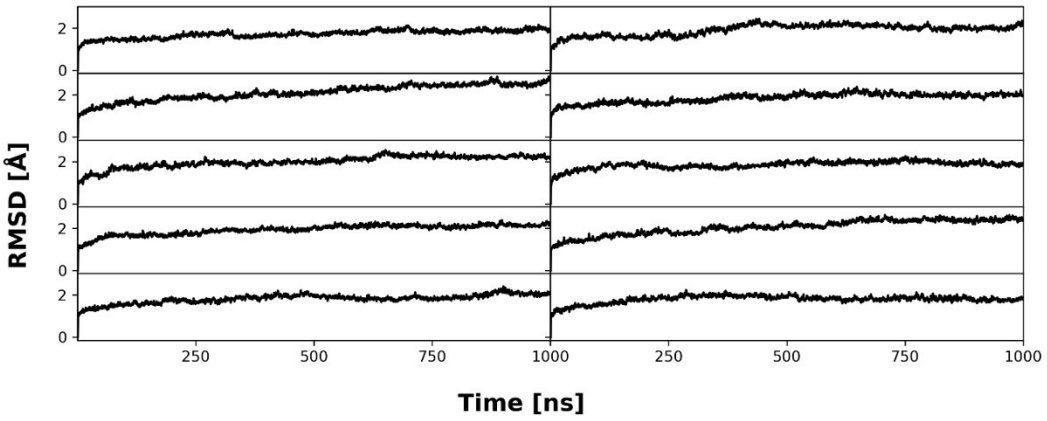

Figure S10: Backbone (C, CA, N) RMSD of nAChR during 10 replicas of 1 µs long MD simulations with respect to the first frame of the production run.

Supplemental Tables

Table S1: List of commercially obtained test compounds.

#	Compound	Salt	Purity	Supplier
1	Bunazosin	-	≥ 95%	Angene (Honk Kong, China)
2	C-021	-	≥ 97%	BIONET – KeyOrganics Ltd (Cornwall, United Kingdom)
3	Cycloguanil	HCl	≥ 95%	Otava Ltd (Kiew, Ukraine)
4	MS012	-	≥ 90%	TimTec, LLC (Newark, United States)
5	PTMD01-0019C	-	≥ 85%	ChemBridge Corporation (San Diego, United States)
6	PTMD01-0020C	-	≥ 90%	Enamine Ltd (Kiew, Ukraine)
7	PTMD01-0021C	-	≥ 85%	ChemBridge Corporation (San Diego, United States)
8	PTMD01-0022C	-	≥ 85%	ChemBridge Corporation (San Diego, United States)
9	PTMD01-0023C	-	≥ 90%	Enamine Ltd (Kiew, Ukraine)
10	PTMD01-0024C	-	≥ 85%	ChemBridge Corporation (San Diego, United States)
11	PTMD01-0025C	-	≥ 90%	Enamine Ltd (Kiew, Ukraine)
12	PTMD99-0001C	HI	≥ 90%	Enamine Ltd (Kiew, Ukraine)
13	PTMD99-0002C	-	≥ 90%	UkrOrgSynthesis Ltd. (Kiew, Ukraine)
14	PTMD99-0004C	2 HCl	≥ 85%	ChemBridge Corporation (San Diego, United States)
15	PTMD99-0005C	-	≥ 90%	ChemBridge Corporation (San Diego, United States)
16	PTMD99-0006C	-	≥ 85%	ChemBridge Corporation (San Diego, United States)
17	PTMD99-0008C	H_2SO_4	≥ 90%	Vitas-M Laboratory Ltd (Causeway Bay, Hong Kong)
18	PTMD99-0009C	HBr	≥ 90%	Enamine Ltd (Kiew, Ukraine)
19	PTMD99-0010C	2 HCl	≥ 85%	ChemBridge Corporation (San Diego, United States)
20	PTMD99-0011C	-	≥ 85%	ChemBridge Corporation (San Diego, United States)
21	PTMD99-0013C	HCl	≥ 90%	ChemBridge Corporation (San Diego, United States)
22	PTMD99-0014C	HCl	≥ 90%	Enamine Ltd (Kiew, Ukraine)
23	PTMD99-0015C	-	≥ 85%	ChemBridge Corporation (San Diego, United States)
24	PTMD99-0016C	-	≥ 85%	ChemBridge Corporation (San Diego, United States)
25	PTMD99-0020C	-	≥ 85%	ChemBridge Corporation (San Diego, United States)
26	PTMD99-0021C	-	≥ 85%	ChemBridge Corporation (San Diego, United States)
27	PTMD99-0023C	2 HCl	≥ 85%	ChemBridge Corporation (San Diego, United States)
28	PTMD99-0024C	2 HCl	≥ 85%	ChemBridge Corporation (San Diego, United States)
29	PTMD99-0025C	2 HCl	≥ 85%	ChemBridge Corporation (San Diego, United States)
30	PTMD99-0026C	2 HCl	≥ 85%	ChemBridge Corporation (San Diego, United States)
31	PTMD99-0028C	2 HCl	≥ 85%	ChemBridge Corporation (San Diego, United States)
32	PTMD99-0029C	2 HCl	≥ 85%	ChemBridge Corporation (San Diego, United States)
33	PTMD99-0031C	2 HCl	≥ 85%	ChemBridge Corporation (San Diego, United States)
34	PTMD99-0032C	HCl	≥ 90%	Maybridge Ltd (Cornwall, United Kingdom)
35	PTMD99-0035C	HCl	≥ 90%	Otava Ltd (Kiew, Ukraine)
36	PTMD99-0036C	HCl	≥ 90%	ChemBridge Corporation (San Diego, United States)
37	PTMD99-0038C	HCl	≥ 95%	Otava Ltd (Kiew, Ukraine)
38	PTMD99-0041C	HCl	≥ 85%	ChemBridge Corporation (San Diego, United States)
39	PTMD99-0044C	HCl	≥ 90%	Maybridge Ltd (Cornwall, United Kingdom)
40	PTMD99-0045C	HCl	≥ 90%	Maybridge Ltd (Cornwall, United Kingdom)
41	UNC0379	-	≥ 98%	TargetMol (Boston, United States)
42	ZT-12-037-01	-	≥ 98%	TargetMol (Boston, United States)

Table S2: All analogs of UNC0646 tested for affinity to MB327-PAM-1 in nAChR determined in MS Binding Assays based on a two-dimensional similarity search.

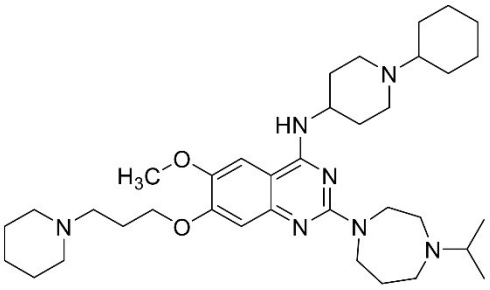

UNC0646

pK_i = 5.83 ± 0.05[a]

Remaining marker binding: 21 ± 3 %[b]

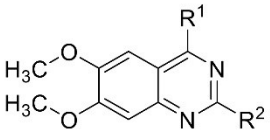

Compound	R^1	R^2	Remaining marker binding [%][b]
C-021	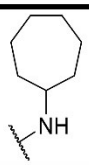	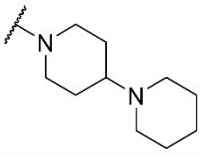	63 ± 2
ZT-12-037-01	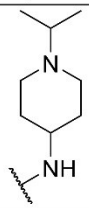	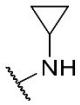	66 ± 5
MS012	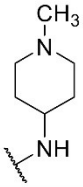	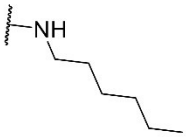	83 ± 6
UNC0379	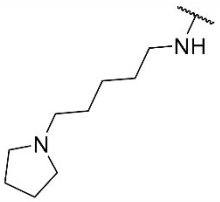	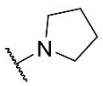	59 ± 4
Bunazosin		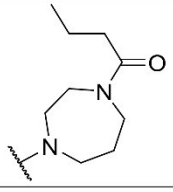	90 ± 7

PTMD01-0019C		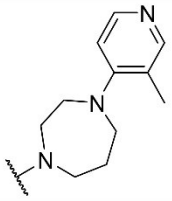	47 ± 3
PTMD01-0020C		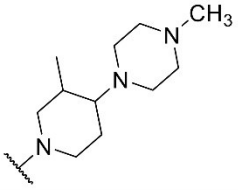	73 ± 7
PTMD01-0021C		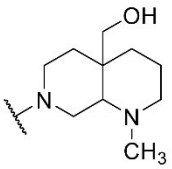	87 ± 2
PTMD01-0022C		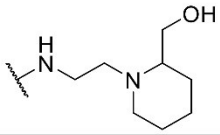	108 ± 10
PTMD01-0023C		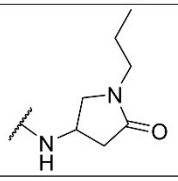	98 ± 3
PTMD01-0024C		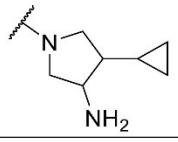	83 ± 4
PTMD01-0025C		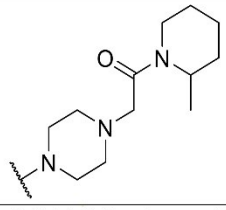	81 ± 5

[a] The pK_i value of UNC0646 has been reported in ref. [XXX Nitsche *et al.*, unpublished].

[b] Characterized by UNC0642 MS Binding Assays; Percentage of remaining reporter ligand binding in the presence of test compounds as compared to 100% reporter ligand binding in the absence of a competitor. Results are based on thirty measurements for UNC0646 and three measurements for all other compounds at a test compound concentration of 10 µM and a reporter ligand concentration of 1 µM. Mean and standard deviation are displayed.

Table S3: Results of affinity testing to MB327-PAM-1 in nAChR determined in MS Binding Assays of initial compounds ordered based on structure-based screening.

Name	Structure	Remaining marker binding [%][a]
PTMD99-0001C (**3**)	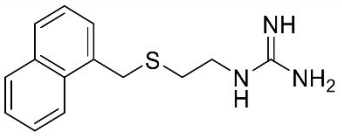	88 ± 5
PTMD99-0002C	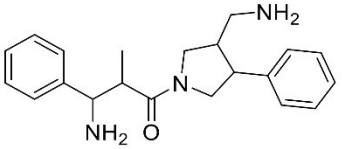	101 ± 9
PTMD99-0004C	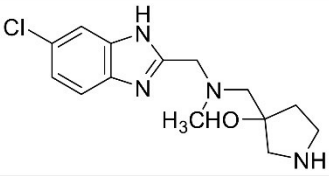	92 ±7
PTMD99-0005C	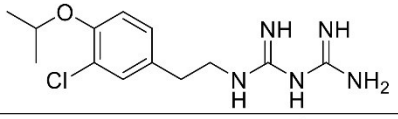	101 ± 3
PTMD99-0006C (**13**)	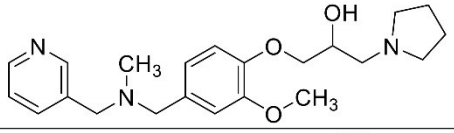	93 ± 7
PTMD99-0008C	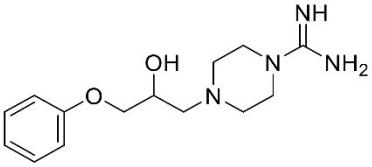	95 ± 4
PTMD99-0009C	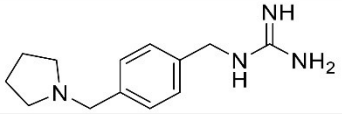	92 ± 9
PTMD99-0010C (**14**)	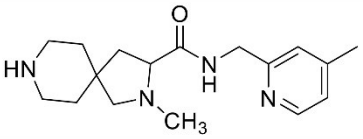	96 ± 5
PTMD99-0011C	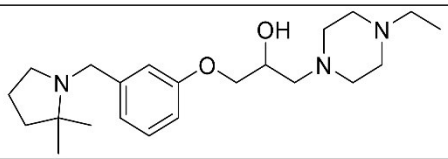	95 ± 7
PTMD99-0013C	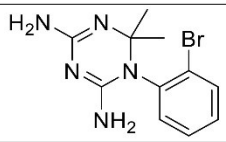	101 ± 6

PTMD99-0014C (**15**)	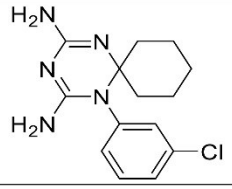	94 ± 6
PTMD99-0015C	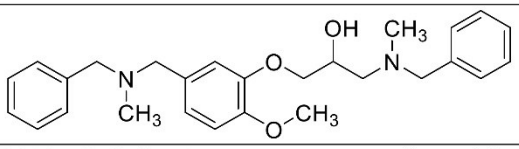	98 ± 8

[a] Characterized by UNC0642 MS Binding Assays; Percentage of remaining reporter ligand binding in the presence of test compounds as compared to 100% reporter ligand binding in the absence of a competitor. If not stated otherwise, results are based on three measurements at a test compound concentration of 10 µM and a reporter ligand concentration of 1 µM. Mean and standard deviation are displayed.

Table S4: Results of affinity testing of compounds analogous to the best hits from the initially ordered compounds based on structure-based screening.

Name	Structure	Remaining marker binding [%][a]
PTMD99-0016C (**4**)	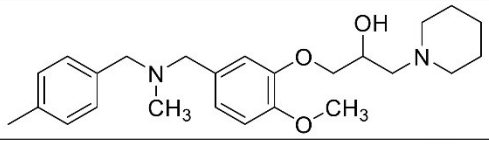	78 ± 3
PTMD99-0020C (**16**)	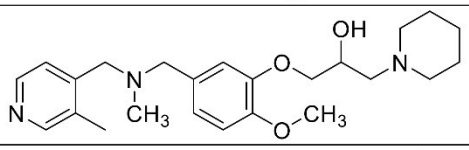	97 ± 4
PTMD99-0021C	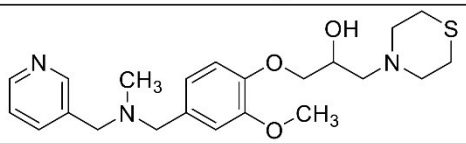	107 ± 11
PTMD99-0023C (**17**)	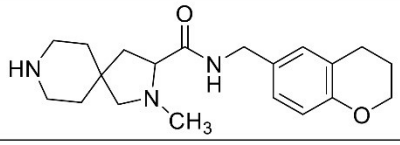	108 ± 4
PTMD99-0024C (**18**)	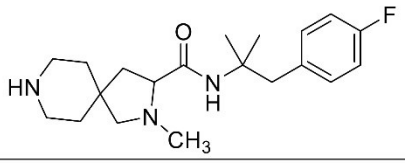	99 ± 6
PTMD99-0025C (**19**)	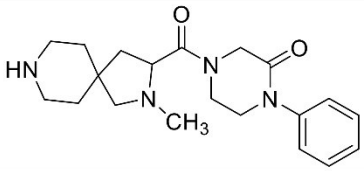	100 ± 6
PTMD99-0026C (**5**)	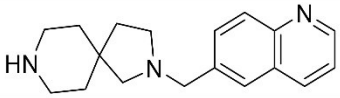	90 ± 5
PTMD99-0028C (**20**)	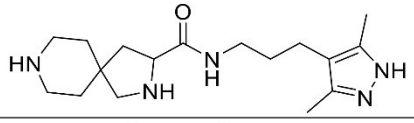	101 ± 7
PTMD99-0029C	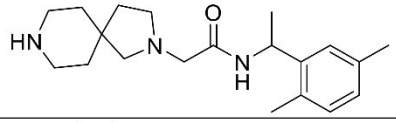	98 ± 4
PTMD99-0031C	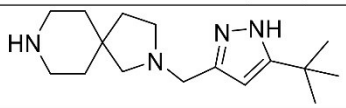	101 ± 8
PTMD99-0032C	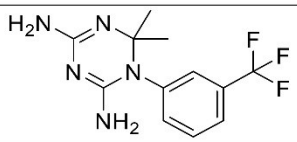	98 ± 6

PTMD99-0035C	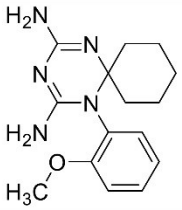	109 ± 8
PTMD99-0036C	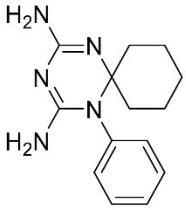	93 ± 4
PTMD99-0038C	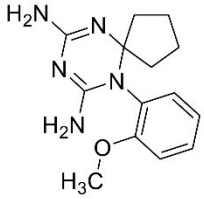	100 ± 4
Cycloguanil (**6**)	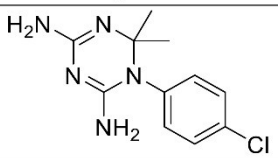	76 ± 3
PTMD99-0041C	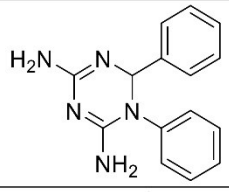	81 ± 3
PTMD99-0044C	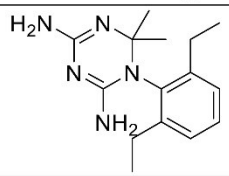	106 ± 6
PTMD99-0045C	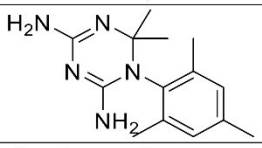	95 ± 8

[a] Characterized by UNC0642 MS Binding Assays; Percentage of remaining reporter ligand binding in the presence of test compounds as compared to 100% reporter ligand binding in the absence of a competitor. If not stated otherwise, results are based on three measurements at a test compound concentration of 10 µM and a reporter ligand concentration of 1 µM. Mean and standard deviation are displayed.

Analytical Data

6-Methoxy-2-(piperidin-1-yl)-7-[3-(piperidin-1-yl)propoxy]-*N*-[5-(pyrrolidin-1-yl)pentyl]quinazolin-4-amine (1k): mp.: 54 °C. R_f = 0.34 [10% (3 M NH_3 in MeOH) in CH_2Cl_2]. IR (film): $\tilde{\nu}$ = 2935, 1581, 1493, 1244, 754 cm^{-1}. ^1H NMR (500 MHz, CD_2Cl_2): δ = 1.37-1.47 (m, 2 H, CH_2CH$_2$CH$_2$NCH$_2$CH$_2$CH$_2$O), 1.48-1.55 (m, 2 H, CH_2CH$_2$CH$_2$NH), 1.55-1.61 (m, 8 H, CH$_2$CH_2CH$_2$NC, CH$_2$CH_2CH$_2$NCH$_2$CH$_2$CH$_2$O), 1.62-1.70 (m, 4 H, CH_2CH$_2$CH$_2$NC, CH_2CH$_2$CH$_2$CH$_2$NH), 1.74 (p, J = 7.0 Hz, 2 H, CH_2CH$_2$NH), 1.80-1.89 [m, 4 H, CH_2CH$_2$N(CH$_2$)$_5$NH], 2.00 (p, J = 6.9 Hz, 2 H, CH_2CH$_2$O), 2.22-2.42 (m, 4 H, CH_2NCH$_2$CH$_2$CH$_2$O), 2.42-2.48 (m, 2 H, CH_2CH$_2$CH$_2$O), 2.57-2.66 [m, 2 H, CH_2(CH$_2$)$_4$NH], 2.66-2.84 [m, 4 H, CH_2N(CH$_2$)$_5$NH], 3.53-3.64 (m, 2 H, CH_2NH), 3.73-3.84 (m, 4 H, CH$_2$NC), 3.89 (s, 3 H, CH$_3$O), 4.11 (t, J = 6.7 Hz, 2 H, CH$_2$O), 5.77 (s, 1 H, NH), 6.84 (s, 1 H, CHCOCH$_2$), 6.98 (s, 1 H, CHCOCH$_3$). ^{13}C NMR (126 MHz, CD_2Cl_2): δ = 23.82 [CH$_2$CH$_2$N(CH$_2$)$_5$NH], 24.94 (CH$_2$CH$_2$CH$_2$NCH$_2$CH$_2$CH$_2$O), 25.17 (CH$_2$CH$_2$CH$_2$NH), 25.57 (CH$_2$CH$_2$CH$_2$NC), 26.41 (CH$_2$CH$_2$NCH$_2$CH$_2$CH$_2$O)*, 26.46 (CH$_2$CH$_2$NC)*, 27.05 (CH$_2$CH$_2$O), 28.02 [CH$_2$(CH$_2$)$_3$NH], 29.19 (CH$_2$CH$_2$NH), 41.36 (CH$_2$NH), 45.39 (CH$_2$NC), 54.41 [CH$_2$N(CH$_2$)$_5$NH], 55.00 (CH$_2$NCH$_2$CH$_2$CH$_2$O), 55.97 (CH$_2$CH$_2$CH$_2$O), 56.31 [CH$_2$(CH$_2$)$_4$NH], 56.96 (CH$_3$O), 67.57 (CH$_2$O), 102.41 (CHCOCH$_3$), 103.30 (CCNH), 106.82 (CHCOCH$_2$), 145.83 (COCH$_3$), 149.62 (CCCNH), 154.35 (COCH$_2$), 159.04 (CNCNH), 159.49 (CNH). HRMS-EI m/z $[M]^+$ calcd. for $C_{31}H_{50}N_6O_2$: 538.3995, found: 538.3989.

***N*^{1}-Cyclohexyl-*N*^{2}-{6-methoxy-7-[3-(piperidin-1-yl)propoxy]quinazolin-4-yl}-*N*^{1}-methylethane-1,2-diamine (2b):** R_f = 0.38 [10% (3 M NH_3 in MeOH) in CH_2Cl_2]. IR (film): $\tilde{\nu}$ = 3020, 1641, 1215 cm^{-1}. ^1H NMR (500 MHz, CD_2Cl_2): δ = 1.03-1.16 (m, 1 H, CH_2CH$_2$CH$_2$CHN), 1.19-1.37 (m, 4 H, CH_2CH_2CHN), 1.37-1.47 (m, 2 H, CH_2CH$_2$CH$_2$NCH$_2$CH$_2$CH$_2$O), 1.47-1.59 (m, 4 H, CH_2CH$_2$NCH$_2$CH$_2$CH$_2$O), 1.59-1.66 (m, 1 H, CH_2CH$_2$CH$_2$CHN), 1.77-1.87 (m, 4 H, CH_2CH_2CHN), 2.02 (p, J = 6.8 Hz, 2 H, CH_2CH$_2$O), 2.32 (s, 3 H, CH$_3$N), 2.34-2.43 (m, 4 H, CH_2NCH$_2$CH$_2$CH$_2$O), 2.43-2.52 (m, 3 H, CH_2CH$_2$CH$_2$O, CH$_2$CHN), 2.68-2.88 (m, 2 H, CH_2CH$_2$NH), 3.53-3.67 (m, 2 H, CH_2NH), 3.94 (s, 3 H, CH$_3$O), 4.16 (t, J = 6.7 Hz, 2 H, CH$_2$O), 6.50 (d, J = 13.6 Hz, 1 H, NH), 6.95 (s, 1 H, CHCOCH$_3$), 7.14 (s, 1 H, CHCOCH$_2$), 8.43 (s, 1 H, CHNCNH). ^{13}C NMR (126 MHz, CD_2Cl_2): δ = 24.97 (CH$_2$CH$_2$CH$_2$NCH$_2$CH$_2$CH$_2$O), 26.35 (CH$_2$CH$_2$CHN), 26.52 (CH$_2$CH$_2$NCH$_2$CH$_2$CH$_2$O), 26.68 (CH$_2$CH$_2$O), 27.02 (CH$_2$CH$_2$CH$_2$CHN), 29.26 (CH$_2$CHN), 37.08 (CH$_3$N), 38.38 (CH$_2$NH), 52.08 (CH$_2$CH$_2$NH), 55.03 (CH$_2$NCH$_2$CH$_2$CH$_2$O), 55.91 (CH$_2$CH$_2$CH$_2$O), 56.39 (CH$_3$O), 63.59 (CH$_2$$C$HN), 67.87 (CH$_2$O), 100.42 ($C$HCOCH$_3$), 108.83 ($C$HCOCH$_2$), 109.02 (14), 146.84 (15), 149.46 (12), 154.21 (11), 154.49 (CHNCNH), 158.65 (19). HRMS-ESI m/z $[M+H]^+$ calcd. for $C_{26}H_{42}N_5O_2$: 456.3339, found: 456.3334.

6-Methoxy-*N*-[3-(4-methylpiperazin-1-yl)butyl]-7-[3-(piperidin-1-yl)propoxy]quinazolin-4-amine (2c): mp.: 85 °C. R_f = 0.22 [10% (3 M NH_3 in MeOH) in CH_2Cl_2]. IR (film): $\tilde{\nu}$ = 2100, 1622, 1504, 1338, 1217 cm^{-1}. ^1H NMR (500 MHz, CD_2Cl_2): δ = 1.05 (d, J = 6.6 Hz, 3 H, CH_3CH), 1.37-1.49 (m, 2 H, CH_2CH$_2$CH$_2$NCH$_2$CH$_2$CH$_2$O), 1.51-1.61 (m, 4 H, CH_2CH$_2$NCH$_2$CH$_2$CH$_2$O), 1.65-1.97 (m, 2 H, CH_2CH$_2$NH), 1.98-2.08 (m, 2 H, CH_2CH$_2$O), 2.26 (s, 3 H, CH$_3$N), 2.28-2.62 (m, 12 H, CH_2CH_2NCH$_3$, CH_2NCH_2CH$_2$CH$_2$O), 2.64-2.77 (m, 2 H, CH_2CH$_2$NCH$_3$), 2.78-2.96 (m, 1 H, CHCH$_3$), 3.58-3.70 (m, 1 H, CH_2NH), 3.72-3.85 (m, 1 H, CH_2NH), 3.97 (s, 3 H, CH$_3$O), 4.17 (t, J = 6.6 Hz, 2 H, CH$_2$O), 6.71 (s, 1 H, NH), 7.05 (s, 1 H, CHCOCH$_3$), 7.15 (s, 1 H, CHCOCH$_2$), 8.43 (s, 1 H, CHNCNH). ^{13}C NMR (126 MHz, CD_2Cl_2): δ = 13.74 (CH$_3$CH), 24.92 (CH$_2$CH$_2$CH$_2$NCH$_2$CH$_2$CH$_2$O), 26.47 (CH$_2$CH$_2$NCH$_2$CH$_2$CH$_2$O), 26.98 (CH$_2$CH$_2$O), 32.20 (CH$_2$CH$_2$NH), 40.71 (CH$_2$NH), 46.07 (CH$_3$N), 48.75 (CH$_2$CH$_2$NCH$_3$), 55.01 (CH$_2$NCH$_2$CH$_2$CH$_2$O), 55.93 (CH$_2$NCH$_3$, CH$_2$CH$_2$CH$_2$O), 57.61 (CH$_3$O), 59.32 (CHCH$_3$), 67.81 (CH$_2$O), 102.33 (CHCOCH$_3$), 108.99 (CHCOCH$_2$), 109.06 (CCNH), 147.20 (CCCNH), 149.40 (COCH$_3$), 154.51 (CHNCNH, COCH$_2$), 158.94 (CNH). HRMS-ESI m/z $[M+H]^+$ calcd. for $C_{26}H_{43}N_6O_2$: 471.3447, found: 471.3443.

6-Methoxy-7-[3-(piperidin-1-yl)propoxy]-4-[4-(pyrrolidin-1-yl)piperidin-1-yl]quinazoline (2d): IR (film): $\tilde{\nu}$ = 2937, 1643, 1504, 1209 cm^{-1}. ^{1}H NMR (500 MHz, CD_2Cl_2): δ = 1.36-1.49 (m, 2 H, $CH_2CH_2CH_2NCH_2CH_2CH_2O$), 1.49-1.59 (m, 4 H, $CH_2CH_2NCH_2CH_2CH_2O$), 1.69-1.82 (m, 6 H, CH_2CHN, CH_2CH_2NCH), 1.98-2.10 (m, 4 H, CH_2CHN, CH_2CH_2O), 2.28 (tt, J = 10.2, 4.0 Hz, 1 H, $CHNCH_2$), 2.32-2.43 (m, 4 H, $CH_2NCH_2CH_2CH_2O$), 2.46 (t, J = 7.1 Hz, 2 H, $CH_2CH_2CH_2O$), 2.51-2.64 (m, 4 H, CH_2NCH), 3.04-3.15 (m, 2 H, CH_2NC), 3.94 (s, 3 H, CH_3O), 4.04-4.14 (m, 2 H, CH_2NC), 4.18 (t, J = 6.7 Hz, 2 H, CH_2O), 7.11 (s, 1 H, $CHCOCH_3$), 7.19 (s, 1 H, $CHCOCH_2$), 8.55 (s, 1 H, CHNCN). ^{13}C NMR (126 MHz, CD_2Cl_2): δ = 23.74 (CH_2CH_2NCH), 24.96 ($CH_2CH_2CH_2NCH_2CH_2CH_2O$), 26.52 ($CH_2CH_2NCH_2CH_2CH_2O$), 26.98 ($CH_2CH_2O$), 32.07 ($CH_2CHN$), 49.09 ($CH_2CH_2CHN$), 51.78 ($CH_2NCH$), 55.03 ($CH_2NCH_2CH_2CH_2O$), 55.89 ($CH_2CH_2CH_2O$), 56.31 ($CH_3O$), 62.21 ($CHNCH_2$), 67.92 ($CH_2O$), 103.89 ($CHCOCH_3$), 108.49 ($CHCOCH_2$), 111.84 ($CCHCOCH_3$), 149.03 ($COCH_3$), 149.47 ($CCCNCH_2$), 153.34 ($CHNCN$), 154.41 ($COCH_2$), 164.49 ($CNCH_2$). HRMS-ESI m/z $[M+H]^+$ calcd. for $C_{26}H_{40}N_5O_2$: 454.3182, found: 454.3177.

***N*-[1-(Azepan-1-yl)-2-methylpropan-2-yl]-6-methoxy-7-[3-(piperidin-1-yl)propoxy]quinazolin-4-amine (2e):** Hygroscopic. R_f = 0.30 [5% (7 M NH_3 in MeOH) in CH_2Cl_2]. IR (film): $\tilde{\nu}$ = 2926, 1643, 1498 cm^{-1}. ^{1}H NMR (500 MHz, CD_2Cl_2): δ = 1.38-1.47 (m, 2 H, $CH_2CH_2CH_2NCH_2CH_2CH_2O$), 1.52-1.62 (m, 10 H, CH_3C, $CH_2CH_2NCH_2CH_2CH_2O$), 1.62-1.78 (m, 8 H, $CH_2CH_2CH_2NCH_2CNH$), 2.03 (p, J = 6.9 Hz, 2 H, CH_2CH_2O), 2.26-2.46 (m, 4 H, $CH_2NCH_2CH_2CH_2O$), 2.46-2.57 (m, 2 H, $CH_2CH_2CH_2O$), 2.75 (s, 2 H, CH_2CNH), 2.82-2.96 (m, 4 H, CH_2NCH_2CNH), 3.95 (s, 3 H, CH_3O), 4.16 (t, J = 6.6 Hz, 2 H, CH_2O), 6.84 (s, 1 H, NH), 6.93 (s, 1 H, $CHCOCH_3$), 7.12 (s, 1 H, $CHCOCH_2$), 8.40 (s, 1 H, $CHNCNH$). ^{13}C NMR (126 MHz, CD_2Cl_2): δ = 24.91 ($CH_2CH_2CH_2NCH_2CH_2CH_2O$), 25.77 ($CH_3C$), 26.45 ($CH_2CH_2NCH_2CH_2CH_2O$), 26.97 ($CH_2CH_2O$), 27.51 ($CH_2CH_2CH_2NCH_2CNH$), 29.59 ($CH_2CH_2NCH_2CNH$), 54.36 ($CH_3C$), 55.00 ($CH_2NCH_2CH_2CH_2O$), 55.91 ($CH_2CH_2CH_2O$), 56.38 ($CH_3O$), 58.82 ($CH_2NCH_2CNH$), 67.81 ($CH_2O$), 69.97 ($CH_2CNH$), 100.45 ($CHCOCH_3$), 109.02 ($CHCOCH_2$), 109.86 ($CCNH$), 146.93 ($CCCNH$), 149.32 ($COCH_3$), 153.88 ($COCH_2$), 154.04 ($CHNCNH$), 158.64 (NCNH). HRMS-ESI m/z $[M+H]^+$ calcd. for $C_{27}H_{44}N_5O_2$: 470.3495, found: 470.3492.

***N*-(1-Propan-2-ylpiperidin-4-yl)-6-methoxy-7-[3-(piperidin-1-yl)propoxy]quinazolin-4-amine (2f):** mp.: 166 °C. R_f = 0.18 [10% (4 M NH_3 in MeOH) in CH_2Cl_2]. IR (film): $\tilde{\nu}$ = 2933, 1593, 1506, 1254 cm^{-1}. ^{1}H NMR (500 MHz, CD_3OD): δ = 1.14 (d, J = 6.6 Hz, 6 H, CH_3CH), 1.45-1.56 (m, 2 H, $CH_2CH_2CH_2NCH_2CH_2CH_2O$), 1.57-1.69 (m, 4 H, $CH_2CH_2NCH_2CH_2CH_2O$), 1.69-1.81 (m, 2 H, CH_2CHNH), 2.04-2.18 (m, 4 H, CH_2CH_2O, CH_2CHNH), 2.38-2.48 (m, 2 H, CH_2NCH), 2.48-2.60 (m, 4 H, $CH_2NCH_2CH_2CH_2O$), 2.60-2.69 (m, 2 H, $CH_2CH_2CH_2O$), 2.82 (hept, J = 6.5 Hz, 1 H, CH_3CH), 2.98-3.09 (m, 2 H, CH_2NCH), 3.97 (s, 3 H, CH_3O), 4.09-4.30 (m, 3 H, CH_2O, $CHNH$), 7.07 (s, 1 H, CHCN), 7.60 (s, 1 H, CHCCN), 8.30 (s, 1 H, CHNCNH). ^{13}C NMR (126 MHz, CD_3OD): δ = 18.47 (CH_3CH), 25.04 ($CH_2CH_2CH_2NCH_2CH_2CH_2O$), 26.38 ($CH_2CH_2NCH_2CH_2CH_2O$), 27.00 ($CH_2CH_2O$), 32.37 ($CH_2CHNH$), 48.83 ($CH_2NCH$), 49.84 ($CHNH$), 55.46 ($CH_2NCH_2CH_2CH_2O$), 56.06 ($CH_3CH$), 56.82 ($CH_3O$), 57.00 ($CH_2CH_2CH_2O$), 68.32 ($CH_2O$), 102.94 ($CHCCN$), 107.81 ($CHCN$), 110.17 ($CCNH$), 146.65 ($CCCNH$), 150.87 ($CH_3OC$), 154.28 ($CHNCNH$), 155.48 ($CH_2OC$), 159.65 (CNH). HRMS-ESI m/z $[M+H]^+$ calcd. for $C_{25}H_{40}N_5O_2$: 442.3182, found: 442.3175.

***N*-(1-Propan-2-ylpiperidin-4-yl)-6-methoxy-7-[3-(piperidin-1-ylmethyl)pyrrolidin-1-yl]quinazolin-4-amine (2g):** mp.: 244 °C. R_f = 0.35 [10% (3 M NH_3 in MeOH) in CH_2Cl_2]. IR (film): $\tilde{\nu}$ = 2935, 1612, 1504, 1363 cm^{-1}. ^{1}H NMR (500 MHz, CD_2Cl_2): δ = 1.04 (d, J = 6.6 Hz, 6 H, CH_3CH), 1.33-1.47 (m, 2 H, $CH_2CH_2CH_2N$), 1.47-1.60 (m, 6 H, $CH_2CH_2CH_2N$, CH_2CHNH), 1.60-1.78 (m, 1 H, $CH_2CH_2CHCH_2N$), 2.02-2.09 (m, 1 H, $CH_2CH_2CHCH_2N$), 2.09-2.17 (m, 2 H, CH_2CHNH), 2.19-2.44 (m, 8 H, $CH_2NCH_2CHCH_2N$,

C*H*$_2$CH$_2$CHNH), 2.49 (hept, *J* = 7.0 Hz, 1 H, C*H*CH$_2$N), 2.76 (hept, *J* = 6.4 Hz, 1 H, CH$_3$C*H*), 2.83-2.93 (m, 2 H, C*H*$_2$CH$_2$CHNH), 3.26 (dd, *J* = 10.2, 7.2 Hz, 1 H, CHC*H*$_2$NC), 3.51-3.62 (m, 3 H, C*H*$_2$NC), 3.90 (s, 3 H, CH$_3$O), 4.10-4.26 (m, 1 H, C*H*NH), 5.01-5.18 (m, 1 H, NH), 6.76 (s, 1 H, C*H*COCH$_3$), 6.79 (s, 1 H, C*H*CNCH$_2$), 8.34 (s, 1 H, CHNC). ^{13}C NMR (126 MHz, CD_2Cl_2): δ = 18.46 (*C*H$_3$CH), 24.97 (*C*H$_2$CH$_2$CH$_2$N), 26.55 (CH$_2$*C*H$_2$CH$_2$N), 30.45 (*C*H$_2$CHCH$_2$N), 33.37 (*C*H$_2$CHNH), 36.58 (*C*HCH$_2$N), 48.05 (*C*H$_2$CH$_2$CHNH), 48.85 (CHNH), 50.56 (*C*H$_2$CH$_2$CHCH$_2$N), 54.85 (CH$_3$*C*H), 55.41 (CH$_2$CH$_2$*C*H$_2$N), 55.84 (CN*C*H$_2$CH), 56.33 (CH$_3$O), 63.20 (*C*H$_2$CHCH$_2$NC), 100.12 (*C*HCOCH$_3$), 106.53 (*C*CNH), 109.46 (*C*HCNCH$_2$), 145.49 (*C*NCH$_2$), 147.48 (*C*CCNH), 150.16 (*C*OCH$_3$), 154.18 (*C*HNCNH), 157.71 (CNH). HRMS-ESI m/z [M+H]$^+$ calcd. for $C_{27}H_{43}N_6O$: 467.3498; found: 467.3489.

4-Chloro-6-methoxy-2-(piperidin-1-yl)-7-[3-(piperidin-1-yl)propoxy]quinazoline (8): mp.: 138 °C. R_f = 0.35 (15% MeOH in CH_2Cl_2 IR (film): ṽ = 2931, 1626, 1585, 1495, 1238, 754 cm^{-1}. ^{1}H NMR (500 MHz, CD_3OD): δ = 1.59-1.70 (m, 6 H, C*H*$_2$CH$_2$CH$_2$NCH$_2$CH$_2$CH$_2$O, C*H*$_2$CH$_2$NC), 1.70-1.77 (m, 2 H, C*H*$_2$CH$_2$CH$_2$NC), 1.77-1.89 (m, 4 H, C*H*$_2$CH$_2$NCH$_2$CH$_2$CH$_2$O), 2.15-2.37 (m, 2 H, C*H*$_2$CH$_2$O), 2.87-3.17 (m, 6 H, C*H*$_2$NC*H*$_2$CH$_2$CH$_2$O), 3.81-3.88 (m, 4 H, CH$_2$NC), 3.95 (s, 3 H, CH$_3$O), 4.25 (t, *J* = 5.8 Hz, 2 H, CH$_2$O), 7.00 (s, 1 H, CHCOCH$_2$), 7.26 (s, 1 H, C*H*COCH$_3$). ^{13}C NMR (126 MHz, CD_3OD): δ = 23.72 (*C*H$_2$CH$_2$CH$_2$NCH$_2$CH$_2$CH$_2$O), 25.29 (*C*H$_2$CH$_2$NCH$_2$CH$_2$CH$_2$O), 25.74 (*C*H$_2$CH$_2$O)*, 25.92 (*C*H$_2$CH$_2$CH$_2$NC)*, 26.88 (*C*H$_2$CH$_2$NC), 46.31 (*C*H$_2$NC), 55.01 (*C*H$_2$NCH$_2$CH$_2$CH$_2$O), 56.54 (CH$_3$O), 56.73 (*C*H$_2$CH$_2$CH$_2$O), 68.09 (CH$_2$O), 104.82 (*C*HCOCH$_3$), 106.56 (*C*HCOCH$_2$), 113.18 (*C*CCl), 148.82 (*C*OCH$_3$), 152.67 (*C*CCCl), 157.42 (*C*OCH$_2$), 158.93 (*C*NCH$_2$), 160.90 (CCl). HRMS-ESI m/z [M+H]$^+$ calcd. for $C_{22}H_{32}ClN_4O_2$: 419.224, found: 419.2206.

4-Chloro-6-methoxy-7-[3-(piperidin-1-yl)propoxy]quinazoline (9) [5, 6]**:** mp.: 106 °C. R_f = 0.21 [5% (4 M NH_3 in MeOH) in CH_2Cl_2]. IR (film): ṽ = 2933, 2358, 1500, 1232, 1020 cm^{-1}. ^{1}H NMR (500 MHz, DMSO-d_6) δ = 1.31-1.43 (m, 2 H, C*H*$_2$CH$_2$CH$_2$NCH$_2$CH$_2$CH$_2$O), 1.45-1.54 (m, 4 H, C*H*$_2$CH$_2$NCH$_2$CH$_2$CH$_2$O), 1.95 (p, *J* = 6.7 Hz, 2 H, C*H*$_2$CH$_2$O), 2.26-2.38 (m, 4 H, C*H*$_2$NCH$_2$CH$_2$CH$_2$O), 2.38-2.43 (m, 2 H, C*H*$_2$CH$_2$CH$_2$O), 4.00 (s, 3 H, CH$_3$O), 4.25 (t, *J* = 6.4 Hz, 2 H, CH$_2$O), 7.38 (s, 1 H, CHCN), 7.44 (s, 1 H, CHCCN), 8.86 (s, 1 H, CHN). ^{13}C NMR (126 MHz, DMSO-d_6) δ = 24.13 (*C*H$_2$CH$_2$CH$_2$NCH$_2$CH$_2$CH$_2$O), 25.60 (*C*H$_2$CH$_2$NCH$_2$CH$_2$CH$_2$O), 25.92 (*C*H$_2$CH$_2$O), 54.11 (*C*H$_2$NCH$_2$CH$_2$CH$_2$O), 54.93 (*C*H$_2$CH$_2$CH$_2$O), 56.21 (*C*H$_3$O), 67.65 (CH$_2$O), 102.30 (*C*HCCN), 107.32 (*C*HCN), 118.48 (*C*CCl), 148.60 (*C*CCCl), 151.49 (CH$_3$O*C*), 152.19 (CHN), 156.11 (CH$_2$O*C*), 157.84 (CCl). HRMS-ESI m/z [M+H]$^+$ calcd. for $C_{17}H_{23}ClN_3O_2$: 336.1479, found: 336.1476. The analytical data agree with those previously reported in the literature [5, 6].

7-Fluoro-*N*-(1-propan-2-ylpiperidin-4-yl)-6-methoxyquinazolin-4-amine (10): mp.: 233 °C (decomposition). R_f = 0.48 [10% (3 M NH_3 in MeOH) in CH_2Cl_2]. IR (film): ṽ = 2968, 1593, 1537, 1045 cm^{-1}. ^{1}H NMR (500 MHz, CD_2Cl_2): δ = 1.04 (d, *J* = 6.6 Hz, 6 H, C*H*$_3$CH), 1.52-1.64 (m, 2 H, C*H*$_2$CHNH), 2.11-2.20 (m, 2 H, C*H*$_2$CHNH), 2.31-2.42 (m, 2 H, C*H*$_2$CH$_2$CHNH), 2.71-2.84 (m, 1 H, CH$_3$C*H*), 2.83-2.96 (m, 2 H, C*H*$_2$CH$_2$CHNH), 4.00 (s, 3 H, CH$_3$O), 4.15-4.31 (m, 1 H, C*H*NH), 5.43 (d, *J* = 7.6 Hz, 1 H, NH), 7.02 (d, *J* = 8.6 Hz, 1 H, C*H*COCH$_3$), 7.44 (d, *J* = 12.0 Hz, 1 H, CHCF), 8.48 (s, 1 H, C*H*NCNH). ^{13}C NMR (126 MHz, CD_2Cl_2): δ = 18.43 (*C*H$_3$CH), 33.01 (*C*H$_2$CHNH), 48.00 (*C*H$_2$CH$_2$CHNH), 49.23 (CHNH), 54.86 (CH$_3$*C*H), 56.96 (CH$_3$O), 102.29 (d, *J* = 3.5 Hz, *C*HCOCH$_3$), 111.90 (*C*CNH), 114.04 (d, *J* = 17.6 Hz, *C*HCF), 146.26 (d, *J* = 12.0 Hz, *C*CHCF), 147.82 (d, *J* = 13.0 Hz, *C*OCH$_3$), 154.79 (*C*HNCNH), 156.64 (d, *J* = 255.1 Hz, CF), 158.12 (CNH). HRMS-ESI m/z [M+H]$^+$ calcd. for $C_{17}H_{24}FN_4O$: 319.1934, found: 319.1929.

Supplemental References

1. Chevillard, F., et al., *Binding-Site Compatible Fragment Growing Applied to the Design of beta2-Adrenergic Receptor Ligands.* J. Med. Chem., 2018. **61**(3): p. 1118-1129.
2. *ROCS 3.4.1.0*. OpenEye Scientific Software: Santa Fe, NM.
3. Chemical Computing Group, U., *Molecular Operating Environment (MOE)*. 2021: 1010 Sehrbooke St. West, Suite #910, Montreal, QC, Canada, H3A, 2R7.
4. Roe, D.R. and T.E. Cheatham, 3rd, *PTRAJ and CPPTRAJ: Software for Processing and Analysis of Molecular Dynamics Trajectory Data.* J. Chem. Theory Comput., 2013. **9**(7): p. 3084-95.
5. Hennequin, L.F., et al., *Quinazoline Derivatives as Angiogenesis Inhibitors (WO-2000047212-A1)*, W.I.P. Organization, Editor. 2000.
6. Ravez, S., et al., *Inhibition of tumor cell growth and angiogenesis by 7-Aminoalkoxy-4-aryloxy-quinazoline ureas, a novel series of multi-tyrosine kinase inhibitors.* Eur. J. Med. Chem., 2014. **79**: p. 369-381.

3.4 Vierte Publikation

„Synthesis and Biological Evaluation of Novel MB327 Analogs as Resensitizers for Desensitized Nicotinic Acetylcholine Receptors after intoxication with Nerve Agents"

3.4.1 Zusammenfassung der Ergebnisse

Bispyridiniumverbindungen, allen voran MB327, gelten als die bisher am besten untersuchten Verbindungen im Rahmen der Entwicklung neuer sogenannter „Resensitizer". Die Forschung an diesen Verbindungen ist von großer Bedeutung, da sie die Therapie von Organophosphatvergiftungen, welche z.B. bei Exposition gegenüber Nervenkampfstoffen auftreten, erheblich verbessern könnten. Die Besonderheit dieser Wirkstoffe besteht darin, dass sie den nikotinischen Acetylcholinrezeptor (nAChR) durch allosterische Modulation von einem desensitisierten, nicht-funktionalen Zustand zurück in einen funktionalen Zustand bringen können. Im Idealfall erlangen die aufgrund von desensitisierten nAChRs paralysierten Muskel, welche zu fatalen Vergiftungssymptomen wie z.B. Atemstillstand führen können, so ihre Funktionalität zurück. Von den bisher untersuchten Bispyridiniumverbindungen zeigen bereits einige einen solchen Muskelkraft-wiederherstellenden Effekt. Allerdings schließen die hierfür erforderlichen, hohen Substanzkonzentrationen und die damit zusammenhängende geringe therapeutische Breite die Verwendung von MB327 und dessen Analoga als Wirkstoffe aus. Deshalb zielten weitere Bestrebungen auf eine Optimierung der Affinität und intrinsischen Aktivität von MB327-Analoga gegenüber der allosterischen MB327-PAM-1-Bindungsstelle am nAChR ab. Zuletzt sind einige asymmetrische Bispyridiniumverbindungen aufgefallen, die eine Aminofunktion in der 4-Position an einer der beiden Pyridinium-Untereinheiten tragen und dabei eine vergleichsweise hohe Muskelkraft-wiederherstellende Aktivität besitzen.

Im Rahmen der in diesem Manuskript beschriebenen Studie wurden weitere zu dieser Gruppe von Substanzen analoge Verbindungen synthetisiert und sowohl hinsichtlich ihres Muskelkraft-wiederherstellenden Effekts als auch hinsichtlich ihrer Affinität zur MB327-PAM-1-Bindungsstelle charakterisiert. Hierfür wurde einmal, für die Bestimmung der intrinsischen Aktivität, ein auf Soman-vergifteten Rattendiaphragmen basierendes Testsystem verwendet und zudem für die Affinitätsbestimmung der kürzlich entwickelte UNC0642-MS-Bindungsassay. Von den neun neu synthetisierten

Analoga fielen vor allem drei (PTM0069, PTM0071 und PTM0072) bei der Untersuchung ihrer Aktivität am Soman-vergifteten Muskel auf. Im Gegensatz zu den bisher untersuchten Bispyridiniumverbindungen zeigten PTM0069, PTM0071 und PTM0072 bereits bei zweistellig mikromolaren Testkonzentrationen einen beachtlichen Muskelkraft-wiederherstellenden Effekt. Um einen vergleichbaren Effekt mit MB327 zu bewirken, muss dieses in einer etwa zehnfach höheren Konzentration eingesetzt werden. Interessanterweise korreliert die erhöhte intrinsische Aktivität für PTM0069 und PTM0071 auch mit einer erhöhten Affinität zur MB327-PAM-1-Bindungsstelle. Im Vergleich zu MB327 waren die in dieser Arbeit ermittelten pK_i-Werte für PTM0069 und PTM0071 um etwa 0.5 bzw. 0.8 log-Einheiten höher.

Ähnlich wie bei bereits untersuchten Bispyridiniumverbindungen ist für die neu synthetisierten Substanzen zu beobachten, dass die Muskelkraft in den Rattendiaphragmen-basierten *ex vivo* Versuchen nach initialer Wiederherstellung wieder sinkt, wenn die Konzentration der Testverbindung weiter erhöht wird. Um diesem Phänomen weiter nachzugehen, wurden in dieser Arbeit erstmalig entsprechende Versuche mit Bispyridiniumverbindungen am nicht-vergifteten Muskel durchgeführt. Interessanterweise legen die Ergebnisse dieser Experimente nahe, dass die Bispyridiniumverbindungen in relativ hohen Konzentrationen einen negativen Effekt auf die Muskelkraft haben können. Es ist deshalb anzunehmen, dass der bei den Experimenten mit Soman-vergifteten Rattendiaphragmen beobachtete, biphasische Verlauf der Muskelkraftwiederherstellung auf zwei gegenläufige Effekte zurückgeht.

Zusätzlich zu den MB327-Analoga mit einer zusätzlichen Aminofunktion umfasst diese Arbeit auch die Synthese und die biologische Charakterisierung von zwei weiteren neuen MB327-Analoga. Die Strukturvorschläge für diese Verbindungen gehen auf *in silico* Versuche zurück. Beide Verbindungen, PTMD90-0012 und PTMD90-0015, zeigen einen Muskelkraft-wiederherstellenden Effekt, wenngleich dieser nicht so hoch wie bei den oben beschriebenen Bispyridiniumverbindungen mit zusätzlicher Aminofunktion ist. Die *in silico* Experimente, die zur Identifizierung der beiden Verbindungen geführt hatten, legen nahe, dass bei der Bindung der Substanzen Wasser aus der Bindetasche verdrängt wird. Im Einklang damit wurde für PTMD90-0012 ein im Vergleich zu MB327 um etwa 0.3 log-Einheiten höherer pK_i-Wert gefunden.

3.4.2 Erklärung zum Eigenanteil

Die neuen Testverbindungen wurden von Tamara Bernauer synthetisiert. Für die *in silico* Experimente war Jesko Kaiser verantwortlich und Thomas Seeger für die *ex vivo* Versuche. Die in dieser Publikation beschriebenen MS-Bindungsexperimente wurden von mir eigenständig durchgeführt und ausgewertet. Das Manuskript hat Tamara Bernauer erstellt, einschließlich des Abschnitts zur Interpretation der Ergebnisse der MS-Bindungsstudien, bei dem sie von mir unterstützt wurde. Die Abschnitte inklusive Grafiken und Tabellen zu den *in silico* Experimenten und den *ex vivo* Versuchen wurden von Jesko Kaiser bzw. Thomas Seeger verfasst. Unter Beteiligung von Christoph G. W. Gertzen und Georg Höfner geht die Interpretation der Ergebnisse maßgeblich auf Tamara Bernauer, Jesko Kaiser, Thomas Seeger und mich zurück und erfolgte in enger Abstimmung mit Holger Gohlke, Klaus T. Wanner und Franz F. Paintner, die auch die Korrektur übernahmen. Zur Korrektur haben ferner Karin. V. Niessen, Dirk Steinritz und Franz Worek beigetragen.

Synthesis and Biological Evaluation of Novel MB327 Analogs as Resensitizers for Desensitized Nicotinic Acetylcholine Receptors after Intoxication with Nerve Agents

Tamara Bernauer[a], Valentin Nitsche[a], Jesko Kaiser[b], Christoph G.W. Gertzen[b], Georg Höfner[a], Karin V. Niessen[c], Thomas Seeger[c], Dirk Steinritz[c], Franz Worek[c], Holger Gohlke[b,d], Klaus T. Wanner[a] and Franz F. Paintner*[a]

[a] Department of Pharmacy - Center for Drug Research
Ludwig-Maximilians-Universität München
Butenandtstraße 5-13, 81377 Munich (Germany)
E-mail: Franz.Paintner@cup.uni-muenchen.de

[b] Institute for Pharmaceutical and Medicinal Chemistry
Heinrich Heine Universität Düsseldorf
Universitätsstraße 1, 40225 Düsseldorf (Germany)

[c] Bundeswehr Institute of Pharmacology and Toxicology
Neuherbergstraße 11, 80937 Munich (Germany)

[d] John von Neumann Institute for Computing (NIC), Jülich Supercomputing Centre (JSC), Institute of Biological Information Processing (IBI-7: Structural Biochemistry) & Institute of Bio- and Geosciences (IBG-4: Bioinformatics)
Forschungszentrum Jülich
Wilhelm-Johnen-Straße, 52428 Jülich (Germany)

Author ORCID

Tamara Bernauer: 0000-0001-9570-1253

Valentin Nitsche: 0009-0000-3351-1227

Jesko Kaiser: 0000-0002-6429-0911

Christoph Gertzen: 0000-0002-9562-7708

Georg Höfner: 0000 0002 7957 4503

Karin Niessen: 0009-0008-6810-5294

Thomas Seeger: 0009-0007-5713-4367

Dirk Steinritz: 0000-0002-2073-5683

Franz Worek: 0000-0003-3531-3616

Holger Gohlke: 0000-0001-8613-1447

Klaus Wanner: 0000-0003-4399-1425

Franz Paintner: 0000-0002-6795-586X

Abstract

Poisoning with organophosphorus compounds, which can lead to a cholinergic crisis due to the inhibition of acetylcholinesterase and the subsequent accumulation of acetylcholine (ACh) in the synaptic cleft, is a serious problem for which treatment options are currently insufficient. Our approach to broadening the therapeutic spectrum is to use agents that interact directly with desensitized nicotinic acetylcholine receptors (nAChRs) in order to induce functional recovery after ACh overstimulation. Although MB327, one of the most prominent compounds investigated in this context, has already shown positive properties in terms of muscle force recovery, this compound is not suitable for use as a therapeutic agent due to its insufficient potency. By means of *in silico* studies based on our recently presented allosteric binding pocket at the nAChR, i.e. the MB327-PAM-1 binding site, three promising 4-aminopyridinium ion-substituted MB327 analogs (PTM0056, PTM0062 and PTM0063) were identified. In this study, we present the synthesis and biological evaluation of a series of new 4-aminopyridinium ion-substituted analogs of the aforementioned compounds (PTM0064-PTM0072), as well as hydroxy-substituted analogs of MB327 (PTMD90-0012 and PTMD90-0015) designed to substitute energetically unfavorable water clusters identified during molecular dynamics simulations. The compounds were characterized in terms of their binding affinity towards the aforementioned binding site by applying the UNC0642 MS Binding Assays and in terms of their muscle force reactivation in rat diaphragm myography. More potent compounds were identified compared to MB327, as some of them showed a higher affinity towards MB327-PAM-1 and also a higher recovery of neuromuscular transmission at lower compound concentrations. To improve the treatment of organophosphate poisoning, direct targeting of nAChRs with appropriate compounds is a key step, and this study is an important contribution to this research.

1 Introduction

The verified use of sarin in the Syrian war in 2013 (Dolgin, 2013; Pita and Domingo, 2014) and 2017 (OPCW, 2017), as well as the politically motivated Novichok attack on Russian opposition politician Alexei Navalny in 2020 (Steindl et al., 2021), provide clear evidence that highly toxic organophosphorus nerve agents still pose a major threat to military personnel and civilians, even after their international ban by the Chemical Weapons Convention in 1997 (Thakur and Haru, 2007). Intoxication with organophosphorus compounds (OPCs) leads to the irreversible inhibition of acetylcholinesterase (AChE), resulting in an uncontrolled accumulation of acetylcholine (ACh) in the synaptic cleft of cholinergic neurons. As a result, cholinergic signaling is disrupted by overstimulation of muscarinic and nicotinic acetylcholine receptors (mAChRs and nAChRs, respectively) (Koelle, 1981; Maselli and Leung, 1993; Massoulié et al., 1993). This condition, known as a “cholinergic crisis”, can be life-threatening due to respiratory paralysis as a result of the disruption of nAChR-mediated neuromuscular transmission (Brown and Brix, 1998; Thiermann et al., 2010). Standard treatment for nerve agent poisoning currently includes a muscarinic acetylcholine receptor antagonist, e.g. atropine, to reduce mAChR overstimulation and an oxime-based AChE reactivator, e.g. obidoxime. According to Sheridan et al. (Sheridan et al., 2005) neuromuscular blockers (competitive nAChR antagonists) are not suitable for the treatment of nerve agent poisoning. Hence, reactivation of inhibited AChE appears to be crucial to counteract nicotinic overstimulation. However, despite decades of effort, there is still no universally applicable AChE reactivator that can efficiently cleave all OPC-AChE conjugates (Worek et al., 2020).

Therefore, there is an urgent need to develop novel antidotes to counteract desensitization of muscle-type nAChRs as a result of overstimulation. One approach is to use agents that directly target the nAChR to restore its function after it has been desensitized by overstimulation (Sheridan et al., 2005; Turner et al., 2011).

Indeed, a number of bispyridinium salts, such as the prototypical compound MB327 (Figure 1), are able to restore the function of desensitized nAChR of *Torpedo californica* (recently reclassified as *Tetronarce californica*) in *in vitro* experiments by interacting directly with the receptor most likely via an allosteric mechanism (Niessen et al., 2016; Niessen et al., 2018; Seeger et al., 2012; Sichler et al., 2018). Since the *Torpedo californica* nAChR has a high sequence identity to the rat and human muscle-type nAChRs, it is reasonable to assume that MB327 has similar effects on the desensitized nAChRs of the latter species as well. Indeed, in *ex vivo* experiments, MB327 shows a muscle force-restoring effect on both soman-poisoned rat diaphragms and soman-poisoned human intercostal muscles, which is thought to be due to the resensitization of desensitized nAChR (Niessen et al., 2018; Seeger et al., 2012). In addition, MB327 (or the corresponding methanesulfonate salt MB399, respectively) in combination with the mAChR antagonist hyoscine and the indirect parasympathomimetic physostigmine, was shown to increase the survival rates of guinea pigs poisoned with sarin or tabun in *in vivo* studies (Timperley et al., 2012; Turner et al., 2011). Despite these promising results, MB327 is not suitable for human use due to its narrow therapeutic window. Nevertheless, MB327 is a promising starting point for further investigation.

Recently, based on blind docking experiments and molecular dynamics simulations, we proposed a new allosteric binding site of MB327 at the muscle-type nAChR, termed MB327-PAM-1 (Kaiser et al., 2023). This binding site is located at the transition from the extracellular to the trans-membrane region and, according to a rigidity analysis, is expected to exert an allosteric effect on the orthosteric binding pocket upon binding of MB327. The amino acids interacting with MB327 in this binding site, predominantly glutamate residues, are highly conserved within the different nAChR subunits as well as in different species. Accordingly, comparable resensitizing effects of MB327 should be observable on desensitized nAChR of different species (e.g. *Torpedo californica*, rats and humans).

However, recently published results also show that bispyridinium compounds related to MB327 have inhibitory activity on the nAChR, most likely mediated via the orthosteric binding site (Epstein et al., 2021). Indeed, free ligand diffusion MD simulations performed by us indicated that MB327 also has affinity for the orthosteric binding site (Kaiser et al., 2023). The fact that the muscle force restoring activity of MB327 on soman-poisoned rat diaphragms is lost at higher concentrations after a peak at 300 µM may be explained by this inhibitory activity (Niessen et al., 2018).

The binding mode of MB327 in the MB327-PAM-1 binding pocket indicates that one of the two *tert*-butyl groups projects into a polar region of the binding pocket. This allowed us to predict structural modifications of MB327 that led to the more potent resensitizers PTM0062 (**1**) and PTM0063 (**2**), which have a more polar substituent, i.e., an amino and a methylamino group, respectively, instead of one of the two *tert*-butyl residues of MB327 (Figure 1) (Kaiser et al., 2023). Interestingly, the recently described dimethylamino analog PTM0056 (**3**) (Figure 1), which has a less polar substituent than PTM0062 (**1**) or PTM0063 (**2**), also shows a slightly higher affinity for the MB327-PAM-1 binding site than MB327 (Rappenglück et al., 2018) and a muscle force-restoring activity comparable to PTM0062 (**1**) and PTM0063 (**2**) in

preliminary, unpublished *ex vivo* studies with soman-poisoned rat diaphragm hemispheres. Therefore, PTM0056 (**3**) appeared to be a promising starting point for the development of new, possibly even more potent, resensitizers for the desensitizied muscle-typ nAChR.

In this study, we report the development of a series of non-symmetric MB327 analogs derived from PTM0062 (**1**), PTM0063 (**2**) and PTM0056 (**3**), respectively, as resensitizers for desensitized muscle-type nAChRs. To obtain a structurally diverse set of analogs, the 4-amino substituents of compounds **1**-**3** were replaced by either acylamino groups, new dialkylamino groups or cyclic amino groups (e.g. pyrrolidino, piperidino, morpholino and piperazino groups). Furthermore, based on identifying energetically unfavorable water clusters in MB327-PAM-1 using molecular dynamics (MD) simulations in combination with Grid Inhomogeneous Solvent Theory (GIST) computations (Lazaridis, 1998; Nguyen et al., 2011; Nguyen et al., 2012; Ramsey et al., 2016), we designed novel MB327 analogs potentially able to substitute these water clusters. To determine the affinities of the newly developed compounds at the MB327-PAM-1 binding site of *Torpedo*-nAChR, our recently developed UNC0642 MS Binding Assays were applied. To gain insight into the intrinsic activity of some selected representatives of the newly developed compounds, their ability to restore muscle force was also investigated in *ex vivo* experiments with soman-poisoned rat diaphragms. Some of the newly developed compounds showed a slightly higher affinity for the MB327-PAM-1 binding site of *Torpedo*-nAChR than the prototypical compound MB327 and a comparable or even higher muscle force-restoring effect on soman-poisoned rat diaphragms at lower concentrations than MB327.

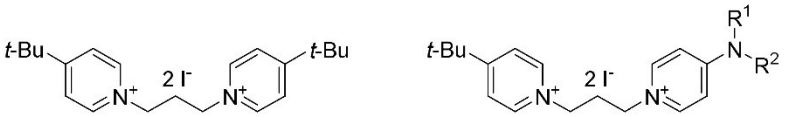

MB327

PTM0062 (**1**): $R^1 = R^2 = H$
PTM0063 (**2**): $R^1 = CH_3$, $R^2 = H$
PTM0056 (**3**): $R^1 = R^2 = CH_3$

Figure 1. Chemical structures: MB327, PTM0062 (**1**), PTM0063 (**2**) and PTM0056 (**3**).

2 Material and Methods

2.1 Synthesis of novel MB327 analogs

Microwave reactions were carried out on a Discover SP microwave system by *CEM GmbH* in glass vials. All chemicals were used as purchased from commercial sources. Solvents used for crystallization were distilled before use. Melting points were determined with a Büchi 510 melting point apparatus and are uncorrected. For IR spectroscopy, an FT-IR Spectrometer 1600 from *PerkinElmer* was used. High-resolution mass spectrometry was performed on a Finnigan MAT 95 (EI) or a Finnigan LTQ FT (ESI). ^{1}H and ^{13}C NMR spectra were recorded on a Bruker BioSpin Avance III HD 400 and 500 MHz at 25 °C. For data processing, MestReNova (Version 14.1.0) from Mestrelab Research S.L. 2019, and for calibration, the solvent signal (CD_3OD) was used. Using PTM0064 (**6a**) as an example, the signal assignment in the NMR spectra of the bispyridinium compounds is shown (see Supporting information). Unless otherwise noted, the purity of the test compounds was ≥ 98%, determined using quantitative ^{1}H NMR spectroscopy using TraceCERTS® ethyl 4-(dimethylamino)benzoate from *Sigma Aldrich* as internal calibrant (Cushman et al., 2014; Pauli et al., 2014).

All target compounds synthesized in the context of this study were cataloged with a certain PTM and PTMD number, respectively (Pharmacy and Toxicology Munich and Pharmacy and Toxicology Munich and Düsseldorf, respectively).

General Procedure (GP): Synthesis of non-symmetric MB327 analogs by *N*-alkylation with 4

A solution of 4-(*tert*-butyl)-1-(3-iodopropyl)pyridin-1-ium iodide (**4**) (Rappenglück et al., 2018) (1.0 equiv) and the corresponding 4-amino-substituted pyridine **5** (1.05-1.1 equiv) or 7-hydroxychinoline (**7**) in acetonitrile (2.0-2.7 mL/mmol) was stirred at 90 °C under microwave irradiation (150 W) for 1 h unless otherwise stated. The reaction mixture was concentrated in vacuo, and the residue was purified by recrystallization from different solvent mixtures.

4-Acetamido-1-{3-[4-(*tert*-butyl)pyridin-1-ium-1-yl]propyl}pyridin-1-ium diiodide (PTM0064, 6a): According to the GP, with **4** (431 mg, 1.00 mmol, 1.0 equiv) and **5a** (150 mg, 1.10 mmol, 1.1 equiv) in MeCN (2.0 mL). Recrystallization from EtOAc/EtOH/MeOH (1:2:1) afforded **6a** (529 mg, 93%) as a yellow solid. m.p. 259 °C; ^{1}H NMR (400 MHz, CD_3OD): δ = 1.45 (s, 9 H), 2.27 (s, 3 H), 2.71-2.80 (m, 2 H), 4.66-4.72 (m, 2 H), 4.77-4.83 (m, 2 H), 8.12-8.16 (m, 2 H), 8.16-8.20 (m, 2 H), 8.79-8.86 (m, 2 H), 8.96-9.02 (m, 2 H); ^{13}C NMR (101 MHz, CD_3OD): δ = 24.61, 30.21, 33.27, 37.68, 57.42, 58.32, 116.48, 126.90, 145.43, 146.32, 154.33, 172.69, 173.27; IR (KBr): □ = 2964, 1645, 1518, 1207 cm^{-1}; HRMS (ESI): *m/z* calcd for $C_{19}H_{27}N_3OI_2$-I$^-$: 440.1199 [*M*-I]$^+$; found: 440.1185.

4-[(*tert*-Butoxycarbonyl)amino]-1-{3-[4-(*tert*-butyl)pyridin-1-ium-1-yl]propyl}-pyridin-1-ium diiodide (PTM0065, 6b): According to the GP, a solution of **4** (323 mg, 0.750 mmol, 1.0 equiv) and **5b** (157 mg, 0.810 mmol, 1.08 equiv) in MeCN (2.0 mL) was stirred under microwave irradiation (150 W) at 60 °C for 15 h. Recrystallization from Et_2O/DMF (10:1) afforded **6b** (431 mg, 92%) as a yellow solid. Purity: 94%. m.p. 117 °C; ^{1}H NMR (400 MHz, CD_3OD): δ = 1.45 (s, 9 H), 1.56 (s, 9 H), 2.67-2.79 (m, 2 H), 4.59-4.67 (m, 2 H), 4.74-4.82 (m, 2 H), 7.87-8.02 (m, 2 H), 8.20-8.14 (m, 2 H), 8.68-8.76 (m, 2 H), 8.91-9.01 (m, 2 H); ^{13}C NMR

(101 MHz, CD_3OD): δ = 28.25, 30.21, 33.19, 37.68, 57.16, 58.38, 84.27, 115.30, 126.90, 145.41, 145.85, 153.10, 155.64, 173.30; IR (KBr): □ = 2967, 1643, 1531, 1148 cm^{-1}; HRMS (ESI): *m/z* calcd for $C_{22}H_{33}N_3O_2I_2$-I^-: 498.1618 [*M*-I]$^+$; found: 498.1600.

4-[Benzyl(methyl)amino]-1-{3-[4-(*tert*-butyl)pyridin-1-ium-1-yl]propyl}pyridin-1-ium diiodide (PTM0066, 6c): According to the GP, with **4** (323 mg, 0.750 mmol, 1.0 equiv) and **5c** (164 mg, 0.830 mmol, 1.1 equiv) in MeCN (2.0 mL). Recrystallization from EtOAc/EtOH/MeOH (10:5:1) afforded **6c** (354 mg, 75%) as a yellow solid. m.p. 185 °C; ^{1}H NMR (400 MHz, CD_3OD): δ = 1.45 (s, 9 H), 2.56-2.70 (m, 2 H), 3.34 (s, 3 H), 4.40 (t, *J* = 7.6 Hz, 1 H), 4.74 (t, *J* = 7.7 Hz, 2 H), 4.90 (s, 2 H), 7.03-7.19 (m, 2 H), 7.24-7.29 (m, 2 H), 7.29-7.41 (m, 3 H), 8.13-8.19 (m, 2 H), 8.20-8.40 (m, 2 H), 8.91-8.97 (m, 2 H); ^{13}C NMR (101 MHz, CD_3OD): δ = 30.20, 33.14, 37.67, 39.70, 55.41, 56.75, 58.52, 109.83, 126.86, 127.82, 129.11, 130.21, 136.21, 143.72, 145.38, 158.26, 173.24; IR (KBr): □ = 2967, 1645, 1556, 1193 cm^{-1}; HRMS (ESI): *m/z* calcd for $C_{25}H_{33}N_3I_2$-I^-: 502.1719 [*M*-I]$^+$; found: 502.1703.

4-(*tert*-Butyl)-1-{3-[4-(diethylamino)pyridin-1-ium-1-yl]propyl}pyridin-1-ium diiodide (PTM0067, 6d): According to the GP, with **4** (431 mg, 1.00 mmol, 1.0 equiv) and **5d** (165 mg, 1.10 mmol, 1.1 equiv) in MeCN (2.0 mL). Recrystallization from EtOAc/EtOH (2.5:1) afforded **6d** (419 mg, 72%) as a yellow solid. m.p. 217 °C; ^{1}H NMR (400 MHz, CD_3OD): δ = 1.27 (t, *J* = 7.2 Hz, 6 H), 1.45 (s, 9 H), 2.60-2.71 (m, 2 H), 3.64 (q, *J* = 7.2 Hz, 4 H), 4.41 (t, *J* = 7.7 Hz, 2 H), 4.78 (t, *J* = 7.8 Hz, 2 H), 7.01-7.08 (m, 2 H), 8.13-8.21 (m, 2 H), 8.24-8.31 (m, 2 H), 8.97-9.02 (m, 2 H); ^{13}C NMR (101 MHz, CD_3OD): δ = 12.21, 30.23, 33.20, 37.66, 46.46, 55.15, 58.49, 109.23, 126.86, 143.44, 145.41, 156.42, 173.11; IR (KBr): □ = 2968, 1648, 1561, 1197 cm^{-1}; HRMS (ESI): *m/z* calcd for $C_{21}H_{33}N_3I_2$-I^-: 454.1719 [*M*-I]$^+$; found: 454.1704.

4-(*tert*-Butyl)-1-{3-[4-(pyrrolidin-1-yl)pyridin-1-ium-1-yl]propyl}pyridin-1-ium diiodide (PTM0068, 6e): According to the GP, with **4** (431 mg, 1.00 mmol, 1.0 equiv) and **5e** (159 mg, 1.05 mmol, 1.05 equiv) in MeCN (2.0 mL). Recrystallization from EtOAc/*i*-PrOH (1.1:1) afforded **6e** (457 mg, 79%) as a yellow solid. m.p. 178 °C; ^{1}H NMR (400 MHz, CD_3OD): δ = 1.45 (s, 9 H), 2.10-2.15 (m, 4 H), 2.60-2.69 (m, 2 H), 3.55-3.60 (m, 4 H), 4.40 (t, *J* = 7.7 Hz, 2 H), 4.76 (t, *J* = 7.8 Hz, 2 H), 6.86-6.91 (m, 2 H), 8.15-8.18 (m, 2 H), 8.24-8.29 (m, 2 H), 8.96-9.00 (m, 2 H); ^{13}C NMR (101 MHz, CD_3OD): δ = 26.14, 30.21, 33.22, 37.66, 49.83, 55.26, 58.52, 109.87, 126.86, 143.01, 145.40, 155.23, 173.15; IR (KBr): □ = 2961, 1647, 1561, 1192 cm^{-1}; HRMS (ESI): *m/z* calcd for $C_{21}H_{31}N_3I_2$-I^-: 452.1563 [*M*-I]$^+$; found: 452.1545.

4-(*tert*-Butyl)-1-{3-[4-(piperidin-1-yl)pyridin-1-ium-1-yl]propyl}pyridin-1-ium diiodide (PTM0069, 6f): According to the GP, with **4** (216 mg, 0.500 mmol, 1.0 equiv) and **5f** (85.2 mg, 0.530 mmol, 1.05 equiv) in MeCN (1.0 mL). Recrystallization from EtOAc/*i*-PrOH (1:1.2) afforded **6f** (245 mg, 83%) as a yellow solid. m.p. 240 °C; ^{1}H NMR (400 MHz, CD_3OD): δ = 1.45 (s, 9 H), 1.69-1.76 (m, 4 H), 1.76-1.85 (m, 2 H), 2.58-2.71 (m, 2 H), 3.69-3.76 (m, 4 H), 4.39 (t, *J* = 7.6 Hz, 2 H), 4.77 (t, *J* = 7.7 Hz, 4 H), 7.12-7.20 (m, 2 H), 8.13-8.20 (m, 2 H), 8.21-8.29 (m, 2 H), 8.95-9.02 (m, 2 H); ^{13}C NMR (101 MHz, CD_3OD): δ = 24.93, 26.73, 30.22, 33.14, 37.66, 49.17, 55.07, 58.51, 109.45, 126.86, 143.58, 145.41, 156.92, 173.13; IR (KBr): □ = 2956, 1648, 1547, 1194 cm^{-1}; HRMS (ESI): *m/z* calcd for $C_{22}H_{33}N_3I_2$-I^-: 466.1719 [*M*-I]$^+$; found: 466.1711.

4-(*tert*-Butyl)-1-[3-(4-morpholinopyridin-1-ium-1-yl)propyl]pyridin-1-ium diiodide (PTM0070, 6g): According to the GP, with **4** (431 mg, 1.00 mmol, 1.00 equiv) and **5g** (172 mg, 1.10 mmol, 1.05 equiv) in MeCN (2.0 mL). Recrystallization from EtOAc/EtOH (1:1.4) afforded **6g** (518 mg, 87%) as a yellow solid. m.p. 222 °C; ^{1}H NMR (400 MHz, CD_3OD): δ = 1.45 (s, 9 H), 2.62-2.72 (m, 2 H), 3.69-3.76 (m, 4 H), 3.80-3.85 (m, 4 H), 4.45 (t, *J* = 7.7 Hz, 2 H), 4.78 (t, *J* = 7.8 Hz, 2 H), 7.13-7.27 (m, 2 H), 8.14-8.20 (m, 2 H), 8.33-8.40 (m, 2 H), 8.97-9.04 (m, 2 H); ^{13}C NMR (101 MHz, CD_3OD): δ = 30.23, 33.21, 37.66, 47.73, 55.33, 58.44, 67.15, 109.72, 126.86, 143.86, 145.41, 157.85, 173.11; IR (KBr): □ = 2964, 1650, 1545, 1193 cm^{-1}; HRMS (ESI): *m/z* calcd for $C_{21}H_{31}N_3OI_2$-I$^-$: 468.1512 [*M*-I]$^+$; found: 468.1493.

4-[4-(*tert*-Butoxycarbonyl)piperazin-1-yl]-1-{3-[4-(*tert*-butyl)pyridin-1-ium-1-yl]propyl}-pyridin-1-ium diiodide (PTM0071, 6h): According to the GP, with **4** (216 mg, 0.500 mmol, 1.0 equiv) and **5h** (145 mg, 0.550 mmol, 1.1 equiv) in MeCN (1.0 mL). Recrystallization from EtOAc/EtOH (2:1) afforded **6h** (320 mg, 92%) as a yellow solid. m.p. 149 °C; ^{1}H NMR (500 MHz, CD_3OD): δ = 1.45 (s, 9 H), 1.49 (s, 9 H), 2.61-2.69 (m, 2 H), 3.62-3.68 (m, 4 H), 3.76-3.80 (m, 4 H), 4.42 (t, *J* = 7.6 Hz, 2 H), 4.75 (t, *J* = 7.7 Hz, 2 H), 7.19-7.23 (m, 2 H), 8.15-8.19 (m, 2 H), 8.31-8.36 (m, 2 H), 8.95-8.99 (m, 2 H); ^{13}C NMR (126 MHz, CD_3OD): δ = 28.59, 30.21, 33.17, 37.67, 43.60, 47.12, 55.38, 58.48, 81.95, 109.85, 126.86, 143.79, 145.40, 156.17, 157.71, 173.22; IR (KBr): □ = 2967, 1649, 1416, 1169 cm^{-1}; HRMS (ESI): *m/z* calcd for $C_{26}H_{40}N_4O_2I_2$-I$^-$: 567.2196 [*M*-I]$^+$; found: 567.2180.

4-(1-{3-[4-(*tert*-Butyl)pyridin-1-ium-1-yl]propyl}pyridin-1-ium-4-yl)piperazin-1-ium triiodide (PTM0072, 6i): A solution of **6h** (69.4 mg, 0.100 mmol, 1.0 equiv) and iodo(trimethyl)silane (80.0 mg, 0.400 mmol, 4.0 equiv) in MeCN (2.0 mL) was stirred under argon at rt for 2 h. **6i** (71.3 mg, 99%) was afforded after filtration of the reaction mixture as a yellow solid. m.p. 109 °C; ^{1}H NMR (400 MHz, CD_3OD): δ = 1.45 (s, 9 H), 2.65-2.75 (m, 2 H), 3.47-3.55 (m, 4 H), 4.03-4.12 (m, 4 H), 4.52 (t, *J* = 7.5 Hz, 2 H), 4.75-4.86 (m, 2 H), 7.33-7.39 (m, 2 H), 8.14-8.20 (m, 2 H), 8.45-8.52 (m, 2 H), 9.01-9.06 (m, 2 H); ^{13}C NMR (101 MHz, CD_3OD): δ = 30.23, 33.27, 37.65, 44.04, 44.65, 55.66, 58.33, 110.83, 126.84, 144.37, 145.44, 158.02, 173.07; IR (KBr): □ = 2963, 1647, 1549, 1191 cm^{-1}; HRMS (ESI): *m/z* calcd for $C_{21}H_{33}N_4I_3$-H$^+$-2I$^-$: 467.1671 [*M*-I-I-H]$^+$; found: 467.1663.

1-{3-[4-(*tert*-Butyl)pyridin-1-ium-1-yl]propyl}-7-hydroxyquinolin-1-ium diiodide (PTMD90-0012, 8): According to the GP, a solution of **4** (431 mg, 1.00 mmol, 1.0 equiv) and **7** (163 mg, 1.10 mmol, 1.1 equiv) in MeCN (2.0 mL) was stirred under microwave irradiation (150 W) at 90 °C for 3 h. Recrystallization from EtOH/EtOAc (2:1.5) afforded **8** (167 mg, 29%) as a yellow solid. m.p. 263 °C; ^{1}H NMR (400 MHz, CD_3OD): δ = 1.45 (s, 9 H), 2.76-2.89 (m, 2 H), 4.89-4.96 (m, 2 H), 5.09-5.19 (m, 2 H), 7.56 (dd, *J* = 9.0, 2.1 Hz, 1 H), 7.68 (d, *J* = 2.2 Hz, 1 H), 7.81 (dd, *J* = 8.1, 6.1 Hz, 1 H), 8.11-8.22 (m, 2 H), 8.29 (d, *J* = 9.1 Hz, 1 H), 8.95-9.04 (m, 3 H), 9.31 (dd, *J* = 6.1, 1.4 Hz, 1 H); ^{13}C NMR (101 MHz, CD_3OD): δ = 30.20, 31.59, 37.68, 54.85, 58.50, 101.59, 119.39, 123.77, 126.81, 126.88, 134.57, 142.53, 145.41, 148.20, 148.99, 167.19, 173.30; IR (film): □ = 2968, 1628, 1209, 849 cm^{-1}; HRMS (ESI): *m/z* calcd for $C_{21}H_{26}N_2OI_2$-H$^+$-2I$^-$: 321.1967 [*M*-I-I-H]$^+$; found: 321.1961.

1,1'-(2-Hydroxypropan-1,3-diyl)bis[4-(*tert*-butyl)pyridin-1-ium] dibromide (PTMD90-0015, 11): A mixture of **9** (108 µL, 229 mg, 1.00 mmol, 1.0 equiv) and **10** (352 µL, 325 mg, 2.40 mmol, 2.4 equiv) was stirred at 145 °C for 2 h. The reaction mixture was

concentrated in vacuo and the residue was purified by recrystallization from EtOAc/EtOH (1:2) to afford **11** (196 mg, 40%) as a colorless solid. m.p. 248 °C; ^{1}H NMR (400 MHz, CD_3OD): δ = 1.45 (s, 18 H), 4.43-4.69 (m, 3 H), 4.97-5.22 (m, 2 H), 8.11-8.24 (m, 4 H), 8.83-9.01 (m, 4 H); ^{13}C NMR (101 MHz, CD_3OD): δ = 30.19, 37.70, 63.74, 71.06, 126.42, 146.09, 173.58; IR (film): □ = 2972, 1643, 1468, 1117 cm^{-1}; HRMS (ESI): *m/z* calcd for $C_{21}H_{32}N_2OBr_2$-H^+-2Br^-: 327.2436 [*M*-Br-Br-H]$^+$; found: 327.2430.

2.2 UNC0642 MS Binding Assays

Competitive MS Binding Assays were performed as previously described (Kaiser et al., 2024; Nitsche et al., 2024) apart from one minor difference: in order to obtain competition curves for compounds bearing a 4-aminopyridinium moiety, the non-linear regression function "log(inhibitor) vs. normalized response – Variable slope" (Prism Software v. 6.07, GraphPad Software, La Jolla, CA, USA) was used instead of the recently used function "One site – fit Ki". Statistically significant differences were verified by a two-sided *t*-test (alpha = 0.05).

2.3 Rat diaphragm myography

All procedures using animals followed animal care regulations. Preparation of rat diaphragm hemispheres from male Wistar rats (300 ± 50 g) and experimental protocol of myography was performed as previously described (Nitsche et al., 2024; Seeger et al., 2012). In brief, for all procedures (including wash-out steps, preparation of soman and test compound solutions) aerated Tyrode solution (125 mM NaCl, 24 mM $NaHCO_3$, 5.4 mM KCl, 1 mM $MgCl_2$, 1.8 mM $CaCl_2$, 10 mM glucose, 95% O_2, 5% CO_2; pH 7.4; 25 ± 0.5 °C) was used. After the recording of control muscle force one hour after preparation, the muscles were incubated in the Tyrode solution, containing 3 µM soman for 20 min. Following a 20 min wash-out period, the test compounds were added in ascending concentrations (0.1 µM to 300 µM). The incubation time was 20 min for each concentration. The electric field stimulation was performed with 10 µs pulse width and 2 A amplitudes. The titanic stimulation of 20 Hz, 50 Hz, 100 Hz were applied for 1 s and in 10 min intervals. Measurements on non-toxic muscle were carried out according to the same scheme. Instead of soman, pure Tyrode was incubated. Muscle force was calculated as a time-force integral (area under the curve, AUC) and constrained to values obtained for maximum force generation at the start of the measurements (muscle force in the presence of Tyrode solution without any additives; 100%). All results were expressed in means ± SD (n = 6 - 12). Prism 5.0 (GraphPad Software, San Diego, CA, USA) was used for data analysis.

2.4 MD simulations

The model of the human muscle type nAChR was generated using Modeller with the PDB structure of the α7-nAChR as the template (PDB ID: 7KOX (Noviello et al., 2021). The orthosteric ligand nicotine and a sodium ion in the transmembrane pore were included by aligning the structure of the α3β4-nAChR (PDB ID: 6PV7 (Gharpure et al., 2019) to the homology model. Nicotine was subsequently minimized using SZYBKI (OpenEye Scientific Software, 2021). MB327 was docked in MB327-PAM-1 using MOE with an induced-fit refinement using default parameters (Chemical Computing Group, 2020). Ligand charges

were calculated using Gaussian16 (M. J. Frisch et al., 2016) at the HF 6-31G* level of theory; force field parameters for the ligand were taken from the gaff force field (Wang et al., 2004). Using Packmol-Memgen (Schott-Verdugo and Gohlke, 2019), the system was embedded in a membrane containing 1-palmitoyl-2-oleoyl-*sn*-glycero-3-phosphocholine (POPC) lipids, solvated using the Optimal Point Charge water model (Izadi et al., 2014) with a minimum distance of 12 Å between receptor atoms and the edge of the box, KCl was added in a concentration of 150 mM, and the system was neutralized using Cl^- ions. To perform MD simulations, the AMBER22 package of molecular simulations software (Case et al., 2005; Case et al., 2022), the ff19SB force field (Tian et al., 2020) for the protein, the Lipid17 force field (Gould et al., unpublished) for lipids, the gaff force field for the ligand, and the Joung and Cheatham parameters for monovalent ions were used (Joung and Cheatham, 2008). MD simulations were performed as described previously (Kaiser et al., 2023). In short, a combination of steepest descent and conjugate gradient minimization was performed while gradually decreasing positional harmonic restraints. The system was then heated in a stepwise manner to 300 K, and harmonic restraints on receptor and ligand atoms were gradually removed subsequently. Then, 12 replicas of 1 µs long unbiased MD simulations were performed in the NPT ensemble using semi-isotropic pressure adaptation with the Berendsen barostat. The RMSD, electron density profiles and representative binding modes were computed using CPPTRAJ (Roe and Cheatham, 2013), as implemented in AmberTools (Case et al., 2023).

2.5 GIST computations

GIST (Lazaridis, 1998; Nguyen et al., 2011; Nguyen et al., 2012; Ramsey et al., 2016) computations, as implemented in CPPTRAJ (Roe and Cheatham, 2013), were performed in replicas where MB327 remained in the binding site (distance to I64δ (respectively, I61ε, I61α, I64β) < 5 Å, as done previously (Kaiser et al., 2023) during MD simulations. The backbone of each frame during these MD simulations was aligned to the starting structure of the simulations using CPPTRAJ (Roe and Cheatham, 2013). The middle carbon atom of the C3-linker in MB327 was used as the center of the box for GIST grid generations with grid dimensions of 40 increments along each axis and a grid spacing of 0.5 Å. The results were filtered based on the density of oxygen centers in each voxel compared to bulk density (cutoff: > 1.75) and the solvent free energy (cutoff: > -0.25 kcal mol^{-1}). Visualization of water clusters and manual modification of MB327 to PTMD90-0012 (**8**) and PTMD90-0015 (**11**) was performed using MOE (Chemical Computing Group, 2020).

2.6 Image generation

Images of nAChR in complex with MB327 and its analogs were created using UCSF Chimera (Pettersen et al., 2004).

3 Results and Discussion

3.1 Synthesis of novel MB327 analogs

To identify novel non-symmetric MB327 analogs that should exhibit higher binding affinities to the MB327-PAM-1 binding site as well as higher intrinsic activities compared to MB327, a

series of non-symmetric bispyridinium compounds **6a-6i** with a 4-aminopyridinium ion partial structure derived from compounds **1-3** was synthesized. In addition, based on modeling studies (see chapter 3.3), novel MB327 analogs **8** and **11** with an additional OH function were synthesized with the assumption that this modification should increase the binding affinity by displacing water molecules from the binding pocket.

*Non-symmetric MB327 analogs PTM0064-PTM0072 (**6a-6i**) and PTMD90-0012 (**8**)*

Non-symmetric MB327 analogs **6a-6h** bearing a 4-aminopyridinium ion moiety were readily accessible in one step by *N*-alkylation of 4-aminopyridines **5** with *N*-(3-iodopropyl)pyridinium building block **4**, analogous to the method described by Rappenglück *et al.* (Rappenglück et al., 2018) (Scheme 1). To cover a wider variety of 4-amino substituents in the target compounds, the set of commercially available 4-aminopyridines **5a**, **5b** and **5e-5g** was extended with some building blocks (**5c**, **5d** and **5h**), synthesized according to literature (Hay et al., 2015; Price et al., 2006; Wang et al., 2019). *N*-Alkylation of the pyridines **5a** and **5c-5h** with building block **4** (Rappenglück et al., 2018) was accomplished by stirring the components in acetonitrile at 90 °C under microwave irradiation for 1 h. After removing the reaction solvent, the resulting residues were purified by crystallization to yield the target compounds **6a** and **6c-6h** in good to excellent yields (72-93%) and high purities (≥ 98%). Reaction with *tert*-butyl pyridin-4-ylcarbamate (**5b**), however, required a lower reaction temperature to prevent cleavage of the Boc group as a reaction at 90 °C for 1 h had led to a mixture of product **6b** and 4-amino-analog **1** in a ratio of 3:1. By stirring **5b** with building block **4** at 60 °C for 15 h no side product **1** was observed and the product **6b** was afforded in excellent yield (92%) and sufficient purity (94%). To get the hydroiodide **6i**, the Boc protecting group of **6h** was cleaved by stirring with trimethylsilyl iodide (TMSI) (4.0 equiv) in acetonitrile at room temperature for 1 h (Lott et al., 1979). Thus, compound **6i** was isolated in quantitative yield (99%) and with high purity (100%).

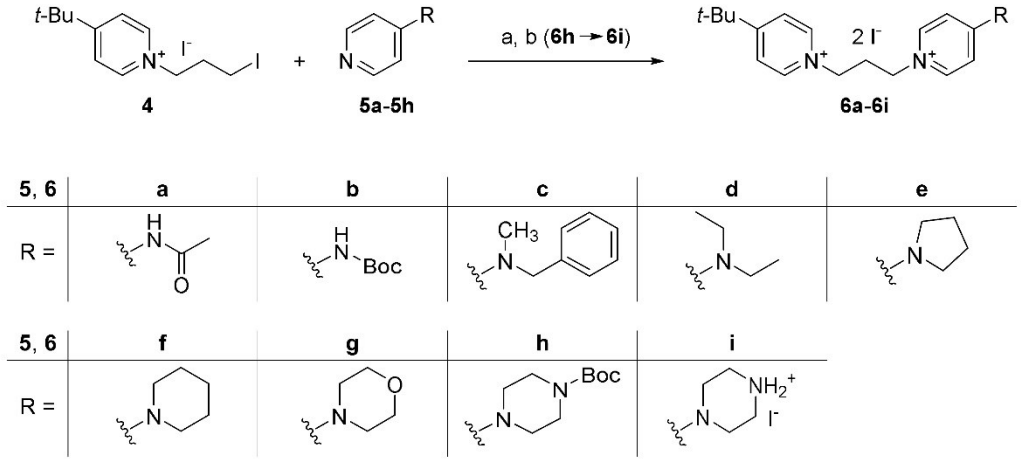

Scheme 1. Synthesis of **6a-6i**. Reagents and conditions: (a) 4-(*tert*-butyl)-1-(3-iodopropyl)pyridin-1-ium iodide (**4**) (1.0 equiv), pyridines **5a-5h** (1.05-1.1 equiv), MeCN, microwave: 150 W, 60-90 °C, 1-15 h, 72-93%; (b) **6i**: **6h** (1.0 equiv), TMSI (4.0 equiv), MeCN, rt, 1 h, 99%.

PTMD90-0012 (**8**) was synthesized from building block **4** (Rappenglück et al., 2018) and 7-hydroxyquinoline (**7**) under the reaction conditions described for bispyridinium compounds **6a-6h**. However, the reaction time had to be increased to 3 h to compensate for the lower reactivity of the sterically more demanding quinoline **7** as compared to the 4-aminopyridines **5**. That way, PTMD90-0012 (**8**) was obtained in 29% yield after recrystallization (purity ≥ 98%) (Scheme 2).

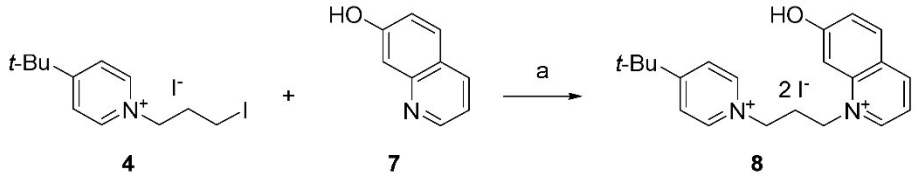

4 **7** **8**

Scheme 2. Synthesis of PTMD90-0012 (**8**). Reagents and conditions: (a) 4-(*tert*-butyl)-1-(3-iodopropyl)pyridin-1-ium iodide (**4**) (1.0 equiv), 7-hydroxyquinoline (**7**) (1.1 equiv), MeCN, microwave: 150 W, 90 °C, 3 h, 29%.

*MB327 analog PTMD90-0015 (**11**)*

The symmetric bispyridinium compound PTMD90-0015 (**11**) with a 2-hydroxypropyl linker between the two pyridinium rings, was synthesized by heating 1,3-dibromopropan-2-ol (**9**) with an excess of 4-*tert*-butylpyridine (**10**) to 145 °C for 2 h. Bis-alkylation product PTMD90-0015 (**11**) was obtained in 40% yield and in high purity (100%) after recrystallization (Scheme 3). In contrast, reaction of **8** with epichlorohydrine or 1,3-dichloropropan-2-ol under the reaction conditions described above led only to the corresponding monosubstituted products.

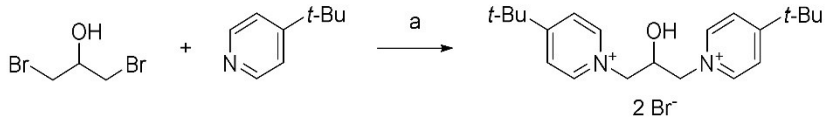

9 **10** **11**

Scheme 3. Synthesis of PTMD90-0015 (**11**). Reagents and conditions: (a) 1,3-dibromopropan-2-ol (**9**) (1.0 equiv), 4-*tert*-butylpyridine (**10**) (2.4 equiv), 145 °C, 2 h, 40%.

3.2 Biological evaluation

Affinity to the MB327-PAM-1 binding site of Torpedo californica nAChR

All of the newly developed compounds presented in this study, i.e. PTM0064-PTM0072 (**6a-6i**), PTMD90-0012 (**8**) and PTMD90-0015 (**11**) as well as MB327 and its recently reported analogs PTM0062 (**1**) (Kaiser et al., 2023), PTM0063 (**2**) (Kaiser et al., 2023) and PTM0056 (**3**) (Rappenglück et al., 2018) were evaluated for their binding affinity towards the MB327-PAM-1 binding site of *Torpedo californica* nAChR by means of the recently introduced UNC0642 MS Binding Assays (Table 1) (Kaiser et al., 2024; Nitsche et al., 2024). First, for economic reasons, all test compounds were studied at a single concentration of 10 µM and a reporter ligand concentration of 1 µM. For a set of selected compounds also the

binding affinity constants (pK_i values) were determined in full-scale MS competition experiments.

Table 1. Binding affinities of bispyridinium compounds for the MB327-PAM-1 binding site of *Torpedo californica* nAChR, determined in UNC0642 MS Binding Assays.

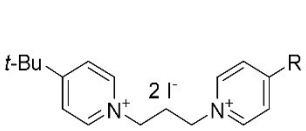

MB327, 1-3, 6a-6i

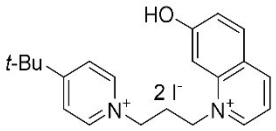

8

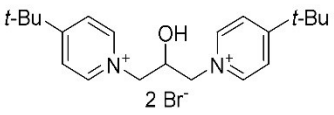

11

Entry	Compound	R	Remaining Reporter Ligand Binding [%][a]	PTM code
1	**MB327**		102 ± 9 (pK_i = 3.40 ± 0.04[b])	-
2	**1**		93 ± 5	0062[c]
3	**2**	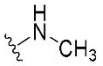	92 ± 1	0063[c]
4	**3**	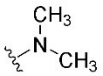	90 ± 5	0056[d]
5	**6a**	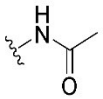	90 ± 6	0064
6	**6b**	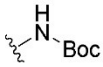	90 ± 4	0065
7	**6c**	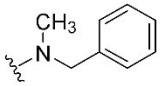	85 ± 8*	0066
8	**6d**	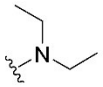	91 ± 11	0067
9	**6e**		85 ± 0.5*	0068
10	**6f**	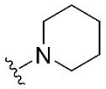	73 ± 6** (pK_i = 3.96 ± 0.08)	0069
11	**6g**	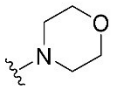	90 ± 8	0070
12	**6h**	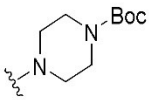	64 ± 8** (pK_i = 4.17 ± 0.02)	0071
13[e]	**6i**	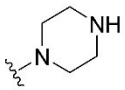	83 ± 5*	0072

14	**8**	-	93 ± 9 (pK_i = 3.69 ± 0.03)	D90-0012
15	**11**	-	98 ± 5 (pK_i = 3.29 ± 0.05)	D90-0015

[a] The results of UNC0642 MS Binding Assays are given as percentages representing the remaining reporter ligand binding (UNC0642, 1 µM) in presence of 10 µM test compound as compared to 100% reporter ligand binding in the absence of a competitor. Values are given as means ± SD of triplicate experiments, except for MB327, which was determined in two experiments from a triplicate determination each. The pK_i values given in brackets represent means ± SEM of three independent experiments determined in UNC0642 MS Binding Assays in full scale competition experiments (mean Hill coefficient = 0.45-0.61).
[b] pK_i value of MB327 from (Nitsche et al., 2024).
[c] Compound from (Kaiser et al., 2023).
[d] Compound from (Rappenglück et al., 2018).
[e] Compound tested as hydroiodide.
* Asterisks indicate statistically significantly higher values for the remaining reporter ligand binding of the respective compound compared to the MB327 value (* $p < 0.05$, ** $p < 0.01$, based on a two-sided *t*-test)

Residual reporter ligand binding in the presence of 10 µM of the respective compounds listed in Table 1 range from 102% ± 9% for MB327 (Table 1, entry 1) to 64% ± 8% for the *N*-Boc-piperazino derivative PTM0071 (**6h**, Table 1, entry 12). Substitution of one of the two 4-*tert*-butyl residues of MB327 by an amino [PTM0062 (**1**), 93% ± 5%, Table 1, entry 2], an *N*-methylamino [PTM0063 (**2**), 92% ± 1%, Table 1, entry 3], or dimethylamino group [PTM0056 (**3**), 90% ± 5%, Table 1, entry 4] results in a nominal yet not statistically significant reduction of residual reporter ligand binding as compared to MB327. This is also true for compounds PTM0064 (**6a**, 90% ± 6%, Table 1, entry 5) and PTM0065 (**6b**, 90% ± 4%, Table 1, entry 6) displaying an *N*-acetamido- and an *N*-*tert*-butoxycarbonylamino moiety, respectively effecting a reduction to 90% of remaining reporter ligand binding. According to the data obtained for **1-3** and **6a-6b** the capability of the nitrogen substituents, present in these compounds to participate in hydrogen bonding seems to have only little if any influence on the binding affinities, the remaining reporter ligand binding amounting in any case to about 90%. Likewise, when the dimethylamino group in PTM0056 (**3**, 90% ± 5%, Table 1, entry 4) is replaced by a sterically more demanding *N*,*N*-diethylamino moiety, the binding affinity of the resulting PTM0067 (**6d**) remains with 91% ± 11% virtually unaltered (remaining reporter ligand binding, Table 1, entry 8). Although **1-3** as well as **6a**, **6b** and **6d** effect remaining reporter ligand binding nominally below that of MB327 (Table 1, entry 1), for none of these compounds the observed differences are statistically significant. However, for the *N*-benzyl-*N*-methylamino derivative PTM0066 (**6c**) with an enlarged lipophilic domain, remaining reporter ligand binding reaches 85% ± 8% (Table 1, entry 7), which is statistically significantly lower than that of MB327 (102% ± 9%, Table 1, entry 1).

Notably, the pyrrolidino and the piperidino substituted derivatives PTM0068 (**6e**) and PTM0069 (**6f**), of which the former can be considered as a cyclic analog of the diethylamino substituted **6d,** reduce remaining reporter ligand binding to 85% ± 0.5% (Table 1, entry 9) and 73% ± 6% (Table 1, entry 10), both values being also statistically significantly below than that of MB327 (102% ± 9%, Table 1, entry 1).

Upon transition from the piperidino-substituted bispyridinium salt **6f** to the more polar morpholino-substituted analog PTM0070 (**6g**), again a decline in binding affinity is observed

with the remaining reporter ligand binding increasing to 90% ± 8% (Table 1, entry 11). However, for the nitrogen analog of the morpholino derivative **6g**, the piperazino derivative PTM0072 (**6i**), the decline in binding affinity compared to **6f** displaying a piperidino residue (73% ± 6%, Table 1, entry 10) was less pronounced, with the remaining reporter ligand binding amounting to 83% ± 5% (Table 1, entry 13). Obviously, the binding affinity-diminishing effect of the additional heteroatom seems to be less distinct for the piperazino derivative **6i** than for the morpholino derivative **6g** (as compared to the piperidino analog **6f**), which can be possibly attributed to the capability **6i** to act as a hydrogen bridge acceptor and donor.

Remarkably, the hydrogen bridge donor capability appears to be of minor importance, as upon attachment of an *N*-Boc substituent to the piperazino moiety of **6i** resulting in PTM0071 (**6h**, Table 1, entry 12), the binding affinity is distinctly improved despite the absence of the formerly present NH group. Thus, a remaining reporter ligand binding of 64% ± 8% could be measured for this compound, which is statistically significantly lower than that of the piperazino-substituted compound **6i** (Table 1, entry 13). Hence, the piperidino-substituted compound **6f** (Table 1, entry 10) and the *N*-Boc-piperazino derivative **6h** (Table 1, entry 12) possess the highest binding affinities for the MB327-PAM-1 binding site of the nAChR of the compounds evaluated in this study.

Modeling studies (see chapter 3.3) indicated, that the presence of an OH function in ligands of the MB327-PAM-1 binding site might be favorable for the binding affinity by displacing water molecules present in the binding pocket. In particular, the MB327 analog **11** with an OH function in the spacer linking the two pyridinium subunits in the molecule as well as **8** with a 7-hydroxyquinolinium replacing one of the two pyridinium subunits in MB327 were expected to possess improved binding affinities. Hence, the binding affinities of PTMD90-0015 (**11**) and PTMD90-0012 (**8**) were studied. Both compounds, however, show no or only a negligible improvement of the binding affinity compared to MB327 (Table 1, entry 1), the remaining reporter ligand binding amounting to 98% ± 5% for **11** (Table 1, entry 15) and 93% ± 9% for **8** (Table 1, entry 14). Although no clear improvement of the binding affinity could be achieved with **11** and **8**, the results indicate that the presence of an additional polar OH function is tolerated in the binding pocket.

Finally, for a small set of compounds, the pK_i values as a more accurate measure of the binding affinity were determined in full-scale competitive MS Binding Assays. This set comprised the two compounds **6f** and **6h**, which had shown the highest binding affinities in the single point determinations described above (reduction of the remaining reporter ligand binding to < 75%) as well as the two OH function-containing derivatives **8** and **11,** which had emerged as candidate compounds for testing from modeling studies. Notably, the piperidino derivative **6f** (Table 1, entry 10) exhibits a pK_i of 3.96 ± 0.08, which was approximately 0.5 log units and thus statistically significantly higher than the pK_i of MB327 previously determined to be 3.40 ± 0.04 (Table 1, entry 1) (Nitsche et al., 2024). The *N*-Boc-piperazino derivative **6h** (Table 1, entry 12) showed an even higher pK_i of 4.17 ± 0.02, as to be expected from the preliminary binding data (remaining reporter ligand binding 64% ± 5%), exceeding that of MB327 by approximately 0.8 log units. For the MB327 analog **11** with an OH function as part of the propan-1,3-diyl spacer (Table 1, entry 15), the pK_i value (3.29 ± 0.05) matched that of MB327 within the limits of error. For the 7-hydroxyquinolinium derivative **8** (Table 1, entry 14), a pK_i value of 3.69 ± 0.03 was found, almost 0.3 log units higher than that of MB327, which is statistically significantly different, indicating the higher binding affinity of this compound compared to MB327.

Evaluation of muscle force recovery in soman-poisoned rat diaphragm hemispheres

In addition to the binding affinities, the intrinsic activities of a selection of the test compounds have been determined by means of an *ex vivo* assay based on rat diaphragm hemispheres. In this assay dissected rat diaphragm hemispheres are treated with a solution containing 3 µM soman. Whereas upon indirect electric field stimulation commonly carried out at frequencies of 20 Hz, 50 Hz and 100 Hz, unpoisoned rat diaphragms undergo muscle contractions, in case of poisoned samples no or only very faint contractions occur. This inhibition further does not vanish, when the poisoned samples are freed from the toxin by washing, typically performed as a control, as this has no effect on the irreversible inhibition of the AChE by the nerve agent. The positive intrinsic activity of the test compounds becomes apparent, when their addition to the poisoned muscle preparations, typically performed in increasing concentrations from 0.1-300 µM, affects a recovery of the muscle force of the soman-impaired rat diaphragm hemispheres. Muscle force inhibition reappears, when samples are subjected to a subsequent washout step, which is due to the irreversible inactivation of the AChE and indicative of the reversibility of the receptor-mediated resensitizing effect of the test compounds.

For the characterization of the muscle force restoring potency of soman-poisoned rat diaphragms in the aforementioned test system, the piperidino- and the *N*-Boc-piperazino derivatives **6f** and **6h** were selected as they had shown the highest binding affinities among the new test compounds presented in this study. In addition, the piperazino derivative **6i**, closely related to **6h**, the *N*,*N*-dimethylamino-substituted compound **3** as parent compound, as well as the hydroxy-substituted compounds **8** and **11** as analogs of MB327 devoid of an amino-substituent were evaluated in this test system.

Since it is known, that the largest efficacy is observed at low stimulation frequencies (Seeger et al., 2012), only the results of experiments performed at 20 Hz will be presented (Figure 2) and discussed in the following. The data of measurements carried out at higher frequencies (50 Hz, 100 Hz) can be found in the Supporting Information (SI, Figure S2).

As reference, the published data obtained for MB327 in the test system have been included in Figure 2 (Niessen et al., 2018). As previously reported, MB327 addition (Figure 2A) leads to a concentration-dependent reactivation of soman-impaired muscle. The recovery gradually increases with the MB327 concentration (Figure 2A). At a MB327 concentration of 100 µM, the muscle force recovery amounts to 14.8% ± 9.2%, reaches 30.2% ± 9.5% at 300 µM (both values statistically significantly different from the value obtained for the soman-poisoned muscle), to finally decrease to 4.2% ± 4.2% at 1000 µM MB327 (not shown in Figure 2A)(Niessen et al., 2018).

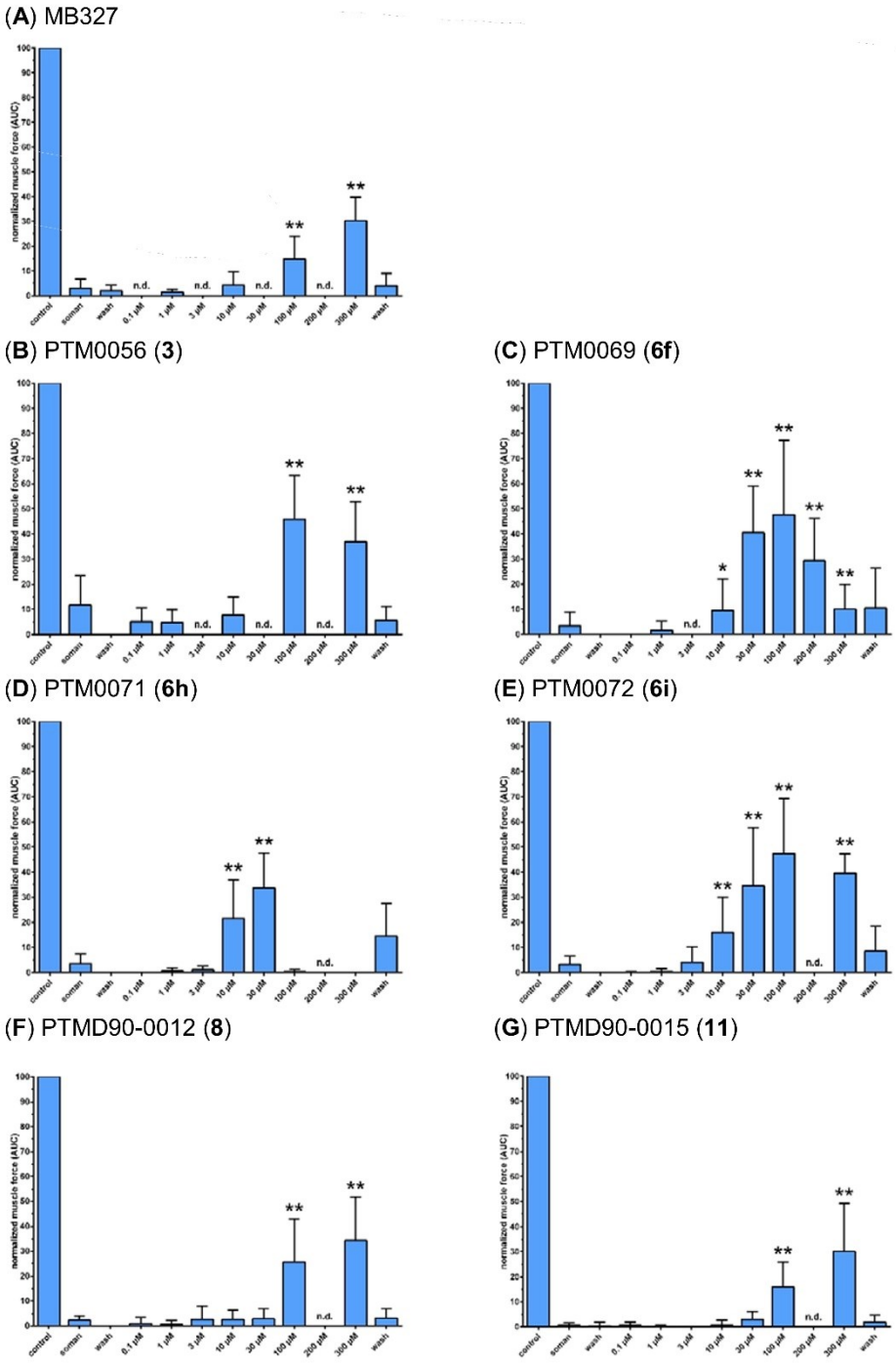

Figure 2: Concentration-dependent restoration of muscle force of soman-poisoned rat diaphragms by (**A**) MB327 (Niessen et al., 2018), (**B**) PTM0056 (**3**), (**C**) PTM0069 (**6f**), (**D**) PTM0071 (**6h**), (**E**) PTM0072 (**6i**), (**F**) PTMD90-0012 (**8**) and (**G**) PTMD90-0015 (**11**). For indirect stimulation, a frequency of 20 Hz was applied. Data are shown as % of control and are given as mean ± SD (n = 4-25). Asterisks indicate statistically significantly higher values for the respective compound concentration

compared to the soman value (* $p < 0.05$, ** $p < 0.01$, based on a two-sided *t*-test). n.d.: not determined.

Similar to MB327, the analogs **3**, **6f**, **6h** and **6i** exhibiting a 4-amino group at one of the two pyridinium subunits instead of a *tert*-butyl moiety (present in MB327) lead to an increase of the regeneration of the muscle force of soman-poisoned rat diaphragms with increasing concentrations, whereas the onset and the size of this effect differ. The *N*,*N*-dimethylamino-substituted analog **3** shows its maximum recovery at a concentration of 100 µM (45.8% ± 17.4%), which statistically significantly exceeds that of MB327 ($p < 0.01$) at the same concentration (14.8% ± 9.2%). However, the reactivation decreases nominally at 300 µM to 37.0% ± 15.8%, approximating that of MB327 at the same concentration (30.2% ± 9.5%). At a compound concentration of 100 µM, the results for the piperidino- and the piperazino-substituted compounds **6f** (47.5% ± 29.8%) and **6i** (47.3% ± 21.8%) are comparable to the value observed for the dimethylamino derivative **3**, which are also nominally the highest values of all three compounds. At concentrations above 100 µM, alike observed for the dimethylamino derivative **3**, the muscle force declines again for **6f** as well as **6i**, which is in the case of **6i** with 39.5% ± 7.7% muscle force recovery at 300 µM compound concentration far less pronounced than for **6f** with 10.0% ± 9.8% (statistically significant, $p < 0.01$%; **6f** at 200 µM 29.3% ± 16.8%). The *N*-Boc-piperazino derivative **6h** induces a rather strong muscle force recovery already at 10 µM with a value amounting to 21.7% ± 15.3%, which is nominally the highest for all tested compounds at this concentration, which further increases at 30 µM to 33.8% ± 13.8% followed by a sharp drop to almost 0% (0.3% ± 0.8%) at 100 µM (0.0% ± 0.0% at 300 µM). This strong muscle force recovery effect of **6h** at a low concentration might be a result of its high binding affinity, which is the highest of all compounds studied.

Notably, all three MB327 analogs with cyclic amino residues exert already at a concentration of 10 µM a muscle force recovery that is statistically significantly higher than that of the soman-poisoned but untreated muscle, whereas this is neither the case for the dimethylamino derivative **3** nor for MB327. For the piperidino derivative **6f,** the respective recovery of muscle force at 10 µM amounts to 9.5% ± 12.7%, for the *N*-Boc-piperazino analog **6h** to 21.7% ± 15.3% and the piperazino derivative **6i** to 16.0% ± 14.1%. Statistical significance of muscle force recovery over the soman-poisoned but untreated muscle as reference value is reached for these three compounds also at a test compound concentration of 30 µM (**6f**, 40.6% ± 18.5%; **6h**, 33.8% ± 13.8%; **6i**, 34.5% ± 23.2%). Yet, it remains unclear, whether this is also the case for the dimethylamino derivative **3** and MB327, as data for these two compounds when applied at 30 µM are missing.

The two MB327 analogs featuring an additional hydroxy group either in the spacer, **11**, or as part of a quinolinium moiety, **8**, show very similar effects in terms of muscle force regeneration after soman-intoxication. Also, muscle force recovery effected by **11** and **8** at concentrations of 100 µM and 300 µM is statistically significant as compared to the soman value. Thereby, the values for muscle force recovery of soman-poisoned muscle amounted for **11** to 15.9% ± 9.9% at 100 µM and to 30.1% ± 19.1% at 300 µM, whereas those for **8** are higher with 25.6% ± 17.5% at 100 µM and 34.3% ± 17.5% at 300 µM. For both compounds, no decrease in muscle force could be observed up to the highest concentration of 300 µM studied.

Finally, the effects of test compounds that were still available in sufficient amounts, i.e., of MB327 and the dimethylamino **3**, the piperidino **6f** as well as the quinolinium derivative **8,** on the muscle force of rat diaphragm hemispheres not been poisoned with soman were studied (SI, Figure S3). These experiments were carried out in analogy to those for the determination of muscle force recovery of soman-poisoned rat diaphragm hemispheres. Accordingly, the muscle force of rat diaphragm hemispheres not exposed to soman was measured as a function of increasing concentrations of the test compounds under indirect electric field stimulation at 20 Hz, 50 Hz and 100 Hz. Data from analogous experiments performed in parallel but without the application of test compounds served as reference by unveiling the loss of muscle force purely due to the washing steps. MB327 and dimethylamino derivative **3** showed no inhibitory effect up to the maximum concentration of 300 µM, as did the quinolinium derivative **8** up to 200 µM as the highest concentration still feasible due to a shortage of the compound. For the piperidino derivative **6f**, however, although the muscle force remained unaffected up to a concentration of 100 µM, a distinct reduction occurred at a concentration of 300 µM. The latter might explain the bell-shaped curve observed for this compound, **6f**, in the muscle force recovery experiments of soman-poisoned rat diaphragm hemispheres (Figure 2C). The positive effect of **6f** on soman-poisoned rat diaphragms mediated by binding to the MB327-PAM-1 binding site of the nAChR might be counteracted by a direct negative effect on muscle force, mediated by different binding sites, which seems to become dominating at concentrations above 100 µM of **6f,** leading to the observed decline of muscle force recovery in soman-poisoned muscles (Figure 2C) above this concentration.

3.3 Substituting energetically unfavorable water clusters using *in silico* methods

We performed unbiased MD simulations (12 replicas of 1 µs length each) of the human nAChR with MB327 bound to the recently identified allosteric binding site MB327-PAM-1 in all five subunits (Kaiser et al., 2023). During the simulations, the receptor and membrane stayed structurally invariant shortly after the simulations started (SI, Figure S4, S5). MB327 mostly or completely remained within the binding sites in between the α- and δ-subunits (ten out of twelve replicas) as well as in between the α- and ε-subunits (twelve out of twelve replicas) using the distance of heavy atoms of MB327 to heavy atoms of I64δ (respectively I61ε) to characterize unbinding as done previously (Kaiser et al., 2023). For these two binding sites, Grid Inhomogeneous Solvent Theory (GIST) computations (Lazaridis, 1998; Nguyen et al., 2011; Nguyen et al., 2012; Ramsey et al., 2016) were subsequently performed to identify potential energetically unfavorable water clusters (Figure 3B, SI, Figure S6A). We then visualized the docked MB327 binding mode and representative MB327 structures from MD simulations in the presence of such water clusters and manually created new MB327 analogs with substituents replacing these water clusters. Initially, during the first few replicas (5 out of 12) of MD simulations and subsequent GIST computations, a network of energetically unfavorable water molecules near the linker of MB327 was identified between E65α, V66α, and Q68α (SI, Figure S7). Based on these preliminary results, PTMD90-0015 (**11**) was designed. However, after completion of the MD simulations, the hydroxyl group located at the C3-linker would not result in replacing energetically unfavorable water molecules as indicated by GIST. Hence, PTMD90-0012 (**8**) was designed based on the results after 1 µs long simulations (Figure 3C, SI, Figure S6B), such that it should substitute energetically unfavorable water molecules in close proximity to I63ε, E65ε, and E204ε

(respectively L66δ, E68δ, and E210δ). As only the analogs based on the docked structure [PTMD90-0012 (**8**)] and those based on the initial MD simulations results [PTMD90-0015 (**11**)] could be synthesized, they were subsequently tested for affinity and resensitizing potential.

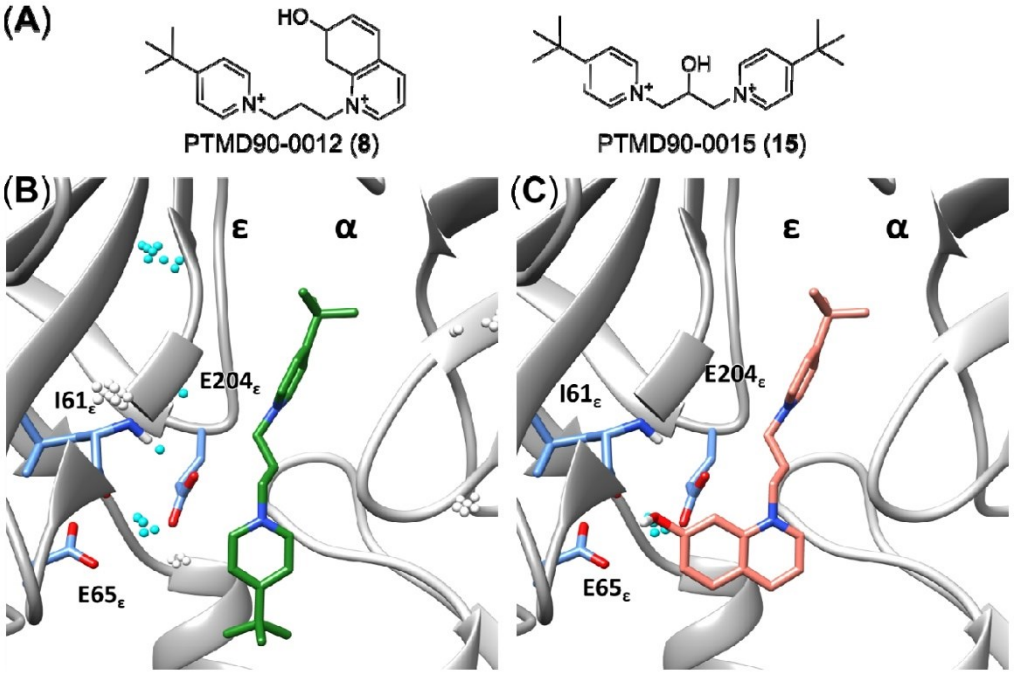

Figure 3: Design of MB327 analogs based on substituting water clusters in MB327-PAM-1. **A)** Structure of the MB327 analogs PTMD90-0012 (**8**) and PTMD90-0015 (**11**). **B)** MB327 (green) binding in between the α- and ε-subunit. Water clusters identified during GIST computations are shown as spheres. Water clusters within 5 Å of MB327 are shown in cyan. **C)** Proposed binding mode of PTMD90-0012 (**8**) (salmon) in between the α- and ε-subunit. Modification of MB327 to PTMD90-0012 (**8**) (salmon) leads to a substitution of a water cluster located in proximity to $I63_{\varepsilon}$, $E65_{\varepsilon}$, and $E204_{\varepsilon}$; for $I61_{\varepsilon}$, the backbone atoms are shown in addition to the side chain.

4 Conclusion

The recently developed non-symmetric MB327 analogs PTM0062 (**1**), PTM0063 (**2**) and PTM0056 (**3**), which have an amino, methylamino or dimethylamino group in place of one of the two *tert*-butyl residues of MB327, respectively, show higher muscle force restoring activity on soman-poisoned rat diaphragms than MB327. They are therefore promising starting points for the development of new resensitizers for desensitized muscle-type nAChRs as antidots for OPC poisoning.

In the present study, a series of new non-symmetric MB327 analogs, PTM0064-PTM0072 (**6a-6i**), with a 4-amino-substituted pyridinium ion substructure derived from compounds **1-3**, were synthesized and evaluated for their binding affinity towards the MB327-PAM-1 binding site of *Torpedo californica* nAChR using the recently introduced UNC0642 MS Binding

Assays. In addition, selected compounds were evaluated for their intrinsic activity on soman-poisoned rat diaphragms in myography assays.

Among the compounds evaluated in this study, the piperidino derivative PTM0069 (**6f**) and the *N*-Boc-piperazino derivative PTM0071 (**6h**) showed the highest affinities for the MB327-PAM-1 binding site of the nAChR. The pK_i values for **6f** and **6h** exceeded that of MB327 by approximately 0.5 and 0.8 log units, respectively. PTMD90-0015 (**11**), designed to substitute unfavorable water clusters in MB327 PAM-1 after preliminary MD simulations, showed reduced affinity towards MB327-PAM-1 and no beneficial resensitizing effects compared to MB327. These results are concordant with that the hydroxy group located at the C3-linker would not result in replacing energetically unfavored water molecules as indicated by GIST after 1 µs long MD simulations. By contrast, PTMD90-0012 (**8**), designed using extended MD data, showed a statistically significant increase of affinity compared to MB327. Likely, this may result from replacing energetically unfavored water molecules close to $I63_{\varepsilon}$, $E65_{\varepsilon}$, and $E204_{\varepsilon}$ (or $L66_{\delta}$, $E68_{\delta}$, and $E210_{\delta}$) with the 7-hydroxy quinazoline moiety.

Ex vivo studies in soman-poisoned rat diaphragms showed a clear muscle force restoring activity for all compounds tested [PTM0069 (**6f**), PTM0071 (**6h**), PTM0056 (**3**), PTM0072 (**6i**), PTMD90-0012 (**8**), and PTMD90-0015 (**11**)]. In particular, compounds PTM0069 (**6f**), PTM0071 (**6h**) and PTM0072 (**6i**), which all have a cyclic amino residue instead of one of the two *tert*-butyl residues of MB327, showed a statistically significantly higher activity at lower concentrations than MB327. Thus, to achieve muscle force recovery comparable to that of the aforementioned compounds, MB327 must be used at a tenfold higher concentration. This could be due to the fact that PTM0069 (**6f**) and PTM0071 (**6h**), in particular, but also PTM0072 (**6i**) have statistically significantly higher binding affinities for the MB327-PAM-1 binding site than MB327. It is noteworthy that the recovery of muscle force with PTM0069 (**6f**) and PTM0071 (**6h**) at higher concentrations decreased significantly immediately after reaching the maximum value, a phenomenon also observed for MB327. Experiments with PTM0069 (**6f**) and rat diaphragms that had not been poisoned with soman showed that in the presence of higher concentrations of PTM0069 (**6f**), a significant inhibition of muscle force occurs, which is reversible as it almost completely disappears after a subsequent washout step. Interestingly, this reversible inhibition occurs in the same concentration range in which the muscle force restoring effect of compound **6f** decreases in the experiments with soman-poisoned rat diaphragms.

Taken together, this indicates that the positive resensitizing effect mediated by binding to the MB327-PAM-1 binding site is counteracted by a muscle force inhibitory effect becoming generally prominent at higher concentrations that appears to be due to reversible binding to a different binding site.

Therefore, future efforts must focus, on the one hand, on further increasing the affinity of new compounds for the MB327-PAM-1 binding site and, on the other hand, on reducing the direct muscle inhibitory effect.

5 Supporting Information

Supplementary data associated with this article can be found in the online version at doi: xxx

6 Acknowledgments

This work was supported by the German Ministry of Defence (E/ U2AD/KA019/IF558). We are grateful for computational support and infrastructure provided by the "Zentrum für Informations- und Medientechnologie" (ZIM) at the Heinrich Heine University Düsseldorf and the computing time provided by the John von Neumann Institute for Computing (NIC) to HG on the supercomputer JUWELS at Jülich Supercomputing Center (JSC) (user IDs: HKF7, VSK33, nAChR). HG is grateful to OpenEye Scientific Software for granting a Free Public Domain Research License.

7 Conflict of interest

The authors declare no conflict of interest.

8 Keywords

neurological agents • nicotinic acetylcholine receptor • MB327-PAM-1 binding site • bispyridinium salts • Resensitizer • *in silico* studies • myographic studies

9 References

Brown, M.A., Brix, K.A., 1998. Review of health consequences from high-, intermediate- and low-level exposure to organophosphorus nerve agents. Journal of Applied Toxicology 18, 393-408.

Case, D.A., Aktulga, H.M., Belfon, K., Cerutti, D.S., Cisneros, G.A., Cruzeiro, V.W.D., Forouzesh, N., Giese, T.J., Götz, A.W., Gohlke, H., Izadi, S., Kasavajhala, K., Kaymak, M.C., King, E., Kurtzman, T., Lee, T.-S., Li, P., Liu, J., Luchko, T., Luo, R., Manathunga, M., Machado, M.R., Nguyen, H.M., O'Hearn, K.A., Onufriev, A.V., Pan, F., Pantano, S., Qi, R., Rahnamoun, A., Risheh, A., Schott-Verdugo, S., Shajan, A., Swails, J., Wang, J., Wei, H., Wu, X., Wu, Y., Zhang, S., Zhao, S., Zhu, Q., Cheatham, T.E., III, Roe, D.R., Roitberg, A., Simmerling, C., York, D.M., Nagan, M.C., Merz, K.M., Jr., 2023. AmberTools. Journal of Chemical Information and Modeling 63, 6183-6191.

Case, D.A., Cheatham, T.E., 3rd, Darden, T., Gohlke, H., Luo, R., Merz, K.M., Jr., Onufriev, A., Simmerling, C., Wang, B., Woods, R.J., 2005. The Amber biomolecular simulation programs. J Comput Chem 26, 1668-1688.

Case, D.A., H.M., A., Belfon, K., Ben-Shalom, I.Y., Berryman, J.T., Brozell, S.R., Cerutti, D.S., Cheatham, T.E., 3rd, Cisneros, G.A., Cruzeiro, V.W.D., Darden, T.A., Duke, R.E., Giambasu, G., Gilson, M.K., Gohlke, H., Goetz, A.W., Harris, R., Izadi, S., Izmailov, S.A., Kasavajhala, K., Kaymak, M.C., King, E., Kovalenko, A., Kurtzmann, T., Lee, T.S., Le Grand, S., Li, P., Lin, C., Liu, J., Luchko, T., Luo, R., Machado, M., Man, V., Manathunga, M., Merz, K.M., Miao, Y., Mikhailovskii, O., Monard, G., Nguyen, H., O'Hearn, K.A., Onufriev, A., Pan, F., Pantano, S., Qi, R., Rahnamoun, A., Roe, D.R., Roitberg, A., Sagui, E., Schott-Verdugo, S., Shajan, A., Shen, J., Simmerling, C.L., Skrynnikov, N.R., Smith, J., Swails, J., Walker, R.C., Wang, J., Wang, J., Wei, H., Wolf, R.M., Wu, X., Xiong, Y., Xue, Y., York, D.M., Zhao,

S., Kollmann, P.A., 2022. Amber 2022. vol. Amber 2022. University of California, San Francisco.

Chemical Computing Group, U., 2020. Molecular Operating Environment (MOE). vol. 2019.01, 1010 Sehrbooke St. West, Suite #910, Montreal, QC, Canada, H3A, 2R7.

Cushman, M., Georg, G.I., Holzgrabe, U., Wang, S., 2014. Absolute Quantitative 1H NMR Spectroscopy for Compound Purity Determination. Journal of Medicinal Chemistry 57, 9219-9219.

Dolgin, E., 2013. Syrian gas attack reinforces need for better anti-sarin drugs. Nature Medicine 19, 1194-1195.

Epstein, M., Bali, K., Piggot, T.J., Green, A.C., Timperley, C.M., Bird, M., Tattersall, J.E.H., Bermudez, I., Biggin, P.C., 2021. Molecular determinants of binding of non-oxime bispyridinium nerve agent antidote compounds to the adult muscle nAChR. Toxicology Letters 340, 114-122.

Gharpure, A., Teng, J., Zhuang, Y., Noviello, C.M., Walsh, R.M., Jr., Cabuco, R., Howard, R.J., Zaveri, N.T., Lindahl, E., Hibbs, R.E., 2019. Agonist Selectivity and Ion Permeation in the alpha3beta4 Ganglionic Nicotinic Receptor. Neuron 104, 501-511 e506.

Hay, D.A., Rogers, C.M., Fedorov, O., Tallant, C., Martin, S., Monteiro, O.P., Müller, S., Knapp, S., Schofield, C.J., Brennan, P.E., 2015. Design and synthesis of potent and selective inhibitors of BRD7 and BRD9 bromodomains. MedChemComm 6, 1381-1386.

Izadi, S., Anandakrishnan, R., Onufriev, A.V., 2014. Building Water Models: A Different Approach. J Phys Chem Lett 5, 3863-3871.

Joung, I.S., Cheatham, T.E., III, 2008. Determination of Alkali and Halide Monovalent Ion Parameters for Use in Explicitly Solvated Biomolecular Simulations. The Journal of Physical Chemistry B 112, 9020-9041.

Kaiser, J., Gertzen, C.G.W., Bernauer, T., Höfner, G., Niessen, K.V., Seeger, T., Paintner, F.F., Wanner, K.T., Worek, F., Thiermann, H., Gohlke, H., 2023. A novel binding site in the nicotinic acetylcholine receptor for MB327 can explain its allosteric modulation relevant for organophosphorus-poisoning treatment. Toxicology Letters 373, 160-171.

Kaiser, J., Gertzen, C.G.W., Bernauer, T., Nitsche, V., Höfner, G., Niessen, K.V., Seeger, T., Paintner, F.F., Wanner, K.T., Steinritz, D., Worek, F., Gohlke, H., 2024. Identification of ligands binding to MB327-PAM-1, a binding pocket relevant for resensitization of nAChRs. Toxicology Letters, submitted. Preprint bioRxiv doi: https://doi.org/10.1101/2023.12.21.572862.

Koelle, G.B., 1981. Organophosphate poisoning—An overview. Fundamental and Applied Toxicology 1, 129-134.

Lazaridis, T., 1998. Inhomogeneous Fluid Approach to Solvation Thermodynamics. 1. Theory. The Journal of Physical Chemistry B 102, 3531-3541.

Lott, R.S., Chauhan, V.S., Stammer, C.H., 1979. Trimethylsilyl iodide as a peptide deblocking agent. Journal of the Chemical Society, Chemical Communications, 495-496.

M. J. Frisch, G.W.T., H. B. Schlegel, G. E. Scuseria,, M. A. Robb, J.R.C., G. Scalmani, V. Barone,, G. A. Petersson, H.N., X. Li, M. Caricato, A. V. Marenich,, J. Bloino, B.G.J., R.

Gomperts, B. Mennucci, H. P. Hratchian,, J. V. Ortiz, A.F.I., J. L. Sonnenberg, D. Williams-Young,, F. Ding, F.L., F. Egidi, J. Goings, B. Peng, A. Petrone,, T. Henderson, D.R., V. G. Zakrzewski, J. Gao, N. Rega,, G. Zheng, W.L., M. Hada, M. Ehara, K. Toyota, R. Fukuda,, J. Hasegawa, M.I., T. Nakajima, Y. Honda, O. Kitao, H. Nakai,, T. Vreven, K.T., J. A. Montgomery, Jr., J. E. Peralta,, F. Ogliaro, M.J.B., J. J. Heyd, E. N. Brothers, K. N. Kudin,, V. N. Staroverov, T.A.K., R. Kobayashi, J. Normand,, K. Raghavachari, A.P.R., J. C. Burant, S. S. Iyengar,, J. Tomasi, M.C., J. M. Millam, M. Klene, C. Adamo, R. Cammi,, J. W. Ochterski, R.L.M., K. Morokuma, O. Farkas,, J. B. Foresman, a.D.J.F., 2016. Gaussian16. vol. Revision A.03. Gaussian Inc., Wallingford CT.

Maselli, R.A., Leung, C., 1993. Analysis of anticholinesterase-induced neuromuscular transmission failure. Muscle & Nerve 16, 548-553.

Massoulié, J., Pezzementi, L., Bon, S., Krejci, E., Vallette, F.-M., 1993. Molecular and cellular biology of cholinesterases. Progress in Neurobiology 41, 31-91.

Nguyen, C., Gilson, M.K., Young, T., 2011. Structure and Thermodynamics of Molecular Hydration via Grid Inhomogeneous Solvation Theory. arXiv, 1108.4876.

Nguyen, C.N., Young, T.K., Gilson, M.K., 2012. Grid inhomogeneous solvation theory: hydration structure and thermodynamics of the miniature receptor cucurbit[7]uril. J Chem Phys 137, 044101.

Niessen, K.V., Muschik, S., Langguth, F., Rappenglück, S., Seeger, T., Thiermann, H., Worek, F., 2016. Functional analysis of Torpedo californica nicotinic acetylcholine receptors in multiple activation states by SSM-based electrophysiology. Toxicology Letters 247, 1-10.

Niessen, K.V., Seeger, T., Rappenglück, S., Wein, T., Höfner, G., Wanner, K.T., Thiermann, H., Worek, F., 2018. In vitro pharmacological characterization of the bispyridinium non-oxime compound MB327 and its 2- and 3-regioisomers. Toxicology Letters 293, 190-197.

Nitsche, V., Höfner, G., Kaiser, J., Gertzen, C.G.W., Seeger, T., Niessen, K.V., Steinritz, D., Worek, F., Gohlke, H., Paintner, F.F., Wanner, K.T., 2024. MS Binding Assays with UNC0642 as reporter ligand for the MB327 binding site of the nicotinic acetylcholine receptor. Toxicology Letters 392, 94-106.

Noviello, C.M., Gharpure, A., Mukhtasimova, N., Cabuco, R., Baxter, L., Borek, D., Sine, S.M., Hibbs, R.E., 2021. Structure and gating mechanism of the α7 nicotinic acetylcholine receptor. Cell 184, 2121-2134.e2113.

OPCW, 2017. OPCW Director-General Shares Incontrovertible Laboratory Results Concluding Exposure to Sarin, 19.04.2017.

OpenEye Scientific Software, I., 2021. SZYBKI. OpenEye Scientific Software, Santa Fe, NM.

Pauli, G.F., Chen, S.-N., Simmler, C., Lankin, D.C., Gödecke, T., Jaki, B.U., Friesen, J.B., McAlpine, J.B., Napolitano, J.G., 2014. Importance of Purity Evaluation and the Potential of Quantitative 1H NMR as a Purity Assay. Journal of Medicinal Chemistry 57, 9220-9231.

Pettersen, E.F., Goddard, T.D., Huang, C.C., Couch, G.S., Greenblatt, D.M., Meng, E.C., Ferrin, T.E., 2004. UCSF Chimera—A visualization system for exploratory research and analysis. Journal of Computational Chemistry 25, 1605-1612.

Pita, R., Domingo, J., 2014. The Use of Chemical Weapons in the Syrian Conflict. Toxics 2, 391-402.

Price, K.E., Mason, B.P., Bogdan, A.R., Broadwater, S.J., Steinbacher, J.L., McQuade, D.T., 2006. Microencapsulated Linear Polymers: "Soluble" Heterogeneous Catalysts. Journal of the American Chemical Society 128, 10376-10377.

Ramsey, S., Nguyen, C., Salomon-Ferrer, R., Walker, R.C., Gilson, M.K., Kurtzman, T., 2016. Solvation thermodynamic mapping of molecular surfaces in AmberTools: GIST. Journal of Computational Chemistry 37, 2029-2037.

Rappenglück, S., Sichler, S., Höfner, G., Wein, T., Niessen, K.V., Seeger, T., Paintner, F.F., Worek, F., Thiermann, H., Wanner, K.T., 2018. Synthesis of a Series of Non-Symmetric Bispyridinium and Related Compounds and Their Affinity Characterization at the Nicotinic Acetylcholine Receptor. ChemMedChem 13, 2653-2663.

Roe, D.R., Cheatham, T.E., 3rd, 2013. PTRAJ and CPPTRAJ: Software for Processing and Analysis of Molecular Dynamics Trajectory Data. J Chem Theory Comput 9, 3084-3095.

Schott-Verdugo, S., Gohlke, H., 2019. PACKMOL-Memgen: A Simple-To-Use, Generalized Workflow for Membrane-Protein-Lipid-Bilayer System Building. J Chem Inf Model 59, 2522-2528.

Seeger, T., Eichhorn, M., Lindner, M., Niessen, K.V., Tattersall, J.E.H., Timperley, C.M., Bird, M., Green, A.C., Thiermann, H., Worek, F., 2012. Restoration of soman-blocked neuromuscular transmission in human and rat muscle by the bispyridinium non-oxime MB327 in vitro. Toxicology 294, 80-84.

Sheridan, R.D., Smith, A.P., Turner, S.R., Tattersall, J.E.H., 2005. Nicotinic Antagonists in the Treatment of Nerve Agent Intoxication. Journal of the Royal Society of Medicine 98, 114-115.

Sichler, S., Höfner, G., Rappenglück, S., Wein, T., Niessen, K.V., Seeger, T., Worek, F., Thiermann, H., Paintner, F.F., Wanner, K.T., 2018. Development of MS Binding Assays targeting the binding site of MB327 at the nicotinic acetylcholine receptor. Toxicology Letters 293, 172-183.

Steindl, D., Boehmerle, W., Körner, R., Praeger, D., Haug, M., Nee, J., Schreiber, A., Scheibe, F., Demin, K., Jacoby, P., Tauber, R., Hartwig, S., Endres, M., Eckardt, K.-U., 2021. Novichok nerve agent poisoning. The Lancet 397, 249-252.

Thakur, R., Haru, E., 2007. The Chemical Weapons Convention: Implementation, Challenges, Opportunities.

Thiermann, H., Seeger, T., Gonder, S., Herkert, N., Antkowiak, B., Zilker, T., Eyer, F., Worek, F., 2010. Assessment of neuromuscular dysfunction during poisoning by organophosphorus compounds. Chemico-Biological Interactions 187, 265-269.

Tian, C., Kasavajhala, K., Belfon, K.A.A., Raguette, L., Huang, H., Migues, A.N., Bickel, J., Wang, Y., Pincay, J., Wu, Q., Simmerling, C., 2020. ff19SB: Amino-Acid-Specific Protein Backbone Parameters Trained against Quantum Mechanics Energy Surfaces in Solution. J Chem Theory Comput 16, 528-552.

Timperley, C.M., Bird, M., Green, C., Price, M.E., Chad, J.E., Turner, S.R., Tattersall, J.E., 2012. 1, 1′-(Propane-1, 3-diyl) bis (4-tert-butylpyridinium) di (methanesulfonate) protects guinea pigs from soman poisoning when used as part of a combined therapy. MedChemComm 3, 352-356.

Turner, S.R., Chad, J.E., Price, M., Timperley, C.M., Bird, M., Green, A.C., Tattersall, J.E.H., 2011. Protection against nerve agent poisoning by a noncompetitive nicotinic antagonist. Toxicology Letters 206, 105-111.

Wang, J., Wolf, R.M., Caldwell, J.W., Kollman, P.A., Case, D.A., 2004. Development and testing of a general amber force field. Journal of Computational Chemistry 25, 1157-1174.

Wang, X., Long, C.-Y., Su, M.-H., Qu, Y.-X., Li, S.-H., Zhang, X.-J., Huang, S.-J., Wang, X.-Q., 2019. Rapid Amination of Methoxy Pyridines with Aliphatic Amines. Organic Process Research & Development 23, 1587-1593.

Worek, F., Thiermann, H., Wille, T., 2020. Organophosphorus compounds and oximes: a critical review. Archives of Toxicology 94, 2275-2292.

Supporting Information

Synthesis and Biological Evaluation of Novel MB327 Analogs as Resensitizers for Desensitized Nicotinic Acetylcholine Receptors after Intoxication with Nerve Agents

Tamara Bernauer[a], Valentin Nitsche[a], Jesko Kaiser[b], Christoph G.W. Gertzen[b], Georg Höfner[a], Karin V. Niessen[c], Thomas Seeger[c], Dirk Steinritz[c], Franz Worek[c], Holger Gohlke[b,d], Klaus T. Wanner[a] and Franz F. Paintner*[a]

[a] T. Bernauer, V. Nitsche, Dr. G. Höfner, Prof. Dr. K. T. Wanner, Prof. Dr. F. F. Paintner
Department of Pharmacy, Center for Drug Research
Ludwig-Maximilians-Universität München
Butenandtstrasse 5-13, 81377 Munich (Germany)
E-mail: Franz.Paintner@cup.uni-muenchen.de

[b] J. Kaiser, Dr. C. G. W. Gertzen, Prof. Dr. H. Gohlke
Institute for Pharmaceutical and Medicinal Chemistry
Heinrich Heine Universität Düsseldorf
Universitätsstrasse 1, 40225 Düsseldorf (Germany)

[c] Dr. K. V. Niessen, Dr. T. Seeger, Prof. Dr. D. Steinritz, Prof. Dr. F. Worek
Bundeswehr Institute of Pharmacology and Toxicology
Neuherbergstrasse 11, 80937 Munich (Germany)

[d] Prof. Dr. H. Gohlke
John von Neumann Institute for Computing (NIC), Jülich Supercomputing Centre (JSC), Institute of Biological Information Processing (IBI-7: Structural Biochemistry) & Institute of Bio- and Geosciences (IBG-4: Bioinformatics)
Forschungszentrum Jülich
Wilhelm-Johnen-Strasse, 52428 Jülich (Germany)

Table of Content

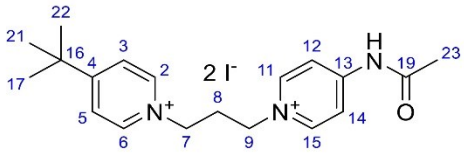

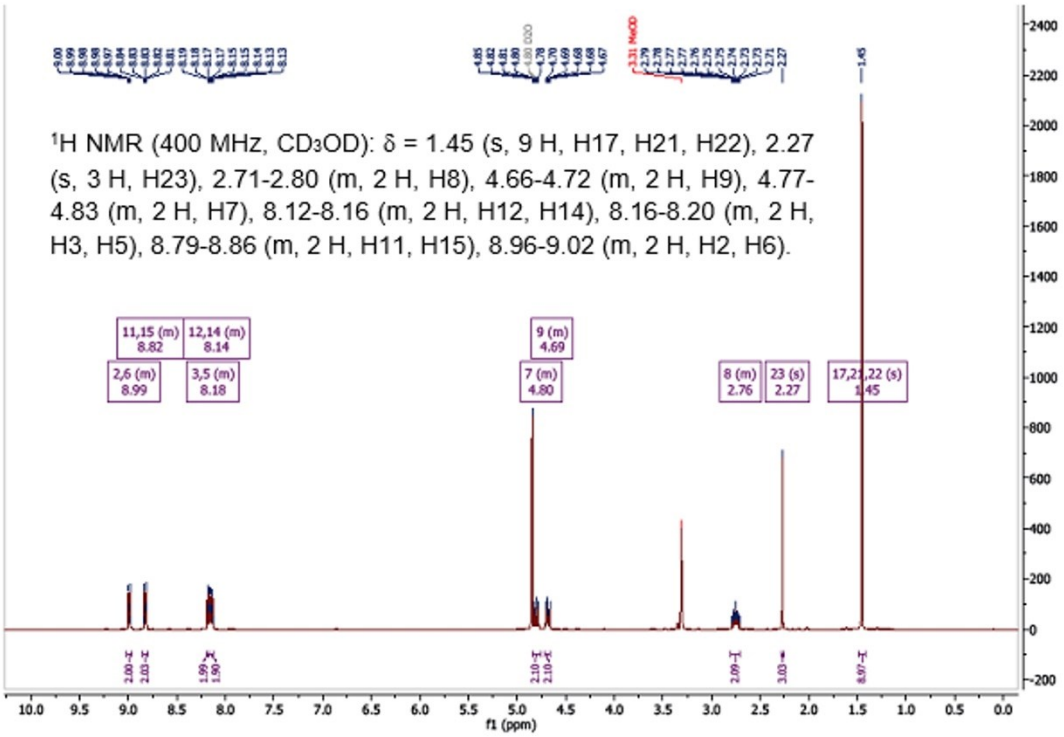

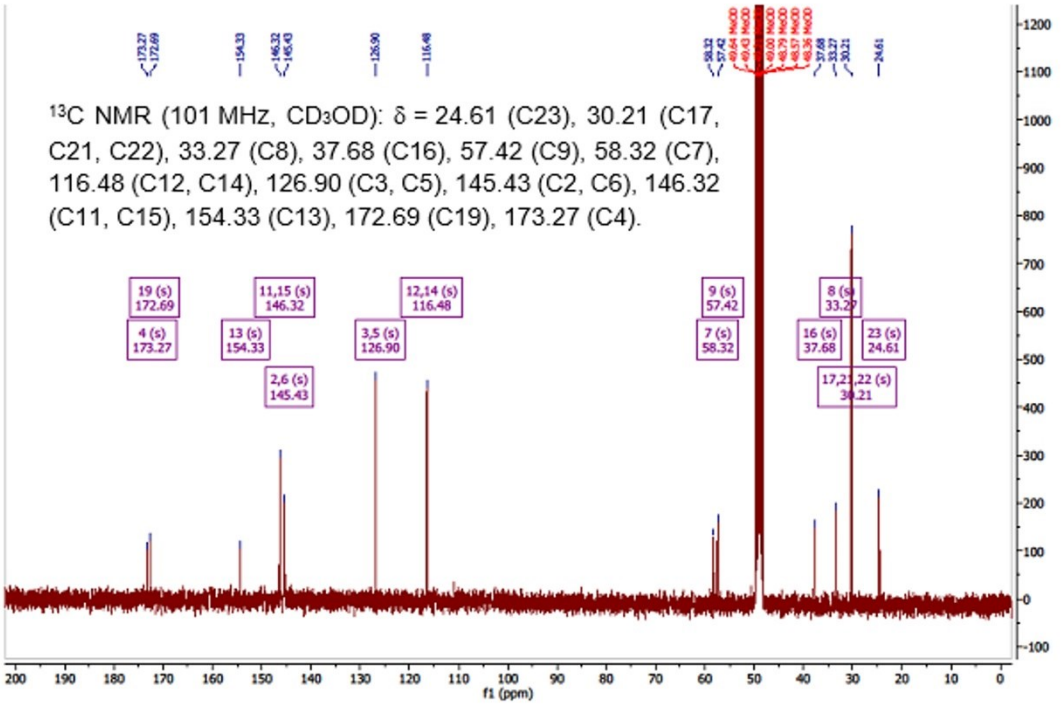

Figure S1: ^{1}H and ^{13}C NMR spectrum of PTM0064 (**6a**), as an example of a non-symmetric bispyridinium compound, with signals assigned.

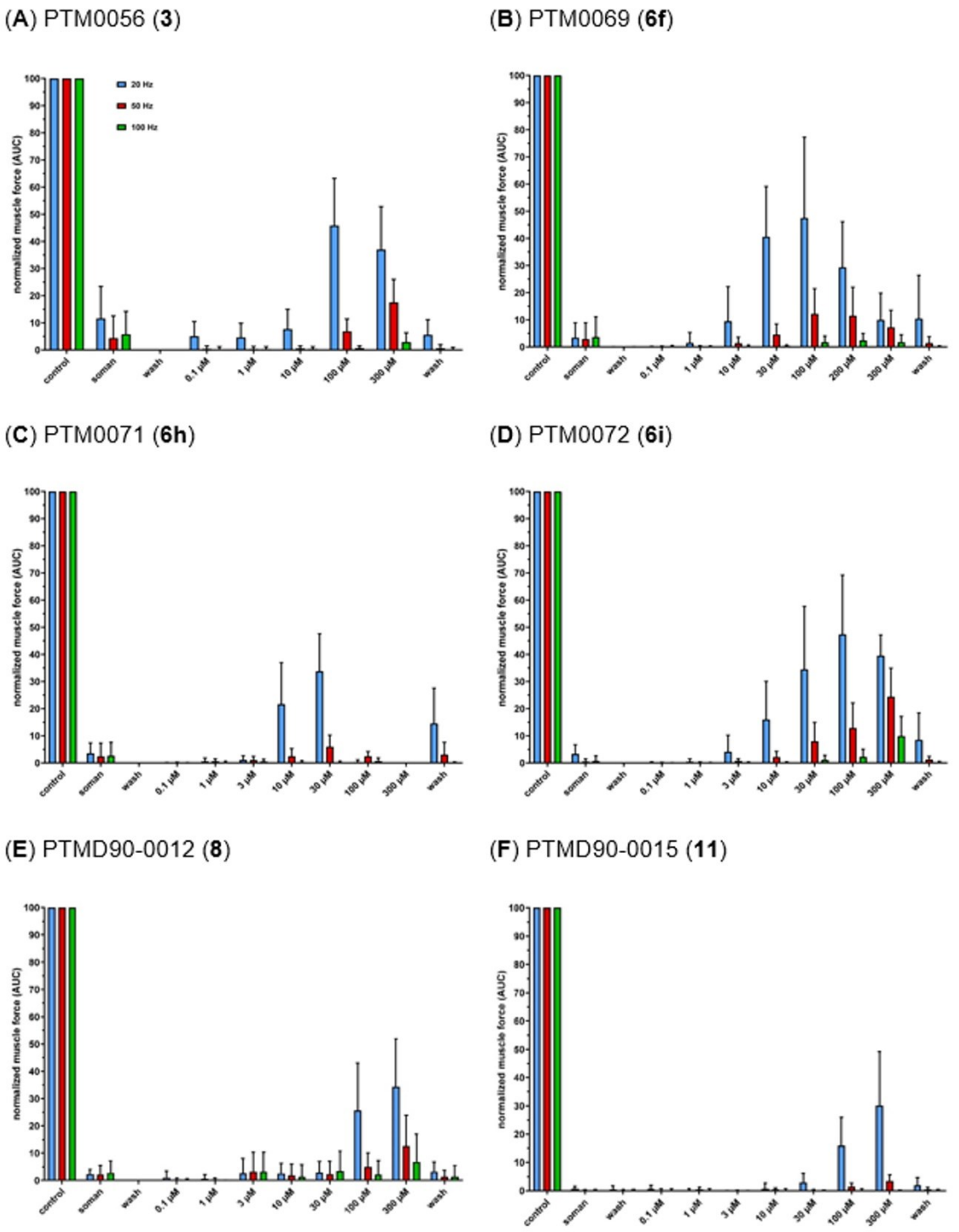

Figure S2: Concentration-dependent restoration of the muscle force by (**A**) PTM0056 (**3**), (**B**) PTM0069 (**6f**), (**C**) PTM0071 (**6h**), (**D**) PTM0072 (**6i**), (**E**) PTMD90-0012 (**8**), (**F**) PTMD90-0015 (**11**) of rat diaphragm preparations after poisoning with soman (3 µM). For indirect stimulation, a frequency of 20 Hz, 50 Hz and 100 Hz was applied. Data are shown as % of control and are given as mean ± SD (n = 4-25).

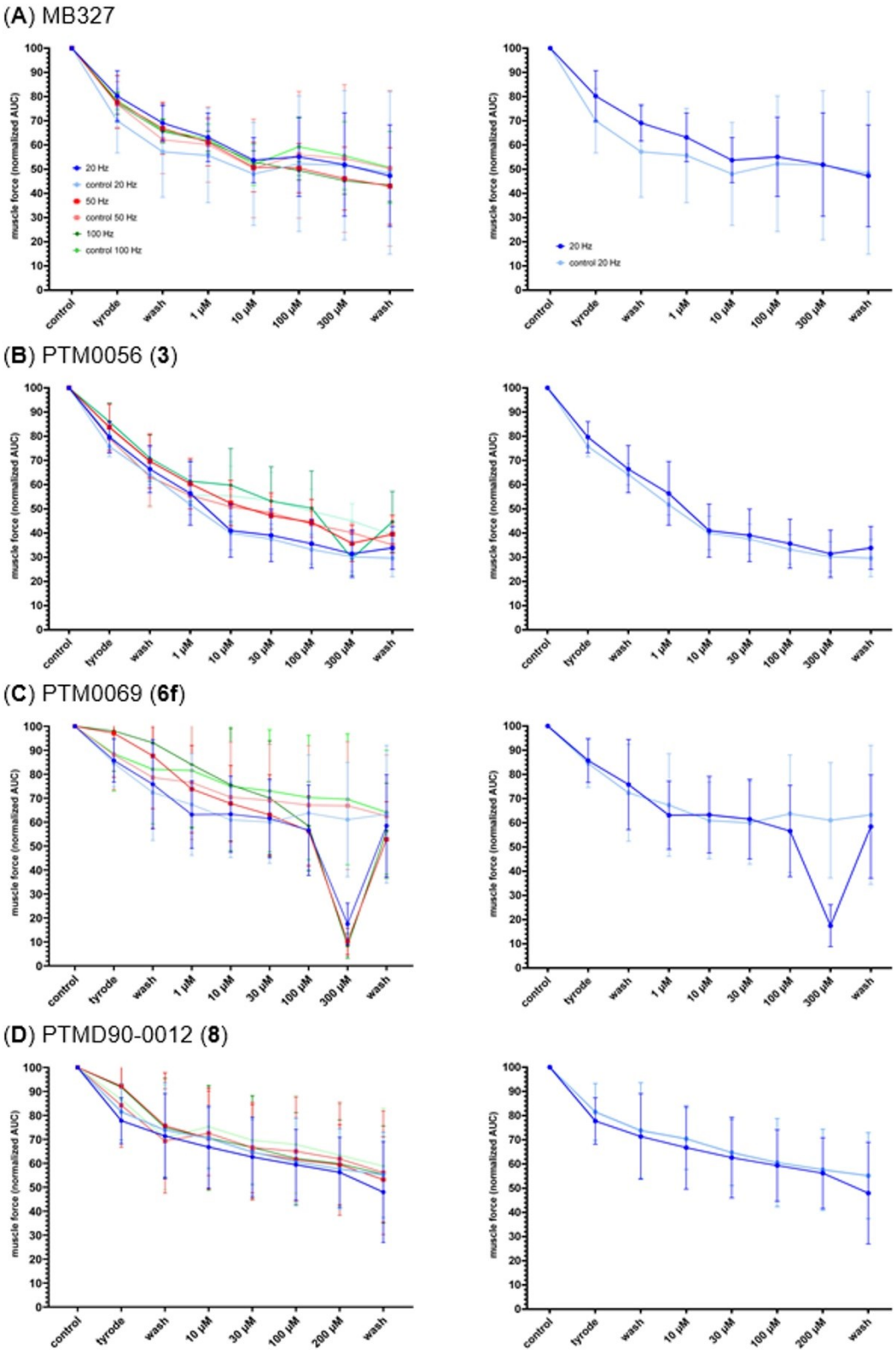

Figure S3: Muscle force of unpoisoned rat diaphragms after treatment with (**A**) MB327, (**B**) PTM0056 (**3**), (**C**) PTM0069 (**6f**) and (**D**) PTMD90-0012 (**8**). For indirect stimulation, a frequency of 20 Hz, 50 Hz and 100 Hz was applied. Muscle force generation was presented as the area under the curve normalized to muscle force under control conditions at the start of the measurement.

5

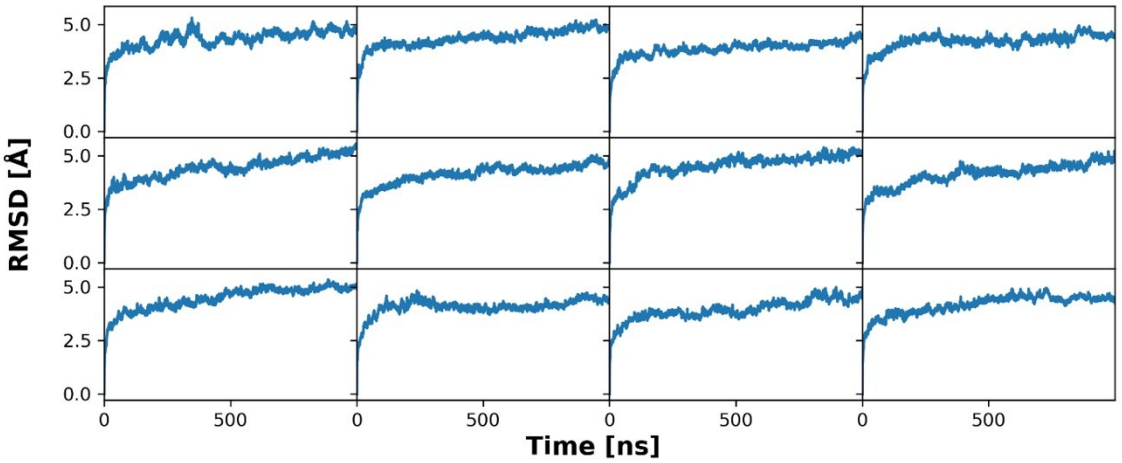

Figure S4: Backbone (C, CA, N) RMSD of 12 replicas of 1 µs long MD simulations of MB327 bound to the human nAChR compared to the first frame of each simulation.

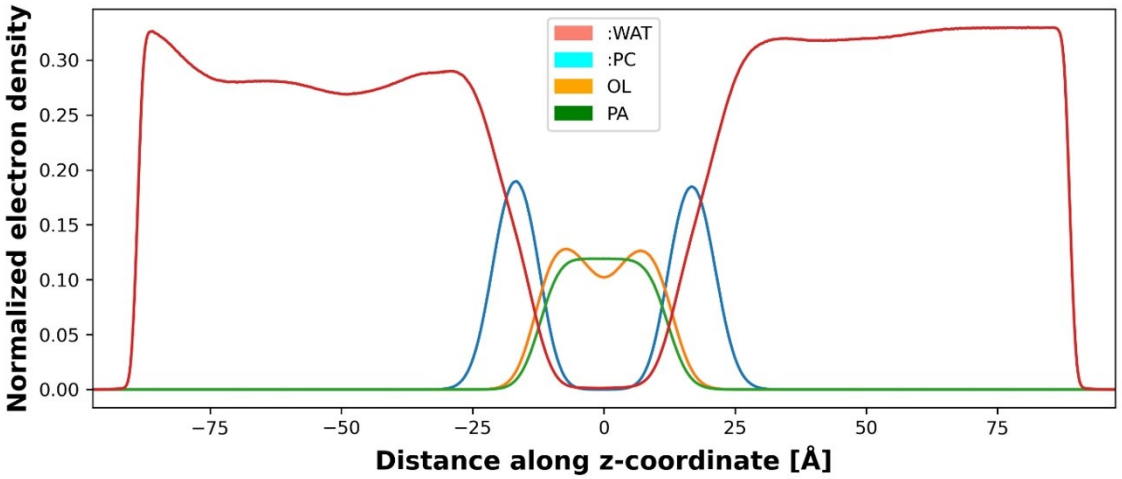

Figure S5: Normalized electron density of water and membrane components averaged over all replicas during MD simulations.

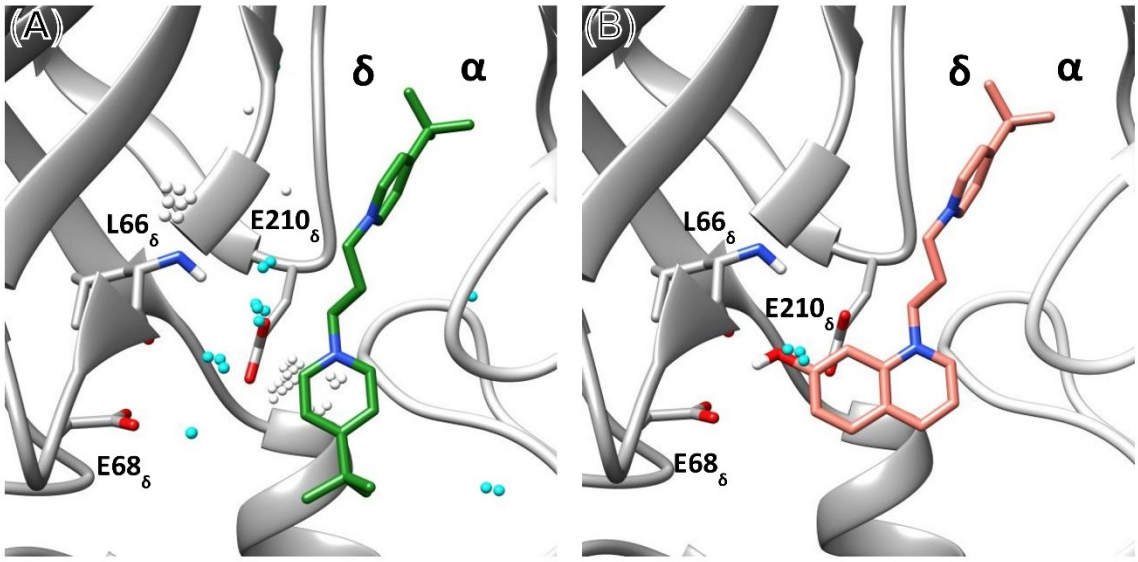

Figure S6: MB327 analog based on substituting water molecules in the allosteric MB327-PAM-1 binding pocket between the α- and δ-subunit. **A)** MB327 binding in between the α- and δ-subunit. Water clusters as identified by GIST are shown as spheres; clusters within 5 Å of MB327 are colored cyan. **B)** Proposed binding mode of PTMD90-0012 (salmon) in between the α- and δ-subunit. Modification of MB327 to PTMD90-0012 (salmon) leads to a substitution of a water cluster located in proximity to $L66_{\delta}$, $E68_{\delta}$, and $E210_{\delta}$. For $L66_{\delta}$, the backbone atoms are shown in addition to the side chain.

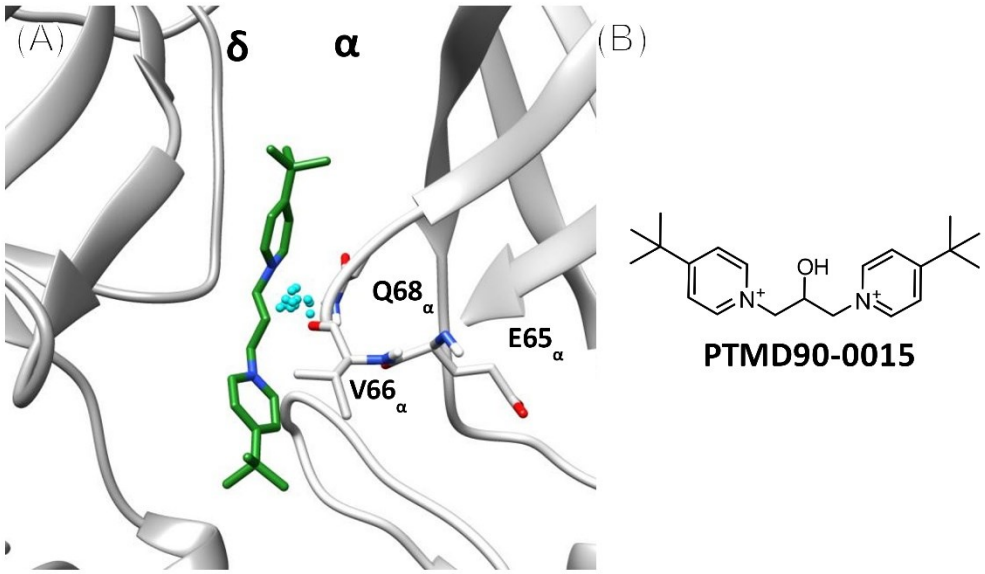

Figure S7: Initial water cluster leading to the design of PTMD90-0015. **A)** During the first few replicas (5 out of 12) of MD simulations of MB327 in MB327-PAM-1, an energetically unfavorable cluster of water molecules was identified in between the backbone atoms of $E65_{\alpha}$, $V66_{\alpha}$, and $Q68_{\alpha}$ close to the C3-linker of MB327 in a representative binding mode during MD simulations (*k*-means clustering based on MB327 atoms ligand between the α- and δ-subunit). Based on these preliminary results, **B)** PTMD90-0015 was designed. This water cluster was later only observed in between the δ- and α-subunit. However, there, no docked or representative structure from MD simulations was in the range to form interactions with the protein after modification of MB327 to PTMD90-0015.

3.5 Fünfte Publikation (Manuskript)

"Structure-Affinity Relationship of Quinazoline Derivatives as Potential Resensitizers of Desensitized nAChRs After Nerve Agent Intoxication"

3.5.1 Zusammenfassung der Ergebnisse

Bei der Suche nach allosterischen Modulatoren, die den nikotinischen Acetylcholinrezeptor (nAChR) nach Desensitisierung in einen funktionalen Zustand zurückführen (sogenannte „Resensitizer"), wurden bisher hauptsächlich Bispyridiniumverbindungen untersucht. „Resensitizer" des nAChRs werden dringend benötigt, um das Therapieschema bei Vergiftungen mit Organophosphatverbindungen zu verbessern. Zuletzt wurde entdeckt, dass einige Substanzen, die alle auf einem Chinazolin-Gerüst basieren, dieselbe Bindungsstelle wie MB327 – die wohl prominenteste der bisher untersuchten Bispyridiniumverbindungen – adressieren. Die Chinazolin-basierten Verbindungen sind für die Weiterentwicklung von „Resensitizern" besonders interessant, da ihre Affinität zur MB327-Bindungsstelle des nAChRs deutlich höher ist als die von MB327. Um die Struktur-Affinitäts-Beziehungen der Chinazolin-basierten Verbindungen hinsichtlich der MB327-PAM-1-Bindungsstelle des nAChRs besser zu verstehen, wurden in dieser Arbeit zahlreiche Verbindungen mit einem Chinazolin-Grundgerüst synthetisiert. Durch das Anwenden und Anpassen literaturbekannter Methoden konnte eine große Breite an verschiedenartig substituierten Chinazolinen hergestellt werden. Diese sind als systematisch abgewandelte Analoga von UNC0646 – der Verbindung mit der bis dato höchsten Affinität zur MB327-Bindungsstelle des nAChRs – zu verstehen. Des Weiteren wurde das Chinazolin-Grundgerüst mit neuartigen Resten substituiert, um so den Strukturraum von UNC0646-Analoga noch ausgiebiger zu untersuchen. Alle neu synthetisierten Verbindungen wurden mit Hilfe des kürzlich entwickelten UNC0642-MS-Bindungsassays hinsichtlich ihrer Affinität zur MB327-PAM-1-Bindungsstelle untersucht. In einigen Fällen wurden, um zusätzlich Erkenntnisse zu erlangen, auch kommerziell verfügbare Verbindungen in diese Untersuchungen miteinbezogen. Die mit der Untersuchung der zahlreichen, mit diversen Resten in 2-, 4- und 7-Position substituierten Chinazolinderivate gewonnenen Erkenntnisse ermöglichen erste Rückschlüsse, welche Strukturelemente für die Affinität der UNC0646-Analoga zur MB327-Bindungsstelle des nAChRs von besonderer Bedeutung sind – und stellen

damit insbesondere für *in silico* Experimente eine wichtige Grundlage dar. Die in dieser Arbeit gewonnen Daten sind deshalb von immensem Wert für die zielgerichtete Weiterentwicklung von „Resensitizern“ des nAChRs, auch wenn von den insgesamt mehr als 50 untersuchten Verbindungen nur eine Substanz, UNC0631, eine geringfügig gesteigerte Affinität (pK_i = 6.04 ± 0.04) im Vergleich zu UNC0646 (pK_i = 5.83 ± 0.05) aufweist.

3.5.2 Erklärung zum Eigenanteil

Das Manuskript wurde gemeinsam von Tamara Bernauer und mir verfasst. Die in der Arbeit beschriebenen Synthesen wurden von Tamara Bernauer durchgeführt. Die Untersuchung der in diesem Manuskript gezeigten Testverbindungen hinsichtlich ihrer Affinität durch MS-Bindungsexperimente wurde eigenständig von mir durchgeführt und die entsprechenden Ergebnisse von mir ausgewertet. Der Abschnitt zur Synthese inklusive aller Grafiken und Tabellen und jener zur biologischen Prüfung wurde von Tamara Bernauer bzw. mir erstellt. Das Konzept für das Manuskript wurde im Wesentlichen von Tamara Bernauer und mir entwickelt. Auch die Ergebnisse wurden von uns interpretiert. Bei Beidem wurden wir von Georg Höfner, Klaus T. Wanner und Franz F. Paintner unterstützt. Vor der Abgabe der Dissertation haben Klaus T. Wanner und Franz F. Paintner das Manuskript korrigiert. Derzeit ist geplant, noch einen Beitrag zu *in silico* Studien von Jesko Kaiser, Christoph G. W. Gertzen und Holger Gohlke vor der Publikation in das Manuskript aufzunehmen. Das Manuskript wird aller Voraussicht nach bei Toxicology Letters eingereicht werden, soll vorher aber noch den Kooperationspartnern bei der Bundeswehr, d.h. Thomas Seeger, Karin V. Niessen, Dirk Steinritz und Franz Worek zur Korrektur vorgelegt werden.

Structure-Affinity Relationship of Quinazoline Derivatives as Potential Resensitizers of Desensitized nAChRs After Nerve Agent Intoxication

Tamara Bernauer[+][a], Valentin Nitsche[+][a], Georg Höfner[a], Karin V. Niessen[b], Thomas Seeger[b], Dirk Steinritz[b], Franz Worek[b], Klaus T. Wanner[a] and Franz F. Paintner*[a]

[a] T. Bernauer, V. Nitsche, Dr. G. Höfner, Prof. Dr. K. T. Wanner, Prof. Dr. F. F. Paintner
Department of Pharmacy - Center for Drug Research
Ludwig-Maximilians-Universität München
Butenandtstrasse 5-13, 81377 Munich (Germany)
E-mail: Franz.Paintner@cup.uni-muenchen.de

[b] Dr. K. V. Niessen, Dr. T. Seeger, Prof. Dr. D. Steinritz, Prof. Dr. F. Worek
Bundeswehr Institute of Pharmacology and Toxicology
Neuherbergstrasse 11, 80937 Munich (Germany)

[+] These authors contributed equally to this work.

Author ORCID

Tamara Bernauer: 0000-0001-9570-1253

Valentin Nitsche: 0009-0000-3351-1227

Georg Höfner: 0000 0002 7957 4503

Karin Niessen: 0009-0008-6810-5294

Thomas Seeger: 0009-0007-5713-4367

Dirk Steinritz: 0000-0002-2073-5683

Franz Worek: 0000-0003-3531-3616

Klaus Wanner: 0000-0003-4399-1425

Franz Paintner: 0000-0002-6795-586X

Abstract

In order to improve the therapy in case of organophosphorus compound poisoning, which eventually leads to death if not treated properly, one promising approach seems to be the development of allosteric modulators of the nicotinic acetylcholine receptor (nAChR), so called resensitizers. Recently, it was found that quinazoline-based compounds may propose very promising candidates for this purpose, as several of them, for example UNC0646, display the highest yet known affinities for the corresponding binding site of the nAChR. With the intention to gain a better understanding regarding structure-affinity relationships within this class of compounds, we present the syntheses and the evaluation (via MS binding experiments) of a remarkable number of UNC0646 analogs in this study. On the one hand, our results show, how to easily access a variety of UNC0646 analogs with different substituents in positions 2, 4 and 7 of the quinazoline. Furthermore, the results of MS Binding Assays for this plethora of compounds are of great value regarding the specific design of novel, ideally more affine (and therefore hopefully more potent) quinazoline-based compounds in the future.

1 Introduction

Organophosphorus compounds (OPCs), commonly used as pesticides (Freire and Koifman, 2013) but also as chemical weapons, e.g. in the brutal civil war in Syria (Dolgin, 2013; OPCW, 2017; Pita and Domingo, 2014), can cause severe health damage upon exposure. They interfere with the cholinergic system, where the formed OPC-acetylcholinesterase (AChE) complexes prevent the necessary cleavage of the neurotransmitter acetylcholine (ACh) in the synaptic cleft of cholinergic neurons, so that the accumulated ACh triggers overstimulation of the associated muscarinic (mAChRs) and nicotinic acetylcholine receptors (nAChRs) (Brown and Brix, 1998; Maselli and Leung, 1993; Massoulié et al., 1993; Thiermann et al., 2010). The resulting so-called "cholinergic crisis" manifests itself in mild poisoning, e.g. by abdominal cramping and vomiting; severe poisoning is life-threatening if medical treatment is inadequate because of the onset of respiratory arrest (Newmark, 2007). The most common approach to counteract overstimulation of the affected receptors involves, on the one hand, the degradation of ACh catalyzed by AChE reactivated by oxime drugs and, on the other hand, the antagonization of ACh at the mAChR by administration of atropine to reduce neuronal signal transduction (Shih et al., 2007; Thiermann and Worek, 2022; Worek et al., 2005). However, the current treatment approach has major gaps, as present oxime drugs show only limited efficacy on specific OPC-AChE complexes, and despite extensive research in this field, no universal oxime therapy has yet been presented (Worek et al., 2020). At the same time, there are no competitive nAChR antagonists that act directly on the corresponding receptors, which is why the receptors rapidly enter a desensitized state with interrupted cholinergic signal transduction (Papke, 2014). Therefore, an important approach to improve OPC treatment is to directly address the nAChR with allosteric ligands, so-called resensitizers, in order to reactivate the inactive nAChRs (Sheridan et al., 2005; Turner et al., 2011).

Initially, bispyridinium compounds such as MB327 were investigated for this purpose, whereby beneficial pharmacological aspects could be detected in various *in vitro*, *ex vivo* as well as *in vivo* experiments (Niessen et al., 2016; Niessen et al., 2018; Seeger et al., 2012; Timperley et al., 2012; Turner et al., 2011). Nevertheless, both the affinity to the nAChR and the potency of MB327, were insufficient to be applicable as a therapeutic agent (Kassa et al., 2022; Price et al., 2016). Detailed *in silico* studies of the binding mode led to the identification of an allosteric binding pocket (MB327-PAM-1) (Kaiser et al., 2023). And even while our recently synthesized MB327 analogs have shown that the development of more potent bispyridinium compounds with higher binding affinity to the nAChR and higher muscle reactivation ability is possible (Bernauer et al., 2024; Kaiser et al., 2023; Rappenglück et al., 2018a, b), it again became clear that the potency of the compounds is far from meeting the requirements for a drug candidate.

Moving away from the syntheses of compounds based on MB327, we have therefore dedicated ourselves to the search for a new compound class with higher affinity towards the MB327-PAM-1 binding site, which would benefit their use as therapeutic agents. To this purpose, we recently screened two compound libraries with our [$^2H_6$]MB327 MS Binding Assay, identifying a series of quinazoline derivatives, specifically UNC0646 (**1**), UNC0642 (**2**), and UNC0638 (**3**), which have a distinctly higher affinity towards the MB327-PAM-1 binding site than the so far investigated bispyridinium compounds, showing K_i values around low micromolar concentrations (Figure 1) (Sichler et al., 2024). Based on these new quinazoline-based ligands, with the highest yet known affinities towards the binding site of interest, we developed an alternative MS Binding Assay with UNC0642 (**2**) as the reporter ligand and UNC0638 (**3**) as the internal standard, which provides a valuable alternative for characterizing binding

affinities of ligands towards the MB327-PAM-1 binding site of *Torpedo*-nAChR (Nitsche et al., 2024). Applying this assay, it was proven, that UNC0646 (**1**) is the allosteric ligand with the highest yet known binding affinity of $pK_i = 5.83 \pm 0.05$ making this compound an indispensable candidate as a new scaffold structure for the development of new derivatives.

Initial *in silico* studies involving flexible docking studies and MD simulations to analyze the binding behavior of UNC0646 (**1**) to the receptor identified strong binding interactions (in the form of salt bridge binding) of the substituent in the 4-position with glutamate residues in the binding pocket. Further, but probably weaker interactions between the ligand and the glutamate residues are conceivable, whereby the diazepane in the 2-position appears to be the less important (Nitsche et al., 2024). Broadening the spectrum of consideration by synthesizing and characterizing structurally different UNC0646 analogs in our MS Binding Assay showed that some increased flexibility of the substituents in the 4-position was beneficial in terms of binding, and thus even replacing the basic side chain in the 7-position with a methoxy residue was tolerated in this case (Kaiser et al., 2024). These initial indications of the binding behavior of UNC0646 (**1**) are helpful, but for further development of more comprehensive structure-affinity relationships the characterization of a large group of analogs with systematic structural variations is essential so that new potential allosteric nAChR modulators can be designed rationally. Especially considering that UNC0646 (**1**) does not meet the standard criteria for a drug candidate in terms of molecular weight, it is of great importance to find out, which components of the molecule are particularly important for its affinity, in order to reduce its size and ideally further enhance its affinity.

In this work, we synthesized a variety of UNC0646 analogs with quinazoline scaffold and varying substituents in the 2-, 4-, and 7-position. These compounds, along with commercially acquired ones, were then investigated using the newly developed UNC0642 MS Binding Assay, evaluating their binding affinities towards the *Torpedo*-nAChR. First, by systematic structural simplification of the individual substituents starting from UNC0646 (**1**), their relevance concerning binding affinity was investigated. In addition, we generated simplified, rapidly synthesizable quinazoline compounds in which either the 2-position was unsubstituted, or the basic side chain in the 7-position was reduced in size in order to improve the efficiency of the investigation of the binding behavior of UNC0646 analogs.

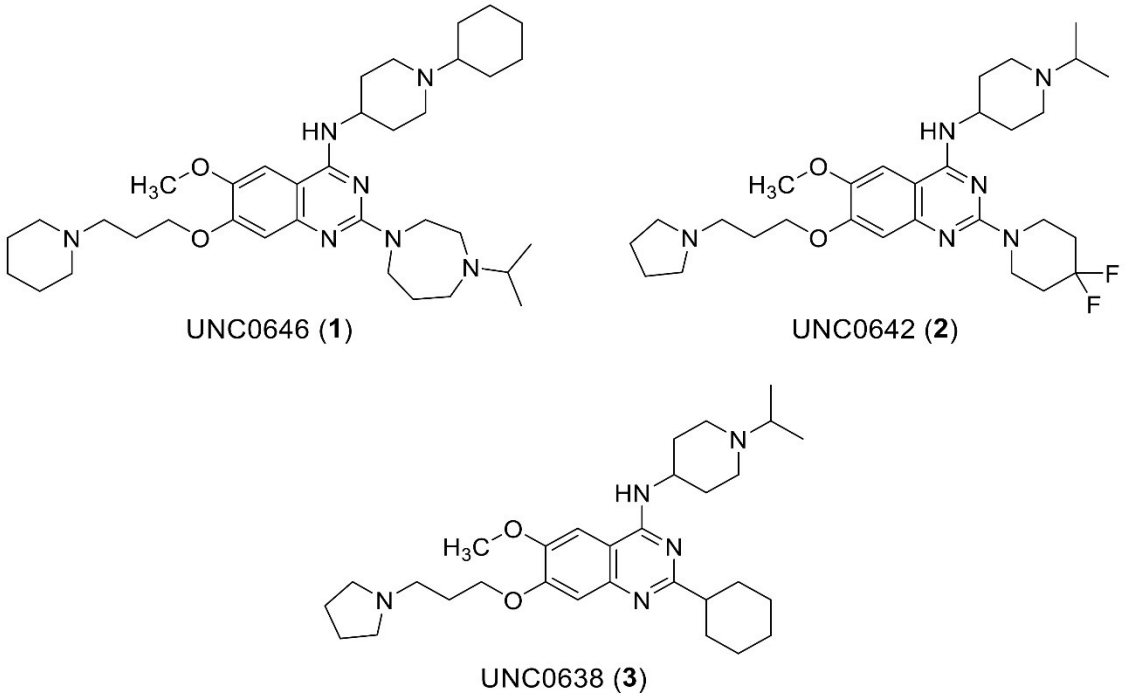

Figure 1. Quinazoline-based ligands towards MB327-PAM-1: UNC0646 (**1**), UNC0642 (**2**) and UNC0638 (**3**).

2 Material and Methods

All target compounds synthesized in the context of this study were cataloged with a certain PTMD number (Pharmacy and Toxicology Munich and Düsseldorf).

2.1 Chemistry

All chemicals were used as purchased from commercial sources. Solvents used for purification were distilled before use. Amines, which could only be purchased as the respective hydrochloride salts (1-cyclohexylpiperidin-4-amine dihydrochloride, 1-(cyclohexylmethyl)-piperidin-4-amine dihydrochloride and 5-pyrrolidin-1-ylpentan-1-amine dihydrochloride) were converted into the free bases before use (Mellstedt et al., 2020). Anhydrous reactions were carried out under argon atmosphere in vacuum-dried glassware. For Microwave reactions, a Discover SP microwave system by CEM GmbH was used. TLC-Analysis was performed on plates purchased from Merck (silica gel $60F_{254}$ on aluminum sheet). Flash chromatography was carried out using Merck silica gel 60 (40-63 mm mesh size) as stationary phase. Melting points were determined with a Büchi 510 melting point instrument and are uncorrected. IR spectra were recorded on a PerkinElmer FT-IR Spectrometer 1600 as films. ^{1}H and ^{13}C NMR spectra were recorded with a Bruker BioSpin Avance III HD 400 and 500 MHz at 25 °C. For data processing, MestReNova (Version 14.1.0) from Mestrelab Research S.L. 2019, and for calibration, the solvent signal (CD_2Cl_2, CD_3OD or $CDCl_3$) was used. Due to signal overlap in 2D-NMR, signals that could not be unambiguously assigned were marked with *. The purity of all test compounds was ≥ 95% as determined using quantitative NMR using TraceCERT® ethyl 4-(dimethylamino)benzoate from Merck as internal calibrant (Cushman et al., 2014; Pauli et al., 2014). High-resolution MS spectra were recorded with a Finnigan MAT 95 (EI) or a Finnigan LTQ FT (ESI). The analytical data of the synthesized compounds described below, obtained using the described methods, can be found in the Supporting Information.

The following compounds were prepared according to literature:

4-Chloro-6-methoxy-2-(piperidin-1-yl)-7-[3-(piperidin-1-yl)propoxy]quinazoline (**8**) (Kaiser et al., 2024), 4-chloro-6-methoxy-7-[3-(piperidin-1-yl)propoxy]quinazoline (**15**) (Kaiser et al., 2024), 7-fluoro-*N*-(1-isopropylpiperidin-4-yl)-6-methoxyquinazolin-4-amine (**22**) (Kaiser et al., 2024), 4-(*tert*-butyl)-1-(3-iodopropyl)pyridin-1-ium iodide (Rappenglück et al., 2018a).

General procedures

Synthesis of 4-amino-substituted 2-chloroquinazolines (GP1): A solution of the respective 2,4-dichloroquinazoline **6** or **24** (1.0 equiv), the corresponding amine (1.1 equiv) and *N*,*N*-diisopropylethylamine (DIEA) (3.0 equiv) in dry THF (4 mL/mmol) was stirred at rt for 48 h. The reaction mixture was concentrated in vacuo and the crude product was purified by flash chromatography [5% to 15% 3 M NH_3 (in MeOH) in CH_2Cl_2]. Synthesized compounds: **7** (yellow solid, 64% yield, 96% purity), **10a** (yellow solid, 86% yield, 99% purity), **10b** (yellow solid, 48% yield, 97% purity), **10c** (colorless solid, 86% yield, 96% purity), **25** (colorless solid,

81% yield, 95% purity), **26** (colorless solid, 65% yield, 99% purity), **27** (pale yellow solid, 98% yield, 98% purity).

Synthesis of 2,4-diamino-substituted quinazolines (GP2): A mixture of the respective 4-amino-substituted 2-chloroquinazoline **7**, **10**, **12**, **25**, **26** or **27** (1.0 equiv) and the corresponding amine (5.0 equiv) in toluene (2-5 mL/mmol) was stirred at 130 °C under microwave irradiation (300 W) for 50 min. The reaction mixture was concentrated in vacuo and the crude product was purified by flash chromatography [5% to 20% 3 M NH_3 (in MeOH) in CH_2Cl_2]. Synthesized compounds: **9a** (colorless solid, 89% yield, 97% purity), **9b** (colorless solid, 89% yield, 99% purity), **11a** (pale yellow solid, 89% yield, 95% purity), **11b** (colorless solid, 62% yield, 98% purity), **11c** (red solid, 91% yield, 98% purity), **14** (yellow oil, 99% yield, 97% purity), **28a** (yellow, hygroscopic solid, 90% yield, 97% purity), **28b** (yellow solid, 94% yield, 97% purity), **28c** (yellow solid, 97% yield, 97% purity), **31** (red solid, > 99% yield, 95% purity), **32a** (pale yellow solid, 91% yield, 95% purity), **32b** (pale yellow solid, 67% yield, 98% purity), **32c** (pale yellow solid, 84% yield, 98% purity), **32d** (colorless solid, 97% yield, 98% purity).

Synthesis of 4-amino-substituted quinazolin-2-amines (GP3): A solution of the respective 4-amino-substituted 2-chloroquinazoline **7** or **27** (1.0 equiv) and NaN_3 (1.1 equiv) in EtOH/AcOH (4:1) (6.7 mL/mmol) was stirred at 90 °C for 2 h. After cooling down, 10% Pd/C (0.10 equiv) and hydrazine hydrate (1.5 equiv) were gradually added and the mixture was again stirred at 90 °C for 2 h. The cold reaction mixture was filtered over a pad of celite, washed with EtOH and the solvent was removed in vacuo. The crude product was purified by flash chromatography [10% 3 M NH_3 (in MeOH) in CH_2Cl_2 or 5% to 10% 7 M NH_3 (in MeOH) in CH_2Cl_2]. Synthesized compounds: **9e** (colorless solid, 49% yield, 99% purity) and **16b** (colorless solid, 16% yield, 97% purity) as a side-product, **32e** (colorless solid, 78% yield, 96% purity) and **32f** (colorless solid, 5% yield, 95% purity) as a side-product.

Synthesis of 4-amino-substituted quinazolines (GP4): A solution of the respective 4-chloroquinazoline **8**, **15**, **17**, **29** or **33** (1.0 equiv), the corresponding amine (2.0 equiv) and *N*,*N*-diisopropylethylamine (DIEA) (3.0 equiv) in *i*-PrOH (5 mL/mmol) was stirred at 160 °C under microwave irradiation (200 W) for 15 min to 1 h. The reaction mixture was concentrated in vacuo and the crude product was purified by flash chromatography [5% to 15% 3 M NH_3 (in MeOH) in CH_2Cl_2]. Synthesized compounds: **9c** (colorless solid, 70% yield, 98% purity), **9f** (colorless solid, 58% yield, 99% purity), **16a** (colorless solid, 62% yield, 98% purity), **16b** (yellow solid, 94% yield, 95% purity), **16c** (colorless solid, 69% yield, 97% purity), **16d** (colorless solid, 82% yield, 100% purity), **16e** (colorless solid, 85% yield, 99% purity), **16f** (pale yellow solid, 83% yield, 98% purity), **18** (colorless solid, > 99% yield, 96% purity), **30a** (pale yellow, hygroscopic solid, 84% yield, 95% purity), **30b** (colorless solid, 64% yield, 97% purity), **34a** (pale yellow, hygroscopic solid, 86% yield, 99% purity), **34b** (colorless solid, 68% yield, 99% purity), **34c** (colorless solid, 73% yield, 97% purity).

***Mitsunobu*-reaction on quinazolin-7-ol 19 (GP5):** To a slurry of quinazolin-7-ol **19** (1.0 equiv), the corresponding alcohol (3.5-4.0 equiv) and PPh_3 (5.5 equiv) in dry THF (14.5 mL/mmol) at 0 °C diisopropyl azodicarboxylate (DIAD; 5.0 equiv) was added in portions. The resulting solution was stirred at rt for 20 h. The reaction mixture was concentrated in vacuo and the crude product was purified by flash chromatography [20% MeOH in CH_2Cl_2 or 10% 3 M NH_3 (in MeOH) in CH_2Cl_2]. Synthesized compounds: **20a** (colorless solid, 63% yield, 99% purity), **20c** (colorless solid, 79% yield, 99% purity), **20d** (colorless solid, 69% yield, 98%

purity), **20e** (colorless solid, 59% yield, 97% purity), **20f** (colorless solid, 46% yield, 100% purity), **20g** (colorless solid, 58% yield, 95% purity), **20h** (colorless solid, 78% yield, 96% purity), **21** (colorless solid, 92% yield, 99% purity).

Synthesis of 7-amino-substituted quinazolines (GP6): A mixture of 7-fluoroquinazolin-4-amine **22** (1.0 equiv), the corresponding amine (5.0 equiv) and K_2CO_3 (1.1 equiv) in *N*-methyl-2-pyrrolidone (NMP) (1.3 mL/mmol) was stirred at 135 °C for 20 h. The reaction mixture was concentrated in vacuo and the crude product was purified by flash chromatography [5% to 20% 3 or 7 M NH_3 (in MeOH) in CH_2Cl_2]. Synthesized compounds: **23a** (pale yellow solid, 78% yield, 95% purity), **23b** (pale yellow solid, 84% yield, 97% purity), **23c** (colorless solid, 24% yield, 98% purity).

Synthesis of 4-chlor-2-(piperidin-1-yl)quinazolines (GP7): A solution of the respective 2,4-dichloroquinazoline **4** or **24** (1.0 equiv) and 1-methylpiperidine (1.2-2.0 equiv) in 1,4-dioxane (2.5 mL/mmol) was stirred at 150 °C under microwave irradiation (300 W) for 1 h. The reaction mixture was concentrated in vacuo and the crude product was purified by flash chromatography (CH_2Cl_2). Synthesized compounds: **33** (yellow solid, 132 mg, 86% yield, 100% purity) and **29** (yellow solid, 81% yield, 95% purity).

2,4-Dichloro-6-methoxyquinazolin-7-ol (5) (Doig et al., 2014)**:** A mixture of **4** (3.35 g, 10.0 mmol, 1.0 equiv) and 5% Pd on alumina (1.70 g, 0.800 mmol, 0.08 equiv) in THF (130 mL) was stirred under H_2 atmosphere (1 bar) on ice for 6 h. The mixture was filtered and concentrated in vacuo to give **5** without further purification as a pale yellow solid (2.48 g, > 99% yield, 95% purity).

2,4-Dichloro-6-methoxy-7-[3-(piperidin-1-yl)propoxy]quinazoline (6) (Vital et al., 2023)**:** To a slurry of **5** (245 mg, 1.00 mmol, 1.0 equiv), PPh_3 (344 mg, 1.30 mmol, 1.3 equiv), 3-piperidin-1-ylpropan-1-ol (200 µL, 188 mg, 1.25 mmol, 1.25 equiv) and dry THF (2.0 mL) was added di-tert-butyl azodicarboxylate (DBAD) (305 mg, 1.30 mmol, 1.3 equiv) in portions at 0 °C. The resulting solution was stirred overnight at rt and concentrated under reduced pressure. Purification by flash chromatography (10% MeOH in CH_2Cl_2) afforded **6** as a red solid (301 mg, 81% yield, 97% purity).

***N*^{4}-(1-Cyclohexylpiperidin-4-yl)-6-methoxy-*N*^{2},*N*^{2}-dimethyl-7-[3-(piperidin-1-yl)propoxy]-quinazoline-2,4-diamine (9d):** A mixture of **7** (98.1 mg, 0.190 mmol, 1.0 equiv) solved in dimethylamine (2 M in THF) (0.95 µL, 1.90 mmol, 10 equiv) was heated for 48 h at 100 °C in a pressure vessel. The mixture was cooled down and concentrated in vacuo. **9d** was purified with flash chromatography [7% 3 M NH_3 (in MeOH) in CH_2Cl_2] and obtained as a red solid (84.8 mg, 85% yield, 96% purity).

2-Chloro-6-methoxy-7-[3-(piperidin-1-yl)propoxy]quinazoline (12) and 6-methoxy-7-[3-(piperidin-1-yl)propoxy]quinazoline (13): A mixture of **6** (370 mg, 1.00 mmol, 1.0 equiv), 10% Pd/C (23.7 mg, 20.0 µmol, 0.02 equiv) and NEt_3 (209 µL, 152 mg, 1.50 mmol, 1.5 equiv) in EtOAc (2.0 mL) was stirred under H_2 atmosphere at rt for 4 h. The mixture was filtered and concentrated in vacuo. **12** (203 mg, 61% yield, 98% purity) and **13** (57.8 mg, 19% yield, 96% purity) were isolated after flash chromatography [5% 3 M NH_3 (in MeOH) in CH_2Cl_2] as colorless resp. pale yellow solids.

4-[(1-Isopropylpiperidin-4-yl)oxy]-6-methoxy-7-[3-(piperidin-1-yl)propoxy]quinazoline (16g): NaH (60% in mineral oil, 24.0 mg, 0.600 mmol, 2.0 equiv) was added at 0 °C to a

solution of 1-propan-2-ylpiperidin-4-ol (92.7 µL, 90.5 mg, 0.600 mmol, 2.0 equiv) in THF (1.1 mL). After stirring for 20 min, **15** (101 mg, 0.300 mmol, 1.0 equiv) was added and the mixture was stirred for a further 3 h at 0 °C. The reaction mixture was quenched with H_2O (0.5 mL). The phases were separated and the aqueous phase was washed with CH_2Cl_2 (3 × 1 mL). The combined organic phases were washed with brine (2 mL), dried over Na_2SO_4, filtrated and concentrated. **16g** (122 mg, 92% yield, 95% purity) was isolated after flash chromatography [7% 3 M NH_3 (in MeOH) in CH_2Cl_2] as a pale yellow solid.

4-[(1-Isopropylpiperidin-4-yl)amino]-6-methoxyquinazolin-7-ol (19): A suspension of **18** (1.42 g, 3.50 mmol, 1.0 equiv), cyclohexa-1,4-diene (3.41 mL, 2.89 g, 35.0 mmol, 10 equiv) and 10% Pd/C (518 mg, 438 µmol, 0.125 equiv) in EtOH (34 mL) was stirred under reflux for 2 h. After cooling, the catalyst was filtered off and the filtrate was concentrated in vacuo to yield **19** (1.16 g, > 99% yield, 95% purity) without further purification as a yellow solid.

***N*-(1-Isopropylpiperidin-4-yl)-6-methoxy-7-[4-(piperidin-1-yl)butoxy]quinazolin-4-amine (20b):** A mixture of **21** (102 mg, 0.250 mmol, 1.0 equiv) and KI (83.0 mg, 0.500 mmol, 2.0 equiv) in piperidine (2.49 mL, 2.15 g, 25.0 mmol, 100 equiv) was stirred at 50 °C for 48 h. **20b** (98.0 mg, 86% yield, 98% purity) was isolated by flash chromatography [10% 3 M NH_3 (in MeOH) in CH_2Cl_2] as a colorless solid.

4-(*tert*-Butyl)-1-[3-({4-[(1-isopropylpiperidin-4-yl)amino]-6-methoxyquinazolin-7-yl}oxy)-propyl]pyridin-1-ium chloride (20i) A mixture of **19** (79.1 mg, 0.250 mmol, 1.0 equiv), 4-(*tert*-butyl)-1-(3-iodopropyl)pyridin-1-ium iodide (119 mg, 0.275 mmol, 1.1 equiv) and K_2CO_3 (173 mg, 1.25 mmol, 5.0 equiv) in DMF (0.625 mL) was stirred overnight at rt. The reaction mixture was filtrated, concentrated and purified by flash chromatography [10% 3 M NH_3 (in MeOH) in CH_2Cl_2]. To obtain the product as chloride salt, the isolated quinazoline was resolved in CH_2Cl_2 (2 mL) and extracted with NaCl (958 mg, 10.0 mmol, 40 equiv) in NaOH solution (8 M, 10 mL). The aqueous phase was extracted with CH_2Cl_2 (3 × 10 mL). The combined organic phase was dried over $MgSO_4$, filtrated, and concentrated to yield **20i** (39.1 mg, 30% yield, 97% purity) as a brown solid.

2.2 Determination of Binding Affinities

The affinity of the test compounds for the MB327-PAM-1 binding site of *Torpedo*nAChR was determined by a competitive UNC0642 MS Binding Assay as described previously (Kaiser et al., 2024; Nitsche et al., 2024). General information on the test compounds from commercial sources can be found in the Supporting Information (Table S1). These were employed in the form given in Table S1.

3 Results and Discussion

3.1 Chemistry

To gain further insight into the structure-affinity relationships of UNC0646 analogs regarding their binding to the MB327-PAM-1 binding site of nAChR, a series of related quinazoline derivatives was synthesized. While retaining the 5,8-unsubstituted 6-methoxyquinazoline scaffold, the UNC0646 structure was varied at the 2-, 4-, and/or 7-positions.

The first two sets of compounds investigated (**9a-9e** and **16b** and **11a-11c** and **14**, respectively) consist of structurally closely related analogs of UNC0646 (**1**), in which the residues at either the 2- or 4-position have been gradually reduced in size, as shown in Figure 2.

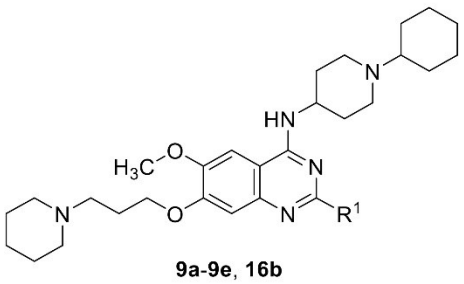

9a-9e, **16b**

	9a	**9b**	**9c**
R^1 =	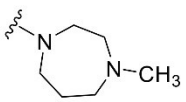	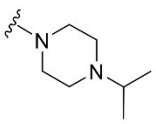	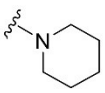

	9d	**9e**	**16b**
R^1 =	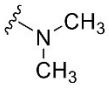		

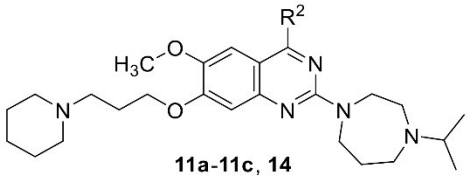

11a-11c, **14**

	11a	**11b**	**11c**	**14**
R^2 =	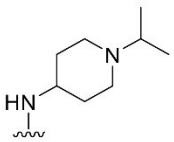	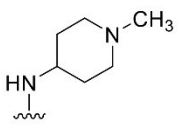		

Figure 2. Structures of target compounds **9a-9e**, **11a-11c**, **14** and **16**.

The key building block for the target compounds **9a**, **9b**, **9d** and **9e**, which differ from UNC0646 (**1**) only in the substituents at the 2-position, is the 2-chloroquinazoline **7**, which was readily accessible in three steps starting from the commercially available building block **4** (Scheme 1).

In the first step, the benzyl ether protecting group was cleaved with hydrogen over a Pd/Al catalyst according to a method described in the literature. (Doig et al., 2014). The yield of 2,4-dichloroquinazolin-7-ol (**5**) was thereby increased from 77% to nearly 100% by extending the reaction time from 2 h as described by Doig et al. to 6 h in this work. In the next step, starting from compound **5**, the 3-(piperidin-1-yl)propoxy side chain was introduced at position 7 of the quinazoline scaffold via a *Mitsunobu* reaction. Accordingly, the quinazolin-7-ol **5** was reacted with 1.25 equivalents of 3-(piperidin-1-yl)propan-1-ol and 1.3 equivalents each of PPh_3 and DBAD (THF, rt, 20 h) to give compound **6** (Vital et al., 2023) in very good yield (81%). Finally, the chlorine atom at the 4-position of 2,4-dichloquinazoline **6** was selectively substituted by reaction with 1.1 equivalents of 1-cyclohexylpiperidin-4-amine under well-established reaction conditions (3.0 equivalents of DIEA, THF, rt, 48 h) (Liu et al., 2011) to give the desired product **7** in 64% yield.

The UNC0646 analogs **9a** and **9b**, which contain a 1-methyl-1,4-diazepane and 1-propan-2-ylpiperazino group, respectively, at the 2-position of the quinazoline ring, were readily obtained starting from building block **7** by microwave-assisted reaction with the corresponding secondary amines (Kaiser et al., 2024; Sundriyal et al., 2017). With a 5-fold excess of secondary amine (toluene, microwave irradiation, 300 W, 130 °C, 50 min), the 2,4-diamino-quinazoline derivatives **9a** (Liu et al., 2011) and **9b** were obtained in high yields of 89% each. The synthesis of compound **9d**, which has a dimethylamino group at the 2-position, required adapted reaction conditions due to the volatility of dimethylamine, as a microwave synthesis as described for **9a** and **9b** was not possible due to the high pressure developed. Therefore, compound **7** was reacted in a conventional manner with dimethylamine in a pressure tube (Venkatesan et al., 2008). The reaction with a tenfold excess of dimethylamine at 100 °C (THF, 48 h) afforded the target compound **9d** in a very good yield (85%). To obtain the 2-aminoquinazoline **9e** starting from **7**, a two-step one-pot strategy known from the literature (Mohamed and Rao, 2015) based on an azide intermediate was used, since the direct reaction of 4-amino-substituted 2-chloroquinazolines, such as intermediate **7**, with ammonia usually gives poor yields (Aubin et al., 2010; Borzenko et al., 2015). Therefore, the chlorine atom was first replaced by an azide group by reacting **7** with 1.1 equivalents of NaN_3 (EtOH, AcOH, rt to 90 °C, 2 h). The resulting crude azide product was then reduced with 1.5 equivalents of hydrazine hydrate in the presence of Pd/C (rt to 90 °C, 2 h) to give the primary amine **9e**. In addition to the desired target compound **9e**, which was obtained in 49% yield, the by-product **16b** was also formed (16% yield).

Finally, the target compounds **9c** and **9f**, which have a piperidine residue at the 2-position, **9f** being an analog of UNC0631 (**35**) (see Table 1), were readily accessible in one step from the recently described 4-chloroquinazoline building block **8** (Kaiser et al., 2024). Thus, heating of compound **8** with 2.0 equivalents of the corresponding 4-aminopiperidines under microwave irradiation (3.0 equivalents DIEA, *i*-PrOH, 160 °C, 15 min) (Kaiser et al., 2024) afforded **9c** and **9f** in 70% and 58% yields, respectively.

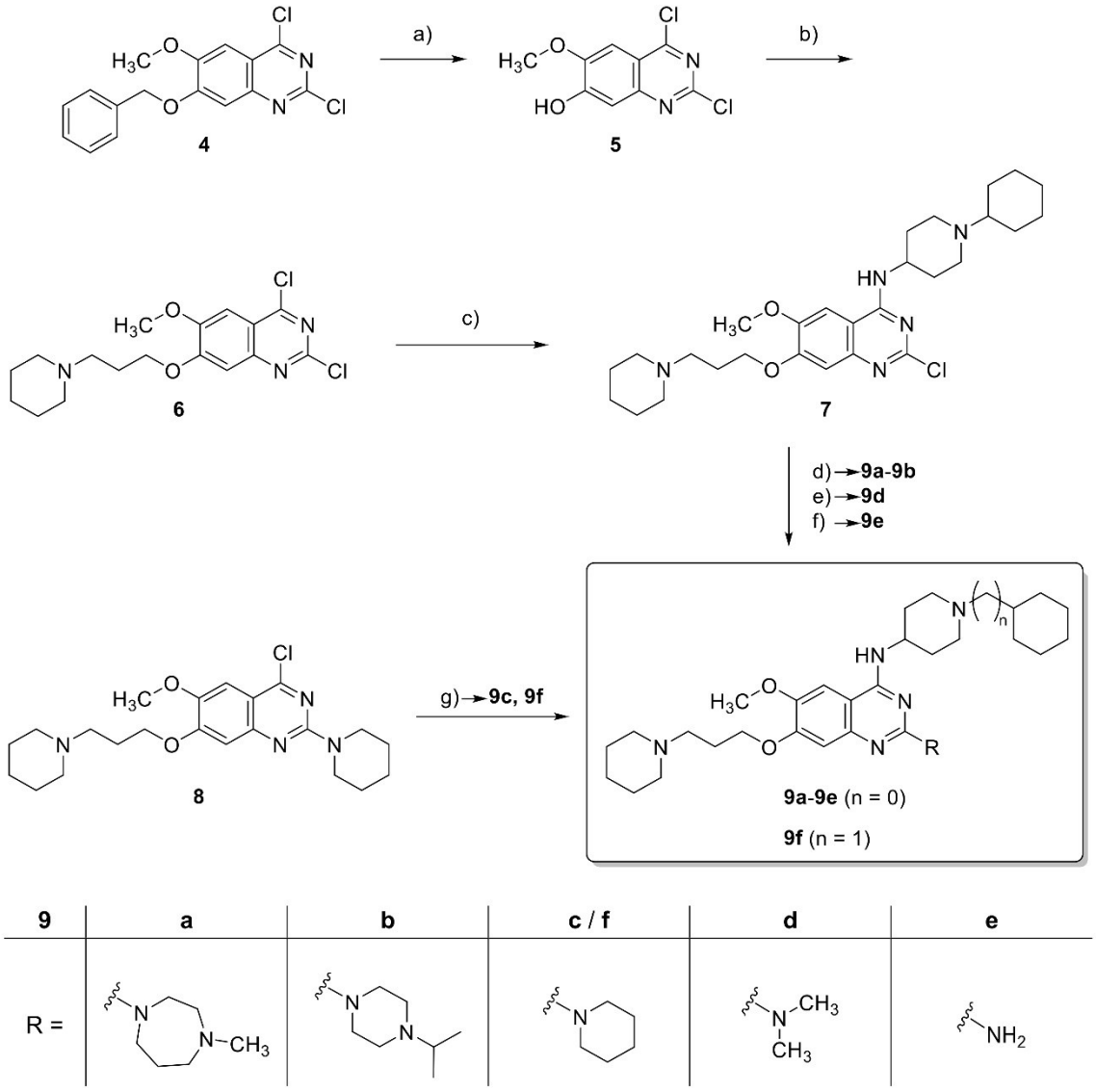

9	a	b	c / f	d	e
R =					

Scheme 1. Reagents and conditions: (a) H_2, 5% Pd/Al (0.08 equiv), THF, 0 °C, 6 h, > 99%; (b) 3-piperidin-1-ylpropan-1-ol (1.25 equiv), PPh_3 (1.3 equiv), DBAD (1.3 equiv), THF, rt, 20 h, 81%; (c) 1-cyclohexylpiperidin-4-amine (1.1 equiv), DIEA (3.0 equiv), THF, rt, 48 h, 64%; (d) 1-methyl-1,4-diazepane or 1-propan-2-ylpiperazine (5.0 equiv), toluene, microwave: 300 W, 130 °C, 50 min; **9a**: 89%, **9b**: 89% (e) dimethylamine (10 equiv), THF, 100 °C, 48 h, 85%; (f) 1. NaN_3 (1.1 equiv), 4:1 EtOH, glacial AcOH, rt to 90 °C, 2 h; 2. 10% Pd/C (0.01 equiv), hydrazine hydrate (1.5 equiv), rt to 90 °C, 2 h, 49% (over two steps); (g) 1-cyclohexylpiperidin-4-amine or 1-(cyclohexylmethyl)piperidin-4-amine (2.0 equiv), DIEA (3.0 equiv), *i*-PrOH, microwave: 200 W, 160 °C, 15 min; **9c**: 70%, **9f**: 58%.

The desired UNC0646 analogs **11a** (UNC618) (Jiang et al., 2017; Liu et al., 2011), **11b** and **11c**, which have amine residues at the 4-position that are gradually reduced in size compared to those of UNC0646 (**1**), were prepared analogously to compounds **9a** and **9b**. First, the intermediates **10a** (Davis et al., 2016; Vital et al., 2023), **10b** and **10c**, which are analogous to compound **7** (see above), were prepared by reacting compound **6** with 1-isopropylpiperidin-4-amine, 1-methylpiperidin-4-amine and methylamine, respectively. The desired compounds **10a**-**10c** were obtained in 48-86% yields. Intermediates **10a**-**10c** were then reacted with 1-isopropyl-1,4-diazepane to afford the target compounds **11a**-**11c** in fair to excellent yields (62-91%) (Scheme 2).

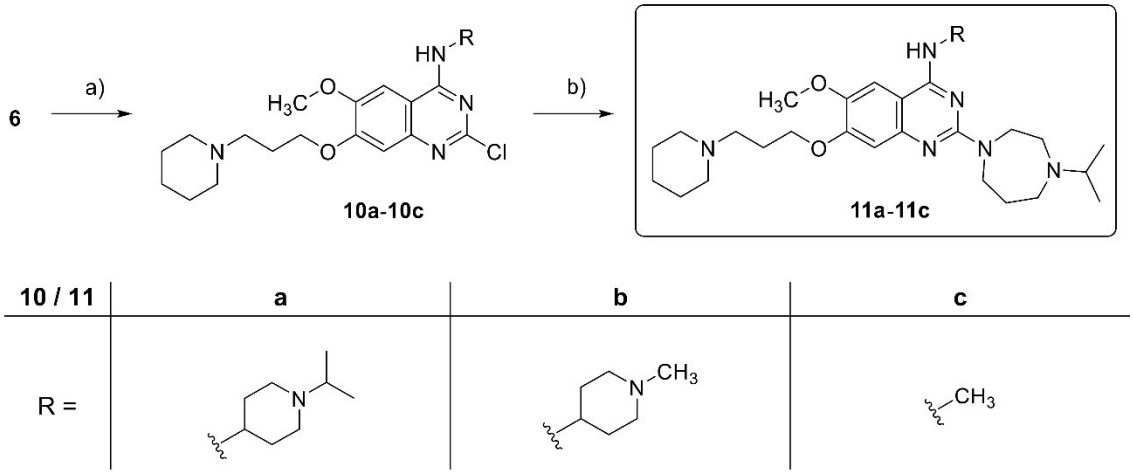

10 / 11	a	b	c
R =			

Scheme 2. Reagents and conditions: (a) 1-propan-2-ylpiperidin-4-amine or 1-methylpiperidin-4-amine or methanamine (1.1 equiv), DIEA (3.0 equiv), THF, rt, 48 h, **10a**: 86%, **10b**: 48%, **10c**: 86%; (b) 1-propan-2yl-1,4-diazepane (5.0 equiv), toluene, microwave: 300 W, 130 °C, 50 min; **11a**: 89%, **11b**: 62%, **11c**: 91%.

The synthesis of the 4-unsubstituted UNC0646 analog **14** was carried out starting from the 2,4-dichloroquinazoline building block **6**, as no appropriate 4-unsubstituted 2-chloroquinazoline building block was commercially available (Scheme 3). Since it is generally not possible to selectively replace the chloro substituent at the 2-position of 2,4-dichloroquinazolines by reaction with secondary amine nucleophiles, since the 4-substituted products are preferentially formed (see above) (Yamamoto and Shinnkai, 2004), the chloro substituent at the 4-position first had to be selectively removed by reductive means. This was accomplished according to a procedure described in the literature (Abe et al., 1998), by hydrogenolysis with hydrogen over Pd/C in the presence of NEt_3, yielding 2-chloroquinazoline **12** as the major product (61% yield) and the double reduction product **13** as a minor component (19% yield). Finally, the desired product **14** was prepared from **12** and 1-isopropyl-1,4-diazepane under the same reaction conditions as described for the syntheses of **11a**-**11c**, whereby **14** could be isolated in quantitative yield.

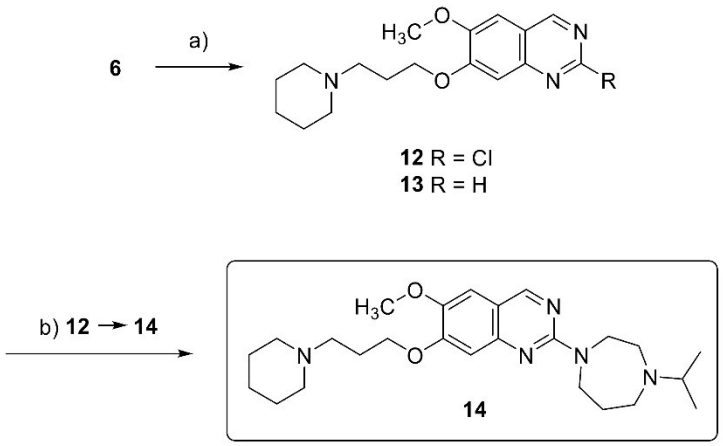

Scheme 3. Reagents and conditions: (a) H_2, 10% Pd/C (0.02 equiv), NEt_3 (1.5 equiv), EtOAc, rt, 4 h, **12**: 61%, **13**: 19%; (b) 1-isopropyl-1,4-diazepane (5.0 equiv), toluene, microwave: 300 W, 130 °C, 50 min, 99%.

As we have recently shown (Kaiser et al., 2024), 2-unsubstituted UNC0646 analogs also exhibit a distinct affinity for the MB327-PAM-1 binding site. Therefore, two series of additional 2-unsubstituted UNC0646 analogs were synthesized in which the substituents at the 4-position (**16a-16g**) and at the 7-position (**20a-20i** and **23a-23c**), respectively, were varied (Table 2 and Table 3).

Starting from building block **15** known from the literature (Kaiser et al., 2024), the target compounds **16a-16f** were readily accessible in one step (62-94% yield) by reacting **15** with 2.0 equivalents of the corresponding amines using well-established microwave-assisted reaction conditions (3.0 equivalents DIEA, *i*-PrOH, 160 °C, 15-60 min) (Kaiser et al., 2024; Liu et al., 2011) (Scheme 4). Quinazoline derivative **16g** bearing a (1-isopropylpiperidin-4-yl)oxy-substituent at the 4-position was obtained in 92% yield by reacting **15** with 2.0 equivalents of 1-propan-2-ylpiperidin-4-ol in the presence of NaH (2.0 equivalents, THF, rt, 3 h) (Scheme 4) (Gharat et al., 2015).

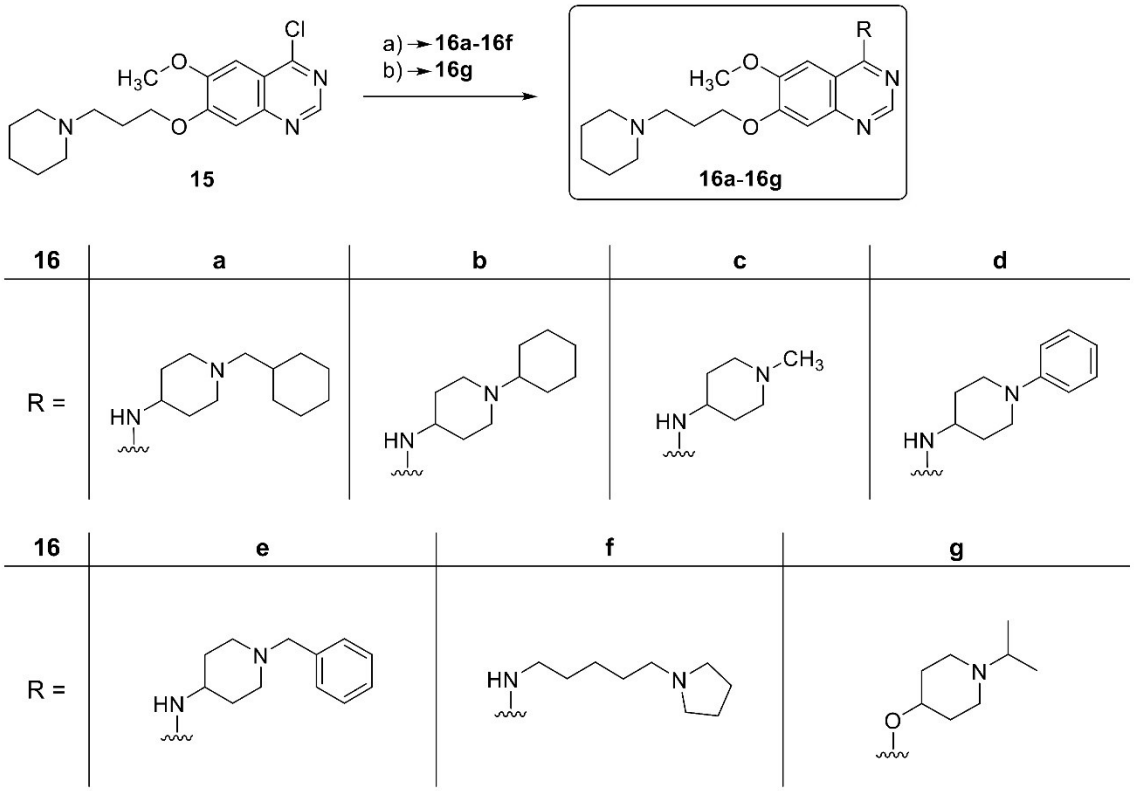

Scheme 4. Reagents and conditions: (a) corresponding amines (2.0 equiv), DIEA (3.0 equiv), *i*-PrOH, microwave: 200 W, 160 °C, 15-60 min, **16a**: 62%, **16b**: 94%, **16c**: 69%, **16d**: 82%, **16e**: 85%, **16f**: 83%; (b) 1-propan-2-ylpiperidin-4-ol (2.0 equiv), NaH (60%, 2.0 equiv), THF, rt, 3 h, 92%.

In addition to the UNC0646 analogs **16a-16g**, the 2-unsubstituted quinazoline derivatives **20a-20i** and **23a-23c** were synthesized, bearing a uniform (1-isopropypiperidin-4-yl)amino residue at the 4-position and varying basic side chains at the 7-position. These side chains are not only linked to the quinazoline backbone via an ether function (compounds **20a-20i**), but also via amino functions (compounds **23a-23c**).

The key building block **19** for the synthesis of the compounds **20a-20i** was prepared in only two steps and in almost quantitative yield from the commercially available building block **17** (Scheme 5). In the first step, the substitution of the chlorine at the 4-position was achieved quantitatively by reaction with 2.0 equivalents of 1-propan-2-ylpiperidin-4-amine (3.0 equivalents DIEA, *i*-PrOH, microwave irradiation, 160 °C, 15 min). In a second step, the benzyl ether protecting group of the resulting building block **18** was cleaved using 10 equivalents of cyclohexa-1,4-diene over a Pd/C catalyst (EtOH, reflux, 2 h) (Liu et al., 2010), to give quinazolin-7-ol **19**.The subsequent introduction of the basic side chains at the 7-position of the quinazoline to generate the target compounds **20a** (Kaiser et al., 2024) and **20c-20h** was accomplished in one step via a *Mitsunobu* reaction (5.5 equivalents PPh_3, 5.0 equivalents DIAD, THF, rt, 20 h) (Liu et al., 2011) using 3.5-4.0 equivalents of the corresponding aminoalcohols (46-79% yield). Target compound **20b**, bearing a 4-(piperidin-1-yl)butoxy side chain, was prepared in an alternative two-step procedure. A *Mitsunobu* reaction with the corresponding amino alcohol 4-(piperidin-1-yl)butan-1-ol is not possible in this case, since the intermediate alkoxyphosphonium ion formed from it cyclizes to a 5-azaspiro[4.5]decan-5-ium ion, which is not reactive enough for alkylation reactions (Gmeiner et al., 1994). Therefore, in a first step, quinazolin-7-ol **19** was converted to the 7-(4-chlorobutoxy)quinazoline **21** via a *Mitsunobu* reaction with 4.0 equivalents of 4-chloro-butan-1-ol (5.5 equivalents PPh_3, 5.0 equivalents DIAD, THF, rt, 20 h) (Liu et al., 2011). The subsequent reaction with piperidine (2.0 equivalents, KI, 50 °C, 20 h) (Fagan et al., 2019) then afforded the desired product **20b** in good overall yield (79% over two steps). The synthesis of the hybrid compound **20i**, which carries a partial structure of the prototypical ligand MB327 as a side chain, was also carried out starting from the key building block **19**. Thus, quinazolin-7-ol **19** was first alkylated with 1.1 equivalents of 4-(*tert*-butyl)-1-(3-iodopropyl)pyridin-1-ium iodide (Rappenglück et al., 2018a) (5.0 equivalents K_2CO_3, DMF, rt, 20 h) to obtain the corresponding iodine salt as crude product. After basic extraction of this salt (aqueous NaOH, CH_2Cl_2) in the presence of a large excess of sodium chloride, the desired product **20i** was obtained as the chloride salt (30% yield).

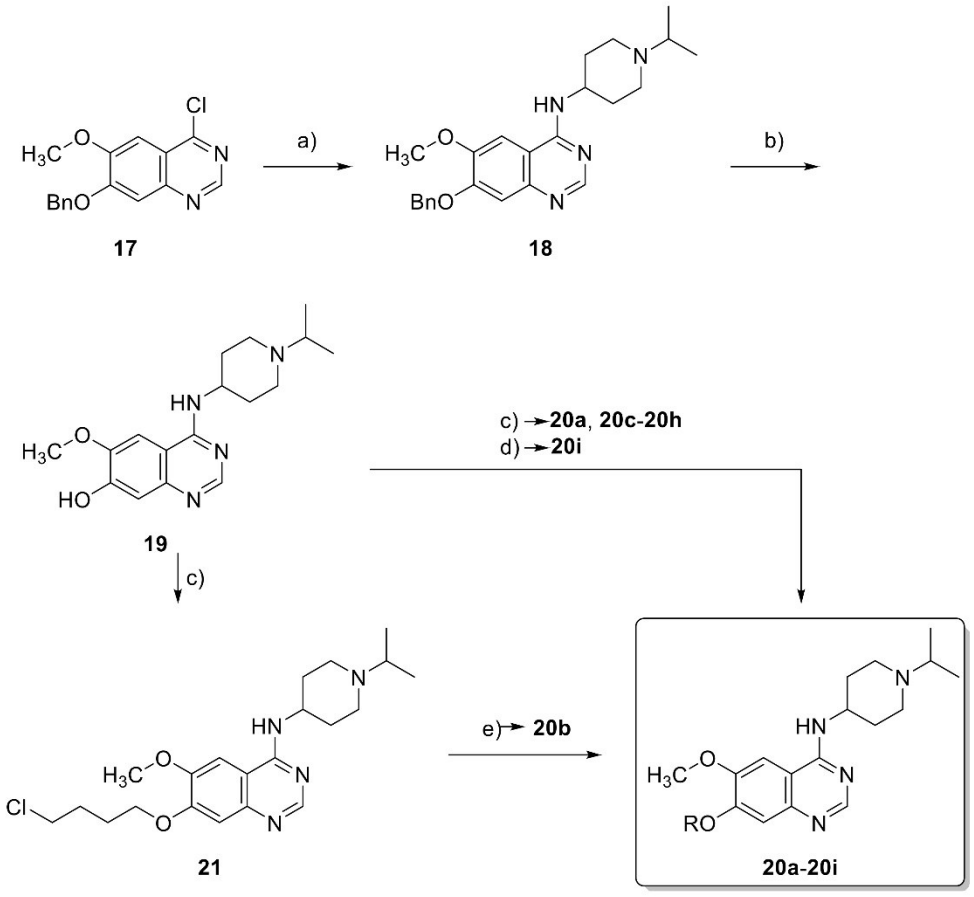

20	a	b	c
R =	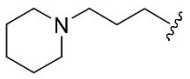	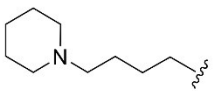	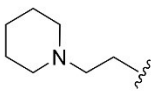

20	d	e	f
R =	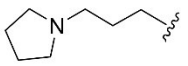	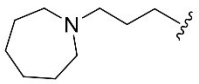	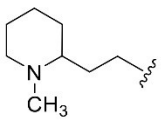

20	g	h	i
R =	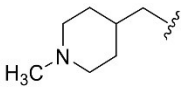	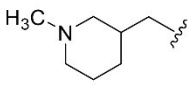	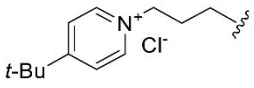

Scheme 5. Reagents and conditions: (a) 1-propan-2-ylpiperidin-4-amine (2.0 equiv), DIEA (3.0 equiv), *i*-PrOH, microwave: 200 W, 160 °C, 15 min, > 99%; (b) cyclohexa-1,4-diene (10 equiv), 10% Pd/C (0.125 equiv), EtOH, reflux, 2 h, > 99%; (c) corresponding aminoalcohols (3.5-4.0 equiv) or 4-chlorobutan-1-ol (4.0 equiv), PPh_3 (5.5 equiv), DIAD (5.0 equiv), THF, rt, 20 h, **20a**: 63%, **20c**: 79%, **20d**: 69%, **20e**: 59%, **20f**: 46%, **20g**: 58%, **20h**: 78%, **21**: 92%; (d) 1. 4-(*tert*-butyl)-1-(3-iodopropyl)pyridin-1-ium iodide (1.1 equiv), K_2CO_3 (5.0 equiv), DMF, rt, 20 h; 2. NaCl, NaOH (8 M), rt, 30% (over two steps); (e) KI (2.0 equiv), piperidine, 50 °C, 20 h, 86%.

Finally, the 7-amino-substituted target compounds **23a-23c** were readily accessible in a single step starting from the recently described 7-fluoroquinazoline building block **22** (Kaiser et al., 2024). Nucleophilic substitution of the fluorine atom with 5.0 equivalents of the corresponding primary or secondary amine (1.1 equivalents K_2CO_3, NMP, 135 °C, 20 h) (Harris et al., 2005; Kaiser et al., 2024) afforded the desired products **23a-23c** in 24-84% yields (Scheme 6).

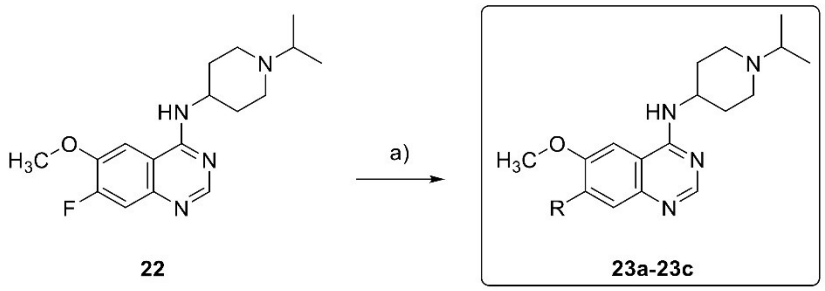

23	a	b	c
R =	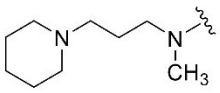	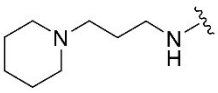	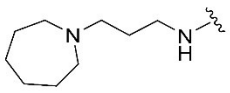

Scheme 6. Reagents and conditions: (a) 3-piperidin-1-ylpropan-1-amine, *N*-methyl-3-piperidin-1-ylpropan-1-amine or 3-(azepan-1-yl)propan-1-amine (5.0 equiv), K_2CO_3 (1.1 equiv), NMP, 135 °C, 20 h, **23a**: 78%, **23b**: 84%, **23c**: 24%.

In addition to the UNC0646 analogs with gradually reduced residues at the 2- and 4-positions (**9a**-**9e**, **11a**-**11c**, **14** and **16b**), the UNC0646 analog **31**, which in contrast to UNC0646 (**1**) bears a methoxy substituent at the 7-position instead of a basic 3-(piperidin-1-yl)propoxy side chain, was of particular interest. As we have recently shown, individual UNC0646 analogs with a 6,7-dimethoxyquinazoline scaffold also exhibit remarkable binding affinities to the MB327-PAM-1 binding site of nAChR (Kaiser et al., 2024). To further investigate the binding behavior of such compounds, we prepared a series of additional UNC0646 analogs with a 6,7-dimethoxyquinazoline scaffold and various substituents at the 2- and 4-positions (**28a**-**28c**, **30a**-**30b**, **31** and **32a**-**32f**) (Table 4). Most of these compounds were accessible in a simple two-step procedure starting from the commercially available 2,4-dichloroquinazoline **24** (Scheme 7 and Scheme 8).

By reaction **24** with 1.1 equivalents of the corresponding primary amines under same reaction conditions as described for the synthesis of **7** from **6** (see above), the intermediates **25**-**27** were prepared according to literature (Ma et al., 2014; Somnarin et al., 2022; Sundriyal et al., 2017; Wang et al., 2019). Deviating from the literature procedures, the reaction time was increased from 2-20 h (47-86% yield) to 48 h, which clearly increased the yields (65-98% yield).The subsequent reaction of the intermediates **25**-**27** with 5.0 equivalents of 1-methyl-1,4-diazepane or 1-propan-2-yl-1,4-diazepane under the established reaction conditions (see above for synthesis of **9a** and **9b**) afforded the desired products **28a**, **28b**-**28c** (Sundriyal et al., 2017) and **31** in excellent yield (94 to > 99%).

For an efficient synthesis of a structurally diverse series of 2,4-diaminoquinazolines starting from readily available 2,4-dichloroquinazolines, it would be of great advantage to be able to replace the chlorine atoms at the 2- and 4-positions by amino groups in any order. As already observed in the synthesis of intermediates **7**, **10a**-**10c** and **25**-**27**, reactions of 2,4-dichloroquinazolines with primary and secondary amines are highly regioselective at the 4-position. However, Yoshida et al. showed that in the case of 2,4-dichloroquinazoline, the chlorine atom at the 2-position is selectively substituted with amino groups by reaction with tertiary *N*-methylamines with cleavage of the methyl group (Yoshida and Taguchi, 1992). Indeed, the reaction of 2,4-dichloroquinazoline **24** with 2.0 equivalents of 1-methylpiperidine under adapted, microwave-assisted reaction conditions (1,4-dioxane, 300 W, 150 °C, 1 h) (Kaiser et al., 2024) afforded 2-piperidinoquinazoline **29** as the sole product in 81% yield. With intermediate **29** in hand, the desired compounds **30a** (Ma et al., 2014) and **30b** (Sundriyal et al., 2017) were prepared in good yields (84% and 64%, respectively) by reaction with 2.0 equivalents of 5-pyrrolidin-1-ylpentan-1-amine and 1-propan-2-ylpiperidin-4-amine, respectively, under the same reaction conditions as described for the synthesis of **9c** and **9f** (see above).

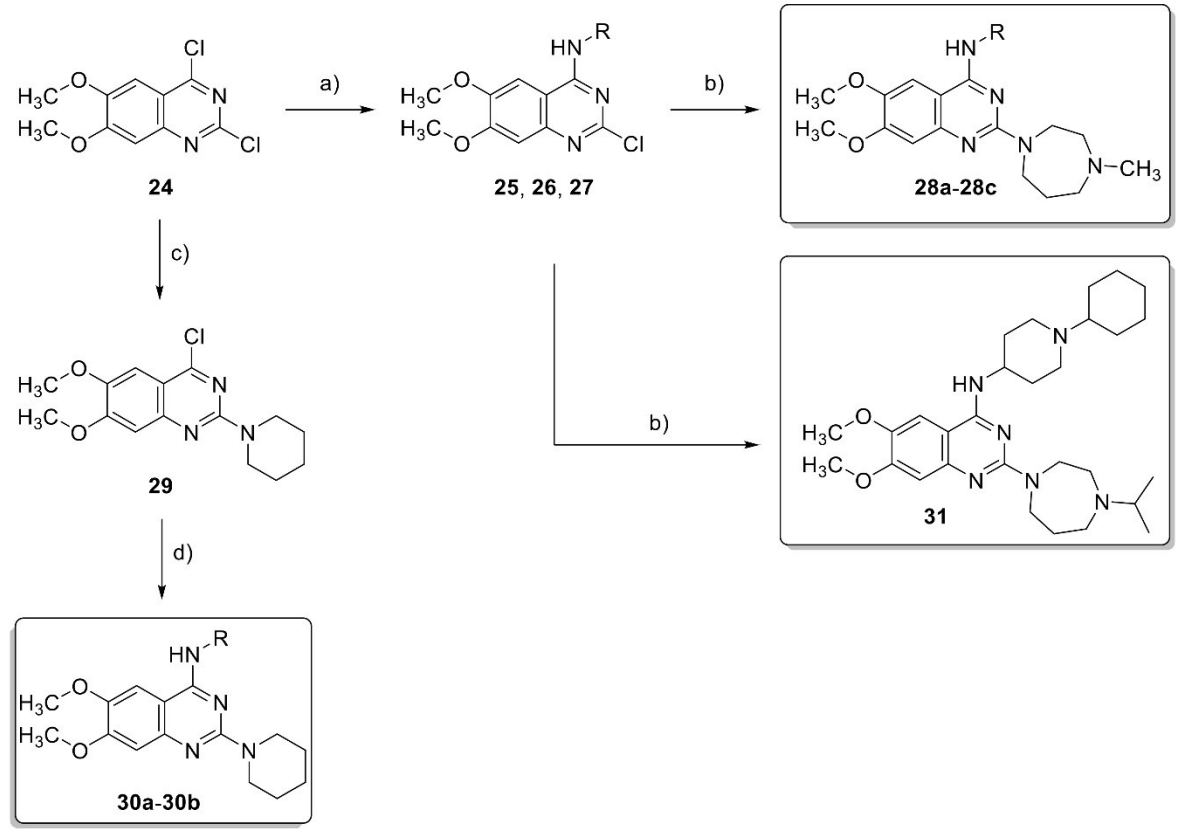

Scheme 7. Reagents and conditions: (a) 5-pyrrolidin-1-ylpentan-1-amine, 1-cyclohexylpiperidin-4-amine or 1-propan-2-ylpiperidin-4-amine (1.1 equiv), DIEA (3.0 equiv), THF, rt, 48 h, **25**: 81%, **26**: 65%, **27**: 98%; (b) 1-methyl-1,4-diazepane or 1-propan-2-yl-1,4-diazepane (5.0 equiv), toluene, microwave: 300 W, 130 °C, 50 min; **28a**: 90%, **28b**: 94%, **28c**: 97%, **31**: > 99%; (c) 1-methylpiperidine (2.0 equiv), 1,4-dioxane, microwave: 300 W, 150 °C, 1 h, 81%; (d) 5-pyrrolidin-1-ylpentan-1-amine or 1-propan-2-ylpiperidin-4-amine (2.0 equiv), DIEA (3.0 equiv), *i*-PrOH, microwave: 200 W, 160 °C, 15 min, **30a**: 84%, **30b**: 64%.

To investigate the effects of different amino substituents at the 2-position (Kaiser et al., 2024) on the binding affinity of 2,4-diamino-substituted 6,7-dimethoxyquinazolines, a series of compounds **32a**-**32f** derived from compounds **28c** and **30b**, respectively, were synthesized (Scheme 8). Using the known substitution procedure, compounds **32a**-**32d** were readily obtained by analogy with compound **28c** starting from intermediate **27**. Thus, reacting **27** with a 5-fold excess of the corresponding secondary amines gave the desired compounds **32a**-**32c** and **32d** (Cui et al., 2020) in 67 to 97% yield. The synthesis of 2-aminoquinazoline **32e** followed a two-step, one-pot azide-based procedure analogous to the synthesis of compound **9e** described above. By replacing the chlorine atom of **27** with an azide group and subsequent reduction of the intermediate, the primary amine **32e** was obtained in good yield (78%). As in the analogous synthesis of **9e**, the corresponding 2-unsubstituted by-product was also formed here (**32f**, 5% yield).

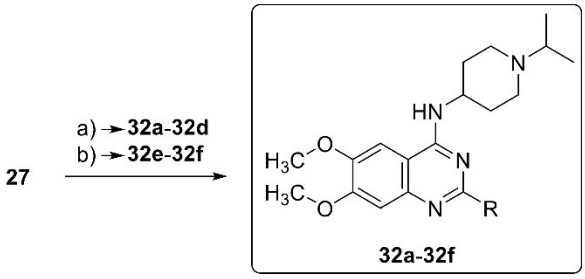

32	a	b	c
R =	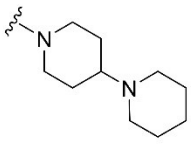	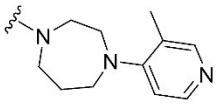	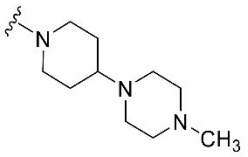

32	d	e	f
R =	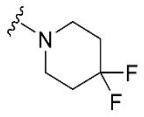		

Scheme 8. Reagents and conditions: (a) corresponding amines (5.0 equiv), toluene, microwave: 130 °C, 50 min; **32a**: 91%, **32b**: 67%, **32c**: 84%, **32d**: 97%; (b) 1. NaN_3 (1.1 equiv), 4:1 EtOH, glacial AcOH, rt to 90 °C, 2 h; 2. 10% Pd/C (0.01 equiv), hydrazine hydrate (1.5 equiv), rt to 90 °C, 2 h, **32e**: 78% (two steps), **32f**: 5% (two steps).

The last series of test compounds, 4-amino-substituted 2-piperidinoquinazolines bearing a benzyloxy group at the 7-position, **34a**-**34c** (Table 5), were synthesized in two steps starting from the commercially available building block **4** analogously to the compounds **30a**-**30b** described above. Intermediate **33** was obtained in 86% yield by regioselective nucleophilic displacement of the 2-chloro substituent of **4** with 1.2 equivalents of 1-methylpiperidine. Subsequent reaction with 2.0 equivalents of the corresponding amines afforded the target compounds **34a**-**34c** in good to high yield (68-86%) (Scheme 9).

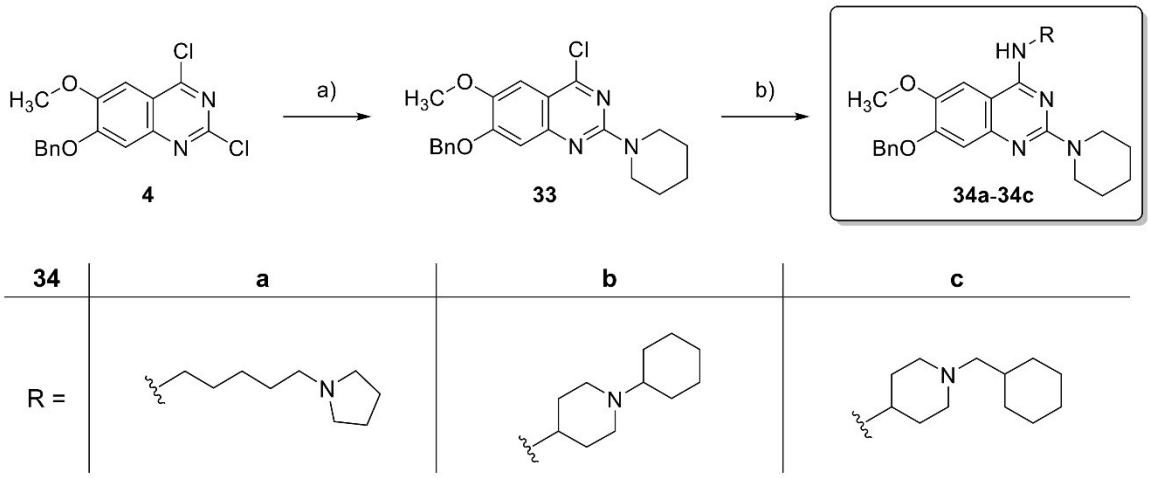

Scheme 9. Reagents and conditions: (a) 1-methylpiperidine (1.2 equiv), 1,4-dioxane, 150 °C (300 W), 1 h, 86%; (b) 5-pyrrolidin-1-ylpentan-1-amine, 1-cyclohexylpiperidin-4-amine or 1-(cyclohexylmethyl)-piperidin-4-amine (2.0 equiv), DIEA (3.0 equiv), *i*-PrOH, microwave: 200 W, 160 °C, 15 min, **34a**: 86%, **34b**: 68%, **34c**: 73%.

3.2 Biological evaluation

All compounds synthesized as part of this study supplemented by compounds from commercial sources, that appeared of interest because of structural relations, were characterized regarding their affinity towards the MB327 binding site of the nAChR. To this end the recently developed UNC0642 MS Binding Assay for the MB327-PAM-1 binding site was used. Based on the obtained data first structure-affinity relationships for the studied quinazoline derivatives were established. For economic reasons test compounds were studied at a single concentration, i.e. of 10 µM, in the UNC0642 MS Binding Assays with the concentration of the reporter ligand UNC0642 (**2**) being set to 1 µM. As deduced from affinity calculation for competitive binding and as known from previous studies based on this setup, it can be assumed that compounds with binding affinities comparable to that of UNC0646 (**1**, $pK_i = 5.83 \pm 0.05$) lead to a distinct reduction of specific reporter ligand binding, i.e. to about ~ 20% (Kaiser et al., 2024). Accordingly, compounds with binding affinities in the range of that of UNC0646 (**1**) including those with binding affinities up to nearly 100 µM should be clearly identifiable. In the following the discussion and interpretation of the test results is divided into five categories corresponding to the respective compound classes with the data being listed in five individual tables.

At first, compounds derived from UNC0646 (**1**), exhibiting the highest yet known affinity towards the MB327-PAM-1 binding site of the nAChR, by varying the structure and in particular reducing the size of the substituents in 2- and 4-position were studied (see Table 1).

In one set of compounds the substituents of UNC0646 (**1**, Table 1, Entry 1) in 4-, 6- and 7-position remained unchanged whereas the 4-isopropyl-1,4-diazepan-1-yl residue of UNC0646 (**1**) in 2-position of the quinazoline scaffold was gradually reduced in size. In the individual compounds thus in this position either a 4-methyl-1,4-diazepan-1-yl (**9a**, Table 1, Entry 2), a 4-isopropylpiperazin-1-yl (**9b**, Table 1, Entry 3) or a piperidin-1-yl residue (**9c**, Table 1, Entry 4) is present. Furthermore, compounds with even smaller substituents in the 2-position, i.e. a *N*,*N*-dimethylamino (**9d**, Table 1, Entry 5), an amino function (**9e**, Table 1, Entry 6) or just hydrogen were studied (**16b**, Table 1, Entry 7). In the latest case with only hydrogen in 2-position the lowest binding affinity in this series of compounds is observed, which is still characterized by a significant reduction of reporter ligand binding down to 50 ± 5% (Table 1, Entry 7). Remarkably, for the test compounds with a 1,4-diazepan-1-yl (**9a**), a piperazin-1-yl (**9b**), a dimethylamino (**9d**) and an amino residue (**9e**) the remaining reporter ligand binding ranged from 23% to 27% (Table 1, Entries 2, 3, 5, 6). The binding affinities of these compounds are thus very similar to each other and to that of UNC0646 (**1**, 21 ± 3%). In case of the 2-piperidin-1-yl substituted quinazoline derivative **9c** the affinity to the MB327-PAM-1 binding site seems somewhat higher with the remaining reporter ligand binding amounting to 11 ± 3% (Table 1, Entry 4). Though this value is even below the remaining reporter ligand binding of UNC0646 (**1**) as competitor (21 ± 3%, Table 1, Entry 1), the pK_i values determined for **9c** ($pK_i = 5.83 \pm 0.02$) and UNC0646 (**1**, $pK_i = 5.83 \pm 0.05$) (in full scale competition experiments) indicate, that the binding affinities for both compounds are the same.

According to the result from recent *in silico* studies, residues in 2-position of the quinazoline derivatives exhibit only minor interactions with the receptor (Kaiser et al., 2024; Nitsche et al., 2024). This may explain the very similar binding affinities observed for **1** and **9a-9e**. The

relatively strong decline of the binding affinity in case of **16b** might be due to the decreased basicity of the quinazoline ring resulting from the lack of an amino group in 2-position as a mesomeric donor.

The second set of compounds comprises derivatives of UNC0646 (**1**) in which the substituent in 2-position is left unchanged whereas the substituents in 4-position are delineated from the original 1-cyclohexylpiperidin-4-amino residue by a stepwise reduction of the size of the latter. Thus, in 4-position a 1-isopropylpiperidin-4-amino (**11a**, Table 1, Entry 8), a 1-methylpiperidin-4-amino (**11b**, Table 1, Entry 9) a *N*-methylamino residue (**11c**, Table 1, Entry 10), or only a hydrogen (**14**, Table 1, Entry 11) is present. Upon reduction of the terminal *N*-cyclohexyl residue within the substituent in 4-position (**1**, Table 1, Entry 1) to an isopropyl moiety (**11a**, Table 1, Entry 8) or methyl group (**11b**, Table 1 Entry 9), a nominal increase of the remaining reporter ligand binding from 21 ± 3% to 33 ± 6% and 37 ± 4%, respectively, is observed. This nominal increase of remaining reporter ligand binding corresponding to a decrease of binding affinity further continued when only a *N*-methylamino group (**11c**, 39 ± 5%, Table 1, Entry 10) or finally only a hydrogen atom (**14**, 44 ± 8%, Table 1, Entry 11) was present. Thus, a comparably large *N*-alkyl residue attached to the piperidin-4-amino substituent in 4-position of the quinazoline skeleton as in **1** appears favorable for the binding affinity for the MB327-PAM-1 binding site (compare binding affinity of **1** to binding affinity of **11a** and **11b**), though the influence of the 4-substituent overall is moderate (compare binding affinity of **1** to binding affinity of **11c** and **14**). This trend of larger *N*-alkyl residues attached to the piperidine nitrogen of the 4-substituent of the quinazoline moiety resulting in higher binding affinities continued for the UNC0646 analog UNC0631 (**35**, Table 1, Entry 13). The latter by exhibiting a cyclohexylmethyl residue instead of the smaller cyclohexyl moiety present in UNC0646 (**1**) gives rise to a remaining reporter ligand binding of 12 ± 0.5%, which is significantly lower than that of UNC0646 (**1**, 21 ± 3%). The higher binding affinity of **35** as compared to **1** is further corroborated by the pK_i value determined for this compound, which by amounting to 6.04 ± 0.04 (pK_i, **35**) is significantly higher than that of **1** (pK_i = 5.83 ± 0.05).

Having studied the influence of the substituents in 2- and 4-position of the quinazoline ring on the affinity of the UNC0646 analogs, also the relevance of the side chain in 7-position, in particular of the terminal piperidine ring should be evaluated. To this end, the 3-(piperidin-1-yl)propoxy substituent in this position was replaced by a methoxy group. According to the remaining reporter ligand binding of 65 ± 7% found for the respective compound, the UNC0646 analog **31** (Table 1, Entry 12), the binding affinity of this compound is distinctly lower than that of UNC0646 (**1**, remaining reporter ligand binding 21 ± 3%) but still significant. Hence, the 7-substituent in UNC0646 (**1**) significantly contributes to the binding affinity of this compound, but may be partly omitted, i.e. reduced to a methoxy group, while still a reasonable binding affinity remains.

As in preliminary experiments a substitution of the residue in 2-position of the original quinazoline derivative UNC0646 (**1**) with a piperidino moiety and an exchange of the terminal cyclohexyl group in the 4-substituent of **1** by a cyclohexylmethyl residue had yielded a reduction of remaining reporter ligand binding indicating the potential to enhance binding affinities, it was assumed that a combination of both measures might further improve the binding affinity (compare remaining reporter ligand binding of **9c** and **35** with **1**). For compound **9f** (Table 1, Entry 14) comprising the aforementioned structural adaptations a value of 6 ± 1% for the remaining reporter ligand was found, which is distinctly lower than the values observed for **9c** (11 ± 3%) and **35** (12 ± 0.5%) and thus points to an increase in binding affinity as

compared to the aforementioned compounds as well as of UNC0646 (**1**). According to the pK_i value, that has finally been determined in full scale competition experiments for the hybrid compound **9f**, the binding affinity of this compound, **9f**, by amounting to 5.84 ± 0.03 (pK_i) is, however, in the same range as that of the precursor compounds **9c** (pK_i = 5.83 ± 0.02) and **35** (pK_i = 6.04 ± 0.04) as well as of the reference compound UNC0646 (**1**, pK_i = 5.83 ± 0.05).

Table 1: Binding affinities of analogues of UNC0646 (**1**) with varying structures of the substituents in 2- and 4-position for the MB327-PAM-1 binding site of *Torpedo*-nAChR. [a] 'reporter ligand binding' refers to the remaining binding of the reporter ligand (UNC0642, 1 µM) in presence of the respective test compound (10 µM) as % value ± SD; see Material and Methods for details. [b] 'reporter ligand binding' and/or pK_i value have been reported previously (Kaiser et al., 2024; Nitsche et al., 2024).

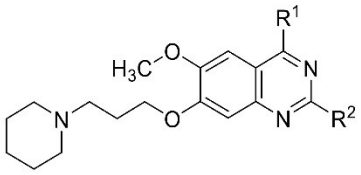	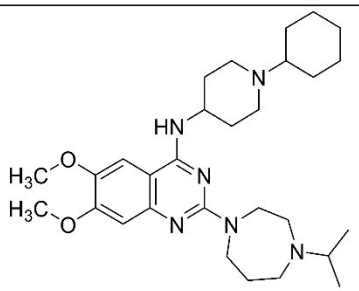
1, **9a-9f**, **11a-11c**, **14**, **16b**, **35**	**31**

Entry	Compound	R^1	R^2	reporter ligand binding [%] [a]	PTMD01 code
1	**1** (UNC0646)	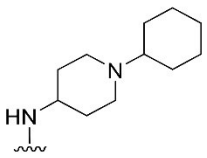	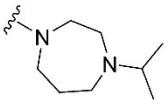	21 ± 3 (n = 30) pK_i = 5.83 ± 0.05 [b]	-
2	**9a**		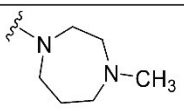	23 ± 2	47L
3	**9b**		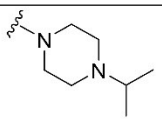	26 ± 5	71
4	**9c**		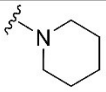	11 ± 3 pK_i = 5.83 ± 0.02	49
5	**9d**		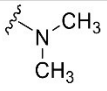	23 ± 4	48
6	**9e**			27 ± 2	65
7	**16b**			50 ± 5 (n = 12) [b]	04

Continued next page

Table 1 *(continued)*

Entry	Compound	R^1	R^2	reporter ligand binding [%] [a]	PTMD01 code
8	**11a** (UNC618)	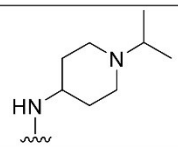	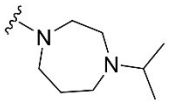	33 ± 6	-
9	**11b**	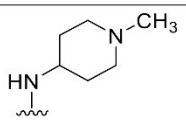		37 ± 4	45
10	**11c**			39 ± 5	46
11	**14**			44 ± 8	40
12	**31**	-	-	65 ± 7 (n = 9)	01
13	**35** (UNC0631)	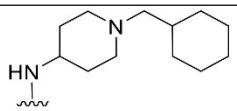	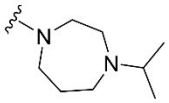	12 ± 0.5 pK_i = 6.04 ± 0.04	-
14	**9f**	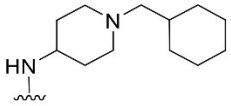	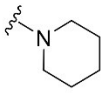	6 ± 1 pK_i = 5.84 ± 0.03	70

For the UNC0646 (**1**) analog **16b** differing from **1** by the lack of a 2-substituent the remaining reporter ligand binding by amounting to 50 ± 5% was found as described above to be distinctly higher than that of the reference compound UNC0646 (**1**, 21 ± 3%; see Table 1, Entry 1 and 7). Though the binding affinity of **16b** is thus significantly lower than that of **1**, it is still of a decent size. Hence, analogs of this compound, **16b**, with varying substituents in 4-position should be studied with regard to their binding affinities, as this might supplement the so far established structure affinity relationships. The compounds selected in this context, the synthesis of which is comparably easy to accomplish, are listed in Table 2.

The first subset of compounds to be discussed regarding their binding affinities comprises the quinazoline derivatives **16b**, **20a**, **16c** and **16a** (Table 2, Entries 1-4). These compounds differ with regard to their *N*-alkyl substituents attached to the terminal amino group of the piperidin-4-amino residue in 4-position of the quinazoline system, which are a cyclohexyl, an isopropyl, a methyl and a cyclohexylmethyl group. As observed before for the UNC0646 analogs **11a**-**11c** and **35** (see Table 1) also for **16b**, **20a**, **16c** and **16a** (Table 2, Entries 1-4) the binding affinity increases, which is mirrored by a decrease in remaining reporter ligand binding, in parallel to the increasing size of the aforementioned *N*-alkyl substituents. Thus, while **16a** with a *N*-cyclohexylmethyl residue effects a remaining reporter ligand binding of 41 ± 4%, this value goes continuously up to 50 ± 5% for the *N*-cyclohexyl (**16b**), 63 ± 4% for the *N*-isopropyl (**20a**) and finally to 80 ± 2% for the *N*-methyl derivative (**16c**).

In addition, the effect of the substitution of the *N*-cyclohexyl residue present in **16a** and the *N*-cyclohexylmethyl moiety in **16b** by a phenyl (→ **16d**) and a benzyl group (→ **16e**),

respectively, on the remaining reporter ligand binding has been evaluated. These structural variations have, however, no significant effect on the binding affinity, the remaining reporter ligand binding amounting to 50 ± 3% for the phenyl and 46 ± 3% for the benzyl derivative **16d** and **16e**, respectively, which values are identical or at least very close to those observed for the saturated analogs **16b** (50 ± 5%, Table 2, Entry 2) and **16a** (41 ± 4%, Table 2, Entry 1).

In a recent study a quinazoline derivative with a 5-(pyrrolidin-1-yl)pentan-1-amino residue in the 4-position of **9c** instead of the 1-cyclohexylpiperidin-4-amino residue was found to remain a similar binding affinity as the original compound **9c** (Kaiser et al., 2024). When an analogous exchange was undertaken for **16b** the binding affinity of the resulting compound **16f** (remaining reporter ligand binding 65 ± 5%, Table 2, Entry 7) was, to some extent lower than that of the reference compound (**16b**, remaining reporter ligand binding 50 ± 5%, Table 2, Entry 2).

When the secondary amino function attached to the 4-position of **20a** was replaced by an ether oxygen, to expand the structure affinity relationship study, the thus modified compound **16g** showed a decreased binding affinity (as compared to **20a**, 63 ± 4%, Table 2, Entry 2). Interestingly, with 74 ± 4% the value of the remaining reporter ligand binding for this compound, **16g** (Table 2, Entry 8), is still of a reasonable size indicating that even an ether function instead of an amino function is tolerated in 4-position of the quinazoline. When, however, a substituent in 4-position of the quinazoline ring is omitted in this series of compounds listed in Table 2, then as can be seen from the data obtained for **13** any binding affinity appears to be lost (remaining reporter ligand binding 100 ± 7%, Table 2, Entry 9).

Finally, also the commercially available drug Tandutinib (**36**) structurally related to the compounds in Table 2 was included in this study. The remaining reporter ligand binding for this compound describing its affinity amounted to 66 ± 6% (Table 2, Entry 10). Though, this binding affinity is relatively low, it is still of reasonable size, indicating that Tandutinib (**36**) known as an inhibitor of the FMS-like tyrosine kinase 3, is also as a ligand of the MB327-PAM-1 binding site of the nAChR.

Table 2: Binding affinities of UNC0646 analogs devoid of a 2-substituent but with varying 4-substituents for the MB327-PAM-1 binding site of the *Torpedo*-nAChR. [a] 'reporter ligand binding' refers to the remaining binding of the reporter ligand (UNC0642, 1 µM) in presence of the respective test compound (10 µM) as % value ± SD; see Material and Methods for details. [b] 'reporter ligand binding' has been reported previously (Kaiser et al., 2024).

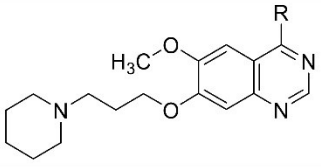

13, 16a-16g, 20a, 36

Entry	Compound	R	reporter ligand binding [%] [a]	PTMD01 code
1	**16a**	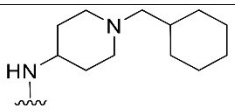	41 ± 4	07

Continued next page

Table 2 *(continued)*

Entry	Compound	R	reporter ligand binding [%] [a]	PTMD01 code
2	**16b**	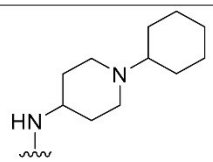	50 ± 5 (n = 12) [b]	04
3	**20a**	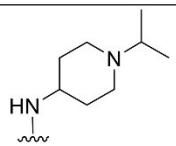	63 ± 4 (n = 6) [b]	05
4	**16c**	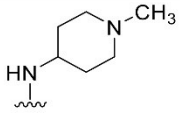	80 ± 2	06
5	**16d**	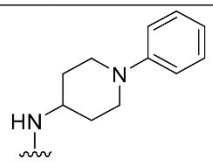	50 ± 3	08
6	**16e**	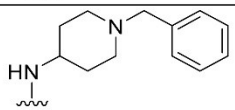	46 ± 3	09
7	**16f**	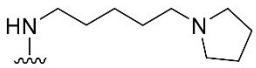	65 ± 5	51
8	**16g**	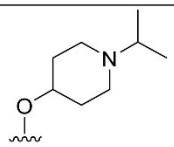	74 ± 4	54
9	**13**		100 ± 7	52
10	**36** (Tandutinib)	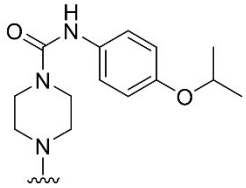	66 ± 6	-

Next, the binding affinities of UNC0646 analogs devoid of a 2-substituent but with varying 7-substituents for the MB327-PAM-1 binding site were studied. The structures of these analogs and their binding affinities again determined by means of UNC0642 MS Binding Assays are listed in Table 3.

First, the influence of the chain length of the spacer between the ether and the amino function of the side chain in 7-position of the quinazoline scaffold on the binding affinity was studied by extending as well as shortening it by one methylene group leading from **20a** with a propan-1,3-diyl (Table 3, Entry 1) to **20b** with a butan-1,4-diyl (Table 3, Entry 2) and **20c** with an ethan-1,2-diyl chain (Table 3, Entry 3), respectively. This, however, did not have any significant effect

on the binding affinity, the remaining reporter ligand binding amounting to 63 ± 4% (**20a**), 64 ± 3% (**20b**) and 63 ± 2% (**20c**), respectively, and thus stays almost constant.

Furthermore, the effect of the terminal heterocycle of the side chain in the 7-position of **20a** on the binding affinity was studied. When the respective piperidine ring of **20a** is exchanged by a pyrrolidine-1-yl and azepan-1-yl moiety resulting in **20d** and **20e**, respectively, the remaining reporter ligand binding of **20a** of 63 ± 4% (Table 3, Entry 1) increases to 76 ± 5% for **20d** (Table 3, Entry 4) whereas it descends to 55 ± 5% for **20e** (Table 3, Entry 5). Hence, there is a clear trend, according to which an increase of the ring size of the terminal azaheterocycle of the 7-substituent in these quinazoline derivatives gives rise to improved binding affinities.

In the compounds **20f**, **20g** and **20h**, the attachment point of the spacer in the 7-substituent of the quinazoline derivative **20a** is shifted from the nitrogen to the 2-, 4- and 3-position of the terminal piperidine ring, respectively, in combination with adapted spacer lengths. Whereas for the derivative **20g** (Table 3, Entry 7), in which the piperidine ring is linked via the 4-position with the rest of the molecule, the remaining reporter ligand is with 63 ± 1% nominally identical with that of **20a** (63 ± 4%, Table 3, Entry 1), that of **20f** and **20h** attached via the 2- and 3-position, respectively, is higher (**20f**, 71 ± 7%, Table 3, Entry 6; **20h**, 79 ± 7%, Table 3, Entry 8). Thus, these variations appear to have no (**20g**) or only a negative effect on the binding affinity (**20f** and **20h**).

To gain insight on the significance of the ether function in the 7-position of **20a** for the binding affinity, a set of derivatives of **20a**, in which the ether function had been replaced by an amino group, was included in this study as well. When this ether function is replaced by a methylamino group leading to **23a** with a tertiary amino function a clear decrease of binding affinity with the remaining reporter ligand binding ascending to 71 ± 1% occurs (Table 3, Entry 10) as compared to 63 ± 4% for **20a** (Table 3, Entry 1). Interestingly, for **23b** the remaining reporter ligand binding is significantly lower (54 ± 4%; Table 3, Entry 11) than that of the original compound **20a** (63 ± 4%). A further decline of the remaining reporter ligand binding to 45 ± 7% and thus increase of the binding affinity is even observed for the azepan-1-yl analog **23c** (Table 3, Entry 12). The latter improvement is likely to be assigned to the presence of the azepane ring, which also in case of the quinazoline derivative **20a** (Table 3, Entry 1) with an ether function gives rise to an increase in binding affinity when the piperidine ring (in **20a**) is enlarged to an azepane ring (→ **20e**, Table 3, Entry 5). In any case, a secondary amino group instead of an ether function in 7-position of the quinazoline scaffold is according to the above-described results well tolerated giving even rise to a slight increase of the binding affinity.

With MB327 as a prototypic ligand of the MB327-PAM-1 binding site, well characterized in various *in vitro* and *in vivo* assays, in mind we thought it worthwhile to replace the piperidine ring in the side chain in 7-position of **20a** by a 4-*tert*-butylpyridinium group and to thus partly mimic MB327 as a bispyridinium salt comprising two such moieties. The remaining reporter ligand binding found for the respective hybrid compound **20i** (Table 3, Entry 9) is by amounting to 79 ± 2%, however, distinctly higher than that of **20a** (Table 3, Entry 1, 63 ± 4%), thus indicating the reduced binding affinity effected by the performed modification.

To shed some light on the question of the importance of the side chain in 7-position comprising a piperidino moiety for the binding affinity of **20a**, the more basically substituted compounds **18**, **32f** and **22** (Table 3, Entries 13-15) with a benzyloxy, methoxy or a fluoro substituent in

this position, respectively, were also included in this study. The remaining reporter ligand binding found for these compounds are by amounting to 96 ± 2% (**18**), 92 ± 8% (**32f**) and 88 ± 2% (**22**) far higher than that of **20a** (63 ± 4%) indicating a distinct loss of binding affinity due to the structural variations, the binding affinities becoming very low to negligible.

Table 3: Binding affinities of UNC0646 analogs devoid of a 2-substituent but with varying 7-substituents for the MB327 binding site of the *Torpedo*-nAChR. [a] 'reporter ligand binding' refers to the remaining binding of the reporter ligand (UNC0642, 1 µM) in presence of the respective test compound (10 µM) as % value ± SD; see Material and Methods for details. [b] 'reporter ligand binding' has been reported previously (Kaiser et al., 2024).

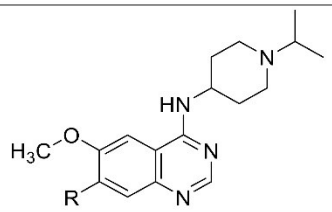

18, **20a-20i**, **22**, **23a-23c**, **32f**

Entry	Compound	R	reporter ligand binding [%] [a]	PTMD01 code
1	**20a**	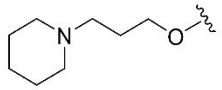	63 ± 4 (n = 6) [b]	05
2	**20b**	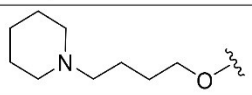	64 ± 3	16
3	**20c**	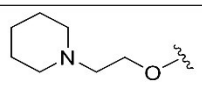	63 ± 2	10
4	**20d**	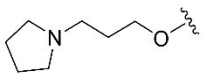	76 ± 5	12
5	**20e**	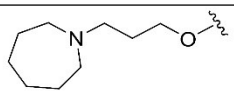	55 ± 5	11
6	**20f**	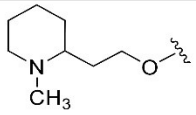	71 ± 7	13
7	**20g**	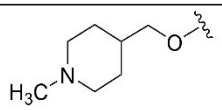	63 ± 1	14
8	**20h**	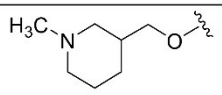	79 ± 7	15
9	**20i**	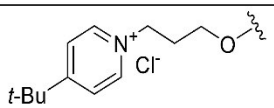	79 ± 2	17
10	**23a**	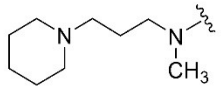	71 ± 1	41

Continued next page

Table 3 *(continued)*

Entry	Compound	R	reporter ligand binding [%] [a]	PTMD01 code
11	**23b**	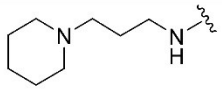	54 ± 4 (n = 6)	42
12	**23c**	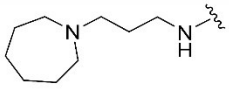	45 ± 7	63
13	**18**	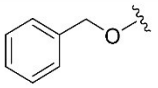	96 ± 2	68
14	**32f**	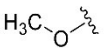	92 ± 8	69
15	**22**		88 ± 2	72

For the transformation of UNC0646 (**1**) into its analog **31** by exchange of the 3-(piperidin-1-yl)propoxy group in 7-position by a methoxy substituent, as already outlined above, a distinct decline in binding affinity has been observed reflected by an increase of the remaining reporter ligand binding from 21 ± 3% for **1** to 65 ± 7% for **31**. But for a compound of this size, **31** being notably smaller than **1**, this binding affinity is still reasonable. Moreover, for some analogs of **31** promising results had been reported in a recent study (Kaiser et al., 2024). Hence, a set of analogs of **31** for which the substituents in 2- and 4-position are varied but the 6,7-dimethoxyquinazoline scaffold is kept constant should be studied for their binding affinity for the MB327-PAM-1 binding site.

When as a first measure, the 4-isopropyl-1,4-diazepan-1-yl substituent in 2-position was reduced in size by replacing the isopropyl by a methyl group, the remaining reporter ligand binding goes nominally down from 65 ± 7% for **31** to 57 ± 4% for **28b** (Table 4, Entry 4). Though this might indicate an increase in binding affinity, this change lacks statistical significance.

A reduction of the size of the 4-substituent in **28b** by replacement of the terminal hexyl by an isopropyl group, however, leads to a distinct decrease in binding affinity, the remaining reporter ligand binding increasing from 57 ± 4% for **28b** (Table 4, Entry 4) to 74 ± 1% for **28c** (Table 4, Entry 6). This is in line with a former observation, according to which large *N*-alkyl residues as in the 1-cyclohexylpiperidin-4-amino rest in 4-position are more favorable for higher binding affinities (compare listed data for **16a**-**16c** and **20a**, Table 2, and in addition the listed data for **11a**, **11b**, **1** and **35**, Table 1). Similarly, as already observed for the analogs **16b** and **16e** (Table 2, Entry 2 and 6) differing by the terminal *N*-substituent of the piperidin-4-amino residue in 4-position of the quinazoline scaffold, i.e. a cyclohexyl versus a benzyl group, this switch has here, as well, no significant influence on the binding affinity. Thus, whereas for the *N*-cyclohexyl analog **28b** the remaining reporter ligand binding amounts 57 ± 4%, the *N*-benzyl analog **37**, gives rise to a nominal increase to 64 ± 4% (Table 4, Entry 3) which is, however, not statistically significant.

In a two-dimensional *in silico* similarity search for UNC0646 analogs, among 6,7-dimethoxyquinazoline derivatives one compound (UNC0379) with a 5-(pyrrolidin-1-yl)pentan-

1-amino moiety in 4-position with promising binding affinity has been found. In the present set of compounds, **28a** exhibiting the same residue (5-(pyrrolidin-1-yl)pentan-1-amino moiety) the remaining reporter ligand binding amounted 56 ± 3% that is in the same range as for **28b** (57 ± 4%) with a 1-cyclohexylpiperidin-4-amino residue known from UNC0646. For **30a**, which is formally deduced from **28a** by exchange of the 4-methyl-1,4-diazepan-1-yl by a piperidine residue in 2-position a decrease of the remaining reporter ligand binding from 56 ± 3% (for **28a**) to 48 ± 5% (for **30a**) is observed. This change, however, does not reflect an increase in binding affinity, as the difference does lack statistical significance. Still, a positive effect of the presence of the 5-(pyrrolidin-1-yl)pentan-1-amino moiety on the binding affinity becomes apparent, when compound **30a** is compared to **30b**, both exhibiting a piperidine ring in 2-position. Here, the exchange of the substituent in 2-position, i.e. of the 1-isopropylhexylpiperidin-4-amino (in **30b**) by a 5-(pyrrolidin-1-yl)pentan-1-amino residue (in **30a**) leads to a decline of the remaining reporter ligand binding from 66 ± 5% (**30b**, Table 4, Entry 11) to 48 ± 5% (**30a**, Table 4, Entry 1) indicating an increase in binding affinity.

As already described above, for the quinazoline derivative **28c** exhibiting a 4-methyl-1,4-diazepan-1-yl moiety in 2- and a 1-isopropylpiperidin-4-amino residue in 4-position only a modest binding affinity has been found (remaining reporter ligand binding 74 ± 1%, Table 4, Entry 6). Yet, it seemed of interest to explore to what extent the binding affinity of this compound, **28c**, depends on the structure of the substituent in 2-position. Hence, we investigated the binding affinity of analogs of **28c**, for which the structure of the 2-substituent was altered, whereas that of all other substituent was kept constant.

For **32a** with an 1,4´-bipiperidine moiety, **32c** with an 4-(4-methlypiperazin1-yl)piperidine moiety, **32d** with a 4,4-difluoropiperidine and **30b** with a piperidine ring in 2-position the remaining reporter ligand binding varied only to a small extent, the values reaching from 64% to 66%. Thus, the binding affinities of these derivatives delineated from **28c** are very similar to that of the original compound, **28c**, exhibiting a remaining reporter ligand binding of 74 ± 1% (Table 4, Entry 6).

In a related study the (3-methylpyridin-4-yl)-1,4-diazepan-1-yl located in in the 4-position of a quinazoline derivative has been found to mediate a positive effect on the binding affinity of the respective test compound (Kaiser et al., 2024). Interestingly, this is the case here, too, as compound **32b** with the aforementioned substituent in 2-position exhibits a distinct increase in binding affinity as compared to **28c**, the remaining reporter ligand binding of **32b** ranging with 41 ± 9% (Table 4, Entry 8) significantly below the 74 ± 1% of **28c** (Table 4, Entry 6).

For the two UNC0646 (**1**, Table 1, Entry 1) analogs **9e** (Table 1, Entry 6) and **16b** (Table 1, Entry 7), in which the 4-isopropyl-1,4-diazepane residue of **1** in the 2-position of the molecule has been replaced by a primary amino group (**9e**) or just an hydrogen (**16b**), the binding affinity remained in the first case almost unchanged (remaining reporter ligand binding 27 ± 2%) or in the second case was lowered but remained still reasonable (50 ± 5%). A similar trend is observed upon transition from **28c** to its analogs **32e** and **32f**, that can be considered as parent compounds. When instead of the 4-methyl-1,4-diazepane substituent in 2-position of **28c** a primary amino group is present (**32e**) the remaining reporter ligand binding is with 75 ± 2% almost identical with that of **28c** (74 ± 1%). In case of the in 2-position unsubstituted analog of **28c**, **32f**, the binding affinity decreases and as it starts already at a low level for **28c** (remaining reporter ligand binding 74 ± 1%) it this time almost vanishes (remaining reporter ligand binding 92 ± 8%).

By exhibiting a primary amino function in 2- and 4-position of 6,7-dimethoxyquinazoline compound **40** it comprises all of the most fundamental structural features of the compound listed in Table 4. As this compound, **40**, as well its analogs **38** and **39** with more complex amino substituents in the 2-position, a piperazine ring and a 4-furanoylpiperazine moiety, were commercially available, they were included in this study. Whereas the diamino substituted quinazoline derivative **40** seems to be devoid of any binding affinity (remaining reporter ligand binding 95 ± 8%), the presence of the two larger substituents in **38** and **39** appears to mediate a slight increase of the binding affinity which remains, however, still modest (remaining reporter ligand binding 83 ± 7% and 85 ± 5% for **38** and **39**, respectively).

Table 4: Binding affinities of 6,7-dimethoxyquinazoline analogs of UNC0646 for the MB327 binding site of the *Torpedo*-nAChR. [a] 'reporter ligand binding' refers to the remaining binding of the reporter ligand (UNC0642, 1 µM) in presence of the respective test compound (10 µM) as % value ± SD; see Material and Methods for details.

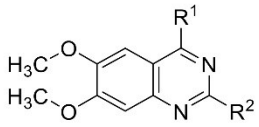
28a-28c, **30a-30b**, **31**, **32a-32f**, **37-40**

Entry	Compound	R^1	R^2	reporter ligand binding [%] [a]	PTMD01 code
1	**30a**	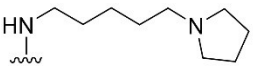	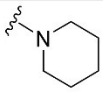	48 ± 5	61L
2	**28a**	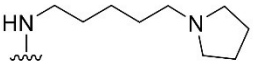	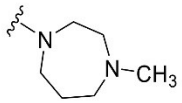	56 ± 3	59
3	**37** (BIX01294)	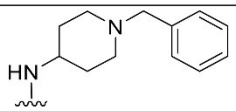		64 ± 4	-
4	**28b**	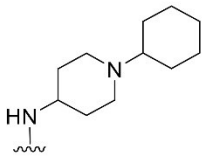		57 ± 4	02
5	**31**		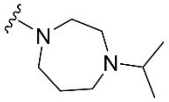	65 ± 7 (n = 9)	01

Continued next page

Table 3 *(continued)*

Entry	Compound	R^1	R^2	reporter ligand binding [%] [a]	PTMD01 code
6	**28c**	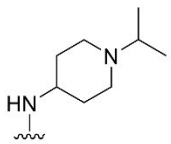	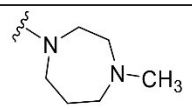	74 ± 1	03
7	**32a**		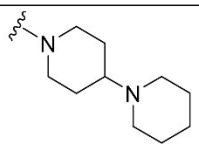	64 ± 6	55
8	**32b**		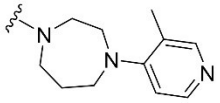	41 ± 9	56
9	**32c**		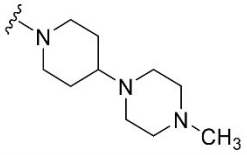	64 ± 8	57
10	**32d**		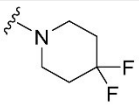	70 ± 2 (n = 2)	58L
11	**30b**		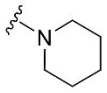	66 ± 5	60L
12	**32e**			75 ± 2	64
13	**32f**			92 ± 8	69
14	**38**		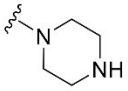	83 ± 7	18C
15	**39** (Prazosin)		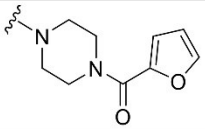	85 ± 5	-
16	**40**			95 ± 8	73C

During this study various analogs of UNC0646 (**1**) have been synthesized using 7-benzyloxy-2,4-dichloro-6-methoxyquinazoline (**4**) as a key compound. Thereby, the 7-benzyloxy residue in **4** served as starting point for the establishment of various ω-aminoalkoxy side chains in this position of the final test compounds as they are common for UNC0646 (**1**) and respective analogs. With the building block **4** at hand, it seemed worthwhile to also study the binding affinities of UNC0646 analogs that can be directly delineated from **4** leaving the substituents in 6- and 7-position unchanged. That was expected to provide further information regarding the necessity of a basic side chain in 7-position of quinazoline analogs of UNC0646 (**1**) for effecting reasonable binding affinities. Hence, the test compounds **34a**-**34c** were studied, all of which are characterized by a 6-methoxy-7-benzyloxyquinazoline substructure, a piperidine ring in 2-position and various basic residues in 4-position. The piperidine ring in 2-position had been chosen, as it mediates a similar binding affinity as the 4-isopropyl-1,4-diazepan-1-yl substituent in UNC0646 though it is distinctly smaller (Table 1, Entries 1 and 4). As the UNC0646 analog **9c** also the 7-benzyloxy substituted quinazoline derivative **34b** contains a 1-cyclohexylpiperidin-4-amino residue in 4-position as does UNC0646 (**1**). Remarkably, compound **34b** exerts a reduction of reporter ligand binding down to 26 ± 1%, which is in the same range as the remaining reporter ligand binding of UNC0646 (**1**, 21 ± 3%, Table 1, Entry 1) and **9c** (11 ± 3%, Table 1, Entry 4). Upon substitution of the 1-cyclohexylpiperidin-4-amino group in 4-position by a 5-(pyrrolidin-1-yl)pentan-1-amino residue the binding affinity even further increases, the remaining reporter ligand binding decreasing to 15 ± 1% (Table 5, Entry 1). Hence, high binding affinities may even be reached without a basic group being part of the substituent in 7-position of the quinazoline system.

For the UNC0646 analog **9c** upon transition to **9f** with an extra methylene group in the side chain in 4-position (1-cyclohexylmethylpiperidin-4-amino instead of a 1-cyclohexylpiperidin-4-amino residue) the high binding affinity is retained [remaining reporter ligand binding of **9c**, 11 ± 3% (pK_i = 5.83 ± 0.02) for **9f**, 6 ± 1% (pK_i = 5.84 ± 0.03)]. In contrast, for **34c** a lower binding affinity than for **34b** is observed, though the former differs from the latter in the same way as **9f** and **9c** by an extra methylene group in the 4-substituent of the quinazoline system. These different trends might possibly arise from different binding modes for quinazoline derivatives with a basic group as part of the 7-substituent and those with a 7-benzyloxy group.

Being commercially available the quinazoline derivative **41** (Table 5, Entry 4) with a 7-benzyloxy residue alike **34a-34c** was included in this study, as well. With a remaining reporter ligand binding of 67 ± 3% (Table 5, Entry 4) the binding affinity of this compound with a 4-substituent that was now smaller than that of **34b** (1-methylpiperidin-4-amino instead of a 1-cyclohexylpiperidin-4-amino group) and which carried a 1,4-diazepane instead of a piperidine ring in 2-position was poor, too.

In any case, considering these results, quinazoline derivatives related to UNC0646 (**1**) but equipped with a benzyloxy residue instead of a side chain with an amino function in 7-position appear to deserve further exploration as ligands of the MB327 binding site.

Table 5: Binding affinities of 2,4-disubstituted 7-(benzyloxy)-6-methoxyquinazoline derivatives for the MB327 binding site of the *Torpedo*-nAChR. [a] 'reporter ligand binding' refers to the remaining binding of the reporter ligand (UNC0642, 1 µM) in presence of the respective test compound (10 µM) as % value ± SD; see Material and Methods for details.

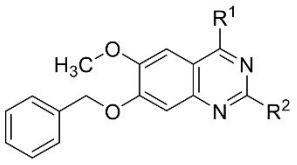

34a-**34c**, **41**

Entry	Compound	R^1	R^2	reporter ligand binding [%] [a]	PTMD01 code
1	**34a**	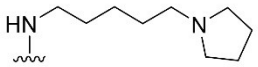	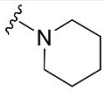	15 ± 1	62
2	**34b**	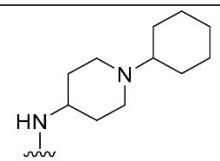	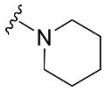	26 ± 1	66
3	**34c**	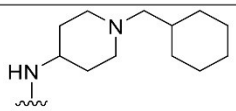	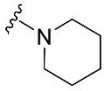	53 ± 2	67
4	**41** (TM2-115)	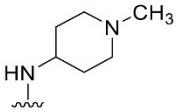	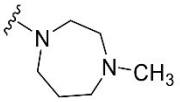	67 ± 3	-

4 Conclusion

In this study we successfully synthesized a remarkable number of yet unknown analogs of UNC0646 (**1**), which represented the compound with the highest known affinity towards the MB327-PAM-1 binding site of the nAChR at the begin of this study. This binding site is of great interest as it is thought that organophosphorus compound poisoning therapy will benefit from compounds mediating allosteric effects through this binding site.

Adapting literature known methods, this plethora of compounds could be synthesized with high efficiency in one- to four-step syntheses, introducing a wide variety of substituents to positions 2, 4 and 7 of the quinazoline scaffold. By applying this strategy, we were able to, on the one hand, get access to strategically, only slightly modified UNC0646 analogs to subsequently examine the influence of the corresponding substituents. On the other hand, we accomplished the synthesis of quinazoline-based compounds that structurally differed a little more from UNC0646 (**1**) in order to further explore the chemical space around UNC0646 (**1**).

Expanded with structurally matching compounds that were commercially available, all compounds synthesized in this study were evaluated regarding their affinity towards the above-mentioned binding site. For this purpose, a recently developed MS Binding Assay, utilizing UNC0642 (**2**) as reporter ligand, was applied. Even though here only one compound, UNC0631 (**35**) ($pK_i = 6.04 \pm 0.04$), showed an increased affinity compared to UNC0646 (**1**) ($pK_i = 5.83 \pm 0.05$), the generated data is of great value. This is because the results of the competitive MS binding experiments at a single test compound concentration, which investigated more than 50 quinazoline-based compounds, allow to draw conclusions regarding structure-affinity relationships within this class of compounds, not yet possible to this extent.

The gained information is crucial in order to purposefully design new quinazoline-based compounds, ideally addressing the MB327-PAM-1 binding site with high affinity plus ideally having lower molecular weight than UNC0646 (**1**). These compounds would then display promising candidates to be further evaluated in terms of other characteristics, e.g. regarding their intrinsic activity in order to develop novel therapeutics against organophosphorus intoxications.

5 Supporting Information

Supplementary data associated with this article can be found in the online version at doi: xxx.

6 Acknowledgments

This work was supported by the German Ministry of Defence (E/ U2AD/KA019/IF558).

7 Conflict of interest

The authors declare no conflict of interest.

8 Keywords

neurological agents • nicotinic acetylcholine receptor • quinazolines • structure-affinity relationships • MS Binding Assay

9 References

Abe, Y., Kayakiri, H., Satoh, S., Inoue, T., Sawada, Y., Inamura, N., Asano, M., Aramori, I., Hatori, C., Sawai, H., Oku, T., Tanaka, H., 1998. A Novel Class of Orally Active Non-Peptide Bradykinin B2 Receptor Antagonists. 3. Discovering Bioisosteres of the Imidazo[1,2-a]pyridine Moiety. Journal of Medicinal Chemistry 41, 4062-4079.

Aubin, Y., Fischmeister, C., Thomas, C.M., Renaud, J.-L., 2010. Direct amination of aryl halides with ammonia. Chemical Society Reviews 39, 4130-4145.

Bernauer, T., Nitsche, V., Kaiser, J., Gertzen, C.G.W., Höfner, G., Niessen, K.V., Seeger, T., Steinritz, D., Worek, F., Gohlke, H., Wanner, K.T., Paintner, F.F., 2024. Synthesis and Biological Evaluation of Novel MB327 Analogs as Resensitizers for Desensitized Nicotinic Acetylcholine Receptors after Intoxication with Nerve Agents. bioRxiv, 2024.2002.2009.579646.

Borzenko, A., Rotta-Loria, N.L., MacQueen, P.M., Lavoie, C.M., McDonald, R., Stradiotto, M., 2015. Nickel-Catalyzed Monoarylation of Ammonia. Angewandte Chemie 127, 3844-3848.

Brown, M.A., Brix, K.A., 1998. Review of health consequences from high-, intermediate- and low-level exposure to organophosphorus nerve agents. Journal of Applied Toxicology 18, 393-408.

Cui, R., Yin, C., Deng, X., Zhang, T., 2020. STK19 inhibitors for treatment of cancer. Trustees of Boston University, Xiamen University.

Cushman, M., Georg, G.I., Holzgrabe, U., Wang, S., 2014. Absolute Quantitative 1H NMR Spectroscopy for Compound Purity Determination. Journal of Medicinal Chemistry 57, 9219-9219.

Davis, I., Jin, J., Janzen, W.P., Pattenden, S., Jayakody, C., 2016. A novel compound for the treatment of ewing sarcoma and high-throughput assays for identifying small molecules that modulate aberrant chromatin accessibility. Google Patents.

Doig, P., Boriack-Sjodin, P.A., Dumas, J., Hu, J., Itoh, K., Johnson, K., Kazmirski, S., Kinoshita, T., Kuroda, S., Sato, T.-o., Sugimoto, K., Tohyama, K., Aoi, H., Wakamatsu, K., Wang, H., 2014. Rational design of inhibitors of the bacterial cell wall synthetic enzyme GlmU using virtual screening and lead-hopping. Bioorganic & Medicinal Chemistry 22, 6256-6269.

Dolgin, E., 2013. Syrian gas attack reinforces need for better anti-sarin drugs. Nature Medicine 19, 1194-1195.

Fagan, V., Johansson, C., Gileadi, C., Monteiro, O., Dunford, J.E., Nibhani, R., Philpott, M., Malzahn, J., Wells, G., Faram, R., Cribbs, A.P., Halidi, N., Li, F., Chau, I., Greschik, H., Velupillai, S., Allali-Hassani, A., Bennett, J., Christott, T., Giroud, C., Lewis, A.M., Huber,

K.V.M., Athanasou, N., Bountra, C., Jung, M., Schüle, R., Vedadi, M., Arrowsmith, C., Xiong, Y., Jin, J., Fedorov, O., Farnie, G., Brennan, P.E., Oppermann, U., 2019. A Chemical Probe for Tudor Domain Protein Spindlin1 to Investigate Chromatin Function. Journal of Medicinal Chemistry 62, 9008-9025.

Freire, C., Koifman, S., 2013. Pesticides, depression and suicide: a systematic review of the epidemiological evidence. International journal of hygiene and environmental health 216, 445-460.

Gharat, L.A., Banerjee, A., Khairatkar-Joshi, N., Kattige, V.G., 2015. Bicyclic compounds as mPGES-1 inhibitors. Google Patents.

Gmeiner, P., Junge, D., Kaertner, A., 1994. Enantiomerically pure amino alcohols and diamino alcohols from L-aspartic acid. Application to the synthesis of epi-and diepislaframine. The Journal of Organic Chemistry 59, 6766-6776.

Harris, C.S., Kettle, J.G., Williams, E.J., 2005. Facile synthesis of 7-amino anilinoquinazolines via direct amination of the quinazoline core. Tetrahedron Letters 46, 7381-7384.

Jiang, Y.-H., Kim, Y., Lee, H.-M., Jin, J., Roth, B.L., 2017. Preparation of quinazolin-4-amine derivatives as histone methyltransferase G9a inhibitors and methods for the treatment of Prader-willi syndrome. Duke University, The University of North Carolina at Chapel Hill.

Kaiser, J., Gertzen, C.G.W., Bernauer, T., Höfner, G., Niessen, K.V., Seeger, T., Paintner, F.F., Wanner, K.T., Worek, F., Thiermann, H., Gohlke, H., 2023. A novel binding site in the nicotinic acetylcholine receptor for MB327 can explain its allosteric modulation relevant for organophosphorus-poisoning treatment. Toxicology Letters 373, 160-171.

Kaiser, J., Gertzen, C.G.W., Bernauer, T., Nitsche, V., Höfner, G., Niessen, K.V., Seeger, T., Paintner, F.F., Wanner, K.T., Steinritz, D., Worek, F., Gohlke, H., 2024. Identification of ligands binding to MB327-PAM-1, a binding pocket relevant for resensitization of nAChRs. bioRxiv, p. 2023.2012.2021.572862.

Kassa, J., Timperley, C.M., Bird, M., Green, A.C., Tattersall, J.E.H., 2022. Influence of Experimental End Point on the Therapeutic Efficacy of Essential and Additional Antidotes in Organophosphorus Nerve Agent-Intoxicated Mice. Toxics, vol. 10.

Liu, F., Barsyte-Lovejoy, D., Allali-Hassani, A., He, Y., Herold, J.M., Chen, X., Yates, C.M., Frye, S.V., Brown, P.J., Huang, J., Vedadi, M., Arrowsmith, C.H., Jin, J., 2011. Optimization of Cellular Activity of G9a Inhibitors 7-Aminoalkoxy-quinazolines. Journal of Medicinal Chemistry 54, 6139-6150.

Liu, F., Chen, X., Allali-Hassani, A., Quinn, A.M., Wigle, T.J., Wasney, G.A., Dong, A., Senisterra, G., Chau, I., Siarheyeva, A., Norris, J.L., Kireev, D.B., Jadhav, A., Herold, J.M., Janzen, W.P., Arrowsmith, C.H., Frye, S.V., Brown, P.J., Simeonov, A., Vedadi, M., Jin, J., 2010. Protein Lysine Methyltransferase G9a Inhibitors: Design, Synthesis, and Structure Activity Relationships of 2,4-Diamino-7-aminoalkoxy-quinazolines. Journal of Medicinal Chemistry 53, 5844-5857.

Ma, A., Yu, W., Li, F., Bleich, R.M., Herold, J.M., Butler, K.V., Norris, J.L., Korboukh, V., Tripathy, A., Janzen, W.P., 2014. Discovery of a selective, substrate-competitive inhibitor of the lysine methyltransferase SETD8. Journal of medicinal chemistry 57, 6822-6833.

Maselli, R.A., Leung, C., 1993. Analysis of anticholinesterase-induced neuromuscular transmission failure. Muscle & Nerve 16, 548-553.

Massoulié, J., Pezzementi, L., Bon, S., Krejci, E., Vallette, F.-M., 1993. Molecular and cellular biology of cholinesterases. Progress in Neurobiology 41, 31-91.

Mellstedt, H., Bystrom, S., Vagberg, J., Olsson, E., 2020. 2-phenyl-3H-imidazo [4, 5-B] pyridine derivates useful as inhibitors of mammalian tyrosine kinase ROR1 activity. Google Patents.

Mohamed, T., Rao, P.P., 2015. Facile approaches toward the synthesis of N4-monosubstituted quinazolin-2, 4-diamines. Tetrahedron letters 56, 6882-6885.

Newmark, J., 2007. Nerve Agents. The Neurologist 13, 20-32.

Niessen, K.V., Muschik, S., Langguth, F., Rappenglück, S., Seeger, T., Thiermann, H., Worek, F., 2016. Functional analysis of Torpedo californica nicotinic acetylcholine receptors in multiple activation states by SSM-based electrophysiology. Toxicology Letters 247, 1-10.

Niessen, K.V., Seeger, T., Rappenglück, S., Wein, T., Höfner, G., Wanner, K.T., Thiermann, H., Worek, F., 2018. In vitro pharmacological characterization of the bispyridinium non-oxime compound MB327 and its 2- and 3-regioisomers. Toxicology Letters 293, 190-197.

Nitsche, V., Höfner, G., Kaiser, J., Gertzen, C.G.W., Seeger, T., Niessen, K.V., Steinritz, D., Worek, F., Gohlke, H., Paintner, F.F., Wanner, K.T., 2024. MS Binding Assays with UNC0642 as reporter ligand for the MB327 binding site of the nicotinic acetylcholine receptor. Toxicology Letters 392, 94-106.

OPCW, 2017. OPCW Director-General Shares Incontrovertible Laboratory Results Concluding Exposure to Sarin, 19.04.2017.

Papke, R.L., 2014. Merging old and new perspectives on nicotinic acetylcholine receptors. Biochemical Pharmacology 89, 1-11.

Pauli, G.F., Chen, S.-N., Simmler, C., Lankin, D.C., Gödecke, T., Jaki, B.U., Friesen, J.B., McAlpine, J.B., Napolitano, J.G., 2014. Importance of Purity Evaluation and the Potential of Quantitative 1H NMR as a Purity Assay. Journal of Medicinal Chemistry 57, 9220-9231.

Pita, R., Domingo, J., 2014. The Use of Chemical Weapons in the Syrian Conflict. Toxics 2, 391-402.

Price, M.E., Docx, C.J., Rice, H., Fairhall, S.J., Poole, S.J.C., Bird, M., Whiley, L., Flint, D.P., Green, A.C., Timperley, C.M., Tattersall, J.E.H., 2016. Pharmacokinetic profile and quantitation of protection against soman poisoning by the antinicotinic compound MB327 in the guinea-pig. Toxicology Letters 244, 154-160.

Rappenglück, S., Sichler, S., Höfner, G., Wein, T., Niessen, K.V., Seeger, T., Paintner, F.F., Worek, F., Thiermann, H., Wanner, K.T., 2018a. Synthesis of a Series of Non-Symmetric Bispyridinium and Related Compounds and Their Affinity Characterization at the Nicotinic Acetylcholine Receptor. ChemMedChem 13, 2653-2663.

Rappenglück, S., Sichler, S., Höfner, G., Wein, T., Niessen, K.V., Seeger, T., Paintner, F.F., Worek, F., Thiermann, H., Wanner, K.T., 2018b. Synthesis of a Series of Structurally Diverse MB327 Derivatives and Their Affinity Characterization at the Nicotinic Acetylcholine Receptor. ChemMedChem 13, 1806-1816.

Seeger, T., Eichhorn, M., Lindner, M., Niessen, K.V., Tattersall, J.E.H., Timperley, C.M., Bird, M., Green, A.C., Thiermann, H., Worek, F., 2012. Restoration of soman-blocked neuromuscular transmission in human and rat muscle by the bispyridinium non-oxime MB327 in vitro. Toxicology 294, 80-84.

Sheridan, R.D., Smith, A.P., Turner, S.R., Tattersall, J.E.H., 2005. Nicotinic Antagonists in the Treatment of Nerve Agent Intoxication. Journal of the Royal Society of Medicine 98, 114-115.

Shih, T.-M., Rowland, T.C., McDonough, J.H., 2007. Anticonvulsants for Nerve Agent-Induced Seizures: The Influence of the Therapeutic Dose of Atropine. Journal of Pharmacology and Experimental Therapeutics 320, 154.

Sichler, S., Höfner, G., Nitsche, V., Niessen, K.V., Seeger, T., Worek, F., Paintner, F.F., Wanner, K.T., 2024. Screening for new ligands of the MB327-PAM-1 binding site of the nicotinic acetylcholine receptor. Toxicology Letters 394, 23-31.

Somnarin, T., Pobsuk, N., Chantakul, R., Panklai, T., Temkitthawon, P., Hannongbua, S., Chootip, K., Ingkaninan, K., Boonyarattanakalin, K., Gleeson, D., Paul Gleeson, M., 2022. Computational design, synthesis and biological evaluation of PDE5 inhibitors based on N2,N4-diaminoquinazoline and N2,N6-diaminopurine scaffolds. Bioorganic & Medicinal Chemistry 76, 117092.

Sundriyal, S., Chen, P.B., Lubin, A.S., Lueg, G.A., Li, F., White, A.J.P., Malmquist, N.A., Vedadi, M., Scherf, A., Fuchter, M.J., 2017. Histone lysine methyltransferase structure activity relationships that allow for segregation of G9a inhibition and anti-Plasmodium activity. MedChemComm 8, 1069-1092.

Thiermann, H., Seeger, T., Gonder, S., Herkert, N., Antkowiak, B., Zilker, T., Eyer, F., Worek, F., 2010. Assessment of neuromuscular dysfunction during poisoning by organophosphorus compounds. Chemico-Biological Interactions 187, 265-269.

Thiermann, H., Worek, F., 2022. Pro: Oximes should be used routinely in organophosphate poisoning. British Journal of Clinical Pharmacology 88, 5064-5069.

Timperley, C.M., Bird, M., Green, C., Price, M.E., Chad, J.E., Turner, S.R., Tattersall, J.E., 2012. 1, 1′-(Propane-1, 3-diyl) bis (4-tert-butylpyridinium) di (methanesulfonate) protects guinea pigs from soman poisoning when used as part of a combined therapy. MedChemComm 3, 352-356.

Turner, S.R., Chad, J.E., Price, M., Timperley, C.M., Bird, M., Green, A.C., Tattersall, J.E.H., 2011. Protection against nerve agent poisoning by a noncompetitive nicotinic antagonist. Toxicology Letters 206, 105-111.

Venkatesan, A.M., Dehnhardt, C., Chen, Z., Santos, O.D., Santos, E.D., Curran, K., Ayral-Kaloustian, S., Chen, L., 2008. Amino-substituted quinazoline derivatives as inhibitors of β-cantenin/Tcf-4 pathway and cancer treatment agents and their preparation. Wyeth.

Vital, T., Wali, A., Butler, K.V., Xiong, Y., Foster, J.P., Marcel, S.S., McFadden, A.W., Nguyen, V.U., Bailey, B.M., Lamb, K.N., 2023. MS0621, a novel small-molecule modulator of Ewing sarcoma chromatin accessibility, interacts with an RNA-associated macromolecular complex and influences RNA splicing. Frontiers in Oncology 13.

Wang, P.G., Kondengaden, M.S., Zhang, Q., Zang, L., 2019. Histone deacetylase and histone methyltransferase inhibitors and methods of making and use of the same. Google Patents.

Worek, F., Szinicz, L., Eyer, P., Thiermann, H., 2005. Evaluation of oxime efficacy in nerve agent poisoning: Development of a kinetic-based dynamic model. Toxicology and Applied Pharmacology 209, 193-202.

Worek, F., Thiermann, H., Wille, T., 2020. Organophosphorus compounds and oximes: a critical review. Archives of Toxicology 94, 2275-2292.

Yamamoto, Y., Shinnkai, I., 2004. Science of Synthesis - Category 2, Hetarenes and Related Ring Systems, Stuttgart, pp. 573-749.

Yoshida, K., Taguchi, M., 1992. Reaction of N-substituted cyclic amines with 2, 4-dichloroquinazoline, 2, 4-dichloropyrimidine, and its 5-methyl derivative. Journal of the Chemical Society, Perkin Transactions 1, 919-922.

Supporting Information

Structure-Affinity Relationship of Quinazoline Derivatives as Potential Resensitizers of Desensitized nAChRs After Nerve Agent Intoxication

Tamara Bernauer[+][a], Valentin Nitsche[+][a], Georg Höfner[a], Karin V. Niessen[b], Thomas Seeger[b], Dirk Steinritz[b], Franz Worek[b], Klaus T. Wanner[a] and Franz F. Paintner*[a]

[a] T. Bernauer, V. Nitsche, Dr. G. Höfner, Prof. Dr. K. T. Wanner, Prof. Dr. F. F. Paintner
Department of Pharmacy - Center for Drug Research
Ludwig-Maximilians-Universität München
Butenandtstrasse 5-13, 81377 Munich (Germany)
E-mail: Franz.Paintner@cup.uni-muenchen.de

[b] Dr. K. V. Niessen, Dr. T. Seeger, Prof. Dr. D. Steinritz, Prof. Dr. F. Worek
Bundeswehr Institute of Pharmacology and Toxicology
Neuherbergstrasse 11, 80937 Munich (Germany)

[+] These authors contributed equally to this work.

Table of Content

Table S1: Commercially obtained test compounds.

#	Compound	Salt	Purity	Supplier
1	BIX01294	3 HCl	≥ 97%	Activate Scientific GmbH (Prien, Germany)
2	Prazosin	HCl	≥ 99%	Angene (Honk Kong, China)
3	PTMD01-0018C	-	≥ 98%	Merck (Darmstadt, Germany)
4	PTMD01-0073C	2 HCl	≥ 95%	BLDpharm (Kaiserslautern, Germany)
5	Tandutinib	-	≥ 98%	MedChemExpess (New Jersey, USA)
6	TM2-115	-	≥ 99%	Excenen Pharma & Tech (Guangzhou, China)
7	UNC0631	-	≥ 99%	MedChemExpess (New Jersey, USA)

Experimental Procedures and Analytical Data of Synthesized Compounds

2,4-Dichloro-6-methoxyquinazolin-7-ol (5) (Doig et al., 2014)

mp.: 184 °C. IR (film): $\tilde{\nu}$ = 1632, 1514, 1257, 1180 cm^{-1}. ^{1}H NMR (500 MHz, CD_3OD): δ = 4.06 (s, 3 H, CH_3O), 7.15 (s, 1 H, C*H*COH), 7.42 (s, 1 H, C*H*$COCH_3$). ^{13}C NMR (126 MHz, CD_3OD): δ = 56.95 (CH_3O), 103.98 (*C*H$COCH_3$), 109.96 (*C*HCOH), 118.35 (*C*CH$COCH_3$), 151.82 (*C*CHCOH), 152.78 (*C*OCH_3), 154.05 (*C*NCCHCOH), 158.62 (*C*CCH$COCH_3$), 161.12 (COH). HRMS-EI m/z $[M]^+$ calcd. for $C_9H_6Cl_2N_2O_2$: 243.9806, found: 243.9803.

2,4-Dichloro-6-methoxy-7-[3-(piperidin-1-yl)propoxy]quinazoline (6) (Vital et al., 2023)

mp.: 106 °C. R_f = 0.27 (10% MeOH in CH_2Cl_2). IR (film): $\tilde{\nu}$ = 2935, 1643, 1506, 1240 cm^{-1}. ^{1}H NMR (500 MHz, CD_3OD): δ = 1.43–1.58 [m, 2 H, C*H*$_2$CH$_2$CH$_2$N(CH$_2$)$_3$O], 1.58–1.75 [m, 4 H, C*H*$_2$CH$_2$N(CH$_2$)$_3$O], 2.09–2.20 (m, 2 H, C*H*$_2$CH$_2$O), 2.45–2.63 [m, 4 H, C*H*$_2$N(CH$_2$)$_3$O], 2.63–2.72 (m, 2 H, *C*H$_2$CH$_2$CH$_2$O), 4.03 (s, 3 H, CH_3O), 4.28 (t, *J* = 6.1 Hz, 2 H, CH_2O), 7.30 (s, 1 H, C*H*$COCH_2$), 7.45 (s, 1 H, C*H*$COCH_3$). ^{13}C NMR (126 MHz, CD_3OD): δ = 24.83 [*C*H$_2$CH$_2$CH$_2$N(CH$_2$)$_3$O], 26.22 [*C*H$_2$CH$_2$N(CH$_2$)$_3$O], 26.67 (*C*H$_2$CH$_2$O), 55.39 [*C*H$_2$N(CH$_2$)$_3$O], 56.76 (*C*H$_2$CH$_2$CH$_2$O), 56.95 (CH_3O), 69.09 (CH_2O), 103.74 (*C*H$COCH_3$), 107.54 (*C*H$COCH_2$), 118.97 (*C*CCl), 151.82 (*C*CCCl), 153.58 (*C*OCH_3), 154.22 (C*C*Cl), 159.06 (*C*OCH_2), 161.19 (CHCN*C*Cl). HRMS-ESI m/z $[M+H]^+$ calcd. for $C_{17}H_{22}Cl_2N_3O_2$: 370.1089, found: 370.1087.

2-Chloro-*N*-(1-cyclohexylpiperidin-4-yl)-6-methoxy-7-[3-(piperidin-1-yl)propoxy]quinazolin-4-amine (7)

According to GP1 with **6** (278 mg, 0.750 mmol, 1.0 equiv), 1-cyclohexylpiperidin-4-amine (150 mg, 0.825 mmol, 1.1 equiv) and DIEA (400 µL, 297 mg, 2.25 mmol, 3.0 equiv) in THF (3 mL). Purification by flash chromatography [5% to 10% 3 M NH_3 (in MeOH) in CH_2Cl_2] afforded **7** as yellow solid (249 mg, 64% yield, 96% purity). mp.: 89 °C. R_f = 0.32 [10% 3 M NH_3 (in MeOH) in CH_2Cl_2]. IR (film): $\tilde{\nu}$ = 2927, 2360, 1587, 1510, 1443, 1255 cm^{-1}. ^{1}H NMR (500 MHz, CD_2Cl_2): δ = 1.03–1.17 (m, 1 H, 10), 1.18–1.32 (m, 4 H, CH$_2$C*H*$_2$C*H*$_2$CHN), 1.35–1.48 [m, 2 H, C*H*$_2$CH$_2$CH$_2$N(CH$_2$)$_3$O], 1.49–1.66 [m, 6 H, C*H*$_2$CHNH, C*H*$_2$CH$_2$CH$_2$CHN, C*H*$_2$CH$_2$N(CH$_2$)$_3$O], 1.74–1.88 (m, 4 H, CH$_2$C*H*$_2$C*H*$_2$CHN), 2.00 (p, *J* = 6.8 Hz, 2 H, C*H*$_2$CH$_2$O), 2.06–2.19 (m, 2 H, C*H*$_2$CHNH), 2.25–2.40 [m, 5 H, C*H*$_2$N(CH$_2$)$_3$O, CHN], 2.41–2.54 (m, 4 H, C*H*$_2$CH$_2$CHNH, C*H*$_2$CH$_2$CH$_2$O), 2.81–2.97 (m, 2 H, C*H*$_2$CH$_2$CHNH), 3.94 (s, 3 H, CH_3), 4.10–4.26 (m, 3 H, CH_2O, CHNH), 5.44 (d, *J* = 7.8 Hz, 1 H, NH), 6.83 (s, 1 H, C*H*$COCH_3$), 7.08 (s, 1 H, C*H*$COCH_2$). ^{13}C NMR (126 MHz, CD_2Cl_2): δ = 24.97 [*C*H$_2$CH$_2$CH$_2$N(CH$_2$)$_3$O], 26.51 [*C*H$_2$CH$_2$N(CH$_2$)$_3$O]*, 26.54 (CH$_2$*C*H$_2$CH$_2$CHN)*, 26.85 (*C*H$_2$CH$_2$CH$_2$CHN)**, 26.94 (*C*H$_2$CH$_2$O)**, 29.29 (CH$_2$CH$_2$*C*H$_2$CHN), 33.27 (CH$_2$*C*H$_2$CHNH), 48.34 (*C*H$_2$CH$_2$CHNH), 49.41 (CHNH), 55.03 [*C*H$_2$N(CH$_2$)$_3$O], 55.83 (*C*H$_2$CH$_2$CH$_2$O), 56.76 (CH_3O), 64.09 (CHN), 68.04 (*C*H$_2$O), 100.38 (*C*H$COCH_3$), 106.91 (*C*CH$COCH_3$), 108.37 (*C*H$COCH_2$), 148.49 (*C*CCNH), 149.72 (*C*OCH_3), 155.07 (*C*OCH_2), 156.29 (CCl), 159.52 (CNH). HRMS-ESI m/z $[M+H]^+$ calcd. for $C_{28}H_{43}ClN_5O_2$: 516.3105, found: 516.3096.

***N*-(1-Cyclohexylpiperidin-4-yl)-6-methoxy-2-(4-methyl-1,4-diazepan-1-yl)-7-[3-(piperidin-1-yl)propoxy]quinazolin-4-amine (9a)** (Liu et al., 2011)

According to GP2 with **7** (92.9 mg, 0.180 mmol, 1.0 equiv) and 1-methyl-1,4-diazepane (115 µL, 106 mg, 0.900 mmol, 5.0 equiv) in toluene (0.9 mL). **9a** was isolated by flash chromatography [10% to 20% 3 M NH_3 (in MeOH) in CH_2Cl_2] as colorless solid (95.0 mg, 89% yield, 97% purity). mp.: 82 °C. R_f = 0.22 [10% 3 M NH_3 (in MeOH) in CH_2Cl_2]. IR (film): $\tilde{\nu}$ = 2933, 2854, 1579, 1495, 1246 cm^{-1}. ^1H NMR (500 MHz, CD_2Cl_2): δ = 1.05–1.18 (m, 1 H, CH_2CH$_2$CH$_2$CHN), 1.21–1.33 (m, 4 H, CH$_2$CH_2CH_2CHN), 1.37–1.49 [m, 2 H, CH_2CH$_2$CH$_2$N(CH$_2$)$_3$O], 1.52–1.71 [m, 7 H, CH_2CH$_2$N(CH$_2$)$_3$O, CH$_2$CH_2CHNH, CH_2CH$_2$CH$_2$CHN], 1.78–1.82 (m, 2 H, CH$_2$CH_2CH$_2$CHN), 1.84–1.92 (m, 2 H, CH$_2$CH$_2$CH_2CHN), 1.93–2.06 (m, 4 H, CH_2CH$_2$O, CH$_3$NCH$_2$CH_2CH$_2$N), 2.09–2.24 (m, 2 H, CH$_2$CH_2CHNH), 2.34 (s, 3 H, CH$_3$N), 2.35–2.50 (m, 9 H, CH_2NCH_2CH$_2$CH$_2$O, CHN, CH_2CH$_2$CHNH), 2.51–2.57 (m, 2 H, CH$_3$NCH_2CH$_2$CH$_2$N), 2.64–2.72 (m, 2 H, CH$_3$NCH_2CH$_2$N), 2.84–3.04 (m, 2 H, CH_2CH$_2$CHNH), 3.83 (t, J = 6.4 Hz, 2 H, CH$_3$NCH$_2$CH$_2$CH_2N), 3.88 (s, 3 H, CH$_3$O), 3.89–3.96 (m, 2 H, CH$_3$NCH$_2$CH_2N), 4.02–4.09 (m, 1 H, CHNH), 4.11 (t, J = 6.7 Hz, 2 H, CH$_2$O), 5.07 (d, J = 7.2 Hz, 1 H, NH), 6.75 (s, 1 H, CHCOCH$_3$), 6.82 (s, 1 H, CHCOCH$_2$). ^{13}C NMR (126 MHz, CD_2Cl_2): δ = 24.94 [CH$_2$CH$_2$CH$_2$N(CH$_2$)$_3$O], 26.43 (CH$_2$$CH_2CH_2$CHN)*, 26.46 [$CH_2CH_2$N(CH$_2$)$_3$O]*, 26.76 ($CH_2CH_2$O), 27.05 ($CH_2CH_2CH_2$CHN), 28.26 (CH$_3NCH_2$$CH_2CH_2$N), 29.13 (CH$_2CH_2$$CH_2$CHN), 32.99 (CH$_2$$CH_2$CHNH), 46.20 (CH$_3NCH_2CH_2$$CH_2$N)**, 46.26 (CH$_3NCH_2$$CH_2$N)**, 46.83 (CH$_3$N), 48.55 ($CH_2CH_2$CHNH), 49.10 (CHNH), 55.01 [CH$_2$N(CH$_2$)$_3$O], 55.96 (CH$_2$CH$_2$CH$_2$O), 56.88 (CH$_3$O), 57.60 (CH$_3$NCH$_2$CH$_2$CH$_2$N), 59.11 (CH$_3$NCH$_2$CH$_2$N), 64.30 (CHN), 67.59 (CH$_2$O), 101.89 (CHCOCH$_3$), 102.95 (CCNH), 107.02 (CHCOCH$_2$), 145.63 (COCH$_3$), 150.55 (CCCNH), 154.52 (COCH$_2$), 158.47 (CNH), 159.31 (CNCNH). HRMS-ESI m/z $[M+H]^+$ calcd. for $C_{34}H_{56}N_7O_2$: 594.4495, found: 594.4488.

***N*-(1-Cyclohexylpiperidin-4-yl)-2-(4-isopropylpiperazin-1-yl)-6-methoxy-7-[3-(piperidin-1-yl)propoxy]quinazolin-4-amine (9b)**

According to GP2 with **7** (206 mg, 0.400 mmol, 1.0 eq) and 1-propan-2-ylpiperazine (292 µL, 262 mg, 2.00 mmol, 5.0 equiv) in toluene (2.0 mL). **9b** was isolated by flash chromatography [10% to 15% 3 M NH_3 (in MeOH) in CH_2Cl_2] as colorless solid (216 mg, 89% yield, 99% purity). mp.: 83 °C. R_f = 0.51 [10% 3 M NH_3 (in MeOH) in CH_2Cl_2]. IR (film): $\tilde{\nu}$ = 2098, 1626, 1448, 1245 cm^{-1}. ^1H NMR (500 MHz, CD_2Cl_2): δ = 1.05 (d, J = 6.5 Hz, 6 H, CH_3CH), 1.07–1.19 (m, 1 H, CH_2CH$_2$CH$_2$CHN), 1.20–1.34 (m, 4 H, CH$_2$CH_2CH_2CHN), 1.35–1.47 [m, 2 H, CH_2CH$_2$CH$_2$N(CH$_2$)$_3$O], 1.47–1.58 [m, 6 H, CH_2CHNH, CH_2CH$_2$N(CH$_2$)$_3$O], 1.58–1.66 (m, 1 H, CH_2CH$_2$CH$_2$CHN), 1.75–1.88 (m, 4 H, CH$_2$CH_2CH_2CHN), 1.99 (p, J = 6.8 Hz, 2 H, CH_2CH$_2$O), 2.07–2.19 (m, 2 H, CH_2CHNH), 2.24–2.48 (m, 9 H, CHNCH_2CH$_2$CHNH, CH_2NCH_2CH$_2$CH$_2$O), 2.49–2.59 (m, 4 H, CH_2NCHCH$_3$), 2.70 (hept, J = 6.6 Hz, 1 H, CH$_3$CH), 2.84–2.99 (m, 2 H, CH_2CH$_2$CHNH), 3.61–3.81 (m, 4 H, CH$_2$NC), 3.88 (s, 3 H, CH$_3$O), 3.97–4.19 (m, 3 H, CHNH, CH$_2$O), 5.05 (d, J = 7.2 Hz, 1 H, NH), 6.74 (s, 1 H, CHCOCH$_3$), 6.82 (s, 1 H, CHCOCH$_2$). ^{13}C NMR (126 MHz, CD_2Cl_2): δ = 18.65 (CH$_3$CH), 24.99 [CH$_2$CH$_2$CH$_2$N(CH$_2$)$_3$O], 26.52 (CH$_2$$CH_2CH_2$CHN)*, 26.55 [CH$_2CH_2$N(CH$_2$)$_3$O]*, 26.88 (CH$_2CH_2$$CH_2$CHN), 27.11 ($CH_2CH_2$O), 29.32 (CH$_2CH_2$$CH_2$CHN), 33.32 ($CH_2$CHNH), 44.88 ($CH_2$NC), 48.54 ($CH_2CH_2$CHNH), 49.19 ($CH_2$NCHCH$_3$), 49.20 (CHNH), 54.93 (CH$_3$$C$H), 55.04 [$CH_2$N(CH$_2$)$_3$O], 55.96 ($CH_2CH_2CH_2$O), 56.85 (CH$_3$O), 64.13 (CH$_2CH_2CH_2$$C$HN), 67.62 (CH$_2$O), 101.79 ($C$HCOCH$_3$), 103.29 ($C$CNH),

107.18 (*C*HCOCH$_2$), 145.98 (*C*OCH$_3$), 149.72 (*C*CCNH), 154.54 (*C*OCH$_2$), 158.58 (CNH), 159.27 (*C*NCNH). HRMS-ESI m/z [M+H$^+$]$^+$ calcd. for $C_{35}H_{58}N_7O_2$: 608.4652; found: 608.4662.

N-(1-Cyclohexylpiperidin-4-yl)-6-methoxy-2-(piperidin-1-yl)-7-[3-(piperidin-1-yl)propoxy]quinazolin-4-amine (9c)

According to GP4 with **8** (83.8 mg, 0.200 mmol, 1.0 equiv), 1-cyclohexylpiperidin-4-amine (72.9 mg, 0.400 mmol, 2.0 equiv) and DIEA (107 µL, 79.1 mg, 0.600 mmol, 3.0 equiv) in *i*-PrOH (1.0 mL) for 15 min. **9c** (78.8 mg, 70% yield, 98% purity) was isolated by flash chromatography [7% to 15% 3 M NH_3 (in MeOH) in CH_2Cl_2] as colorless solid. mp.: 92 °C. R_f = 0.38 [10% 3 M NH_3 (in MeOH) in CH_2Cl_2]. IR (film): $\tilde{\nu}$ = 2929, 1579, 1491, 1244, 754 cm^{-1}. ^{1}H NMR (500 MHz, CD_2Cl_2): δ = 1.04–1.18 (m, 1 H, C*H*$_2$CH$_2$CH$_2$CHN), 1.22–1.28 (m, 4 H, CH$_2$C*H*$_2$C*H*$_2$CHN), 1.38–1.46 [m, 2 H, C*H*$_2$CH$_2$CH$_2$N(CH$_2$)$_3$O], 1.47–1.54 (m, 2 H, C*H*$_2$CHNH), 1.54–1.62 [m, 8 H, C*H*$_2$CH$_2$NC, C*H*$_2$CH$_2$N(CH$_2$)$_3$O], 1.62–1.68 (m, 2 H, C*H*$_2$CH$_2$CH$_2$NC), 1.68–1.74 (m, 1 H, C*H*$_2$CH$_2$CH$_2$CHN), 1.75–1.88 (m, 4 H, CH$_2$C*H*$_2$C*H*$_2$CHN), 1.99 (p, *J* = 6.9 Hz, 2 H, C*H*$_2$CH$_2$O), 2.08–2.19 (m, 2 H, C*H*$_2$CHNH), 2.27–2.49 (m, 9 H, C*H*$_2$CH$_2$CHNH, C*H*$_2$NC*H*$_2$CH$_2$CH$_2$O, CHN), 2.82–2.96 (m, 2 H, C*H*$_2$CH$_2$CHNH), 3.74–3.79 (m, 4 H, CH$_2$NC), 3.87 (s, 3 H, CH$_3$O), 4.01–4.15 (m, 3 H, C*H*NH, CH$_2$O), 5.02 (d, *J* = 7.2 Hz, 1 H, NH), 6.74 (s, 1 H, C*H*COCH$_3$), 6.81 (s, 1 H, C*H*COCH$_2$). ^{13}C NMR (126 MHz, CD_2Cl_2): δ = 24.99 [CH$_2$CH$_2$CH$_2$N(CH$_2$)$_3$O], 25.60 (*C*H$_2$CH$_2$CH$_2$NC), 26.40 (*C*H$_2$CH$_2$NC)*, 26.52 (*C*H$_2$CH$_2$CHN)*, 26.54 [*C*H$_2$CH$_2$N(CH$_2$)$_3$O]*, 26.87 (*C*H$_2$CH$_2$CH$_2$CHN)*, 27.11 (*C*H$_2$CH$_2$O), 29.31 (*C*H$_2$CHN), 33.30 (*C*H$_2$CHNH), 45.36 (*C*H$_2$NC), 48.54 (*C*H$_2$CH$_2$CHNH), 49.16 (CHNH), 55.04 [*C*H$_2$N(CH$_2$)$_3$O], 55.98 (*C*H$_2$CH$_2$CH$_2$O), 56.87 (CH$_3$O), 64.14 (CHN), 67.60 (CH$_2$O), 101.87 (*C*HCOCH$_3$), 103.05 (*C*CNH), 107.11 (*C*HCOCH$_2$), 145.77 (*C*OCH$_3$), 149.92 (*C*CCNH), 154.49 (*C*OCH$_2$), 158.58 (CNH), 159.26 (CNCNH). HRMS-ESI m/z [M+H]$^+$ calcd. for $C_{33}H_{53}N_6O_2$: 565.4230, found: 565.4229.

N^4-(1-Cyclohexylpiperidin-4-yl)-6-methoxy-*N*^{2},*N*^{2}-dimethyl-7-[3-(piperidin-1-yl)propoxy]-quinazoline-2,4-diamine (9d)

mp.: 84 °C. R_f = 0.32 [10% 3 M NH_3 (in MeOH) in CH_2Cl_2]. IR (film): $\tilde{\nu}$ = 2931, 1628, 1581, 1427, 1246 cm^{-1}. ^{1}H NMR (500 MHz, CD_2Cl_2): δ = 1.03–1.19 (m, 1 H, C*H*$_2$CH$_2$CH$_2$CH), 1.21–1.34 (m, 4 H, CH$_2$C*H*$_2$C*H*$_2$CH), 1.42 [t, *J* = 5.9 Hz, 2 H, C*H*$_2$CH$_2$CH$_2$N(CH$_2$)$_3$O], 1.47–1.69 [m, 7 H, C*H*$_2$CHNH, C*H*$_2$CH$_2$CH$_2$CH, C*H*$_2$CH$_2$N(CH$_2$)$_3$O], 1.70–1.89 (m, 4 H, CH$_2$C*H*$_2$C*H*$_2$CH), 1.99 (p, *J* = 6.9 Hz, 2 H, C*H*$_2$CH$_2$O), 2.09–2.22 (m, 2 H, C*H*$_2$CHNH), 2.24–2.52 (m, 9 H, C*H*$_2$CH$_2$CHNH, C*H*N, C*H*$_2$NC*H*$_2$CH$_2$CH$_2$O), 2.87–3.00 (m, 2 H, C*H*$_2$CH$_2$CHNH), 3.16 (s, 6 H, CH$_3$N), 3.87 (s, 3 H, CH$_3$O), 4.05–4.21 (m, 3 H, CH$_2$O, C*H*NH), 5.04 (d, *J* = 7.2 Hz, 1 H, NH), 6.74 (s, 1 H, C*H*COCH$_3$), 6.83 (s, 1 H, C*H*COCH$_2$). ^{13}C NMR (126 MHz, CD_2Cl_2): δ = 24.98 [CH$_2$CH$_2$CH$_2$N(CH$_2$)$_3$O], 26.49 (CH$_2$*C*H$_2$CH$_2$CH)*, 26.52 [CH$_2$CH$_2$N(CH$_2$)$_3$O]*, 26.84 (CH$_2$CH$_2$CH$_2$CH), 27.10 (*C*H$_2$CH$_2$O), 29.24 (CH$_2$CH$_2$*C*H$_2$CH), 33.21 (*C*H$_2$CHNH), 37.12 (CH$_3$N), 48.57 (*C*H$_2$CH$_2$CHNH), 49.18 (CHNH), 55.03 [*C*H$_2$N(CH$_2$)$_3$O], 55.97 (*C*H$_2$CH$_2$CH$_2$O), 56.88 (CH$_3$O), 64.19 (CHN), 67.61 (*C*H$_2$O), 101.91 (*C*HCOCH$_3$), 102.77 (*C*CNH), 107.04 (*C*HCOCH$_2$), 145.66 (*C*OCH$_3$), 149.93 (*C*CCNH), 154.52 (*C*OCH$_2$), 158.43 (CNH), 159.93 (*C*NCH$_3$). HRMS-ESI m/z [M+H]$^+$ calcd. for $C_{30}H_{49}N_6O_2$: 525.3917, found: 525.3909.

N^4-(1-Cyclohexylpiperidin-4-yl)-6-methoxy-7-[3-(piperidin-1-yl)propoxy]quinazoline-2,4-diamine (9e) and *N*-(1-cyclohexylpiperidin-4-yl)-6-methoxy-7-[3-(piperidin-1-yl)propoxy]quinazolin-4-amine (16b)

According to a GP3, with **7** (196 mg, 0.380 mmol, 1.0 equiv) and NaN_3 (27.2 mg, 0.418 mmol, 1.1 equiv) in EtOH/AcOH (4:1) (2.54 mL) and afterwards 10% Pd/C (45.0 mg, 38.0 µmol, 0.10 equiv) and hydrazine hydrate (28.5 µL, 28.5 mg, 0.570 mmol, 1.5 equiv). **9e** (92.6 mg, 49% yield, 99% purity) and **16b** (29.6 mg, 16% yield, 97% purity, analytic see below) were isolated by flash chromatography [10% 3 M NH_3 (in MeOH) in CH_2Cl_2] as colorless solids. **9e**: mp.: 143 °C. R_f = 0.32 [10% 3 M NH_3 (in MeOH) in CH_2Cl_2]. IR (film): $\tilde{\nu}$ = 2935, 2089, 1624, 1454, 1213, 754 cm^{-1}. ^1H NMR (500 MHz, CD_2Cl_2): δ = 1.04–1.19 (m, 1 H, CH_2CH$_2$CH$_2$CH), 1.20–1.32 (m, 4 H, CH$_2$CH_2CH_2CH), 1.35–1.46 [m, 2 H, CH_2CH$_2$CH$_2$N(CH$_2$)$_3$O], 1.53–1.65 [m, 7 H, CH_2CHNH, CH_2CH$_2$CH$_2$CH, CH_2CH$_2$N(CH$_2$)$_3$O], 1.66–1.90 (m, 4 H, CH$_2$CH_2CH_2CH), 2.00 (p, *J* = 6.8 Hz, 2 H, CH_2CH$_2$O), 2.07–2.16 (m, 2 H, CH_2CHNH), 2.21–2.52 (m, 9 H, CH_2NC*H*, CH_2NCH_2CH$_2$CH$_2$O), 2.87–3.00 (m, 2 H, CH_2NCH), 3.89 (s, 3 H, CH$_3$O), 4.10 (t, *J* = 6.6 Hz, 2 H, CH$_2$O), 4.12–4.21 (m, 1 H, C*H*NH), 4.84 (s, 2 H, NH$_2$), 5.38 (s, 1 H, NH), 6.79 (s, 1 H, C*H*COCH$_2$), 6.82 (s, 1 H, C*H*COCH$_3$). ^{13}C NMR (126 MHz, CD_2Cl_2): δ = 24.92 [*C*H$_2$CH$_2$CH$_2$N(CH$_2$)$_3$O], 26.42 (CH$_2$*C*H$_2$CH$_2$CH)*, 26.45 [*C*H$_2$CH$_2$N(CH$_2$)$_3$O]*, 26.77 (*C*H$_2$CH$_2$CH$_2$CH)**, 26.95 (*C*H$_2$CH$_2$O)**, 29.13 (CH$_2$CH$_2$*C*H$_2$CH), 32.99 (*C*H$_2$CHNH), 48.53 (*C*H$_2$NCH), 48.73 (CHNH), 54.99 [*C*H$_2$N(CH$_2$)$_3$O], 55.91 (*C*H$_2$CH$_2$CH$_2$O), 56.87 (CH$_3$O), 64.22 (CH$_2$CH$_2$CH$_2$*C*H), 67.66 (CH$_2$O), 101.94 (*C*HCOCH$_3$), 103.84 (*C*CNH), 106.07 (*C*HCOCH$_2$), 146.56 (*C*OCH$_3$), 148.01 (*C*CCNH), 154.72 (*C*OCH$_2$), 159.36 (CNH), 159.77 (CNH$_2$). HRMS-EI m/z $[M]^+$ calcd. for $C_{28}H_{44}N_6O_2$: 496.3526; found: 496.3524.

***N*-[1-(Cyclohexylmethyl)piperidin-4-yl]-6-methoxy-2-(piperidin-1-yl)-7-[3-(piperidin-1-yl)propoxy]quinazolin-4-amine (9f)**

According to GP4 with **8** (168 mg, 0.400 mmol, 1.0 equiv), 1-(cyclohexylmethyl)piperidin-4-amine (157 mg, 0.800 mmol, 2.0 equiv) and DIEA (213 µL, 158 mg, 1.20 mmol, 3.0 equiv) in *i*-PrOH (2.0 mL) for 15 min. **9f** (134 mg, 58% yield, 99% purity) was isolated by flash chromatography [7% 3 M NH_3 (in MeOH) in CH_2Cl_2] as colorless solid. mp.: 75 °C. R_f = 0.49 [10% 3 M NH_3 (in MeOH) in CH_2Cl_2]. IR (film): $\tilde{\nu}$ = 2931, 1579, 1493, 1244, 756 cm^{-1}. ^1H NMR (500 MHz, CD_2Cl_2): δ = 0.77–0.96 (m, 2 H, CH$_2$CH$_2$CH_2CH), 1.10–1.33 (m, 3 H, CH_2CH_2CH$_2$CH$_2$CH), 1.40–1.45 (m, 2 H, CH_2CH$_2$CH$_2$NCH$_2$), 1.46–1.53 (m, 1 H, CH$_2$CH$_2$CH$_2$C*H*), 1.53–1.74 (m, 15 H, CH_2CH_2CH$_2$NC, CH_2CHNH, CH$_2$CH_2CH$_2$NCH$_2$, CH_2CH_2CH$_2$CH), 1.74–1.81 (m, 2 H, CH$_2$CH$_2$CH_2CH), 1.99 (p, *J* = 6.9 Hz, 2 H, CH$_2$CH_2CH$_2$O), 2.04–2.18 (m, 6 H, CH_2NCH_2CH_2CHNH), 2.38 (s, 4 H, CH$_2$CH$_2$CH_2NCH$_2$), 2.44 (t, *J* = 7.1 Hz, 2 H, CH_2CH$_2$CH$_2$O), 2.72–2.98 (m, 2 H, CH_2CH$_2$CHNH), 3.73–3.81 (m, 4 H, CH$_2$CH$_2$CH_2NC), 3.87 (s, 3 H, CH$_3$O), 4.11 (t, *J* = 6.7 Hz, 3 H, C*H*NH, CH$_2$CH$_2$CH_2O), 5.04 (d, *J* = 7.2 Hz, 1 H, NH), 6.74 (s, 1 H, C*H*COCH$_3$), 6.81 (s, 1 H, C*H*COCH$_2$). ^{13}C NMR (126 MHz, CD_2Cl_2): δ = 24.96 (*C*H$_2$CH$_2$CH$_2$NCH$_2$), 25.59 (*C*H$_2$CH$_2$CH$_2$NC), 26.40 (CH$_2$*C*H$_2$CH$_2$NCH$_2$)*, 26.49 (CH$_2$*C*H$_2$CH$_2$NC)*, 26.62 (CH$_2$*C*H$_2$CH$_2$CH), 27.07 (CH$_2$*C*H$_2$CH$_2$O), 27.30 (*C*H$_2$CH$_2$CH$_2$CH), 32.28 (CH$_2$CH$_2$*C*H$_2$CH), 32.75 (*C*H$_2$CHNH), 35.79 (CH$_2$CH$_2$CH$_2$*C*H), 45.37 (CH$_2$CH$_2$*C*H$_2$NC), 48.85 (CHNH), 53.55 (*C*H$_2$CH$_2$CHNH), 55.02 (CH$_2$CH$_2$*C*H$_2$NCH$_2$), 55.97 (*C*H$_2$CH$_2$CH$_2$O), 56.85 (CH$_3$O), 66.08 (CH*C*H$_2$N), 67.59 (CH$_2$CH$_2$*C*H$_2$O), 101.84 (*C*HCOCH$_3$), 103.06 (*C*CNH), 107.09 (*C*HCOCH$_2$), 145.78 (*C*OCH$_3$), 149.87 (*C*CCNH), 154.49 (*C*OCH$_2$), 158.61 (CNH), 159.22 (*C*NCNH). HRMS-ESI m/z $[M+H^+]^+$ calcd. for $C_{34}H_{55}N_6O_2$: 579.4386; found: 579.4392.

2-Chloro-*N*-(1-isopropylpiperidin-4-yl)-6-methoxy-7-[3-(piperidin-1-yl)propoxy]quinazolin-4-amine (10a) (Davis et al., 2016; Vital et al., 2023)

According to GP1 with **6** (43.3 mg, 0.110 mmol, 1.0 equiv), 1-propan-2-ylpiperidin-4-amine (19.1 µL, 17.2 mg, 0.121 mmol, 1.1 equiv) and DIEA (58.7 µL, 43.5 mg, 0.330 mmol, 3.0 equiv) in THF (440 µL). Purification by flash chromatography [5% to 10% 3 M NH_3 (in MeOH) in CH_2Cl_2] afforded **10a** as yellow solid (45.1 mg, 86% yield, 99% purity). mp.: 81 °C. R_f = 0.27 [10% 3 M NH_3 (in MeOH) in CH_2Cl_2]. IR (film): $\tilde{\nu}$ = 2931, 1622, 1589, 1510, 1443 cm^{-1}. ^1H NMR (500 MHz, CD_2Cl_2): δ = 1.07 (d, J = 6.6 Hz, 6 H, CH_3CH), 1.37–1.48 [m, 2 H, CH_2CH$_2$CH$_2$N(CH$_2$)$_3$O], 1.51–1.59 [m, 4 H, CH_2CH$_2$N(CH$_2$)$_3$O], 1.59–1.81 (m, 2 H, CH_2CHNH), 2.01 (p, J = 6.8 Hz, 2 H, CH_2CH$_2$O), 2.09–2.19 (m, 2 H, CH_2CHNH), 2.24–2.53 (m, 8 H, CH_2CH$_2$CHNH, CH_2NCH_2CH$_2$CH$_2$O), 2.81 (h, J = 6.6 Hz, 1 H, CH$_3$CH), 2.88–2.99 (m, 2 H, CH_2CH$_2$CHNH), 3.96 (s, 3 H, CH$_3$O), 4.15 (t, J = 6.6 Hz, 2 H, CH$_2$O), 4.17–4.29 (m, 1 H, CHNH), 5.45 (d, J = 7.9 Hz, 1 H, NH), 6.83 (s, 1 H, CHCOCH$_3$), 7.08 (s, 1 H, CHCOCH$_2$). ^{13}C NMR (126 MHz, CD_2Cl_2): δ = 18.35 (*C*H$_3$CH), 24.93 [*C*H$_2$CH$_2$CH$_2$N(CH$_2$)$_3$O], 26.49 [*C*H$_2$CH$_2$N(CH$_2$)$_3$O], 26.90 (*C*H$_2$CH$_2$O), 32.83 (*C*H$_2$CHNH), 47.86 (*C*H$_2$CH$_2$CHNH), 49.18 (CHNH), 55.01 [*C*H$_2$N(CH$_2$)$_3$O], 55.04 (CH$_3$*C*H), 55.82 (*C*H$_2$CH$_2$CH$_2$O), 56.79 (CH$_3$O), 68.03 (CH$_2$O), 100.36 (*C*HCOCH$_3$), 106.91 (*C*CNH), 108.39 (*C*HCOCH$_2$), 148.51 (*C*CCNH), 149.75 (*C*OCH$_3$), 155.08 (*C*OCH$_2$), 156.25 (CCl), 159.52 (CNH). HRMS-ESI m/z $[M+H]^+$ calcd. for $C_{25}H_{39}ClN_5O_2$: 476.2792, found: 476.2797.

2-Chloro-6-methoxy-*N*-(1-methylpiperidin-4-yl)-7-[3-(piperidin-1-yl)propoxy]quinazolin-4-amine (10b)

According to GP1 with **6** (148 mg, 0.400 mmol, 1.0 equiv), 1-methylpiperidin-4-amine (58.1 µL, 52.9 mg, 0.440 mmol, 1.1 equiv) and DIEA (213 µL, 158 mg, 1.20 mmol, 3.0 equiv) in THF (1.6 mL). Purification by flash chromatography [5% to 10% 3 M NH_3 (in MeOH) in CH_2Cl_2] afforded **10b** as yellow solid (86.1 mg, 48% yield, 97% purity). mp.: 82 °C. R_f = 0.24 [10% 3 M NH_3 (in MeOH) in CH_2Cl_2]. IR (film): $\tilde{\nu}$ = 2929, 1587, 1510, 1441, 1255 cm^{-1}. ^1H NMR (500 MHz, CD_2Cl_2): δ = 1.37–1.50 [m, 2 H, CH_2CH$_2$CH$_2$N(CH$_2$)$_3$O], 1.50–1.59 [m, 4 H, CH_2CH$_2$N(CH$_2$)$_3$O], 1.59–1.70 (m, 2 H, CH$_2$CH_2CHNH), 2.01 (p, J = 6.8 Hz, 2 H, CH_2CH$_2$O), 2.07–2.14 (m, 2 H, CH$_2$CH_2CHNH), 2.14–2.23 (m, 2 H, CH_2CH$_2$CHNH), 2.28 (s, 3 H, CH$_3$N), 2.38 [s, 4 H, CH_2N(CH$_2$)$_3$O], 2.46 (t, J = 7.1 Hz, 2 H, CH_2CH$_2$CH$_2$O), 2.69–2.97 (m, 2 H, CH_2CH$_2$CHNH), 3.95 (s, 3 H, CH$_3$O), 4.15 (t, J = 6.6 Hz, 2 H, CH$_2$O), 4.17–4.25 (m, 1 H, CHNH), 5.43 (d, J = 7.7 Hz, 1 H, NH), 6.84 (s, 1 H, *C*HCOCH$_3$), 7.08 (s, 1 H, CHCOCH$_2$). ^{13}C NMR (126 MHz, CD_2Cl_2): δ = 24.91 [*C*H$_2$CH$_2$CH$_2$N(CH$_2$)$_3$O], 26.46 [*C*H$_2$CH$_2$N(CH$_2$)$_3$O], 26.87 (*C*H$_2$CH$_2$O), 32.58 (*C*H$_2$CHNH), 46.37 (CH$_3$N), 48.51 (CHNH), 54.96 (*C*H$_2$CH$_2$CHNH), 55.00 [*C*H$_2$N(CH$_2$)$_3$O], 55.81 (*C*H$_2$CH$_2$CH$_2$O), 56.78 (CH$_3$O), 68.02 (CH$_2$O), 100.36 (*C*HCOCH$_3$), 106.93 (*C*CNH), 108.38 (*C*HCOCH$_2$), 148.50 (*C*CCNH), 149.75 (*C*OCH$_3$), 155.08 (*C*OCH$_2$), 156.25 (CCl), 159.57 (CNH). HRMS-ESI m/z $[M+H]^+$ calcd. for $C_{23}H_{35}ClN_5O_2$: 448.2479, found: 448.2474.

2-Chloro-6-methoxy-*N*-methyl-7-[3-(piperidin-1-yl)propoxy]quinazolin-4-amine (10c)

According to GP1 with **6** (222 mg, 0.600 mmol, 1.0 equiv), methanamine (2 M in THF) (330 µL, 0.660 mmol, 1.1 equiv) and DIEA (320 µL, 237 mg, 1.80 mmol, 3.0 equiv) in THF (2.07 mL).

Purification by flash chromatography [5% 3 M NH_3 (in MeOH) in CH_2Cl_2] afforded **10c** as colorless solid (187 mg, 86% yield, 96% purity). mp.: 63 °C. R_f = 0.34 [10% 3 M NH_3 (in MeOH) in CH_2Cl_2]. IR (film): $\tilde{\nu}$ = 1624, 1510, 1244, 1022 cm^{-1}. ^1H NMR (500 MHz, CD_2Cl_2): δ = 1.34–1.47 [m, 2 H, CH_2CH_2CH_2N(CH_2)$_3$O], 1.48–1.66 [m, 4 H, CH_2CH_2N(CH_2)$_3$O], 2.01 (p, J = 6.8 Hz, 2 H, CH_2CH_2O), 2.32–2.41 [m, 4 H, CH_2N(CH_2)$_3$O], 2.45 (t, J = 7.1 Hz, 2 H, CH_2CH_2CH_2O), 3.16 (d, J = 4.8 Hz, 3 H, CH_3NH), 3.93 (s, 3 H, CH_3O), 4.15 (t, J = 6.6 Hz, 2 H, CH_2O), 5.59–5.78 (m, 1 H, NH), 6.85 (s, 1 H, CHCOCH_3), 7.09 (s, 1 H, CHCOCH_2). ^{13}C NMR (126 MHz, CD_2Cl_2): δ = 25.11 [$CH_2CH_2CH_2N(CH_2)_3O$], 26.67 [$CH_2CH_2N(CH_2)_3O$], 27.07 (CH_2CH_2O), 28.81 (CH_3NH), 55.18 [$CH_2N(CH_2)_3O$], 55.98 ($CH_2CH_2CH_2O$), 56.76 (CH_3O), 68.20 (CH_2O), 100.41 ($CHCOCH_3$), 107.25 (CCNH), 108.51 ($CHCOCH_2$), 148.35 (CCCNH), 149.96 ($COCH_3$), 155.19 ($COCH_2$), 156.45 (CCl), 161.05 (CNH). HRMS-ESI m/z $[M+H]^+$ calcd. for $C_{18}H_{26}ClN_4O_2$: 365.1744, found: 365.1740.

2-(4-Isopropyl-1,4-diazepan-1-yl)-*N*-(1-isopropylpiperidin-4-yl)-6-methoxy-7-[3-(piperidin-1-yl)propoxy]quinazolin-4-amine (11a) (Jiang et al., 2017; Liu et al., 2011)

According to GP2 with **10a** (100 mg, 0.210 mmol, 1.0 equiv) and 1-propan-2-yl-1,4-diazepane (170 µL, 152 mg, 1.05 mmol, 5.0 equiv) in toluene (1.0 mL). **11a** was isolated by flash chromatography [10% to 15% 3 M NH_3 (in MeOH) in CH_2Cl_2] as pale yellow solid (109 mg, 89% yield, 95% purity). mp.: 52 °C. R_f = 0.25 [10% 3 M NH_3 (in MeOH) in CH_2Cl_2]. IR (film): $\tilde{\nu}$ = 2931, 2094, 1630, 1248 cm^{-1}. ^1H NMR (500 MHz, CD_2Cl_2): δ = 1.00 (d, J = 6.6 Hz, 6 H, CH_3CHNCH_2CH_2N), 1.05 (d, J = 6.6 Hz, 6 H, CH_3CHNCH_2CH_2CH), 1.37–1.48 [m, 2 H, CH_2CH_2CH_2N(CH_2)$_3$O], 1.50–1.65 (m, 6 H, CH_2CH_2NCH_2CH_2CH_2O, CH_2CHNH), 1.89 (p, J = 6.1 Hz, 2 H, CH_2CH_2CH_2NC), 1.99 (p, J = 6.9 Hz, 2 H, CH_2CH_2O), 2.13–2.18 (m, 2 H, CH_2CHNH), 2.29–2.42 [m, 6 H, CH_2CH_2CHNH, CH_2N(CH_2)$_3$O], 2.44 (t, J = 7.1 Hz, 2 H, CH_2CH_2CH_2O), 2.53–2.62 (m, 2 H, CH_2CH_2CH_2NC), 2.72–2.82 (m, 3 H, CH_3CHNCH_2CH_2CHNH, NCH_2CH_2NC), 2.85–2.92 (m, 2 H, CH_2CH_2CHNH), 2.92–2.98 (m, 1 H, CH_3CHNCH_2CH_2NC), 3.81–3.85 (m, 2 H, NCH_2CH_2CH_2NC), 3.85–3.93 (m, 5 H, CH_3O, NCH_2CH_2NC), 4.00–4.17 (m, 3 H, CH_2O, CHNH), 5.12 (d, J = 7.1 Hz, 1 H, NH), 6.78 (s, 1 H, CHCOCH_3), 6.82 (s, 1 H, CHCOCH_2). ^{13}C NMR (126 MHz, CD_2Cl_2): δ = 18.45 (CH_3CHNCH_2CH_2NC), 18.45 (CH_3CHNCH_2CH_2CHNH), 24.95 [$CH_2CH_2CH_2N(CH_2)_3O$], 26.48 [$CH_2CH_2N(CH_2)_3O$], 27.06 (CH_2CH_2O), 29.03 (NCH_2CH_2CH_2NC), 33.00 (NCH_2CH_2CHNH), 45.89 (NCH_2CH_2CH_2NC), 48.08 (NCH_2CH_2NC, CH_2CH_2CHNH), 49.17 (CHNH), 50.89 (NCH_2CH_2CH_2NC), 52.45 (NCH_2CH_2NC), 54.97 (CH_3CHNCH_2CH_2CHNH), 55.01 [$CH_2N(CH_2)_3O$], 55.96 ($CH_2CH_2CH_2O$), 56.06 (CH_3CHNCH_2CH_2NC), 56.88 (CH_3O), 67.59 (CH_2O), 102.01 ($CHCOCH_3$), 102.98 (CCNH), 106.99 ($CHCOCH_2$), 145.56 ($COCH_3$), 149.95 (CCCNH), 154.48 ($COCH_2$), 158.54 (CNH), 158.83 (CNCNH). HRMS-ESI m/z $[M+H]^+$ calcd. for $C_{33}H_{56}N_7O_2$: 582.4495, found: 582.4488.

2-(4-Isopropyl-1,4-diazepan-1-yl)-6-methoxy-*N*-(1-methylpiperidin-4-yl)-7-[3-(piperidin-1-yl)propoxy]quinazolin-4-amine (11b)

According to GP2 with **10b** (58.2 mg, 0.130 mmol, 1.0 equiv) and 1-propan-2-yl-1,4-diazepane (105 µL, 94.3 mg, 0.650 mmol, 5.0 equiv) in toluene (0.6 mL). **11b** was isolated by flash chromatography [10% to 15% 3 M NH_3 (in MeOH) in CH_2Cl_2] as colorless solid (44.9 mg, 62% yield, 98% purity). mp.: 68 °C. R_f = 0.15 [10% 3 M NH_3 (in MeOH) in CH_2Cl_2]. IR (film): $\tilde{\nu}$ = 2935, 1628, 1579, 1497, 1248 cm^{-1}. ^1H NMR (500 MHz, CD_3OD): δ = 1.07 (d, J = 6.6 Hz,

6 H, C*H*$_3$CH), 1.45–1.58 [m, 2 H, C*H*$_2$CH$_2$CH$_2$N(CH$_2$)$_3$O], 1.60–1.69 [m, 4 H, C*H*$_2$CH$_2$N(CH$_2$)$_3$O], 1.69–1.82 (m, 2 H, C*H*$_2$CHNH), 1.90–2.01 (m, 2 H, CH$_2$C*H*$_2$CH$_2$NC), 2.03–2.15 (m, 4 H, C*H*$_2$CHNH, C*H*$_2$CH$_2$O), 2.16–2.24 (m, 2 H, C*H*$_2$NCH$_3$), 2.33 (s, 3 H, CH$_3$N), 2.54 [s, 4 H, C*H*$_2$N(CH$_2$)$_3$O], 2.59–2.65 (m, 2 H, C*H*$_2$CH$_2$CH$_2$O), 2.65–2.75 (m, 2 H, C*H*$_2$CH$_2$CH$_2$NC), 2.79–2.93 (m, 2 H, NC*H*$_2$CH$_2$NC), 2.93–3.05 (m, 3 H, CH$_3$C*H*, C*H*$_2$NCH$_3$), 3.86 (t, *J* = 6.2 Hz, 2 H, CH$_2$CH$_2$C*H*$_2$NC), 3.89 (s, 5 H, CH$_3$O, NCH$_2$C*H*$_2$NC), 4.08–4.26 (m, 3 H, CH$_2$O, C*H*NH), 6.91 (s, 1 H, C*H*COCH$_2$), 7.42 (s, 1 H, C*H*COCH$_3$). ^{13}C NMR (126 MHz, CD$_3$OD): δ = 18.31 (*C*H$_3$CH), 25.07 [*C*H$_2$CH$_2$CH$_2$N(CH$_2$)$_3$O], 26.40 [*C*H$_2$CH$_2$N(CH$_2$)$_3$O], 27.06 (*C*H$_2$CH$_2$O), 29.11 (CH$_2$*C*H$_2$CH$_2$NC), 32.34 (*C*H$_2$CHNH), 46.24 (CH$_3$N), 46.50 (CH$_2$CH$_2$*C*H$_2$NC), 47.99 (NCH$_2$*C*H$_2$NC), 48.49 (CHNH), 51.73 (*C*H$_2$CH$_2$CH$_2$NC), 52.68 (N*C*H$_2$CH$_2$NC), 55.47 [*C*H$_2$N(CH$_2$)$_3$O], 56.04 (*C*H$_2$NCH$_3$), 56.62 (CH$_3$*C*H), 56.87 (CH$_3$O), 57.08 (*C*H$_2$CH$_2$CH$_2$O), 68.06 (CH$_2$O), 104.31 (*C*HCOCH$_3$), 104.77 (*C*CNH), 106.27 (*C*HCOCH$_2$), 147.03 (*C*OCH$_3$), 149.18 (*C*CCNH), 155.18 (*C*OCH$_2$), 159.60 (*C*NCNH), 160.13 (CNH). HRMS-ESI m/z [M+H]$^+$ calcd. for C$_{31}$H$_{52}$N$_7$O$_2$: 554.4182, found: 554.4176.

2-(4-Isopropyl-1,4-diazepan-1-yl)-6-methoxy-*N*-methyl-7-[3-(piperidin-1-yl)propoxy]quinazolin-4-amine (11c)

According to GP2 with **10c** (146 mg, 0.400 mmol, 1.0 equiv) and 1-propan-2-yl-1,4-diazepane (324 µL, 290 mg, 2.00 mmol, 5.0 equiv) in toluene (2.0 mL). **11c** was isolated by flash chromatography [10% 3 M NH$_3$ (in MeOH) in CH$_2$Cl$_2$] as red solid (171 mg, 91% yield, 98% purity). mp.: 66 °C. *R*$_f$ = 0.29 [10% 3 M NH$_3$ (in MeOH) in CH$_2$Cl$_2$]. IR (film): ṽ = 2937, 2360, 1585, 1497, 1215 cm^{-1}. ^{1}H NMR (400 MHz, CD$_2$Cl$_2$): δ = 0.99 (d, *J* = 6.6 Hz, 6 H, C*H*$_3$CH), 1.36–1.47 [m, 2 H, C*H*$_2$CH$_2$CH$_2$N(CH$_2$)$_3$O], 1.52–1.61 [m, 4 H, C*H*$_2$CH$_2$N(CH$_2$)$_3$O], 1.80–1.93 (m, 2 H, CH$_2$C*H*$_2$CH$_2$NC), 1.99 (p, *J* = 6.9 Hz, 2 H, C*H*$_2$CH$_2$O), 2.25–2.40 [m, 4 H, C*H*$_2$N(CH$_2$)$_3$O], 2.43 (t, *J* = 7.1 Hz, 2 H, C*H*$_2$CH$_2$CH$_2$O), 2.50–2.65 (m, 2 H, C*H*$_2$CH$_2$CH$_2$NC), 2.67–2.81 (m, 2 H, NC*H*$_2$CH$_2$NC), 2.83–3.01 (m, 1 H, CH$_3$C*H*), 3.09 (d, *J* = 4.7 Hz, 3 H, C*H*$_3$NH), 3.76–3.99 (m, 7 H, CH$_2$NC, CH$_3$O), 4.11 (t, *J* = 6.7 Hz, 2 H, CH$_2$O), 5.18–5.29 (m, 1 H, NH), 6.76 (s, 1 H, C*H*COCH$_3$), 6.81 (s, 1 H, C*H*COCH$_2$). ^{13}C NMR (101 MHz, CD$_2$Cl$_2$): δ = 18.52 (*C*H$_3$CH), 25.00 [*C*H$_2$CH$_2$CH$_2$N(CH$_2$)$_3$O], 26.55 [*C*H$_2$CH$_2$N(CH$_2$)$_3$O], 27.13 (*C*H$_2$CH$_2$O), 28.24 (CH$_3$NH), 29.30 (CH$_2$*C*H$_2$CH$_2$NC), 45.97 (CH$_2$CH$_2$*C*H$_2$NC), 48.45 (NCH$_2$*C*H$_2$NC), 51.03 (*C*H$_2$CH$_2$CH$_2$NC), 52.46 (N*C*H$_2$CH$_2$NC), 55.04 [*C*H$_2$N(CH$_2$)$_3$O], 55.94 (CH$_3$*C*H), 55.98 (*C*H$_2$CH$_2$CH$_2$O), 56.68 (CH$_3$O), 67.61 (*C*H$_2$O), 101.78 (*C*HCOCH$_3$), 103.12 (*C*CNH), 107.02 (*C*HCOCH$_2$), 145.54 (*C*OCH$_3$), 149.80 (*C*CCNH), 154.42 (*C*OCH$_2$), 159.01 (*C*NCN$_2$), 159.89 (CNH). HRMS-ESI m/z [M+H]$^+$ calcd. for C$_{26}$H$_{43}$N$_6$O$_2$: 471.3447, found: 471.3442.

2-Chloro-6-methoxy-7-[3-(piperidin-1-yl)propoxy]quinazoline (12)

mp.: 127 °C. *R*$_f$ = 0.59 [10% 3 M NH$_3$ (in MeOH) in CH$_2$Cl$_2$]. IR (film): ṽ = 2935, 1616, 1504, 1246 cm^{-1}. ^{1}H NMR (500 MHz, CD$_2$Cl$_2$): δ = 1.38–1.48 [m, 2 H, C*H*$_2$CH$_2$CH$_2$N(CH$_2$)$_3$O], 1.53–1.58 [m, 4 H, C*H*$_2$CH$_2$N(CH$_2$)$_3$O], 2.05 (p, *J* = 6.8 Hz, 2 H, C*H*$_2$CH$_2$O), 2.38 [s, 4 H, C*H*$_2$N(CH$_2$)$_3$O], 2.46 (t, *J* = 7.1 Hz, 2 H, C*H*$_2$CH$_2$CH$_2$O), 3.99 (s, 3 H, CH$_3$O), 4.24 (t, *J* = 6.6 Hz, 2 H, CH$_2$O), 7.12 (s, 1 H, C*H*COCH$_3$), 7.25 (s, 1 H, C*H*COCH$_2$), 9.00 (s, 1 H, CHNCCl). ^{13}C NMR (126 MHz, CD$_2$Cl$_2$): δ = 24.94 [*C*H$_2$CH$_2$CH$_2$N(CH$_2$)$_3$O], 26.51 [*C*H$_2$CH$_2$N(CH$_2$)$_3$O], 26.80 (*C*H$_2$CH$_2$O), 55.02 [*C*H$_2$N(CH$_2$)$_3$O], 55.72 (*C*H$_2$CH$_2$CH$_2$O), 56.60 (CH$_3$O), 68.48 (CH$_2$O),

104.17 (*C*HCOCH$_3$), 106.77 (*C*HCOCH$_2$), 119.77 (*C*CHCOCH$_3$), 150.59 (*C*CHCOCH$_2$), 151.66 (*C*OCH$_3$), 156.21 (CCl), 157.43 (*C*OCH$_2$), 159.45 (*C*HNCCl). HRMS-ESI m/z [M+H]$^+$ calcd. for $C_{17}H_{23}ClN_3O_2$: 336.1479, found: 336.1471.

6-Methoxy-7-[3-(piperidin-1-yl)propoxy]quinazoline (13)

mp.: 98 °C. R_f = 0.49 [10% 3 M NH$_3$ (in MeOH) in CH$_2$Cl$_2$]. IR (film): $\tilde{\nu}$ = 2937, 1618, 1502, 1234 cm^{-1}. ^{1}H NMR (500 MHz, CD$_2$Cl$_2$): δ = 1.39–1.46 [m, 2 H, C*H*$_2$CH$_2$CH$_2$N(CH$_2$)$_3$O], 1.53–1.59 [m, 4 H, C*H*$_2$CH$_2$N(CH$_2$)$_3$O], 2.05 (p, *J* = 6.8 Hz, 2 H, C*H*$_2$CH$_2$O), 2.25–2.43 [m, 4 H, C*H*$_2$N(CH$_2$)$_3$O], 2.47 (t, *J* = 7.1 Hz, 2 H, C*H*$_2$CH$_2$CH$_2$O), 3.99 (s, 3 H, CH$_3$O), 4.24 (t, *J* = 6.7 Hz, 2 H, CH$_2$O), 7.11 (s, 1 H, C*H*COCH$_3$), 7.31 (s, 1 H, C*H*COCH$_2$), 9.06 (s, 1 H, C*H*NCCHCOCH$_2$), 9.12 (s, 1 H, C*H*CCHCOCH$_3$). ^{13}C NMR (126 MHz, CD$_2$Cl$_2$): δ = 24.95 [CH$_2$CH$_2$CH$_2$N(CH$_2$)$_3$O], 26.52 [CH$_2$CH$_2$N(CH$_2$)$_3$O], 26.89 (CH$_2$CH$_2$O), 55.02 [CH$_2$N(CH$_2$)$_3$O], 55.80 (CH$_2$CH$_2$CH$_2$O), 56.49 (CH$_3$O), 68.24 (CH$_2$O), 104.23 (*C*HCOCH$_3$), 107.49 (*C*HCOCH$_2$), 121.32 (*C*CHCOCH$_3$), 148.46 (*C*CHCOCH$_2$), 151.35 (*C*OCH$_3$), 154.34 (*C*HNCCHCOCH$_2$), 156.25 (*C*OCH$_2$), 156.93 (*C*HCCHCOCH$_3$). HRMS-ESI m/z [M+H]$^+$ calcd. for $C_{17}H_{24}N_3O_2$: 302.1869, found: 302.1861.

2-(4-Isopropyl-1,4-diazepan-1-yl)-6-methoxy-7-[3-(piperidin-1-yl)propoxy]quinazoline (14)

According to GP2 with **12** (101 mg, 0.300 mmol, 1.0 equiv) and 1-isopropyl-1,4-diazepane (243 µL, 218 mg, 1.50 mmol, 5.0 equiv) in toluene (1.5 mL). **14** was isolated by flash chromatography [10% 3 M NH$_3$ (in MeOH) in CH$_2$Cl$_2$] as yellow oil (131 mg, 99% yield, 97% purity). Hygroscopic. R_f = 0.33 [10% 3 M NH$_3$ (in MeOH) in CH$_2$Cl$_2$]. IR (film): $\tilde{\nu}$ = 2931, 1593, 1493, 1223, 1153 cm^{-1}. ^{1}H NMR (500 MHz, CD$_2$Cl$_2$): δ = 0.98 (d, *J* = 6.6 Hz, 6 H, C*H*$_3$CH), 1.36–1.51 [m, 2 H, C*H*$_2$CH$_2$CH$_2$N(CH$_2$)$_3$O], 1.51–1.60 [m, 4 H, C*H*$_2$CH$_2$N(CH$_2$)$_3$O], 1.80–1.94 (m, 2 H, CNCH$_2$C*H*$_2$CH$_2$N), 2.01 (p, *J* = 6.9 Hz, 2 H, C*H*$_2$CH$_2$O), 2.38 [s, 4 H, C*H*$_2$N(CH$_2$)$_3$O], 2.44 (t, *J* = 7.1 Hz, 2 H, C*H*$_2$CH$_2$CH$_2$O), 2.51–2.63 (m, 2 H, CNCH$_2$CH$_2$C*H*$_2$N), 2.67–2.82 (m, 2 H, CNCH$_2$C*H*$_2$N), 2.90 (hept, *J* = 6.6 Hz, 1 H, CH$_3$C*H*), 3.79–3.96 (m, 7 H, CNCH$_2$, CH$_3$O), 4.17 (t, *J* = 6.8 Hz, 2 H, CH$_2$O), 6.89 (s, 1 H, C*H*COCH$_2$), 6.90 (s, 1 H, C*H*COCH$_3$), 8.74 (s, 1 H, CHNC). ^{13}C NMR (126 MHz, CD$_2$Cl$_2$): δ = 18.52 (*C*H$_3$CH), 24.99 [CH$_2$CH$_2$CH$_2$N(CH$_2$)$_3$O], 26.55 [CH$_2$CH$_2$N(CH$_2$)$_3$O], 27.01 (CH$_2$CH$_2$O), 29.12 (CNCH$_2$CH$_2$CH$_2$N), 46.19 (CN*C*H$_2$CH$_2$CH$_2$N), 48.68 (CN*C*H$_2$CH$_2$N), 51.15 (CNCH$_2$CH$_2$CH$_2$N), 52.08 (CNCH$_2$CH$_2$N), 55.05 [CH$_2$N(CH$_2$)$_3$O], 55.88 (CH$_2$CH$_2$CH$_2$O), 55.93 (CH$_3$CH), 56.32 (CH$_3$O), 67.88 (CH$_2$O), 105.55 (CHCO)*, 105.76 (CHCO)*, 114.18 (*C*CHCOCH$_3$), 147.10 (*C*OCH$_3$), 150.66 (*C*CHCOCH$_2$), 156.21 (*C*OCH$_2$), 158.43 (*C*HNC), 159.44 (*C*NCH$_2$). HRMS-ESI m/z [M+H]$^+$ calcd. for $C_{25}H_{40}N_5O_2$, 442.3182, found: 442.3177.

***N*-[1-(Cyclohexylmethyl)piperidin-4-yl]-6-methoxy-7-[3-(piperidin-1-yl)propoxy]-quinazolin-4-amine (16a)**

According to GP4 with **15** (67.2 mg, 0.200 mmol, 1.0 equiv), 1-(cyclohexylmethyl)piperidin-4-amine (78.5 mg, 0.400 mmol, 2.0 equiv) and DIEA (107 µL, 79.1 mg, 0.600 mmol, 3.0 equiv)

in *i*-PrOH (1.0 mL) for 15 min. **16a** (61.8 mg, 62% yield, 98% purity) was isolated by flash chromatography [7% to 8% 3 M NH_3 (in MeOH) in CH_2Cl_2] as colorless solid. mp.: 194 °C. R_f = 0.43 [10% 3 M NH_3 (in MeOH) in CH_2Cl_2]. IR (film): $\tilde{\nu}$ = 2927, 1589, 1504, 1458, 1252, 754 cm^{-1}. ^1H NMR (500 MHz, CD_2Cl_2): δ = 0.78–0.96 (m, 2 H, CH_2CHCH$_2$N), 1.12–1.34 (m, 3 H, CH_2CH_2CH$_2$CHCH$_2$N), 1.36–1.46 [m, 2 H, CH_2CH$_2$CH$_2$N(CH$_2$)$_3$O], 1.46–1.53 (m, 1 H, C*H*CH$_2$N), 1.53–1.59 [m, 4 H, CH_2CH$_2$N(CH$_2$)$_3$O], 1.59–1.63 (m, 2 H, CH$_2$CH_2CHNH), 1.63–1.74 (m, 3 H, CH_2CH_2CH$_2$CHCH$_2$N), 1.74–1.82 (m, 2 H, CH_2CHCH$_2$N), 1.96–2.05 (m, 2 H, CH_2CH$_2$O), 2.05–2.18 (m, 6 H, CH_2NCH_2CH_2CHNH), 2.29–2.42 [m, 4, CH_2N(CH$_2$)$_3$O], 2.45 (t, *J* = 7.1 Hz, 2 H, CH_2CH$_2$CH$_2$O), 2.78–2.93 (m, 2 H, CH_2CH$_2$CHNH), 3.95 (s, 3 H, CH$_3$O), 4.16 (t, *J* = 6.6 Hz, 2 H, CH$_2$O), 4.18–4.28 (m, 2 H, C*H*NH), 5.24 (d, *J* = 7.7 Hz, 1 H, NH), 6.85 (s, 1 H, C*H*CCNH), 7.15 (s, 1 H, C*H*CCCNH), 8.43 (s, 1 H, C*H*NCNH). ^{13}C NMR (126 MHz, CD_2Cl_2): δ = 24.96 [*C*H$_2$CH$_2$CH$_2$N(CH$_2$)$_3$O], 26.52 [*C*H$_2$CH$_2$N(CH$_2$)$_3$O], 26.61 (*C*H$_2$CH$_2$CHCH$_2$N), 27.01 (*C*H$_2$CH$_2$O), 27.31 (*C*H$_2$CH$_2$CH$_2$CH), 32.26 (*C*H$_2$CHCH$_2$N), 32.90 (*C*H$_2$CHNH), 35.79 (*C*HCH$_2$N), 48.76 (*C*HNH), 53.49 (*C*H$_2$CH$_2$CHNH), 55.03 [*C*H$_2$N(CH$_2$)$_3$O], 55.90 (*C*H$_2$CH$_2$CH$_2$O), 56.68 (CH$_3$O), 66.00 (CH*C*H$_2$N), 67.90 (CH$_2$O), 100.09 (*C*HCCNH), 108.69 (*C*CNH), 108.97(*C*HCCCNH), 147.17 (*C*CCNH), 149.57 (*C*OCH$_3$), 154.29 (*C*HNCNH), 154.33 (*C*OCH$_2$), 157.98 (CNH). HRMS-ESI m/z $[M+H]^+$ calcd. for $C_{29}H_{46}N_5O_2$: 496.3651, found: 496.3644.

N-(1-Cyclohexylpiperidin-4-yl)-6-methoxy-7-[3-(piperidin-1-yl)propoxy]-quinazolin-4-amine (16b)

According to GP4 with **15** (33.6 mg, 0.100 mmol, 1.0 equiv), 1-cyclohexylpiperidin-4-amine (36.5 mg, 0.200 mmol, 2.0 equiv) and DIEA (53.3 µL, 39.6 mg, 0.300 mmol, 3.0 equiv) in *i*-PrOH (0.5 mL) for 15 min. **16b** (45.2 mg, 94% yield, 95% purity) was isolated by flash chromatography [5% to 10% 3 M NH_3 (in MeOH) in CH_2Cl_2] as yellow solid. mp.: 168 °C. R_f = 0.50 [10% 4 M NH_3 (in MeOH) in CH_2Cl_2]. IR (film): $\tilde{\nu}$ = 2929, 1620, 1504, 1217, 735 cm^{-1}. ^1H NMR (400 MHz, CD_3OD): δ = 1.09–1.23 (m, 1 H, CH_2CH$_2$CH$_2$CHN), 1.25–1.42 (m, 4 H, CH_2CH_2CHN), 1.44–1.58 [m, 2 H, CH_2CH$_2$CH$_2$N(CH$_2$)$_3$O], 1.61–1.72 [m, 5 H, CH_2CH$_2$CH$_2$CHN, CH_2CH$_2$N(CH$_2$)$_3$O], 1.72–1.83 (m, 2 H, CH_2CHNH), 1.83–1.92 (m, 2 H, CH_2CH$_2$CHN), 1.92–2.05 (m, 2 H, CH_2CHN), 2.06–2.17 (m, 4 H, CH_2CHNH, CH_2CH$_2$O), 2.38–2.47 (m, 1 H, CH$_2$C*H*N), 2.47–2.55 (m, 2 H, CH_2CH$_2$CHNH), 2.55–2.62 [m, 4 H, CH_2N(CH$_2$)$_3$O], 2.62–2.70 (m, 2 H, CH_2CH$_2$CH$_2$O), 3.02–3.13 (m, 2 H, CH_2CH$_2$CHNH), 3.97 (s, 3 H, CH$_3$O), 4.13–4.20 (m, 3 H, C*H*NH, CH$_2$O), 7.07 (s, 1 H, C*H*CCCNH), 7.60 (s, 1 H, C*H*CCNH), 8.30 (s, 1 H, C*H*NCNH). ^{13}C NMR (101 MHz, CD_3OD): δ = 25.00 [CH$_2$CH$_2$CH$_2$N(CH$_2$)$_3$O], 26.35 [*C*H$_2$CH$_2$N(CH$_2$)$_3$O], 26.97 (*C*H$_2$CH$_2$O), 27.09 (*C*H$_2$CH$_2$CHN), 27.29 (*C*H$_2$CH$_2$CH$_2$CHN), 29.52 (*C*H$_2$CHN), 32.41 (*C*H$_2$CHNH), 49.28 (*C*H$_2$CH$_2$CHNH), 49.85 (*C*HNH), 55.45 [*C*H$_2$N(CH$_2$)$_3$O], 56.82 (CH$_3$O), 56.99 (*C*H$_2$CH$_2$CH$_2$O), 65.28 (CH$_2$*C*HN), 68.31 (CH$_2$O), 102.94 (*C*HCCNH), 107.82 (*C*HCCCNH), 110.17 (*C*CNH), 146.65 (*C*CCNH), 150.87 (CH$_3$O*C*), 154.28 (*C*NCNH), 155.47 (CH$_2$O*C*), 159.64 (CNH). HRMS-ESI m/z $[M+H]^+$ calcd. for $C_{28}H_{44}N_5O_2$: 482.3495, found: 482.3490.

6-Methoxy-*N*-(1-methylpiperidin-4-yl)-7-[3-(piperidin-1-yl)propoxy]quinazolin-4-amine (16c)

According to GP4 with **15** (33.6 mg, 0.100 mmol, 1.0 equiv), 1-methylpiperidin-4-amine (26.4 µL, 24.5 mg, 0.200 mmol, 2.0 equiv) and DIEA (53.3 µL, 39.6 mg, 0.300 mmol,

3.0 equiv) in *i*-PrOH (0.5 mL) for 15 min. **16c** (28.7 mg, 69% yield, 97% purity) was isolated by flash chromatography [5% to 10% 3 M NH_3 (in MeOH) in CH_2Cl_2] as colorless solid. mp.: 210 °C (decomposition). R_f = 0.26 [10% 4 M NH_3 (in MeOH) in CH_2Cl_2]. IR (film): $\tilde{\nu}$ = 2931, 1591, 1254, 1049 cm^{-1}. ^1H NMR (500 MHz, CD_3OD): δ = 1.48–1.59 [m, 2 H, CH_2CH_2CH_2N(CH_2)$_3$O], 1.63–1.72 [m, 4 H, CH_2CH_2N(CH_2)$_3$O], 1.73–1.85 (m, 2 H, CH_2CHNH), 2.04–2.11 (m, 2 H, CH_2CHNH), 2.11–2.17 (m, 2 H, CH_2CH_2O), 2.21–2.28 (m, 2 H, CH_2NCH_3), 2.35 (s, 3 H, CH_3N), 2.64 [bs, 4 H, CH_2N(CH_2)$_3$O], 2.68–2.76 (m, 2 H, CH_2CH_2CH_2O), 2.93–3.04 (m, 2 H, CH_2NCH_3), 3.98 (s, 3 H, CH_3O), 4.14–4.26 (m, 3 H, CH_2O, C*H*NH), 7.07 (s, 1 H, C*H*CCCNH), 7.60 (s, 1 H, C*H*CCNH), 8.31 (s, 1 H, C*H*NCNH). ^{13}C NMR (126 MHz, CD_3OD): δ = 24.78 [CH_2CH_2CH_2N(CH_2)$_3$O], 26.16 [CH_2CH_2N(CH_2)$_3$O], 26.76 (CH_2CH_2O), 32.26 (CH_2CHNH), 46.18 (CH_3N), 55.37 [CH_2N(CH_2)$_3$O], 55.92 (CH_2NCH_3), 56.82 (CH_3O), 56.95 (CH_2CH_2CH_2O), 68.24 (CH_2O), 102.93 (*C*HCCNH), 107.83 (*C*HCCCNH), 110.22 (*C*CNH), 146.63 (*C*CCNH), 150.84 (CH$_3$O*C*), 154.30 (*C*HNCNH), 155.40 (CH$_2$O*C*), 159.69 (CNH). HRMS-ESI m/z $[M+H]^+$ calcd. for $C_{23}H_{36}N_5O_2$: 414.1869, found: 414.2864.

6-Methoxy-*N*-(1-phenylpiperidin-4-yl)-7-[3-(piperidin-1-yl)propoxy]quinazolin-4-amine (16d)

According to GP4 with **15** (67.2 mg, 0.200 mmol, 1.0 equiv), 1-phenylpiperidin-4-amine (74.2 mg, 0.400 mmol, 2.0 equiv) and DIEA (107 µL, 79.1 mg, 0.600 mmol, 3.0 equiv) in *i*-PrOH (1.0 mL) for 15 min. **16d** (77.7 mg, 82% yield, 100% purity) was isolated by flash chromatography [10% 3 M NH_3 (in MeOH) in CH_2Cl_2] as colorless solid. mp.: 207 °C (decomposition). R_f = 0.49 [10% 4 M NH_3 (in MeOH) in CH_2Cl_2]. IR (film): $\tilde{\nu}$ = 2935, 1589, 1504, 1215, 756 cm^{-1}. ^1H NMR (500 MHz, CD_2Cl_2): δ = 1.37–1.47 [m, 2 H, CH_2CH_2CH_2N(CH_2)$_3$O], 1.49–1.63 [m, 4 H, CH_2CH_2N(CH_2)$_3$O], 1.74 (qd, *J* = 11.9, 11.9, 11.9, 4.0 Hz, 2 H, CH_2CHNH), 2.03 (p, *J* = 6.9, 6.9, .9, 6.9 Hz, 2 H, CH_2CH_2O), 2.21–2.30 (m, 2 H, CH_2CHNH), 2.39 [s, 4 H, CH_2N(CH_2)$_3$O], 2.44–2.52 (m, 2 H, CH_2CH_2CH_2O), 2.97 (td, *J* = 12.4, 12.4, 2.5 Hz, 2 H, CH_2CH_2CHNH), 3.69–3.78 (m, 2 H, CH_2CH_2CHNH), 3.94 (s, 3 H, CH_3O), 4.16 (t, *J* = 6.7, 6.7 Hz, 2 H, CH_2O), 4.36–4.50 (m, 1 H, C*H*NH), 5.34 (s, 1 H, NH), 6.82 (t, *J* = 7.3, 7.3 Hz, 1 H, C*H*CHCHCN), 6.88 (s, 1 H, C*H*CCNH), 6.93–7.01 (m, 2 H, CHC*H*CHCN), 7.16 (s, 1 H, C*H*CCCNH), 7.21–7.30 (m, 2 H, CHCHC*H*CN), 8.46 (s, 1 H, C*H*NCNH). ^{13}C NMR (126 MHz, CD_2Cl_2): δ = 24.90 [CH_2CH_2N(CH_2)$_3$O], 26.44 [CH_2N(CH_2)$_3$O], 26.92 (CH_2CH_2O), 32.34 (CH$_2$CH_2CHNH), 48.57 (CHNH), 49.14 (CH_2CH_2CHNH), 54.99 [CH_2N(CH_2)$_3$O], 55.87 (CH_2CH_2CH_2O), 56.67 (CH_3O), 67.88 (CH_2O), 100.06 (*C*HCCNH), 108.72 (*C*CNH), 108.98 (*C*HCCCNH), 116.75 (CH*C*HCHCN), 119.61 (*C*HCHCHCN), 129.46 (CHCH*C*HCN), 147.22 (*C*CCNH), 149.64 (*C*OCH$_3$), 151.76 (CHCHCH*C*N), 154.24 (*C*HNCNH), 154.37 (*C*OCH$_2$), 157.94 (CNH). HRMS-ESI m/z $[M+H]^+$ calcd. for $C_{28}H_{38}N_5O_2$: 476.3026, found: 476.3019.

N-(1-Benzylpiperidin-4-yl)-6-methoxy-7-[3-(piperidin-1-yl)propoxy]quinazolin-4-amine (16e)

According to GP4 with **15** (67.2 mg, 0.200 mmol, 1.0 equiv), 1-benzylpiperidin-4-amine (83.2 µL, 77.7 mg, 0.400 mmol, 2.0 equiv) and DIEA (107 µL, 79.1 mg, 0.600 mmol, 3.0 equiv) in *i*-PrOH (1.0 mL) for 15 min. **16e** (83.1 mg, 85% yield, 99% purity) was isolated by flash chromatography [10% 3 M NH_3 (in MeOH) in CH_2Cl_2] as colorless solid. mp.: 164 °C. R_f = 0.32 [10% 4 M NH_3 (in MeOH) in CH_2Cl_2]. IR (film): $\tilde{\nu}$ = 2931, 1589, 1504, 1458, 1217, 746 cm^{-1}. ^1H NMR (400 MHz, CD_2Cl_2): δ = 1.37–1.48 [m, 2 H, CH_2CH_2CH_2N(CH_2)$_3$O], 1.48–1.75 [m, 6 H,

CH_2CH_2CHNH, $CH_2CH_2N(CH_2)_3O$], 1.97–2.08 (m, 2 H, CH_2CH_2O), 2.08–2.17 (m, 2 H, CH_2CH_2CHNH), 2.17–2.27 (m, 2 H, CH_2CH_2CHNH), 2.29–2.43 [m, 4 H, $CH_2N(CH_2)_3O$], 2.43–2.53 (m, 2 H, $CH_2CH_2CH_2O$), 2.84–2.98 (m, 2 H, CH_2CH_2CHNH), 3.53 (s, 2 H, CCH_2N), 3.95 (s, 3 H, CH_3O), 4.16 (t, J = 6.6 Hz, 2 H, CH_2O), 4.19–4.31 (m, 1 H, $CHNH$), 5.18–5.26 (m, 1 H, NH), 6.85 (s, 1 H, $CHCCNH$), 7.15 (s, 1 H, $CHCCCNH$), 7.21–7.28 (m, 1 H, $CHCHCHCCH_2N$), 7.28–7.37 (m, 4 H, $CHCHCCH_2N$), 8.43 (s, 1 H, $CHNCNH$). ^{13}C NMR (101 MHz, CD_2Cl_2): δ = 24.90 [$CH_2CH_2CH_2N(CH_2)_3O$], 26.43 [$CH_2CH_2N(CH_2)_3O$], 26.92 (CH_2CH_2O), 32.85 (CH_2CH_2CHNH), 48.62 (CH_2CH_2CHNH), 52.93 (CH_2CH_2CHNH), 54.99 [$CH_2N(CH_2)_3O$], 55.87 ($CH_2CH_2CH_2O$), 56.68 (CH_3O), 63.31 (CCH_2N), 67.85 (CH_2O), 100.05 ($CHCCNH$), 108.69 ($CCNH$), 108.99 ($CHCCCNH$), 127.28 ($CHCHCHCCH_2N$), 128.53 ($CHCHCCH_2N$), 129.38 ($CHCCH_2N$), 139.39 (CCH_2N), 147.18 ($CCCNH$), 149.57 ($COCH_3$), 154.27 ($CHNCNH$), 154.31 ($COCH_2$), 157.96 (CNH). HRMS-ESI m/z $[M+H]^+$ calcd. for $C_{29}H_{40}N_5O_2$: 490.3182, found: 490.3176.

6-Methoxy-7-[3-(piperidin-1-yl)propoxy]-*N*-[5-(pyrrolidin-1-yl)pentyl]quinazolin-4-amine (16f)

According to GP4 with **15** (101 mg, 0.300 mmol, 1.0 equiv), 5-pyrrolidin-1-ylpentan-1-amine (93.8 mg, 0.600 mmol, 2.0 equiv) and DIEA (160 µL, 119 mg, 0.900 mmol, 3.0 equiv) in *i*-PrOH (1.5 mL) for 1 h. **16f** (114 mg, 83% yield, 98% purity) was isolated by flash chromatography [10% to 15% 3 M NH_3 (in MeOH) in CH_2Cl_2] as pale yellow solid. mp.: 103 °C. R_f = 0.41 [15% 3 M NH_3 (in MeOH) in CH_2Cl_2]. IR (film): $\tilde{\nu}$ = 2937, 1593, 1460, 1217, 754 cm^{-1}. ^{1}H NMR (500 MHz, CD_2Cl_2): δ = 1.38–1.46 [m, 2 H, $CH_2CH_2CH_2N(CH_2)_3O$], 1.47–1.53 (m, 2 H, $CH_2CH_2CH_2NH$), 1.54–1.58 [m, 4 H, $CH_2CH_2N(CH_2)_3O$], 1.58–1.65 [m, 2 H, $CH_2(CH_2)_3NH$], 1.69–1.76 (m, 2 H, CH_2CH_2NH), 1.76–1.84 [m, 4 H, $CH_2CH_2N(CH_2)_5NH$], 2.01 (p, J = 6.9 Hz, 2 H, CH_2CH_2O), 2.31–2.42 [m, 4 H, $CH_2N(CH_2)_3O$], 2.45 (t, J = 7.2 Hz, 2 H, $CH_2CH_2CH_2O$), 2.53 [t, J = 7.2 Hz, 2 H, $CH_2(CH_2)_4NH$], 2.56–2.62 [m, 4 H, $CH_2N(CH_2)_5NH$], 3.56–3.71 (m, 2 H, CH_2NH), 3.95 (s, 3 H, CH_3O), 4.15 (t, J = 6.7 Hz, 2 H, CH_2O), 5.90 (t, J = 5.6 Hz, 1 H, NH), 7.07 (s, 1 H, $CHCOCH_3$), 7.14 (s, 1 H, $CHCOCH_2$), 8.43 (s, 1 H, $CHNCNH$). ^{13}C NMR (126 MHz, CD_2Cl_2): δ = 23.82 [$CH_2CH_2N(CH_2)_5NH$], 24.96 [$CH_2CH_2CH_2N(CH_2)_3O$], 25.22 ($CH_2CH_2CH_2NH$), 26.51 [$CH_2CH_2N(CH_2)_3O$], 27.00 (CH_2CH_2O), 28.52 [$CH_2(CH_2)_3NH$], 29.43 (CH_2CH_2NH), 41.58 (CH_2NH), 54.47 [$CH_2N(CH_2)_5NH$], 55.02 [$CH_2N(CH_2)_3O$], 55.90 ($CH_2CH_2CH_2O$), 56.39 [$CH_2(CH_2)_4NH$], 56.79 (CH_3O), 67.85 (CH_2O), 100.72 ($CHCOCH_3$), 108.83 ($CHCOCH_2$), 108.91 ($CCNH$), 146.98 ($CCCNH$), 149.52 ($COCH_3$), 154.21 ($COCH_2$), 154.32 ($CHNCNH$), 158.84 (CNH). HRMS-ESI m/z $[M+H]^+$ calcd. for $C_{26}H_{42}N_5O_2$: 456.3339, found: 456.3333.

4-[(1-Isopropylpiperidin-4-yl)oxy]-6-methoxy-7-[3-(piperidin-1-yl)propoxy]quinazoline (16g)

mp.: 93 °C. R_f = 0.38 [7% 3 M NH_3 (in MeOH) in CH_2Cl_2]. IR (film): $\tilde{\nu}$ = 2935, 1502, 1427, 1211, 754 cm^{-1}. ^{1}H NMR (500 MHz, CD_2Cl_2): δ = 1.05 (d, J = 6.5 Hz, 6 H, CH_3CH), 1.32–1.48 [m, 2 H, $CH_2CH_2CH_2N(CH_2)_3O$], 1.49–1.62 [m, 4 H, $CH_2CH_2N(CH_2)_3O$], 1.83–1.93 (m, 2 H, CH_2CHO), 2.03 (p, J = 6.8 Hz, 2 H, CH_2CH_2O), 2.08–2.18 (m, 2 H, CH_2CHO), 2.25–2.42 [m, 4 H, $CH_2N(CH_2)_3O$], 2.42–2.52 (m, 4 H, $CH_2CH_2CH_2O$, CH_2CH_2CHO), 2.76 (h, J = 6.6 Hz, 1 H, CH_3CH), 2.80–2.91 (m, 2 H, CH_2CH_2CHO), 3.97 (s, 3 H, CH_3O), 4.19 (t, J = 6.7 Hz, 2 H, CH_2O), 5.35 (dt, J = 8.5, 4.2 Hz, 1 H, CHO), 7.23 (s, 1 H, $CHCOCH_2$), 7.36 (s, 1 H, $CHCOCH_3$),

8.56 (s, 1 H, CHNCO). ^{13}C NMR (126 MHz, CD_2Cl_2): δ = 18.46 (*C*H$_3$CH), 24.96 [*C*H$_2$CH$_2$CH$_2$N(CH$_2$)$_3$O], 26.52 [*C*H$_2$CH$_2$N(CH$_2$)$_3$O], 26.97 (*C*H$_2$CH$_2$O), 31.82 (*C*H$_2$CHO), 46.44 (*C*H$_2$CH$_2$CHO), 54.77 (CH$_3$*C*H), 55.03 [*C*H$_2$N(CH$_2$)$_3$O], 55.87 (*C*H$_2$CH$_2$CH$_2$O), 56.42 (CH$_3$O), 68.01 (CH$_2$O), 73.20 (CHO), 101.69 (*C*HCOCH$_3$), 107.87 (*C*HCOCH$_2$), 111.30 (C*C*CO), 149.00 (*C*CCO), 150.27 (*C*OCH$_3$), 153.30 (*C*HNCO), 155.28 (*C*OCH$_2$), 165.09 (*C*OCH). HRMS-ESI m/z [M+H]$^+$ calcd. for $C_{25}H_{39}N_4O_3$: 443.3022, found: 443.3019.

7-Benzyloxy-*N*-(1-isopropylpiperidin-4-yl)-6-methoxyquinazolin-4-amine (18)

According to GP4 with **17** (1.27 g, 4.00 mmol, 1.0 equiv), 1-propan-2-ylpiperidin-4-amine (1.29 mL, 1.16 g, 8.00 mmol, 2.0 equiv) and DIEA (2.08 mL, 1.58 g, 12.0 mmol, 3.0 equiv) in *i*-PrOH (20 mL) for 15 min. **18** (1.63 g, > 99% yield, 96% purity) was isolated by flash chromatography [10% 3 M NH_3 (in MeOH) in CH_2Cl_2] as colorless solid. mp.: 192 °C (decomposition). R_f = 0.35 [10% 4 M NH_3 (in MeOH) in CH_2Cl_2]. IR (film): $\tilde{\nu}$ = 2966, 1589, 1504, 1252, 752 cm^{-1}. ^{1}H NMR (500 MHz, $CDCl_3$): δ = 1.07 (d, *J* = 6.6 Hz, 6 H, C*H*$_3$CH), 1.52–1.73 (m, 2 H, C*H*$_2$CH), 2.11–2.23 (m, 2 H, C*H*$_2$CH), 2.34–2.45 (m, 2 H, C*H*$_2$CH$_2$CH), 2.70–2.83 (m, 1 H, CH$_3$C*H*), 2.87–2.97 (m, 2 H, C*H*$_2$CH$_2$CH), 4.01 (s, 3 H, CH$_3$O), 4.18–4.29 (m, 1 H, C*H*NH), 5.12 (d, *J* = 7.7 Hz, 1 H, NH), 5.27 (s, 2 H, CH$_2$O), 6.81 (s, 1 H, C*H*CCNH), 7.22 (s, 1 H, *C*HCCCNH), 7.29–7.34 (m, 1 H, C*H*CHCHCCH$_2$O), 7.35–7.41 (m, 2 H, C*H*CHCCH$_2$O), 7.44–7.51 (m, 2 H, C*H*CCH$_2$O), 8.52 (s, 1 H, C*H*NCNH). ^{13}C NMR (126 MHz, $CDCl_3$): δ = 18.59 (*C*H$_3$C), 32.99 (*C*H$_2$CH), 47.82 (*C*H$_2$CH$_2$CH), 48.63 (CHNH), 54.65 (CH$_3$*C*), 56.59 (CH$_3$O), 70.91 (CH$_2$O), 99.77 (*C*HCCNH), 108.78 (*C*CNH), 109.69 (*C*HCCCNH), 127.57 (*C*HCCH$_2$O), 128.35 (*C*HCHCHCCH$_2$O), 128.86 (*C*HCHCCH$_2$O), 135.60 (*C*CH$_2$O), 146.70 (*C*CCNH), 149.46 (CH$_3$O*C*), 153.59 (CH$_2$O*C*), 154.23 (*C*HNCNH), 157.70 (CNH). HRMS-ESI m/z [M+H]$^+$ calcd. for $C_{24}H_{31}N_4O_2$: 407.2447, found: 407.2441.

4-[(1-Isopropylpiperidin-4-yl)amino]-6-methoxyquinazolin-7-ol (19)

mp.: 166 °C. R_f = 0.18 [15% 4 M NH_3 (in MeOH) in CH_2Cl_2]. IR (film): $\tilde{\nu}$ = 2359, 1633, 1489, 1427, 1352 cm^{-1}. ^{1}H NMR (400 MHz, CD_3OD): δ = 1.15 (d, *J* = 6.6 Hz, 6 H, C*H*$_3$CH), 1.65–1.83 (m, 2 H, C*H*$_2$CHNH), 2.02–2.21 (m, 2 H, C*H*$_2$CHNH), 2.34–2.53 (m, 2 H, CH$_2$N), 2.85 (hept, *J* = 6.6 Hz, 1 H, CH$_3$C*H*), 2.94–3.12 (m, 2 H, CH$_2$N), 4.00 (s, 3 H, CH$_3$O), 4.21 (tt, *J* = 11.4, 4.2 Hz, 1 H, C*H*NH), 6.94 (s, 1 H, C*H*COH), 7.57 (s, 1 H, C*H*CCNH), 8.25 (s, 1 H, C*H*NCNH). ^{13}C NMR (126 MHz, CD_3OD): δ = 18.40 (*C*H$_3$CH), 32.29 (*C*H$_2$CHNH), 49.17 (CH$_2$N), 49.74 (CHNH), 56.20 (CH$_3$*C*H), 56.65 (CH$_3$O), 102.49 (*C*HCCNH), 108.41 (*C*CNH), 109.53 (*C*HCOH), 145.87 (*C*CCNH), 151.00 (CH$_3$O*C*), 153.21 (*C*HNCNH), 156.86 (COH), 159.59 (CNH). HRMS-ESI m/z [M+H]$^+$ calcd. for $C_{17}H_{25}N_4O_2$: 317.1978, found: 317.1973.

***N*-(1-Propan-2-ylpiperidin-4-yl)-6-methoxy-7-[3-(piperidin-1-yl)propoxy]quinazolin-4-amine (20a)** (Kaiser et al., 2024)**.**

According to GP5, with **19** (127 mg, 0.400 mmol, 1.0 equiv), 3-piperidin-1-ylpropan-1-ol (224 µL, 211 mg, 1.40 mmol, 3.5 equiv), PPh_3 (0.589 g, 2.20 mmol, 5.5 equiv) and DIAD (413 µL, 426 mg, 2.00 mmol, 5.0 equiv) in THF (5.8 mL). Purification by flash chromatography [10% 3 M NH_3 (in MeOH) in CH_2Cl_2] afforded **20a** (111 mg, 63% yield, 99% purity) as colorless solid. The characterization data of **20a** match the reported (Kaiser et al., 2024).

_N_-(1-Isopropylpiperidin-4-yl)-6-methoxy-7-[4-(piperidin-1-yl)butoxy]quinazolin-4-amine (20b)

mp.: 191 °C. R_f = 0.41 [10% 4 M NH_3 (in MeOH) in CH_2Cl_2]. IR (film): $\tilde{\nu}$ = 2927, 1624, 1504, 1460, 1252 cm^{-1}. ^1H NMR (500 MHz, CD_2Cl_2): δ = 1.04 (d, J = 6.6 Hz, 6 H, CH_3CH), 1.36–1.46 [m, 2 H, CH_2CH$_2$CH$_2$N(CH$_2$)$_4$O], 1.48–1.61 [m, 6 H, CH_2CH$_2$N(CH$_2$)$_4$O, CH_2CHNH], 1.62–1.75 (m, 2 H, CH_2CH$_2$CH$_2$O), 1.82–1.94 (m, 2 H, CH_2CH$_2$O), 2.09–2.18 (m, 2 H, CH_2CHNH), 2.20–2.54 [m, 8 H, CH_2NCH_2(CH$_2$)$_3$O, CH_2CH$_2$CHNH], 2.76 (hept, J = 6.6 Hz, 1 H, CH$_3$CH), 2.83–2.93 (m, 2 H, CH_2CH$_2$CHNH), 3.95 (s, 3 H, CH$_3$O), 4.13 (t, J = 6.7 Hz, 2 H, CH$_2$O), 4.15–4.26 (m, 1 H, CHNH), 5.25 (d, J = 7.7 Hz, 1 H, NH), 6.86 (s, 1 H, CHCCNH), 7.13 (s, 1 H, CHCCCNH), 8.43 (s, 1 H, CHNCNH). ^{13}C NMR (126 MHz, CD_2Cl_2): δ = 18.45 (*C*H$_3$CH), 23.81 (*C*H$_2$CH$_2$CH$_2$O), 25.01 [*C*H$_2$CH$_2$CH$_2$N(CH$_2$)$_4$O], 26.53 [*C*H$_2$CH$_2$N(CH$_2$)$_4$O], 27.37 (*C*H$_2$CH$_2$O), 33.23 (*C*H$_2$CHNH), 48.02 (*C*H$_2$CH$_2$CHNH), 49.04 (*C*HNH), 54.85 (CH$_3$*C*H), 55.01 [*C*H$_2$N(CH$_2$)$_4$O], 56.69 (CH$_3$O), 59.16 [*C*H$_2$(CH$_2$)$_3$O], 69.26 (CH$_2$O), 100.10 (*C*HCCNH), 108.67 (*C*CNH), 108.87 (*C*HCCCNH), 147.17 (*C*CCNH), 149.58 (CH$_3$O*C*), 154.28 (*C*HNCNH), 154.33 (CH$_2$O*C*), 157.97 (CNH). HRMS-ESI m/z [M+H]$^+$ calcd. for $C_{26}H_{42}N_5O_2$: 456.3339, found: 456.3331.

_N_-(1-Isopropylpiperidin-4-yl)-6-methoxy-7-[2-(piperidin-1-yl)ethoxy]quinazolin-4-amine (20c)

According to GP5, with **19** (127 mg, 0.400 mmol, 1.0 equiv), 2-piperidin-1-ylethan-1-ol (215 µL, 209 mg, 1.60 mmol, 4.0 equiv), PPh_3 (0.589 g, 2.20 mmol, 5.5 equiv) and DIAD (413 µL, 426 mg, 2.00 mmol, 5.0 equiv) in THF (5.8 mL). Purification by flash chromatography [10% 3 M NH_3 (in MeOH) in CH_2Cl_2] afforded **20c** (136 mg, 79% yield, 99% purity) as colorless solid. mp.: 185 °C. R_f = 0.21 [15% 4 M NH_3 (in MeOH) in CH_2Cl_2]. IR (film): $\tilde{\nu}$ = 1643, 1460, 1252 cm^{-1}. ^1H NMR (500 MHz, CD_2Cl_2): δ = 1.04 (d, J = 6.6 Hz, 6 H, CH_3CH), 1.36–1.47 (m, 2 H, CH_2CH$_2$CH$_2$NCH$_2$CH$_2$O), 1.54–1.63 (m, 6 H, CH_2CHNH, CH_2CH$_2$NCH$_2$CH$_2$O), 2.12–2.17 (m, 2 H, CH_2CHNH), 2.32–2.40 (m, 2 H, CH_2CH$_2$CHNH), 2.42–2.54 (m, 4 H, CH_2NCH$_2$CH$_2$O), 2.78 (s, 1 H, CH$_3$CH), 2.78–2.81 (m, 2 H, CH_2CH$_2$O), 2.84–2.93 (m, 2 H, CH_2CH$_2$CHNH), 3.96 (s, 3 H, CH$_3$O), 4.15–4.27 (m, 3 H, CH$_2$O, CHNH), 5.27 (d, J = 7.7 Hz, 1 H, NH), 6.87 (s, 1 H, CHCCNH), 7.14 (s, 1 H, CHCCCNH), 8.43 (s, 1 H, CHNCNH). ^{13}C NMR (126 MHz, CD_2Cl_2): δ = 18.45 (*C*H$_3$CH), 24.71 (*C*H$_2$CH$_2$CH$_2$NCH$_2$CH$_2$O), 26.43 (*C*H$_2$CH$_2$NCH$_2$CH$_2$O), 33.22 (*C*H$_2$CHNH), 48.02 (*C*H$_2$CH$_2$CHNH), 49.06 (CHNH), 54.84 (CH$_3$*C*H), 55.43 (*C*H$_2$NCH$_2$CH$_2$O), 56.68 (CH$_3$O), 58.02 (*C*H$_2$CH$_2$O), 67.04 (CH$_2$O), 100.19 (*C*HCCNH), 108.80 (CCNH), 109.01 (*C*HCCCNH), 147.13 (*C*CCNH), 149.49 (CH$_3$O*C*), 153.75 (CH$_2$O*C*), 154.33 (*C*HNCNH), 157.98 (CNH). HRMS-ESI m/z [M+H]$^+$ calcd. for $C_{24}H_{38}N_5O_2$: 428.3026, found: 428.3020.

_N_-(1-Isopropylpiperidin-4-yl)-6-methoxy-7-[3-(pyrrolidin-1-yl)propoxy]-quinazolin-4-amine (20d)

According to GP5, with **19** (127 mg, 0.400 mmol, 1.0 equiv), 3-pyrrolidin-1-ylpropan-1-ol (227 µL, 218 mg, 1.60 mmol, 4.0 equiv), PPh_3 (0.589 g, 2.20 mmol, 5.5 equiv) and DIAD (413 µL, 426 mg, 2.00 mmol, 5.0 equiv) in THF (5.8 mL). Purification by flash chromatography [10% 3 M NH_3 (in MeOH) in CH_2Cl_2] afforded **20d** (119 mg, 69% yield, 98% purity) as colorless solid. mp.: 162 °C. R_f = 0.18 [15% 4 M NH_3 (in MeOH) in CH_2Cl_2]. IR (film): $\tilde{\nu}$ = 2964, 1593,

1506, 1254 cm^{-1}. ^{1}H NMR (500 MHz, CD_2Cl_2): δ = 1.11 (d, *J* = 6.6 Hz, 6 H, C*H*$_3$CH), 1.69–1.78 (m, 2 H, C*H*$_2$CHNH), 1.77–1.82 [m, 4 H, C*H*$_2$CH$_2$N(CH$_2$)$_3$O], 2.09 (p, *J* = 6.8 Hz, 2 H, C*H*$_2$CH$_2$O), 2.12–2.21 (m, 2 H, C*H*$_2$CHNH), 2.38–2.53 (m, 2 H, C*H*$_2$CH$_2$CHNH), 2.53–2.62 [m, 4 H, C*H*$_2$N(CH$_2$)$_3$O], 2.61–2.73 (m, 2 H, C*H*$_2$CH$_2$CH$_2$O), 2.90 (hept, *J* = 6.6 Hz, 1 H, CH$_3$C*H*), 2.96–3.10 (m, 2 H, C*H*$_2$CH$_2$CHNH), 3.96 (s, 3 H, CH$_3$O), 4.19 (t, *J* = 6.6 Hz, 3 H, CH$_2$O), 4.22–4.37 (m, 1 H, C*H*NH), 5.44 (d, *J* = 7.7 Hz, 1 H, NH), 6.91 (s, 1 H, C*H*CCNH), 7.15 (s, 1 H, C*H*CCCNH), 8.42 (s, 1 H, C*H*NCNH). ^{13}C NMR (126 MHz, CD_2Cl_2): δ = 18.14 (*C*H$_3$CH), 23.90 [*C*H$_2$CH$_2$N(CH$_2$)$_3$O], 28.61 (*C*H$_2$CH$_2$O), 32.36 (*C*H$_2$CHNH), 48.07 (*C*H$_2$CH$_2$CHNH), 48.44 (CHNH), 53.05 (*C*H$_2$CH$_2$CH$_2$O), 54.46 [*C*H$_2$N(CH$_2$)$_3$O], 55.51 (CH$_3$*C*H), 56.73 (CH$_3$O), 67.65 (CH$_2$O), 100.27 (*C*HCCNH), 108.79 (*C*CNH), 108.91 (*C*HCCCNH), 147.13 (*C*CCNH), 149.59 (CH$_3$O*C*), 154.20 (*C*HNCNH), 154.27 (CH$_2$O*C*), 157.98 (CNH). HRMS-ESI m/z [M+H]$^+$ calcd. for $C_{24}H_{38}N_5O_2$: 428.3026, found: 428.3021.

7-[3-(Azepan-1-yl)propoxy]-*N*-(1-isopropylpiperidin-4-yl)-6-methoxyquinazolin-4-amine (20e)

According to GP5, with **19** (127 mg, 0.400 mmol, 1.0 equiv), 3-(azepan-1-yl)propan-1-ol (273 µL, 265 mg, 1.60 mmol, 4.0 equiv), PPh_3 (0.589 g, 2.20 mmol, 5.5 equiv) and DIAD (413 µL, 426 mg, 2.00 mmol, 5.0 equiv) in THF (5.8 mL). Purification by flash chromatography [10% 3 M NH_3 (in MeOH) in CH_2Cl_2] afforded **20e** (108 mg, 59% yield, 97% purity) as colorless solid. mp.: 167 °C. R_f = 0.44 [15% 4 M NH_3 (in MeOH) in CH_2Cl_2]. IR (film): $\tilde{\nu}$ = 2926, 1622, 1593, 1460, 1252 cm^{-1}. ^{1}H NMR (500 MHz, CD_2Cl_2): δ = 1.05 (d, *J* = 6.6 Hz, 6 H, C*H*$_3$CH), 1.48–1.80 [m, 10 H, C*H*$_2$CHNH, C*H*$_2$C*H*$_2$CH$_2$N(CH$_2$)$_3$O], 2.00 (p, *J* = 6.8 Hz, 2 H, C*H*$_2$CH$_2$O), 2.08–2.23 (m, 2 H, C*H*$_2$CHNH), 2.28–2.45 (m, 2 H, C*H*$_2$CH$_2$CHNH), 2.58–2.67 (m, 6 H, C*H*$_2$NC*H*$_2$CH$_2$CH$_2$O), 2.72–2.84 (m, 1 H, CH$_3$C*H*), 2.86–2.96 (m, 2 H, C*H*$_2$CH$_2$CHNH), 3.96 (s, 3 H, CH$_3$O), 4.11–4.28 (m, 3 H, C*H*NH, CH$_2$O), 5.27–5.31 (m, 1 H, NH), 6.88 (s, 1 H, C*H*CCNH), 7.15 (s, 1 H, C*H*CCCNH), 8.42 (s, 1 H, C*H*NCNH). ^{13}C NMR (126 MHz, CD_2Cl_2): δ = 18.40 (*C*H$_3$CH), 27.43 [*C*H$_2$CH$_2$CH$_2$N(CH$_2$)$_3$O], 27.81 (*C*H$_2$CH$_2$O), 28.82 [*C*H$_2$CH$_2$N(CH$_2$)$_3$O], 33.04 (*C*H$_2$CHNH), 48.04 (*C*H$_2$CH$_2$CHNH), 48.92 (*C*HNH), 54.93 (*C*H$_2$CH$_2$CH$_2$O), 54.93 (CH$_3$*C*H), 55.86 [*C*H$_2$N(CH$_2$)$_3$O], 56.70 (CH$_3$O), 67.84 (CH$_2$O), 100.18 (*C*HCCNH), 108.70 (*C*CNH), 108.88 (*C*HCCCNH), 147.13 (*C*CCNH), 149.58 (CH$_3$O*C*), 154.25 (*C*HNCNH), 154.39 (CH$_2$O*C*), 157.99 (CNH). HRMS-ESI m/z [M+H]$^+$ calcd. for $C_{26}H_{42}N_5O_2$: 456.3339, found: 456.3334.

N-(1-Isopropylpiperidin-4-yl)-6-methoxy-7-[2-(1-methylpiperidin-2-yl)ethoxy]-quinazolin-4-amine (20f)

According to GP5, with **19** (127 mg, 0.400 mmol, 1.0 equiv), 2-(1-methylpiperidin-2-yl)ethan-1-ol (246 µL, 241 mg, 1.60 mmol, 4.0 equiv), PPh_3 (0.589 g, 2.20 mmol, 5.5 equiv) and DIAD (413 µL, 426 mg, 2.00 mmol, 5.0 equiv) in THF (5.8 mL). Purification by flash chromatography [10% 3 M NH_3 (in MeOH) in CH_2Cl_2] afforded **20f** (81.0 mg, 46% yield, 100% purity) as colorless solid. mp.: 208 °C. R_f = 0.56 [15% 4 M NH_3 (in MeOH) in CH_2Cl_2]. IR (film): $\tilde{\nu}$ = 1624, 1506, 1252, 1217 cm^{-1}. ^{1}H NMR (500 MHz, CD_2Cl_2): δ = 1.04 (d, *J* = 6.6 Hz, 6 H, C*H*$_3$CH), 1.21–1.34 (m, 1 H, C*H*$_2$CH$_2$CH$_2$NCH$_3$), 1.36–1.47 [m, 1 H, C*H*$_2$(CH$_2$)$_3$NCH$_3$], 1.47–1.76 (m, 7 H, C*H*$_2$CHNH, C*H*$_2$C*H*$_2$C*H*$_2$CHC*H*$_2$CH$_2$O), 1.93–2.04 (m, 1 H, C*H*$_2$CH$_2$O), 2.04–2.18 (m, 4 H, C*H*$_2$CHNH, C*H*NC*H*$_2$), 2.26 (s, 3 H, CH$_3$N), 2.32–2.42 (m, 2 H, C*H*$_2$CH$_2$CHNH), 2.71–2.78 (m, 1 H, CH$_3$C*H*), 2.78–2.84 (m, 1 H, CH$_3$NC*H*$_2$), 2.84–2.94 (m, 2 H, C*H*$_2$CH$_2$CHNH), 3.95 (s, 3 H,

CH_3O), 4.11–4.28 (m, 3 H, C*H*NH, CH_2O), 5.22–5.29 (m, 1 H, NH), 6.86 (s, 1 H, C*H*CCNH), 7.15 (s, 1 H, C*H*CCCNH), 8.43 (s, 1 H, C*H*NCNH). ^{13}C NMR (126 MHz, CD_2Cl_2): δ = 18.46 (CH_3CH), 24.74 ($CH_2CH_2CH_2NCH_3$), 26.11 ($CH_2CH_2NCH_3$), 31.40 [$CH_2(CH_2)_3NCH_3$], 32.32 (CH_2CH_2O), 33.23 (CH_2CHNH), 43.23 (CH_3N), 48.02 (CH_2CH_2CHNH), 49.05 (CHNH), 54.82 (CH_3CH), 56.69 (CH_3O), 57.25 (CH_2NCH_3), 61.46 ($CHNCH_3$), 66.58 (CH_2O), 100.14 (*C*HCCNH), 108.71 (*C*CNH), 108.96 (*C*HCCCNH), 147.16 (*C*CCNH), 149.53 (CH_3OC), 154.29 (CH_2OC), 154.30 (*C*HNCNH), 157.98 (CNH). HRMS-ESI m/z $[M+H]^+$ calcd. for $C_{25}H_{40}N_5O_2$: 442.3182, found: 442.2176.

N-(1-Isopropylpiperidin-4-yl)-6-methoxy-7-[(1-methylpiperidin-4-yl)methoxy]-quinazolin-4-amine (20g)

According to GP5, with **19** (127 mg, 0.400 mmol, 1.0 equiv), (1-methylpiperidin-4-yl)methanol (200 µL, 218 mg, 1.60 mmol, 4.0 equiv), PPh_3 (0.589 g, 2.20 mmol, 5.5 equiv) and DIAD (413 µL, 426 mg, 2.00 mmol, 5.0 equiv) in THF (5.8 mL). Purification by flash chromatography [10% 3 M NH_3 (in MeOH) in CH_2Cl_2] afforded **20g** (99.6 mg, 58% yield, 95% purity) as colorless solid. mp.: 156 °C. R_f = 0.31 [15% 4 M NH_3 (in MeOH) in CH_2Cl_2]. IR (film): $\tilde{\nu}$ = 1643, 1504, 1254 cm^{-1}. ^{1}H NMR (500 MHz, CD_2Cl_2): δ = 1.06 (d, *J* = 6.6 Hz, 6 H, CH_3CH), 1.36–1.47 (m, 2 H, CH_2CHCH_2O), 1.59–1.68 (m, 2 H, CH_2CHNH), 1.72–1.91 (m, 3 H, CH_2CHCH_2O), 1.91–1.99 (m, 2 H, CH_2NCH_3), 2.09–2.18 (m, 2 H, CH_2CHNH), 2.23 (s, 3 H, CH_3N), 2.32–2.47 (m, 2 H, CH_2CH_2CHNH), 2.75–2.83 (m, 1 H, CH_3CH), 2.83–2.88 (m, 2 H, CH_2NCH_3), 2.88–2.97 (m, 2 H, CH_2CH_2CHNH), 3.92–3.99 (m, 5 H, CH_3O, CH_2O), 4.15–4.31 (m, 1 H, C*H*NH), 5.34–5.36 (m, 1 H, NH), 6.88 (s, 1 H, C*H*CCNH), 7.11 (s, 1 H, C*H*CCCNH), 8.42 (s, 1 H, C*H*NCNH). ^{13}C NMR (126 MHz, CD_2Cl_2): δ = 18.35 (CH_3CH), 29.48 (CH_2CCH_2O), 32.92 (CH_2CHNH), 35.41 ($CHCH_2O$), 46.62 (CH_3N), 48.03 (CH_2CH_2CHNH), 48.85 (CHNH), 55.06 (CH_3CH), 55.72 (CH_2NCH_3), 56.76 (CH_3O), 73.88 (CH_2O), 100.31 (*C*HCCNH), 108.73 (*C*CNH), 108.90 (*C*HCCCNH), 147.14 (*C*CCNH), 149.64 (CH_3OC), 154.26 (*C*HNCNH), 154.38 (CH_2OC), 157.98 (CNH). HRMS-ESI m/z $[M+H]^+$ calcd. for $C_{24}H_{38}N_5O_2$: 428.3026, found: 428.3020.

N-(1-Isopropylpiperidin-4-yl)-6-methoxy-7-[(1-methylpiperidin-3-yl)methoxy]-quinazolin-4-amine (20h)

According to GP5, with **19** (127 mg, 0.400 mmol, 1.0 equiv), (1-methylpiperidin-3-yl)methanol (213 µL, 215 mg, 1.60 mmol, 4.0 equiv), PPh_3 (0.589 g, 2.20 mmol, 5.5 equiv) and DIAD (413 µL, 426 mg, 2.00 mmol, 5.0 equiv) in THF (5.8 mL). Purification by flash chromatography [10% 3 M NH_3 (in MeOH) in CH_2Cl_2] afforded **20h** (133 mg, 78% yield, 96% purity) as colorless solid. mp.: 169 °C. R_f = 0.31 [15% 4 M NH_3 (in MeOH) in CH_2Cl_2]. IR (film): $\tilde{\nu}$ = 1643, 1506, 1460, 1254 cm^{1}. ^{1}H NMR (500 MHz, CD_2Cl_2): δ = 1.04 (d, *J* = 6.6 Hz, 6 H, CH_3CH), 1.07–1.16 (m, 1 H, $CH_2CH_2CH_2NCH_3$), 1.53–1.59 (m, 2 H, CH_2CHNH), 1.59–1.74 (m, 2 H, $CH_2CH_2NCH_3$), 1.76–1.87 (m, 2 H, $CH_2CH_2CH_2NCH_3$, $CHCH_2NCH_3$), 1.93–2.01 (m, 1 H, $CH_2CH_2CH_2NCH_3$), 2.09–2.17 (m, 2 H, CH_2CHNH), 2.17–2.21 (m, 1 H, $CHCH_2O$), 2.23 (s, 3 H, CH_3N), 2.32–2.42 (m, 2 H, CH_2CH_2CHNH), 2.62–2.72 (m, 1 H, CH_2NCH_3), 2.77 (hept, *J* = 6.6 Hz, 1 H, CH_3CH), 2.84–2.96 (m, 3 H, CH_2CH_2CHNH, $CHCH_2NCH_3$), 3.87–4.03 (m, 5 H, CH_3O, CH_2O), 4.12–4.28 (m, 1 H, C*H*NH), 5.25 (d, *J* = 7.7 Hz, 1 H, NH), 6.86 (s, 1 H, C*H*CCNH), 7.12 (s, 1 H, C*H*CCCNH), 8.43 (s, 1 H, C*H*NCHNH). ^{13}C NMR (126 MHz, CD_2Cl_2): δ = 18.45 (CH_3CH), 25.17 ($CH_2CH_2CH_2NCH_3$), 27.20 ($CH_2CH_2CH_2NCH_3$), 33.21 (CH_2CHNH), 36.52 ($CHCH_2O$), 46.92 (CH_3N), 48.02 (CH_2CH_2CHNH), 49.04 (*C*HNH), 54.86 (CH_3CH), 56.64

($CH_2CH_2CH_2NCH_3$), 56.78 (CH_3O), 59.53 ($CHCH_2NCH_3$), 72.30 (CH_2O), 100.27 (*C*HCCNH), 108.74 (*C*CNH), 108.98 (*C*HCCCNH), 147.16 (*C*CCNH), 149.63 (CH_3OC), 154.29 (*C*HNCNH), 154.37 (CH_2OC), 157.97 (CNH). HRMS-ESI m/z $[M+H]^+$ calcd. for $C_{24}H_{38}N_5O_2$: 428.3026, found: 428.3020.

4-(*tert*-Butyl)-1-[3-({4-[(1-isopropylpiperidin-4-yl)amino]-6-methoxyquinazolin-7-yl}oxy)-propyl]pyridin-1-ium chloride (20i)

mp.: 182 °C (decomposition). R_f = 0.23 [20% 3 M NH_3 (in MeOH) in CH_2Cl_2]. IR (film): $\tilde{\nu}$ = 1641, 1506, 1462, 1254, 1217 cm^{-1}. ^1H NMR (500 MHz, CD_2Cl_2): δ = 1.04 (d, *J* = 6.6 Hz, 6 H, C*H*$_3$CH), 1.40 (s, 9 H, CH_3C), 1.62–1.69 (m, 2 H, C*H*$_2$CHNH), 2.06–2.15 (m, 2 H, C*H*$_2$CHNH), 2.31–2.42 (m, 2 H, C*H*$_2$CH$_2$CHNH), 2.68 (p, *J* = 6.2 Hz, 2 H, CH_2CH_2O), 2.76 (h, *J* = 6.6 Hz, 1 H, CH$_3$C*H*), 2.83–2.94 (m, 2 H, C*H*$_2$CH$_2$CHNH), 4.00 (s, 3 H, CH_3O), 4.13–4.31 (m, 3 H, C*H*NH, CH_2O), 5.11 (t, *J* = 6.7 Hz, 2 H, C*H*$_2$CH$_2$CH$_2$O), 5.58 (d, *J* = 7.7 Hz, 1 H, NH), 7.03 (s, 1 H, C*H*COCH$_3$), 7.11 (s, 1 H, C*H*COCH$_2$), 7.90–8.01 (m, 2 H, C*H*CCCH$_3$), 8.43 (s, 1 H, C*H*NCNH), 9.19–9.27 (m, 2 H, C*H*CHCCCH$_3$). ^{13}C NMR (126 MHz, CD_2Cl_2): δ = 18.45 (*C*H$_3$CH), 30.15 (*C*H$_3$C), 30.87 (*C*H$_2$CH$_2$O), 33.09 (*C*H$_2$CHNH), 37.08 (CH_3C), 48.09 (*C*H$_2$CH$_2$CHNH), 49.23 (CHNH), 54.81 (CH_3C), 57.13 (CH_3O), 58.52 (*C*H$_2$CH$_2$CH$_2$O), 65.11 (CH_2O), 101.12 (*C*HCOCH$_3$), 109.56 (*C*CNH), 109.68 (*C*HCOCH$_2$), 125.80 (*C*HCCCH$_3$), 144.70 (*C*HCHCCCH$_3$), 146.85 (*C*CCNH), 149.20 (*C*OCH$_3$), 152.88 (*C*OCH$_2$), 154.52 (*C*HNCNH), 158.09 (CNH), 172.18 (*C*CCH$_3$). HRMS-ESI m/z $[M-Cl]^+$ calcd. for $C_{29}H_{42}N_5O_2$: 492.33385; found: 492.3327.

7-(4-Chlorobutoxy)-*N*-(1-isopropylpiperidin-4-yl)-6-methoxyquinazolin-4-amine (21)

According to GP5, with **19** (127 mg, 0.400 mmol, 1.0 equiv), 4-chlorobutan-1-ol (188 µL, 204 mg, 1.60 mmol, 4.0 equiv) PPh_3 (0.589 g, 2.20 mmol, 5.5 equiv) and DIAD (413 µL, 426 mg, 2.00 mmol, 5.0 equiv) in THF (5.8 mL). Purification by flash chromatography (20% MeOH in CH_2Cl_2) afforded **21** (150 mg, 92% yield, 99% purity) as colorless solid. mp.: 187 °C. R_f = 0.43 (20% MeOH in CH_2Cl_2). IR (film): $\tilde{\nu}$ = 2964, 1622, 1593, 1460, 1252 cm^{-1}. ^1H NMR (500 MHz, CD_2Cl_2): δ = 1.06 (d, *J* = 6.6 Hz, 6 H, C*H*$_3$CH), 1.58–1.67 (m, 2 H, C*H*$_2$CHNH), 1.94–2.08 (m, 4 H, ClCH$_2$C*H*$_2$C*H*$_2$CH$_2$O), 2.12–2.20 (m, 2 H, C*H*$_2$CHNH), 2.31–2.46 (m, 2 H, C*H*$_2$CH$_2$CHNH), 2.74–2.86 (m, 1 H, CH$_3$C*H*), 2.87–2.97 (m, 2 H, C*H*$_2$CH$_2$CHNH), 3.63–3.69 (m, 2 H, $ClCH_2$), 3.96 (s, 3 H, CH_3O), 4.13–4.17 (m, 2 H, CH_2O), 4.17–4.28 (m, 1 H, C*H*NH), 5.30 (bs, 1 H, NH), 6.88 (s, 1 H, C*H*CCNH), 7.13 (s, 1 H, C*H*CCCNH), 8.43 (s, 1 H, C*H*NCNH). ^{13}C NMR (126 MHz, CD_2Cl_2): δ = 18.52 (*C*H$_3$CH), 26.96 (ClCH$_2$*C*H$_2$), 29.98 (ClCH$_2$CH$_2$*C*H$_2$), 33.13 (*C*H$_2$CHNH), 45.46 ($ClCH_2$), 48.18 (*C*H$_2$CH$_2$CHNH), 49.05 (CHNH), 55.18 (CH_3CH), 56.87 (CH_3O), 68.67 (CH_2O), 100.38 (*C*HCCNH), 109.00 (*C*CNH), 109.10 (*C*HCCCNH), 147.26 (*C*CCNH), 149.72 (CH_3OC), 154.28 (CH_2OC), 154.46 (*C*HNCNH), 158.14 (CNH). HRMS-ESI m/z $[M+H]^+$ calcd. for $C_{21}H_{31}ClN_4O_2$: 407.2214, found: 407.2207.

N^4-(1-Isopropylpiperidin-4-yl)-6-methoxy-N^7-methyl-N^7-[3-(piperidin-1-yl)propyl]quinazoline-4,7-diamine (23a)

According to GP6, with **22** (159 mg, 0.500 mmol, 1.0 equiv), *N*-methyl-3-piperidin-1-ylpropan-1-amine (457 µL, 411 mg, 2.50 mmol, 5.0 equiv) and K_2CO_3 (76.0 mg, 0.550 mmol, 1.1 equiv)

in NMP (650 µL). Purification by flash chromatography [7% to 15% 3 M NH_3 (in MeOH) in CH_2Cl_2] afforded **23a** (176 mg, 78% yield, 95% purity) as pale yellow solid. mp.: 242 °C. R_f = 0.28 [10% 3 M NH_3 (in MeOH) in CH_2Cl_2]. IR (film): $\tilde{\nu}$ = 2927, 1643, 1502, 1244 cm^{-1}. ^1H NMR (500 MHz, CD_2Cl_2): δ = 1.04 (d, J = 6.6 Hz, 6 H, CH_3CH), 1.34–1.46 [m, 2 H, CH_2CH$_2$CH$_2$N(CH$_2$)$_3$NC], 1.46–1.64 [m, 6 H, CH_2CHNH, CH_2CH$_2$N(CH$_2$)$_3$NC], 1.74 (tt, J = 9.5, 6.5 Hz, 2 H, CH_2CH$_2$NC), 2.09–2.18 (m, 2 H, CH_2CHNH), 2.18–2.46 (m, 8 H, CH_2CH$_2$CHNH, CH_2NCH$_2$CH$_2$CH$_2$NC), 2.77 (hept, J = 6.6 Hz, 1 H, CH$_3$CH), 2.83–2.97 (m, 5 H, CH_2CH$_2$CHNH, CH$_3$N), 3.19–3.32 (m, 2 H, CH$_2$NC), 3.95 (s, 3 H, CH$_3$O), 4.13–4.26 (m, 1 H, CHNH), 5.21 (d, J = 7.7 Hz, 1 H, NH), 6.80 (s, 1 H, CHCOCH$_3$), 7.07 (s, 1 H, CHCNCH$_3$), 8.39 (s, 1 H, CHNCNH). ^{13}C NMR (126 MHz, CD_2Cl_2): δ = 18.44 (*C*H$_3$CH), 24.96 [*C*H$_2$CH$_2$CH$_2$N(CH$_2$)$_3$NC], 25.21 (*C*H$_2$CH$_2$NC), 26.49 [*C*H$_2$CH$_2$N(CH$_2$)$_3$NC], 33.24 (*C*H$_2$CHNH), 40.10 (*C*H$_3$NC), 48.03 (*C*H$_2$CH$_2$CHNH), 48.91 (CHNH), 53.37 (*C*H$_2$NC), 54.88 (CH$_3$*C*H), 54.95 [*C*H$_2$N(CH$_2$)$_3$NC], 56.17 (CH$_3$O), 57.15 (*C*H$_2$CH$_2$CH$_2$NC), 99.84 (*C*HCOCH$_3$), 108.71 (*C*CNH), 114.71 (*C*HCNCH$_3$), 146.88 (*C*CCNH), 148.29 (*C*NCH$_3$), 151.96 (*C*OCH$_3$), 154.09 (*C*NCNH), 157.86 (CNH). HRMS-ESI m/z $[M+H]^+$ calcd. for $C_{26}H_{43}N_6O$: 455.3498; found: 455.3492.

N^4-(1-Isopropylpiperidin-4-yl)-6-methoxy-*N*^{7}-[3-(piperidin-1-yl)propyl]quinazoline-4,7-diamine (23b)

According to GP6, with **22** (127 mg, 0.400 mmol, 1.0 eq), 3-piperidin-1-ylpropan-1-amine (328 µL, 293 mg, 2.00 mmol, 5.0 equiv) and K_2CO_3 (60.8 mg, 0.440 mmol, 1.1 equiv) in NMP (520 µL). Purification by flash chromatography [5% to 15% 3 M NH_3 (in MeOH) in CH_2Cl_2] afforded **23b** (148 mg, 84% yield, 97% purity) as pale yellow solid. mp.: 251 °C. R_f = 0.32 [10% 3 M NH_3 (in MeOH) in CH_2Cl_2]. IR (film): $\tilde{\nu}$ = 2935, 1620, 1525, 1433, 1213 cm^{-1}. ^1H NMR (500 MHz, CD_2Cl_2): δ = 1.05 (d, J = 6.6 Hz, 6 H, CH_3CH), 1.41–1.52 [m, 2 H, CH_2CH$_2$CH$_2$N(CH$_2$)$_3$NH], 1.52–1.60 (m, 2 H, CH_2CHNH), 1.60–1.67 [m, 4 H, CH_2CH$_2$N(CH$_2$)$_3$NH], 1.85 (p, J = 6.1 Hz, 2 H, CH_2CH$_2$NH), 2.08–2.18 (m, 2 H, CH_2CHNH), 2.30–2.45 [m, 6 H, CH_2CH$_2$CHNH, CH_2N(CH$_2$)$_3$NH], 2.47 (t, J = 6.1 Hz, 2 H, CH_2CH$_2$CH$_2$NH), 2.78 (hept, J = 6.6 Hz, 1 H, CH$_3$CH), 2.83–2.97 (m, 2 H, CH_2CH$_2$CHNH), 3.29 (t, J = 6.2 Hz, 2 H, CH_2NH), 3.96 (s, 3 H, CH$_3$O), 4.18 (tdt, J = 11.5, 8.1, 4.3 Hz, 1 H, CHNH), 5.00–5.18 (m, 1 H, CHNH), 6.38–6.63 (m, 1 H, NHCH$_2$), 6.66 (s, 1 H, CHCNH), 6.71 (s, 1 H, CHCOCH$_3$), 8.34 (s, 1 H, CHNCNH). ^{13}C NMR (126 MHz, CD_2Cl_2): δ = 18.42 (*C*H$_3$CH), 24.98 [*C*H$_2$CH$_2$CH$_2$N(CH$_2$)$_3$NH], 25.23 (*C*H$_2$CH$_2$NH), 26.42 [*C*H$_2$CH$_2$N(CH$_2$)$_3$NH], 33.33 (*C*H$_2$CHNH), 43.97 (CH$_2$NH), 48.08 (*C*H$_2$CH$_2$CHNH), 48.81 (CHNH), 54.94 (CH$_3$*C*H), 55.20 [*C*H$_2$N(CH$_2$)$_3$NH], 55.98 (CH$_3$O), 58.89 (*C*H$_2$CH$_2$CH$_2$NH), 97.46 (*C*HCOCH$_3$), 103.13 (*C*HCNH), 104.94 (*C*CNHCH), 144.68 (*C*NHCH$_2$), 147.66 (*C*CCNHCH), 147.93 (*C*OCH$_3$), 153.90 (*C*HNCNH), 157.88 (*C*NHCH). HRMS-EI m/z $[M]^+$ calcd. for $C_{25}H_{40}N_6O$: 440.3264; found: 440.3259.

N^7-[3-(Azepan-1-yl)propyl]-*N*^{4}-(1-isopropylpiperidin-4-yl)-6-methoxyquinazoline-4,7-diamine (23c)

According to GP6, with **22** (111 mg, 0.350 mmol, 1.0 equiv), 3-(azepan-1-yl)propan-1-amine (320 µL, 288 mg, 1.75 mmol, 5.0 equiv) and K_2CO_3 (53.2 mg, 0.385 mmol, 1.1 equiv) in NMP (455 µL). Purification by flash chromatography [7% to 12% (7 M NH_3 (in MeOH) in CH_2Cl_2] afforded **23c** (38.0 mg, 24% yield, 98% purity) as colorless solid. mp.: 220 °C (decomposition). R_f = 0.42 [10% (7 M NH_3 (in MeOH) in CH_2Cl_2]. IR (film): $\tilde{\nu}$ = 2929, 1620, 1527, 1215, 754 cm^{-1}.

^{1}H NMR (500 MHz, CD_2Cl_2): δ = 1.03 (d, *J* = 6.6 Hz, 6 H, C*H*$_3$CH), 1.49–1.58 (m, 2 H, C*H*$_2$CHNH), 1.62–1.73 (m, 8 H, C*H*$_2$C*H*$_2$CH$_2$N(CH$_2$)$_3$NH), 1.83 (p, *J* = 6.2 Hz, 2 H, C*H*$_2$CH$_2$NH), 2.08–2.16 (m, 2 H, C*H*$_2$CHNH), 2.31–2.41 (m, 2 H, C*H*$_2$CH$_2$CHNH), 2.59–2.65 (m, 6 H, C*H*$_2$NC*H*$_2$CH$_2$CH$_2$NH), 2.69–2.80 (m, 1 H, CH$_3$C*H*), 2.84–2.91 (m, 2 H, C*H*$_2$CH$_2$CHNH), 3.27–3.33 (m, 2 H, C*H*$_2$NH), 3.96 (s, 3 H, CH$_3$O), 4.17 (tdt, *J* = 11.6, 8.3, 4.3 Hz, 1 H, C*H*NH), 5.07 (d, *J* = 7.7 Hz, 1 H, CHN*H*), 6.11 (t, *J* = 4.9 Hz, 1 H, CH$_2$N*H*), 6.68 (s, 1 H, C*H*CCCNH), 6.70 (s, 1 H, C*H*CCNH), 8.34 (s, 1 H, C*H*NCNH). ^{13}C NMR (126 MHz, CD_2Cl_2): δ = 18.47 (*C*H$_3$CH), 26.50 (*C*H$_2$CH$_2$NH), 27.32 [CH$_2$CH$_2$CH$_2$N(CH$_2$)$_3$NH]*, 28.65 [CH$_2$*C*H$_2$CH$_2$N(CH$_2$)$_3$NH]*, 33.44 (*C*H$_2$CHNH), 43.72 (*C*H$_2$NH), 48.07 (*C*H$_2$CH$_2$CHNH), 48.86 (*C*HNH), 54.81 (CH$_3$*C*H), 56.08 (CH$_3$O), 56.36 [*C*H$_2$N(CH$_2$)$_3$NH], 58.01 (*C*H$_2$CH$_2$CH$_2$NH), 97.51 (*C*HCCNH), 103.42 (*C*HCCCNH), 105.04 (*C*CNHCH), 144.53 (*C*NHCH$_2$), 147.59 (*C*OCH$_3$), 148.02 (*C*CCNHCH), 154.01 (*C*HNCNH), 157.89 (*C*NHCH). HRMS-EI m/z [M]$^+$ calcd. for $C_{26}H_{42}N_6O$: 454.3420; found: 454.3423.

2-Chloro-6,7-dimethoxy-*N*-[5-(pyrrolidin-1-yl)pentyl]quinazolin-4-amine (25) (Ma et al., 2014)

According to GP1 with **24** (264 mg, 1.00 mmol, 1.0 equiv), 5-pyrrolidin-1-ylpentan-1-amine (172 mg, 1.10 mmol, 1.1 equiv) and DIEA (533 µL, 396 mg, 3.00 mmol, 3.0 equiv) in THF (4.0 mL). Purification by flash chromatography [10% to 15% 3 M NH_3 (in MeOH) in CH_2Cl_2] afforded **25** as colorless solid (308 mg, 81% yield, 95% purity). mp.: 54 °C. R_f = 0.30 [10% 3 M in NH_3 MeOH) in CH_2Cl_2]. IR (film): ṽ = 1624, 1512, 1429, 1244 cm^{-1}. ^{1}H NMR (500 MHz, CD_2Cl_2): δ = 1.42–1.52 (m, 2 H, C*H*$_2$CH$_2$CH$_2$NH), 1.52–1.62 [m, 2 H, C*H*$_2$(CH$_2$)$_3$NH], 1.68–1.79 [m, 6 H, C*H*$_2$(CH$_2$)$_3$NCH$_2$C*H*$_2$], 2.36–2.52 (m, 6 H, C*H*$_2$NC*H*$_2$), 3.62 (td, *J* = 7.1, 5.4 Hz, 2 H, C*H*$_2$NH), 3.93 (d, *J* = 1.5 Hz, 6 H, CH$_3$O), 5.99 (t, *J* = 5.5 Hz, 1 H, NH), 6.97 (s, 1 H, C*H*CCNH), 7.06 (s, 1 H, C*H*CCCNH). ^{13}C NMR (126 MHz, CD_2Cl_2): δ = 23.82 (*C*H$_2$CH$_2$N(CH$_2$)$_5$NH), 25.23 (*C*H$_2$CH$_2$CH$_2$NH), 28.94 [*C*H$_2$(CH$_2$)$_3$NH], 29.36 (*C*H$_2$CH$_2$NH), 41.97 (CH$_2$NH), 54.47 (*C*H$_2$N(CH$_2$)$_5$NH), 56.39 (*C*H$_2$(CH$_2$)$_4$NH), 56.47 (CH$_3$O)*, 56.65 (CH$_3$O)*, 100.58 (C*H*CCNH), 107.25 (*C*CNH), 107.51 (*C*HCCCNH), 148.29 (*C*CCNH), 149.54 (*C*CHCCNH), 155.44 (*C*CHCCCNH), 156.40 (CCl), 160.42 (CNH). HRMS-ESI m/z [M+H]$^+$ calcd. for $C_{19}H_{28}ClN_4O_2$: 379.1901, found: 379.1894.

2-Chloro-*N*-(1-cyclohexylpiperidin-4-yl)-6,7-dimethoxyquinazolin-4-amine (26) (Sundriyal et al., 2017)

According to GP1 with **24** (132 mg, 0.500 mmol, 1.0 equiv), 1-cyclohexylpiperidin-4-amine (102 mg, 0.550 mmol, 1.1 equiv) and DIEA (267 µL, 198 mg, 1.50 mmol, 3.0 equiv) in THF (2.0 mL). Purification by flash chromatography [5% 3 M NH_3 (in MeOH) in CH_2Cl_2] afforded **26** as colorless solid (132 mg, 65% yield, 99% purity). mp.: 169 °C. R_f = 0.23 [5% 4 M NH_3 (in MeOH) in CH_2Cl_2]. IR (film): ṽ = 2925, 2360, 1585, 1508, 1254 cm^{-1}. ^{1}H NMR (500 MHz, $CDCl_3$): δ = 1.03–1.18 (m, 1 H, C*H*$_2$CH$_2$CH$_2$CHN), 1.18–1.32 (m, 4 H, C*H*$_2$C*H*$_2$CHN), 1.53–1.70 (m, 3 H, C*H*$_2$CH$_2$CH$_2$CHN, C*H*$_2$CHNH), 1.74–1.93 (m, 4 H, C*H*$_2$C*H*$_2$CHN), 2.13–2.22 (m, 2 H, C*H*$_2$CHNH), 2.29–2.40 (m, 1 H, CHN), 2.40–2.53 (m, 2 H, CH$_2$N), 2.90–3.00 (m, 2 H, CH$_2$N), 3.97 (s, 3 H, C*H*$_3$OCCHCN), 3.99 (s, 3 H, C*H*$_3$OCCHCCN), 4.16–4.32 (m, 1 H, C*H*NH), 5.26–5.35 (m, 1 H, NH), 6.77 (s, 1 H, C*H*CCNH), 7.13 (s, 1 H, C*H*CCCNH). ^{13}C NMR (126 MHz, $CDCl_3$): δ = 26.20 (*C*H$_2$CH$_2$CHN), 26.50 (*C*H$_2$CH$_2$CH$_2$CHN), 29.05 (*C*H$_2$CHN), 32.91 (*C*H$_2$CHNH), 48.07 (CH$_2$N), 48.8 (*C*HNH), 56.40 (CH$_3$O), 56.52(CH$_3$O), 63.95 (CHN),

99.62 (*C*HCCNH), 106.78 (*C*CNH), 107.56 (*C*HCCCNH), 148.25 (*C*CCNH), 149.17 ($CH_3OCCHCCNH$), 155.11 ($CH_3OCCHCCCNH$), 156.38 (CCl), 159.20 (CNH). The characterization data of **26** match the reported (Sundriyal et al., 2017).

2-Chloro-*N*-(1-isopropylpiperidin-4-yl)-6,7-dimethoxyquinazolin-4-amine (27) (Somnarin et al., 2022; Wang et al., 2019)

According to GP1 with **24** (1.32 g, 5.00 mmol, 1.0 equiv), 1-propan-2-ylpiperidin-4-amine (869 mL, 782 mg, 5.50 mmol, 1.1 equiv) and DIEA (2.67 mL, 1.98 g, 15.0 mmol, 3.0 equiv) in THF (20 mL). Purification by flash chromatography [5% to 10% 3 M NH_3 (in MeOH) in CH_2Cl_2] afforded **27** as pale yellow solid (1.79 g, 98% yield, 98% purity). mp.: 106 °C. R_f = 0.32 [10% 3 M NH_3 (in MeOH) in CH_2Cl_2]. IR (film): $\tilde{\nu}$ = 2964, 1585, 1512, 1254 cm^{-1}. ^1H NMR (500 MHz, $CDCl_3$): δ = 1.04 (d, *J* = 6.6 Hz, 6 H, CH_3CH), 1.59 (qd, *J* = 11.8, 3.8 Hz, 2 H, CH_2CHNH), 2.07–2.19 (m, 2 H, CH_2CHNH), 2.34 (td, *J* = 11.8, 2.5 Hz, 2 H, CH_2N), 2.75 (hept, *J* = 6.6 Hz, 1 H, CH_3CH), 2.87 (dt, *J* = 12.1, 3.8 Hz, 2 H, CH_2N), 3.92 (d, *J* = 4.0 Hz, 6 H, CH_3O), 4.23 (tdt, *J* = 11.6, 8.2, 4.2 Hz, 1 H, C*H*NH), 5.71 (d, *J* = 7.8 Hz, 1 H, NH), 6.90 (s, 1 H, C*H*CCNH), 7.07 (s, 1 H, CHCN). ^{13}C NMR (126 MHz, $CDCl_3$): δ = 18.47 (CH_3CH), 32.57 (CH_2CHNH), 47.66 (CH_2N), 48.91 (CHNH), 54.62 (CH_3CH), 56.31 (CH_3O), 56.41 (CH_3O), 100.03 (*C*HCCNH), 106.88 (*C*CNH), 107.26 (*C*HCN), 148.10 (*C*CCNH), 149.07 (*C*CHCCNH), 155.00 (*C*CHCN), 156.30 (CCl), 159.29 (CNH). HRMS-ESI m/z $[M+H]^+$ calcd. for $C_{18}H_{26}ClN_4O_2$: 365.1744, found: 365.1741.

6,7-Dimethoxy-2-(4-methyl-1,4-diazepan-1-yl)-*N*-[5-(pyrrolidin-1-yl)pentyl]quinazolin-4-amine (28a)

According to GP2 with **25** (152 mg, 0.400 mmol, 1.0 equiv) and 1-methyl-1,4-diazepane (256 µL, 235 mg, 2.00 mmol, 5.0 equiv) in toluene (2.0 mL). **28a** was isolated by flash chromatography [7% to 12% 3 M NH_3 (in MeOH) in CH_2Cl_2] as yellow, hygroscopic solid (165 mg, 90% yield, 97% purity). mp.: 57 °C. R_f = 0.22 [10% 3 M NH_3 (in MeOH) in CH_2Cl_2]. IR (film): $\tilde{\nu}$ = 2935, 1630, 1583, 1495, 1240, 752 cm^{-1}. ^1H NMR (500 MHz, CD_2Cl_2): δ = 1.42–1.51 (m, 2 H, C$H_2CH_2CH_2NH$), 1.52–1.62 [m, 2 H, C$H_2(CH_2)_3NH$], 1.66–1.78 [m, 6 H, C$H_2CH_2N(CH_2)_3CH_2$], 1.91–2.01 (m, 2 H, $NCH_2CH_2CH_2NC$), 2.32 (s, 3 H, CH_3N), 2.42–2.55 [m, 8 H, $NCH_2CH_2CH_2NC$, C$H_2NCH_2(CH_2)_4NH$], 2.62–2.69 (m, 2 H, NCH_2CH_2NC), 3.53–3.60 (m, 2 H, CH_2NH), 3.81–3.86 (m, 2 H, $NCH_2CH_2CH_2NC$), 3.87 (s, 3 H, CH_3OCCHCCNH), 3.90 (s, 3 H, CH_3OCCHCCCNH), 3.91–3.96 (m, 2 H, NCH_2CH_2NC), 5.38 (s, 1 H, NH), 6.79 (s, 1 H, C*H*CCCNH), 6.80 (s, 1 H, C*H*CCNH). ^{13}C NMR (126 MHz, CD_2Cl_2): δ = 23.85 ($CH_2CH_2N(CH_2)_5NH$), 25.52 ($CH_2CH_2CH_2NH$), 28.43 ($NCH_2CH_2CH_2NC$), 29.03 [$CH_2(CH_2)_3NH$], 29.80 (CH_2CH_2NH), 41.61 (CH_2NH), 46.28 ($NCH_2CH_2CH_2NC$), 46.36 (NCH_2CH_2NC), 46.94 (CH_3N), 54.49 ($CH_2N(CH_2)_5NH$), 56.14 ($CH_3OCCHCCCNH$), 56.65 ($CH_2(CH_2)_4NH$, $CH_3OCCHCCNH$), 57.68 ($NCH_2CH_2CH_2NC$), 59.20 (NCH_2CH_2NC), 101.62 (*C*HCCNH), 103.14 (*C*CNH), 106.20 (*C*HCCCNH), 145.43 (*C*CHCCNH), 149.90 (*C*CCNH), 154.86 (*C*CHCCCNH), 159.02 (*C*NCNH), 159.26 (CNH). HRMS-EI m/z $[M]^+$ calcd. for $C_{25}H_{40}N_6O_2$: 456.3213, found: 456.3210.

***N*-(1-Cyclohexylpiperidin-4-yl)-6,7-dimethoxy-2-(4-methyl-1,4-diazepan-1-yl)quinazolin-4-amine (28b)** (Sundriyal et al., 2017)

According to GP2 with **26** (60.7 mg, 0.150 mmol, 1.0 equiv) and 1-methyl-1,4-diazepane (96.2 µL, 88.3 mg, 0.750 mmol, 5.0 equiv) in toluene (0.3 mL). **28b** was isolated by flash chromatography [10% 3 M NH_3 (in MeOH) in CH_2Cl_2] as yellow solid (67.8 mg, 94% yield, 97% purity). mp.: 94 °C. R_f = 0.49 [10% 4 M NH_3 (in MeOH) in CH_2Cl_2]. IR (film): $\tilde{\nu}$ = 2931, 1579, 1427, 1246 cm^{-1}. ^1H NMR (500 MHz, CD_2Cl_2): δ = 1.05–1.17 (m, 1 H, CH_2CH$_2$CH$_2$CHN), 1.19–1.34 (m, 4 H, CH$_2$CH_2CH_2CHN), 1.46–1.58 (m, 2 H, CH$_2$CH_2CHNH), 1.58–1.66 (m, 1 H, CH_2CH$_2$CH$_2$CHN), 1.75–1.86 (m, 4 H, CH$_2$CH_2CH_2CHN), 1.89–1.99 (m, 2 H, CH$_3$NCH$_2$CH_2CH$_2$N), 2.09–2.20 (m, 2 H, CH$_2$CH_2CHNH), 2.27–2.36 (m, 4 H, CH$_3$N, CHN), 2.36–2.44 (m, 2 H, CH_2CH$_2$CHNH), 2.47–2.55 (m, 2 H, CH$_3$NCH_2CH$_2$CH$_2$N), 2.61–2.68 (m, 2 H, CH$_3$NCH_2CH$_2$N), 2.87–2.95 (m, 2 H, CH_2CH$_2$CHNH), 3.83 (t, J = 6.4, 6.4 Hz, 2 H, CH$_3$NCH$_2$CH$_2$CH_2N), 3.87 (s, 3 H, CH_3OCCHCCNH), 3.88–3.94 (m, 5 H, CH$_3$NCH$_2$CH_2N, CH_3OCCHCCCNH), 3.97–4.12 (m, 1 H, CHNH), 5.08 (d, J = 7.2 Hz, 1 H, NH), 6.75 (s, 1 H, CHCCNH), 6.79 (s, 1 H, CHCCCNH). ^{13}C NMR (126 MHz, CD_2Cl_2): δ = 26.51 (CH$_2$$CH_2CH_2$CHN), 26.86 ($CH_2CH_2CH_2$CHN), 28.41 (CH$_3NCH_2$$CH_2CH_2$N), 29.30 (CH$_2CH_2$$CH_2$CHN), 33.31 (CH$_2$$CH_2$CHNH), 46.25 (CH$_3NCH_2CH_2$$CH_2$N), 46.41 (CH$_3NCH_2$$CH_2$N), 46.92 (CH$_3$N), 48.56 ($CH_2CH_2$CHNH), 49.34 (CH$_2CH_2$$C$HNH), 56.13 ($CH_3$OCCHCCCNH), 56.67 ($CH_3$OCCHCCNH), 57.65 (CH$_3NCH_2CH_2CH_2$N), 59.15 (CH$_3NCH_2CH_2$N), 64.13 (CHN), 101.56 (CHCCNH), 103.05 (CCNH), 106.23 (CHCCCNH), 145.42 (CH$_3$OCCHCCNH), 150.03 (CCCNH), 154.91 (CH$_3$OCCHCCCNH), 158.49 (CNH), 158.98 (CNCNH). HRMS-ESI m/z $[M+H]^+$ calcd. for $C_{27}H_{43}N_6O_2$: 483.3447, found: 483.3442.

_N_-(1-Isopropylpiperidin-4-yl)-6,7-dimethoxy-2-(4-methyl-1,4-diazepan-1-yl)-quinazolin-4-amine (28c) (Sundriyal et al., 2017)

According to GP2 with **27** (91.2 mg, 0.250 mmol, 1.0 equiv) and 1-methyl-1,4-diazepane (160 µL, 147 mg, 1.25 mmol, 5.0 equiv) in toluene (0.5 mL). **28c** was isolated by flash chromatography [5% 3 M NH_3 (in MeOH) in CH_2Cl_2] as yellow solid (107 mg, 97% yield, 97% purity). mp.: 89 °C. R_f = 0.57 [15% 3 M NH_3 (in MeOH) in CH_2Cl_2]. IR (film): $\tilde{\nu}$ = 2935, 1579, 1495, 1246 cm^{-1}. ^1H NMR (500 MHz, $CDCl_3$): δ = 1.09 (d, J = 6.6 Hz, 6 H, CH_3CH), 1.55–1.69 (m, 2 H, CH_2CHNH), 2.02 (p, J = 6.2 Hz, 2 H, CH_2CH$_2$NCH$_3$), 2.13–2.22 (m, 2 H, CH_2CHNH), 2.29–2.37 (m, 2 H, CH_2NCH), 2.37 (s, 3 H, CH$_3$N), 2.52–2.62 (m, 2 H, NCH$_2$CH$_2$CH_2NCH$_3$), 2.67–2.74 (m, 2 H, NCH$_2$CH_2NCH$_3$), 2.78 (h, J = 6.6 Hz, 1 H, CH$_3$CH), 2.89–2.99 (m, 2 H, CH_2NCH), 3.88 (t, J = 6.4 Hz, 2 H, NCH_2CH$_2$CH$_2$NCH$_3$), 3.92 (s, 3 H, CH_3OCCHCCN), 3.94 (s, 3 H, CH_3OCCHCN), 3.96–4.00 (m, 2 H, NCH_2CH$_2$NCH$_3$), 4.02–4.13 (m, 1 H, CHNH), 5.02 (d, J = 7.2 Hz, 1 H, NH), 6.71 (s, 1 H, CHCCN), 6.90 (s, 1 H, CHCN). ^{13}C NMR (126 MHz, $CDCl_3$): δ = 18.70 (CH$_3$CH), 27.93 (NCH$_2$$CH_2CH_2NCH_3$), 32.61 ($CH_2$CHNH), 45.93 (NCN$CH_2$), 46.02 (NCN$CH_2$), 46.84 (CH$_3$N), 47.93 ($CH_2$NCH), 48.72 (CHNH), 54.80 (CH$_3$$C$H), 56.11 ($CH_3$OCCHCN), 56.51 ($CH_3$OCCHCCN), 57.50 (NCH$_2CH_2$$CH_2NCH_3$), 59.07 (NCH$_2$$CH_2NCH_3$), 100.91 ($C$HCCN), 102.88 ($C$CNH), 106.14 ($C$HCN), 145.16 (CH$_3OC$CHCCN), 149.57 ($C$CCNH), 154.46 (CH$_3OC$CHCN), 158.16 (CNH), 158.67 (CNCNH). HRMS-ESI m/z $[M+H]^+$ calcd. for $C_{24}H_{39}N_6O_2$: 443.3134, found: 443.3127.

4-Chloro-6,7-dimethoxy-2-(piperidin-1-yl)quinazoline (29)

According to GP7 with **24** (793 mg, 3.00 mmol, 1.0 equiv) and 1-methylpiperidine (733 µL, 601 mg, 6.00 mmol, 2.0 equiv) in 1,4-dioxane (7.5 mL). **29** was isolated by flash chromatography (CH_2Cl_2) as yellow solid (744 mg, 81% yield, 95% purity). mp.: 126 °C.

R_f = 0.34 (CH_2Cl_2). IR (film): $\tilde{\nu}$ = 2935, 2852, 1585, 1495, 1238, 754 cm^{-1}. ^1H NMR (500 MHz, CD_2Cl_2): δ = 1.57–1.65 (m, 4 H, CH_2CH_2N), 1.65–1.72 (m, 2 H, CH_2CH_2CH_2N), 3.77–3.86 (m, 4 H, CH_2N), 3.92 (s, 3 H, CH_3OCCHCCCl), 3.95 (s, 3 H, CH_3OCCHCCCCl), 6.88 (s, 1 H, CHCCCCl), 7.16 (s, 1 H, CHCCCl). ^{13}C NMR (126 MHz, CD_2Cl_2): δ = 25.27 (*C*H_2CH_2CH_2N), 26.23 (*C*H_2CH_2N), 45.49 (CH_2N), 56.36 (*C*H_3OCCHCCCl), 56.55 (*C*H_3OCCHCCCCl), 103.99 (*C*HCCCl), 105.11 (*C*HCCCCl), 112.31 (*C*CCl), 147.73 (*C*CHCCCl), 151.97 (*C*CCCl), 157.41 (*C*CHCCCCl), 158.10 (*C*NCCl), 159.85 (CCl). HRMS-ESI m/z $[M+H]^+$ calcd. for $C_{15}H_{19}ClN_3O_2$: 308.1166, found: 308.1161.

6,7-Dimethoxy-2-(piperidin-1-yl)-*N*-[5-(pyrrolidin-1-yl)pentyl]quinazolin-4-amine (30a)
(Ma et al., 2014)

According to GP4 with **29** (123 mg, 0.400 mmol, 1.0 equiv), 5-pyrrolidin-1-ylpentan-1-amine (125 mg, 0.800 mmol, 2.0 equiv) and DIEA (213 µL, 158 mg, 1.20 mmol, 3.0 equiv) in *i*-PrOH (2.0 mL) for 15 min. **30a** (144 mg, 84% yield, 95% purity) was isolated by flash chromatography [5% to 7% 3 M NH_3 (in MeOH) in CH_2Cl_2] as pale yellow, hygroscopic solid. mp.: 58 °C. R_f = 0.15 [5% 3 M NH_3 (in MeOH) in CH_2Cl_2]. IR (film): $\tilde{\nu}$ = 2933, 1583, 1215, 756 cm^{-1}. ^1H NMR (500 MHz, CD_2Cl_2): δ = 1.40–1.50 (m, 2 H, CH_2CH_2CH_2NH), 1.51–1.62 [m, 6 H, CH_2CH_2CH_2NC, CH_2(CH_2)$_3$NH], 1.62–1.69 (m, 2 H, CH_2CH_2CH_2NC), 1.69–1.78 [m, 6 H, CH_2CH_2N(CH_2)$_3$CH_2], 2.35–2.49 (m, 6 H, CH_2NCH_2), 3.51–3.61 (m, 2 H, CH_2NH), 3.74–3.83 (m, 4 H, CH_2CH_2CH_2NC), 3.87 (s, 3 H, CH_3OCCHCCNH), 3.90 (s, 3 H, CH_3OCCHCCCNH), 5.29 (t, *J* = 6.5 Hz, 1 H, NH), 6.77 (s, 1 H, C*H*CCNH), 6.80 (s, 1 H, C*H*CCCNH). ^{13}C NMR (126 MHz, CD_2Cl_2): δ = 23.86 (*C*H_2CH_2N(CH_2)$_5$NH), 25.56 (*C*H_2CH_2CH_2NH)*, 25.59 (*C*H_2CH_2CH_2NC)*, 26.42 (CH_2*C*H_2CH_2NC), 29.23 [*C*H_2(CH_2)$_3$NH], 29.85 (*C*H_2CH_2NH), 41.61 (CH_2NH), 45.31 (CH_2CH_2*C*H_2NC), 54.50 (*C*H_2N(CH_2)$_5$NH), 56.14 (*C*H_3OCCHCCCNH), 56.60 (*C*H_3OCCHCCNH), 56.69 (*C*H_2(CH_2)$_4$NH), 101.48 (*C*HCCNH), 103.22 (*C*CNH), 106.27 (*C*HCCCNH), 145.63 (*C*CHCCNH), 149.79 (*C*CCNH), 154.88 (*C*CHCCCNH), 159.29 (*C*NCNH)**, 159.38 (CNH)**. HRMS-EI m/z $[M]^+$ calcd. for $C_{24}H_{37}N_5O_2$: 427.2947, found: 427.2940.

***N*-(1-Isopropylpiperidin-4-yl)-6,7-dimethoxy-2-(piperidin-1-yl)quinazolin-4-amine (30b)**
(Sundriyal et al., 2017)

According to GP4 with **29** (123 mg, 0.400 mmol, 1.0 equiv), 1-propan-2-ylpiperidin-4-amine (126 µL, 114 mg, 0.800 mmol, 2.0 equiv) and DIEA (213 µL, 158 mg, 1.20 mmol, 3.0 equiv) in *i*-PrOH (2.0 mL) for 15 min. **30b** (106 mg, 64% yield, 97% purity) was isolated by flash chromatography [5% to 7% 3 M NH_3 (in MeOH) in CH_2Cl_2] as colorless solid. mp.: 87 °C. R_f = 0.15 [5% 3 M NH_3 (in MeOH) in CH_2Cl_2]. IR (film): $\tilde{\nu}$ = 2935, 1579, 1493, 1246, 754 cm^{-1}. ^1H NMR (500 MHz, CD_2Cl_2): δ = 1.04 (d, *J* = 6.6 Hz, 6 H, CH_3CH), 1.39–1.76 (m, 8 H, CH_2CH_2CH_2NC, CH_2CHNH), 2.08–2.21 (m, 2 H, CH_2CHNH), 2.28–2.39 (m, 2 H, CH_2CH_2CHNH), 2.76 (hept, *J* = 6.6 Hz, 1 H, CH_3C*H*), 2.83–2.94 (m, 2 H, CH_2CH_2CHNH), 3.73–3.81 (m, 4 H, CH_2NC), 3.88 (s, 3 H, CH_3OCCHCCNH), 3.90 (s, 3 H, CH_3OCCHCCCNH), 4.02–4.16 (m, 1 H, C*H*NH), 5.03 (d, *J* = 7.2 Hz, 1 H, NH), 6.73 (s, 1 H, C*H*CCNH), 6.80 (s, 1 H, C*H*CCCNH). ^{13}C NMR (126 MHz, CD_2Cl_2): δ = 18.49 (*C*H_3CH), 25.59 (*C*H_2CH_2CH_2NC), 26.40 (*C*H_2CH_2NC), 33.12 (*C*H_2CHNH), 45.35 (*C*H_2NC), 48.07 (*C*H_2CH_2CHNH), 49.12 (CHNH), 54.88 (CH_3*C*H), 56.15 (*C*H_3OCCHCCCNH), 56.68 (*C*H_3OCCHCCNH), 101.44 (*C*HCCNH), 103.13 (*C*CNH), 106.29 (*C*HCCCNH), 145.66 (CH_3O*C*CHCCNH), 149.89 (*C*CCNH), 154.95

(*C*CHCCCNH), 158.60 (CNH), 159.25 (*C*NCNH). HRMS-EI m/z $[M]^+$ calcd. for $C_{23}H_{35}N_5O_2$: 413.2791, found: 413.2781.

N-(1-Cyclohexylpiperidin-4-yl)-2-(4-isopropyl-1,4-diazepan-1-yl)-6,7-dimethoxyquinazolin-4-amine (31)

According to GP2 with **26** (40.5 mg, 0.100 mmol, 1.0 equiv) and 1-propan-2-yl-1,4-diazepane (81.1 µL, 72.6 mg, 0.500 mmol, 5.0 equiv) in toluene (0.5 mL). **31** was isolated by flash chromatography [5% 3 M NH_3 (in MeOH) in CH_2Cl_2] as red solid (52.6 mg, > 99% yield, 95% purity). mp.: 86 °C. R_f = 0.17 [5% 4 M NH_3 (in MeOH) in CH_2Cl_2]. IR (film): $\tilde{\nu}$ = 2929, 1579, 1496, 1248 cm^{-1}. ^1H NMR (500 MHz, $CDCl_3$): δ = 1.01 (d, *J* = 6.5 Hz, 6 H, C*H*$_3$CH), 1.05–1.19 (m, 1 H, C*H*$_2$CH$_2$CH$_2$CHN), 1.19–1.34 (m, 4 H, CH$_2$C*H*$_2$CHN), 1.52–1.62 (m, 2 H, C*H*$_2$CHNH), 1.62–1.68 (m, 1 H, C*H*$_2$CH$_2$CH$_2$CHN), 1.75–1.86 (m, 2 H, C*H*$_2$CH$_2$CHN), 1.86–2.00 (m, 4 H, NCH$_2$C*H*$_2$CH$_2$NC, C*H*$_2$CHN), 2.14–2.22 (m, 2 H, C*H*$_2$CHNH), 2.29–2.37 (m, 1 H, CH$_2$C*H*N), 2.37–2.45 (m, 2 H, C*H*$_2$CH$_2$CHNH), 2.51–2.64 (m, 2 H, NC*H*$_2$CH$_2$CH$_2$NC), 2.72–2.82 (m, 2 H, NC*H*$_2$CH$_2$NC), 2.87–3.01 (m, 3 H, CH$_3$C*H*, C*H*$_2$CH$_2$CHNH), 3.84–3.90 (m, 2 H, NCH$_2$CH$_2$C*H*$_2$NC), 3.90–3.95 (m, 5 H, NCH$_2$C*H*$_2$NC, C*H*$_3$OCCHCCN), 3.95 (s, 3 H, C*H*$_3$OCCHCCCN), 4.02–4.12 (m, 1 H, C*H*NH), 4.90 (d, *J* = 7.1 Hz, 1 H, NH), 6.68 (s, 1 H, CHCCN), 6.88 (s, 1 H, CHCCCN). ^{13}C NMR (126 MHz, $CDCl_3$): δ = 18.68 (*C*H$_3$CH), 26.22 (CH$_2$*C*H$_2$CH$_2$CHN), 26.53 (*C*H$_2$CH$_2$CH$_2$CHN), 28.83 (NCH$_2$*C*H$_2$CH$_2$NC), 29.12 (CH$_2$CH$_2$*C*H$_2$CHN), 33.01 (CH$_2$*C*H$_2$CHNH), 45.84 (NCH$_2$CH$_2$*C*H$_2$NC), 47.81 (NCH$_2$*C*H$_2$NC), 48.34 (*C*H$_2$CH$_2$CHNH), 48.89 (CHNH), 50.77 (N*C*H$_2$CH$_2$CH$_2$NC), 52.33 (N*C*H$_2$CH$_2$NC), 55.30 (CH$_3$*C*H), 56.13 (*C*H$_3$OCCHCCCN), 56.55 (*C*H$_3$OCCHCCN), 63.97 (CH$_2$*C*HN), 100.89 (*C*HCCN), 102.87 (*C*CN), 106.28 (*C*HCCCN), 145.04 (CH$_3$O*C*CHCCN), 149.89 (*C*CCNH), 154.43 (CH$_3$O*C*CHCCCN), 158.19 (CNH), 158.86 (*C*NCNH). HRMS-ESI m/z $[M+H]^+$ calcd. for $C_{29}H_{47}N_6O_2$: 511.3760, found: 511.3755.

2-[(1,4'-Bipiperidin)-1'-yl]-*N*-(1-isopropylpiperidin-4-yl)-6,7-dimethoxyquinazolin-4-amine (32a)

According to GP2 with **27** (109 mg, 0.300 mmol, 1.0 equiv) and 1-piperidin-4-ylpiperidine (260 mg, 1.50 mmol, 5.0 equiv) in toluene (1.5 mL). **32a** was isolated by flash chromatography [5% to 10% 3 M NH_3 (in MeOH) in CH_2Cl_2] as pale yellow solid (135 mg, 91% yield, 95% purity). mp.: 107 °C. R_f = 0.36 [10% 3 M NH_3 (in MeOH) in CH_2Cl_2]. IR (film): $\tilde{\nu}$ = 2929, 2360, 1579, 1246, 754 cm^{-1}. ^1H NMR (500 MHz, CD_2Cl_2): δ = 1.04 (d, *J* = 6.6 Hz, 6 H, C*H*$_3$CH), 1.38–1.50 (m, 4 H, C*H*$_2$CH$_2$CH$_2$NCHC*H*$_2$CH$_2$NC), 1.50–1.57 (m, 6 H, CH$_2$C*H*$_2$CH$_2$NCH, C*H*$_2$CHNH), 1.78–1.87 (m, 2 H, CHC*H*$_2$CH$_2$NC), 2.10–2.20 (m, 2 H, C*H*$_2$CHNH), 2.26–2.39 (m, 2 H, C*H*$_2$CH$_2$CHNH), 2.41–2.56 (m, 5 H, CH$_2$CH$_2$C*H*$_2$NC*H*), 2.68–2.82 (m, 3 H, CH$_2$NC, CH$_3$C*H*), 2.83–2.96 (m, 2 H, C*H*$_2$CH$_2$CHNH), 3.88 (s, 3 H, C*H*$_3$OCCHCCNH), 3.90 (s, 3 H, C*H*$_3$OCCHCN), 4.08 (dtd, *J* = 11.2, 7.0, 3.8 Hz, 1 H, C*H*NH), 4.80–4.93 (m, 2 H, CH$_2$NC), 5.05 (d, *J* = 7.2 Hz, 1 H, NH), 6.73 (s, 1 H, C*H*CCNH), 6.80 (s, 1 H, C*H*CCCNH). ^{13}C NMR (126 MHz, CD_2Cl_2): δ = 18.51 (*C*H$_3$CH), 25.38 (*C*H$_2$CH$_2$CH$_2$NCH), 26.99 (CH$_2$*C*H$_2$CH$_2$NCH), 28.45 (CH*C*H$_2$CH$_2$NC), 33.13 (*C*H$_2$CHNH), 44.29 (CHCH$_2$*C*H$_2$NC), 48.07 (*C*H$_2$CH$_2$CHNH), 49.16 (CHNH), 50.62 (CH$_2$CH$_2$*C*H$_2$NCH), 54.83 (CH$_3$*C*H), 56.15 (*C*H$_3$OCCHCCCNH), 56.67 (*C*H$_3$OCCHCCNH), 63.72 (*C*HCH$_2$CH$_2$NC), 101.41 (*C*HCCNH), 103.20 (*C*CNH), 106.30 (*C*HCCCNH), 145.76 (*C*H$_3$O*C*CHCCNH), 149.83 (*C*CCNH), 154.96 (CH$_3$O*C*CHCCCNH),

158.64 (CNH), 159.08 (NCNCNH). HRMS-EI m/z $[M]^+$ calcd. for $C_{28}H_{44}N_6O_2$: 496.3526, found: 496.3518.

N-(1-Isopropylpiperidin-4-yl)-6,7-dimethoxy-2-[4-(3-methylpyridin-4-yl)-1,4-diazepan-1-yl]quinazolin-4-amine (32b)

According to GP2 with **27** (182 mg, 0.500 mmol, 1.0 equiv) and 1-(3-methylpyridin-4-yl)-1,4-diazepane (503 mg, 2.50 mmol, 5.0 equiv) in toluene (2.5 mL). **32b** was isolated by flash chromatography [5% 3 M NH_3 (in MeOH) in CH_2Cl_2] as pale yellow solid (174 mg, 67% yield, 98% purity). mp.: 76 °C. R_f = 0.44 [10% 3 M NH_3 (in MeOH) in CH_2Cl_2]. IR (film): $\tilde{\nu}$ = 2096, 1581, 1497, 1246, 754 cm^{-1}. ^1H NMR (500 MHz, CD_2Cl_2): δ = 1.04 (d, *J* = 6.6 Hz, 6 H, C*H*$_3$CH), 1.48–1.59 (m, 2 H, C*H*$_2$CHNH), 2.03–2.10 (m, 2 H, NCH$_2$C*H*$_2$CH$_2$NCH), 2.10–2.18 (m, 2 H, C*H*$_2$CHNH), 2.27 (s, 3 H, CH$_3$C), 2.30–2.35 (m, 2 H, C*H*$_2$CH$_2$CHNH), 2.75 (hept, *J* = 6.6 Hz, 1 H, CH$_3$C*H*), 2.85–2.91 (m, 2 H, C*H*$_2$CH$_2$CHNH), 3.24–3.29 (m, 2 H, NC*H*$_2$CH$_2$CH$_2$NCH), 3.43–3.48 (m, 2 H, NC*H*$_2$CH$_2$NC), 3.88 (s, 3 H, C*H*$_3$OCCHCCNH), 3.89–3.96 (m, 5 H, NCH$_2$CH$_2$C*H*$_2$NCH, C*H*$_3$OCCHCN), 4.01–4.12 (m, 3 H, NCH$_2$C*H*$_2$NC, C*H*NH), 5.09 (d, *J* = 7.2 Hz, 1 H, NH), 6.75 (s, 1 H, C*H*CCNH), 6.77 (d, *J* = 5.6 Hz, 1 H, C*H*CCCH$_3$), 6.81 (s, 1 H, C*H*CCCNH), 8.10–8.15 (m, 2 H, C*H*NC*H*CCH$_3$). ^{13}C NMR (126 MHz, CD_2Cl_2): δ = 18.05 (*C*H$_3$C), 18.50 (*C*H$_3$CH), 28.54 (NCH$_2$*C*H$_2$CH$_2$NCH), 33.19 (*C*H$_2$CHNH), 46.21 (NCH$_2$CH$_2$*C*H$_2$NCH), 48.09 (NCH$_2$*C*H$_2$NC, *C*H$_2$CH$_2$CHNH), 49.33 (CHNH), 52.74 (N*C*H$_2$CH$_2$CH$_2$NCH), 53.90 (N*C*H$_2$CH$_2$NC), 54.85 (CH$_3$*C*H), 56.16 (*C*H$_3$OCCHCN), 56.69 (*C*H$_3$OCCHCCNH), 101.47 (*C*HCCNH), 103.21 (*C*CNH), 106.29 (*C*HCCCNH), 112.87 (*C*HCCCH$_3$), 124.19 (CH$_3$*C*), 145.66 (CH$_3$O*C*CHCCNH), 148.43 (*C*HNCHCCH$_3$), 149.99 (*C*CCNH), 152.58 (*C*HCCH$_3$), 154.99 (CH$_3$O*C*CHCN), 158.60 (CNH), 158.70 (*C*NCH$_2$CH$_2$N*C*). HRMS-EI m/z $[M]^+$ calcd. for $C_{29}H_{41}N_7O_2$: 519.3322, found: 519.3317.

N-(1-Isopropylpiperidin-4-yl)-6,7-dimethoxy-2-[4-(4-methylpiperazin-1-yl)piperidin-1-yl]quinazolin-4-amine (32c)

According to GP2 with **27** (182 mg, 0.500 mmol, 1.0 equiv) and 1-methyl-4-piperidin-4-ylpiperazine (482 mg, 2.50 mmol, 5.0 equiv) in toluene (2.5 mL). **32c** was isolated by flash chromatography [7% to 10% 3 M NH_3 (in MeOH) in CH_2Cl_2] as pale yellow solid (214 mg, 84% yield, 98% purity). mp.: 111 °C. R_f = 0.22 [10% 3 M NH_3 (in MeOH) in CH_2Cl_2]. IR (film): $\tilde{\nu}$ = 2939, 2810, 1579, 1248, 752 cm^{-1}. ^1H NMR (500 MHz, CD_2Cl_2): δ = 1.10 (d, *J* = 6.6 Hz, 6 H, C*H*$_3$CH), 1.37–1.50 (m, 2 H, C*H*$_2$CH$_2$NC), 1.60–1.74 (m, 2 H, C*H*$_2$CHNH), 1.82–1.90 (m, 2 H, C*H*$_2$CH$_2$NC), 2.13–2.21 (m, 2 H, C*H*$_2$CHNH), 2.22 (s, 3 H, CH$_3$N), 2.27–2.51 (m, 7 H, C*H*NC*H*$_2$CH$_2$NCH$_3$, C*H*$_2$CH$_2$CHNH), 2.58 (s, 4 H, C*H*$_2$NCH$_3$), 2.74–2.84 (m, 2 H, C*H*$_2$NC), 2.84–2.91 (m, 1 H, CH$_3$C*H*), 2.91–3.02 (m, 2 H, C*H*$_2$CH$_2$CHNH), 3.88 (s, 3 H, C*H*$_3$OCCHCCNH), 3.90 (s, 3 H, C*H*$_3$OCCHCCCNH), 4.13 (dtd, *J* = 11.1, 7.0, 3.7 Hz, 1 H, C*H*NH), 4.78–4.88 (m, 2 H, C*H*$_2$NC), 5.15 (d, *J* = 7.3 Hz, 1 H, NH), 6.76 (s, 1 H, C*H*CCNH), 6.82 (s, 1 H, C*H*CCCNH). ^{13}C NMR (126 MHz, CD_2Cl_2): δ = 18.27 (*C*H$_3$CH), 28.78 (*C*H$_2$CH$_2$NC), 32.49 (*C*H$_2$CHNH), 44.05 (*C*H$_2$NC), 46.17 (CH$_3$N), 48.08 (*C*H$_2$CH$_2$CHNH), 48.75 (CHNH), 49.38 (*C*H$_2$NCH$_3$), 55.35 (CH$_3$*C*H), 55.98 (*C*H$_2$CH$_2$NCH$_3$), 56.17 (*C*H$_3$OCCHCCCNH), 56.68 (*C*H$_3$OCCHCCNH), 62.82 (*C*HNCH$_2$CH$_2$NCH$_3$), 101.41 (*C*HCCNH), 103.21 (*C*CNH), 106.23 (*C*HCCCNH), 145.86 (CH$_3$O*C*CHCCNH), 149.67 (*C*CCNH), 155.01 (CH$_3$O*C*CHCCCNH), 158.65 (CNH), 158.96 (*C*NCNH). HRMS-EI m/z $[M]^+$ calcd. for $C_{28}H_{45}N_7O_2$: 511.3635, found: 511.3628.

2-(4,4-Difluoropiperidin-1-yl)-*N*-(1-isopropylpiperidin-4-yl)-6,7-dimethoxyquinazolin-4-amine (32d) (Cui et al., 2020)

According to GP2 with **27** (182 mg, 0.500 mmol, 1.0 equiv) and 4,4-difluoropiperidine (319 mg, 2.50 mmol, 5.0 equiv) in toluene (2.5 mL). **32d** was isolated by flash chromatography [5% 3 M NH_3 (in MeOH) in CH_2Cl_2] as colorless solid (218 mg, 97% yield, 98% purity). mp.: 88 °C. R_f = 0.23 [5% 3 M NH_3 (in MeOH) in CH_2Cl_2]. IR (film): $\tilde{\nu}$ = 2968, 1581, 1495, 1211, 756 cm^{-1}. ^1H NMR (500 MHz, CD_2Cl_2): δ = 1.04 (d, J = 6.6 Hz, 6 H, CH_3CH), 1.51–1.59 (m, 2 H, CH_2CHNH), 1.90–2.06 (m, 4 H, CH_2CF_2), 2.09–2.19 (m, 2 H, CH_2CHNH), 2.27–2.41 (m, 2 H, CH_2CH_2CHNH), 2.76 (hept, J = 6.6 Hz, 1 H, CH_3CH), 2.83–2.92 (m, 2 H, CH_2CH_2CHNH), 3.89 (s, 3 H, CH_3OCCHCCNH), 3.91 (s, 3 H, CH_3OCCHCCCNH), 3.94–4.00 (m, 4 H, C$H_2CH_2CF_2$), 4.01–4.13 (m, 1 H, CHNH), 5.11 (d, J = 7.3 Hz, 1 H, NH), 6.75 (s, 1 H, CHCCNH), 6.83 (s, 1 H, CHCCCNH). ^{13}C NMR (126 MHz, CD_2Cl_2): δ = 18.49 (CH_3CH), 33.12 (CH_2CHNH), 34.19 (t, J = 22.3 Hz, CH_2CF_2), 41.49 (t, J = 5.0 Hz, $CH_2CH_2CF_2$), 48.04 (CH_2CH_2CHNH), 49.29 (CHNH), 54.84 (CH_3CH), 56.19 (CH_3OCCHCCCNH), 56.67 (CH_3OCCHCCNH), 101.24 (CHCCNH), 103.49 (CCNH), 106.43 (CHCCCNH), 123.51 (t, J = 241.2 Hz, CF_2), 146.23 (CCHCCNH), 149.58 (CCCNH), 155.09 (CCHCCCNH), 158.57 (CNCNH), 158.85 (CNH). HRMS-EI m/z $[M]^+$ calcd. for $C_{23}H_{33}F_2N_5O_2$: 449.2602, found: 449.2597.

***N*⁴-(1-Isopropylpiperidin-4-yl)-6,7-dimethoxyquinazoline-2,4-diamine (32e) and *N*-(1-isopropylpiperidin-4-yl)-6,7-dimethoxyquinazolin-4-amine (32f)**

According to GP3, with **27** (146 mg, 0.400 mmol, 1.0 equiv) and NaN_3 (28.6 mg, 0.440 mmol, 1.1 equiv) in EtOH/AcOH (4:1) (2.68 mL) and afterwards 10% Pd/C (47.4 mg, 40.0 µmol, 0.10 equiv) and hydrazine hydrate (30.0 µL, 30.0 mg, 0.600 mmol, 1.5 equiv). **32e** (108 mg, 78% yield, 96% purity) and **32f** (6.20 mg, 5% yield, 95% purity) were isolated by flash chromatography [5% to 10% (7 M NH_3 (in MeOH) in CH_2Cl_2] as colorless solids. **32e**: mp.: 113 °C. R_f = 0.27 [10% (7 M NH_3 (in MeOH) in CH_2Cl_2]. IR (film): $\tilde{\nu}$ = 1624, 1585, 1429, 1248, 754 cm^{-1}. ^1H NMR (500 MHz, CD_2Cl_2): δ = 1.03 (d, J = 6.6 Hz, 6 H, CH_3CH), 1.44–1.59 (m, 2 H, CH_2CH), 2.05–2.18 (m, 2 H, CH_2CH), 2.26–2.40 (m, 2 H, CH_2N), 2.75 (hept, J = 6.6 Hz, 1 H, CH_3CH), 2.82–2.94 (m, 2 H, CH_2N), 3.88 (s, 3 H, CH_3OCCHCCNH), 3.89 (s, 3 H, CH_3OCCHCCCNH), 4.12 (tdt, J = 10.6, 7.3, 3.9 Hz, 1 H, CHNH), 4.61 (s, 2 H, NH_2), 4.98–5.23 (m, 1 H, NH), 6.76 (s, 1 H, CHCCNH), 6.79 (s, 1 H, CHCCCNH). ^{13}C NMR (126 MHz, CD_2Cl_2): δ = 18.48 (CH_3CH), 33.28 (CH_2CH), 48.04 (CH_2N), 48.82 (CHNH), 54.79 (CH_3CH), 56.18 (CH_3OCCHCCCNH), 56.67 (CH_3OCCHCCNH), 101.34 (CHCCNH), 104.07 (CCNH), 106.14 (CHCCCNH), 146.29 (CCHCCNH), 149.31 (CCCNH), 155.07 (CCHCCCNH), 159.37 (CNH), 160.07 (CNH_2). HRMS-ESI m/z $[M+H]^+$ calcd. for $C_{18}H_{28}N_5O_2$: 346.2243, found: 346.2236. **32f**: mp.: 241 °C (decomposition). R_f = 0.39 [10% (7 M NH_3 (in MeOH) in CH_2Cl_2]. IR (film): $\tilde{\nu}$ = 1626, 1506, 1473, 1252 cm^{-1}. ^1H NMR (500 MHz, CD_2Cl_2): δ = 1.03 (d, J = 6.6 Hz, 6 H, CH_3CH), 1.51–1.65 (m, 2 H, CH_2CHNH), 2.04–2.20 (m, 2 H, CH_2CHNH), 2.27–2.42 (m, 2 H, CH_2CH_2CHNH), 2.75 (hept, J = 6.6 Hz, 1 H, CH_3CH), 2.80–2.95 (m, 2 H, CH_2CH_2CHNH), 3.94 (s, 3 H, CH_3OCCHCCNH), 3.95 (s, 3 H, CH_3OCCHCCCNH), 4.12–4.27 (m, 1 H, CHNH), 5.36 (d, J = 7.6 Hz, 1 H, NH), 6.89 (s, 1 H, CHCCNH), 7.14 (s, 1 H, CHCCCNH), 8.44 (s, 1 H, CHNCNH). ^{13}C NMR (126 MHz, CD_2Cl_2): δ = 18.45 (CH_3CH), 33.19 (CH_2CHNH), 48.02 (CH_2CH_2CHNH), 49.08 (CHNH), 54.81 (CH_3CH), 56.38 (CH_3O)*, 56.58 (CH_3O)*, 100.02

(*C*HCCNH), 108.12 (*C*HCCCNH), 108.86 (*C*CNH), 147.11 (*C*CCNH), 149.41 (*C*CHCCNH), 154.33 (*C*HNCNH), 154.81 (*C*CHCCCNH), 158.03 (CNH). HRMS-ESI m/z $[M+H]^+$ calcd. for $C_{18}H_{27}N_4O_2$: 331.2134, found: 331.2128.

7-(Benzyloxy)-4-chloro-6-methoxy-2-(piperidin-1-yl)quinazoline (33)

According to GP7 with **4** (138 mg, 0.400 mmol, 1.0 equiv) and 1-methylpiperidine (58.6 mL, 48.1 mg, 0.480 mmol, 1.2 equiv) in 1,4-dioxane (1.0 mL). **33** was isolated by flash chromatography (CH_2Cl_2) as yellow solid (132 mg, 86% yield, 100% purity). mp.: 162 °C. R_f = 0.84 (CH_2Cl_2). IR (film): $\tilde{\nu}$ = 2929, 1626, 1583, 1491, 1240 cm^{-1}. ^1H NMR (500 MHz, CD_2Cl_2): δ = 1.57–1.65 (m, 4 H, CH_2CH_2N), 1.65–1.73 (m, 2 H, CH_2CH_2CH_2N), 3.76–3.85 (m, 4 H, CH_2N), 3.93 (s, 3 H, CH_3O), 5.20 (s, 2 H, CH_2O), 6.95 (s, 1 H, C*H*COCH$_2$), 7.19 (s, 1 H, C*H*COCH$_3$), 7.34–7.40 (m, 1 H, C*H*CHCHCC), 7.40–7.45 (m, 2 H, C*H*CHC), 7.45–7.51 (m, 2 H, C*H*CCH$_2$O). ^{13}C NMR (126 MHz, CD_2Cl_2): δ = 25.27 (*C*H$_2$CH$_2$CH$_2$N), 26.24 (*C*H$_2$CH$_2$N), 45.48 (CH$_2$N), 56.45 (CH$_3$O), 71.22 (CH$_2$O), 104.25 (*C*HCOCH$_3$), 106.28 (*C*HCOCH$_2$), 112.45 (*C*CCl), 128.26 (*C*HCCH$_2$O), 128.76 (*C*HCHCHC), 129.08 (*C*HCHC), 136.37 (*C*CH$_2$O), 147.90 (*C*OCH$_3$), 151.83 (*C*CCCl), 156.43 (*C*OCH$_2$), 158.09 (*C*NCCl), 159.88 (CCl). HRMS-ESI m/z $[M+H]^+$ calcd. for $C_{21}H_{23}ClN_3O_2$: 384.1479, found: 384.1474.

7-(Benzyloxy)-6-methoxy-2-(piperidin-1-yl)-*N*-[5-(pyrrolidin-1-yl)pentyl]quinazolin-4-amine (34a)

According to GP4 with **33** (154 mg, 0.400 mmol, 1.0 equiv), 5-pyrrolidin-1-ylpentan-1-amine (125 mg, 0.800 mmol, 2.0 equiv) and DIEA (213 µL, 158 mg, 1.20 mmol, 3.0 equiv) in *i*-PrOH (2.0 mL) for 15 min. **34a** (173 mg, 86% yield, 99% purity) was isolated by flash chromatography [5% 3 M NH_3 (in MeOH) in CH_2Cl_2] as pale yellow, hygroscopic solid. mp.: 66 °C. R_f = 0.17 [5% 3 M NH_3 (in MeOH) in CH_2Cl_2]. IR (film): $\tilde{\nu}$ = 2933, 1579, 1491, 1244, 756 cm^{-1}. ^1H NMR (500 MHz, CD_2Cl_2): δ = 1.39–1.51 (m, 2 H, CH_2CH$_2$CH$_2$NH), 1.52–1.68 [m, 8 H, CH_2CH_2CH$_2$NC,CH_2(CH$_2$)$_3$NH], 1.68–1.78 [m, 6 H, CH_2CH$_2$N(CH$_2$)$_3$CH_2], 2.31–2.52 [m, 6 H, CH$_2$CH_2NCH_2(CH$_2$)$_4$NH], 3.53–3.61 (m, 2 H, CH_2NH), 3.74–3.82 (m, 4 H, CH$_2$CH$_2$CH_2NC), 3.89 (s, 3 H, CH$_3$O), 5.15 (s, 2 H, CH$_2$O), 5.37 (t, J = 5.5 Hz, 1 H, NH), 6.82 (s, 1 H, C*H*COCH$_3$), 6.86 (s, 1 H, C*H*COCH$_2$), 7.31–7.38 (m, 1 H, C*H*CHCHC), 7.38–7.44 (m, 2 H, C*H*CHC), 7.44–7.49 (m, 2 H, C*H*CCH$_2$O). ^{13}C NMR (126 MHz, CD_2Cl_2): δ = 23.83 [*C*H$_2$CH$_2$N(CH$_2$)$_5$NH], 25.52 (*C*H$_2$CH$_2$CH$_2$NH)*, 25.58 (*C*H$_2$CH$_2$CH$_2$NC)*, 26.42 (*C*H$_2$CH$_2$NC), 29.15 [*C*H$_2$(CH$_2$)$_3$NH], 29.76 (*C*H$_2$CH$_2$NH), 41.60 (*C*H$_2$NH), 45.31 (*C*H$_2$NC), 54.47 [*C*H$_2$N(CH$_2$)$_5$NH], 56.63 [*C*H$_2$(CH$_2$)$_4$NH], 56.75 (CH$_3$O), 70.83 (CH$_2$O), 101.94 (*C*HCOCH$_3$), 103.50 (*C*CNH), 107.51 (*C*HCOCH$_2$), 128.19 (*C*HCCH$_2$O), 128.51 (*C*HCHCHC), 128.98 (*C*HCHC), 137.03 (*C*CH$_2$O), 145.80 (*C*OCH$_3$), 149.64 (*C*CCNH), 153.95 (*C*OCH$_2$), 159.29 (*C*NCNH)*, 159.38 (CNH)*. HRMS m/z $[M]^+$ calcd. for $C_{30}H_{41}N_5O_2$: 503.3260, found: 503.2079.

7-(Benzyloxy)-*N*-(1-cyclohexylpiperidin-4-yl)-6-methoxy-2-(piperidin-1-yl)quinazolin-4-amine (34b)

According to GP4 with **33** (154 mg, 0.400 mmol, 1.0 equiv), 1-cyclohexylpiperidin-4-amine (146 mg, 0.800 mmol, 2.0 equiv) and DIEA (213 µL, 158 mg, 1.20 mmol, 3.0 equiv) in *i*-PrOH (2.0 mL) for 15 min. **34b** (145 mg, 68% yield, 99% purity) was isolated by flash

chromatography [5% 3 M NH_3 (in MeOH) in CH_2Cl_2] as colorless solid. mp.: 192 °C. R_f = 0.32 [5% 3 M NH_3 (in MeOH) in CH_2Cl_2]. IR (film): $\tilde{\nu}$ = 2931, 2852, 1579, 1491, 1246, 754 cm^{-1}. ^1H NMR (500 MHz, CD_2Cl_2): δ = 1.03–1.18 (m, 1 H, CH_2CH$_2$CH$_2$CH), 1.19–1.32 (m, 4 H, CH$_2$CH_2CH_2CH), 1.45–1.72 (m, 9 H, CH_2CH_2CH$_2$N, CH_2CHNH, CH_2CH$_2$CH$_2$CH), 1.74–1.90 (m, 4 H, CH$_2$CH_2CH_2CH), 2.09–2.20 (m, 2 H, CH_2CHNH), 2.27–2.36 (m, 1 H, CH$_2$CH$_2$CH$_2$C*H*), 2.38–2.46 (m, 2 H, CH_2NCH), 2.83–2.96 (m, 2 H, CH_2NCH), 3.71–3.82 (m, 4 H, CH$_2$CH$_2$CH_2N), 3.89 (s, 3 H, CH_3O), 3.99–4.15 (m, 1 H, C*H*NH), 5.05 (d, *J* = 7.2 Hz, 1 H, NH), 5.15 (s, 2 H, CH_2O), 6.77 (s, 1 H, C*H*COCH$_3$), 6.86 (s, 1 H, C*H*COCH$_2$), 7.32–7.38 (m, 1 H, C*H*CHCHC), 7.38–7.44 (m, 2 H, CHC*H*CHC), 7.44–7.50 (m, 2 H, CHCHC*H*C). ^{13}C NMR (126 MHz, CD_2Cl_2): δ = 25.58 (*C*H$_2$CH$_2$CH$_2$N), 26.41 (CH$_2$*C*H$_2$CH$_2$N)*, 26.51 (CH$_2$*C*H$_2$CH$_2$CH)*, 26.87 (*C*H$_2$CH$_2$CH$_2$CH), 29.29 (CH$_2$CH$_2$*C*H$_2$CH), 33.26 (*C*H$_2$CHNH), 45.33 (CH$_2$CH$_2$*C*H$_2$N), 48.54 (*C*H$_2$NCH), 49.18 (CHNH), 56.83 (CH_3O), 64.15 (CH$_2$CH$_2$CH$_2$*C*H), 70.83 (CH_2O), 101.86 (*C*HCOCH$_3$), 103.39 (*C*CNH), 107.56 (*C*HCOCH$_2$), 128.18 (CHCH*C*HC), 128.51 (*C*HCHCHC), 128.98 (CH*C*HCHC), 137.01 (*C*CH$_2$O), 145.83 (*C*OCH$_3$), 149.77 (*C*CCNH), 154.02 (*C*OCH$_2$), 158.58 (CNH), 159.26 (*C*NCNH). HRMS-ESI m/z $[M+H^+]^+$ calcd. for $C_{32}H_{44}N_5O_2$: 530.3495; found: 530.3499.

7-(Benzyloxy)-*N*-[1-(cyclohexylmethyl)piperidin-4-yl]-6-methoxy-2-(piperidin-1-yl)quinazolin-4-amine (34c)

According to GP4 with **33** (154 mg, 0.400 mmol, 1.0 equiv), 1-(cyclohexylmethyl)piperidin-4-amine (157 mg, 0.800 mmol, 2.0 equiv) and DIEA (213 µL, 158 mg, 1.20 mmol, 3.0 equiv) in *i*-PrOH (2.0 mL) for 15 min. **34c** (158 mg, 73% yield, 97% purity) was isolated by flash chromatography [5% to 10% 3 M NH_3 (in MeOH) in CH_2Cl_2] as colorless solid. mp.: 181 °C. R_f = 0.35 [5% 3 M NH_3 (in MeOH) in CH_2Cl_2]. IR (film): $\tilde{\nu}$ = 2924, 2360, 1576, 1491, 1246, 754 cm^{-1}. ^1H NMR (500 MHz, CD_2Cl_2): δ = 0.75–0.99 (m, 2 H, CH_2CHCH$_2$N), 1.12–1.34 (m, 3 H, CH_2CH_2CH$_2$CH), 1.41–1.53 (m, 1 H, C*H*CH$_2$N), 1.53–1.74 (m, 11 H, CH_2CH_2CH$_2$N, CH_2CHNH, CH_2CH_2CH$_2$CH), 1.75–1.81 (m, 2 H, CH_2CHCH$_2$N), 1.97–2.27 (m, 6 H, CH_2NCH_2CH_2CHNH), 2.68–2.98 (m, 2 H, CH_2CH$_2$CHNH), 3.71–3.83 (m, 4 H, CH$_2$NC), 3.89 (s, 3 H, CH_3O), 4.04–4.17 (m, 1 H, C*H*NH), 5.06 (d, *J* = 7.1 Hz, 1 H, NH), 5.15 (s, 2 H, CH_2O), 6.77 (s, 1 H, C*H*COCH$_3$), 6.87 (s, 1 H, C*H*COCH$_2$), 7.27–7.38 (m, 1 H, C*H*CHCHC), 7.38–7.43 (m, 2 H, CHC*H*CHC), 7.44–7.53 (m, 2 H, CHCHC*H*C). ^{13}C NMR (126 MHz, CD_2Cl_2): δ = 25.57 (*C*H$_2$CH$_2$CH$_2$N), 26.40 (CH$_2$*C*H$_2$CH$_2$N)*, 26.62 (CH$_2$*C*H$_2$CH$_2$CH)*, 27.30 (*C*H$_2$CH$_2$CH$_2$CH), 32.28 (CH$_2$CH$_2$*C*H$_2$CH), 32.72 (*C*H$_2$CHNH), 35.78 (CH$_2$CH$_2$CH$_2$*C*H), 45.35 (CH$_2$CH$_2$*C*H$_2$N), 48.88 (CHNH), 53.55 (*C*H$_2$CH$_2$CHNH), 56.82 (CH_3O), 66.06 (CH*C*H$_2$N), 70.84 (CH_2O), 101.83 (*C*HCOCH$_3$), 103.38 (*C*CNH), 107.52 (*C*HCOCH$_2$), 128.19 (CHCH*C*HC), 128.52 (*C*HCHCHC), 128.98 (CH*C*HCHC), 137.00 (CHCHCH*C*), 145.85 (*C*OCH$_3$), 149.70 (*C*CCNH), 154.03 (*C*OCH$_2$), 158.60 (CNH), 159.20 (*C*NCNH). HRMS-ESI m/z $[M+H^+]^+$ calcd. for $C_{33}H_{46}N_5O_2$: 544.3652; found: 544.3657.

Supplemental References

Cui, R., Yin, C., Deng, X., Zhang, T., 2020. STK19 inhibitors for treatment of cancer. Trustees of Boston University, Xiamen University.

Davis, I., Jin, J., Janzen, W.P., Pattenden, S., Jayakody, C., 2016. A novel compound for the treatment of ewing sarcoma and high-throughput assays for identifying small molecules that modulate aberrant chromatin accessibility. Google Patents.

Doig, P., Boriack-Sjodin, P.A., Dumas, J., Hu, J., Itoh, K., Johnson, K., Kazmirski, S., Kinoshita, T., Kuroda, S., Sato, T.-o., Sugimoto, K., Tohyama, K., Aoi, H., Wakamatsu, K., Wang, H., 2014. Rational design of inhibitors of the bacterial cell wall synthetic enzyme GlmU using virtual screening and lead-hopping. Bioorganic & Medicinal Chemistry 22, 6256-6269.

Jiang, Y.-H., Kim, Y., Lee, H.-M., Jin, J., Roth, B.L., 2017. Preparation of quinazolin-4-amine derivatives as histone methyltransferase G9a inhibitors and methods for the treatment of Prader-willi syndrome. Duke University, The University of North Carolina at Chapel Hill.

Kaiser, J., Gertzen, C.G.W., Bernauer, T., Nitsche, V., Höfner, G., Niessen, K.V., Seeger, T., Paintner, F.F., Wanner, K.T., Steinritz, D., Worek, F., Gohlke, H., 2024. Identification of ligands binding to MB327-PAM-1, a binding pocket relevant for resensitization of nAChRs. bioRxiv, p. 2023.2012.2021.572862.

Liu, F., Barsyte-Lovejoy, D., Allali-Hassani, A., He, Y., Herold, J.M., Chen, X., Yates, C.M., Frye, S.V., Brown, P.J., Huang, J., Vedadi, M., Arrowsmith, C.H., Jin, J., 2011. Optimization of Cellular Activity of G9a Inhibitors 7-Aminoalkoxy-quinazolines. Journal of Medicinal Chemistry 54, 6139-6150.

Ma, A., Yu, W., Li, F., Bleich, R.M., Herold, J.M., Butler, K.V., Norris, J.L., Korboukh, V., Tripathy, A., Janzen, W.P., 2014. Discovery of a selective, substrate-competitive inhibitor of the lysine methyltransferase SETD8. Journal of medicinal chemistry 57, 6822-6833.

Somnarin, T., Pobsuk, N., Chantakul, R., Panklai, T., Temkitthawon, P., Hannongbua, S., Chootip, K., Ingkaninan, K., Boonyarattanakalin, K., Gleeson, D., Paul Gleeson, M., 2022. Computational design, synthesis and biological evaluation of PDE5 inhibitors based on N2,N4-diaminoquinazoline and N2,N6-diaminopurine scaffolds. Bioorganic & Medicinal Chemistry 76, 117092.

Sundriyal, S., Chen, P.B., Lubin, A.S., Lueg, G.A., Li, F., White, A.J.P., Malmquist, N.A., Vedadi, M., Scherf, A., Fuchter, M.J., 2017. Histone lysine methyltransferase structure activity relationships that allow for segregation of G9a inhibition and anti-Plasmodium activity. MedChemComm 8, 1069-1092.

Vital, T., Wali, A., Butler, K.V., Xiong, Y., Foster, J.P., Marcel, S.S., McFadden, A.W., Nguyen, V.U., Bailey, B.M., Lamb, K.N., 2023. MS0621, a novel small-molecule modulator of Ewing sarcoma chromatin accessibility, interacts with an RNA-associated macromolecular complex and influences RNA splicing. Frontiers in Oncology 13.

Wang, P.G., Kondengaden, M.S., Zhang, Q., Zang, L., 2019. Histone deacetylase and histone methyltransferase inhibitors and methods of making and use of the same. Google Patents.

4 Zusammenfassung der Arbeit

Organophosphatvergiftungen, die nach Exposition gegenüber Nervenkampfstoffen oder bestimmten Insektiziden auftreten, können tödlich enden, wenn sie nicht adäquat therapiert werden. Allerdings weist das derzeitige Behandlungsschema Lücken auf und berücksichtigt nicht alle an der Entstehung der Vergiftungssymptome beteiligten biologischen Funktionsmoleküle. Bei einer Organophosphatvergiftung wird primär die für den Abbau des Neurotransmitters Acetylcholin verantwortliche Acetylcholinesterase (AChE) blockiert, wodurch es als Folge eines unkontrollierten Anstiegs der Neurotransmitterkonzentration zu einer Fehlfunktion der muskarinischen (mAChR) und nikotinischen Acetylcholinrezeptoren (nAChR) kommt. Die für eine Organophosphat-Intoxikation bekannten schwerwiegenden Symptome sind die Folge. Die derzeit für die Therapie einer Organophosphatvergiftung eingesetzten Arzneistoffe entfalten ihre Wirkung entweder an der AChE oder am mAChR. Der nAChR wird nicht direkt adressiert – lediglich die Behandlung der AChE wirkt sich indirekt positiv auf die Funktionalität des nAChRs aus. Um die Erfolgschancen einer Therapie von Organophosphatvergiftungen zu erhöhen, ist es zwingend notwendig, auch Wirkstoffe zur Verfügung zu haben, die mit ihrer Wirkung direkt am nAChR ansetzen.

Die andauernde Überstimulation des nAChRs mit dem Neurotransmitter Acetylcholin, die während einer Organophosphatvergiftung stattfindet, führt dazu, dass dieser von einem funktionalen Zustand in einen desensitisierten Zustand übergeht, in welchem er nicht mehr aktivierbar ist. Die nAChR-vermittelte Reizweiterleitung ist dadurch gestört. Die resultierenden Probleme sind vielfältig und drastisch, wenn man bedenkt, dass auch die Signalübertragung von Nerven- auf Muskelzellen von funktionsfähigen nAChRs abhängt (Atemmuskulatur!). Ein in letzter Zeit intensiv bearbeitetes Forschungsfeld beschäftigt sich mit der Entwicklung sogenannter „Resensitizer“. Das sind Substanzen, die den nAChR als allosterische Modulatoren von einem desensitisierten in einen funktionalen Zustand zurückführen. Als solche Modulatoren wurden bisher am eingehendsten Bispyridiniumverbindungen untersucht, mit MB327 als einem der wichtigsten Vertreter dieser Substanzklasse. Obwohl mit den Bispyridiniumverbindungen bereits beachtliche Erfolge erzielt werden konnten, ist keine der bisher bekannten Substanzen als Wirkstoffkandidat geeignet. Dies liegt unter anderem daran, dass die Affinität der Substanzen zur allosteren MB327-PAM-1-Bindungsstelle, die die Wirkung von „Resensitizern“ vermittelt, vergleichsweise gering

ist. Auf der Suche nach Verbindungen mit deutlich höherer Affinität zu dieser allosteren Bindungsstelle wurden vor Beginn dieser Arbeit die Substanzen UNC0638, UNC0642 und UNC0646 identifiziert. Zu Beginn der vorliegenden Dissertation galten diese Substanzen als die mit der höchsten bekannten Affinität zur MB327-PAM-1-Bindungsstelle. Besonders interessant erscheinen diese drei Verbindungen, da sie alle auf einem Chinazolin-Grundgerüst beruhen und sich auch hinsichtlich der Struktur der Substituenten sehr ähnlich sind. Es ist deshalb anzunehmen, dass es weitere strukturverwandte Verbindungen gibt, die eine noch höhere Affinität zur MB327-Bindungsstelle und damit ein besonders hohes Potenzial als „Resensitizer“ aufweisen.

Ziel dieser Arbeit war es, im ersten Schritt einen MS-Bindungsassay zu entwickeln, der eine der Verbindungen UNC0638, UNC0642 oder UNC0646 als Reporterliganden verwendet. Dies gelang mit der Etablierung des UNC0642-MS-Bindungsassays. Gegenüber dem auf [$^2H_6$]MB327 basierenden MS-Bindungsassay, der bis dahin für die Untersuchung der MB327-Bindungsstelle verwendet worden war, bietet der neu entwickelte Assay den Vorteil, dass der verwendete Reporterligand, UNC0642, kommerziell verfügbar und der Assay somit leichter einzurichten ist. Zudem zählt der für den neuen MS-Bindungsassay verwendete Reporterligand, UNC0642, zu den drei Verbindungen mit den höchsten bekannten Affinitäten zur MB327-Bindungsstelle des nAChRs. Der UNC0642-MS-Bindungsassay kann deshalb als robuster als der [$^2H_6$]MB327-MS-Bindungsassay angesehen werden. Mit dem neu entwickelten MS-Bindungsassay wurde erstmalig die Bindung von UNC0642 am nAChR (in Form des *Torpedo californica*-nAChRs) in Sättigungsexperimenten charakterisiert. Der hier ermittelte K_d-Wert von 6.7 ± 0.4 µM bestätigt die hohe Affinität von UNC0642 zum nAChR. Die Annahme, dass es sich bei der adressierten Bindungsstelle tatsächlich um MB327-PAM-1 handelt, wurde durch die Ergebnisse einzelner Kompetitionsexperimente mit ausgewählten Referenzsubstanzen bekräftigt. Außerdem unterstützen die Ergebnisse aus *in silico* Studien und aus *ex vivo* Versuchen diese Hypothese. Mit Hilfe der *in silico* Studien gelang es für UNC0646 den Bindemodus in der MB327-PAM-1-Bindetasche abzuleiten. In den *ex vivo* Experimenten ließ sich zeigen, dass UNC0642 und dessen Analoga in der Lage sind, die Muskelkraft von mit Nervenkampfstoff vergifteten Muskeln zumindest teilweise wiederherzustellen (hier: Soman-vergiftete Rattendiaphragmen).

Im Weiteren kam der von mir entwickelte UNC0642-MS-Bindungsassay für die Bestimmung der Affinität von Testsubstanzen zur MB327-PAM-1-Bindungsstelle des nAChRs zum Einsatz.

So wurde der UNC0642-MS-Bindungsassay verwendet, um für die in *in silico* Screenings identifizierten Hits die Affinität zu bestimmen. Auf der Suche nach strukturell neuartigen Liganden für die MB327-PAM-1-Bindungsstelle wurden durch computergestützte Berechnungen vier neue Chemotypen identifiziert. Vertreter von zwei der vier vorgeschlagenen Chemotypen waren in kompetitiven UNC0642-MS-Bindungsassays bei einer Konzentration von 10 µM in der Lage, die Bindung des in einer Konzentration von 1 µM eingesetzten Reporterliganden signifikant zu reduzieren. Diese beiden Verbindungen, namentlich Cycloguanil und PTMD99-0016C, weisen somit eine nennenswerte Affinität gegenüber der MB327-PAM-1-Bindungsstelle auf. Für Cycloguanil wurden weitere Untersuchungen angestellt, die zum einen zeigen, dass dessen Affinität sogar signifikant höher als die von MB327 ist und dass es zudem einen Muskelkraft-wiederherstellenden Effekt bei Soman-vergifteten Rattendiaphragmen besitzt. Die neu identifizierten Chemotypen bilden somit vielversprechende Ansatzpunkte für die Weiterentwicklung von „Resensitizern“ des nAChRs.

Mit Hilfe des UNC0642-MS-Bindungsassays wurden des Weiteren auch neue, erstmalig hergestellte Bispyridiniumverbindungen hinsichtlich ihrer Affinität zur MB327-Bindungsstelle des nAChRs charakterisiert. Es handelte sich hierbei hauptsächlich um Verbindungen mit einem 4-Aminopyridinium-Motiv. Diese sollten gezielt untersucht werden, da entsprechende Analoga zuvor beachtliche Ergebnisse in *ex vivo* Versuchen mit Soman-vergifteten Rattenmuskeln gezeigt hatten. Auch von den neu synthetisierten Verbindungen zeichneten sich einzelne durch eine beträchtliche Wiederherstellung der Muskelkraft bei vergleichsweise niedrigen Substanzkonzentrationen aus. Von den Verbindungen PTM0069, PTM0071 und PTM0072, welche bei der Muskelkraftwiederherstellung besonders aktiv waren, zeigen die beiden ersten im UNC0642-MS-Bindungsassays auch eine deutlich höhere Affinität zur MB327-PAM-1-Bindungsstelle als MB327.

Nicht zuletzt fungierte der UNC0642-MS-Bindungsassay als essenzielles Werkzeug bei der Bestimmung der Affinitäten von mehrfach substituierten Chinazolinen in Bezug auf die MB327-Bindungsstelle des nAChRs. Durch die Untersuchung zahlreicher entsprechender Analoga, deren Substituenten am Chinazolin-Grundgerüst

systematisch variiert worden waren, konnten wertvolle Daten generiert werden, die Rückschlüsse darüber zulassen, welche Strukturelemente für die Bindung von Substanzen dieser Klasse an die MB327-PAM-1-Bindungsstelle besonders wichtig sind. Diese Bindungsdaten stellen zudem eine wichtige Grundlage für weitere computergestützte Berechnungen zur Weiterentwicklung neuer Liganden für die MB327-Bindungsstelle dar. Darüber hinaus wurde in den entsprechenden Untersuchungen mit UNC0631 eine zu UNC0646 analoge Verbindung mit einem im Vergleich dazu geringfügig höheren pK_i-Wert identifiziert.

Der in dieser Arbeit entwickelte UNC0642-MS-Bindungsassay bietet gegenüber dem [$^2H_6$]MB327-MS-Bindungsassay, welcher bisher die einzige Möglichkeit bot, die MB327-Bindungsstelle des nAChRs zu untersuchen, klare Vorteile und kann als attraktive Alternative zu diesem angesehen werden. Durch die Anwendung des neu etablierten Assays wurden zahlreiche Verbindungen verschiedener Substanzklassen hinsichtlich ihrer Affinität zur MB327-PAM-1-Bindungsstelle untersucht. Die erzielten Ergebnisse liefern wertvolle Erkenntnisse für die Weiterentwicklung von „Resensitizern“ des nAChRs und könnten damit eine wichtige Grundlage für die Verbesserung der Behandlung von Organophosphatvergiftungen schaffen.

5 Abkürzungsverzeichnis

5-HT	5-Hydroxytryptamin
ACh	Acetylcholin
AChE	Acetylcholinesterase
Cys	Cystein
ESI	Elektrospray-Ionisation
FDA	engl.: *Food and Drug Administration*
GABA	γ-Aminobuttersäure
K_i	Dissoziationsgleichgewichtskonstante des Inhibitors
K_d	Dissoziationsgleichgewichtskonstante des Reporterliganden
LC	engl.: *Liquid Chromatography*
MS	Massenspektrometrie
mAChR	muskarinischer Acetylcholinrezeptor
nAChR	nikotinischer Acetylcholinrezeptor
PAM	Positiv Allosterischer Modulator
PDB	engl.: *Protein Data Bank*
Ser	Serin

6 Literaturverzeichnis

1. Schrader G., *Die insektiziden Phosphorsäureester.* Angewandte Chemie, 1957. **69**(3): p. 86-90.
2. Timperley C.M., *Highly-toxic fluorine compounds*, in *Fluorine Chemistry at the Millennium*. 2000.
3. Sidell F.R., *Nerve Agents*, in *Textbook of Military Medicine - Medical Aspects of Chemical and Biological Warfare*. 1997.
4. Chai P.R., Hayes B.D., Erickson T.B., Boyer E.W., *Novichok agents: a historical, current, and toxicological perspective.* Toxicol Commun, 2018. **2**(1): p. 45-48.
5. Costanzi S., Machado J.H., Mitchell M., *Nerve Agents: What They Are, How They Work, How to Counter Them.* ACS Chem Neurosci, 2018. **9**(5): p. 873-885.
6. Quitschau M., Schuhmann T., Piel J., von Zezschwitz P., Grond S., *The New Metabolite (S)-Cinnamoylphosphoramide from Streptomyces sp. and Its Total Synthesis.* European Journal of Organic Chemistry, 2008. **2008**(30): p. 5117-5124.
7. Höfer M., *Chemische Kampfstoffe: Ein Überblick.* Chemie in unserer Zeit, 2002. **36**(3): p. 148-155.
8. OPCW, *Report of the OPCW: S2013735.* 2013.
9. OPCW, *Report of the OPCW: S15102017.* 2017.
10. OPCW, *Report of the OPCW: S15482017.* 2017.
11. OPCW, *Report of the OPCW: S16122018.* 2018.
12. OPCW, *Report of the OPCW: S16362018.* 2018.
13. OPCW, *Report of the OPCW: S16712018.* 2018.
14. OPCW, *Statement of the OPCW: EC87NAT14.* 2018.
15. OPCW, *Report of the OPCW: S19062020.* 2020.
16. Steindl D., Boehmerle W., Korner R., Praeger D., Haug M., Nee J., Schreiber A., Scheibe F., Demin K., Jacoby P., Tauber R., Hartwig S., Endres M., Eckardt K.U., *Novichok nerve agent poisoning.* Lancet, 2021. **397**(10270): p. 249-252.
17. John H., van der Schans M.J., Koller M., Spruit H.E.T., Worek F., Thiermann H., Noort D., *Fatal sarin poisoning in Syria 2013: forensic verification within an international laboratory network.* Forensic Toxicol, 2018. **36**(1): p. 61-71.
18. OPCW, *Chemical Weapons Convention.* 2020.
19. Buckley N.A., Roberts D., Eddleston M., *Overcoming apathy in research on organophosphate poisoning.* BMJ, 2004. **329**(7476): p. 1231-3.
20. Eddleston M. and Phillips M.R., *Self poisoning with pesticides.* BMJ, 2004. **328**(7430): p. 42-4.
21. Gunnell D., Eddleston M., Phillips M.R., Konradsen F., *The global distribution of fatal pesticide self-poisoning: systematic review.* BMC Public Health, 2007. **7**: p. 357.
22. Mew E.J., Padmanathan P., Konradsen F., Eddleston M., Chang S.S., Phillips M.R., Gunnell D., *The global burden of fatal self-poisoning with pesticides 2006-15: Systematic review.* J Affect Disord, 2017. **219**: p. 93-104.
23. Böhm S., *Cholinerge Systeme*, in *Pharmakologie und Toxikologie*. 2016.
24. Starke K., *Pharmakologie cholinerger Systeme*, in *Allgemeine und spezielle Pharmakologie und Toxikologie*. 2013.
25. Bear M.F., Connors B.W., Paradiso M.A., *Neurowissenschaften*. 2018.
26. Silbernagl S., Despopoulos A., Draguhn A., *Taschenatlas Physiologie*. 2012.

27. Hampel H., Mesulam M.M., Cuello A.C., Farlow M.R., Giacobini E., Grossberg G.T., Khachaturian A.S., Vergallo A., Cavedo E., Snyder P.J., Khachaturian Z.S., *The cholinergic system in the pathophysiology and treatment of Alzheimer's disease.* Brain, 2018. **141**(7): p. 1917-1933.
28. Martorana A., Esposito Z., Koch G., *Beyond the cholinergic hypothesis: do current drugs work in Alzheimer's disease?* CNS Neurosci Ther, 2010. **16**(4): p. 235-45.
29. Contestabile A., *The history of the cholinergic hypothesis.* Behav Brain Res, 2011. **221**(2): p. 334-40.
30. Craig L.A., Hong N.S., McDonald R.J., *Revisiting the cholinergic hypothesis in the development of Alzheimer's disease.* Neurosci Biobehav Rev, 2011. **35**(6): p. 1397-409.
31. Halder N. and Lal G., *Cholinergic System and Its Therapeutic Importance in Inflammation and Autoimmunity.* Front Immunol, 2021. **12**: p. 660342.
32. Bohnen N.I., Yarnall A.J., Weil R.S., Moro E., Moehle M.S., Borghammer P., Bedard M.A., Albin R.L., *Cholinergic system changes in Parkinson's disease: emerging therapeutic approaches.* Lancet Neurol, 2022. **21**(4): p. 381-392.
33. Papke R.L., Brunzell D.H., De Biasi M., *Cholinergic Receptors and Addiction.* Curr Top Behav Neurosci, 2020. **45**: p. 123-151.
34. Terry A.V., *Role of the central cholinergic system in the therapeutics of schizophrenia.* Curr Neuropharmacol, 2008. **6**(3): p. 286-92.
35. Wang Y., Tan B., Wang Y., Chen Z., *Cholinergic Signaling, Neural Excitability, and Epilepsy.* Molecules, 2021. **26**(8).
36. Sofuoglu M. and Mooney M., *Cholinergic functioning in stimulant addiction: implications for medications development.* CNS Drugs, 2009. **23**(11): p. 939-52.
37. Sarter M., Lustig C., Taylor S.F., *Cholinergic contributions to the cognitive symptoms of schizophrenia and the viability of cholinergic treatments.* Neuropharmacology, 2012. **62**(3): p. 1544-53.
38. Oleksak P., Novotny M., Patocka J., Nepovimova E., Hort J., Pavlik J., Klimova B., Valis M., Kuca K., *Neuropharmacology of Cevimeline and Muscarinic Drugs-Focus on Cognition and Neurodegeneration.* Int J Mol Sci, 2021. **22**(16).
39. Lotti M., *Clinical Toxicology of Acetylcholinesterase Agents in Humans*, in *Hayes Handbook of Pesticide Toxicology*. 2010.
40. Soukup O., Tobin G., Kumar U.K., Binder J., Proska J., Jun D., Fusek J., Kuca K., *Interaction of nerve agent antidotes with cholinergic systems.* Curr Med Chem, 2010. **17**(16): p. 1708-18.
41. Field M.J. and Wymore T.W., *Multiscale modeling of nerve agent hydrolysis mechanisms: a tale of two Nobel Prizes.* Physica Scripta, 2014. **89**(10).
42. Colovic M.B., Krstic D.Z., Lazarevic-Pasti T.D., Bondzic A.M., Vasic V.M., *Acetylcholinesterase inhibitors: pharmacology and toxicology.* Curr Neuropharmacol, 2013. **11**(3): p. 315-35.
43. Worek F., Eyer P., Aurbek N., Szinicz L., Thiermann H., *Recent advances in evaluation of oxime efficacy in nerve agent poisoning by in vitro analysis.* Toxicol Appl Pharmacol, 2007. **219**(2-3): p. 226-34.
44. Thiermann H., Aurbek N., Worek F., *Treatment of Nerve Agent Poisoning*, in *Chemical Warfare Toxicology - Volume 2: Management of Poisoning*. 2016.
45. Newmark J., *Therapy for nerve agent poisoning.* Arch Neurol, 2004. **61**(5): p. 649-52.
46. Holmstedt B., *Pharmacology of Organophosphorus Cholinesterase Inhibitors.* Pharmacological Reviews, 1959. **11**(3): p. 567.

47. Hulse E.J., Davies J.O., Simpson A.J., Sciuto A.M., Eddleston M., *Respiratory complications of organophosphorus nerve agent and insecticide poisoning. Implications for respiratory and critical care.* Am J Respir Crit Care Med, 2014. **190**(12): p. 1342-54.
48. Eyer P., Szinicz L., Thiermann H., Worek F., Zilker T., *Testing of antidotes for organophosphorus compounds: experimental procedures and clinical reality.* Toxicology, 2007. **233**(1-3): p. 108-19.
49. Worek F., Thiermann H., Wille T., *Oximes in organophosphate poisoning: 60 years of hope and despair.* Chem Biol Interact, 2016. **259**(Pt B): p. 93-98.
50. Thiermann H. and Worek F., *Pro: Oximes should be used routinely in organophosphate poisoning.* Br J Clin Pharmacol, 2022. **88**(12): p. 5064-5069.
51. Costa L.G., *Current issues in organophosphate toxicology.* Clin Chim Acta, 2006. **366**(1-2): p. 1-13.
52. Masson P., Nachon F., Lockridge O., *Structural approach to the aging of phosphylated cholinesterases.* Chem Biol Interact, 2010. **187**(1-3): p. 157-62.
53. Thiermann H., Szinicz L., Eyer P., Felgenhauer N., Zilker T., Worek F., *Lessons to be learnt from organophosphorus pesticide poisoning for the treatment of nerve agent poisoning.* Toxicology, 2007. **233**(1-3): p. 145-54.
54. Sirin G.S., Zhou Y., Lior-Hoffmann L., Wang S., Zhang Y., *Aging mechanism of soman inhibited acetylcholinesterase.* J Phys Chem B, 2012. **116**(40): p. 12199-207.
55. Worek F., Thiermann H., Wille T., *Organophosphorus compounds and oximes: a critical review.* Arch Toxicol, 2020. **94**(7): p. 2275-2292.
56. Worek F., Szinicz L., Eyer P., Thiermann H., *Evaluation of oxime efficacy in nerve agent poisoning: development of a kinetic-based dynamic model.* Toxicol Appl Pharmacol, 2005. **209**(3): p. 193-202.
57. Aman S., Paul S., Chowdhury F.R., *Management of Organophosphorus Poisoning: Standard Treatment and Beyond.* Crit Care Clin, 2021. **37**(3): p. 673-686.
58. Sheridan R.D., *Nicotinic antagonists in the treatment of nerve agent intoxication.* Journal of the Royal Society of Medicine, 2005. **98**(3): p. 114-115.
59. Changeux J.P., *The nicotinic acetylcholine receptor: the founding father of the pentameric ligand-gated ion channel superfamily.* J Biol Chem, 2012. **287**(48): p. 40207-15.
60. Stroud R.M., McCarthy M.P., Shuster M., *Nicotinic acetylcholine receptor superfamily of ligand-gated ion channels.* Biochemistry, 1990. **29**(50): p. 11009-23.
61. Lester H.A., Dibas M.I., Dahan D.S., Leite J.F., Dougherty D.A., *Cys-loop receptors: new twists and turns.* Trends Neurosci, 2004. **27**(6): p. 329-36.
62. Le Novere N., Corringer P.J., Changeux J.P., *The diversity of subunit composition in nAChRs: evolutionary origins, physiologic and pharmacologic consequences.* J Neurobiol, 2002. **53**(4): p. 447-56.
63. Unwin N., *Nicotinic acetylcholine receptor and the structural basis of neuromuscular transmission: insights from Torpedo postsynaptic membranes.* Q Rev Biophys, 2013. **46**(4): p. 283-322.
64. Papke R.L., *Merging old and new perspectives on nicotinic acetylcholine receptors.* Biochem Pharmacol, 2014. **89**(1): p. 1-11.
65. Zhang J., Xue F., Liu Y., Yang H., Wang X., *The structural mechanism of the Cys-loop receptor desensitization.* Mol Neurobiol, 2013. **48**(1): p. 97-108.

66. Corradi J. and Bouzat C., *Understanding the Bases of Function and Modulation of alpha7 Nicotinic Receptors: Implications for Drug Discovery.* Mol Pharmacol, 2016. **90**(3): p. 288-99.
67. Karlin A., *Emerging structure of the nicotinic acetylcholine receptors.* Nat Rev Neurosci, 2002. **3**(2): p. 102-14.
68. Sine S.M. and Engel A.G., *Recent advances in Cys-loop receptor structure and function.* Nature, 2006. **440**(7083): p. 448-55.
69. Giniatullin R., Nistri A., Yakel J.L., *Desensitization of nicotinic ACh receptors: shaping cholinergic signaling.* Trends Neurosci, 2005. **28**(7): p. 371-8.
70. Wang H. and Sun X., *Desensitized nicotinic receptors in brain.* Brain Res Brain Res Rev, 2005. **48**(3): p. 420-37.
71. Nemecz A., Prevost M.S., Menny A., Corringer P.J., *Emerging Molecular Mechanisms of Signal Transduction in Pentameric Ligand-Gated Ion Channels.* Neuron, 2016. **90**(3): p. 452-70.
72. Noviello C.M., Gharpure A., Mukhtasimova N., Cabuco R., Baxter L., Borek D., Sine S.M., Hibbs R.E., *Structure and gating mechanism of the alpha7 nicotinic acetylcholine receptor.* Cell, 2021. **184**(8): p. 2121-2134 e13.
73. Millar N.S. and Gotti C., *Diversity of vertebrate nicotinic acetylcholine receptors.* Neuropharmacology, 2009. **56**(1): p. 237-46.
74. Seifert R., *Basiswissen Pharmakologie*. 2018.
75. Galzi J.L., Revah F., Bessis A., Changeux J.P., *Functional architecture of the nicotinic acetylcholine receptor: from electric organ to brain.* Annu Rev Pharmacol Toxicol, 1991. **31**: p. 37-72.
76. Newmark J., *Nerve agents.* Neurologist, 2007. **13**(1): p. 20-32.
77. Itier V. and Bertrand D., *Neuronal nicotinic receptors: from protein structure to function.* FEBS Lett, 2001. **504**(3): p. 118-25.
78. Whittaker V.P., *The historical significance of work with electric organs for the study of cholinergic transmission.* Neurochem Int, 1989. **14**(3): p. 275-87.
79. Millar N.S., *Assembly and subunit diversity of nicotinic acetylcholine receptors.* Biochem Soc Trans, 2003. **31**(Pt 4): p. 869-74.
80. Missias A.C., Chu G.C., Klocke B.J., Sanes J.R., Merlie J.P., *Maturation of the acetylcholine receptor in skeletal muscle: regulation of the AChR gamma-to-epsilon switch.* Dev Biol, 1996. **179**(1): p. 223-38.
81. Mishina M., Takai T., Imoto K., Noda M., Takahashi T., Numa S., Methfessel C., Sakmann B., *Molecular distinction between fetal and adult forms of muscle acetylcholine receptor.* Nature, 1986. **321**(6068): p. 406-11.
82. Unwin N., *Refined structure of the nicotinic acetylcholine receptor at 4A resolution.* J Mol Biol, 2005. **346**(4): p. 967-89.
83. Mnatsakanyan N. and Jansen M., *Experimental determination of the vertical alignment between the second and third transmembrane segments of muscle nicotinic acetylcholine receptors.* J Neurochem, 2013. **125**(6): p. 843-54.
84. Morales-Perez C.L., Noviello C.M., Hibbs R.E., *X-ray structure of the human alpha4beta2 nicotinic receptor.* Nature, 2016. **538**(7625): p. 411-415.
85. Rahman M.M., Teng J., Worrell B.T., Noviello C.M., Lee M., Karlin A., Stowell M.H.B., Hibbs R.E., *Structure of the Native Muscle-type Nicotinic Receptor and Inhibition by Snake Venom Toxins.* Neuron, 2020. **106**(6): p. 952-962.
86. Berman H.M., Westbrook J., Feng Z., Gilliland G., Bhat T.N., Weissig H., Shindyalov I.N., Bourne P.E., *The Protein Data Bank.* Nucleic Acids Res, 2000. **28**(1): p. 235-42.
87. Sehnal D., Bittrich S., Deshpande M., Svobodova R., Berka K., Bazgier V., Velankar S., Burley S.K., Koca J., Rose A.S., *Mol* Viewer: modern web app for*

3D visualization and analysis of large biomolecular structures. Nucleic Acids Res, 2021. **49**(W1): p. W431-W437.
88. Arias H.R., *Localization of agonist and competitive antagonist binding sites on nicotinic acetylcholine receptors.* Neurochem Int, 2000. **36**(7): p. 595-645.
89. Brejc K.v.D., W. J., Klaassen R.V., Schuurmans M., van Der Oost J., Smit A.B., Sixma T.K., *Crystal structure of an ACh-binding protein reveals the ligand-binding domain of nicotinic receptors.* Nature, 2001. **411**(6835): p. 269-76.
90. Changeux J.P., *The nicotinic acetylcholine receptor: a typical 'allosteric machine'.* Philos Trans R Soc Lond B Biol Sci, 2018. **373**(1749).
91. Cecchini M. and Changeux J.P., *The nicotinic acetylcholine receptor and its prokaryotic homologues: Structure, conformational transitions & allosteric modulation.* Neuropharmacology, 2015. **96**(Pt B): p. 137-49.
92. Chatzidaki A. and Millar N.S., *Allosteric modulation of nicotinic acetylcholine receptors.* Biochem Pharmacol, 2015. **97**(4): p. 408-417.
93. Timperley C.M., Bird M., Green C., Price M.E., Chad J.E., Turner S.R., Tattersall J.E.H., *1,1'-(Propane-1,3-diyl)bis(4-tert-butylpyridinium) di(methanesulfonate) protects guinea pigs from soman poisoning when used as part of a combined therapy.* Med. Chem. Commun., 2012. **3**(3): p. 352-356.
94. Turner S.R., Chad J.E., Price M., Timperley C.M., Bird M., Green A.C., Tattersall J.E., *Protection against nerve agent poisoning by a noncompetitive nicotinic antagonist.* Toxicol Lett, 2011. **206**(1): p. 105-11.
95. Seeger T., Eichhorn M., Lindner M., Niessen K.V., Tattersall J.E., Timperley C.M., Bird M., Green A.C., Thiermann H., Worek F., *Restoration of soman-blocked neuromuscular transmission in human and rat muscle by the bispyridinium non-oxime MB327 in vitro.* Toxicology, 2012. **294**(2-3): p. 80-4.
96. Niessen K.V., Muschik S., Langguth F., Rappenglück S., Seeger T., Thiermann H., Worek F., *Functional analysis of Torpedo californica nicotinic acetylcholine receptors in multiple activation states by SSM-based electrophysiology.* Toxicol Lett, 2016. **247**: p. 1-10.
97. Niessen K.V., Seeger T., Rappenglück S., Wein T., Höfner G., Wanner K.T., Thiermann H., Worek F., *In vitro pharmacological characterization of the bispyridinium non-oxime compound MB327 and its 2- and 3-regioisomers.* Toxicol Lett, 2018. **293**: p. 190-197.
98. Sichler S., Höfner G., Rappenglück S., Wein T., Niessen K.V., Seeger T., Worek F., Thiermann H., Paintner F.F., Wanner K.T., *Development of MS Binding Assays targeting the binding site of MB327 at the nicotinic acetylcholine receptor.* Toxicol Lett, 2018. **293**: p. 172-183.
99. Wein T., Höfner G., Rappengluck S., Sichler S., Niessen K.V., Seeger T., Worek F., Thiermann H., Wanner K.T., *Searching for putative binding sites of the bispyridinium compound MB327 in the nicotinic acetylcholine receptor.* Toxicol Lett, 2018. **293**: p. 184-189.
100. Kaiser J., Gertzen C.G.W., Bernauer T., Höfner G., Niessen K.V., Seeger T., Paintner F.F., Wanner K.T., Worek F., Thiermann H., Gohlke H., *A novel binding site in the nicotinic acetylcholine receptor for MB327 can explain its allosteric modulation relevant for organophosphorus-poisoning treatment.* Toxicol Lett, 2023. **373**: p. 160-171.
101. Kassa J., Timperley C.M., Bird M., Green A.C., Tattersall J.E.H., *Influence of Experimental End Point on the Therapeutic Efficacy of Essential and Additional Antidotes in Organophosphorus Nerve Agent-Intoxicated Mice.* Toxics, 2022. **10**(4).

102. Niessen K.V., Tattersall J.E., Timperley C.M., Bird M., Green C., Seeger T., Thiermann H., Worek F., *Interaction of bispyridinium compounds with the orthosteric binding site of human alpha7 and Torpedo californica nicotinic acetylcholine receptors (nAChRs).* Toxicol Lett, 2011. **206**(1): p. 100-4.
103. Niessen K.V., Tattersall J.E., Timperley C.M., Bird M., Green C., Thiermann H., Worek F., *Competition radioligand binding assays for the investigation of bispyridinium compound affinities to the human muscarinic acetylcholine receptor subtype 5 (hM(5)).* Drug Test Anal, 2012. **4**(3-4): p. 292-7.
104. Maguire J.J., Kuc R.E., Davenport A.P., *Radioligand binding assays and their analysis.* Methods Mol Biol, 2012. **897**: p. 31-77.
105. Bylund D.B. and Enna S.J., *Receptor Binding Assays and Drug Discovery.* Adv Pharmacol, 2018. **82**: p. 21-34.
106. Höfner G. and Wanner K.T., *MS Binding Assays*, in *Analyzing Biomolecular Interactions by Mass Spectrometry*. 2015.
107. Wanner K.T., Höfner G., Mannhold R., Kubinyi H., Folkers G., *Mass Spectrometry in Medicinal Chemistry: Applications in Drug Discovery*. 2007.
108. Zepperitz C., Höfner G., Wanner K.T., *MS-binding assays: kinetic, saturation, and competitive experiments based on quantitation of bound marker as exemplified by the GABA transporter mGAT1.* ChemMedChem, 2006. **1**(2): p. 208-17.
109. Hulme E.C. and Trevethick M.A., *Ligand binding assays at equilibrium: validation and interpretation.* Br J Pharmacol, 2010. **161**(6): p. 1219-37.
110. Gesztelyi R., Zsuga J., Kemeny-Beke A., Varga B., Juhasz B., Tosaki A., *The Hill equation and the origin of quantitative pharmacology.* Archive for History of Exact Sciences, 2012. **66**(4): p. 427-438.
111. Neubig R.R., Spedding M., Kenakin T., Christopoulos A., *International Union of Pharmacology Committee on Receptor Nomenclature and Drug Classification. XXXVIII. Update on terms and symbols in quantitative pharmacology.* Pharmacological Reviews, 2003. **55**(4): p. 597-606.
112. Weiland G.A. and Molinoff P.B., *Quantitative analysis of drug-receptor interactions: I. Determination of kinetic and equilibrium properties.* Life Sci, 1981. **29**(4): p. 313-30.
113. Rappenglück S., Sichler S., Höfner G., Wein T., Niessen K.V., Seeger T., Paintner F.F., Worek F., Thiermann H., Wanner K.T., *Synthesis of a Series of Non-Symmetric Bispyridinium and Related Compounds and Their Affinity Characterization at the Nicotinic Acetylcholine Receptor.* ChemMedChem, 2018. **13**(24): p. 2653-2663.
114. Rappenglück S., Sichler S., Höfner G., Wein T., Niessen K.V., Seeger T., Paintner F.F., Worek F., Thiermann H., Wanner K.T., *Synthesis of a Series of Structurally Diverse MB327 Derivatives and Their Affinity Characterization at the Nicotinic Acetylcholine Receptor.* ChemMedChem, 2018. **13**(17): p. 1806-1816.
115. Sichler S., Höfner G., Nitsche V., Niessen K.V., Seeger T., Worek F., Paintner F.F., Wanner K.T., *Screening for new ligands of the MB327-PAM-1 binding site of the nicotinic acetylcholine receptor.* Toxicol Lett, 2024. **394**: p. 23-31.